Preparation of *p*-Vinylacetophenone Copolymer

To a solution of 3 ml. of methylmagnesium bromide (Arapahoe, 3*M* in ether) and 5 ml. of dry tetrahydrofuran was added a solution of 0.5 g. of the 11% cyano copolymer (V) in 15 ml. of tetrahydrofuran. The mixture was stirred for 30 min. and then heated to 40°C. A gel began to form; therefore, the mixture was cooled, stirred vigorously for 30 min., and carefully decomposed with 5% aqueous hydrochloric acid. The mixture was stirred for 12 hr. and the liquid phase was decanted into methanol. The solid which formed was filtered from the solution, washed with methanol; and reprecipitated from chloroform into methanol to yield 0.41 g. of a white polymer (X).

ANAL. Calcd. for $C_{10}H_{10}O$(11%)–C_8H_8(89%): C, 90.77%; H, 7.62%. Found: C, 90.06%; H, 7.43%.

The Grignard reactions were attempted with the 43.5% cyano copolymer IV but only a small amount of conversion was observed at 15°C. and gel formation occurred at 40°C. Only 1–2% of converted polymer could be extracted from the gels.

Analyses were performed by Micro-Tech Laboratories, Skokie, Illinois, and by Alfred Bernhardt, Mikroanalytisches Laboratorium, Mulheim (Ruhr), West Germany.

DISCUSSION

The halogenation of polystyrene may be assumed to yield the *para* isomer almost exclusively, since the *meta* position is electronically unfavored for electrophilic substitution and the *ortho* position is probably effectively hindered by the backbone chain of the polymer. This assumption would appear to be especially valid for the larger iodine atom. To date the only reactions involving these *p*-halogenated polystyrenes that have been reported are the formation of poly-*p*-styryl-lithium from *p*-iodostyrene[2,5] and *p*-bromostyrene[6] polymers.

In the present investigation three *p*-iodostyrene–styrene copolymers were prepared by partial iodination according to the procedure of Braun,[2] and these readily formed *p*-cyanostyrene–styrene copolymers upon heating with cuprous cyanide in *N*-methylpyrrolidinone. Analysis of the products indicated that complete replacement of the iodine had occurred. Polystyrene was sufficiently brominated to form an apparent homopolymer and a 30% *p*-bromostyrene copolymer, and these were treated with cuprous cyanide under the same conditions. Only partial replacement of the bromine could be attained in 4 hr. and longer heating periods brought about considerable gel formation. The *p*-cyanostyrene copolymers were dark grey in color and their solutions were dark brown. These colors may have been due to traces of cuprous iodide, a red-brown solid, trapped in the polymer, for poly *p*-cyanostyrene prepared from the monomer is white.[1] The cyano copolymer prepared from the 65% *p*-iodostyrene

copolymer (I) was insoluble in benzene, chloroform, and tetrahydrofuran and soluble in ketone solvents. The inverse was found for the iodo copolymer I. This change in solubility properties is consistent with the replacement of the iodine by the highly polar cyano group. The 43.5% (IV) and 11% (V) *p*-cyanostyrene copolymers prepared from the corresponding *p*-iodostyrene copolymers II and III retained the solubility properties of the halo polymers. Therefore, IV and V were utilized for further reactions, since a wider choice of solvents was possible and interactions between adjacent groups were diminished.

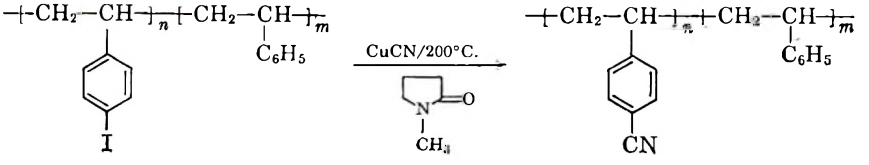

I: n = ca. 65% ($n + m$)
II: n = 43.5% ($n + m$)
III: n = 11% ($n + m$)

IV: n = 43.5% ($n + m$)
V: n = 11% ($n + m$)

All attempts to hydrolyze the *p*-cyanostyrene copolymers to the corresponding *p*-vinylbenzoic acid copolymers failed. No reports of this

TABLE I
Softening Points of the Polymers

Polymer		Softening point, °C.[a]	Solubility			
No.	Description		Bz	$CHCl_3$	THF	Acetone
	Polystyrene	130–140	+	+	+	+
I	*p*-Iodostyrene(65%)–styrene copolymer	170–175	+	+	+	−
II	*p*-Iodostyrene(43.5%)–styrene copolymer	155–165	+	+	+	+
III	*p*-Iodostyrene(11%)–styrene copolymer	160–165	+	+	+	+
IV	*p*-Cyanostyrene(43.5%)–styrene copolymer	160–170	+	+	+	+
V	*p*-Cyanostyrene(11%)–styrene copolymer	140–150	+	+	+	+
VI	Methyl *p*-vinylbenzoate (40%) terpolymer	145–150	+	+	+	+
VII	*p*-Vinylbenzoic acid polymer from VI	200–210	−	−	−	−[b]
VIII	*n*-Butyl-*p*-styrylketimine copolymer	150–153	+	+	+	+
IX	*n*-Butyl-*p*-styrylketone copolymer	125–135	+	+	+	+
X	Methyl-*p*-styrylketone copolymer (*p*-vinylacetophenone copolymer)	145–150	+	+	+	+

[a] Softening points were recorded on a Kofler hot bench.
[b] Soluble in pyridine, swells in aqueous base.

reaction could be found in the current literature although the monomer has been hydrolyzed to the monomer acid by a number of workers.[7] The *p*-cyanostyrene copolymer IV was converted into the methyl *p*-vinylbenzoate copolymer (VI) by reaction with methanol and hydrogen chloride under anhydrous conditions. Analysis indicated that the conversion to ester was about 93%. This conversion was substantiated by the presence of a weak band at 2200 cm.$^{-1}$ in the infrared spectrum indicative of a small amount of unaltered nitrile. The ester copolymer VI was partially hydrolyzed to the *p*-vinylbenzoic acid copolymer under basic conditions. The product (VII) was soluble in pyridine and swelled in aqueous sodium hydroxide solution. Only a crude infrared spectrum could be obtained for VII, and this showed the presence of a relatively large amount of unaltered ester. Apparently poly(methyl *p*-vinylbenzoate) has not been hydrolyzed to the acid polymer, although Marvel[8] has hydrolyzed poly(*sec*-butyl *p*-vinylbenzoate) to an "almost insoluble polymer" with a softening point of 300°C. and a tendency to swell in dilute base. The softening point of VII was 200–210°C. These results offer an interesting contrast with the recent preparation of *p*-vinylbenzoic acid and poly(methyl *p*-vinylbenzoate) by Merrill.[9]

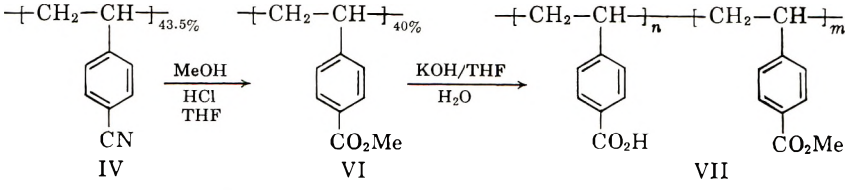

IV VI VII

Braun[5] has reported the reaction of poly-*p*-styryllithium with a number of nitriles to prepare poly-*p*-styrylketones in yields of 25–58%. A somewhat analogous reaction would be that of poly-*p*-cyanostyrene with Grignard reagents. The reaction of the 43.5% cyano copolymer IV with methyl- and *n*-butylmagnesium bromide was accompanied by gel formation, but the 11% cyano copolymer V reacted smoothly. When copolymer

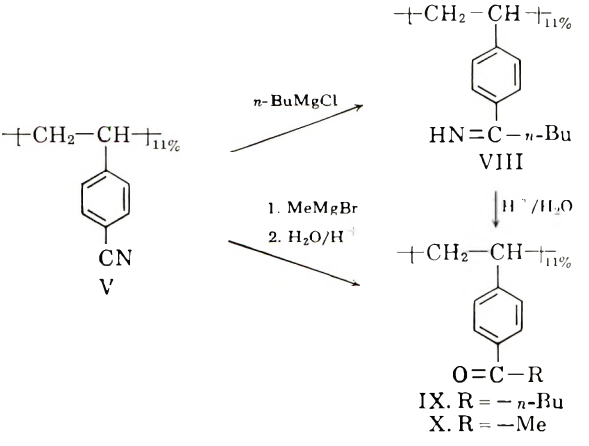

V VIII

IX. R = –*n*-Bu
X. R = –Me

V was treated with *n*-butylmagnesium chloride, the intermediate ketimine (VIII) could be isolated. Analysis indicated that VIII was impure, but attempts to purify it resulted in partial hydrolysis to the ketone. The ketimine VIII was rapidly hydrolyzed to the *n*-butyl-*p*-styrylketone (IX) with aqueous acid. The reaction of V with methylmagnesium bromide followed by hydrolysis with acid yielded an 11% *p*-vinylacetophenone copolymer (X).

References

1. *Styrene, its Polymers and Copolymers*, Am. Chem. Soc. Monograph Series, No. 152, Wiley, New York, 1952.
2. Braun, D., *Makromol. Chem.*, **30**, 85 (1959); *J. Polymer Sci.*, **40**, 578 (1959).
3. Newman, M. S., and H. Boden, *J. Org. Chem.*, **26**, 2525 (1961).
4. Supniewski, J. V., and P. L. Salzberg, *Org. Syn.*, **1**, 46 (1941).
5. Braun, D., *Makromol. Chem.*, **44**, 269 (1961).
6. Leavitt, F. G., and L. V. Matternas, *J. Polymer Sci.*, **45**, 249 (1960).
7. Marvel, C. S., and C. G. Overberger, *J. Am. Chem. Soc.*, **67**, 2250 (1945).
8. Marvel, C. S., *J. Am. Chem. Soc.*, **68**, 2106 (1946).
9. Merrill, S. H., *J. Polymer Sci.*, **61**, 223 (1962).

Résumé

On a préparé des copolymères de *p*-cyanostyrène et de styrène en chauffant des copolymères de *p*-iodostyrène/styrène en présence de cyanure cuivreux dans la *N*-méthylpyrrolidone. Les copolymères de *p*-cyanostyrène ne peuvent pas être hydrolysés afin dérivés de l'acide benzoïque, mais donnèrent le copolymère du *p*-méthyle benzoate de vinyle/styrène par réaction avec le méthanol et l'acide chlorhydrique. Ce copolymère d'ester méthylique fur partiellement hydrolysé en acide libre. On a traité un copolymère de *p*-cyanostyrène (11%)/styrène avec un réactif de Grignard *n*-butylé et méthylé et on obtient des copolymères de *n*-butyl et *p*-styrylcétone méthyleés correspondantes. Dans la réaction avec le chlorure de *n*-butyle, on isole le copolymère intermédiaire de l'imine *n*-butyl-*p*-styrylique.

Zusammenfassung

Copolymere aus *p*-Cyanostyrol und Styrol wurden durch Erhitzen von *p*-Jodstyrol-Styrolcopolymeren mit Kupfer-1-cyanid in *N*-Methylpyrrolidinon dargestellt. Die *p*-Cyanstyrolcopolymeren konnten nicht zu den Benzoesäurederivaten hydrolysiert werden, es war jedoch möglich sie durch Reaktion mit Methanol und Chlorwasserstoff ins Methyl-*p*-vinylbenzoat–Styrolcopolymere umzuwandeln. Dieses Methylestercopolymere wurde partiell zur freien Säure hydrolysiert. Ein *p*-Cyanstyrol (11%)–Styrolcopolymeres wurde zur Bildung der entsprechenden *n*-Butyl- und Methyl-*p*-styrylketoncopolymeren mit *n*-Butyl- und Methyl-Grignardverbindungen behandelt. Bei der Reaktion mit *n*-Butylmagnesiumchlorid wurde als Zwischenprodukt das *n*-Butyl-*p*-styrylketimincopolymere isoliert.

Received December 12, 1962

Journal of Polymer Science

INFORMATION FOR CONTRIBUTORS

1. Manuscripts should be submitted to one of the members of the Editorial Board or to the Editorial Office, c/o H. Mark, Polytechnic Institute of Brooklyn, 333 Jay Street, Brooklyn, New York 11201. Those in Europe should be submitted to Professor G. Smets, University of Louvain, Louvain, Belgium. Address all other correspondence to the publishers, Periodicals Division, John Wiley & Sons, Inc., 605 Third Avenue, New York, New York 10016.
2. Manuscripts for publication that have not been published elsewhere, books for review, and all correspondence regarding papers prior to their acceptance should be submitted to the Editorial Office. The editors desire to receive manuscripts based on original research in any phase of the chemistry and physics of large molecules.
3. It is the preference of the editors that papers be published in the English language. However, if the author desires that his paper be published in French or German, it is necessary that a particularly complete and comprehensive synopsis be furnished.
4. Manuscripts should be submitted in duplicate (one *original*, one carbon copy), typed *double space* throughout, on a *heavy* grade of paper, with margins of one inch on both sides.
5. A short synopsis of the main contributions in the paper is required in *triplicate*. This synopsis should be carefully prepared, for it will appear in English, in French, and in German, and is automatically the source of most abstracts. A summary of the whole paper, not the conclusions alone, should form the synopsis.
6. The paper should be reasonably subdivided into sections and, if necessary, subsections. Please refer to any issue of this Journal for examples.
7. The references should be numbered consecutively in the order of their appearance and should be complete, including authors' initials and—for unpublished lectures or symposia—the title of the paper, the date, and the name of the sponsoring society. Please compile references on a separate sheet at the end of the manuscript.
8. Please do not use footnotes to the text. Materials intended for footnotes should be inserted at the appropriate point in the manuscript proper and marked for "small type" (or inserted in the text as parenthetical material).
9. Please supply numbers and titles for all tables. All table columns should have an explanatory heading.
10. It is particularly important that all figures be submitted in a form suitable for reproduction. Good glossy photographs are required for halftone reproductions. For line drawings (graphs, etc.), the figures must be drawn clearly with India ink on heavy white paper, Bristol board, drawing linen, or coordinate paper with a very light blue background. The India ink lettering of graphs must be large, clear, and "open" so that letters and numbers do not fill in when reduced for publication. It is the usual practice to submit drawings that are twice the size of the final engravings; the maximum final size of figures for this journal is $4\frac{1}{2} \times 7\frac{1}{2}$ inches.

    It is the author's responsibility to obtain written permission to reproduce material which has appeared in another publication.

    If in doubt about the preparation of illustrations suitable for reproduction, please consult the publisher at the address given above in paragraph *1* and ask for a sample drawing.
11. Please supply legends for all figures and compile these on a separate sheet.

12. Authors are cautioned to type—wherever possible—all mathematical and chemical symbols, equations, and formulas. If these must be handwritten, please write clearly and leave ample space above and below for printer's marks; please use only ink. All Greek or unusual symbols should be identified in the margin the first time they are used. Please distinguish in the margins of the manuscript between capital and small letters of the alphabet wherever confusion may arise (e.g., k, K, κ). Please underline with a wavy line all vector quantities. Use fractional exponents to avoid root signs.

    The nomenclature sponsored by the international Union of Chemistry is requested for chemical compounds. Chemical bonds should be correctly placed, and double bonds clearly indicated. Valence is to be indicated by superscript plus and minus signs.

13. Authors will receive 50 reprints of their articles without charge. Additional reprints can be ordered and purchased by filling out the form attached to the galley proof. Page proofs will not be supplied.

14. No manuscript will be returned following publication unless a request for return is made when the manuscript is originally submittee's.

Manuscripts and illustrations not conforming to the style of the Journal will be returned to the author for reworking, thus delaying their appearance.

JOURNAL OF POLYMER SCIENCE: PART A VOL. 2, PP. 513–522 (1964)

Base-Catalyzed Solution Polymerization of Octamethylcyclotetrasiloxane*

MAURICE MORTON, M. A. DEISZ,† and E. E. BOSTICK,‡ *Institute of Rubber Research, University of Akron, Akron, Ohio*

Synopsis

A study has been carried out on the effect of solvent polarity on the base-catalyzed polymerization of octamethylcyclotetrasiloxane. The solvents used were decalin, *p*-chlorotoluene, *o*-dichlorobenzene, and nitrobenzene. In accordance with the ionic mechanism proposed by Grubb and Osthoff, it has been found that the polymerization rate increases with solvent polarity, presumably bp increasing the concentration of silanolate ions. In addition, a better correlation has been obtained between molecular weights and initiator concentration, and the effect of monomer concentration on equilibrium conversion has also been elucidated.

INTRODUCTION

The base-catalyzed polymerization of dimethylsiloxanes has been the subject of some recent investigations. Grubb and Osthoff[1] provided a comprehensive study of the bulk polymerization of octamethylcyclotetrasiloxane (D_4) catalyzed by potassium hydroxide. They found that the polymerization rate was first-order with respect to the monomer and half-order with respect to the initiator, and that the conversion of the cyclic monomer to linear polymer was a reversible process. Their kinetics were consistent with the following mechanism, involving the silanolate ion as the active species in the polymerization reaction:

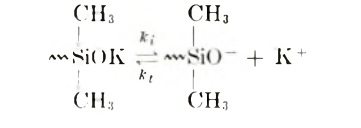

(1)

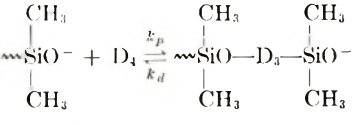

(2)

where k_i, k_t, k_p, and k_d represent the rate constants for initiation, termination, propagation, and depropagation respectively.

They also proposed that the propagation step [eq. (2)] was rate-govern-

* Presented in part at the 130th National Meeting of the American Chemical Society, Atlantic City, New Jersey, September 1956.

† Present address: Shell Development Co., Emeryville, California.

‡ Present address: General Electric Co., Schenectady, New York.

ing, hence the polymerization rate would be first-order with respect to the D_4 and its magnitude would be governed by the extent of the ionization shown in eq. (1). Furthermore, the average chain length of the polymer, at equilibrium, should be given by the ratio of polymer to initiator, since each silanolate is capable of initiating a chain.

On the basis of the above mechanism, it would be expected that the polymerization rate, but not the chain length, should be markedly affected by the polarity of the medium, inasmuch as the latter would be expected to affect reaction (1), but not reaction (2). It was the purpose of this investigation to study the effect of solvents of different polarity on this system.

EXPERIMENTAL

Materials

A. Cyclic Siloxanes. Octamethylcyclotetrasiloxane, D_4, and hexamethylcyclotrisiloxane, D_3, were kindly supplied by the General Electric Company. The compounds were redistilled prior to use, tetramer b.p. 175°C./738 mm. Hg, trimer b.p. 134°C./740 mm. Hg.

B. Potassium Hydroxide Catalyst. This material was also furnished by the General Electric Company as a suspension of potassium hydroxide in D_4. The base content was obtained by stirring an aliquot portion in twice its volume of distilled water and titrating with 1.0*N* hydrochloric acid, a Fisher titrimeter being used to determine the endpoint. The suspension was found to contain 0.0029 g. of potassium hydroxide/g. of suspension.

C. Potassium Silanolate Catalyst. The toluene solution of potassium silanolate, $HO[(CH_3)_2SiO]_xK$ was prepared by refluxing powdered potassium hydroxide and D_3 in toluene, as described by Grubb and Osthoff.[1]

D. Potassium Methoxide Catalyst. A suspension of potassium methoxide in D_4 was prepared under high vacuum conditions. Methyl alcohol was purified by first refluxing over calcium oxide, then distilling. This was followed by degassing at 10^{-5} mm. of mercury. A 0.5-g. portion of potassium was transferred, under benzene, to a flask which was subsequently evacuated and the benzene removed, and 10 ml. of the methyl alcohol was added to the flask. After the reaction was complete, the system was again pumped to remove excess alcohol. The resulting dry potassium methoxide was blended with 20 ml. of purified, degassed D_4 by means of a high speed magnetic stirrer. The suspension was found to contain 0.0374 g. of potassium methoxide/ml. of suspension.

E. Solvents. The four solvents employed were decalin (Matheson, Coleman and Bell, practical grade), *p*-chlorotoluene (Eastman reagent), *o*-dichlorobenzene (Eastman reagent), and nitrobenzene (Eastman reagent). These materials were redistilled prior to use, but the preliminary runs with decalin gave erratic results. In many cases there was no evidence of a polymerization reaction and the appearance of a solid precipitate was noticed. Lesser discrepancies occurred in the *p*-chlorotoluene poly-

merizations. By distilling the solvents over potassium hydroxide pellets (Merck reagent), reproducible results were finally obtained.

Determination of the Rate of Polymerization

The reactions were carried out in round-bottomed flasks equipped with a nitrogen inlet and a reflux condenser with drying tube. D_4 (and solvent in the case of the solution polymerizations) was placed in the flask which was then immersed up to the neck in an oil bath, maintained at 140 ± 0.6°C. After thermal equilibrium had been attained, the catalyst (potassium hydroxide or potassium methoxide) was added, and this point taken as zero reaction time. Nitrogen (prepurified) was bubbled continuously through the polymerizing mass. The rate was then determined by periodically removing the inlet tube and quickly withdrawing about 1 g. of sample by means of a glass tube. The sample was transferred to a tared aluminum cup and then weighed. The quantity of polymer present was found by adding an excess of iodine in toluene solution[2] to the cup containing the sample and drying the whole on an electric hot plate for 15 min. at 230°C. The error attributable to the drying procedure was determined by dissolving a known quantity of dimethyl polymer in D_4 at 140°C., adding potassium hydroxide catalyst, and then sampling the reaction immediately after solubilization of the catalyst. The maximum error in the determination of the quantity of polymer present was found to be ±1.0% of the total polymer.

The silanolate-catalyzed polymerizations were carried out in a manner similar to the potassium hydroxide runs. The solution of silanolate in toluene was placed in the reaction flask and pumped at reduced pressure to

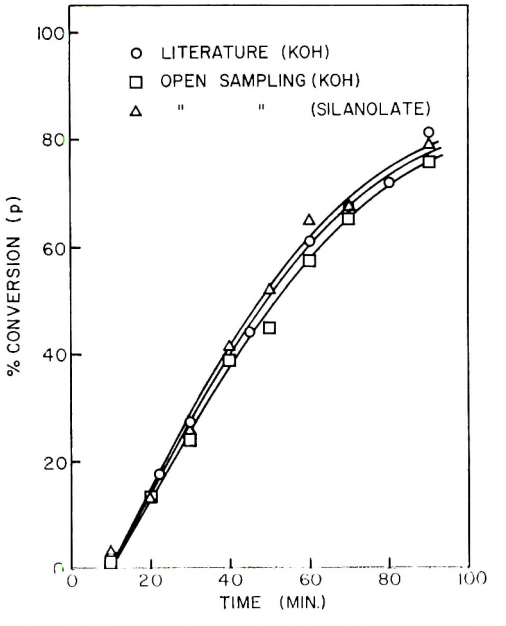

Fig. 1. Bulk polymerization of D_4 at 140°C. with 0.01% KOH.

remove the toluene. D_4 (and solvent in the solution reactions) was added to the flask and the mixture shaken at room temperature until the silanolate was dissolved. Following this the vessel was immersed in the oil bath and given 10 min. to attain thermal equilibrium. The reaction rate was determined as described above for the potassium hydroxide catalyzed polymerizations.

In order to determine the overall accuracy of this type of "open sampling" method, D_4 was polymerized in bulk at 140°C. with 0.01% potassium hydroxide and with potassium silanolate (equivalent to 0.01% potassium hydroxide). The data obtained may be compared in Figure 1 to those given in the literature,[1] where the rate of polymerization was determined by treating samples of partially polymerized D_4 with iodine, and subsequently pumping to constant weight.

It is apparent that the values for the rates of polymerization are nearly equivalent, and the accuracy of the open sampling method can be considered as satisfactory. Subsequent solution polymerization rates were obtained by this procedure.

Determination of Polymer Concentration and Molecular Weight at Equilibrium

Two methods were used to determine the per cent polymer, p_e, present at equilibrium. One approach was to carry out the polymerization for a period of 24 hr. to ensure equilibrium conditions, and then obtain p_e by the open sampling procedure. In the other method, a sample of dimethylsiloxane polymer ($\bar{M}_n$ = 606,000) was dissolved in the appropriate solvent at 140°C. 0.01% potassium hydroxide (based on the siloxane) was added and the depolymerization continued for 24 hr. At the end of this period, p_e was again determined by open sampling.

The average molecular weight, $\bar{M}_n$, of the polymer at equilibrium was calculated from viscosity measurements in toluene at 20°C. by using Barry's equation.[3] A modified Ubbelohde dilution viscometer was used for the measurements. The equilibrium solutions were decatalyzed by first dissolving them in toluene as 2% polymer solutions, then washing in succession with dilute aqueous hydrochloric acid, aqueous sodium bicarbonate, and finally with water. The polymers were recovered by precipitation with excess methanol and subsequently dried under vacuum at 50°C.

RESULTS AND DISCUSSION

Polymerization of D_4 in Different Solvents

The solution polymerizations of D_4 were initially carried out in 50 vol.-% solvent at 140°C., with 0.01% potassium hydroxide (by weight based on the siloxane). With the exception of nitrobenzene system, all of the runs were homogeneous over the entire course of reaction. The polymerization in nitrobenzene behaved differently in that the initially homogeneous solution became turbid within 90 sec. after the addition of catalyst and a sepa-

rate phase containing relatively high molecular weight polymer was obtained.

The data for typical homogeneous runs are plotted in Figure 2 to show

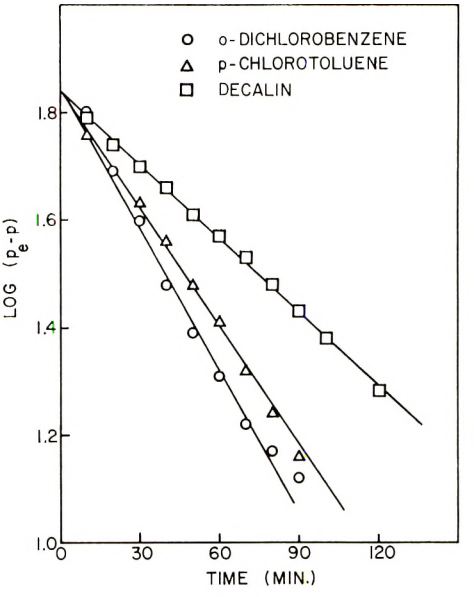

Fig. 2. First-order curves for polymerization of D_4 in 50 vol.-% solvent at 140°C. with 0.01% KOH.

the first-order dependence of rate on D_4. A correction for zero reaction time has already been made here.

In Table I, the first-order polymerization rate constants, k, the per cent polymer present at equilibrium, p_e, and the average molecular weight, $\bar{M}_n$, of the polymer are tabulated for duplicate determination.

TABLE I
Effects of Solvents on D_4 Polymerization
(50 Vol.-% Solvent, 140°C., 0.01% KOH)

Solvent	Dipole moment of solvent μ, D.	$k \times 10^2$, min.$^{-1}$	p_e, %		$\bar{M}_n \times 10^{-5}$	
			Polymerization	Depolymerization	Polymerization	Depolymerization
Decalin	0.00	0.75	68.6	70.4	0.96	1.36
		0.74	66.3	69.8	1.38	0.80
p-Chlorotoluene	1.85	1.25	68.0	69.3	1.59	1.19
		1.15	66.6	70.8	1.68	1.51
o-Dichlorobenzene	2.28	1.52	69.7	68.6	1.20	1.07
		1.58	70.8	68.6	2.00	1.77
		1.52[a]	69.3[a]	—	2.00[a]	—

[a] Potassium silanolate catalyst.

It is apparent from the data in Table I that as the polarity of the solvent increases, the rate of reaction increases, but the concentration of polymer present at equilibrium remains essentially constant. There appears to be a small increase in molecular weight for higher solvent polarity, but the reproducibility of these data is poor. In addition, taking the average value of p_e to be 70.0% for the sake of convenience, the calculated molecular weight for reaction in 50 vol.-% solvent is 392,000. This value is considerably greater than the molecular weights listed in Table I. The reason for lack of agreement probably lies in contamination by chain terminators such as water. Hence no valid comparison of molecular weights can be made.

TABLE II
Polymerization of D_4 in Nitrobenzene
(140°C., 0.01% KOH)

Solvent, vol.-%	$k \times 10^2$, min.$^{-1}$	p_e, %	$\bar{M}_n \times 10^{-5}$
0.00	1.99	92.7	7.20
0.00	2.08	91.7	6.20
1.96	3.05	89.9	6.32
1.96	3.21	88.8	5.31
4.76	4.96	88.6	8.05
4.76	4.90	88.3	6.71
9.10	8.77	85.8	4.51
9.10	8.91	83.6	2.00
16.70	17.10	84.9	4.20
16.70	16.90	83.1	5.24
28.60[a]	—	—	2.21
50.00[b]	—	—	2.04

[a] Polymer separated after 5 min. reaction.
[b] Polymer separated after 1 min. reaction.

Polymerization of D_4 in Nitrobenzene

It was thought of interest to determine the effects of various quantities of nitrobenzene on the polymerization reaction. Several runs were carried out at 140°C. with 0.01% potassium hydroxide in which the ratio of D_4 to nitrobenzene was varied. Typical first-order curves are shown in Figure 3, and the rate constants, equilibrium polymer and final molecular weights are listed in Table II. These systems were all homogeneous, except where indicated.

It appears that relatively small quantities of the highly polar nitrobenzene have the effect of increasing the reaction rate (compared to bulk polymerization) without significantly changing the molecular weight and equilibrium conversion. Unfortunately, the scattering of molecular weight values is quite pronounced and no particular significance can be attached to them. However, the results are in general accord with a recent patent[4] which reports increased rates and molecular weights in the presence of solvents such as nitriles and amides.

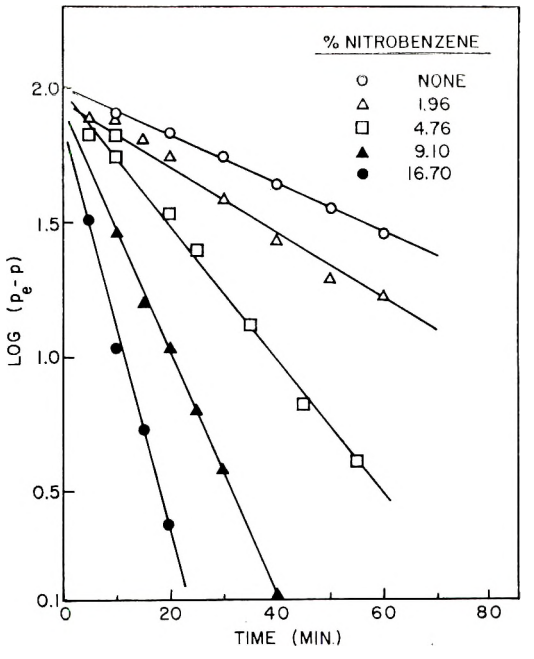

Fig. 3. First-order curves for polymerization of D_4 in nitrobenzene at 140°C. with 0.01% KOH.

Bulk Polymerization of D_4 with Potassium Methoxide as Catalyst

It was believed that the difference in the molecular weight values obtained for duplicate procedures was due to combined effect of silanol condensation and chain degradation, the latter occuring during the course of polymer solubilization prior to removal of the catalyst from the system. The use of potassium hydroxide as catalyst yields chains which are terminated at one end by hydroxyl groups, and condensation (with the formation of water) at elevated temperatures would be expected to take place. Some measure of the condensation reaction may be obtained by replacing the hydroxyl groups with a relatively inactive group, i.e., methoxy.

Consequently, D_4 was polymerized in bulk at 140°C. with potassium methoxide. The catalyst was used in 0.0125% concentration by weight (equivalent to 0.01% potassium hydroxide). The resulting equilibrium conversions, intrinsic viscosities and number-average molecular weights are listed in Table III with the results obtained for the bulk polymerization of D_4 at 140°C. with potassium hydroxide as catalyst. It should be mentioned here that the methoxide-catalyzed runs were sampled only after 24 hr. reaction.

An examination of Table III reveals that the calculated and experimental molecular weights for the methoxide catalyzed reactions are in general agreement. From this it can be assumed that silanol condensation during

TABLE III
Bulk Polymerization of D_4 at 140°C. with Different Catalysts

Catalyst	p_e, %	$[\eta]_{C_7H_8}^{20}$	$\bar{M}_n \times 10^{-5}$ Found	$\bar{M}_n \times 10^{-5}$ Calculated
KOH	92.7	1.47	7.20	5.20
		1.45	7.08	
KOH	91.7	1.33	6.20	5.15
		1.32	6.16	
$KOCH_3$	91.4	1.20	5.30	5.13
		1.20	5.30	
$KOCH_3$	90.7	1.24	5.56	5.09
		1.21	5.31	

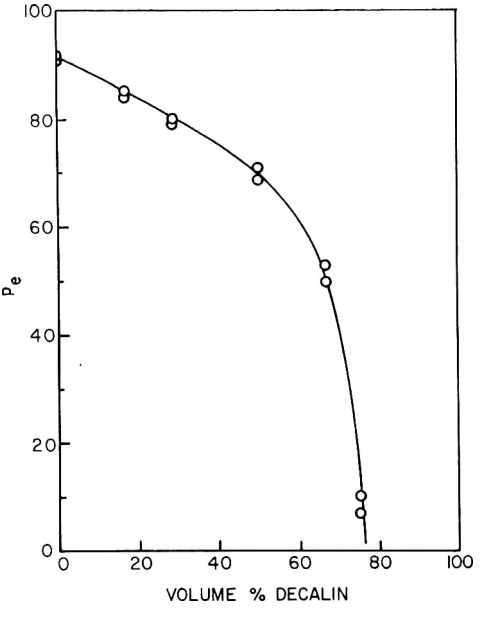

Fig. 4. Effect of solvent concentration on equilibrium for solution polymerization of D_4 at 140°C. with 0.01% KOH.

polymerization occurs only to a negligible extent when potassium methoxide is used as catalyst. In addition, the post-polymerization treatment of the polymer does not appear to have any appreciable influence upon the average molecular weight from the standpoint of chain degradation. However, the procedure does result in the loss of low molecular weight polymer (under 10,000) due to the high solubility of this material.

In the case of the potassium hydroxide polymerizations, which were sampled periodically, it is probable that a small quantity of water as contaminant was introduced during the course of reaction. Consequently, the experimental molecular weight values would be expected to be less than those calculated. It is interesting to note in Table III that the reverse is true,

and it may be concluded that the silanol condensation reaction is appreciable when potassium hydroxide is used as polymerization catalyst.

Effect of Monomer Concentration on Equilibrium

In order to determine the effect of solution concentration upon the equilibrium conversion, D_4 was polymerized in decalin at various degrees of dilution with 0.01% potassium hydroxide at 140°C. The results are presented in Figure 4, wherein the amount of polymer present at equilibrium p_e is shown to decrease with increasing dilution. The curve extrapolates to zero per cent polymer at approximately 77 vol.-% solvent, indicating that polymer will not be formed in solutions more dilute than this critical value. These results are in general agreement with those of Scott[5] who showed that the equilibrium will be shifted in favor of the cyclic siloxanes for polymerization in less concentrated solution.

GENERAL DISCUSSION

The results obtained are consistant with the interpretation of the mechanism of base-catalyzed octamethylcyclotetrasiloxane polymerization presented by Grubb and Osthoff. As expected, the solvents of higher polarity led to an increase in polymerization rate, presumably by permitting a higher degree of dissociation of the silanolate, as shown in eq. (2). Both the polymerization equilibrium and the molecular weights appear to be independent of the solvent medium, as predicted for these systems.

With regard to the effect of initial monomer concentration on the final equilibrium, Dainton and Ivin[6] have shown that the monomer concentration at equilibrium is given by

$$M_e = k_d/k_p$$

and hence is a constant, independent of all variables, except temperature. An examination of Figure 4 indicates that M_e is substantially constant over the range of concentration shown, within the limits of experimental error. There appears to be a tendency for M_e to decrease at higher monomer concentrations, but this may be due to the formation of some low polymeric species, which are known to occur in bulk polymerization and which would tend to raise the p_e values.

Since this is an equilibrium polymerization system, it should be subject to a "ceiling temperature" phenomenon, as determined by measuring the effect of temperature on M_e. However, this was not included in this investigation due to the difficulty in obtaining efficient polymerization systems at different temperatures. Hence an entirely different polymerization system was developed for this purpose, and this will be described in a forthcoming publication.

This work was supported by the Office of the Quartermaster General, Department of the Army, under Contract No. DA 19-129-QM-681.

References

1. Grubb, W. T., and R. C. Osthoff, *J. Am. Chem. Soc.*, **77**, 1405 (1955).
2. Osthoff, R. C., A. M. Bueche, and W. T. Grubb, *J. Am. Chem. Soc.*, **76**, 4659 (1954).
3. Barry, A. J., *J. Appl. Phys.*, **17**, 1020 (1946).
4. Hyde, J. F., U. S. Pat. 2,634,284, April, 1953.
5. Scott, D. W., *J. Am. Chem. Soc.*, **68**, 2294 (1946).
6. Dainton, F. S., and K. J. Ivin, *Nature*, **162**, 705 (1948).

Résumé

On a étudié l'effet de la polarité du solvant sur la polymérisation de l'octaméthylcyclotétrasiloxane catalysée par une base. Les solvants utilisés sont la décaline, le *p*-chlorotoluène, l'*o*-dichlorobenzène et le nitrobenzène. On a trouvé, en accord avec le mécanisme ionique proposé par Grubb et Osthoff, que la vitesse de polymérisation augmente avec la polarité du solvant, probablement par augmentation de la concentration en ions silanolates. En outre, on a obtenu une meilleure corrélation entre les poids moléculaires et la concentration en initiateur, et on a également élucidé l'effet de la concentration en monomère sur l'équilibre de conversion.

Zusammenfassung

Eine Untersuchung des Einflusses der Polarität des Lösungsmittels auf die basenkatalysierte Polymerisation von Octamethylcyclotetrasiloxan wurde durchgeführt. Als Lösungsmittel wurden Dekalin, *p*-Chlortoluol, *o*-Dichlorbenzol und Nitrobenzol verwendet. In Übereinstimmung mit dem von Grubb und Osthoff vorgeschlagenen ionischen Mechanismus wurde festgestellt, dass die Polymerisationsgeschwindigkeit, wahrscheinlich durch Erhöhung der Silanolationenkonzentration, mit der Polarität des Lösungsmittels ansteigt. Zusätzlich wurde eine bessere Korrelation zwischen Molekulargewicht und Starterkonzentration erhalten und ebenso der Einfluss der Monomerkonzentration auf den Gleichgewichtsumsatz aufgeklärt.

Received December 4, 1962

JOURNAL OF POLYMER SCIENCE: PART A VOL. 2, PP. 523–538 (1964)

Anionic Polymerization of Octamethylcyclotetrasiloxane in Tetrahydrofuran Solution*

MAURICE MORTON and E. E. BOSTICK,† *Institute of Rubber Research, University of Akron, Akron, Ohio*

Synopsis

A study has been carried out on the base-catalyzed polymerization of octamethylcyclotetrasiloxane (D_4) in tetrahydrofuran solution by means of various anionic initiators. These included potassium hydroxide, sodium and potassium metal and sodium and potassium naphthalene. Tetrahydrofuran was found to have a very marked accelerating effect on the polymerization rate, presumably by increasing the concentration of the silanolate anions. The rates obtained with the potassium metal and potassium naphthalene were even faster than for the KOH, permitting room temperature polymerization in a few hours. The polymerization temperature was not found to affect the equilibrium conversion of monomer to polymer, indicating very similar activation energies for propagation and depropagation. For polymerizations catalyzed by potassium naphthalene, two molecules of catalyst were found to be consumed per chain formed, with one dihydronaphthalene structure included in the chain.

INTRODUCTION

In a previous paper,[1] some results had been shown on the effect of solvents on the base-catalyzed polymerization of octamethylcyclotetrasiloxane. The behavior of these systems was found to be adequately described by the mechanism proposed by Grubb and Osthoff,[2] in which the silanolate anion is the active species in chain initiation and propagation. Hence, as expected, solvents of higher dielectric constant accelerated the polymerization rate, presumably by increasing the concentration of silanolate ion. However, it was not found possible, in that work, to obtain a good correlation between the kinetics and the chain length of the polymer, presumably due to condensation reactions between terminal hydroxyl groups which occur at the elevated temperatures required for the polymerization (ca. 150°C.). This was demonstrated by the fact that a catalyst like $KOCH_3$, which does not give rise to terminal hydroxyl groups, showed a good correlation between the initiator concentration and the

* Presented in part at the 133rd Meeting, American Chemical Society, San Francisco, April, 1958. Taken in part from the Ph.D. Dissertation of E. E. Bostick, University of Akron, June, 1959.

† Present address: General Electric Co., Research Laboratory, Schenectady, New York.

chain length. In this connection therefore, it was thought of interest to study suitable polymerization systems which could operate at much lower temperatures.

The systems which were considered as most feasible for this purpose were those involving the organoalkali complexes in presence of coordinating solvents, e.g., sodium or potassium naphthalene in tetrahydrofuran. As indicated in our preliminary communication,[3] such systems do indeed lead to a rapid and efficient polymerization of cyclic siloxanes. A detailed description of these studies follows.

EXPERIMENTAL

Materials

Octamethylcyclotetrasiloxane. Octamethylcyclotetrasiloxane, D_4, generously supplied by the General Electric Company, was redistilled from calcium hydride, b.p. 175°C. at 760 mm. pressure. The distillate (n_D^{20} = 1.3968) was then placed over finely ground calcium hydride and degassed by freezing and pumping to 10^{-6} mm. Hg pressure. As needed, the degassed siloxane tetramer was distilled through a $^1/_2 \times 21$ in. column packed with 2 × 4 mm. stainless steel mesh coils into ampules fitted with Eck and Krebs 12-mm. Pyrex breakable seals. The ampules were sealed off under high vacuum, 10^{-6} mm. Hg pressure, and stored at 0°C. until used.

Hexamethylcyclotrisiloxane. Hexamethylcyclotrisiloxane, D_3 (General Electric Company), was recrystallized from benzene (m.p. 64°C.) and redistilled from calcium hydride (b.p. 134°C. at 760 mm. Hg pressure) before use.

Naphthalene. Naphthalene (Eastman Recrystallized) was used as received.

Methyl Iodide. Methyl iodide (Eastman) was redistilled from phosphoric anhydride (Merck Reagent) into 12-mm. ampules fitted with Eck and Krebs breakable seals, and containing a small length of copper turnings. The ampules were sealed under high vacuum and stored in the dark until ready for use.

Calcium Hydride. Calcium hydride (Fisher Laboratory Reagent) was finely ground before use.

Iodine. Iodine (Baker Analyzed Reagent) was dissolved in either anhydrous toluene or anhydrous carbon tetrachloride before use.

Potassium. Potassium ingot (Fisher Laboratory Reagent) was used as received.

Sodium. Sodium ingot (Fisher Laboratory Reagent) was used as received.

Potassium Hydroxide Catalyst. This catalyst was furnished by the General Electric Company as a suspension of KOH in dimethyl siloxane tetramer. The base content was obtained by stirring an aliquot portion

in twice its volume of distilled water and titrating against 0.1*N* HCl with a Fisher Titrimeter to determine the endpoint.

Tetrahydrofuran. Tetrahydrofuran (Merck) was refluxed over sodium for several hours and distilled into a flask containing lumps of sodium and potassium. Naphthalene (Eastman Recrystallized) was added and the flask was fitted to a high vacuum line. Refluxing was continued until sodium and potassium naphthalene complexes were formed, characterized by the appearance of a dark green color. The tetrahydrofuran solution of sodium and potassium naphthalene complexes was then thoroughly degassed by alternate freezing and thawing at a pressure of 10^{-6} mm. Hg. Measured quantities of tetrahydrofuran were flash-distilled from this reservoir as needed.

Benzene. Benzene (Baker reagent grade) was dried over sodium wire before use.

Toluene. Toluene (Baker reagent grade) was dried over sodium wire before use.

Methanol. Methanol (du Pont synthetic) was used as received for polymer precipitations.

Procedures

Preparation of Catalysts

Potassium Silanolate Catalyst. The potassium silanolate catalyst was prepared according to the method of Grubb and Osthoff.[2] Recrystallized hexamethyltrisiloxane, D_3 (13.9 g., 0.0627 moles), was added to 33.3 ml. of toluene in a 100-ml. round-bottom flask equipped with a reflux condenser and Dean-Start trap. To the resulting solution was added 0.935 g. (16.7 mmoles), of finely ground KOH, and the system was refluxed for 24 hr. 0.15 ml. of water was collected in the Dean-Start trap. The toluene was then distilled off and anhydrous octamethylcyclotetrasiloxane added to dissolve the potassium silanolate oil. The solution was found to contain 0.10673 mmoles K/ml. solution.

Potassium Naphthalene. Potassium naphthalene was prepared in a manner previously described[4] for sodium naphthalene.

Base-Catalyzed Polymerization of Octamethylcyclotetrasiloxane

The reactions were carried out in round-bottomed flasks equipped with a nitrogen inlet and a reflux condenser with drying tube. The siloxane tetramer was placed in the flask, which was then immersed up to the neck in an oil bath, maintained at the polymerization temperature ±0.6°C. After thermal equilibrium had been attained, the catalyst (potassium hydroxide) was added, and this point was taken as zero reaction time. Nitrogen (prepurified) was used to flush the reaction flask continuously.

The rate was then determined by periodically removing the inlet tube and quickly withdrawing about 1 g. of sample into a glass tube. The

sample was then transferred to a tared aluminum cup and weighed. The quantity of polymer present was found by adding an excess of iodine in toluene solution to the cup and drying on a hot plate for 15 min. at 230°C. The error attributable to the drying procedure was determined by dissolving a known quantity of dimethyl silicone polymer in tetramer at 140°C., adding KOH, and then sampling the reaction immediately after solubilization of the catalyst. The maximum error in the determination of the polymer present was found to be ± 1.0% of the total polymer.

Polymerization with Potassium Naphthalene Complex

For these polymerizations it was necessary to use a vacuum line technique, such as previously described.[4] The actual polymerization apparatus is shown in Figure 1. The apparatus consisted of (*1*) a tube 3 × 10 cm. fitted with (*2*) an ampule of siloxane tetramer, (*3*) an ampule of initiator (K-naphthalene/THF), (*4*) a standard-taper, ground-glass joint vacuum connection, and (*5*) methyl iodide terminator tube.

The apparatus was evacuated, carefully flamed with an oxygen–natural gas torch, and pumped to 10^{-6} mm. Hg pressure. A measured volume of anhydrous, degassed tetrahydrofuran was distilled into the tube (*1*) and thoroughly pumped to 10^{-6} mm. Hg pressure.

The entire apparatus was then sealed off from the vacuum line. Siloxane tetramer was transferred from the ampule (*2*) to the tube (*1*) by striking the seal with a soft iron nail enclosed in Pyrex tubing. After transfer, the solution was cooled until the tetramer froze out (15°C.). Potassium naphthalene initiator solution was then transferred completely to the tube (*1*) and the sidearm was removed at the constriction (*6*).

Reactants were thoroughly mixed by shaking and the system allowed to warm to room temperature. A slow initial reaction period, usually about 30 min., was noticed. At the end of this induction period, the characteristic green color of K-naphthalene had changed to brown, and the viscosity of the reaction mixture had started to increase markedly.

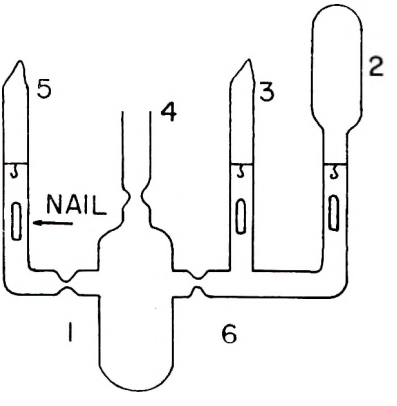

Fig. 1. Polymerization apparatus.

After 3–6 hr., the polymerizing system had become almost immobile due to the viscosity increase. Methyl iodide, which reacted to destroy the brown color, was used to terminate the reaction. Per cent conversion of tetramer to high polymer ($\overline{DP} > 4$) was calculated from duplicate total solids determination, and from vacuum-dried samples (70°C. at 1 mm. Hg pressure).

The polydimethylsiloxane gum was recovered quantitatively and processed by two methods. One involved precipitation of the polymer with methanol from a dilute tetrahydrofuran solution, followed by vacuum drying. The other method consisted of drying at 70°C. at 1 mm. Hg pressure. Equilibrium conversion of polymer, and molecular weight, were determined.

Polymerization with Potassium and Sodium Metals

An ampule, containing a solution of octamethylcyclotetrasiloxane in tetrahydrofuran, was prepared and attached to a mirror assembly similar to the apparatus used for preparation of potassium naphthalene complex. The system was prepared as described for the preparation of the complex, and a mirror was formed by sublimation. After removing the apparatus from the vacuum line in the usual manner, the solution of tetramer in tetrahydrofuran was allowed to contact the mirror. Contact time was maintained constant at 20 min. The mirror tube was shaken during the contact time in order to ensure maximum solution of the metal. During this time, the mirror was somewhat etched as evidenced by loss of lustre in thin areas. After 20 min., the solution was filtered into the receiver, chilled and sealed off.

The solution was allowed to stand at room temperature until polymerization was considered to be complete, usually 24 hr. Termination was by methyl iodide. The polymer was quantitatively recovered for the determination of the equilibrium concentration of polymer (P_e) and molecular weight.

"Seeded" Polymerization

"Seeded" polymer solutions were designated as 20% solutions of tetramer/polymer in tetrahydrofuran, that had been exposed to a potassium mirror as described previously. These solutions were divided into ampules appropriate for addition to increments of tetramer. Tetramer concentrations were adjusted during mixing with "seeded" polymer solutions. All operations were conducted *in vacuo* in apparatus similar to that described for potassium naphthalene polymerizations and shown in Figure 1.

Potassium Determination

Several attempts were made to determine potassium ion concentration in polymer solutions that had been exposed to potassium mirrors. Titration with HCl was found to be inadequate since no indication of alkalinity

was found with various indicators or by a Fisher Titrimeter. Through the courtesy and generous cooperation of the Research Department of the Columbia Southern Chemical Corporation, attempts were made to analyze for potassium by optical methods. Both flame photometry and emission spectrography were employed.

Determination of Polymer Concentration and Molecular Weight at Equilibrium

Flask Reactions. Two methods were used to determine the per cent polymer, P_e, present at equilibrium. One approach was to carry out the polymerization for a period of time sufficient to ensure equilibrium conditions, and then obtain P_e by the open sampling procedure. In the other method (used in the base-catalyzed solution polymerizations), a sample of dimethylsiloxane gum ($\bar{M}_n$ = 606,000) was dissolved in the appropriate solvent and depolymerized in the presence of a basic catalyst (KOH) to the equilibrium point. At that time, P_e was determined by the open sampling technique previously described.

The number-average molecular weight, $\bar{M}_n$ was calculated from viscosity measurements in toluene at 20°C. by use of Barry's equation.[5]

$$[\eta] = 2.00 \times 10^{-4}\bar{M}_n^{0.66}$$

The viscosity-average molecular weight, $\bar{M}_v$, was determined by means of intrinsic viscosity in benzene at 22°C. according to the equation of Yavorsky.[6]

$$[\eta] = 0.617 \times 10^{-3}\bar{M}_v^{0.56}$$

In both cases, a modified Ubbelohde dilution viscometer was used for the measurements.

The base-catalyzed polymers were prepared for viscosity measurements by first dissolving them in toluene as 2% solutions, then decatalyzing by washing the solutions successively with dilute HCl, aqueous $NaHCO_3$, and water. The polymers were recovered by precipitation with excess methanol and were subsequently dried under vacuum at 50°.

Vacuum System Reactions. Polymers from the vacuum system reactions were processed as described above except that termination, or neutralization, was accomplished before opening the reaction vessel, in order to eliminate degradative side reactions. Then, too, some of the polymers were not precipitated but were vacuum-dried only.

A third relationship between intrinsic viscosity and molecular weight, i.e., that of Flory,[7] was used for some of the molecular weight determinations.

$$\log [\eta]^{\mathrm{MEK}}_{30^\circ\mathrm{C.}} = -3.318 + 0.55 \log \bar{M}_v$$

Ultraviolet Absorption Measurements

Low molecular weight polydimethylsiloxanes prepared in THF, with potassium naphthalene as initiator, were terminated with methyl iodide

and precipitated three times from tetrahydrofuran with methanol. The resulting viscous oil was dried for 24 hr. at 70°C. and 1 mm. Hg pressure. A 1-g. portion of this oil was dissolved in 25 ml. of isooctane. A Beckman Model DU spectrophotometer was then used to measure absorption of the polymer solution.

A control sample was prepared from low molecular weight silicone that had been polymerized with KOH catalyst. A solution containing 10% silicone and 1% naphthalene in tetrahydrofuran was precipitated three times with methanol and dried at the same time as the "unknown." Absorption measurements were made on solutions of this polymer in isooctane.

RESULTS AND DISCUSSION

Potassium Hydroxide Catalysis

Although tetrahydrofuran (THF) is not a highly polar solvent (ϵ = 7.58), it is well known as a solvating medium for many reactions. Since the rate of polymerization of D_4 has been found to be accelerated by polar solvents,[1] it is not surprising that the THF should be found to have a similar effect. The results for the polymerization in this solvent, catalyzed by KOH in a high vacuum system, are shown in Table I.

In view of the lower temperature (60°C.) compared to the high temperatures (140°C.) used in absence of THF, it is obvious that this solvent exerts a marked effect in accelerating the polymerization.

Since the above polymerizations were carried out in a high vacuum system, with rigorous exclusion of impurities, it was thought of interest to note the effect of these conditions on the molecular wieght of the polymer. A comparison of such polymerizations, using both KOH and potassium silanolate as catalysts, with similar reactions performed in screw-cap bottles under nitrogen is shown in Table II. It can be seen that the more rigorous conditions of the high vacuum system lead to a much higher molecular weight, presumably by exclusion of moisture or other chain-scission agents. This is especially noticeable in the case of the KOH.

TABLE I
Solution Polymerization of D_4 in THF at 60°C. (50 vol.-% THF, 0.01% KOH)

Time, min.	Conversion, %
10	1.46
20	7.0
30	17.4
40	30.6
60	54.5
75	65.0
90	70.3
1440	71.4

TABLE II
Effect of Conditions on Base-Catalyzed Solution Polymerization of D_4
(Catalyst concentration = 0.2 mmole/100 g. D_4)

Condition	Catalyst	$[\eta]_{C_6H_6}$	$\bar{M}_v \times 10^{-5}$
Vacuum	KOH	1.53	7.7
Bottle	KOH	0.50	1.4
Vacuum	K-silanolate	0.82	3.0
Bottle	K-silanolate	0.44	1.2

Sodium and Potassium Metal Catalysis

In view of the known ability of THF in helping electron-transfer reactions, e.g., from the alkali metals to polynuclear aromatic hydrocarbons, it was thought of interest to note the action of this solvent on the alkali metals in presence of D_4. Actually, the rate of polymerization of D_4 in THF, catalyzed by a sodium mirror, was found to be very slow, taking about 10 days at 25°C. Potassium was found to be much more effective, converting the D_4 to an equilibrium polymer concentration in 3–6 hr. at 25°C. It was first thought that the THF was entering into the reaction as an initiator or by dissolving the potassium metal. However, a sample of THF that had been in contact with a potassium mirror was found to contain no alkalinity, and was incapable of polymerizing D_4. Hence it was concluded that the initial reaction must be the cleavage of the D_4 ring by the potassium itself.

The polymerizations initiated by potassium metal were then subjected to a systematic study as follows. A series of experiments was carried out, a 20% solution of D_4 in THF which had been exposed to a potassium mirror being used as initiator. Very little polymerization occurred at this monomer concentration. Polymerizations were then accomplished by adding different amounts of D_4 to this active initiator solution. The results are shown in Table III. It can be seen that, as expected, the equilibrium conversion increased with D_4 concentration, and the molecular weights reached some very high values ($\sim 10^7$), indicating a very low potassium concentration. This type of high molecular weight poly-

TABLE III
Polymerization of D_4 with "Seed" Polymer Solutions
(Solvent: Tetrahydrofuran, Temp. = 25°C.)

Vol. of "seed," ml.	Vol. D_4, ml.	Vol.-% D_4	Conversion, %	$[\eta]^{25}_{C_6H_6}$	$\bar{M}_v \times 10^{-6}$
—	—	20	8.1	0.115	0.0113
7	2.9	40	49.5	2.28	2.4
10.5	2.1	60	79.7	2.60	2.97
7.4	23	70	87.4	4.94	9.42
13.0	39	80	53.0	5.20	9.88

siloxane is not possible to obtain by the usual atmospheric polymerization with KOH, and is entirely different in appearance from the usual semi-liquid gum. Since its molecular weight is easily 10 times as high, it has the appearance of an elastic gum and is obtained in crumb form.

In view of the rigorous conditions prevailing in the above polymerizations, an attempt was made to determine the relation between the molecular weight and the potassium concentration. Since the latter was obviously very low, the analysis was carried out by means of both flame photometry and emission spectrography. The results are shown in Table IV. Even though a slight trend toward an increase in potassium with decrease in

TABLE IV
Potassium Analysis

Vol.-% D_4	Equilibrium conversion, %	$[\eta]^{20}_{C_7H_8}$	$\bar{M}_n \times 10^{-6}$	Potassium, %	
				Flame	Spectrography
80	89	2.4	1.52	0.001	0.003
$66^{2/3}$	83	2.0	1.15	0.001	0.002
50	75	3.5	2.65	0.001	0.001
$33^{1/3}$	35	1.16	0.50	0.003	0.001
20	6	0.04	0.002	0.005	—

molecular weight can be seen from the flame photometry data, this is not confirmed by the spectrographic results. The only conclusion that may be drawn is that the potassium concentration is extremely low. This is to be expected, in considering the high value of the resulting molecular weights (ca. 10^7) which are not attainable by the usual polymerization methods.

Polymerization with Sodium Naphthalene

The polymerization of D_4 with sodium naphthalene in tetrahydrofuran was found to be slow, requiring 120 hr. at 25°C. to produce a low viscosity oil. Due to the slow rate, even at high catalyst concentrations, the polymerization of D_4 with sodium naphthalene complex was abandoned.

Polymerization with Potassium Naphthalene

As expected for a more active alkali metal, potassium naphthalene was found to be much more effective, only 3–6 hr. being required for the attainment of equilibrium conversion. An important characteristic of this polymerization was the change in color from the green of the naphthalene complex to varying shades of reddish brown, depending on catalyst concentration. This color was found to be destroyed upon contact of the solution with air, water, methanol, etc. Also, upon contact with air, a decrease in viscosity of the solution was found to accompany destruction of the color.

During the early experiments, the polymerized solution was first exposed to air before the polymer was decatalyzed, by acid treatment, and recovered. This resulted in erratic molecular weights, which were consistently lower than predicted.

In subsequent experiments, the polymer was first terminated, *in vacuo*, by means of methyl iodide, thus destroying the color before exposing to the atmosphere. Using this method, the results shown in Table V were obtained. It can be seen that now quite a satisfactory agreement is obtained between the predicted and actual molecular weights, on the basis of two moles of initiator being consumed per chain formed.

TABLE V
Polymerization of D_4 by K-Naphthalene in THF Solution at 25°C.
(50 vol.-% D_4, Conversion ~70%, CH_3I termination)

	Molecular Weight ($\bar{M}_n \times 10^{-5}$)[a]	
$[\eta]^{30}_{MEK}$	Calculated	Found
1.21[b]	11.2	8.5
1.24[b]	11.2	8.8
0.71	4.4	4.0
0.47	2.7	2.6
0.24	1.9	1.4

[a] $\bar{M}_n$(calc.) = g. polymer/1/2 [cat.]; $\bar{M}_n$(found) = $\bar{M}_v$/1.79.
[b] Duplicate polymer samples prepared from same polymerization batch.

Equilibrium Conversion of D_4 to Polymer

Scott's classical study[8] of equilibrium of dimethylsiloxanes and Grubb and Osthoff's investigation[2] of the kinetics of base-catalyzed polymerization of D_4 have both shown the presence of a reverse reaction in this sytem. A polymer chain may depolymerize to yield both tetramer and other cyclics, and, if hydrolytic reagents are present, polymer chain segments as well.

In a rigorous system, contamination should be minimized and the number of chains should be controlled by the agent producing active centers. Scott determined from his work that a minimum concentration of $(CH_3)_2$-SiO units must be present in the form of rings before chain formation can occur. The value he has predicted was 2.2*M* concentration in D units. A series of runs was made in order to find the minimum concentration of tetramer necessary for polymerization to occur at 25°C. in tetrahydrofuran. The results are plotted in Figure 2, where the resulting curve extrapolates to 82 vol.-% tetrahydrofuran. This corresponds to 18 vol.-% D units in the form of cyclics, i.e., a molar concentration of 2.34 in cyclics, as the critical concentration for polymerization. This is surprisingly close to Scott's prediction.

This system would be expected to exhibit a ceiling (or floor) temperature, since the concentration of monomer is found to determine the extent of conversion to polymer. However, between 25 and 60°C., no indication

of a temperature effect on polymer concentration was noticed in these experiments. Furthermore the curve in Figure 2 is very similar to the one previously shown[1] for the polymerization of D_4 by KOH at 140°C. Hence no effect of temperature on the equilibrium polymerization has been noted. Scott's work, as has been discussed, was based on a statistical analysis of both bulk and solution equilibrium systems. On the basis of his results, he also predicted that the equilibrium concentration of various cyclics should be independent of temperature except for the trimer, which, he said, should increase with temperature. The possible existence of a

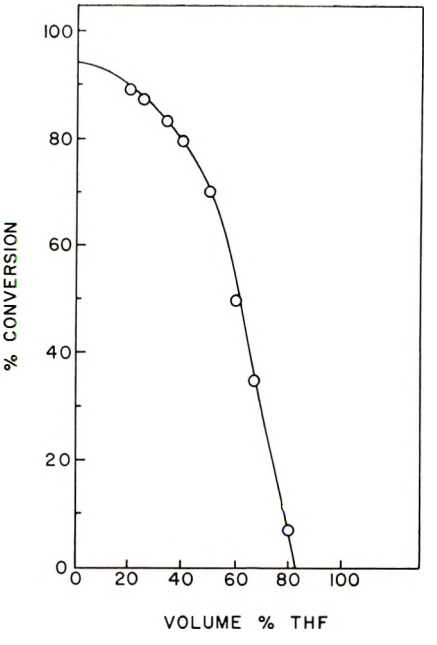

Fig. 2. Effect of dilution on equilibrium polymerization of D_4 in THF at 25°C. (K metal catalyst).

ceiling (or floor) temperature may be considered to depend on the increased trimer concentration. Furthermore, since this is a ring-opening reaction, the heat of the reaction may be relatively small, and the main driving force for polymerization may be the entropy change. Hence, the temperature coefficient for polymerization may be difficult to detect experimentally due to the very small change in conversion with temperature.

Polymerization Mechanisms

Potassium Metal. Since the solvent, tetrahydrofuran, was not found to either react with or dissolve potassium to form an active species capable of initiating polymerization, the initiating reaction may be considered to be a ring-opening by the potassium. Two possible schemes are as follows.

(The two methyl groups attached to each silicon have been removed for simplicity.)

$$(SiO)_4 + 2K \rightarrow \dot{K}:SiO(SiO)_2SiO:\dot{K} \quad (1)$$

$$2(SiO)_4 + 2K \rightarrow 2\,\cdot SiO(SiO)_2SiO:\dot{K} \rightarrow \dot{K}:OSi(OSi)_2OSi:SiO(SiO)_2SiO:\dot{K} \quad (2)$$

Reaction (1) is considered to be the more reasonable course of ring-opening, since the second reaction requires the formation of a Si—Si bond which is not very stable in basic media. Both reactions require electron transfer from two molecules of potassium to effect initiation of polymerization. The resulting silanolate anion is colorless in tetrahydrofuran solution.

Potassium Naphthalene. As in the potassium metal-catalyzed polymerizations, there are at least two schemes that would allow ring-opening of a cyclic siloxane and the ensuing polymerization. The data of Table V show that two molecules of catalyst are consumed per polymer chain formed. Two possible mechanisms were considered. One involved an electron transfer from the naphthalene ion to the siloxane, thereby opening the ring to produce a silanolate anion on one end of the chain and a silicon free radical on the other end. These radicals may then couple to form a chain with a dianion. The naphthalene is regenerated by the reaction.

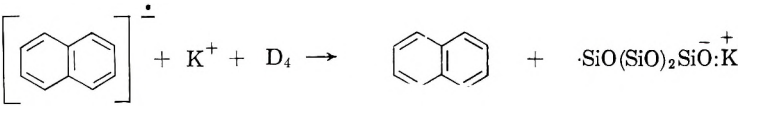

The radical-anion thus formed would couple in similar fashion to reaction (2) above. These reactions would obey the stoichiometry found but should lead to colorless products, since the silanolate anion is known to be colorless in tetrahydrofuran. Furthermore, a silicon-silicon bond would be necessary, and these have been found to be unstable in basic media.[9,10] In order to test for the presence of a silicon-silicon bond, termination with alcoholic KOH was followed by gas analysis. No evolution of hydrogen was detected, hence the following reaction did not occur.

$$\sim\!SiOSiSiOSi\!\sim + 2KOH \rightarrow H_2 + 2KOSiOSi\!\sim$$

Another mechanism requiring two molecules of catalyst is a reaction similar to CO_2 addition to sodium naphthalene reported by Scott et al.[11] and Weissman et al.[12]

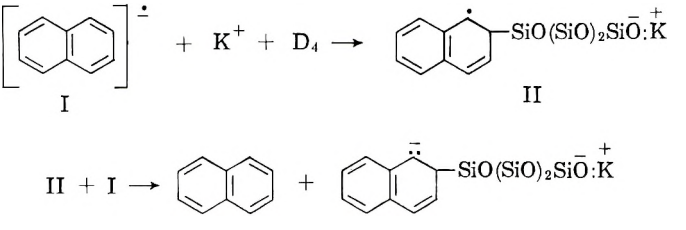

Only the 1,2-dihydronaphthalene is shown, but the 1,4-form may also exist. The dihydronaphthalene anion would account for the color observed in the polymerizations. If the polymer is terminated with methyl iodide and carefully recovered, the dihydronaphthalene structure should be detected by absorption measurements in the ultraviolet region. A sample was thus prepared. The results are shown in Figure 3. A control sample of polydimethylsiloxane, prepared with KOH, was dissolved in tetrahydrofuran containing some naphthalene and treated in the same way as the test sample. No absorption was found for this polymer in the ultraviolet region. The absorption curve illustrated in Figure 3 shows a

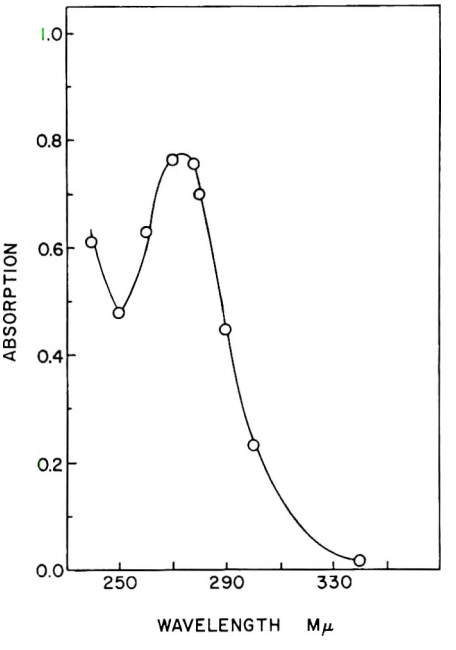

Fig. 3. Ultraviolet absorption spectrum of polydimethylsiloxane prepared with K-naphthalene.

strong maximum at 2715 A. (271.5 mμ). This maximum is near the maximum reported by Morton and De Gouveia.[13] Of course, a mixture of compounds including 1,2- and 1,4-dihydronaphthalene structures must be present which will produce a composite absorption curve.

The presistant brown color associated with the unreacted anion on the dihydronaphthalene should diminish and disappear completely if it is reactive to siloxane tetramer. However, this color was found to remain after a week at 25°C. The fact that color remained does not eliminate reactivity, however, and it is thought that, at higher temperatures, the second anion should react to eventually lead to a colorless silanolate dianion.

Kinetic Studies

It has been shown, in a previous publication,[1] that the base-catalyzed solution polymerization of octamethylcyclotetrasiloxane obeyed the same kinetics as the bulk polymerization, i.e., a first-order dependency of rate on monomer concentration, and a half-order dependency on initiator. This was taken as a confirmation of the Grubb and Osthoff[2] mechanism, in which the weakly-dissociated silanolate ion is presumed to be the active propagating species.

In the present work, tetrahydrofuran was found to have a very profound effect on the polymerization rate, increasing it by 2 or 3 orders of magnitude. This is illustrated by the fact that, in the presence of the THF, the rate at room temperature was approximately the same as the bulk polymerization rate at 140°C. If this effect is due to a marked increase in the dissociation of the potassium silanolate chain ends, it is conceivable that the extent of dissociation may be great enough to affect the kinetics of the system. Thus, if such a dissociation is virtually complete, then the rate should show a first-order dependency on silanolate, i.e., on the initiator concentration.

First-order rate plots for the potassium naphthalene initiated systems at different initiator concentrations are shown in Figure 4, while the

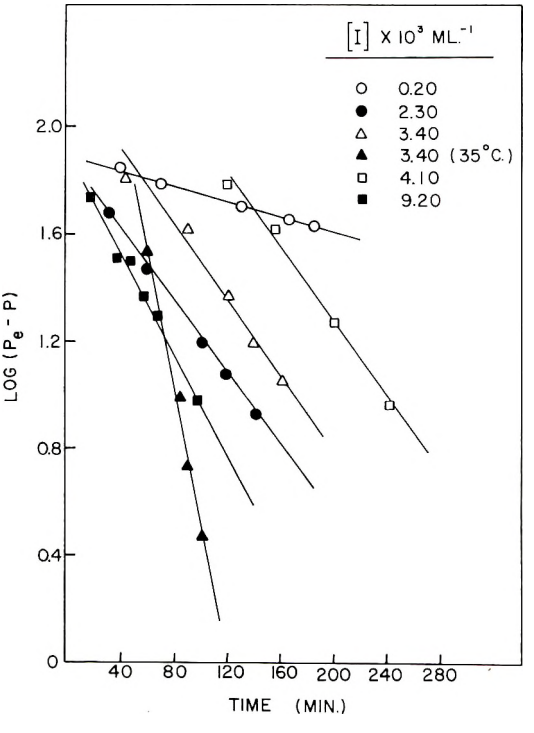

Fig. 4. First-order rate plots for polymerization of D_4 by potassium naphthalene in the at 25°C. (50 wt.-% THF).

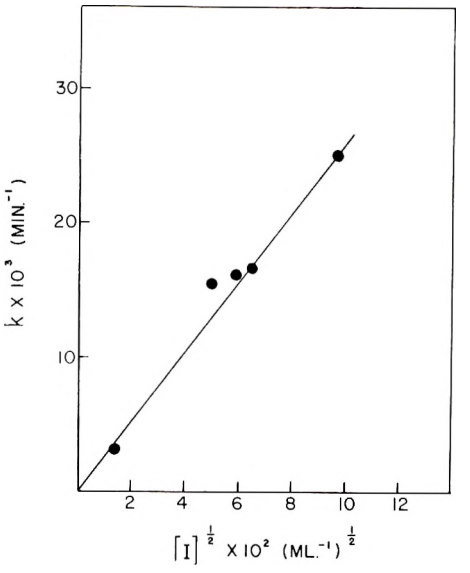

Fig. 5. Dependence of polymerization rate on initiator concentration [I], from data in Fig. 4.

dependence of the first-order rate constants k on initiator concentration is shown in Figure 5. These rate data were obtained by using the total solids method to determine the extent of conversion at different times.

The first-order disappearance rate of the monomer is obvious from Figure 4, even though some of the reactions exhibited an induction period at the start. It can also be readily seen that the polymerization rate still shows a square-root dependency on initiator concentration, as found previously for the other systems.[1,2] Hence, the silanolate ion is still presumably in equilibrium with the undissociated potassium silanolate. It is interesting to note, however, that the dielectric constant of THF is much lower than that of some of the solvents previously used,[1] so that the very marked increase in rate caused by the THF must be ascribed to some other effect, probably an ion solvation phenomenon.

It is also interesting to note that, from the difference in the first-order rates at 25 and 35°C., it was possible to calculate an activation energy of 23 kcal., which compares with the values of 20 kcal. previously found[2] for the bulk polymerization systems at high temperatures. As in the latter case, then, this probably reflects an increase in ion dissociation in both systems.

This research was supported by a grant from the National Science Foundation, G-2630.

References

1. Morton, M., M. A. Deisz, and E. E. Bostick, *J. Polymer Sci.*, **A2**, 513 (1964).
2. Grubb, W. T., and R. C. Osthoff, *J. Am. Chem. Soc.*, **77**, 1405 (1955).
3. Morton, M., A. A. Rembaum, and E. E. Bostick, *J. Polymer Sci.*, **32**, 530 (1958).
4. Morton, M., R. Milkovich, D. B. McIntyre, and J. L. Bradley, *J. Polymer Sci.*, **1A**, 443 (1963).
5. Barry, A. J., *J. Appl. Phys.*, **17**, 1020 (1946).
6. Yavorsky, P. M., private communication.
7. Flory, P. J., L. Mandelkern, J. B. Kinsinger, and W. B. Schultz, *J. Am. Chem. Soc.*, **74**, 3364 (1952).
8. Scott, D. W., *J. Am. Chem. Soc.*, **68**, 2294 (1946).
9. Friedel, C., and H. Ladenburg, *Ann.*, **203**, 251 (1880).
10. Gatterman, L., and K. Weinlig, *Ber.*, **27**, 1946 (1894).
11. Scott, N. D., J. F. Walker, and V. L. Hansby, *J. Am. Chem. Soc.*, **58**, 2443 (1936).
12. Lipkin, D., D. Paul, J. Townsend, and S. I. Weissman, *Science*, **117**, 534 (1953).
13. Morton, R. A., and A. J. A. de Gouveia, *J. Chem. Soc.*, **1934**, 916.

Résumé

On a effectué une étude sur las polymérisation par catalyse basique de l'octaméthylcyclotétrasiloxane (D_4) en solution dans le tétrahydrofuranne avec différents initiateurs anioniques. Ceux-ci comprennent l'hydroxyde de potassium, le sodium et le potassium métalliques et le sodium- et potassium-naphtalène. On a trouvé que le tétrahydrofuranne a un effet remarquable d'accélération sur la polymérisation, vraisemblablement par suite d'un accroissement de la concentration en anions silanolates. Les vitesse obtenues avec le potassium métallique et le potassium-naphtalène sont plus élevées qu'avec la potasse caustique, ce qui permet des polymérisations à température normale en quelques heures. On a trouvé que la température de polymérisation n'affecte pas la conversion d'équilibre de monomère en polymère, ce qui indique des énergies d'activation sensiblement équivalentes pour les réactions de propagation et de dépropagation. Pour la polymérisation avec le potassium-naphtalène, on a trouvé que deux molécules de catalyseur sont consommées par chaîne formée, avec une structure dihydronaphtalène incorporée dans la chaîne.

Zusammenfassung

Die basen-katalysierte Polymerisation von Octamethylcyclotetrasiloxan (D_4) mit verschiedenen anionischen Startern, nämlich Kaliumhydroxyd, Natrium- und Kaliummetall sowie Natrium- und Kaliumnaphthalin, wurde in Tetrahydrofuranlösung untersucht. Tetrahydrofuran hat einen merklichen beschleunigenden Einfluss auf die Polymerisations-geschwindigkeit, wahrscheinlich durch eine Erhöhung der Konzentration der Silanolatanionen. Die mit Kaliummetall und Kaliumnaphthalin erhaltenen Geschwindigkeiten lagen noch höher als mit KOH und ermöglichten eine Polymerisation bei Raumtemperatur innerhalb weniger Stunden. Die Polymerisationstemperatur hatte keinen Einfluss auf das Umwandlungsgleichgewicht des Monomeren zum Polymeren, was beweist, dass die Aktivierungsenergien für Wachstum and Monomerabspaltung sehr ähnlich sind. Bei der Polymerisationskatalyse durch Kaliumnaphthalin wurden zwei Katalysatormoleküle pro gebildeter Kette verbraucht, wobei eine Dihydronaphthalinstruktur in die Kette eingebaut wurde.

Received April 15, 1963
Revised June 28, 1963

JOURNAL OF POLYMER SCIENCE: PART A VOL. 2, PP. 539–586 (1964)

Crosslinked and Noncrosslinked Diisocyanate-Linked Elastomers Containing Substituted Urea Groups*

A. J. HAVLIK and THOR L. SMITH, *Jet Propulsion Laboratory, California Institute of Technology, Pasadena, California*

Synopsis

A study was made of the preparation and properties of diisocyanate-linked elastomers prepared from polyoxypropylene glycol (POPG), toluene-2,4-diisocyanate (TDI), and toluene-2,4-diamine (TDA). The chemical structure and gelation of a series of prepolymers were investigated first. Next, many series of elastomers were prepared at 60°C. in open molds and at 110°C. in closed molds from mixtures in which values of the ratio of isocyanate groups to the sum of the hydroxyl groups and amino groups (R_1) and the ratio of the amino groups to hydroxyl groups (R_2) were systematically varied. Cure at 60°C. gave tough, noncrosslinked elastomers, the properties apparently resulting from interchain attractive forces, while cure at 110°C. gave covalently crosslinked elastomers having rather similar properties. Glass-transition temperatures increased linearly with the concentration of substituted urethane groups but were independent of the concentration of substituted urea groups. An explanation for the surprising behavior is presented. The noncrosslinked elastomers were soluble in *N,N*-dimethylacetamide (DMA) and similar solvents. Intrinsic viscosities in DMA were found to increase with R_1 at constant R_2. Young's modulus, tensile strength, and ultimate elongation were determined between −23 and 82°C. At elevated temperatures, the crosslinked elastomers showed near-equilibrium moduli, while the noncrosslinked ones did not. The number of chains per milliliter for the crosslinked elastomers was calculated from the quantities of excess isocyanate and urea hydrogens, along with an assumed topology for the network. The moduli for both types of elastomers were related to chemical composition. Various relationships between the ultimate properties and equilibrium moduli were evaluated. Extensions up to 5000% with elastic recoveries of better than 90% were noted.

I. INTRODUCTION

Polymers are formed from polyisocyanates and polyfunctional molecules containing active hydrogens[1] or from the isocyanates themselves.[2,3] The materials can serve as the basis for a study on the relationships of physical properties to chemical structure, network topology, chain flexibility, and intermolecular forces in polymers.

The preparation of polymers containing either substituted urethanes, or substituted ureas, substituted biurets, and substituted urethanes has been

* Portions of this paper were originated under studies conducted for the Department of Army Ordnance Corps under Contract No. DA-04-495-Ord-18. Such studies are now conducted for the National Aeronautics and Space Administration under Contract No. NAS 7-100.

discussed in numerous reports[4–43] and in the patent literature.[44–64] Most of these studies reported data for some mechanical property of the polymers containing one or all three of the aforementioned functional groups. In some of these studies, the network structure[12,31] and the presence and type of interchain forces were discussed.[8,19,29,31,34,35,37] Also reported were estimates of the influence of the substituted urethane groups[30] and the substituted urea groups[19] on the glass-transition temperatures T_g and the substituted urea groups on the brittle points.[29]

The dynamic mechanical properties of polyurethanes have been studied over a range of temperatures and the results used to estimate the molecular friction coefficient[65] and the significance of thermal history for mechanical properties.[66]

The importance of the water content of polyurethane materials to the dynamic mechanical properties has been studied.[67] Relationships of the cure to the environment of a polyurethane system have been mentioned.[17,68–70] Little has been done, however, to minimize or control the effects of the environment and study its importance to the preparation and evaluation of polyurethane materials.

In two recent survey articles,[20,31] Saunders discussed the reactions of isocyanates and isocyanate derivatives at elevated temperatures and the relationships between polymer structure and the properties of the polyurethanes. These articles showed that many data have been obtained on the properties of the polyurethanes but concluded that, at the present time, one cannot predict with confidence the contribution of each structural feature present in these polymers. Difficulties in the identification and estimation of functional groups in diisocyanate-linked polymers (e.g., urethanes, ureas, biurets, allophanates, uretidinediones, and triisocyanurates along with other moieties present in these polymers) undoubtedly contribute to this limitation.

Qualitatively, most of the reactions of isocyanates have been known for many years. More recently, investigations have been made of the relative rates of reaction of isocyanates with various model compounds containing active hydrogens or with themselves. The stoichiometry and the kinetics and mechanisms of isocyanate reactions, however, are usually extremely complicated,[10] and much remains to be studied in these areas and in the application of the results to extant problems in the preparation and characterization of the polymers themselves. Control of the factors influencing the stoichiometry and kinetics of the reactions of isocyanates would help the diisocyanate-linked polymers fulfill their potential role as materials for the study of property–structure relationships.

In two previous studies made at the Jet Propulsion Laboratory on the mechanical properties of diisocyanate-linked elastomers,[30,36] the main functional group used to form the elastomer was a urethane by the reaction of an isocyanate with a hydroxyl. One study[30] was made on series of elastomers prepared from polypropylene glycol 2025 (POPG), dipropylene glycol (DPG), trimethylol propane (TMP), and either toluene diiso-

cyanate (TDI) or hexamethylene diisocyanate (HDI). The other study[36] included a series of elastomers prepared from the previously listed monomers and other diisocyanates such as *m*-phenylene diisocyanate, naphthalene 1,5-diisocyanate; polyester diols prepared from ϵ-caprolactone and methyl ϵ-caprolactone; and various commercially available polyols. The mechanical properties (Young's modulus E, tensile strength σ_m, and ultimate elongation ϵ_b) were determined for the elastomers as a function of temperature at a fixed rate. These properties, along with the compositions of the elastomers, specifically the urethane group concentration per kilogram U and the chemical nature of the network chains, were interrelated with the glass-transition temperatures T_g and the crosslink density ν of the various elastomers. The relationships derived from the data on these systems showed that (1) in a given series, the ultimate properties depended upon both U and ν; (2) the T_g increased linearly with U; (3) at equal values of $T - T_g$ and constant ν, the ultimate properties were sensibly independent of U when U was less than about 2 moles/kg., but at larger values of U there was a significant dependence; and (4) for many series of elastomers in which $U = 1.6$, the ultimate elongation and tensile strength appeared to be independent of the type of crosslinker and functions only of the crosslink density, according to the relationships $\sigma_m \propto \nu^{1/2}$ and $\epsilon_b \propto {}^1/_2$.

For the present study, TDI, POPG, TMP, and toluene-2,4-diamine (TDA) were used to prepare a number of diisocyanate-linked polymers. The study consisted of two parts. The first part involved the preparation and characterization of three prepolymers: P-I, prepared from 2 moles of TDI and 1 mole of POPG; P-II prepared from 2 moles of P-I and 1 mole of TDA; and P-III, prepared from 1 mole of P-II and 2 moles of POPG. A high molecular weight polymer, P-IV, prepared from 1 mole of P-I and 1 mole of TDA was also studied. The experimental conditions required for the preparation of these polymers were determined. Marked differences in the rheological behavior of P-I in comparison to P-II, P-III, and P-IV were observed and interpreted on the basis of the intermolecular forces present in these materials. Lithium salts, which lower these intermolecular forces, were successfully used in the preparation of urea-containing elastomers by the prepolymer technique.

For the second part of the study, several series of elastomers were prepared and characterized. Four were prepared from different ratios of P-I to various concentrations of TDA dissolved in POPG; additional series were prepared with either TMP or $LiClO_4$ added to the system composed of POPG, P-I, and TDA. Two sets of curing conditions were employed for these elastomers: one at 60°C. in the presence of ferric acetylacetonate (FeAA) catalyst in open trays, the other at 110°C. in closed molds without FeAA catalyst. Elastomers, with portions of P-I replaced by equivalent quantities of TDI and POPG, were also prepared by the first procedure.

The time-dependent and the time-independent (equilibrium) mechanical properties were obtained on the various elastomers by measuring the stress–strain curves over a wide range of temperatures with an Instron tensile

tester. The glass-transition temperatures were determined for all the elastomers and interrelated with the chemical group contents of the materials. For many of the soluble elastomers, intrinsic viscosity measurements were made in *N*,*N*-dimethylacetamide, and approximate weight per cent sols were determined for some of the insoluble elastomers. Relationships between the time-dependent and independent mechanical properties of the elastomers were determined. The differences between the properties of elastomers with networks formed from either intermolecular forces or covalent chemical bonds are discussed in terms of their chemical structure and network topologies.

II. EXPERIMENTAL MATERIALS AND PROCEDURES

A. Materials

1. Polyoxypropylene Glycol (POPG). One lot of Niax diol PPG 2025 (elastomer grade), obtained from Union Carbide Chemicals Co., New York, N. Y., was used throughout this study. After a preliminary degassing of a large lot of this material, 1500-ml. batches were subjected to a second degassing before use. The procedure consisted of heating the POPG to 125°C. and evacuating with a laboratory vacuum pump for about 6 hr. while a stream of dry nitrogen gas bubbled through the material. Repeated analyses of the same material for hydroxyl content by the acetylation method[71] gave values ranging from 0.97 to 1.06 meq./g., corresponding to average molecular weights of 2060 to 1890 assuming all molecules to be difunctional and only hydroxyl terminated. Although differences of this magnitude are significant, a molecular weight of 2000 for PPG 2025 was used in calculating all formulations. Other analyses showed an unsaturation content of 0.025–0.034 meq./g.,[72] a peroxide content less than 0.001 mmole/g. by the iodine method,[73] a carbonyl content less than 0.01 mmole/g. by infrared spectroscopy,[74] and a water content of less than 0.01% (Karl Fischer method).

2. Toluene Diisocyanate (TDI). This material was purchased from E. I. du Pont de Nemours and Co., Inc., Wilmington, Del., and is reported to be the 2,4-isomer. It was purified by distillation (b.p., 130°C./18 mm.) through a vacuum-jacketed column filled with 0.16 × 0.16 in., type 316 stainless steel protruded packing, purchased from the Scientific Development Co., State College, Pa. The packed section was 18 in. in length and $^3/_4$ in. in diameter. A dry nitrogen atmosphere was used to protect the material from contamination by moisture. Samples so purified gave an isocyanate analysis in the range of 11.4 to 11.5 meq./g. by the di-*n*-butylamine–tetrahydrofuran procedure.[75]

3. Estane. Estane B58301010 was obtained from the B. F. Goodrich Chemical Co., Cleveland, Ohio. This material is reported[76] to be the uncatalyzed reaction product of 2 moles of TDI with 1 mole of PPG 2025. Analysis for isocyanate content was made by the di-*n*-butylamine–tetrahydrofuran procedure using as the solvent a mixture of 200 ml. methanol,

50 ml. water, and about 50 ml. tetrahydrofuran. With samples containing a total of 33 meq. of isocyanate groups, a precision of 0.4% was obtained. Differences in the NCO content for various batches of Estane required some adjustments in formulation of weights. The elastomers of series 1, 2, 3, and 4 (see Table I) were prepared from one batch of Estane with a number-average molecular weight $\bar{M}_n$ of 2522, assuming all molecules to be difunctional and only isocyanate terminated. The elastomers of series 5 through 8 were prepared from Estane, whose isocyanate content ranged from 0.754 to 0.796 meq./g., corresponding to a range of $\bar{M}_n$ of 2510 to 2650. As this material has terminal isocyanate groups, which can react with water, all transfers and weighings were done in the dry-box.

For the preparation of the elastomers, Estane was employed as the source of P-I. The P-I used in the study of the polymers—P-II, P-III, and P-IV—was prepared in the laboratory from 2 moles of TDI and 1 mole of POPG. While the molecular weight of the Estane varied from 2510 to 2650, the laboratory-prepared P-I consistently had an isocyanate content which gave a molecular weight of 2420 ± 70. The quantities of ingredients for the elastomers of series 1, 2, 3, and 4 were calculated from formulas:

$$X = \frac{2CR_2}{R_1(M_3 - M_2)(R_2 + 1) + 2R_2M_1 + 2M_2}$$

$$Y = \frac{C(R_1R_2 + R_1 - 2)}{R_1(M_2 - M_3)(R_2 + 1) - 2R_2M_1 - 2M_2}$$

$$Z = \frac{CR_1(R_2 + 1)}{-R_1(M_2 - M_3)(R_2 + 1) + 2M_1R_2 + 2M_2}$$

$$R_1 = \mathrm{NCO}/(\mathrm{OH} + \mathrm{NH_2})$$

$$R_2 = \mathrm{NH_2}/\mathrm{OH}$$

where C = total weight of ingredients, M_1 = molecular weight of TDA, M_2 = molecular weight of POPG, M_3 = molecular weight of Estane (P-I), X = moles of TDA required, Y = moles of POPG required, and Z = moles of Estane (P-I) required.

For the calculation of the formulation parameters, 1 mole of Estane was considered as a source of 1 mole of POPG and 2 moles of TDI.

4. Toluene-2,4-Diamine (TDA). This material, obtained from Matheson, Coleman and Bell, Inc., East Rutherford, N. J., was purified by a standard method[77] and gave a b.p. of 165°C./15 mm. Analysis of the diamine by a nonaqueous acid–base titrimetric procedure[78] showed it to have a purity of 99.1 ±0.5%.

5. Ferric Acetylacetonate (FeAA). The FeAA was prepared from acetylacetone and ferric chloride.[79]

6. Tetrahydrofuran (THF). The THF was obtained from Industrial Polychemicals Service, Gardena, Calif., and was freshly distilled from sodium wire through a Snyder bubble-cap column before use (b.p., 64–65°C./

760 mm.). Analyses by the iodine method[73] showed a peroxide content of less than 0.001% and a water content (Karl Fischer method) of less than 0.01%.

7. Lithium Perchlorate ($LiClO_4$). Lithium perchlorate was obtained from the American Potash and Chemical Co., Los Angeles, Calif. After drying for 5 hr. at 120–130°C. and less than 10 mm. pressure, the water content (Karl Fischer method) was less than 0.04%. Some difficulty was experienced with this method of analysis and, therefore, a sample was heated under vacuum at 120–130°C. for 22 hr. to constant weight as a check. The two methods gave values in reasonable agreement with each other.

8. *N,N*-Dimethylacetamide (DMA) and *N,N*-Dimethylformamide (DMA). These materials were purchased from the Borden Chemical Co., Monomer-Polymer Laboratories, Philadelphia, Pa. Purification was accomplished by the method of distillation (b.p., 81°C./40 mm.) described by Thomas and Rochow[80] for *N,N*-dimethylformamide.

9. 1,1,1-Trimethylol Propane (TMP). The TMP, obtained from the Celanese Chemical Co., New York, N. Y., was dried at 110°C. under 1–2 mm. pressure for about one week to yield material with a water content of less than 0.01% (Karl Fischer method). The dry TMP was stored in a sealed container in the dry-box.

10. Tetramethyl Urea. This material, obtained from the RSA Corporation, Ardsley, N. Y., was purified by distillation (b.p., 79°C./23–24 mm.) through the vacuum-jacketed, packed column previously described for the purification of TDI.

11. Ethyl Ether. Anhydrous ethyl ether was used as received from Mallinckrodt Chemical Co., St. Louis, Mo., and contained less than 0.01% water.

12. Methylene Chloride. Methylene chloride was obtained from the Braun Chemical Co., Los Angeles, Calif., and was purified by distillation through a Snyder bubble-cap column. After discarding the forerun, the middle fraction was collected and used. It contained less than 0.01% water (Karl Fischer method).

13. Potassium Thiocyanate. This material was Baker's analyzed reagent obtained from J. T. Baker Chemical Co., Phillipsburg, N. J., and was dried for 10 days at 120–130°C. at less than 10 mm. pressure.

14. Lithium Salts. Lithium bromide, lithium chloride, lithium carbonate, and lithium nitrate were Mallinckrodt analytical reagent grade chemicals and were dried for 6–9 days at 120–130°C. and less than 10 mm. pressure.

B. Preparation and Analysis of Prepolymers

All preparations of polymers P-I, P-II, P-III, and P-IV were carried out in oven-baked (110–120°C.) glassware and under anhydrous conditions by use of a dry-box filled with nitrogen, dried by circulation over phosphorus pentoxide (P_2O_5). The dew point inside the box was kept below −20°F., as monitored by an Alnor dew-point meter (manufactured by Illinois Test-

ing Laboratories, Chicago, Ill.). For experiments requiring days or months of time, the reaction mixtures were stored in phosphorus pentoxide-protected desiccators. Additional curing of P-IV was carried out in an open Teflon-coated tray in an oven maintained at 60 ± 5°C. for 18 hr. The preparation of P-III from P-II and POPG was carried out in a round-bottomed flask protected from atmospheric moisture by wax-sealed, standard tapered joints. For isocyanate analysis, samples of the reaction mixture were taken from the reaction vessel after placing it in the dry-box.

While the isocyanate content of TDI and P-I have been carefully investigated by the di-*n*-butylamine–tetrahydrofuran procedure[75] and found to be accurate to 0.4%, a similar study of the isocyanate content of substances such as P-II is not complete. Present results[81] indicate that the isocyanate content of the P-II prepolymer can be obtained with a precision of better than 5%.

C. Preparation and Curing of Elastomers

Elastomers were prepared from different ratios of Estane to various concentrations of TDA dissolved in POPG. Ingredients for the preparation of all the elastomers were weighed and mixed in a dry-box. All glassware used in the preparations was dried in an oven at 110–120°C. and transferred to the dry-box after cooling in a desiccator over P_2O_5.

Toluene-2,4-diamine and POPG were weighed into a tarred flask and heated until the TDA dissolved. For some of the formulations with a high TDA content, this required a temperature of 85–90°C. It was convenient to prepare this solution in excess to simplify subsequent transfer. The prepolymer, Estane, was weighed into a tarred beaker, and the required amount of the POPG–TDA solution was added and thoroughly mixed with a stirring rod. When elastomers of the same formulation were cured at both 110 and 60°C., a double batch of ingredients was mixed (ca. 240 g.) and divided into two equal portions. If the formulation called for catalyst, this was added as a solution of FeAA in THF. A 1-ml. portion of a solution containing 2.5 g. FeAA/100 ml. THF was pipetted into a 120-g. batch immediately before casting. Some separate experiments were made in which the FeAA was added as a solution in POPG; these gave similar results.

The material was cast either into open Teflon-coated trays or into specially designed closed molds which could be used for curing under vacuum or under a nitrogen blanket, and which were shown to hold a pressure of less than 5 mm. for periods greater than 24 hr. The elastomers in open trays were placed in a vacuum chamber and evacuated to 3–5 mm. pressure to remove dissolved gases and bubbles introduced during mixing, as well as the THF. The closed molds were connected directly to the vacuum system and evacuated. A period of 5–10 min. under vacuum was sufficient for samples containing no THF, but 20–30 min. was required for the samples containing THF before foaming ceased and most of the bubbles were removed. The elastomers in open trays were cured in an oven at

60 ±5°C., while those in closed molds were cured under a blanket of nitrogen gas in constant-temperature baths at 110 ±3°C. The weight loss on curing in open trays was less than 0.5 g. (less than 0.4 wt.-%). The standard curing times were 72 hr. at 60°C. and 70 hr. at 110°C. After cure, the sheets were removed from the molds and stored in polyethylene sacks in a refrigerator maintained at about 7°C. The sheets of elastomer were approximately 1/8-in. thick, transparent, and usually bubble-free.

The solubility limit of TDA in POPG (about 20 wt.-% at 90°C.) restricted the formulations that could be made. For example, at a fixed ratio of 1.10, the upper limit of the NH_2/OH ratio was 0.50, while at an NH_2/OH ratio of 0.30, the upper limit for the $NCO/(OH + NH_2)$ ratio was 1.40.

Two other sets of curing conditions were briefly investigated. Cure of the elastomers containing FeAA catalyst at 110°C. under vacuum of a nitrogen blanket led to noticeable decomposition and therefore was not studied further. Selected elastomer formulations with FeAA catalyst were also cured at 60°C. in closed molds under a nitrogen atmosphere or vacuum. These curing conditions led to elastomers with noticeably different mechanical properties than the corresponding formulations cured in open trays. Additional study of these cure conditions is in progress and will be reported in a separate publication.[82]

D. Solubility Determinations

One-gram samples of each elastomer, cut into small pieces (ca. 1 × 1 × 0.3 cm.) were tested by shaking in 50 ml. of DMA at ambient temperatures. The soluble elastomers completely dissolved within 2 hr., while those classed as insoluble did not dissolve completely after 20 days.

E. Glass-Transition Temperatures

The glass-transition temperature T_g of the elastomers was measured with an automatic quartz-tube-type dilatometer.[36,83] Specimens for T_g measurement were prepared by die-cutting disks 1/2 in. in diameter from the elastomer sheets. A number of these disks were stacked to form a cylinder approximately 1.5 in. long. In the dilatometer, the lengths of these cylindrical specimens were monitored by linear variable differential transformers and were recorded while the temperature was decreased slowly and automatically from ambient to −120°C. The temperature was then increased gradually to ambient. Values of T_g obtained from plots of length against temperature while the temperature was decreasing ordinarily agreed within a few degrees with the value obtained while the temperature was increasing. The average of the two values is reported. However, on the basis of several replicate determinations, the values were judged to be precise to ±2.5°C. The T_g of a sample of polyisobutylene obtained from the National Bureau of Standards was determined several times and found to be 199.6 ±1.3°K.,

in good agreement with the previously reported values of 203°K.[84] and 202°K.[85] The rate of change of temperature from −50 to −60°C., a range in which the T_g of the elastomers of the present study are located, was 0.2–0.3°C./min.

F. Viscosity Measurements

Dilute solution viscosities in *N,N*-dimethylacetamide (DMA) of some of the elastomers were determined in Canon-Ubbelohde dilution viscometers at several polymer concentrations. The efflux time for DMA in the viscometers used was about 125 sec. A small kinetic-energy correction was applied, except when efflux times were so high as to make the correction negligible. Viscosity determinations were run in a thermostated bath maintained at 25.00 ±0.02°C.

G. Preparation of Tensile Specimens and Tensile Testing

Ring tensile specimens were cut from the cured elastomer sheets. Details of the equipment and methods used to prepare the ring specimens and monitor them as to their handling, storage history, weight-to-area ratio, the presence of surface defects on the specimen or the development of such defects during the tensile test have been described previously.[86]

Tensile data were obtained from the ring specimens by using an Instron tensile tester. The tensile strengths reported are nominal values, based on the initial cross-sectional area. The strain at ultimate elongation was calculated as $2\Delta C/\pi D_i$, where ΔC is the crosshead displacement and D_i is the inside diameter of the ring. Values of strain prior to rupture were obtained by the use of the same formula, except that the average diameter was used. The dimensions of the rings (average dimensions: 0.90 in. ID × 1.10 in. OD × 0.125 in. thick), in conjunction with the geometry of the Instron, permitted measurement of elongations up to a maximum of 1050%, instead of the less than 900% obtainable from the dumbbell specimens previously employed.[30,36] Furthermore, the ring specimens should permit a more accurate estimation of the ultimate elongations, because the effective gage length should not vary with the strain as it does for the dumbbell specimens. Separate experiments have indicated that the previously reported ultimate elongations[30,36] for dumbbell specimens showing extensibilities of 100–200% are not significantly in error. It appears, however, that values of the ultimate elongation of about 600–800% are relatively too large by about 20 to 30%. Also, as explained elsewhere,[87] the value for the tensile strength is dependent upon the D_0/D_i ratio (where D_0 is the outside diameter of an unstretched ring) and the magnitude by which the force is changing with time prior to the observed rupture point. Taking these factors into consideration for the ring specimens for the elastomers of the present study, the values for the tensile strengths are at most 10% too small.

The Instron tensile tester equipped with a constant-temperature box which surrounded the crosshead and grips used to obtain stress–strain data

on the various elastomers has been discussed previously.[88,89] Tensile data were measured on ring specimens at temperatures ranging from −40 to 82°C. Each series of specimens was conditioned in the constant-temperature box for 10–15 min. before testing was begun. The rings were placed over hooks attached to the crosshead and load cell of the Instron. At test temperatures of 4.5–82°C., a film of castor oil was used on the hooks, while at −23.5 and −40°C., Dow-Corning 200 silicone oil was used as the lubricant. Ring specimens were tested at a crosshead speed of 5 in./min., corresponding to a nominal strain rate of 0.058 sec.$^{-1}$

III. EXPERIMENTAL RESULTS AND DISCUSSION

A. Prepolymer Studies

The prepolymer P-I is formed by reacting under anhydrous conditions 2 moles of TDI with 1 mole of POPG; P-II is formed from 2 moles of P-I and 1 mole of TDA; P-III is formed from 2 moles of POPG and 1 mole of P-II; and P-IV is formed from 1 mole of P-I and 1 mole of TDA:

$$\text{TDI} + \text{POPG} + \text{TDI} \rightarrow \text{P-I}$$
$$\text{P-I} + \text{TDA} + \text{P-I} \rightarrow \text{P-II}$$
$$\text{POPG} + \text{P-II} + \text{POPG} \rightarrow \text{P-III}$$
$$\text{P-I} + \text{TDA} \rightarrow \text{P-IV}$$

At room temperature, the reaction to form P-I requires 200 hr. but only 20 hr. when only 0.03 wt.-% FeAA is added as catalyst. The P-I polymer is a viscous liquid which is terminated mainly by isocyanate groups and does not undergo further polymerization when stored under anhydrous conditions at ambient temperatures. Indeed, samples of P-I prepared in the absence of FeAA catalyst did not show a significant change in isocyanate content after storage under anhydrous conditions at ambient temperatures for two years. Over the same period of time and in the presence of FeAA, however, P-I loses its isocyanate content slowly, probably through dimerization[90] of the isocyanate group. The $\bar{M}_n$ of P-I, as determined from the isocyanate content using the di-*n*-butylamine–tetrahydrofuran procedure, agreed with the expected value of 2348 ±25.

Two methods were tried for the conversion of P-I to a P-II; these are illustrated by eqs. (1) and (2).

At ambient temperatures, the reaction of P-I with water was slow and did not follow the stoichiometry shown above. The reaction is probably complex, as previously reported for model compounds.[91] In contrast to procedure (1), when P-I was reacted with TDA dissolved in dry THF, P-II was formed as shown in eq. (2). The reaction required less than 2 hr. for completion at ambient temperature and appeared to be stoichiometrically reliable, as shown by isocyanate endgroup analyses which gave an $\bar{M}_n$ of 4280 ±200. The P-II formed by this procedure is a rigid gel, and each mole contains, on the average, five benzene rings, two isocyanates, four

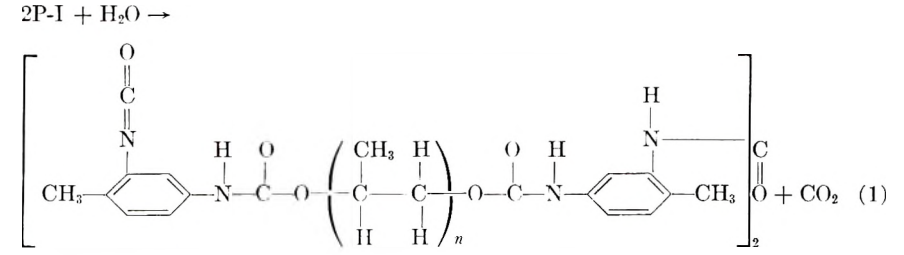

(1)

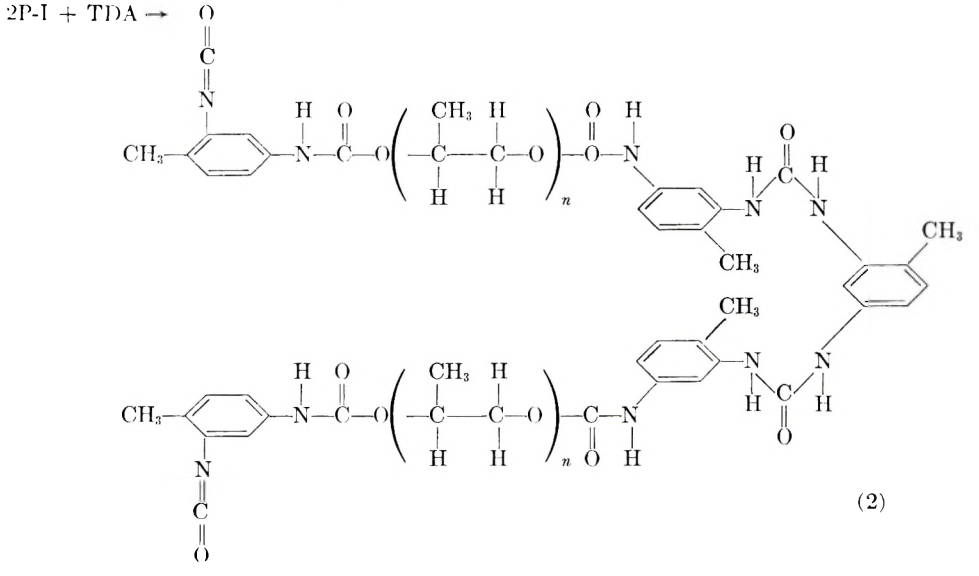

(2)

urethanes, and two urea groups. P-II was also prepared by using TDA dissolved in either ethyl ether or methylene chloride; in each case, the product was a rigid gel like that formed when THF was the solvent.

The gellike P-II is a tough, rubbery material which dissolves in excess THF, DMF, or DMA. At concentrations of about 3 g./100 ml., the THF solution is fluid, but at higher concentrations it is a thixotropic material. Whereas the P-II formed by the TDA reaction is a rigid gel, none of the materials formed by the reaction of water with P-I, as shown in eq. (1), exhibited gellike character. The diisocyanate-terminated P-II was stable for at least two months when stored under anhydrous conditions at ambient temperatures.

Studies also showed that P-II does not gel when it is formed in the presence of suitable quantities of lithium salts, such as lithium perchlorate, nitrate, bromide, etc. This antigelation action is probably the result of the destruction by lithium ions of intermolecular hydrogen bonds formed between urea moieties on different polymer chains.

Separate studies were made of the stability of isocyanate groups toward $LiClO_4$ and THF under anhydrous conditions at ambient temperatures. The results showed that these additives did not change the isocyanate contents of either P-I or P-II.

In order to extend the study of the prepolymers and also to circumvent the necessity of maintaining anhydrous conditions in working with these urea-containing prepolymers, P-III was prepared. The reaction of 2 moles of POPG with 1 mole of P-II in the presence of $LiClO_4$ to yield P-III required 280 hr. at 82°C. The P-III so prepared contained less than 0.10 wt.-% of isocyanate groups, as determined by the di-*n*-butylamine–tetrahydrofuran procedure; furthermore, no isocyanate groups could be detected in the infrared spectrum at 4.4 μ for path lengths up to ca. 500 μ.

The prepolymer P-IV was prepared by reacting equivalent amounts of P-I with TDA for 18 hr. at 60°C. Since the ratio of reacting moieties was close to one, and the reaction of an amine and an isocyanate is rapid, P-IV is a high-molecular-weight polymer. The P-IV had a tensile strength of 860 psi and an elongation of 540% at 25°C., however, it was soluble in solvents such as DMF and DMA and in THF containing a lithium salt. While P-IV is an elastomeric material, a TDI-linked POPG ($\bar{M}$, 2000) polymer with a molecular weight of about 100,000 is a highly viscous, but pourable liquid.[93] This is additional evidence for the introduction by the substituted-urea groups of strong interchain forces into the oxypropylene system.

The antigelation action of the lithium salts in P-II and P-III is dependent on the concentration of the lithium salt present in the prepolymer. The ratios of Li^+/NH_2 found to be effective in preventing the gelation of P-II and P-III were 0.5 and 3, respectively. However, the prepolymers P-II and P-III formed gels when the values for the Li^+/NH_2 ratio were 0.1 and 1, respectively. Other additives such as tetramethyl urea (TMU) and potassium thiocyanate (KSCN), known to be effective in destroying hydrogen bonding in selected protein system,[94] were not antigelation additives for P-II when the ratios $[KSCN]/[NH_2]$ and $[TMU]/NH_2]$ were 0.75.

The action of the antigelation agents is of interest for two reasons: (*1*) the results indicate strongly that interchain forces exist in these systems and that these forces are mainly responsible for the gelation phenomenon; and (*2*) it demonstrates a practical means by which these urea-modified prepolymers can be used for additional synthetic studies. The latter application of the lithium salt additive has been employed successfully in a P-II material which was used to prepare a series of filled and unfilled elastomers.

The gelation behavior of P-II, P-III, and P-IV suggests that the precure or scorch of mixes of diisocyanate-linked polymers containing substituted urea groups, as reported mainly in the patent literature, is the result of strong interchain forces and not necessarily of reactions leading to the formation of a covalently crosslinked network.

B. Chemical Compositions of Elastomers

For the second part of the study, eight separate series of elastomers were prepared; their distinguishing features are given in Table I. Five ratios were used to characterize the stoichiometry and the quantity of functional groups present in a formulation: (*1*) the ratio of isocyanate groups to the

sum of the hydroxyl and amino groups, $NCO/(OH + NH_2)$; (*2*) the ratio of amino groups to hydroxyl groups, NH_2/OH; (*3*) the ratio of the hydroxyl groups from TMP to the total number of hydroxyl groups, OH_{triol}/OH_{total}; (*4*) the ratio of the isocyanate groups from Estane (P-I) to the total number of isocyanate groups, $NCO_{P\text{-}I}/NCO_{total}$, with the remaining NCO introduced with TDI; and (*5*) the ratio of the lithium ions to the amino groups, Li^+/NH_2. The concentrations of the groups given in these ratios and elsewhere (indicated by brackets around the terms), unless specified otherwise, are expressed in equivalents per kilogram of polymer or mixture.

TABLE I
Designations and Cure Conditions for Elastomers Containing Substituted Urea Groups

Series no.	$\frac{NCO}{(OH + NH_2)}$	NH_2/OH	$\frac{OH_{triol}}{OH_{total}}$	$\frac{NCO_{P\text{-}I}}{NCO_{total}}$	Li^+/NH_2	Cure[a]
1[b]	1.10	0.10–0.40	—	1.00	—	A, B
2	1.20	0.10–0.40	—	1.00	—	A, B
3[b]	1.10–1.50	0.20	—	1.00	—	A, B
4[b]	1.10–1.40	0.30	—	1.00	—	A, B
5	1.10	0.20–0.30	0.13	1.00	—	A, B
6	1.10–1.20	0.20–0.30	—	0.75–1.00	—	A
7	1.30	0.30	—	1.00	0.62	A, B
8	1.30	0.30	—	1.00	—	—[c]

[a] Cure A used FeAA catalyst and an open mold at 60°C. for 72 hr., while B used no catalyst and a closed mold at 110°C. for 70 hr.

[b] In separate and earlier preparations of elastomers of series 1, 2, 3, and 4, the ranges for $NCO/(OH + NH_2)$ and NH_2/OH were 1.10, 0.95–1.20, and 0.95–1.30, and 0.00–0.50, 0.20, and 0.30, respectively. When appropriate, the properties of those elastomers which extend the ranges of the formulation parameters of series 1, 3, and 4 (as shown above) are discussed in the text.

[c] Three portions of one batch of polymer cured in closed molds at 110°C. for periods of time ranging from 46.5 to 408 hr.

Two sets of curing conditions were employed. In cure A, elastomer formulations containing about 2.5 mg. of FeAA/100 g. of elastomer were cured in open Teflon-coated trays at 60°C. for 72 hr. In cure B, the same formulations, without FeAA catalyst, were cured at 110°C. for 70 hr. in closed molds.

The effects of the ratios, $NCO/(OH + NH_2)$ or R_1 and NH_2/OH or R_2, on the properties of the polymers were studied in series 1, 2, 3, and 4. The importance of the ratios R_1 and R_2 to the properties of the polymers of series 5 through 8 was not extensively investigated. To assess biuret crosslinks and substituted urea groups in diisocyanate-linked polymers crosslinked with TMP, the arrangement of substituted urea groups in the backbone of the POPG–TDI–TDA terpolymer, and the effect of lithium perchlorate, respectively, on the properties, the polymers of series 5, 6, and 7 were prepared. Series 8 was prepared to determine an adequate period of time for the cure of the isocyanate–hydroxyl–amine system at 110°C.

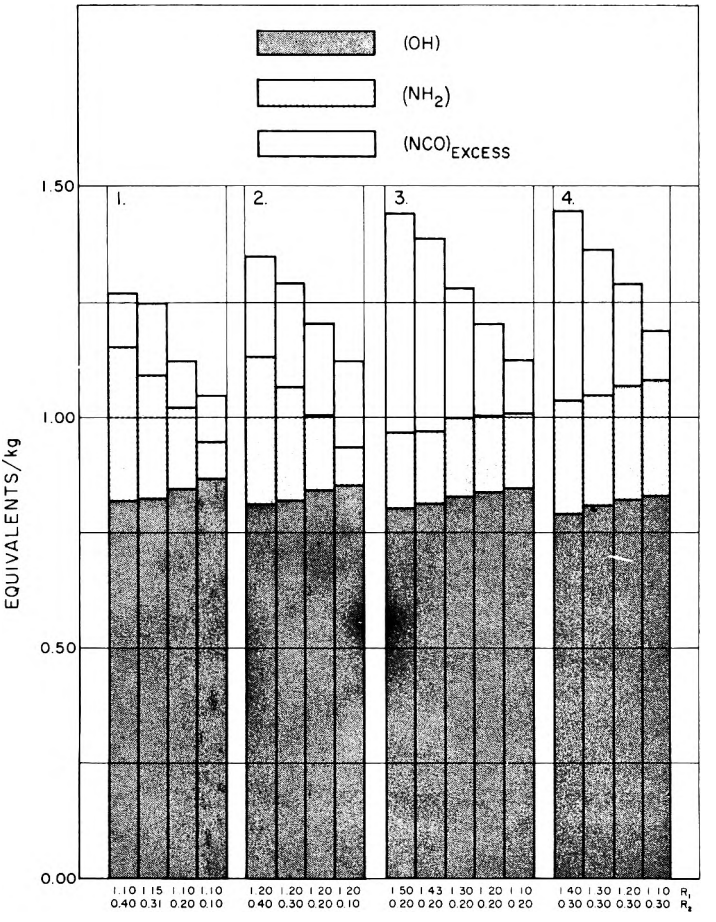

Fig. 1. Equivalents of functional groups used in the preparation of elastomers of series 1, 2, 3, and 4.

The concentrations of the chemical groups per kilogram present in the formulations of series 1, 2, 3, and 4 are represented by the histogram shown in Figure 1. If isocyanate groups react with hydroxyl and amino groups at 60°C. and after 72 hr., in the presence or absence of FeAA catalyst, according to the stoichiometries given by eqs. (3) and (4).

$$\mathrm{ROH} + \mathrm{R'NCO} \rightarrow \mathrm{R'{-}\overset{\displaystyle H}{\underset{|}{N}}{-}\overset{\displaystyle O}{\overset{\|}{C}}{-}O{-}R} \tag{3}$$

$$\mathrm{R''NH_2} + \mathrm{R'NCO} \rightarrow \mathrm{R''{-}\overset{\displaystyle H}{\underset{|}{N}}{-}\overset{\displaystyle O}{\overset{\|}{C}}{-}\overset{\displaystyle H}{\underset{|}{N}}{-}R'} \tag{4}$$

then the excess isocyanate content for the formulations shown in the histogram is given by the expression

$$[\mathrm{NCO}]_{\mathrm{excess}} = [\mathrm{NCO}] - ([\mathrm{NH_2}] + [\mathrm{OH}])$$

The [OH] and [NH_2] shown in the histogram also represent the concentrations of substituted urethanes and substituted urea groups, respectively.

The histogram of Figure 1 shows the hydroxyl or substituted urethane group concentration in the four series to be relatively constant (0.80–0.85 equivalent/kg.) in comparison to the concentrations of amino or substituted ureas and initial or excess isocyanates. The amino or substituted urea group concentrations, however, are relatively constant at two different levels of 0.16 and 0.25 equivalent/kg. in series 3 and 4, respectively. Three experimental errors were committed, and the values for R_1 and R_2 actually used, 1.15 and 1.43, and 0.31, are given rather than those intended, 1.10 and 1.40, and 0.30.

The hydrogens of the substituted urethanes and urea moieties can act as reaction sites for the excess isocyanate under suitable reaction conditions. Studies by Bennet, Saunders, and Hardy[95] on the reaction of either phenyl or *o*-tolyl isocyanates with *N*-phenylurea and ethyl carbanilate indicated that the rate of the isocyanate–urethane reaction was about 1/100 that of the isocyanate–urea reaction. These studies were made at temperatures between 100 and 140°C. and at an isocyanate concentration which is about the same as the $[NCO]_{excess}$ in the formulations of series 1, 2, 3, and 4. This difference in reactivity is supported by the results of the present study with polymers containing these moieties.

The elastomers of series 1, 2, 3, and 4, where $R_1 \geq 1.10$ and $R_2 \geq 0.10$, cured by method B, were insoluble at ambient temperatures in THF, with or without added lithium salts, DMF or DMA. Elastomers from the same batches of ingredients, cured by method A, however, were soluble in DMA. The elastomers of series 7 cured by method B were insoluble in DMA, while those of series 6 and 7 cured by method A were soluble. Also, as expected, the elastomers prepared with TMP (series 5) cured by either methods A or B were insoluble. Except for elastomers of series 5, the data indicate that a three-dimensional network was formed only in those elastomers in which an excess of isocyanate groups and substituted urea hydrogens was present and cure was effected by method B. Thus, the reaction of substituted ureas with excess isocyanate is the main process which leads to a three-dimensional network during cure at 110°C. for 70 hr. Such a reaction is shown by eq. (5):

$$\sim\!\!\sim RNCO + \sim\!\!\sim R''NHCONHR'\sim\!\!\sim \rightarrow \sim\!\!\sim R''\!-\!N\begin{matrix}\diagup\ CONHR\sim\!\!\sim \\ \diagdown\ CONHR'\sim\!\!\sim\end{matrix} \qquad (5)$$

This stoichiometry requires only one hydrogen per substituted urea to be reactive to the $[NCO]_{excess}$. It should be noted, however, that the active hydrogen has not disappeared. Further discussion of this point will be presented when the near-equilibrium moduli of the crosslinked elastomers are discussed.

The histogram in Figure 2 shows the relative amounts of the absolute ex-

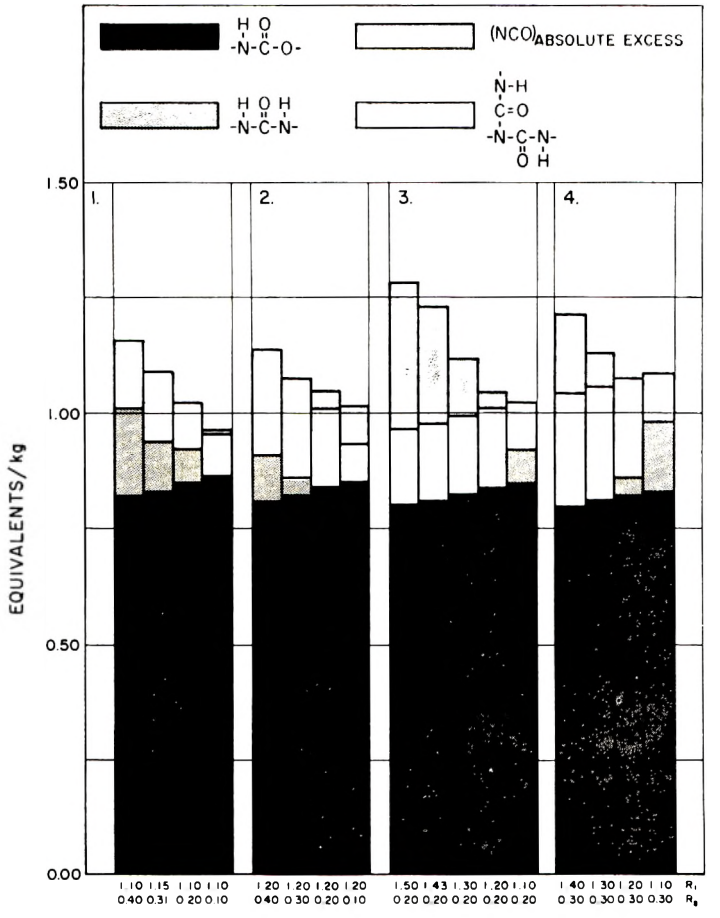

Fig. 2. Potential equivalents of functional groups in elastomers of series 1, 2, 3, and 4.

cess of isocyanate and the substituted urethanes, substituted ureas, and substituted biurets which are present in the elastomers of series 1, 2, 3, and 4 if the isocyanates react only with hydroxyl, amino, and substituted urea hydrogens. The three separate cases considered in the calculation of the compositions shown in Figure 2 are defined by the following expressions.

Case 1. If $[NCO]_{initial} \leq ([NH_2] + [OH])$ and $[NCO]_{initial} \geq [NH_2]$, then [substituted biuret] = 0, [substituted urea] = $[NH_2]$, and $[NCO]_{excess} = 0$.

Case 2. If $[NCO]_{initial} \geq ([NH_2] + [OH])$, $[NCO]_{excess} = [NCO]_{initial} ([NH_2] + [OH])$, and $[NCO]_{excess} \leq [NH_2]$, then [substituted biuret] = $[NCO]_{excess}$, [substituted urea] = $[NH_2] - [NCO]_{excess}$, and $[NCO]_{abs.\ excess} = 0$.

Case 3. If $[NCO]_{initial} > ([NH_2] + [OH])$, $[NCO]_{excess} = [NCO]_{initial} - ([NH_2] + [OH])$, and $[NCO]_{excess} > [NH_2]$, then [substituted biuret] = $[NH_2]$, [substituted urea] = 0, and $[NCO]_{abs.\ excess} = [NCO]_{initial}$ —

$(2[NH_2] + [OH])$, or $[NCO]_{abs.\ excess} = [NCO]_{initial} - ([substituted\ urethane] + 2\ [substituted\ biuret])$; if $([NCO]_{initial} - [NH_2]) \geq [OH]$, then, in all cases, $[OH] = [substituted\ urethanes]$.

The study of the elastomers prepared from POPG, TDI, and TMP by cure A, presented in the previous study,[30] showed that the mechanical properties varied only slightly for NCO/OH ratios greater than 1.05; therefore, the elastomers containing TMP (series 5) for the present study were prepared with an R_1 of 1.10. Elastomers with two levels of R_2, 0.30 and 0.20, at fixed levels of R_1 (1.10) and the (OH_{triol}/OH_{total}) ratio (0.13), were prepared both by cures A and B. The hydroxyl group contents of the two formulations containing TMP were 0.93 equivalent/kg. which is somewhat higher than the 0.80–0.85 equivalent/kg. for the formulations of series 1, 2, 3, and 4. For these formulations, the $[NCO]_{abs.\ excess} = 0$. The concentration of substituted ureas ranges from 0.19 to 0.28 equivalent/kg. for cure A and 0.08 to 0.16 equivalent/kg. for cure B, and the substituted biurets concentration = 0.12 equivalent/kg., assuming that only cure B leads to the formation of biuret structures.

The elastomers of series 6 were prepared with portions of P-I replaced with equivalent quantities of TDI and POPG. This change in ingredients should permit the formation of backbone arrangements in which more of the TDI and TDA molecules are connected directly. In the absence of TDI, the TDA units must be separated by at least one P-I molecule, but in the presence of TDI, the TDA molecules can be linked directly by TDI; e. g.,

$$\sim\!\!\sim\text{P-I—TDA—P-I—TDA—P-I—POPG}\sim\!\!\sim$$
$$\sim\!\!\sim\text{P-I—TDA—TDI—TDA—P-I—POPG}\sim\!\!\sim$$

For formulations with $R_1 = 1.20$ and $R_2 = 0.20$, it was found that there was a limit to the amount of P-I which could be replaced by an equivalent quantity of POPG and TDI. When 25 mole-% or more of the isocyanate originated from TDI, the mixture of POPG, TDI, TDA, and P-I immediately formed a granular gel. This gelation was not observed when 20 mole-% or less of the isocyanate originated from TDI.

Axelrood, Hamilton, and Frisch[40] reported the separation of a greasy powder in attempts to prepare elastomers from POPG-2010, 4,4′-methylene bis(2-chloroaniline) (MOCA), and TDI, in the absence of a metal organic catalyst. It was suggested that, in the absence of catalyst, the isocyanate-amine reaction is considerably faster than the isocyanate-hydroxyl reaction and leads to the formation of a high-melting urea polymer which separates from the mixture. In the POPG–P-I–TDA–TDI system, the granular gel was observed in the presence of FeAA and was dependent upon the amount of free TDI present in the mixture. Apparently, both kinetic and compositional factors are important to the separation process.

The compositions of the formulations and elastomers of series 6, 7, and 8 can be obtained from the histograms shown in Figures 1 and 2. A value

for the additional parameter needed to describe the elastomers of series 7, the Li^+/NH_2 ratio, is given in Table I.

C. Glass-Transition Temperatures

The glass-transition temperature T_g is of great importance in determining the properties of amorphous polymers. As a first approximation, amorphous polymers appear to be in corresponding temperature states at equal values of $T - T_g$. The value for T_g is determined by the cohesive energy density (C.E.D.) of the polymer and possibly by the stiffness of the chains. Increasing the C.E.D. or chain stiffness raises T_g, in general agreement with empirical relationships, as proposed by Marei[96] and Hayes.[97] These relations indicate that T_g increases with increasing C.E.D., although the expression of Hayes also takes into account the chain stiffness with the empirical parameter n. Furthermore, they indicate that the addition of almost any functional group to a hydrocarbon chain will increase T_g. It is currently recognized, however, that such generalizations probably represent oversimplifications.

For copolymeric systems, it has been found that the T_g varies monotonically between the T_g values for the two homopolymers.[98] There are exceptions, however, in the cases of the copolymers of ethylene and other alkenes[99] and the methyl methacrylate–acrylonitrile copolymers.[100] In the latter case, a minimum is observed in the curve relating the T_g of the copolymer to its composition.

In the study of the POPG–TDI–TMP system,[30] the T_g of the diisocyanate-linked polymers was shown to increase linearly with the concentration of the substituted urethane groups. The concentration of substituted urethane in the polymer was taken as equal to the $[NCO]_{initial}$ in a formulation. Since the $[NCO]_{initial}$ was in excess of the $[OH]_{initial}$, the $[NCO]_{initial}$ gives a high estimate for the concentration of substituted urethane. The previous T_g data were replotted against the $[OH]_{initial}$, a more realistic estimate of the substituted urethane concentration, and this led to the equation

$$T_g = 14.9[OH]_{initial} - 71.5 \tag{6}$$

which represents the T_g data as accurately as the previous expression. The importance of $[NCO]_{excess}$ and its progeny to T_g is not known, however.

It is of interest that values of T_g predicted from the equation given by Hayes are in good agreement with the T_g results found in the present and previous studies for non-urea-containing elastomers. For the POPG–TDI system, the method of Hayes predicts the expression $T_g = 13.0[OH]_{initial} - 74.0$, which is in good agreement with eq. (6).

In all of the determinations of T_g made in the present study, only one distinct change in slope could be observed while the change in length of the sample was monitored as a function of temperature over the range 20 to −120°C. In other words, none of the data gave evidence of a first-order transition.

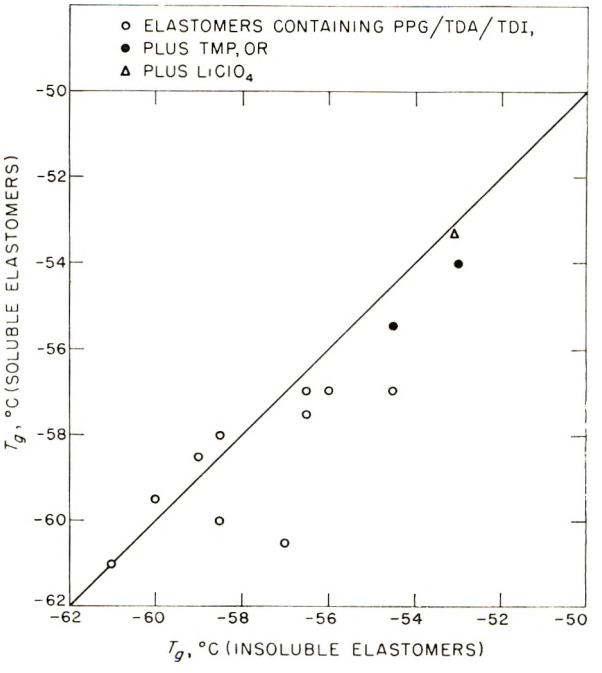

Fig. 3. T_g' of soluble elastomers compared with values of corresponding insoluble elastomers.

Figure 3 shows a plot of the T_g for the insoluble (crosslinked-cure B) versus the soluble (uncrosslinked-cure A) elastomers. The elastomers prepared with TMP by either cure A or B were insoluble but are included in the plot for purposes of comparison. Within the precision of the T_g determination, ± 2.5°C., these data show no discernible differences between a crosslinked and a noncrosslinked elastomer prepared from a given formulation.

The T_g for the elastomers of the present study lead to some surprising results. For these elastomers, even those of series 6, where a change occurred in the distribution of the substituted urea groups, the T_g were adequately represented by eq. (6). Only the elastomers of series 7, which contained $LiClO_4$, were not adequately represented, and they had noticeably higher T_g than predicted by eq. (6). These results show, rather unexpectedly, that the T_g of these diisocyanate-linked elastomers are insensitive to changes in the (substituted urea) concentration. This insensitivity is shown clearly in Figure 4, where the difference between observed values of T_g and values calculated from eq. (3) are plotted against the concentration substituted urea. For these elastomers, the concentration of substituted urethanes varies only from about 0.80 to 0.85 moles/kg., but the concentrations of substituted urea range from 0.08 to 0.40 mole/kg. Only the elastomers containing $LiClO_4$ have higher T_g than the others. For a change of 0.40 mole/kg. in the concentration of substituted urethane, eq. (6) predicts

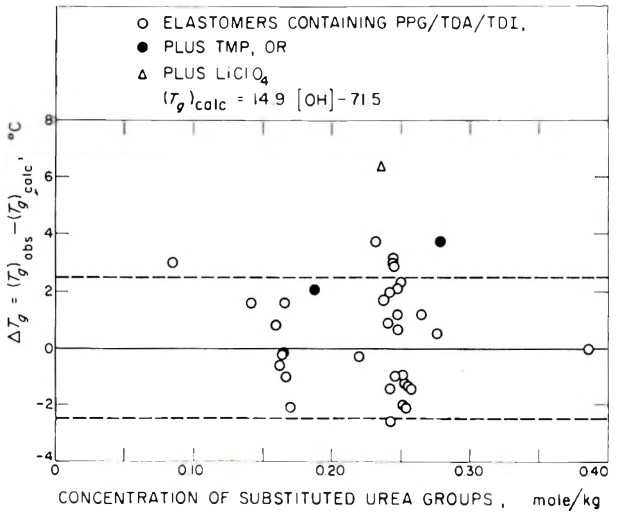

Fig. 4. Insensitivity of T_g to concentration of substituted urea groups.

a change of 6°C. in T_g. Previous reports [101] have indicated that substituted ureas have a larger C.E.D. than substituted urethanes and, hence, a similar change in the substituted urea concentration would be expected to lead to a larger change in T_g. However, Figure 4 shows quite convincingly that the substituted urea groups have no effect on T_g.

Other plots of T_g versus such calculated parameters as [tolylene] or [NCO] were shown to be inadequate for representing the T_g of the present elastomers or of those in previous studies.[30,36] These parameters were tested because they represent different measures of polarity. Other parameters, [NCO]–[substituted urea] and [OH]–[NH_2], which approximately measure polar groups not involved in strongely hydrogen-bonded structures with substituted urea groups, were also found to be inadequate.

The study of the properties of the polymers P-II, P-III, and P-IV, and the mechanical properties of the urea-containing elastomers which will be discussed later, leave little doubt that substituted urea groups introduce strong interchain forces into a substituted urethane–oxypropylene polymer. It is believed that these secondary-type bonds are so strong that the substituted ureas exist in a "frozen state" over the temperature ranges covered in the determinations of T_g (20 to −120°C.) and the mechanical properties (−40 to 82°C.). In such a state, the frozen structures would not affect the value of T_g. The T_g would be determined only by the nature of the chains between aggregates of substituted ureas.

The increase in T_g effected by $LiClO_4$ is, in fact, consistent with this interpretation. The Li salts were shown to act as antigelation agents in the prepolymer studies by reducing the interchain attractive forces. By decreasing these forces, the Li salts free the substituted urea groups and cause an increase in the observed T_g.

The importance of chain flexibility in determining the T_g of a polymer has been emphasized by DiMarzio and Gibbs.[102] They believe that chain stiffness is more important than interchain forces in determining T_g. Thus if the substituted urea groups introduce strong interchain forces but do not increase chain stiffness in the substituted urethane–oxypropylene system, T_g may not change. It is difficult to understand, however, why a larger concentration of rigid tolylene groups should not increase the stiffness of the polymer chain.

D. Solution Viscosities in DMA of Soluble Elastomers

The elastomers of series 1, 2, 3, and 4, prepared by procedure A, were soluble in DMA. Samples of some of the elastomers of series 4 (R_1, 0.95–1.20; R_2, 0.30) were dissolved in DMA and the specific viscosities of the solutions determined at several concentrations. From these data, intrinsic viscosities, $[\eta]$, and k' values were determined from plots of η_{sp}/C versus C and the Huggins' relationship

$$\eta_{sp}/c = [\eta] + k'[\eta]^2 c$$

The results of these determinations are summarized in Table II. These data show that the $[\eta]$ increases as R_1 increases when R_2 is constant. This result suggests that the average size of the polymer molecule increases as the R_1 ratio increases for elastomers cured by procedure A. The essential constancy of k' as the $[\eta]$ increases with increasing R_1 suggests that these are a homologous series of polymers and the number of branches are small.[103] However, a constant value for k' is not as strong evidence for the absence of branching as a variation of k' with $[\eta]$ would be for the presence of branching.[104]

TABLE II
Intrinsic Viscosities and k' Constants of Soluble Elastomers from Series 4

R_1	R_2	$[\eta]^a$	k'
0.95	0.30	0.29	0.42
1.00	0.30	0.46	0.42
1.05	0.30	0.54	0.44
1.10	0.30	0.78	0.60
1.15	0.30	1.04	0.45
1.20	0.30	1.29	0.46

[a] The intrinsic viscosities were determined in *N,N*-dimethylacetamide at 25.00 ±0.02°C.

An estimate of the average molecular weight of the molecules present in the soluble elastomers was made. A substantially linear diisocyanate-linked polymer, prepared from equal molar quantities of TDI and POPG, dissolved in DMA solvent, gave an $[\eta]$ of 0.30 and a k' of 0.46 at 25°C. The same polymer dissolved in benzene solvent showed an $[\eta]$ of 0.35 and a k' of 0.41 at 25°C., corresponding to a viscosity-average molecular weight,

$\bar{M}_v$ of 34,000.[105] Other work[106] has shown that the $[\eta]$ versus M relationship in benzene solvent for POPG's of various molecular weights also applies to POPG ($\bar{M}_n$ = 2000) extended with TDI. Thus, it would be expected that the molecular weight–intrinsic viscosity relationship in DMA solvent for POPG extended with TDI, or P-I extended with TDA, would also be the same. Therefore, the $\bar{M}_v$ of the soluble elastomer of series 4, which has an $[\eta]$ = 0.29, would be above 30,000. Exact values for the $\bar{M}_v$ of the elastomers with larger $[\eta]$ will require a determination of the constants K and a in the Mark-Houwink equation:

$$[\eta] = KM^a$$

The reason for the continuous increase of the average size of the polymer as R_1 increases is not clearly understood. If no side reactions occur, the largest polymer should be formed when the R_1 = 1.00. One explanation for the anomalous behavior might be the hydrolytic conversion of isocyanate to amino groups. Since these elastomers were cured in open trays, and thereby exposed to moisture, this reaction could take place. The conversion would tend to decrease the original value of R_1 and give the appearance that a larger polymer is formed at high values of R_1.

In a similar type of experiment, Murbach and Adicoff[23] observed a shift in the maximum of a plot of $[\eta]$ versus NCO/OH ratio from 1.00 to 1.23 for diisocyanate-linked polymers formed from diphenylmethane-4,4′-diisocyanate, and a copolymer of ethylene oxide and tetrahydrofuran. They explained this shift as the sum of three effects: (*1*) errors in the determination of the hydroxyl content of the glycol, (*2*) reaction of the diisocyanate with traces of water, and (*3*) the formation of dimers from the diisocyanates. Unfortunately, their measurements of $[\eta]$ were made in *N*,*N*-dimethylformamide solvent, a substance recently reported[107] as reactive toward isocyanates. The reactivity of this substance with isocyanates over a range of temperatures from 25 to 150°C. has been confirmed in separate studies at this Laboratory.

Further study of this effect will have to be made, since the reaction of water with isocyanate has been shown to be chemically unpredictable both in the present and in previous studies by Naegli[91] and Goldberg.[108] Also, very little quantitative information exists on the formation of isocyanate dimers and their subsequent reactions.

As will be seen from the discussion of the ultimate properties of the noncrosslinked elastomers, an increase in R_1 at a fixed R_2 leads to an increase in the modulus and tensile strength of the elastomers cured by procedure A. Apparently, the increase in polymer size as R_1 increases raises the total interchain attraction among the polymer molecules within the elastomer and leads to an increase in the modulus and tensile strength.

E. Mechanical Properties

1. Analyses of Stress–Strain Data. The usefulness of stress–strain data for obtaining various types of information regarding the mechanical proper-

ties of elastomers has been discussed previously.[30,88,89] Similar data have been obtained for the present diisocyanate-linked elastomers containing substituted urea, substituted biuret, and substituted urethane groups. Young's modulus, tensile strength, and ultimate elongation were evaluated at a fixed strain rate over a temperature range from −49 to 82°C.

Figure 5 shows stress–strain curves as a function of temperature at a fixed strain rate up to moderate elongations of about 200% for a noncrosslinked and a crosslinked elastomer with $R_1 = 1.20$ and $R_2 = 0.30$. This figure shows the stress level as steadily decreasing as the temperature in-

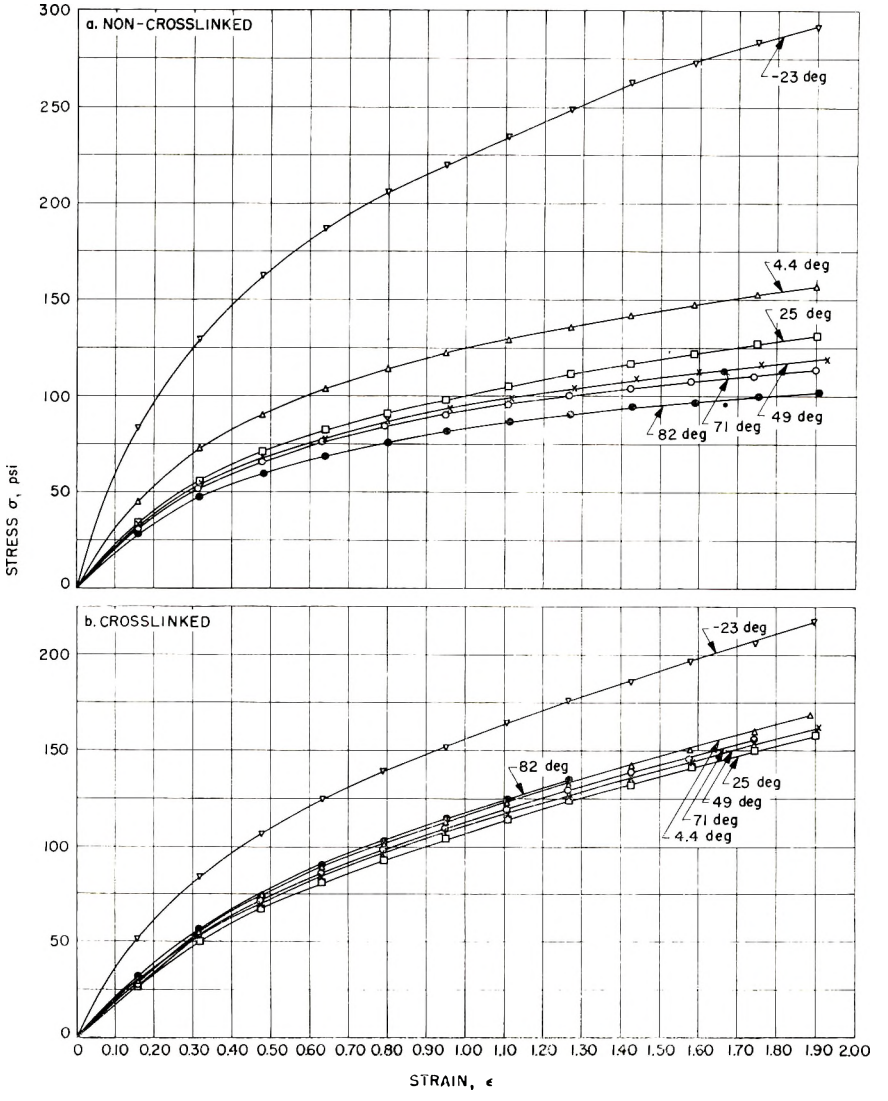

Fig. 5. Stress–strain curves at six different temperatures for noncrosslinked and crosslinked urea-containing elastomers with $R_1 = 1.20$ and $R_2 = 0.30$.

creases at all elongations for the noncrosslinked elastomer, while the crosslinked elastomer manifests an increase in stress between 25 and 49°C. This difference in temperature dependence shown in Figure 5 is typical of the elastomers in all series studied and corresponds to the difference in solubility in DMA mentioned earlier for the crosslinked and noncrosslinked elastomers.

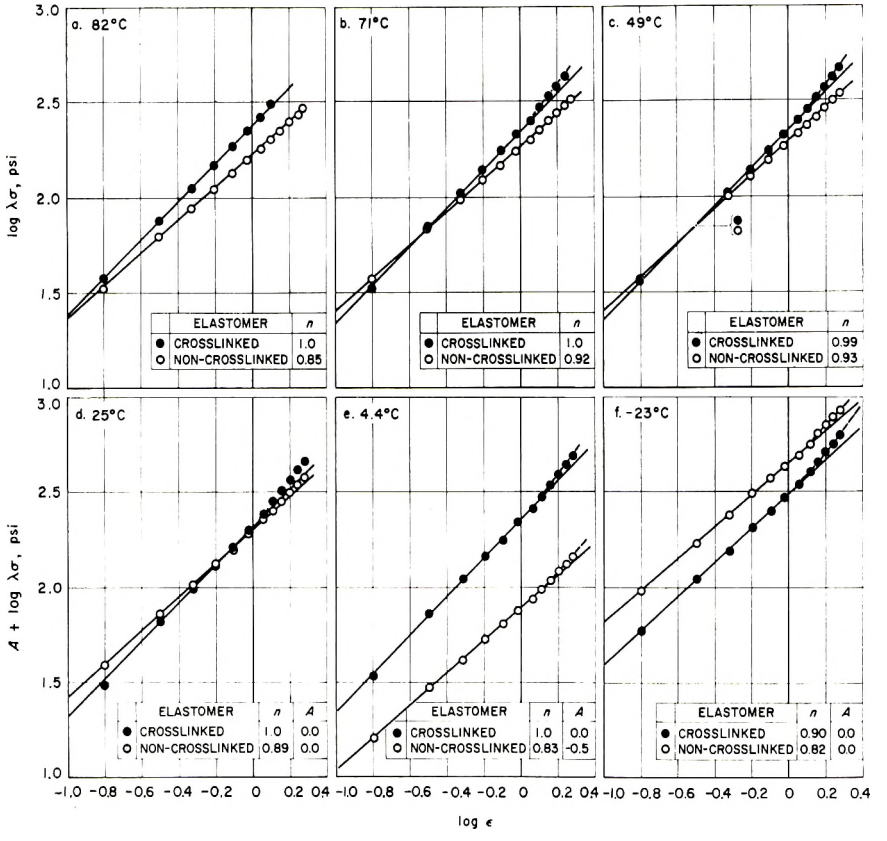

Fig. 6. Double logarithmic plots of stress $\lambda\sigma$ vs. strain ϵ at six different temperatures for crosslinked and noncrosslinked urea-containing elastomers with $R_1 = 1.20$ and $R_2 = 0.30$.

Although no extensions above 200% are shown in Figure 5, many of the specimens of the various crosslinked and noncrosslinked elastomers had extensions well beyond this level. In none was a rapid increase in the stress level apparent for a small increase in the strain, as has been observed for other noncrosslinked diisocyanate-linked elastomers[17] or for other elastomers in general.[109] A rapid increase in the stress level for a small change in strain after an elastomeric material is elongated about 400 to 600% has been ascribed to either crystallization or the ordering of the polymer chains. If similar processes occur upon extension of the urea-containing crosslinked

or noncrosslinked elastomers, they are not manifest from the stress–strain curves.

Because stress–strain curves are nonlinear, it is necessary to linearize them over some finite range of strain in order to obtain reliable values of the moduli. In the earlier study,[30] two equations were evaluated for this purpose:

$$\sigma = (E/3)[\lambda - (1/\lambda^2)]$$

$$\lambda\sigma = E\epsilon^n$$

where σ is the stress based on the original cross-sectional area of the tensile specimen and E is Young's modulus. The quantity λ is $\epsilon + 1$, where ϵ is the strain and equals $\Delta l/l_0$, where Δl is the increase in length and l_0 is the initial length. The first equation is given by the kinetic theory of rubber-like elasticity,[109] and the second is an empirical expression. The previous study[30] showed that the second equation is preferable for representing stress–strain data up to extensions of about 100%. Similar tests were made of these equations with the stress–strain data for the elastomers of the present study, and it was shown[86] that the kinetic theory expression does not represent the data well, even at the low extensions, for either the crosslinked or noncrosslinked elastomers over the temperature range studied. However, double logarithmic plots of the empirical expressions shown in Figure 6 represent stress–strain data up to elongations of about 100% for both the crosslinked and noncrosslinked elastomers. The plots presented in Figure 6 illustrate another basic difference between the stress–strain behavior of the crosslinked and noncrosslinked elastomers. The value for the exponent n is consistently less than one for the noncrosslinked elastomers at all the temperatures studied, while for the crosslinked elastomers, n is less than one only at the lower temperatures. Also, at the higher test temperatures for the crosslinked elastomer, with $R_1 = 1.10$ and $R_2 \leq 0.20$ (not shown by the data given in Fig. 6), n is less than one. It is expected that the exponent n would be unity for equilibrium elastic response and less than unity for nonequilibrium or viscoelastic response. On this basis, the stress–strain curves for the crosslinked materials at elevated temperatures represent equilibrium elastic behavior, but the curves for the noncrosslinked elastomers represent nonequilibrium behavior at all temperatures. The exponent n is a measure of the rate at which stress relaxation occurs during a test; i.e., if n is equal to one, the rate equals zero, and as n decreases, the rate of relaxation increases.

Since the double logarithmic plot of $\lambda\sigma$ versus ϵ best represented the stress–strain curves of both the crosslinked and the noncrosslinked materials, such plots were used to obtain a value for E for the elastomers of series 1 to 8. When the double logarithmic plots were nonlinear, indicating that n was not a constant, values for E and n were determined from the slope of a tangent drawn at $\epsilon = 0.5$.

For many of the specimens of the elastomers, the overall stroke of the Instron apparatus was not large enough to break the ring specimen, and only minimum values could be obtained for the ultimate properties. This behavior was noted for both the noncrosslinked and crosslinked elastomers and was observed only at temperatures below 82°C. For the noncrosslinked elastomers, many of the stress–strain curves showed a maximum stress well before the specimen broke or elongated to the maximum extension obtainable on the Instron apparatus. This behavior was observed primarily in the middle portion of the temperature range covered. Although the phenomenon is rather unusual, it means that the retractive force does not increase during a test at a sufficiently rapid rate to compensate for the decrease in the cross-sectional area of the specimens. In most if not all instances, the maximum is not found on a plot of true stress $\lambda\sigma$ versus ϵ. For the crosslinked elastomers, maxima in the σ versus ϵ curves were not observed.

Both crosslinked and noncrosslinked elastomers showed elastic recoveries of 90% or more within a few minutes after full extension and removal from

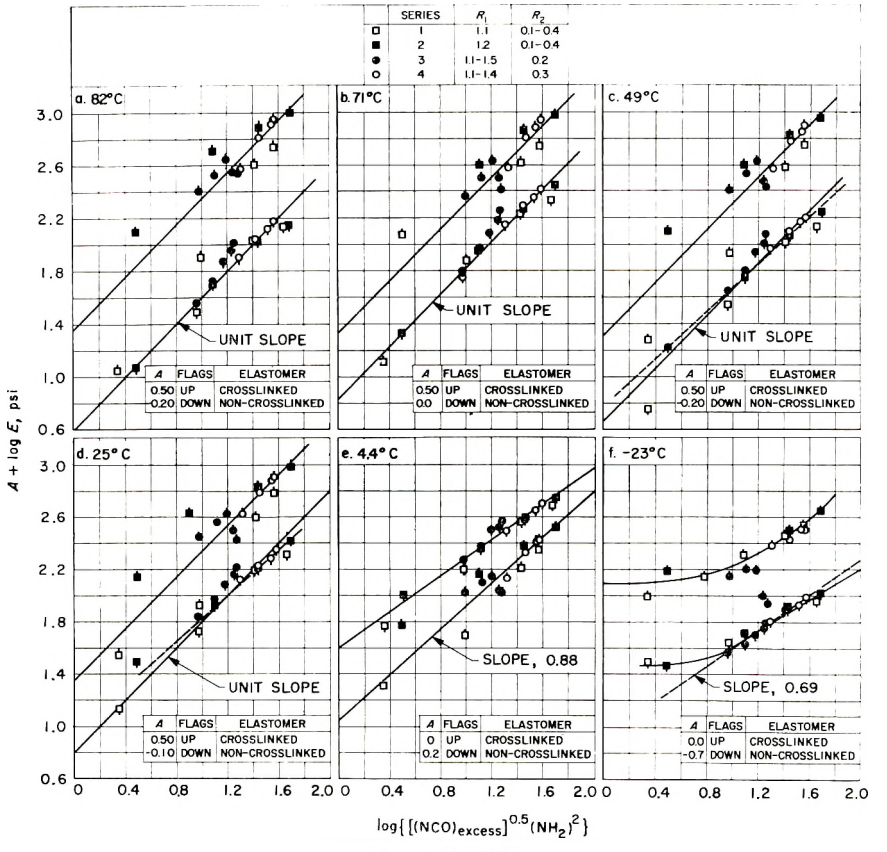

Fig. 7. Log modulus vs. log ($[NCO]_{excess}^{0.5}[NH_2]^2$) at six different temperatures for crosslinked and noncrosslinked elastomers.

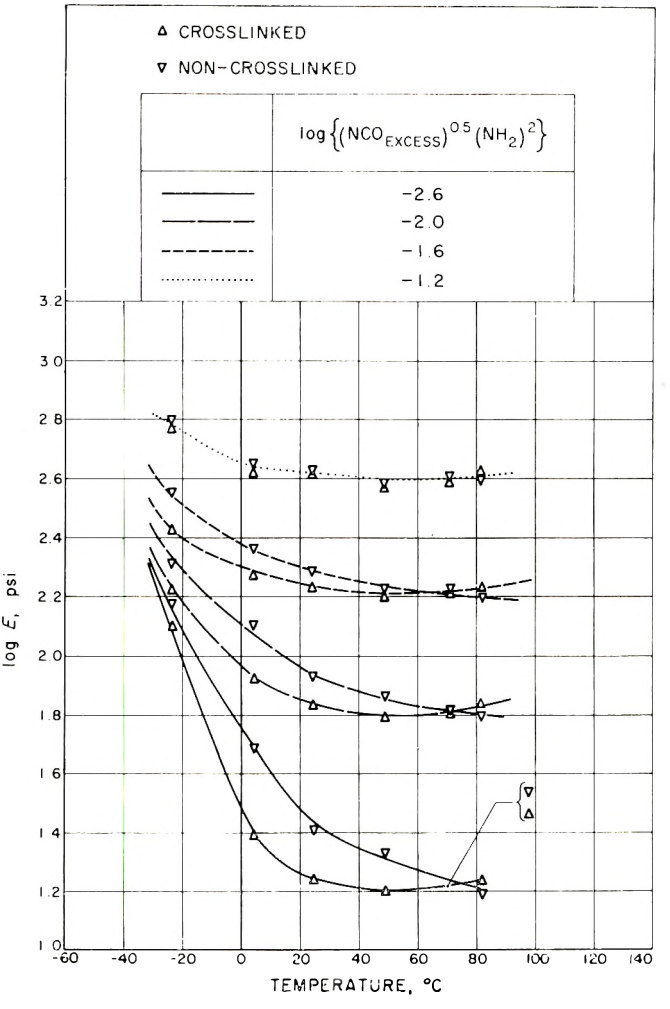

Fig. 8. Log modulus vs. temperature at four levels of the parameter ($[NCO]_{excess}^{0.5}$-$[NH_2]^2$) for crosslinked and noncrosslinked elastomers.

the Instron. One of the crosslinked elastomers ($R_1 = 1.10$ and $R_2 = 0.10$) showed extremely high extension when tested manually as a dumbbell specimen. The 2.4-in. gage section of the specimen was extended to 144 in. (6000%) before rupture. After rupture, the two parts of the specimen returned to an overall dimension which corresponded to an elastic recovery of better than 90%.

2. Moduli *E* of Urea-Containing Diisocyanate-Linked Elastomers. Figure 7 shows the logarithms of E at six different temperatures plotted against the logarithms of the parameter ($[NCO]_{excess}^{0.5}$ $[NH_2]^2$) for the elastomers of series 1, 2, 3, and 4. This parameter gave the best empirical fit of the modulus data for both the crosslinked and noncrosslinked elastomers. At test temperatures of 25°C. and above, lines of unit slope fit the data for

both crosslinked and noncrosslinked elastomers and, thus, at such temperatures, $E = K_c(T)\ ([NCO]^{0.5}_{excess}\ [NH_2]^2)$. At temperatures below 25°C., the E of both types of elastomers becomes less dependent on $([NCO]^{0.5}_{excess}\ [NH_2]^2)$, as indicated in Figure 7 by lines of slope less than unity. Qualitatively, the behavior is expected, because at very low temperatures, the moduli of elastomers are relatively independent of chemical composition. For unknown reasons, at the two lowest test temperatures, the moduli of the noncrosslinked elastomers are less sensitive to compositional changes than the moduli of the crosslinked ones.

Figure 8 shows the log E plotted against temperature for both the crosslinked and noncrosslinked elastomers at four levels of the parameter $([NCO]^{0.5}_{excess}\ [NH_2]^2)$. Values of log E at levels were taken from the lines shown in Figure 7. Figure 8 shows that the E of the noncrosslinked elastomers decreases with increasing temperature at all temperatures, while at the highest temperature, the E of the crosslinked elastomers increase with temperature. This indicates that near-equilibrium values with respect to temperature were obtained for E for the crosslinked elastomers but not for the noncrosslinked elastomers.

At the largest value for the parameter $([NCO]^{0.5}_{excess}\ [NH_2]^2)$, there is little difference between the E for the crosslinked and noncrosslinked elastomers. As the values for the parameter decrease, however, the difference between the E increases, and, surprisingly, the noncrosslinked elastomers have the larger values, except at 82°C.; at this temperature, the moduli for the crosslinked elastomers are slightly higher than for the noncrosslinked ones. In terms of the compositional ratios R_1 and R_2, E increases with R_2 at a fixed R_1 for both the crosslinked and nonlinked elastomers at all test temperatures. For the noncrosslinked elastomers, but not the crosslinked ones, E generally increases at all test temperatures with an increase in R_1 at fixed R_2.

Crosslinks in the urea-containing elastomers are formed mainly by the reaction of isocyanate groups with substituted urea hydrogens. Reaction of four of the hydrogens of the TDA molecule with isocyanate groups leads to tetrafunctional branch points, whereas the reaction of three of the TDA hydrogens would lead to a trifunctional branch point. The latter case would be identical to the crosslinking in a POPG–TDI–TMP system if the isocyanate groups reacted at the same rates with amino and substituted-urea hydrogens and no differences existed between the rates of reactions of isocyanate groups with the hydroxyls of POPG and TMP. When tetrafunctional branch points are formed, the theoretical value of M_c (average molecular weight between crosslinks) is given by the expression

$$M_c = \frac{1}{2}\ \frac{\text{grams of elastomer}}{\text{moles of TDA}}$$

since each mole of TDA contributes 2.0 chains. If trifunctional branch points form, M_c is

$$M_c = \frac{2}{3} \frac{\text{grams of elastomer}}{\text{moles of TDA}}$$

since each mole of TDA contributes 1.5 chains. These calculations of M_c assume that (*1*) the proper stoichiometric quantities of functional groups are present, (*2*) no side reactions occur, (*3*) no monofunctional molecules are present in the reactions, and (*4*) complete reaction occurs. These conditions are not fulfilled by the series of elastomers represented in Table I, or, for that matter, by any other elastomer.

The formulations in which $[NCO]_{excess} = (NH_2)$ and 0.5 $[NH]_2$ correspond to tetrafunctional and trifunctional crosslinking, respectively, and fulfill the requirements of assumption *1*. This may not be sufficient, however, to define a theoretical expression for M_c, since other problems, such as the stoichiometry and statistics of the reaction of isocyanates with urea hydrogens, should be considered. The reaction of the first urea hydrogen with an isocyanate leads to a substituted biuret and the second to a substituted triuret. Continued reaction with the hydrogen sites, which do not disappear, leads to the formation of a block polymer of $(x - 1)$ isocyanate units per unit of hydrogen. These processes are illustrated by eqs. (7).

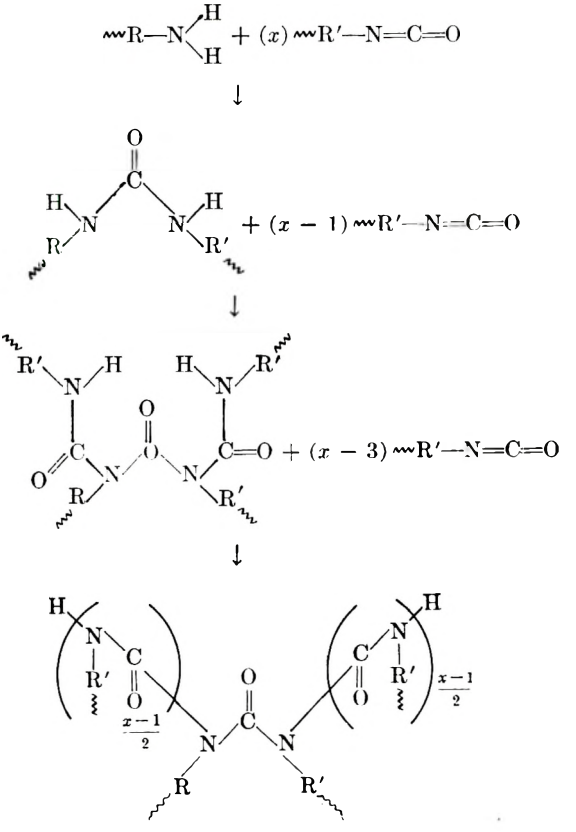

(7)

The occurrence of such processes during the formation of a three-dimensional network would waste isocyanate groups and make a theoretical calculation of M_c difficult. The homopolymerization of isocyanates[2,3] but under somewhat different conditions, and the reported isolation[68] of a material which is believed to be a polybiuret lend support to the possibility that such reactions could occur during cure of the elastomers.

While the many reactions of isocyanates can be used to advantage, they are also responsible for the side reactions and waste of isocyanate groups during the formation of a three-dimensional network. The waste of isocyanate groups by the urea-hydrogen is but one example; others would be the dimerization and trimerization of isocyanates.[90] Also, the ever-present problem of moisture during the preparation and cure of these materials must be considered. In the present study, this interference has been decreased, but not eliminated, in the elastomers cured by procedure B. Studies on the cure of diisocyanate-linked polymers in the presence of FeAA and in vacuum-tight molds (leak rate $< 1 \times 10^{-7}$ cc. helium/sec.) have shown that not only water but also oxygen is important to the cure of these materials.[82]

The presence of monofunctional molecules in the reactants would lead to an imperfect network containing a sol fraction. The POPG used for the preparation of the elastomers shown in Table I contains both carbon—carbon double bonds and carbonyl groups. If these foreign functionalities constitute one end of the polyether chain, the POPG would contain about 7 mole-% of monofunctional molecules. In separate studies on the preparation of substantially linear diisocyanate-linked polymers from POPG and TDI,[110] it was shown that the molecular weight was limited more by nonstoichiometric quantities of reactants than by foreign functional groups present in the POPG. This suggests that the POPG may not contain 7 mole-% of monofunctional molecules. If this were true, the quantity of sol fraction in the elastomers would be more dependent on stoichiometry than on foreign functionalities.

In the absence of side reactions, the time required for the essential completion of a desired reaction will depend upon its rate. The extent of reaction at the gel point increases as the concentration of the crosslinking agent is decreased. Also, as the amount of crosslinking agent is decreased, the quantity of sol fraction to be attached to the three-dimensional network per unit amount of reaction after the gel point becomes larger. For the formation of elastomers with large M_c, the extent of reaction will need to be larger than for those with small M_c before the amount of sol becomes negligible. Side reactions and nonstoichiometric quantities of reactants will consequently be more important for elastomers with large values of M_c, since they will control the attainable extent of reaction and amount of sol.

The equilibrium Young's modulus is predicted by the kinetic theory of rubberlike elasticity to be

$$E_e = 3\nu_e RT \tag{8}$$

where ν_e represents the number of effective chains per milliliter. A value of ν_e can be obtained from the observed equilibrium modulus by use of eq. (8). This value can be compared with that calculated from the concentration of reactants used in preparing the elastomers and an assumed network topology. In this paper, the symbol ν will refer to calculated values and ν_e will refer to those obtained from measured values of the equilibrium modulus. Values of ν for elastomers in series 1, 2, 3, and 4 were calculated from the initial quantities of the reactants. This calculation requires consideration of the relative values of $[NCO]_{excess}$ and $[NH_2]$. Depending on the relative values of these two quantities, as discussed below, at least three different cases must be considered. (For those cases in which the quantities of chemical groups are used to calculate the number of chains per milliliter, the concentrations of chemical groups are expressed in equivalents per milliliter of polymer.)

Case (a). When $[NCO]_{excess} \leq 0.5\ [NH_2]$, it follows that $\nu = 1.5\ [NCO]_{excess}$ and the network would be formed from trifunctional units. These formulas ignore the formation of a mixture of tri- and tetrafunctional crosslinks, as expected on purely statistical grounds. The mixing of crosslink types would lower the calculated value of ν. The formation of either two trifunctional branch points or one tetrafunctional branch point requires two each of NCO and NH groups. However, the two trifunctional branch points contribute 3.0 chains, whereas the one tetrafunctional branch point contributes 2.0 chains. The lowest values for the number of chains would be obtained by considering all the crosslinks to be of the tetra type; this gives $\nu = [NCO]_{excess}$.

Case (b). When $0.5\ [NH_2] < [NCO]_{excess} \leq [NH_2]$, then $\nu = 0.5\ [NH_2] + 0.5\ [NCO]_{excess}$. This equation is based on the existence of both tri- and tetrafunctional junction sites. If it is assumed that only tetrafunctional crosslinking occurs (in practice, this is not likely but does represent an extreme case), then $\nu = [NCO]_{excess}$.

Case (c). When $[NH_2] < [NCO]_{excess} \leq 1.5\ [NH_2]$, then $\nu = 1.5\ [NH_2] - 0.5\ [NCO]_{excess}$. When $[NCO]_{excess} = 1.5\ [NH_2]$, it is assumed that only trifunctional crosslinking occurs. In this case, four chains are attached to each TDA molecule, but one of these is dangling and terminates in a free NCO group.

The calculated and observed values of $E_{82°C.}$ for the elastomers of series 1, 2, 3, and 4 corresponding to cases (*a*), (*b*), and (*c*) are given in Table III. For cases (*a*) and (*b*), the upper and lower limits for E, corresponding to either purely tri- or tetrafunctional and mixed tri- and tetra- or purely tetrafunctional crosslinking, respectively, were calculated. These data show the calculated value or range of values of E to be generally higher than the experimental values, suggesting either incomplete cure of the materials or waste of NCO groups in side reactions as described earlier in this Section. In each instance, however, a change in the formulation parameters leads qualitatively to the predicted change in the observed modulus value. Some of the elastomers were prepared and tested twice as members of

TABLE III
Observed and Calculated E at 82°C. for Crosslinked Elastomers of Series 1, 2, 3, and 4

Case	R_1	R_2	$E_{82°C.}$, psi				Series No.
			Observed	Calculated			
				Tri	Tetra	Tri + Tetra	
a	1.10	0.40	170	212	141	—	1
	1.10	0.30	118	193	128	—	4
b	1.15	0.31	126	—	193	263	1
	1.10	0.20	25, 79	—	128	173	1, 3
	1.20	0.40	312	—	283	347	2
	1.20	0.30	245, 203	—	283	296	2, 4
c	1.10	0.10	3.5	—	—	103	1
	1.20	0.20	159, 104	—	—	199	2, 3
	1.30	0.30	255	—	—	263	4

different series: $R_1 = 1.10$ and $R_2 = 0.20$; $R_1 = 1.20$ and $R_2 = 0.30$; and $R_1 = 1.20$ and $R_2 = 0.20$. In these instances, the agreement between the two experimental values for E are only fair. Good agreement in E, usually within 2 psi, however, was observed for two specimens from a given preparation. This suggests that reproducible cure and test conditions may not have been attained.

To demonstrate that adequate cure was effected after 72 hr. at 110°C., the elastomers of series 8 ($R_1 = 1.30$ and $R_2 = 0.30$) were prepared and tested. Three separate portions of one batch of this formulation were cured for 46, 72, and 408 hr., respectively. The moduli and solubility of the elastomers, each corresponding to a different cure period, were determined. With increasing time of cure, the $E_{71°C.}$ changed from 236 to 221 to 270 psi. After extraction with six separate portions of DMA over a period of 2 months, the samples of elastomers in order of increasing cure time gave sol fractions of 0.11, 0.10, and 0.14. These results suggest that 70 hr. is an adequate period for the cure of the $R_1 = 1.30$ and $R_2 = 0.30$ formulation and for most of the other formulations cured in the closed molds at 110°C. However, for the formulations where $R_1 = 1.10$ and $R_2 \leq 0.20$, the extent of reaction may not have been adequate to minimize the amount of sol fractions, since these elastomers showed $E_{82°C.}$ values markedly lower than those calculated.

Elastomers were also prepared in series 1, 2, 3, and 4 where the $[NCO]_{excess}$ was larger than the 1.5 $[NH_2]$ upper limit of case (*c*). These elastomers were prepared from formulations where $1.5\ [NH_2] < [NCO]_{excess} \leq 3\ [NH_2]$. The observed $E_{82°C.}$ for the elastomers in which $1.5\ [NH_2] < [NCO]_{excess} \leq 2.25\ [NH_2]$ were higher than for the elastomers having the same $[NH_2]$ and $[NCO]_{excess} \leq 1.5\ [NH_2]$, indicating that at these levels of $[NCO]_{excess}$ additional effective crosslinks are formed. This trend did not continue, however, since for elastomers where $2.25\ [NH_2] < [NCO]_{excess} \leq 2.6\ [NH_2]$, the observed $E_{82°C.}$ were lower than for elastomers of the same

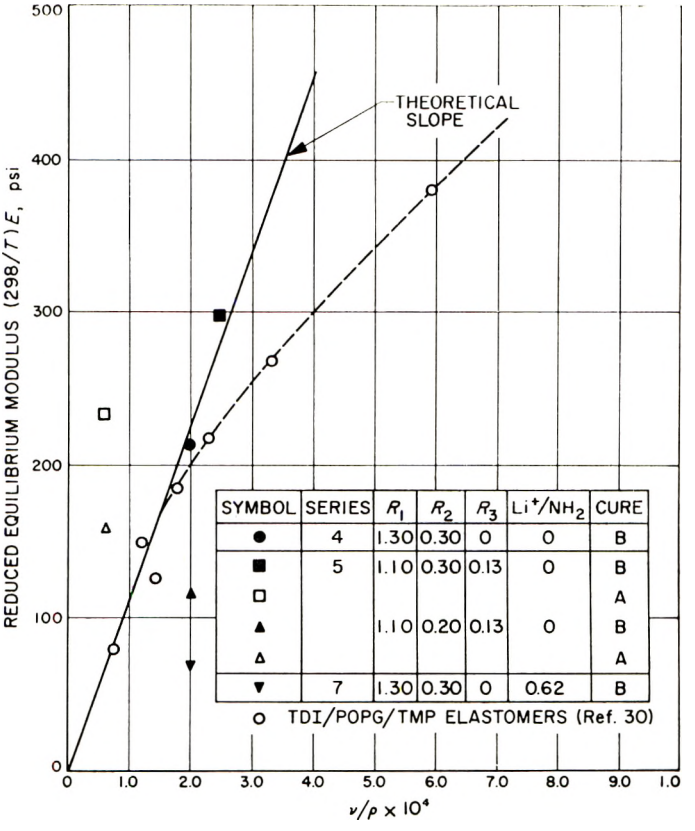

Fig. 9. Dependence of equilibrium modulus on calculated number of chains per gram.

$[NH_2]$ and $[NCO]_{excess} \leq 1.5\ [NH_2]$, indicating that at the highest levels of $[NCO]_{excess}$ the number of effective crosslinks decreased. The use of the large $[NCO]_{excess}$ by certain elastomers of series 1, 2, 3, and 4 may be the result of either continued reaction of the urea hydrogen or other side reactions, as described earlier. The amino groups or their progeny, however, are in some way responsible for the side reactions, since elastomers could not be prepared by procedure B from formulations of P-I, and TDI in the presence of an excess of isocyanate groups.

The modulus values obtained for the elastomers prepared from POPG, P-I, TDA, and TMP (series 5, cures A and B) and POPG, P-I, and $LiClO_4$ (series 7, cure B) increased with temperature above 49°C. The values of E for these elastomers at 71°C. were reduced to 298°K. and are plotted against ν/ρ in Figure 9, where ρ is the density of the elastomer. For the elastomers of series 5 cured by procedure A, the ν was calculated on the basis of crosslinking only by the trifunctional TMP ($\nu = 1.5\ [TMP]$), whereas for those cured by procedure B, crosslinking was considered as arising from both TMP and TDA, with the latter furnishing $\nu = 0.5\ [NH_2] + 0.5\ [NCO]_{excess}$. For the elastomers prepared with $LiClO_4$ (Li^+/NH_2

= 0.62, R_1 = 1.30 and R_2 = 0.30), $[NH_2] \leq [NCO]_{excess} \leq 1.5\ [NH_2]$ and $\nu = 1.5\ [NH_2] - 0.5\ [NCO]_{excess}$. For comparative purposes, similar data for the elastomers prepared in the absence of $LiClO_4$ (R_1 = 130, R_2 = 0.30; series 4) and for elastomers previously prepared from POPG, TDI, and TMP[30] are also shown in Figure 9. It can be seen that for E for the elastomers of series 5 prepared by procedure A increase more rapidly with ν/ρ than the simple theory would predict. Thus, while these elastomers show moduli which increase with temperature above 49°C., indicating the E to be near-equilibrium values, they do not follow the theoretical expression of the simple kinetic theory of rubberlike elasticity. The $E_{298°K.}$ for the elastomers of series 4 and 5 prepared by procedure B follow the $E_{298°K.} - \nu/\rho$ relationship as well as TDI–POPG–TMP materials previously studied. The E for the elastomer prepared with added $LiClO_4$ (series 7, cure B) is markedly lower than predicted by the theoretical relationship between E_e and ν/ρ. The nature of this deviation is probably the result of lower intermolecular forces brought about by the presence of the lithium salt. If this explanation is correct, then it follows that the calculated values of the modulus of the other elastomers are higher than those produced solely by the covalent network. The good agreement between the calculated and observed $E_{82°C.}$ values of some of the elastomers may therefore be fortuitous. Although equilibrium moduli were observed experimentally, this behavior does not prove that the network consists solely of covalent crosslinks. In fact, it is quite likely that multiple stretching would bring about a softening of the rubber. This effect, commonly called the Mullins effect,[34] is attributed to the disruption of secondary linkages. It is the modulus of the network which exists after disruption of secondary linkages which should be compared to that calculated from the covalently linked network.

The E for the noncrosslinked elastomers of series 1, 2, 3, and 4 did not show equilibrium or near-equilibrium behavior. Recently, Weisfeld, Little, and Wolstenholme[37] have ascribed a continued decrease in E with increasing temperature exclusively to breakage of secondary bonds in noncrosslinked diisocyanate-linked elastomers. These workers have analyzed the ordinary modulus–temperature data of diamine-cured diisocyanate-linked polymers and concluded that the secondary bonds are of the hydrogen-bond type. Their procedure will not be applied to the noncrosslinked elastomers of series 1, 2, 3, and 4, since it is not clear at the present time what portion of the increase of E with decreasing temperature, below some temperatures, is caused by a viscosity effect and not entirely by the formation of more and stronger hydrogen-bond-type crosslinks.

The most puzzling aspects regarding the moduli of the crosslinked and noncrosslinked elastomers is the fact that the moduli of the noncrosslinked elastomers are generally higher than those of the crosslinked ones. Yet, the moduli of over half of the crosslinked elastomers were calculated (perhaps fortuitously) rather precisely from the quantities of reactants and an assumed network topology, which is quite reasonable, but the calcu-

lation ignores completely the effect of interchain attractive forces. Perhaps this anomalous finding is the result of cure A bringing about types of reactions different from those considered; consequently, a quantitative comparison of the properties of the two types of elastomers cannot be made in terms of molecular structure because the structure of noncrosslinked elastomers is unknown. It seems certain, however, that the interchain attractive forces in the noncrosslinked materials must have a markedly greater effect on the modulus than do those which exist in the crosslinked ones.

3. Temperature-Dependent Ultimate Mechanical Properties. The studies of diisocyanate-linked elastomers[30,36] have shown that the ultimate properties measured at a fixed strain rate depend on $T - T_g$, the number of effective chains per milliliter ν_e, and the urethane group concentration U, especially for values of U greater than about 2 moles/kg. Since the crosslinked and noncrosslinked elastomers of series 1, 2, 3, and 4 had the same T_g within experimental error, any differences in ultimate properties among these materials should result from differences in ν_e, network imperfections, and the chemical structure of the network chains. Because many of the samples did not reach a maximum stress level or break within the extension range available on the test equipment, the analysis of the ultimate property data of the elastomers of the four series is necessarily limited.

Figure 10 shows the logarithm of the tensile strength σ_m plotted against log $E_{71°C.}$ at six different test temperatures for the noncrosslinked elastomers of series 1, 2, 3, and 4. The quantities were plotted against log $E_{71°C.}$ because $E_{71°C.}$ is proportional to the number of effective chains per milliliter which result from specific interchain attractive forces or from chain entanglements. Each line was drawn with a slope of one, and the data fit this relation well except at the two lower test temperatures of 4.4 and −23°C. This relationship shows that $\sigma_m = K(T)E_{71°C.}$, where $K(T)$ is a function only of temperature. In the previous study,[36] σ_m was related to ν_e through the expression $\sigma_m = K_1(T)\nu_e^{1/2}$. If the $E_{71°C.}$ had been equilibrium values, the present results would have shown that $\sigma_m = K_1(T)\nu_e$. Thus, σ_m would be more dependent on ν_e than the σ_m for the elastomers of previous studies.

Figure 11 shows the logarithm of the tensile strength plotted against log $E_{71°C.}$ at six different temperatures for the crosslinked elastomers of series 1, 2, 3, and 4. Each line was drawn with a unit slope. The data fit this relation, but not as well as in the case of the noncrosslinked elastomers. It follows, however, that the relationship $\sigma_m = K(T)E_{71°C.}$ represents the data reasonably well, except at the two lower test temperatures. Since the $E_{71°C.}$ for the crosslinked elastomers do represent near-equilibrium behavior, $\sigma_m = K_1(T)\nu_e$, and the tensile strength of the crosslinked urea-containing elastomers shows a different dependence on ν_e than that of the elastomers discussed previously[30,36] which were crosslinked with either triols or tetrols. However, neither of these results agrees with the prediction[111] that σ_m should be proportional to $\nu_e^{2/3}$.

For the four series of elastomers, the concentration of substituted urea

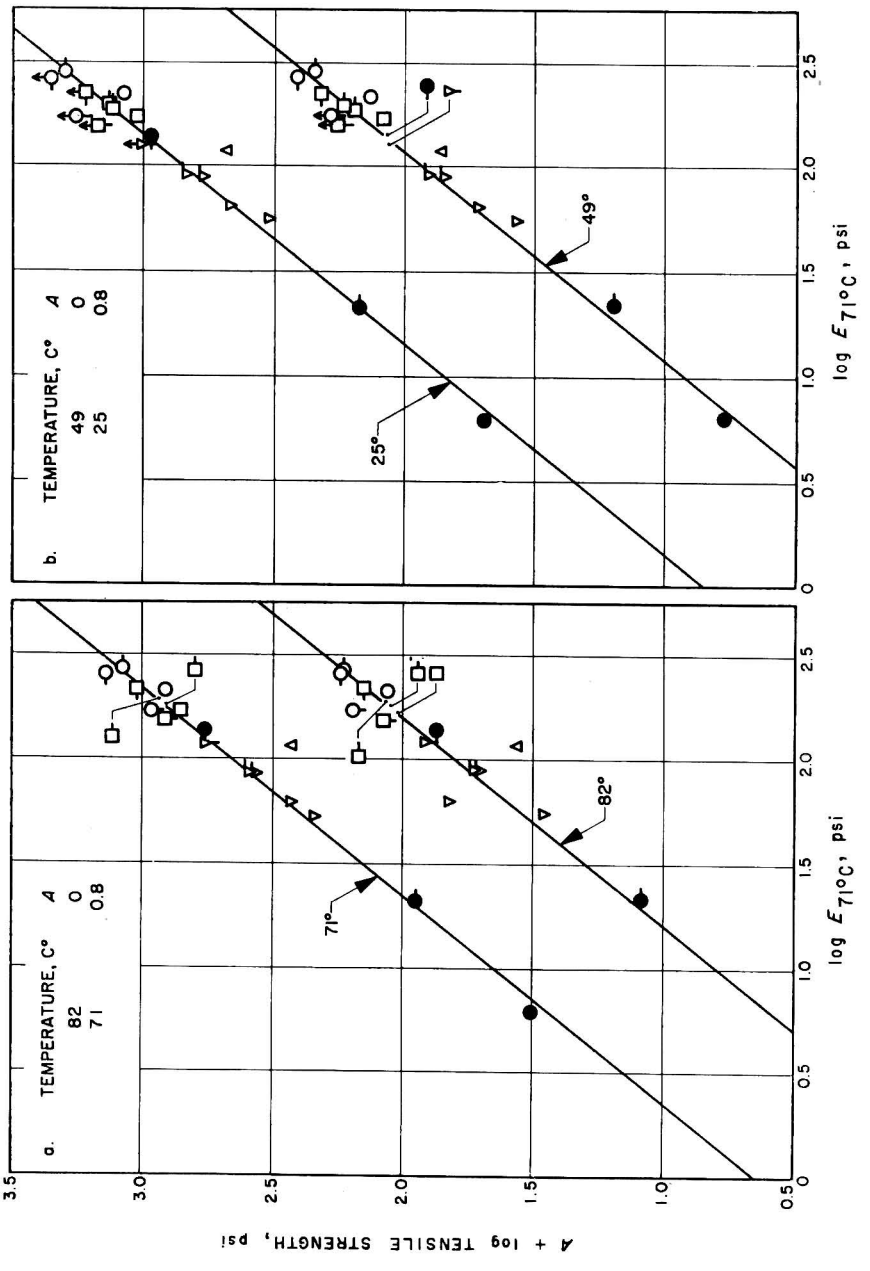
a.
TEMPERATURE, C°
82
71
A
0
0.8
71°
82°
b.
TEMPERATURE, C°
49
25
A
0
0.8
25°
49°
A + log TENSILE STRENGTH, psi
log E 71°C, psi
log E 71°C, psi

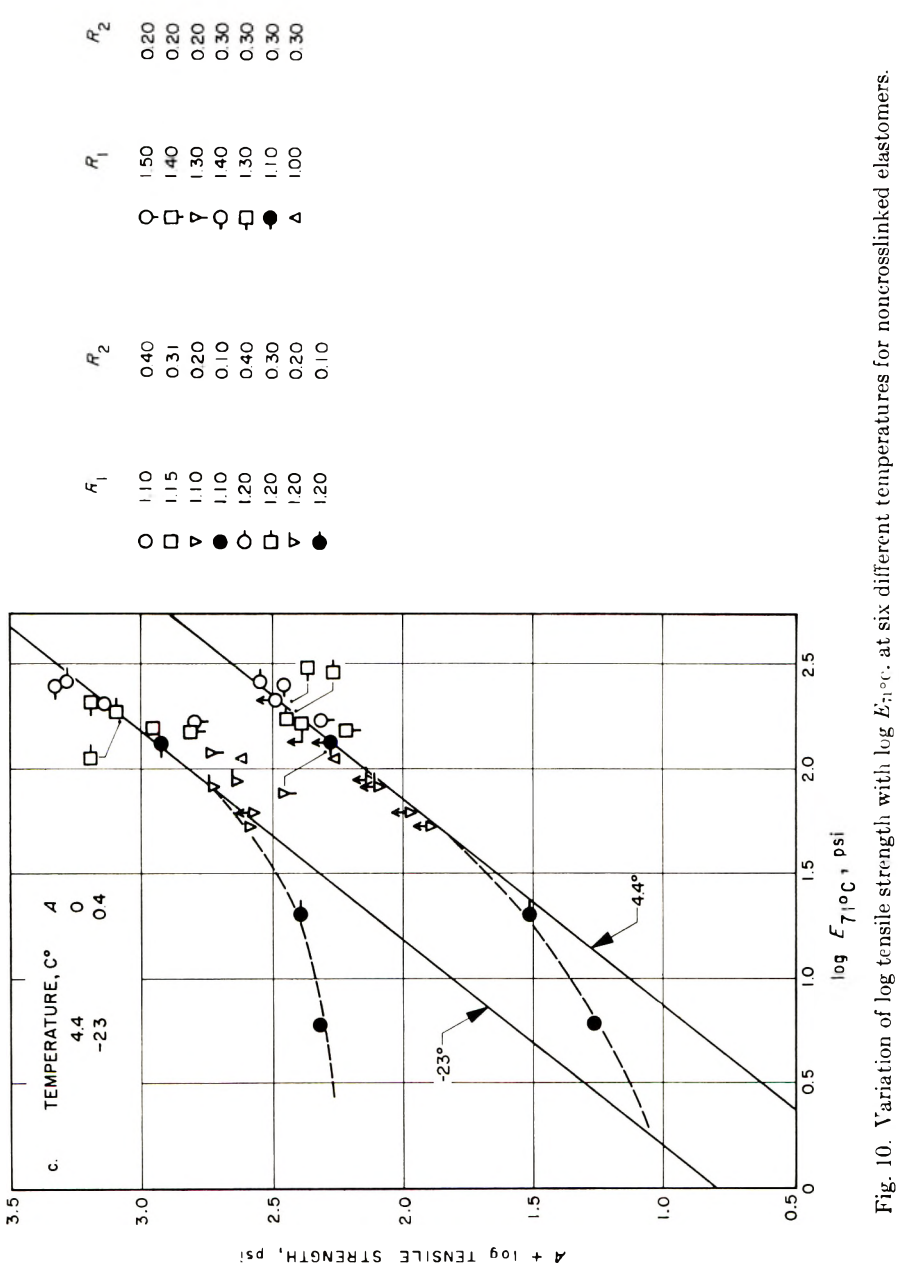

Fig. 10. Variation of log tensile strength with log $E_{71°C}$ at six different temperatures for noncrosslinked elastomers.

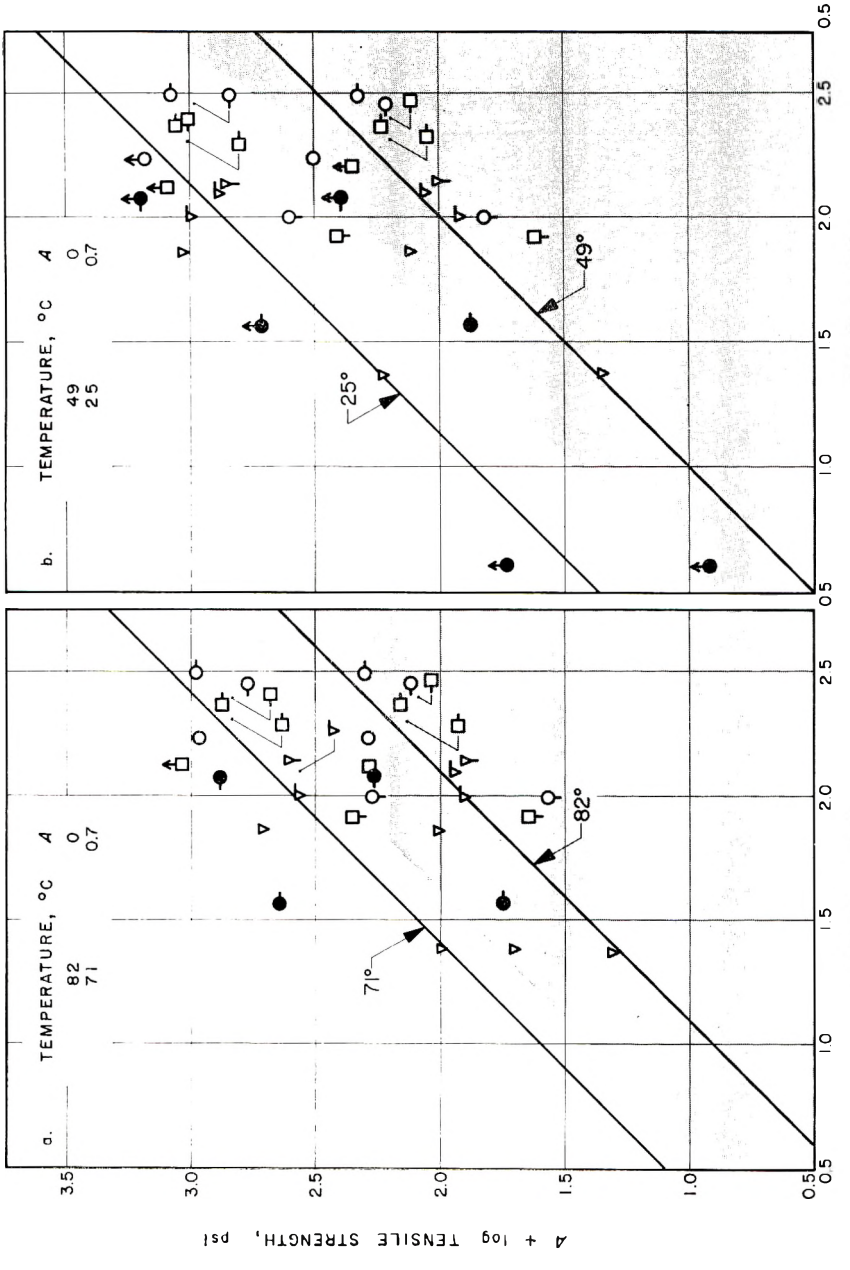
a.
TEMPERATURE, °C
82
71
A
0
0.7
82°
71°
b.
TEMPERATURE, °C
49
25
A
0
0.7
49°
25°
A + log TENSILE STRENGTH, psi
log E_{71°, psi
log E_{71°, psi

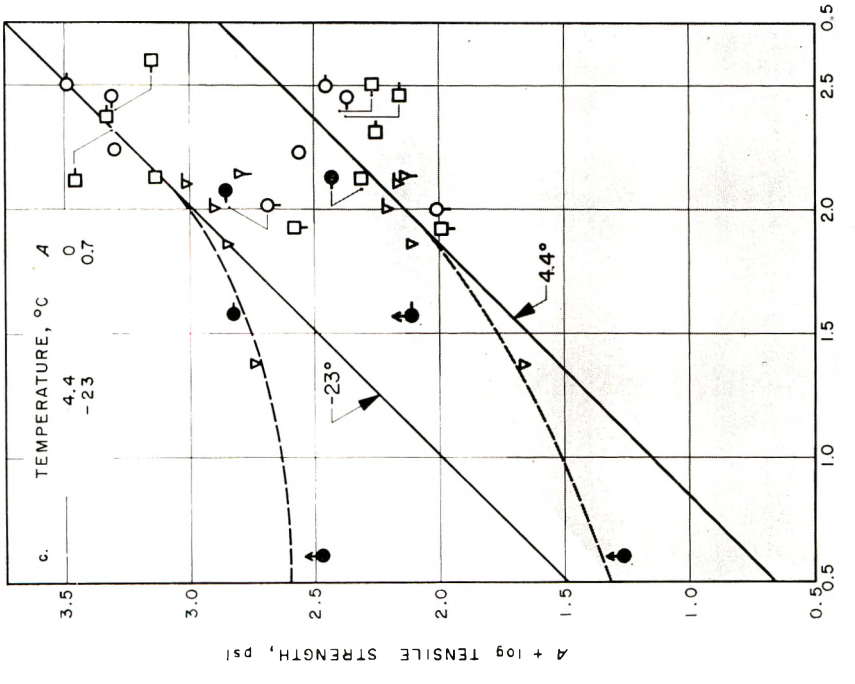

Fig. 11. Variation of log tensile strength with log $E_{7,0}$°c. at six different temperatures for crosslinked elastomers.

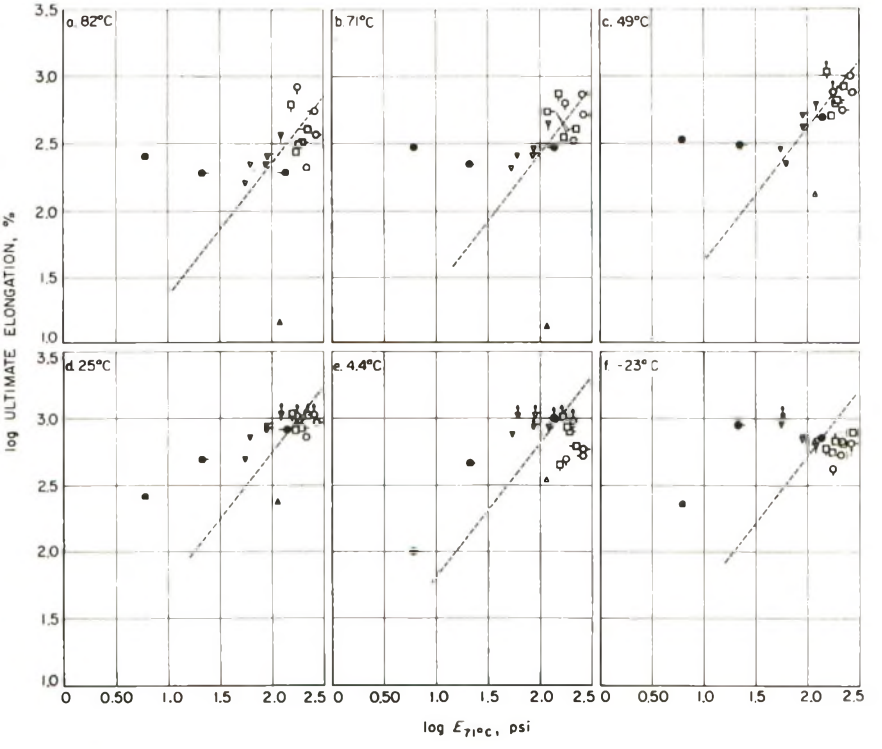

Fig. 12. Variation of log ultimate elongation ($100\epsilon_b$) with log $E_{71°C.}$ at six different temperatures for noncrosslinked elastomers.

groups, substituted biuret groups, and excess isocyanate groups varied widely, as shown in Figures 1 and 2. The relationship between σ_m and $E_{71°C.}$, however, appeared to be independent of these variations, since for either the crosslinked or noncrosslinked elastomers, $K(T)$ appears to be independent of differences in the chemical-group contents of the various elastomers (except that it does depend on whether or not they are crosslinked).

Studies of elastomers, having mobile crosslinks, such as vulcanizates of the carboxylic rubbers crosslinked with metal oxides,[112] have shown these materials to have tensile strengths much higher than any other similar rubber incapable of crystallization. The ability of the mobile crosslinks to relieve local stresses was thought to be mainly responsible for the high tensile strengths.[111] A similar explanation probably would not be applicable to the noncrosslinked elastomers of series 1, 2, 3, and 4, since a comparison of the plots of log σ_m versus log $E_{71°C.}$ in Figures 10 and 11 at a given test temperature shows that the crosslinked elastomers have about the same σ_m as the noncrosslinked elastomers for a fixed value of $E_{71°C.}$, i.e., $K(T)_{\text{crosslinked}} = K(T)_{\text{noncrosslinked}}$ at a given test temperature.

Figures 12 and 13 show the logarithm of the ultimate elongation ($100\ \epsilon_b$) plotted against log $E_{71°C.}$ at six different temperatures for the noncross-

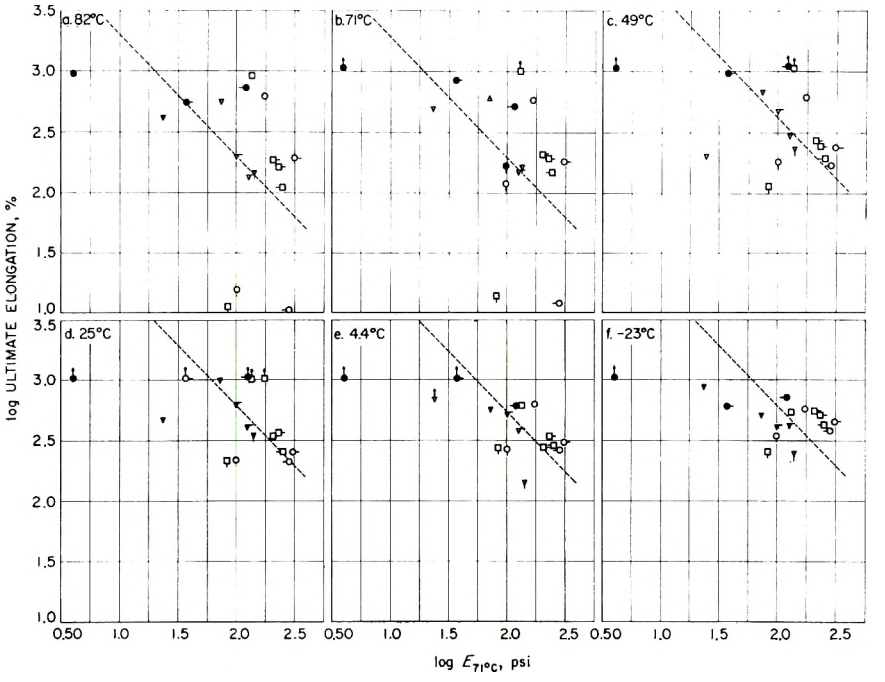

Fig. 13. Variation of log ultimate elongation ($100\epsilon_b$) with log $E_{71°C.}$ at six different temperatures for crosslinked elastomers.

linked and crosslinked elastomers, respectively. The symbols in Figures 12 and 13 present the values of R_1 and R_2 given in Figures 10 and 11 for the noncrosslinked and crosslinked elastomers, respectively. The dotted lines drawn through the data at each temperature represent the relationships $100\epsilon_b = K'(T)E_{71°C.}$ and $100\epsilon_b = K'_1(T)\nu_e^{-1}$ for the noncrosslinked and crosslinked elastomers, respectively. The scatter of the data, however, makes these assignments very tenuous.

Previous studies of ultimate properties showed that the tensile strength always increased when the strain rate was increased or the temperature was decreased, the ultimate elongation usually passing through a maximum with decreasing temperature. The ultimate elongations of the noncrosslinked and crosslinked elastomers of series 1, 2, 3, and 4 usually pass through a maximum with decreasing temperature at a fixed strain rate, as do the tensile strengths of some of the elastomers. A satisfactory explanation cannot be given for this unusual dependence of the tensile strength on temperature. Current theories on the tensile strength of amorphous elastomers[111,113] make no provision for this type of behavior.

The ultimate properties of the elastomers of series 5, 6, and 7 were not extensively investigated. However, elastomers of series 5 prepared from POPG, P-I, TDA, and TMP were compared to the previously studied elastomers[30] prepared from POPG, TDI, and TMP (both by cure A). The elastomers made with and without TDA had calculated M_c values of

17,000 and 6,000, respectively, and experimentally, the same T_g of -53.5 ± 2.5°C. The tensile strengths were about twice as large for the elastomers prepared with TDA at each of two R_2 (0.20 and 0.30) at test temperatures of 49°C. (165 and 220 psi) and 25°C. (240 and 280 psi) and approximately equal at the lower test temperatures. The elastomers prepared with TDA had ultimate elongations of about 300–400% at the higher test temperatures, and these are about twice as large as for the elastomers prepared without TDA. At the lower test temperatures, the ultimate elongations of the two types of elastomers were approximately equal, as might be expected. From the dependence of σ_m and ϵ_b on M_c at equal values of $T - T_g$,[30] it might be assumed, however, that an increase in M_c for elastomers containing TDA would produce a smaller σ_m and a larger ϵ_b in comparison to those without TDA at the high test temperatures. The increase in interchain forces through hydrogen-bonding in the elastomers containing TDA is probably responsible for the observed increase in σ_m.

The ultimate properties of the elastomers of series 6 (cure A), where 10, 15, and 20% portions of P-I were replaced with equivalent quantities of TDI and POPG, were determined at a fixed strain rate at five test temperatures between -23.5 and 71°C. An elastomer (cure A) in which TDI and POPG did not replace P-I showed ϵ_b ranging from 100 to 300% larger than that of the elastomers in which P-I was replaced by POPG–TDI at all test temperatures except -23°C. When 10, 15, and 20% portions of P-I are replaced by POPG–TDI, the σ_m are first enhanced, then decreased to substantially the initial values, and finally diminished to below the initial-value of the elastomer prepared without added TDI at all test temperatures. Because the two different types of elastomers were prepared and cured at different times and probably under different curing environments, the results must be considered tentative.

The ultimate properties of the elastomers containing $LiCO_4$ (series 7) were compared to those of similar elastomers prepared without $LiClO_4$ ($R_1 = 1.30$, $R_2 = 0.30$) by either cure A or B. Analyses of the stress–strain data for the elastomers showed that (*a*) the $LiClO_4$ effected a onefold reduction in the tensile strengths of these elastomers prepared by cure B over a temperature range of 4.5 ($\sigma_m = 120$ psi) to 71°C. ($\sigma_m = 60$ psi) and up to a tenfold reduction of the tensile strength of the elastomers prepared by cure A at test temperatures of 49 and 71°C.; and (*b*) the $LiClO_4$ noticeably increased the ultimate elongation of the elastomers prepared by either cure A or B at all test temperatures.

4. Comparison of Ultimate Properties of Urea-Containing Elastomers and Non-Urea-Containing Elastomers. The previous study[36] presents a comparison of the ultimate properties of various elastomers prepared from a variety of ingredients. This comparison shows that the elastomers having values of U less than 2.0, and prepared with POPG and TDI, HDI, *m*-phenylene, or naphthalene diisocyanates, have essentially the same ultimate properties at equal values of $T - T_g$. In addition, elastomers prepared from POPG, TMP, and TDI and containing between 0 and 20% plasticizer

but roughly identical values of ν_e, have identical values of σ_m and ϵ_b at equal values of $T - T_g$. The diisocyanate linked elastomers prepared with polyesters formed from the copolymerization of ϵ caprolactone and methyl ϵ-caprolactone in either 50/50 or 80/20 mole ratios show noticeably larger ultimate properties, over an extended temperature range, than did corresponding elastomers prepared with POPG. Because the ultimate properties of the elastomers prepared with POPG and of those with both of the polyesters were measured on dumbbell-shaped tensile specimens, reported values of the ultimate elongations which are greater than a few hundred per cent tend to be high, as the effective gage length of such specimens decreases markedly at high elongations. As ultimate properties of the elastomers of series 1, 2, 3, and 4 were determined on ring specimens, the determined values are quite reliable. Such values were found to vary markedly with chemical composition and temperature even though all elastomers had nearly the same T_g. Consequently, a comparison, in separate figures, of the tensile strength and ultimate elongations for the elastomers of series 1, 2, 3, and 4 with the elastomers previously studied for σ_m and ϵ_b would be difficult. It will simply be stated that either the crosslinked or noncrosslinked elastomers of series 1, 2, 3, and 4 generally show markedly better elongations than the previously investigated elastomers in the $T - T_g$ range of 20–130°C. The tensile strengths of the urea-containing elastomers, both crosslinked and noncrosslinked, are similar to those prepared with the 50/50 polyester in the $T - T_g$ range of 60 to 130°C.

CONCLUSION

Two types of elastomers, crosslinked and noncrosslinked, can be prepared from POPG, TDA, and TDI, depending upon cure conditions. The two types can be distinguished from each other by differences in their solubility in polar solvents such as DMA and in the temperature dependence of their stress–strain behavior. The crosslinked elastomers are insoluble in DMA and show equilibrium elastic behavior at elevated temperatures, but such properties are not observed for noncrosslinked elastomers. For the range of cure conditions investigated, reaction of substituted urea hydrogens with excess isocyanate is the main process which leads to a covalent three-dimensional network in the crosslinked elastomers. For many of these elastomers, values for the moduli can be calculated from the quantities of reactants and an assumed network topology. Values of the moduli for the noncrosslinked elastomers are larger than those of the crosslinked ones except at the highest test temperature of (82°C.). This is probably the result of strong interchain forces which appear to have a markedly greater effect on the moduli of the noncrosslinked than on those of the crosslinked elastomers. A quantitative comparison of the interchain forces in the two types of elastomers cannot be made in terms of molecular structure, because the chemical structure for the noncrosslinked elastomers is, for the most part, unknown. This is probably the result of the ambient environment

during cure bringing about reactions different from those considered most likely to occur.

Some insight was gained into the nature of the intermolecular forces present in the urea-containing polymers from studies of prepolymers formed from POPG, TDI, and TDA and of the glass-transition temperatures of numerous elastomers. The gelation of the low molecular weight P-II and P-III prepolymers and the polymer P-IV resulted from strong interchain forces and not from the formation of a covalent three-dimensional network. Furthermore, the values for the glass-transition temperatures of the elastomers suggested that these interchain forces or secondary type bonds formed through substituted ureas are so strong that such groups exist in a "frozen state" over the temperature range investigated (−120 to 82°C.). Lithium salts are antigelation agents for the prepolymers P-II and P-III and raise the glass-transition temperature of the elastomers. These results suggest that the lithium salts interfere with the formation of hydrogen bonds and, as a consequence, the intermolecular forces are lowered.

The ultimate elongations of many of the substituted urea-containing elastomers were extremely large and were not determined under many test conditions; thus, analyses of the ultimate property data are limited. However, for either the crosslinked or noncrosslinked elastomers, the tensile strengths are proportional to $E_{71°C.}$, with the proportionality constants being temperature-dependent. This relationship is independent of the chemical compositions of the various elastomers. A simple relationship between the ultimate elongation and $E_{71°C.}$ could not be established for either the crosslinked or noncrosslinked elastomers. Since certain of the elastomers prepared from POPG, TDI, and TDA exhibited extremely large elongations of 5000%, with elastic recoveries of better than 90%, it is clear that these materials are well suited for further study of large deformations in polymeric materials. However, many of the results of the present study also show that there is a need for further investigation of the quantitative aspects of the detailed chemical structure of diisocyanate-linked elastomers. With this quantitative problem solved, the potential ability of controlled modifications in network topology, chain flexibility, and intermolecular forces recommends diisocyanate-linked polymers as suitable model materials for additional studies of property-structure relationships.

The authors wish to acknowledge the assistance of Messrs. John W. Farrar, Alan B. Magnusson, and John H. Otteman in some of the experimental portions of the study.

References

1. Arnold, R. G., J. A. Nelson, and J. J. Verbanc, *Chem. Revs.*, **57**, 47 (1957).
2. Jones, J. I., and N. G. Savill, *J. Chem. Soc.*, **1957**, 4392.
3. Shashoua, V. E., *Am. Chem. Soc.*, **81**, 3156 (1959).
4. Bayer, O., *Angew. Chem.*, **59**, 257 (1947).
5. Seeger, N. V., T. G. Mastin, E. E. Fauser, F. S. Farson, A. F. Finelli, and E. A. Sinclair, *Ind. Eng. Chem.*, **45**, 2538 (1953).

6. Heiss, H. L., J. H. Saunders, M. R. Morris, B. R. Davis, and E. E. Hardy, *Ind. Eng. Chem.*, **48,** 1498 (1954).

7. Little, J. R., and R. A. Gregg, Paper 51, Division of Paint, Plastics and Printing Ink Chemistry, presented to the 130th American Chemical Society Meeting, Atlantic City, N. J., September 1956.

8. Gregg, R. A., Paper 52, Division of Paint, Plastics, and Printing Ink Chemistry, presented to the 130th American Chemical Society Meeting, Atlantic City, N. J., September 1956.

9. Graham, G. T. E., and R. A. Gregg, Paper 53, Division of Paint, Plastics and Printing Ink Chemistry, presented to the 130th American Chemical Society Meeting, Atlantic City, N. J., September 1956.

10. Farthing, A. C., *Proc. Chem. Soc.*, **1957,** 301.

11. Dickinson, L. A., *Rubber Age*, **82,** 96 (1957).

12. Colodny, P. C., and A. V. Tobolsky, *J. Am. Chem. Soc.*, **79,** 4320 (1957).

13. Dyer, E., and H. Scott, *J. Am. Chem. Soc.*, **79,** 672 (1957).

14. Laakso, T. M., and D. D. Reynolds, *J. Am. Chem. Soc.*, **79,** 5717 (1957).

15. Athey, R. J., J. G. DiPinto, and J. S. Rugg, *Development Products*, Report No. 10, Elastomer Chemicals Department, E. I. du Pont de Nemours and Co., March 15, 1958.

16. Quant, A. J., Sandia Corporation SCR-54, AT-(29-1) p. 789, October, 1958.

17. Schollenberger, C. S., H. Scott, and G. R. Moore, *Rubber World*, **137,** 549 (1958).

18. Trifan, D. S., and J. F. Terenzi, *J. Polymer Sci.*, **28,** 443 (1958).

19. Havlik, A. J., A. B. Magnusson, and T. L. Smith, Paper 8, Division of Polymer Chemistry, presented to the 136th American Chemical Society Meeting, Atlantic City, N. J., September 1959.

20. Saunders, J. H., *Rubber Chem. Technol.*, **32,** 337 (1959).

21. Quant, A. J., *SPE Journal*, **15,** 298 (1959).

22. Axelrood, S. L., and K. C. Frisch, *Rubber Age*, **88,** 465 (1960).

23. Murbach, W. J., and A. Adicoff, *Ind. Eng. Chem.*, **52,** 772 (1960).

24. Wilson, J. E., H. M. Truax, and M. A. Dunn, *J. Appl. Polymer Sci.*, **3,** 343 (1960).

25. Sampson, A. J., and C. F. Blaich, Jr., Paper 10, presented to the 77th Meeting of the Division of Rubber Chemistry of the American Chemical Society, Buffalo, N. Y., May 1960.

26. Blaich, C. F., Jr., and A. J. Sampson, Paper 6, Division of Rubber Chemistry, presented to the 138th American Chemical Society Meeting, Atlantic City, N. J., September 1960.

27. Cluff, E. F., and E. K. Gladding, *J. Appl. Polymer Sci.*, 290 (1960).

28. Saunders, J. H., *Rubber Chem. Technol.*, **33,** 1293 (1960).

29. Heiss, H. L., *Rubber Age*, **88,** 89 (1960).

30. Smith, T. L., and A. B. Magnusson, *J. Polymer Sci.*, **42,** 391 (1960).

31. Saunders, J. H., *Rubber Chem. Technol.*, **33,** 1259 (1960).

32. Fedotova, O. Y., I. P. Losev, N. I. Skripichenko, M. A. Okunchikova, L. V. Bychkova, and M. I. Shtilman, *Vysokomol. Soedin.*, **1,** 1685 (1959).

33. Athey, R. J., *Ind. Eng. Chem.*, **52,** 611 (1960).

34. Trick, G. S., *J. Appl. Polymer Sci.*, **3,** 252 (1960).

35. Illers, K. H., and H. Jacobs, *Makromol. Chem.*, **39,** 234 (1960).

36. Smith, T. L., and A. B. Magnusson, *J. Appl. Polymer Sci.*, **5,** 218 (1961).

37. Weisfeld, L. B., J. R. Little, and W. E. Wolstenholme, *J. Polymer Sci.*, **56,** 455 (1962).

38. Waugaman, C. A., *Modern Plastics*, **39,** No. 2, 146 (1961).

39. Slezak, F., J. Stallings, D. Wagner, and J. Wotiz, *J. Org. Chem.*, **26,** 3137 (1961).

40. Axelrood, S. L., C. W. Hamilton, and K. C. Frisch, *Ind. Eng. Chem.*, **53,** 889 (1961).

41. Axelrood, S. L., C. W. Hamilton, and K. C. Frisch, *Rubber World*, **144**, 85 (1961).
42. Sauer, K., and M. H. Kasparian, *J. Org. Chem.*, **26**, 3498 (1961).
43. Waugaman, C. A., and G. B. Jennings, *Rubber World*, **144**, 72 (1961).
44. Stilmar, F., U.S. Pat. 2,814,606 (November 26, 1957).
45. Dreyfus, H., U.S. Pat. 2,623,867 (December 30, 1952).
46. Seeger, N., U.S. Pat. 2,625,531 (January 13, 1953).
47. Mastin, T. G., and N. Seeger, U.S. Pat. 2,625,535 (January 13, 1953).
48. Rugg, J., U.S. Pat. 2,702,797 (February 22, 1955).
49. Dacey, W. F., R. A. Gregg, and N. W. Hess, U.S. Pat. 2,721,811 (October 25, 1955).
50. Stallman, O., and E. O. Langerak, U.S. Pat. 2,643,250 (June 23, 1953).
51. Gensel, H., and E. Windemuth, U.S. Pat. 2,657,151 (October 27, 1953).
52. Brenschede, W., U.S. Pat. 2,755,266 (July 17, 1956).
53. Lehmann, W., U.S. 2,761,852 (September 4, 1956).
54. Müller, E., and S. Petersen, U.S. Pat. 2,778,810 (January 22, 1957).
55. Stilmar, F. B., U.S. Pat. 2,814,605 (November 26, 1957).
56. Wittbecker, E. L., U.S. Pat. 2,816,879 (December 17, 1957).
57. Hill, F. B., Jr., U.S. Pat. 2,818,404 (December 31, 1957).
58. Saunders, J. H., U.S. Pat. 2,828,291 (March 25, 1958).
59. Carter, A. S., U.S. Pat. 2,830,037 (April 8, 1958).
60. Neher, R., U.S. Pat. 2,833,744 (May 6, 1958).
61. Carter, A. S., and M. L. Ernsberger, U.S. Pat. 2,835,654 (May 20, 1958).
62. Benning, A. F., J. G. Burt, and E. K. Gladding, U.S. Pat. 2,843,568 (July 15, 1958).
63. Seligman, K. L., U.S. Pat. 2,877,212 (March 10, 1959).
64. Seeger, N. V., and T. G. Mastin, U.S. Pat. 2,879,251 (March 24, 1959).
65. [illegible] F., *Colloid Sci.*, **12**, 308 (1957).
66. Jacobs, H., and E. Jenckel, *Makromol. Chem.*, **43**, 132 (1961).
67. Becker, G. W., and H. Oberst, *Kolloid-Z.*, **153**, 1 (1957).
68. Shkapenko, G., G. T. Gmitter, and E. F. Gruber, *Ind. Eng. Chem.*, **52**, 605 (1960).
69. Gruber, E. E., and O. C. Keplinger, *Ind. Eng. Chem.*, **51**, 151 (1959).
70. Keplinger, O., and E. E. Gruber, *Rubber Age*, **87**, 959 (1959).
71. Burns, E. A., and R. F. Muraca, *Anal. Chem.*, **31**, 397 (1959).
72. Burns, E. A., R. F. Muraca, and F. Chang, Progress Report No. 20-345, Jet Propulsion Laboratory, Pasadena, California, January 1, 1958.
73. Siggia, S., *Quantitative Organic Analysis via Functional Groups*, Wiley, New York, 1949.
74. Havlik, A. J., and A. F. Hildebrandt, Paper 34, Division of Polymer Chemistry, presented to the 134th American Chemical Society Meeting, Chicago, September 1958.
75. E. I. du Pont de Nemours & Co., Bulletin C1971.01, E. I. du Pont de Nemours & Co., August 15, 1956.
76. Osborne, M. W., Jr. (B. F. Goodrich Chemical Co., Cleveland, Ohio), private communication.
77. Blatt, A. H., *Organic Synthesis*, Vol. II, Wiley, New York, 1950, p. 160.
78. Havlik, A. J., and J. Perry, unpublished results.
79. Fernelius, W. C., and B. E. Bryant, *Inorganic Synthesis*, Vol. 5, McGraw-Hill New York, 1957, pp. 105–113.
80. Thomas, A. B., and E. G. Rochow, *J. Am. Chem. Soc.*, **79**, 1843 (1957).
81. Havlik, A. J., unpublished results.
82. Havlik, A. J., Technical Report No. 32-334, Jet Propulsion Laboratory, Pasadena, California, September 15, 1962.

83. Landel, R. F., and T. L. Smith, Preprint, Division of Paint, Plastic, and Printing Ink Chemistry, 136th American Chemical Society, Atlantic City, N. J., September 1959.

84. Flory, P. J., *Principles of Polymer Chemistry*, Cornell Univ. Press, Ithaca, N. Y., 1953, p. 53.

85. Ferry, J. D., *Viscoelastic Properties of Polymers*, Wiley, New York, 1961, p. 219.

86. Havlik, A. J., and T. L. Smith, Technical Report No. 32-180 Jet Propulsion Laboratory, Pasadena, California, May 31, 1962.

87. Smith, T. L., Technical Documentary Report No. ASD-TDE-62-572, Stanford Research Institute, Menlo Park, California, June 1962.

88. Smith, T. L., *J. Polymer Sci.*, **32**, 99 (1958).

89. Smith, T. L., *J. Polymer Sci.*, **20**, 89 (1956).

90. Lyman, D. J., *J. Polymer Sci.*, **45**, 49 (1960).

91. Naegeli, C., A. Tyabji, L. Conrad, and K. Litman, *Helv. Chem. Acta*, **21**, 1100 (1938).

92. Alfrey, T., *Mechanical Behavior of High Polymers*, Interscience, New York, 1948, p. 45.

93. Havlik, A. J., and J. Moacanin, unpublished results.

94. Bamford, C. H., A. Eliott, and W. E. Hanby, *Synthetic Polypeptides*, Academic Press, New York, 1956, p. 332.

95. Bennet, W. B., J. H. Saunders, and E. E. Hardy, presented to the Annual Meeting of the Alabama Academy of Science, Tuscaloosa, April, 1954.

96. Marei, A. I., *Kauchuk i Rezina*, **19**, No. 2, 1 (1960).

97. Hayes, R. A., *J. Appl. Polymer Sci.*, **5**, 318 (1961).

98. Wood, L. A., *J. Polymer Sci.*, **28**, 319 (1958).

99. Reding, F. P., Paper GA 10, High Polymer Physics, American Physical Society, March, 1961.

100. Beevers, R. B., and E. F. T. White, *Trans. Faraday Soc.*, **56**, 1529 (1960).

101. Hill, R., and E. E. Walker, *J. Polymer Sci.*, **3**, 609 (1948).

102. DiMarzio, E. A., and J. H. Gibbs, *J. Polymer Sci.*, **40**, 121 (1959).

103. Tompa, H., *Polymer Solutions*, Academic Press, New York, 1957, p. 267.

104. Hobbs, L. M., S. C. Kothari, V. C. Long, and G. C. Sutaria, *J. Polymer Sci.*, **23**, 123 (1956).

105. Moacanin, J.; *J. Appl. Polymer Sci.*, **1**, 272 (1959).

106. Havlik, A. J., R. F. Landel, and J. Moacanin, presented to the Tenth Canadian High Polymer Forum, Ste. Marguerite, Quebec, September 9, 1960.

107. Weiner, M. L., *J. Org. Chem.*, **25**, 2245 (1960).

108. Smeltz, K. C., E. J. Goldberg, I. C. Kogon, W. C. Woodland, submitted for publication; quoted by I. C. Kogon, *J. Org. Chem.*, **25**, 86 (1959).

109. Treolar, L. R. G., *The Physics of Rubberlike Elasticity*, Oxford Univ. Press, London, 1958, p. 2.

110. Havlik, A. J., and J. Moacanin, unpublished results.

111. Bueche, F., *Rubber Chem. Technol.*, **32**, 1269 (1959).

112. Cooper, W., *J. Polymer Sci.*, **28**, 195 (1958).

113. Smith, T. L., *SPE Journal*, **16**, 1211 (1960).

Résumé

On a étudié la préparation et les propriétés d'élastomères contenant des ponts diisocyanates, préparés à partir de polyoxypropylène glycol (POPG), toluène-2,4-diisocyanate (TDI), et toluène-2,4-diamine (TDA). On a étudié tout d'abord la structure chimique et la gélification d'une série de prépolymères. Après cela on a préparé plusieurs séries d'élastomères à 60°C dans des moules ouverts, et à 110°C dans des moules fermés, en faisant varier de façon systématique la rapport entre le nombre de fonctions isocyanates et la somme des fonctions hydroxyles et aminées (R_1), et le rapport entre les fonctions hydroxyles et les fonctions aminées (R_2) dans le mélange. Le traitement à 60°C donne

lieu à la formation d'élastomères non-pontés, avec des propriétés qui résultent des forces attractives entre les chaînes. Le traitement à 110°C donne des polymères pontés avec des liens covalents, possédant des propriétés similaires. Les températures de transition vitreuse augmentent linéairement avec la concentration en fonctions uréthannes substituées, mais elles sont indépendantes du nombre de fonctions urées substituées On propose une explication pour ce comportement surprenant. Les élastomères non-pontés sont solubles dans le *N,N*-diméthylacétamide (DMA) et dans les solvants similaires. Les viscosités intrinsèques dans le DMA augmentent avec R_1, R_2 étant constant. On a déterminé entre −23 et 82°C le module de Young, la résistance à l'élongation, et la limite de l'allongement possible. À haute température, les polymères pontés ont un module quasi d'équilibre, contrairement aux polymères non-pontés. On a calculé pour les élastomères pontés le nombre de chaînes par millilitre à partir de la quantité en exces des atomes d'hydrogène de l'urée ou de l'isocyanate et d'une certaine topologie du réseau. On a relié les modules des deux types d'élastomères avec la composition chimique. On a établi plusieurs relations entre les propriétés limites, et les modules à l'équilibre. On a noté des extensions jusqu'à 5000% avec une récupération élastique de plus de 90%.

Zusammenfassung

Eine Untersuchung der Darstellung und Eigenschaften von Elastomeren aus Polyoxypropylenglykol (POPG) und Toluol-2,4-diisocyanat (TDI) und Toluol-2,4-diamin (TDA) wurde durchgeführt. Zuerst wurde die chemische Struktur und Gelbildung einer Reihe von Vorpolymerisaten untersucht. Dann wurden viele Elastomerreihen bei 60°C in offenen Formen und bei 110°C in geschlossenen Formen aus Mischungen mit systematischer Variierung des Verhältnisses der Isocyanatgruppen zur Summe der Hydroxyl- und Aminogruppen (R_1) und des Verhältnisses der Aminogruppen zu den Hydroxylgruppen (R_2) dargestellt. Die Reaktion bei 60°C lieferte zähe, unvernetzte Elastomere, deren Eigenschaften offenbar durch Anziehungskräfte zwischen den Ketten bedingt waren, während die Reaktion bei 110° zu kovalent vernetzten Elastomeren mit ziemlich ähnlichen Eigenschaften führte. Die Glasumwandlungstemperatur nahm mit der Konzentration an substituierten Urethangruppen linear zu, war aber von der Konzentration substituierter Harnstoffgruppen unabhängig. Eine Erklärung für dieses überraschende Verhalten wird gegeben. Die unvernetzten Elastomeren waren in *N,N*-Dimethylacetamid (DMA) und ähnlichen Lösungsmitteln löslich. Die Viskositätszahlen in DMA nahmen bei konstantem R_2 mit R_1 zu. Young-Modul, Zugfestigkeit und Reissdehnung wurden zwischen −23° und 82°C bestimmt. Bei erhöhter Temperatur besassen die vernetzten Elastomeren nahezu Gleichgewichtswerte für den Modul, nicht aber die unvernetzten. Die Zahl der Ketten pro Milliliter des vernetzten Elastomeren wurde unter Annahme einer bestimmten Netzwerktopologie aus den Beträgen des Überschusses an Isocyanat und Harnstoffwasserstoff berechnet. Der Modul beider Elastomertypen wurde zur chemischen Zusammensetzung in Beziehung gebracht. Verschiedene Beziehungen zwischen Festigkeitseigenschaften und Gleichgewichtsmodul wurden aufgestellt. Dehnungen bis zu 5000% mit elastischer Rückstellung besser als 90% wurden gemessen.

Received February 18, 1963

JOURNAL OF POLYMER SCIENCE: PART A VOL. 2, PP. 587–609 (1964)

Inhibition of the Copper-Catalyzed Oxidation of Polypropylene

R. H. HANSEN, C. A. RUSSELL, T. DE BENEDICTIS, W. M. MARTIN, and J. V. PASCALE, *Bell Telephone Laboratories, Incorporated, Murray Hill, New Jersey*

Synopsis

Thermal oxidation and copper-catalyzed thermal oxidation of polypropylene were studied over a range of elevated temperatures. The apparent activation energy for both of these processes, based on t_{10} induction periods, was 27 kcal./mole. Measurement of the time (t_{10}) required for interaction of 1 g. of polymer with 10 cc. of oxygen was found to be a convenient and expedient technique for estimating the induction period, since this amount of oxygen is sufficient to cause deterioration of physical and dielectric properties of the polymer. In the absence of copper, stabilization of polypropylene comparable to that achieved with polyethylene was observed when antioxidant concentration was increased proportionately to compensate for the larger number of oxidation-susceptible tertiary carbon atoms in polypropylene. However, it was found that thermal antioxidants, even in high concentration, were ineffective protectants for polypropylene when copper was present. Conventional copper chelators and metal deactivators were, at best, only slightly effective in suppressing oxidation catalyzed by copper and usually were unsatisfactory for a variety of other reasons. Oxamide, however, and particularly its less volatile, high melting, disubstituted derivatives, functioned cooperatively with a wide variety of antioxidant systems and were found to comprise a highly effective and useful family of inhibitors of the copper-catalyzed oxidation of polypropylene.

INTRODUCTION

Onset of thermal oxidative degradation in linear and branched polyethylenes can be delayed by addition of small amounts of antioxidants. Incorporation of between 0.01% and 0.1% of a hindered phenol or secondary aromatic amine, for example, suffices to delay oxidative degradation and thus extends the useful service life of the polymer manyfold.

Since unhindered polyolefins which have an abundance of tertiary carbon atoms oxidize more readily than those comprised mainly of primary and secondary carbon atoms,[1] it is likely that much of initial oxidation occurs at branch points. Once initiated, however, oxidation spreads throughout the noncrystalline fraction of the polymer,[2–4] and the extent of oxidation has been used for direct measurements of crystalline content of semicrystalline polymers.[1,4] Sterically hindered branched polymers, such as polystyrene, polyvinylcyclohexane, and polyallylbenzene are less readily oxidized than polyethylene[1] and thus require little or no antioxidant for protection against oxidative degradation. Relatively unhindered branched

polymers such as polybutene-1 and polypropylene, on the other hand, are far more susceptible to thermal oxidation than the unhindered but comparatively unbranched polyethylene.[1] Every second carbon atom in the main chain of polypropylene is a tertiary carbon atom or branch point, a concentration about an order of magnitude greater than that observed for low density polyethylene.[5] It might be expected, therefore, that a proportionate increase in antioxidant concentration could compensate for the greater number of vulnerable tertiary carbon atoms in polypropylene as compared with polyethylene and lead to comparable stabilization. This effect has indeed been observed. For example, 0.1 wt.-% of 4,4′-thiobis-(3-methyl-6-*tert*-butylphenol) in polyethylene affords an induction period in oxygen at 140°C. of about 1000 hr. (as compared with 4 hr. for uninhibited polymer). Isotactic polypropylene containing 0.5 wt.-% of the same inhibitor is found to have an induction period of about 400 hr. at 140°C. (as compared with about 1–2 hr. for unprotected polymer), in good agreement with the stability which might be anticipated from the relative amounts of tertiary carbon atoms in the two polymers and the concentrations of antioxidant used.

This correlation of antioxidant effectiveness in the two polymers is based on the observation that polypropylene is about 50% crystalline at 140°C.[4] and the assumption that all of the antioxidant is to be found in the noncrystalline regions of the polymer. Low density polyethylene is molten at this temperature and is assumed to be completely noncrystalline. Effective antioxidant concentrations at 140°C. are therefore assumed to be 1% for the polypropylene sample and 0.1% for polyethylene. Since much of the initial oxidation occurs at branch points in the noncrystalline portion of a polymer, and since polypropylene has about 17 times as many tertiary carbon atoms as low density polyethylene, it is reasonable to assume that the effective concentration of 1% of antioxidant in polypropylene would result in stabilization 10/17 as great as the stabilization obtained by 0.1% of the same antioxidant in low density polyethylene. The predicted induction period of 600 hr. is in good agreement with the observed value of 400 hr.

Isotactic polypropylene is desirable as a dielectric and structural material because of its low density and the accompanying excellent insulating properties, its high softening point, its low solubility in common solvents and its negligible water absorption, its relative hardness and toughness, and its resistance toward thermal embrittlement and stress cracking. However, it was found that copper, presumably in an oxidized state, catalyzes the thermal oxidation of polypropylene.[6,7] At first it was felt that the decrease in induction period which was observed for uninhibited polypropylene containing copper could be compensated for by the use of proportionately larger amounts of antioxidants or by the use of more effective antioxidant systems. The seriousness of the problem was not realized until it was discovered that oxidative degradation occurred at a drastically rapid rate in the presence of copper even when the polymer contained more than 1% of an antioxidant or combination of antioxidants.[8] A similar effect has been

observed during copper-catalyzed oxidation of gasoline, where normal antioxidant concentration must be quadrupled to counteract the effect of only 1 ppm of dissolved copper.[9]

DISCUSSION

Copper and its compounds are known to act as catalysts for the oxidation of branched organic compounds.[10] For example, copper phthalocyanine has been found to be an effective catalyst for the oxidation of cumene[11] and related compounds.[12] Copper is particularly active as a catalyst for the oxidation of natural rubber[13,14] GR-S rubber,[14] synthetic natural rubber, poly(vinyl formal),[15] petroleum products such as gasoline,[9,16] and a whole host of other branched organic compounds which now include polypropylene.

The catalytic effect of copper on the thermal oxidation of polypropylene is not as drastic in the absence of antioxidants as it is in their presence. However, it can be seen from Figure 1 that oxidation becomes catalytic when copper is present. Without copper, thermal oxidation of polypropylene proceeds normally and autocatalytically. In the presence of copper, however, the autocatalytic period is absent or vestigial and the oxidation reaction rapidly attains a catalytic, constant, and nonaccelerating rate after a shorter "induction period" than observed in the absence of copper.

Oxygen uptake studies of uninhibited polymer in the presence and absence of copper dust and over a range of temperatures show that induction periods vary regularly with temperature. The normally brief induction periods observed for uninhibited polypropylene, presumably due to the abundance of unhindered tertiary carbon atoms, are consistently shortened

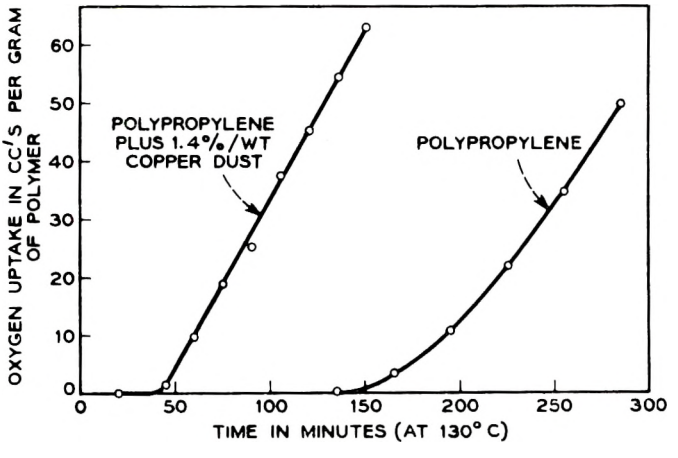

Fig. 1. Catalytic effect of copper on the thermal oxidation of uninhibited polypropylene at 130°C. in oxygen at atmospheric pressure. The addition of 1.4 wt.-% of copper dust decreases the induction period by a factor of about three.

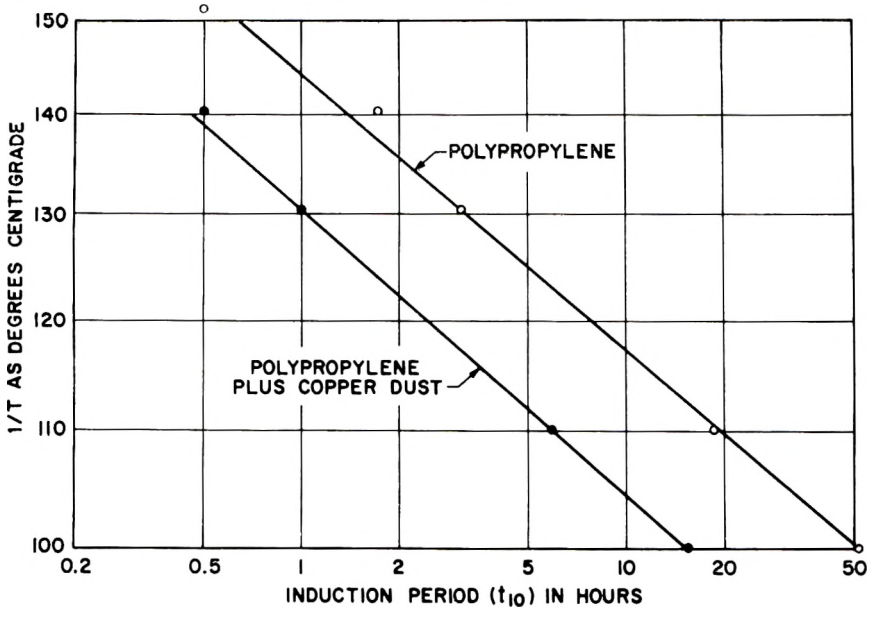

Fig. 2. The effect of temperature on thermal oxidation and copper-catalyzed thermal oxidation of uninhibited polypropylene. Time for interaction of 1 g. of polymer with 10 cc. pure oxygen at atmospheric pressure is plotted against 1/°K.

by a factor of three when about 1.4 wt.-% of finely divided copper dust is present. The linearity of the data plotted in Figure 2 indicates that diffusion of oxygen through the polymer matrix played an unimportant role in the oxidation studies reported here, even at the relatively rapid rates and short induction periods which were observed at higher temperatures or in the presence of copper. Diffusion has been shown to be important in oxidation studies where sample thickness is widely varied.[17,18] This complication was avoided by using uniformly thin samples throughout the present work. Activation energies for diffusion of gases such as oxygen through polyolefins[19] and polypropylene[20] have been reported to be about 10 kcal./mole. Since the observed apparent activation energies for the thermal oxidation and copper-catalyzed thermal oxidation of uninhibited polypropylene were both found to be 27 kcal./mole over a range of temperatures (and, therefore, a range of induction periods), it is believed that there was little or no contribution from or dependence on diffusion effects. The identical apparent activation energies for the oxidation of polypropylene in the absence of and presence of copper also suggest that these reactions follow the same course.

Catalytic interaction of oxygen with polypropylene in the presence of copper is also observed when the polymer contains an antioxidant. The rate of oxidation becomes rapid and constant after a drastically shortened induction period compared with that obtained in the absence of copper. Decreases in induction periods greater than 100-fold have been observed

TABLE I
Catalytic Effect of Copper and Copper Compounds on the Thermal Oxidation of Stabilized Polypropylene

		Induction period t_{10}, hr.			
		At 150°C.		At 140°C.	
	Catalyst	Antioxidant alone	Antioxidant plus 0.5 wt.-% oxanilide	Antioxidant alone	Antioxidant plus 0.5 wt.-% oxanilide
Polymer A[a]	None	120	115	400	450
	Copper dust (1.4 wt.-%)	10	59	35	135
	Cu_2O (1.4 wt.-%)	15	—	8	—
	CuO (1.4 wt.-%)	84	—	71	—
	Copper stearate (0.25 wt.-%)	2	—	4	—
Polymer B[b]	None	190	190	700	800
	Copper dust (1.4 wt.-%)	2	68	3	220
	Cu_2O (1.4 wt.-%)	2	—	—	70
	CuO (1.4 wt.-%)	53	—	200	606
	Copper stearate (0.25 wt.-%)	0.6	8	—	—

[a] Polymer A is stabilized by 0.5 wt.-% of 4,4′-thiobis(3-methyl-6-*tert*-butylphenol).
[b] Polymer B is a commercially stabilized composition.

for a number of antioxidant systems when copper is added, and 10-fold changes are common. For example, the induction period in oxygen at 140°C. for polypropylene stabilized by the addition of 0.5 wt.-% of 4,4′-thio-bis-(3-methyl-6-*tert*-butylphenol) is decreased from about 400 hr. to about 40 hr. by the presence of copper. Similar 90% losses in the effectiveness of this antioxidant in the presence of copper have been observed over a range of temperatures.

Preliminary evidence indicates that copper in an oxidized form, rather than the metal itself, is responsible for the catalysis of the thermal oxidation of polypropylene. Cuprous oxide was found to be a more vigorous polypropylene oxidation catalyst than cupric oxide and seemed to be even more active than freshly-reduced copper. Studies of the catalytic oxidation of carbon monoxide and propylene have shown that, in general, *p*-type semiconductors, such as cuprous oxide, are more active catalysts than *n*-type oxides, and that the latter are more active than insulators such as cupric oxide.[21] This lends credence to a hypothesis that the effect of copper on the thermal oxidation of polypropylene may be another example of catalysis by *p*-type semiconductors. On the other hand, the differences in activity observed between cuprous and cupric oxide in the present study may be due largely to differences in surface area, for copper stearate, which probably is somewhat soluble in the noncrystalline portion of the polymer and which certainly is more dispersible than copper or its oxides, was found to be an extremely active catalyst for the thermal oxidation of polypropylene (see Table I). The present study has also shown that observed induction

periods are dependent on copper concentration and surface area. However, if it is assumed that the oxide film always present on the surface of copper is the catalyst (rather than the metal itself), the apparent dependence on copper concentration is explained. The amount of oxide is certainly very much less than the 1–2% concentration of copper used in these studies and is probably less than the 0.03–0.3% level where a constant value for catalysis of oxidation by metal ions has been observed.[22,23]

It has been shown that the catalyst undergoes a valence change during the oxidation of paraffins catalyzed by manganese and cobalt stearates.[24] It is quite probable that copper oxides or other copper salts, such as the stearate, behave in a similar fashion when they act as catalysts for the oxidation of polypropylene. Thus, it is highly likely that both cuprous and cupric forms of copper are involved in the catalysis, which probably proceeds by a redox process between ionic copper and the hydroperoxides formed during initial autoxidation of the polymer. Propagation of liquid-phase thermal oxidation of hydrocarbons is believed to occur by abstraction of hydrogen atoms by peroxy radicals.[25] Oxidation–reduction reactions between copper salts and hydroperoxides[26–29] are considered to be most pertinent to the mechanism of the copper-catalyzed oxidation of polypropylene. Any interaction which accelerates the production of peroxy radicals will increase the rate of thermal oxidation and decrease the induction period.

The effect of copper catalysis on the oxidative degradation of polypropylene resembles the effect of ultraviolet radiation on the degradation of polyolefins. It is generally agreed that changes caused by oxidation of polymer molecules are responsible for degradation observed during exposure to ultraviolet light (e.g., weathering). Normal and relatively high concentrations of thermal antioxidants cannot cope with the high rate of initiation and propagation of oxidation which accompanies ultraviolet radiation. Similarly, normal and relatively high concentrations of thermal antioxidants are not able to overwhelm copper-catalyzed oxidation. Antioxidants are of greatest benefit where the rate of oxidation is low and usually are not very effective where the rate of initiation or the rate of propagation is high.[30] Ultraviolet light is believed to cause an increase in the rate of branching of the oxidation reaction. Copper salts are believed to accelerate oxidation by catalyzing the decomposition of organic hydroperoxides. The resulting high rate of reaction can thus overwhelm the antioxidant in a manner similar to that resulting from the high rate of reaction obtained by exposure to ultraviolet light. Other mechanisms could be proposed. For example, it is possible that copper may catalyze polypropylene oxidation by aiding in the homolytic cleavage of peroxy compounds. Or, it may assist in the formation of radicals (R·) or otherwise help in the production of peroxy compounds. Further, in acting as a catalyst, it is possible that copper may function by more than one of these or other mechanisms, such as, for example, by interaction with the antioxidant.

Some of the reactions which are believed to be involved in the oxidation of polyolefins are shown in eqs. (1)–(8).[25] The rate of thermal oxidation,

Initiation

$$RH \longrightarrow R\cdot + H\cdot \text{ or } R\cdot + R\cdot \quad (1)$$

$$R\cdot + O_2 \longrightarrow ROO\cdot \quad (2)$$

Propagation

$$ROO\cdot + R'H \longrightarrow ROOH + R'\cdot \quad (3)$$

$$ROOH \longrightarrow RO\cdot + OH\cdot \quad (4)$$

$$2\ ROOH \longrightarrow RO\cdot + ROO\cdot + H_2O \quad (5)$$

$$RO\cdot + R'H \longrightarrow ROH + R'\cdot \quad (6)$$

$$OH\cdot + R'H \longrightarrow HOH + R'\cdot \quad (7)$$

Termination by (1) disproportionation, (2) combination, or (3) by antioxidant:

$$R\cdot + HA \longrightarrow RH + A\cdot \quad (8)$$

after initiation, depends on the rate of the propagation step. Oxidation will obviously proceed more rapidly if the rate of propagation is accelerated by the use of catalysts or elevated temperatures. It has been shown that initiation of the oxidation of polyolefins such as polypropylene can be detected by observing the interaction of the polymer with less than 10^{-5} the amount of oxygen customarily required to estimate induction periods.[31] It has also been shown that oxidation continues homogeneously and autocatalytically from initiation through the induction period over a wide range of temperatures and oxygen uptakes. Thus, oxidation will be initiated on exposure of a polyolefin to oxygen and will continue as long as the polymer is in contact with oxygen. Further, thermal degradation of polypropylene at elevated temperatures in the absence of oxygen has been shown to be due to peroxides already present in the polymer.[32] In order to minimize formation of peroxy compounds and, therefore, obtain maximum protection against oxidative and thermal degradation, it has been suggested that antioxidants should be incorporated immediately after polyolefins are produced.[31]

In an attempt to decrease the amount of free ionic copper available for catalysis of oxidation, conventional chelating agents and metal deactivators[16,33] were added to polypropylene compositions containing thermal antioxidants. All of these materials were found to be unsatisfactory for a variety of reasons. Most of them did not diminish the catalytic activity of copper and copper compounds. Some actually accelerated the already rapid copper-catalyzed oxidation of polypropylene[34] and might be useful in other reactions where oxidation is sought rather than avoided. The best of the conventional deactivators were still only slightly effective in curtailing the catalytic activity of copper. For example, *N,N'*-di-β-naphthyl-*p*-phenylenediamine was found to be a weak inhibitor of the copper-catalyzed oxidation of polypropylene. However, compositions containing this material became quite dark after slight oxidation. In many applications of polymers, discoloration is considered quite objectionable. For example,

the excellent mechanical properties possessed by polypropylene can be utilized to produce a suitably rugged foamed structure which is of great interest as primary wire insulation. To be useful for this purpose it is essential for the composition to be colorless or nearly so in order to permit color coding. Further, it has been shown that azodicarbonamide is an excellent blowing agent for the preparation of expanded polypropylene insulation.[35,36] It was also found that *N,N'*-di-β-naphthyl-*p*-phenylenediamine, a discoloring-type antioxidant, was not compatible with the blowing agent, for an oxidation–reduction reaction in the polymer melt gave rise to a chocolate color and rendered the blowing agent nonfunctional by converting it to a stable hydrazo compound.[35] Other conventional and commercial metal inhibitors or deactivators (as, for example, ethylenediamine tetraacetic acid and its salts, 2,2'-bipyridyl, 8-quinolinol, *N,N'*-disalicylidene-1,2-propanediamine, and benzimidazole) as well as a number of experimental materials either were ineffective or only slightly effective and usually had other disadvantages including instability; incompatibility; water solubility; volatility; formation of highly-colored products; or they reacted with other components of the polypropylene composition.

Oxamide, however, and particularly its less volatile, high melting, disubstituted derivatives were found to be a highly effective and useful new family of inhibitors of the copper-catalyzed oxidation of polypropylene, as is illustrated in Table II. The disadvantages associated with conventional metal deactivators are not observed when the oxamides are used to suppress copper-catalyzed oxidation of polypropylene. Oxamide derivatives which are most effective in a variety of antioxidant systems are those which melt at temperatures above 200°C. and have sufficiently low vapor pressure and water solubility to remain in the polymer during and after processing. The reasons for the poorer performance of the volatile and water-soluble oxamides is obvious, but the need for high melting point may not be immediately apparent. It is believed that the low melting materials may melt and coalesce during processing due to the differences in polarity between the oxamides and the polyolefin. If separation due to oiling out occurs, an effect similar to a lowering of the concentration of copper inhibitor would be observed, and less stabilization would result.

Polymeric oxamides, with high melting points and low volatilities, appear to be somewhat less effective than simple oxamides (see Table II). Presumably the polymeric derivatives are more difficult to disperse than the relatively low molecular weight oxamides. Other polymeric amides such as nylon 6 and nylon 66 are ineffective copper inhibitors. The specificity of the oxamide structure is also indicated by results obtained with simple amides. For example, oxanilide has been found to be very useful as an inhibitor of the copper-catalyzed oxidation of polypropylene while similar materials lacking the oxamide structure, such as carbanilide, phthalamide, and 2,3-quinoxalinediol, were not effective copper inhibitors.

Oxamide and its derivatives are not antioxidants in the usual meaning of the term and do not function as synergistic antioxidants in combination

with conventional thermal antioxidants. For example, the resistance toward thermal oxidation of polypropylene containing 0.5 wt.-% of oxanilide is no greater than that of polypropylene alone. Also, the addition of oxanilide to polypropylene compositions containing antioxidants does not increase resistance toward oxidation in the absence of copper (see Table I, for example). It is believed that the oxamides protect branched polyolefins such as polypropylene against copper-catalyzed thermal oxidation by forming complexes which are not capable of acting as oxidation catalysts, presumably because the nature of this complex interferes with the valence change required in the catalysis of the decomposition of hydroperoxides by copper. Since most compounds which can complex with copper do not inhibit the copper-catalyzed oxidation of polypropylene, other mechanisms to explain the stabilization afforded by the oxamides, such as a heterolytic (nonbranching) decomposition of hydroperoxides or complex formation with hydroperoxides, could be proposed, but a study of the mechanism of inhibition is beyond the scope of the present work.

EXPERIMENTAL PROCEDURE

a. Sample Preparation

As with all unhindered polymers, but especially for highly-branched materials such as polypropylene, it is important to incorporate the antioxidant into the polymer as rapidly as possible in order to minimize thermal oxidation,[17,31] either by short exposure to oxygen at elevated temperatures or by somewhat longer exposure at lower temperatures. For example, extrapolation of data obtained by isothermal oxidation studies performed at elevated temperatures, as shown in Figure 2, indicates that uninhibited polypropylene will be significantly oxidized in a short period of time if air is present. The data presented in Figure 2 indicate that the induction period, a point where the useful properties of the polymer are completely destroyed, is reached in a matter of about a year at 50°C. To minimize initial oxidation, freshly prepared uninhibited polymer was alternately evacuated and flushed with argon several times and then stored in the dark in sealed containers under argon until needed.

Antioxidants were introduced into this fresh uninhibited homopolymer by the preparation of masterbatches in a Brabender Plastograph at about 190°C. under an atmosphere of nitrogen. The use of an inert atmosphere is essential because the presence of air will result in complete degradation of uninhibited polymer in a minute or so at this temperature. Masterbatch concentrates were cut back to desired antioxidant concentrations by diluting banded masterbatch with virgin polymer on a two-roll mill. Oxamide and oxamide derivatives were conveniently added to polypropylene–antioxidant compositions in a Brabender Plastograph at about 190°C. under a nitrogen atmosphere. A 35-g. portion of polypropylene pellets containing a suitable thermal antioxidant was preheated for about 3 min. before fluxing the polymer for 3 min. at 50 rpm. At this point oxamide or one of its de-

TABLE II
Physical Properties and Effectiveness of Oxamide and its Derivatives

Oxamide	Melting point, °C.	Sublimation temperature, °C.[a]	Concentration of oxamide used, wt.-%	Observed induction periods t_{10} of polypropylene–antioxidant compositions containing 1.4 wt.-% of copper dust, hr.[b]			
				0.5% Antioxidant A[c]		0.5% Antioxidant B[d]	
				At 140°C.	At 150°C.	At 140°C.	At 150°C.
Control (antioxidant alone, no copper)	—	—	0	400	120	113	80
Control (antioxidant with copper)	—	—	0	35	10	8	10
Oxamide (ethanediamide)	419[e]	223	0.5	80, 91[b]	31	18	—
N,N'-Di-*n*-octadecyl oxamide	119	270	0.5	68, 78[b]	9	27	—
N,N'-Di-*n*-hexyl oxamide	133	167	0.5	78, 138[b]	50[b]	42	—
N,N'-Bis(2-chlorophenyl) oxamide	—	—	0.5	76	33	44	—
N,N'-Bis(3-chlorophenyl) oxamide	—	—	0.5	—	—	48	—
N,N'-Bis(4-chlorophenyl) oxamide	152	168	0.5	41	14	83	—
N,N'-Diallyl oxamide	156	157	0.5	32	16	11	—
N,N'-Bis(2-pyridyl) oxamide	161	219	0.5	90, 96[b]	72	79	—
N,N'-Di-*n*-propyl oxamide	166	133	0.5	39	—	10	—
N,N'-Dimethyl oxamide	215	145	0.5	38	19	11	—
N,N'-Di-isopropyl oxamide	217	—	0.5	34	—	6	—

N,N'-Dibenzyl oxamide	248	250	0.5	87	16	53	—
N,N'-Diphenyl oxamide	254	236	0.03	—	—	23	—
N,N'-Diphenyl oxamide	254	236	0.10	50	6[b]	27	—
N,N'-Diphenyl oxamide	254	236	0.25	74	37[b]	—	—
N,N'-Diphenyl oxamide	254	236	0.5	138, 130[b]	59, 51[b]	100	80
N,N'-Diphenyl oxamide	254	236	1.0	134	—	109	—
N,N'-Diphenyl oxamide	254	236	3.3	—	—	122	—
N,N'-Bis(4-ethoxyphenyl) oxamide	264	292	0.5	73	24	51	—
N,N'-Bis(4-ethoxyphenyl) oxamide	274	—	0.5	96	34	46	—
Ethylene oxamide	>300	—	0.5	110	—	37	—
Poly(hexamethylene) oxamide	>300	314[f]	0.1	—	—	6	—
Poly(hexamethylene) oxamide	>300	314[f]	0.5	105	—	28	—
Poly(hexamethylene) oxamide	>300	314[f]	1.0	173	—	68	—
Poly(hexamethylene) oxamide	>300	314[f]	2.0	184	—	96	—
Poly(hexamethylene) oxamide	>300	314[f]	3.3	217	—	101	—
Polymeric oxamide derived from 1,4-Bis(aminomethyl)cyclohexane	>300	314[f]	0.5	141	—	42	—
Polymeric oxamide derived from 3,3'-Diamino-di-*n*-propylamine	>300	—	0.5	80	—	65	—
Oxamide copolymer derived from a mixture of 1 part of 1,6-hexanediamine and 3 parts of 1,4-bis(aminomethyl)cyclohexane	>300	—	0.5	107	—	18	—

[a] Temperature at which 50% of the pure oxamide has sublimed from a shallow pan when heated in air at a constant rate of 1°C./min.

[b] In some cases expanded wire insulation was tested. In these instances the polymer also contained about 10% of polyisobutylene.

[c] Antioxidant A = 4,4'-thiobis(3-methyl-6-*tert*-butylphenol).

[d] Antioxidant B = 6,6'-di-*tert*-butyl-4,4'-bi-*o*-cresol.

[e] Reported value.[41]

[f] Decomposes above 300°C. A charred residue (about 20%) was not volatile at 360°C.

rivatives, if used, was added and mixing was continued briefly before 0.5 g. of cleaned copper dust was added, if used, and mixing was again continued for about three minutes. The total time for preparation of the sample, always under a nitrogen atmosphere, did not exceed 9 min. The polymeric composition was removed, pressed flat between aluminum plates, and cooled rapidly. A small aliquot was then pressed into a 10-mil sheet in a polished aluminum picture-frame mold by heating for about 1 min. at about 180°C. in an electrically heated press at a pressure of about 2000 psi. The mold was transferred to a cold press, and the sheet was cooled rapidly under pressure. Samples prepared in this manner were satisfactory for oxidation studies at temperatures of 140°C. since this is close to the temperature at which maximum rate of recrystallization has been reported. At lower temperatures, rate of recrystallization is believed to be more rapid than observed rates of initiation of oxidation. It was found that samples annealed at 120°C. for 3 hr. under N_2 afforded more reproducible oxygen uptake data for samples tested at higher temperatures, possibly because rate of oxidation becomes more rapid while rate of change in polymer morphology decreases at temperatures above 140°C. Since it is likely that a polymer with a higher amorphous (i.e., noncrystalline) content will oxidize more rapidly than one with a lower amorphous content,[3,37] annealing to more representative crystallinity for the tests done at temperatures over 140°C. was deemed desirable and was accepted as standard practice.

Oxamide and its derivatives were purchased, where possible, or synthesized by ammonolysis of diethyl oxalate with the desired amine or diamine. The displacement reactions were carried out in alcohol or in xylene. Aliphatic amines reacted rapidly and exothermally. Reactions were slower with aromatic amines and it was usually necessary to carry them out in refluxing xylene in order to drive off alcohol formed during the displacement reaction. Yields were quantitative or nearly so. Polymeric oxamides were used as prepared but monomeric materials were recrystallized at least once before use, usually from xylene or xylene–acetone solutions. Melting points are listed in Table II.

Clean copper dust was prepared by heating small amounts of electrolytic grade copper powder in a reducing flame to red heat and then cautiously quenching the still-glowing copper in methyl alcohol. Agglomerates resulting from this operation were broken up and put through a 16-mesh Nichrome gauze. The resultant powder was dried in a vacuum oven and stored under nitrogen. A somewhat finer powder was obtained by an alternate method. Fine electrolytic copper dust (10 g.) was washed with trichloroethylene, dried, treated for 1–2 min. (until the copper was bright) with a solution of 13.2 g. ammonium sulfate, 1.1 g. of ammonium persulfate, and 10 ml. of concentrated ammonium hydroxide in 90 ml. of water. After filtration, the dust was washed several times with dilute (10:90) ammonia until the washings were colorless and then with distilled water until the washings were neutral to pH paper. After a final washing with methanol, the dust was vacuum dried and kept under nitrogen.

In order to accelerate the accumulation of data, copper stearate was frequently used as a catalyst for the thermal oxidative degradation of polypropylene. Its greater activity may be due to its ease of dispersion or possibly to a moderate degree of solubility in the polymer. The catalytic effects of reagent grade cuprous oxide and cupric oxide were also investigated (Table I).

In many instances, test samples consisted of expanded insulation on 19-gauge copper wire instead of or in addition to the 10-mil sheet samples described above. A mixture comprised of polypropylene granules containing an antioxidant, azodicarbonamide, and oxamide or an oxamide derivative, if used, was extruded on copper wire by means of a $2^1/_2$-in. commercial machine. Wall thicknesses of the resulting expanded insulation (about 40% expansion) ranged from about 8 to 10 mils. No special precautions were used to clean the wire which probably acquired an oxide surface film during the extrusion process, since it is necessary to preheat the conductor in order to obtain optimum physical properties of the insulation. It was observed that oxamide and its derivatives had no adverse effect on the processing of expanded polypropylene insulation or on the color or physical properties of the finished product. Polypropylene used in the extrusion experiments contained 10% of polyisobutylene which was added in an attempt to improve the low temperature brittleness properties of the polymer.

b. Test Methods

In a few instances the effectiveness of the oxamide type copper inhibitors was studied by oven-aging tests. Samples were visually and manually examined. Cracks or brittleness, an early sign of deterioration (especially in the case of expanded insulation), were considered as points of failure. This type of test is useful for screening materials, but results were generally considered less reliable than oxygen absorption studies and are reported for only one series of samples.

In most instances, effectiveness of the copper inhibitors was determined by measuring oxygen uptake. Isothermal oxygen absorption studies at several elevated temperatures were carried out in pure oxygen at atmospheric pressure by well-known procedures[38] with some minor modifications. The equipment was essentially a Warburg-type apparatus (oil bath or metal block) and oxygen uptake was followed volumetrically, using 13-cc. burets with 0.1 cc. graduations (Corning No. 459050, Drawing XA-6063). At least two duplicate samples, each consisting of 0.1 g. polymer, were tested for all materials. In the case of extruded wire samples, the copper conductor was not removed. Measurements of oxygen uptake were continued until the equivalent of 100 cc./g. polymer had been consumed.

It was observed that degradation of the physical properties of polypropylene compositions could be detected after the interaction of more than about 1 cc. and less than 10 cc. of oxygen/g. of polymer.[1] Similar effects have been observed for other polymeric materials.[3,39,40] Since an oxygen uptake of less than 10 cc./g. polymer is sufficient to impair or destroy the use-

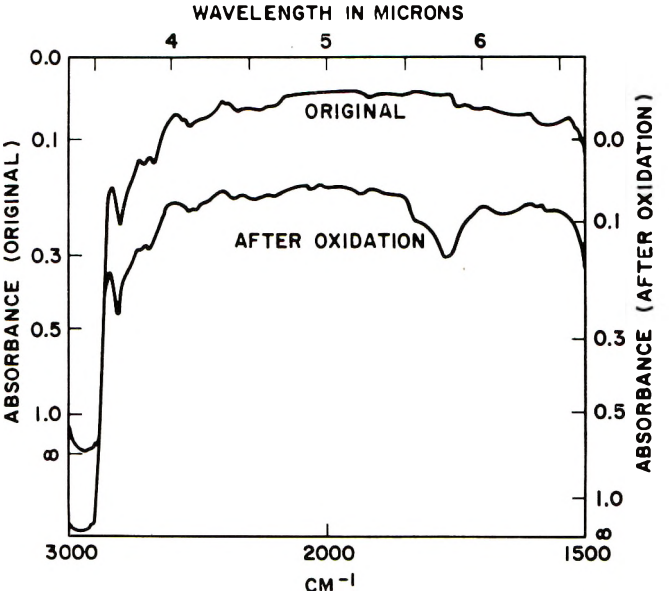

Fig. 3. The effect of partial oxidation (10 cc. oxygen/g. polymer) on the infrared absorption spectrum of polypropylene.

fulness of the polymer and since oxidation of polypropylene compositions containing copper proceeded linearly (without autocatalysis), it was found to be both expedient and convenient to measure failure points by recording time required for interaction with 10 cc. oxygen/g. of polymer. This value, called the t_{10} induction period, was taken as a measure of the time required for deterioration of the polymer even though it represents a relatively early portion of the curve obtained by more complete oxidation. Conventional determination of induction periods (t_i) by back-extrapolation from the steady-state rate agreed well with t_{10} values due to the rapid reactions and the absence of autocatalysis in the presence of copper. Agreement of t_i and t_{10} usually was within experimental error, even when copper was not present (see, for example, Fig. 1).

The effect of a small amount of oxidation can be detected by a variety of techniques other than oxygen uptake studies. Dielectric properties[17] and mechanical properties[1] of polypropylene are greatly impaired or destroyed by slight oxidation, so these properties can be used to study oxidative degradation. Degradation can also be observed by following infrared absorption of the polymer as shown in Figure 3.[17] Here it it seen that 10 cc. oxygen has a marked effect on the absorption characteristics of polypropylene. The increase in absorption in the region between 1700 and 1800 cm.$^{-1}$ is attributed to an increase in carbonyl content which accompanies oxidation of the polymer. Unfortunately, many of the antioxidants used to protect the polymer, as well as the oxamides themselves, contain carbonyl groups and therefore infrared study of the deterioration of stabilized

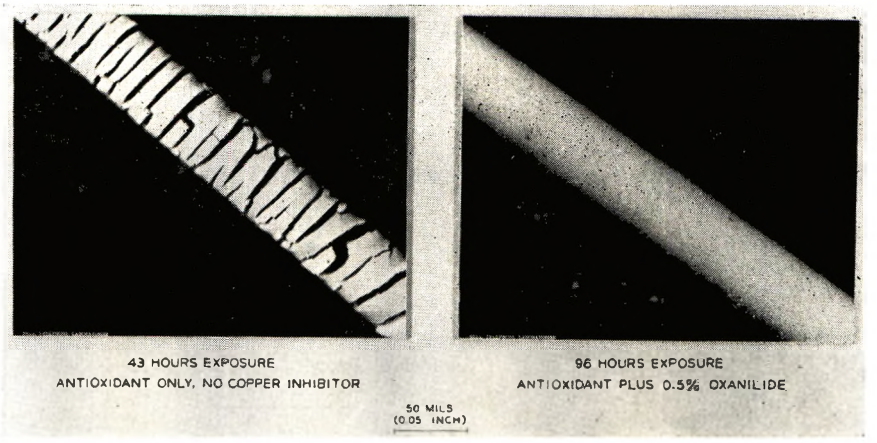

Fig. 4. Improved resistance against copper-catalyzed thermal oxidation obtained by addition of oxanilide to a commercial polypropylene composition is shown by photomicrographs of expanded polypropylene insulated wire samples after exposure in a circulating air oven at 140°C.

compositions is a difficult task. The effect of oxygen on expanded polypropylene insulation on copper wire and the usefulness of oxanilide, a typical oxamide derivative, are shown in Figure 4, where it is seen that the physical properties of the insulation without copper inhibitor are completely destroyed while the addition of oxanilide has protected a similar sample of expanded wire insulation.

RESULTS

Oxamide and particularly its high melting and less volatile derivatives subdue catalysis of oxidation caused by copper by functioning cooperatively

TABLE III
Effect of Oxanilide on the Copper-Catalyzed Oxidation of Several Polypropylene–Antioxidant Compositions

Antioxidant	Induction period t_{10}, hr.					
	At 150°C.			At 140°C.		
	A[a]	AC[b]	AOC[c]	A[a]	AC[b]	AOC[c]
6,6′-Di-*tert*-butyl-4,4′-bi-*o*-cresol	77	10	80	113	8	100
5-*n*-Pentadecylresorcinol	103	7	59	164	12	80
4,4′-Methylenebis(3-methyl-6-*tert*-butylphenol)	35	5	22	77	9	47
2,6-Di(*tert*-butyl)-4-methylphenol	9	2	5	30	4	12
4,4′-Thiobis(3-methyl-6-*tert*-butylphenol)	120	10	59	400	35	135
N-Phenyl-2-naphthylamine	93	22	38	372	52	112

[a] A = Polypropylene containing only 0.5 wt.-% of antioxidant.

[b] AC = Polypropylene containing 0.5 wt.-% of antioxidant and 1.4 wt.-% of copper dust.

[c] AOC = Polypropylene containing 0.5 wt.-% of antioxidant, 0.5 wt.-% of oxanilide, and 1.4 wt.-% of copper dust.

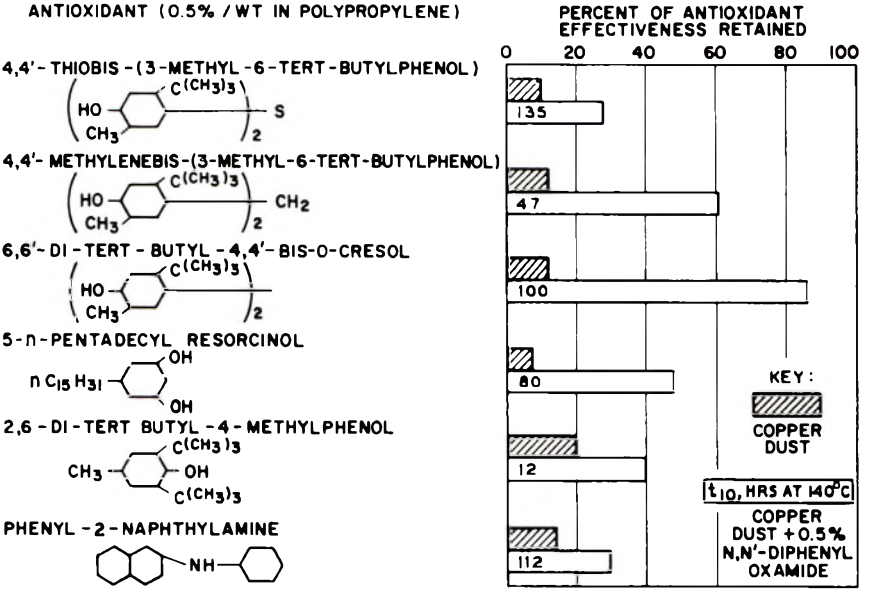

Fig. 5. Oxanilide is an effective inhibitor of copper-catalyzed oxidation of polypropylene. Addition of oxanilide greatly increases resistance of a variety of simple antioxidant–polypropylene compositions toward copper-catalyzed oxidation.

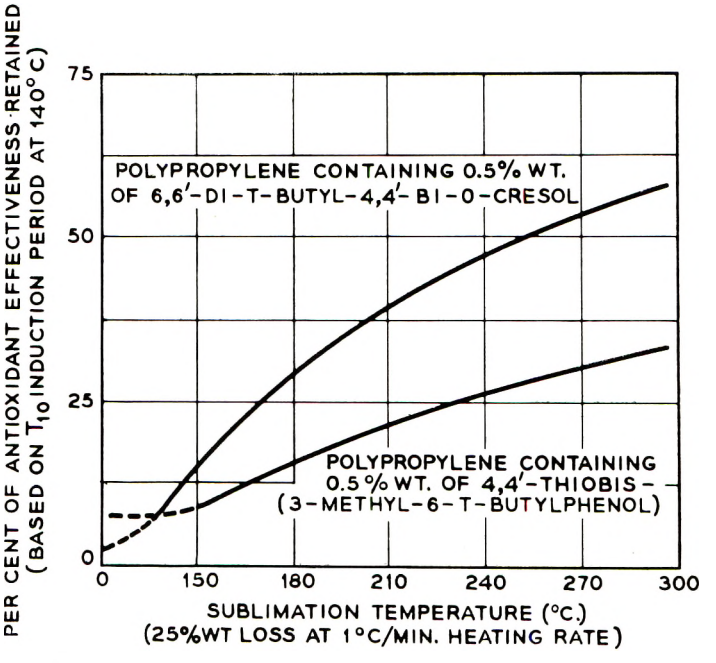

Fig. 6. Effect of volatility of substituted oxamides at constant initial concentration. The least volatile oxamides are the most effective, based on oxygen uptake studies of polypropylene compositions containing 1.4 wt.-% of copper dust and 0.5 wt.-% of oxamide-type copper inhibitors.

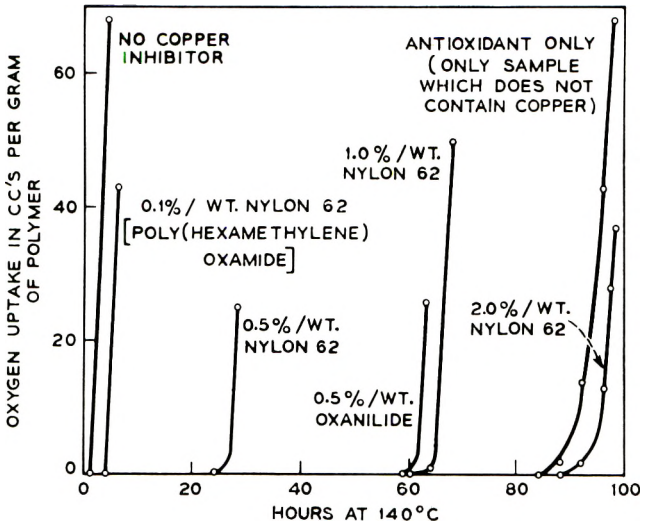

Fig. 7. Finely-divided oxanilide is a more effective copper inhibitor than an equivalent amount of a polymeric oxamide (nylon 62), possibly because of greater ease of dispersion. Complete retention of the effectiveness of the antioxidant (0.5 wt.-% of 6,6′-di-*tert*-butyl-4,4′-bi-*o*-cresol) may be obtained by use of a larger amount of the polymeric oxamide in the polypropylene-antioxidant composition containing 1.4 wt.-% of copper dust.

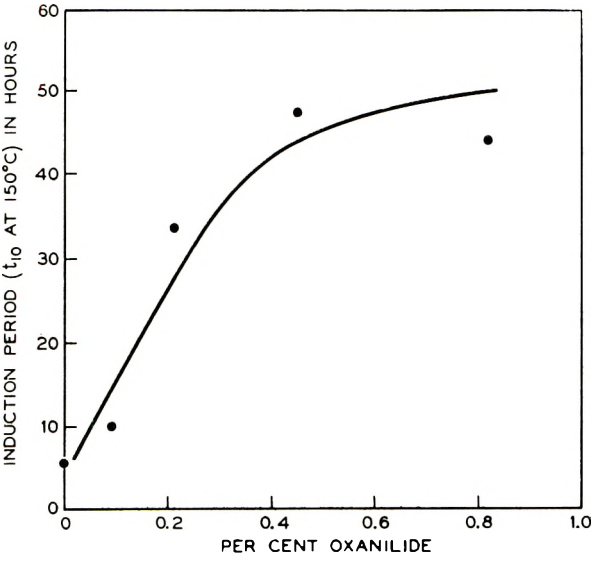

Fig. 8. The effect of finely divided oxanilide on the thermal oxidation of polypropylene containing 0.5 wt.-% of 4,4′-thiobis-(3-methyl-6-*tert*-butylphenol) and 1.4 wt.-% of copper dust indicates that most efficient stabilization is achieved at oxanilide concentrations of between 0.3 and 0.7 wt.-%.

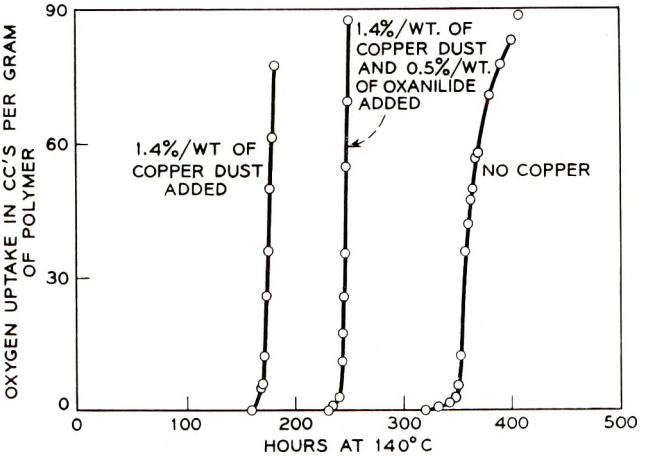

Fig. 9. Oxygen uptake studies of the thermal oxidation and copper-catalyzed thermal oxidation of polybutene-1 containing 0.5 wt.-% of 4,4′-thiobis-(3-methyl-6-*tert*-butylphenol) show that oxanilide also inhibits copper-catalyzed oxidation of this branched polyolefin.

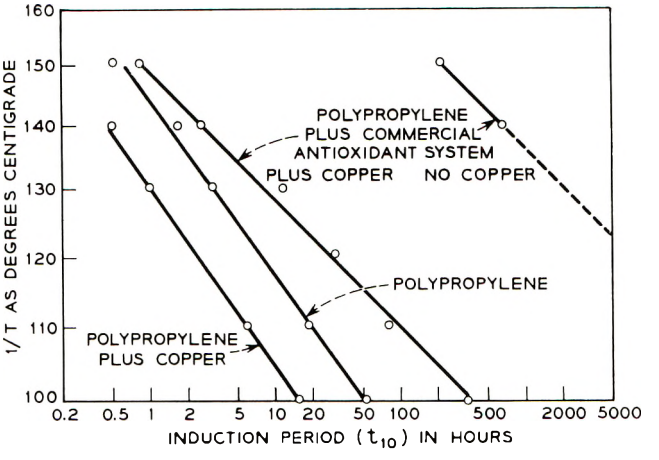

Fig. 10. Comparison of the effect of addition of 1.4 wt.-% of copper dust on the thermal oxidation of uninhibited polypropylene and a well stabilized commercial composition. The effect of copper catalysis has been found to be more drastic in the presence of antioxidants than in their absence. In this instance it is seen that the presence of copper dust decreases the induction periods of the stabilized composition by a factor of more than 100 as compared with a factor of about three for polypropylene alone.

and effectively with a wide variety of antioxidants as shown in Tables II and III and Figure 5. The effect of other forms of copper, such as cuprous oxide, cupric oxide, and copper stearate, and the usefulness of oxanilide in these systems are described in Table I. The efficiency of the oxamide derivative is related to its volatility and melting point as shown in Figure 6 and Table II and to its concentration as shown in Figures 7 and 8 and Table

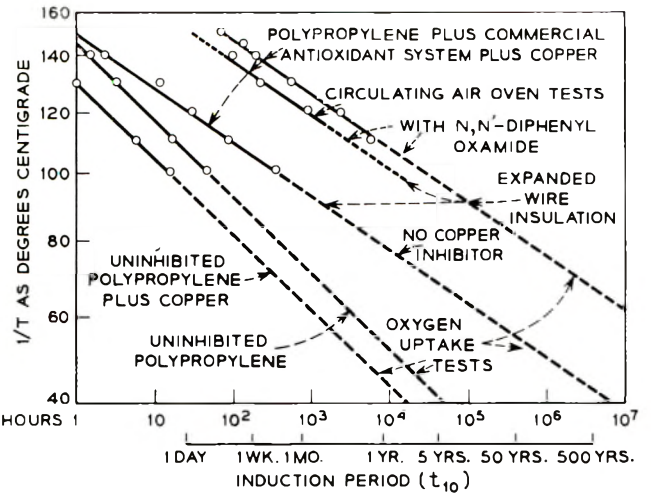

Fig. 11. The usefulness of oxanilide in greatly extending the service life of polypropylene–antioxidant compositions in contact with copper is shown by circulating air oven and oxygen uptake studies of the effect of temperature on the thermal oxidation of expanded wire insulation prepared from a commercially stabilized polypropylene composition. The effect of copper dust on the oxidation of uninhibited polypropylene is shown for comparison.

II. In each instance the t_{10} induction period has been used as a convenient, accurate, and meaningful measure of the resistance of the composition toward oxidative degradation. In all of the data reported, unless otherwise indicated, the concentration of antioxidant used was 0.5 wt.-%, as was the concentration of the oxamide type copper inhibitor. Typical oxygen uptake curves are shown in Figure 9, where it is seen that much of the effectiveness of the antioxidant is restored by the addition of oxanilide (*N,N'*-diphenyl oxamide). At 150°C. the following t_{10} induction periods have been observed for this stabilized polybutene-1 composition: alone, 250 hr.; with copper dust, 92 hr.; and with copper dust and oxanilide, 123 hr.

Oxamide and its derivatives such as oxanilide are useful in multicomponent antioxidant systems as well as the single antioxidant system shown in Figure 9. Oxygen absorption studies of a stabilized commercial composition, as shown in Figure 10, indicate that this material is quite resistant to thermal oxidative degradation in the absence of copper. This same commercial polypropylene–antioxidant system would be severely degraded after less than 5 years at 70°C. in the presence of copper. Addition of 0.5 wt.-% of *N,N'*-diphenyl oxamide to the stabilized composition restores a significant portion of the effectiveness of the antioxidant: estimated service life of this composition is more than 100 years at 70°C. based on extrapolation of results of oxygen absorption studies over a range of temperatures (Fig. 11). Each point on the Arrhenius plot used in making this estimation is an average value based on at least ten samples from at least two separate preparations of expanded polypropylene insulation containing

TABLE IV
Effect of Oxanilide on the Copper-Catalyzed Oxidation of Several Commercial Polypropylene–Antioxidant Compositions

Induction period t_{10} at 150°C., hr.				
Commercial composition alone[a]	Commercial composition and copper dust (1.4 wt.-%)	Commercial composition, copper dust (1.4 wt.-%) and oxanilide (0.5 wt.-%)	Commercial composition and copper stearate (0.25 wt.-%)	Commercial composition, copper stearate (0.25 wt.-%) and oxanilide (0.5 wt.-%)
346	3.2	49	0.5	12
16	2	10	—	—
200	7	55	0.5	12
314	2.2	104	2.5	39
190	2	68	0.6	8

[a] Five different compositions tested. Antioxidant compositions and concentrations not disclosed.

0.5 wt.-% oxanilide (i.e., more than 150 oxygen uptake tests were performed in order to obtain the six points shown). Also shown in Figure 11 are oven-aging tests using the same expanded wire insulation samples. The somewhat lesser amount of stabilization observed in the circulating oven tests may be due to volatilization of the oxanilide (and perhaps the antioxidants as well). However, the material is sufficiently well stabilized to be useful as a composition in contact with copper. Should volatility of the copper inhibitor be a serious problem, polymeric oxamides can be used. The effectiveness of oxanilide with other types of commercial polypropylene–antioxidant compositions is shown in Table IV. In each instance it is seen that the effectiveness of the antioxidant in the presence of copper is greatly improved by the addition of oxanilide.

SUMMARY

Oxamide and its derivatives have been shown to be highly effective and useful inhibitors of the copper-catalyzed oxidation of polypropylene. In compositions containing 0.5% by weight of antioxidant and 0.5 wt.-% of oxamide or a substituted oxamide, between 30 and 80% of the effectiveness of the antioxidant is retained in the presence of copper. Higher concentrations of the oxamide inhibitor result in greater retention of antioxidant effectiveness, and complete restoration of antioxidant effectiveness has been observed in a number of instances. When oxamide or its derivatives are not used, only between 1 and about 15% of the normal induction period for an antioxidant is realizable if copper is present. Apparently antioxidants alone cannot cope with copper catalysis of the thermal oxidation of polypropylene, for increasing the concentration of antioxidant does not significantly increase the stabilization obtained in the presence of copper.

The oxamide family of copper inhibitors are of special interest because they have no adverse effect on processing properties of polypropylene and polybutene-1 or mixtures of these polymers with other polymers, they are relatively innocuous from the standpoint of dielectric and physical properties of the resultant polymeric composition, they are easily dispersed, they are effective and efficient, they do not interact with blowing agents, antioxidants, pigments, or other additives to result in degradation of a desired property, they do not appear to accelerate corrosion of copper, they are relatively permanent, they are stable both during and after processing, they are colorless and do not develop color, and they are inexpensive. In summary, therefore, they permit the use of polypropylene and/or expanded polypropylene where copper must also be present. Polypropylene, polybutene-1, and copolymers or blends based on these materials which contain an effective antioxidant system and an effective copper inhibitor such as oxanilide or other members of the oxamide family can be processed readily and without complication and can be expected to have a useful service life in the presence of copper even at elevated temperatures.

The authors are grateful to a number of members of the Chemical Research Department and Outside Plant Department of Bell Telephone Laboratories for helpful discussions, for their interest in this work, and for assistance in the preparation of samples.

References

1. Hansen, R. H., W. M. Martin, and T. De Benedictis, paper presented at The Conference on Advances in Polymer Science and Technology, The Plastics Institute, London, May 1–3, 1963.

2. Kavafian, G., *J. Polymer Sci.*, **24**, 499 (1957).

3. Hawkins, W. L., W. Matreyek, and F. H. Winslow, *J. Polymer Sci.*, **41**, 1 (1959).

4. Hansen, R. H., F. H. Winslow, W. L. Hawkins, and W. Matreyek, paper presented at the 136th National Meeting of the American Chemical Society, Atlantic City, September 1959.

5. Willbourn, A. H., *J. Polymer Sci.*, **34**, 569 (1959).

6. Lanza, V. L., W. L. Hawkins, and R. H. Hansen, unpublished results.

7. Hawkins, W. L., and F. H. Winslow, *Trans. J. Plastics Inst.*, **29**, 82 (1961).

8. Hawkins, W. L., private communication.

9. Pedersen, C. J., *Ind. Eng. Chem.*, **41**, 924 (1949).

10. See, for example, W. A. Waters in *Organic Chemistry*, Vol. 4, H. Gilman, Ed., Wiley, New York, 1953, p. 1139.

11. Brit. Pat. 801,387, Sept. 10, 1958.

12. U. S. Pat. 2,954,405, Sept. 27, 1960.

13. *Vanderbilt Rubber Handbook*, G. G. Winspear, ed., Vanderbilt, New York, 1958, p. 383.

14. Rao, N. V. C., H. Winn, and J. R. Shelton, *Ind. Eng. Chem.*, **44**, 576 (1952).

15. Beachell, H. C., P. Fotis, and J. Hucks, *J. Polymer Sci.*, **7**, 353 (1951).

16. Watson, R. W., and T. B. Tom, *Ind. Eng. Chem.*, **41**, 918 (1949).

17. Russell, C. A., and J. V. Pascale, *J. Appl. Polymer Sci.*, **7**, 959 (1963).

18. Burnett, J. D., *Ind. Chem. Belg. Suppl.*, **2**, 319 (1959).

19. Barrer, R. M., *Diffusion in and through Solids*, Cambridge University Press, 1941, p. 419.

20. Conner, W. P., and G. D. Schertz, paper presented at the Regional Technical Conference on Polypropylene, Society of Plastics Engineers, Philadelphia, April 1962.

21. See, for example, J. K. Dixon and J. E. Longfield in *Catalysis*, Vol. 7, P. H. Emmett, Ed., Reinhold, New York, 1960.

22. Woodward, A. E., and R. B. Mesrobian, *J. Am. Chem. Soc.*, **75,** 6189 (1953).

23. Tobolsky, A. V., D. J. Metz, and R. B. Mesrobian, *J. Am. Chem. Soc.*, **72,** 1942 (1950).

24. Semenov, N. N., *Some Problems in Chemical Kinetics and Reactivity*, Vol. I, Princeton Univ. Press, Princeton, N. J., 1958, p. 206.

25. See, for example, K. U. Ingold, *Chem. Revs.*, **61,** 563 (1961).

26. Kochi, J. K., et al, *J. Am. Chem. Soc.*, **83,** 2013, 2017, and 3162 (1961).

27. Ivanov, K. I., V. K. Savinova, and E. G. Mikhailova, *Compt. Rend. Acad. Sci. U.R.S.S.*, **25,** 34 (1939); *Chem. Abstr.*, **34,** 3974[3] (1940).

28. Berger, H., and A. F. Bickel, *Trans. Faraday Soc.*, **57,** 1325 (1961).

29. Denney, D. B., D. Z. Denney, and G. Feig, *Tetrahedron Letters*, **15,** 19 (1959).

30. Wagner, A. M., and J. C. Brier, *Ind. Eng. Chem.*, **23,** 40 (1931).

31. Hansen, R. H., and W. M. Martin, paper presented at the Metropolitan Regional Meeting of the New York–North Jersey Sections of the American Chemical Society, New York, January 1962.

32. v. Schooten, J., and P. W. O. Wija, *Thermal Degradation of Polymers*, Society of Chemical Industry Monograph No. 13, London, 1961, p. 432.

33. See, for example, Chaberek, S., and A. E. Martell, *Organic Sequestering Agent*, Wiley, New York, 1959, Chap. 7.

34. Hansen, R. H., and W. M. Martin, unpublished data.

35. Hansen, R. H., *SPE J.*, **18,** 77 (1962).

36. Aamodt, N. O., P. E. Fox, and R. W. Hefty, private communication.

37. Grieveson, B. M., R. N. Haward, and B. Wright, *Thermal Degradation of Polymers*, Society of Chemical Industry Monograph No. 13, London, 1961, p. 413.

38. Hawkins, W. L., R. H. Hansen, W. Matreyek, and F. H. Winslow, *J. Appl. Polymer Sci.*, **1,** 37 (1959).

39. Houwink, R., *Kautschuk*, **17,** 67 (1941); *Chem. Abstr.*, **36,** 6373 (1942).

40. Tobolsky, A. V., *India Rubber World*, **118,** 313 (1948).

41. *Handbook of Chemistry and Physics*, Chemical Rubber Publishing Co., Cleveland, Ohio, 1961.

Résumé

On étudie l'oxydation thermique catalysée au cuivre du polypropylène sur une gamme étendue de températures élevées. L'énergie d'activation apparente pour ces deux processus, basée sur des périodes d'induction t_{10}, est de 27 kcal/mole. On trouve que la mesure de temps (t_{10}) nécessaire à l'interaction d'un gramme de polymère avec 10 cm³ d'oxygène, est une technique facile et rapide d'estimation de la période d'induction puisque cette quantité d'oxygène est suffisante pour déterminer les propriétés physiques et diélectriques du polymère. On observe, en l'absence de cuivre, une stabilisation du polypropylène, comparable à celle obtenue avec le polyéthylène, lorsque la concentration d'antioxydant est augmentée proportionnellement afin de compenser un plus grand nombre d'atomes de carbone tertiaires, susceptibles d'oxydation, dans le polypropylène. Cependant, on constate que les antioxydants thermiques, même en forte concentration, sont des protecteurs peu effectifs pour le polypropylène en présence du cuivre. Les chélates habituels du cuivre, et les désactivants métalliques ne sont finalement que peu effectifs pour supprimer l'oxydation catalysée par le cuivre et ne donnent pas satisfaction pour une séries d'autres raisons. L'oxamide cependant et particulièrement ses dérivés di-substitués moins volatils, à point de fusion élevé, fonctionnent coopérativement avec unde grande variété de systèmes antioxydants et constituent une famille d'inhibiteurs fort effectifs et usuels à l'égard de l'oxydation catalysée au cuivre du polypropylène.

Zusammenfassung

Die thermische und die kupfer-katalysierte thermische Oxydation von Polypropylen wurde in einem Bereich höherer Temperaturen untersucht. Die scheinbare Aktivierungsenergie des Prozesses auf Grundlage der t_{10}-Induktionsperiode betrug 27 kcal/Mol. Die Messung der zur Reaktion von einem Gramm Polymeren mit zehn Kubikzentimeter Sauerstoff erforderlichen Zeit (t_{10} erwies sich als bequeme und brauchbare Methode zur Bestimmung der Induktionsperiode, da diese Sauerstoffmenge zur Verschlechterung der physikalischen und dielektrischen Eigenschaften des Polymeren ausreicht. Bei Abwesenheit von Kupfer wurde bei einer zur Kompensation der grösseren Zahl oxydationsempfindlicher, tertiärer Kohlenstoffatome im Polypropylen ausreichenden Erhöhung der Konzentration des Antioxydans eine der beim Polyäthylen erzielten vergleichbare Stabilisierung erreicht. Es zeigte sich jedoch, dass bei Gegenwart von Kupfer thermische Antioxydantien auch in hoher Konzentration als Schutzmittel für Polypropylen unwirksam waren. Die konventionellen Chelatbildner für Kupfer sowie Metalldesaktivatoren ergaben im besten Falle nur eine schwache Unterdrückung der kupfer-katalysierten Oxydation und waren gewöhnlich aus einer Reihe anderer Gründe unbefriedigend. Dagegen zeigten Oxamid und besonders seine weniger flüchtigen, hochschmelzenden, disubstituierten Derivate eine kooperative Wirkung mit einer Vielfalt von Antioxydanssystemen und erwiesen sich als eine hochwirksame und brauchbare Familie von Inhibitoren für die kupfer-katalysierte Oxydation von Polypropylen.

Received November 5, 1962
Revised December 20, 1962

JOURNAL OF POLYMER SCIENCE: PART A VOL. 2, PP. 611–625 (1964)

An Evaluation of Column Thermal Diffusion As a Means of Polymer Characterization

DAVID L. TAYLOR, *The Institute of Paper Chemistry, Appleton, Wisconsin*

Synopsis

The mechanism of polymer fractionation in a Clusius-Dickel thermal diffusion column was elucidated by a systematic study of the effects of important experimental factors on the separations attainable combined with an analytical description of column operation and recent theories of polymer thermal diffusion. Several polystyrene samples of known molecular weight distribution were studied in toluene and methyl ethyl ketone solvents at varying conditions of temperature gradient (up to 1050°C./cm.), mean temperature (20–45°C.), and concentration (up to 2.4 wt.-%). The thermal diffusion column was of the concentric cylinder type, equipped with thirty sample ports. The degree of separation of polymer from solvent increased with temperature gradients below 40°C./cm., increased slightly with decreased mean temperature, increased markedly with starting concentration, and was greater in toluene at a given concentration. The degree of fractionation was found to increase rapidly with temperature gradient, and was largely independent of concentration in methyl ethyl ketone but increased strongly with concentration in toluene solutions. These effects were interpreted by means of a theoretical calculation of the influence of both ordinary and thermal diffusion on column behavior in conjunction with an evaluation of the radial concentration gradients. The experimental results are in accord with a recent theory of polymer thermal diffusion which predicts that the thermal diffusion coefficient should not be a strong function of molecular weight. The fractionation effect is apparently governed by differences in ordinary diffusion coefficients. The fractionation was greater for higher molecular weights.

INTRODUCTION

Current interest in thermal diffusion of polymers stems from the work of Debye and Bueche[1] in which it was demonstrated that high polymer solutions exhibit a rather large thermal diffusion effect and that some fractionation by molecular size occurs in a Clusius-Dickel column. This study has inspired several workers[2–5] to examine more fully the practicability of thermal diffusion fractionation of high polymers. These efforts have met with some success, but the precise nature of polymer fractionation in a Clusius-Dickel column has been left open to question. Possibly a molecular weight dependence of the thermal diffusion coefficient predicted by Drickamer's theories[6–8] is responsible for the observed fractionation effect, but Ham's recent theory[9,10] indicates that the thermal diffusion coefficient is not greatly dependent on molecular weight for sufficiently large polymer

molecules. It has been suggested[9] that fractionation occurs by ordinary diffusion in a Clusius-Dickel column and that the thermal diffusion separation serves only to produce the required concentration gradients. The object of the present study was an elucidation of the nature of polymer fractionation in a Clusius-Dickel column.

The experimental approach consisted of a systematic study of the effects of important operating factors on the separations attainable combined with an analytical description of column operation and recent theories of polymer thermal diffusion. A single polymer, polystyrene, was chosen as a test specimen for the entire work.

MATERIALS AND EQUIPMENT

A very broad distribution polystyrene having a weight-average molecular weight of 425,000 and a weight-average to number-average ratio of 2.85 was kindly provided by Dr. H. W. McCormick of the Dow Chemical Company. This was polymer B6 described recently by McCormick.[11] Narrow distribution polystyrenes S102 and S111 having weight-average molecular weights of 82,000 and 239,000 and weight to number ratios of 1.05 and 1.08, respectively, were obtained through the International Standard Exchange Program from Dr. H. F. Mark, Brooklyn Polytechnic Institute.

The solvents employed were analytical-grade toluene and methyl ethyl ketone (MEK), dried and redistilled. These represented thermodynamically good and poor solvents, respectively, for polystyrene.

The thermal diffusion column employed throughout the experimental work was of the metallic concentric cylinder type and was obtained from the M. Fink Company, Brecksville, Ohio. The important dimensions were: length of column holding test liquid, 6 ft.; width of annular space, 0.0300 in.; and mean diameter of annulus, 0.6345 in. Thirty equally spaced sample ports connecting with the annulus permitted adequate flexibility of sampling schedules. The column was provided with internal water cooling (3 gal./min. flow) and external electrical heating.

PROCEDURES

All thermal diffusion runs were of at least 9 hr. duration, which was sufficient to insure the attainment of steady-state conditions. The sample concentrations were determined on a weight percentage basis by drying under vacuum at 120°C. All molecular weights of samples were determined by measurement of intrinsic viscosity at 250°C.

Thermal diffusion of a polydisperse polymer solution results in: (*a*) a gross separation of polymer from solvent, and (*b*) a fractionation of polymer molecules of varying molecular weight. These may be termed the *PS* (polymer–solvent) and *PP* (polymer–polymer) separations, respectively. The parameter *PS* was

$$PS = \int_{z_0}^{1} (1 - c/c_0)dz \qquad (1)$$

where z was the distance coordinate along the column in terms of fraction of total column length from bottom, c/c_0 was the concentration at level z in the column relative to the initial concentration c_0, and z_0 was the level where $c = c_0$. Therefore PS is that fraction of the total polymer which has been transferred to regions of concentration greater than c_0. The fractionation parameter PP was defined in the following manner. First an integral molecular weight distribution curve, $G(M)$ versus M, was constructed from the concentration and molecular weight data for a given run by

$$G(M) = \int_z^1 (c/c_0)dz \tag{2}$$

where z was the level corresponding to a molecular weight M. Then PP was calculated as

$$\begin{aligned} PP &= R/R_0 \\ R &= \sum_{n=1}^{9} f(n)|M(0.1n) - M(0.5)| \\ f(n) &= 5 - |5 - n| \end{aligned} \tag{3}$$

where $M(x)$ was the molecular weight corresponding to a value x of $G(M)$, and R_0 was the value of R for the known true $G(M)$ of polymer B6. The $f(n)$ are weighting factors. The range of both PS and PP is zero to unity.

MATHEMATICAL TREATMENT

Because of the extreme concentration dependence of viscosity and diffusion for polymer solutions, a mathematical description of column operation was feasible only for infinitely dilute solutions. Although the Furry-Jones equations[12,13] could be adapted to the present study, a more direct approach was taken through a simple reduction of the general differential transport equations. At infinite dilution, the column convective flows are dependent only on solvent properties and therefore a description of the convective velocity profile can be made independent of the problem of describing the concentration gradients established by the thermal diffusion of solute molecules.

Flow Equation

The general hydrodynamical equation for steady state laminar flow of an incompressible fluid when reduced to the special case of a long annular vertical column filled with a pure liquid and operated with a radial temperature gradient is

$$(1/r)(d/dr)(\eta r dv_z/dr) = \rho g + dp/dz \tag{4}$$

where r,z are the radial and longitudinal coordinates, η is viscosity, v_z the vertical convective velocity, ρ the density, g the gravitational constant, and p the fluid pressure. The associated boundary and integral conditions are

$$v_z = 0$$

when $r = r_c, r_h$

and

$$\int_{r_c}^{r_h} \rho v_z r dr = 0$$

where r_c, r_h locate the cold and hot wall of the column.

Diffusion Problem

For the same special case as for the flow equation, the steady-state equation describing solute transport by thermal diffusion, ordinary diffusion (neglecting diffusion along the column), and bulk convection reduces to

$$(1/r)(\alpha/\alpha r)(rD'c\theta + rD\alpha c/\alpha r) = v_z \alpha c/\alpha z \tag{5}$$

where D and D' are the ordinary and thermal diffusion coefficients, c is concentration, and $\theta = dT/dr$ is the temperature gradient. The equation is separable upon substitution of $c = P(r)Q(z)$:

$$\frac{d^2P}{dr^2} + \left(\frac{\theta D'}{D} + \frac{1}{r} + \frac{\theta \alpha D}{D\alpha T}\right)\frac{dP}{dr} + \left(\frac{\gamma v_z}{D} + \frac{\theta D'}{rD} + \frac{\theta^2 \alpha D'}{D\alpha T}\right)P = 0 \tag{6}$$

where the separation constant $\gamma = -(1/Q)dQ/dz$, which will be referred to as the extinction coefficient, determines the longitudinal concentration dependence. The smallest value of γ consistent with the following boundary and flow conditions was computed:

$$D'P\theta/D + dP/dr = 0 \tag{7}$$

when $r = r_c, r_h$

and

$$\int_{r_c}^{r_h} rPv_z dr = 0 \tag{8}$$

Experimentally, it was found that γ was truly independent of z only at low concentrations of a monodisperse polymer, but an "equivalent γ" may be determined as that value of γ which would produce the measured PS. The quantities γ and PS are related through a material balance by:

$$PS = (1 - \exp\{-\gamma\})^{-1} - \{1 + \ln[\gamma/(1 - \exp\{-\gamma\})]\}(1/\gamma) \tag{9}$$

where γ is expressed in terms of unit column length.

EXPERIMENTAL

PS Separation of Polymer B6

In all cases the polymer was found to concentrate at the bottom of the column. The degree of polymer–solvent separation increased with temperature gradients below 400°C./cm. (temperature difference across

annulus, ΔT = 30°C.) and then remained constant. PS increased slightly with decreased mean temperature $\bar{T}$ (PS = 0.46 and 0.50 for 20 and 45°C., respectively, at ΔT = 20°C. in toluene) but increased markedly with starting concentration (PS = 0.24 and 0.51 for 0.1 and 1.0%, respectively, at ΔT = 50°C., $\bar{T}$ = 45°C. in toluene), both these effects are predictable in terms of the influence of solution viscosity on the velocity of the convection currents: at lower convective velocities, the polymer molecules are not carried as far up the column during their diffusive transfer from the warm stream to the cold stream. At a given initial concentration, PS was about 10% greater in toluene solution than in MEK solely because of the higher toluene solution viscosity.

Fractionation of Polymer B6

Some typical molecular weight distribution curves obtained from thermal diffusion data are shown in Figure 1. The range of molecular weight observed includes, at best, only the middle third of the known distribution of polymer B6 (30% by weight under 2.0×10^5 and 30% over 5.7×10^5 molecular weight). PP was found to increase rapidly with temperature gradient for both solvent systems, as seen in Figure 2.

Any fractionation by column thermal diffusion must be incomplete because every molecular species must be present to some extent in the lower regions of the column. However, it might be hoped that an analytical correction of distribution data extrapolated to infinite dilution could pro-

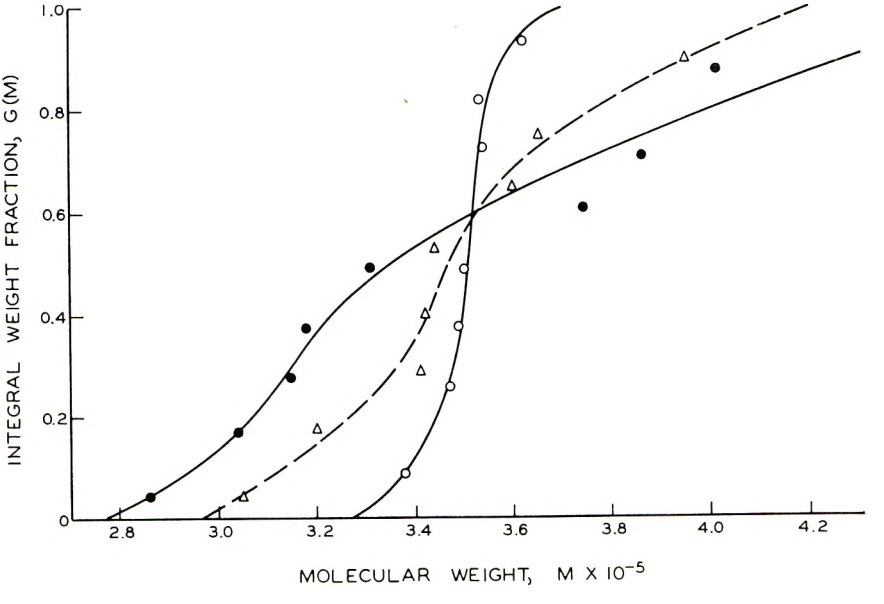

Fig. 1. Effect of ΔT on molecular weight distribution of polymer B6 in toluene (c_0 = 0.50%, $\bar{T}$ = 50 ± 5°C.): (○) run 30, ΔT = 20°C.; (△) run 28, ΔT = 50°C.; (●) run 29, ΔT = 80°C.

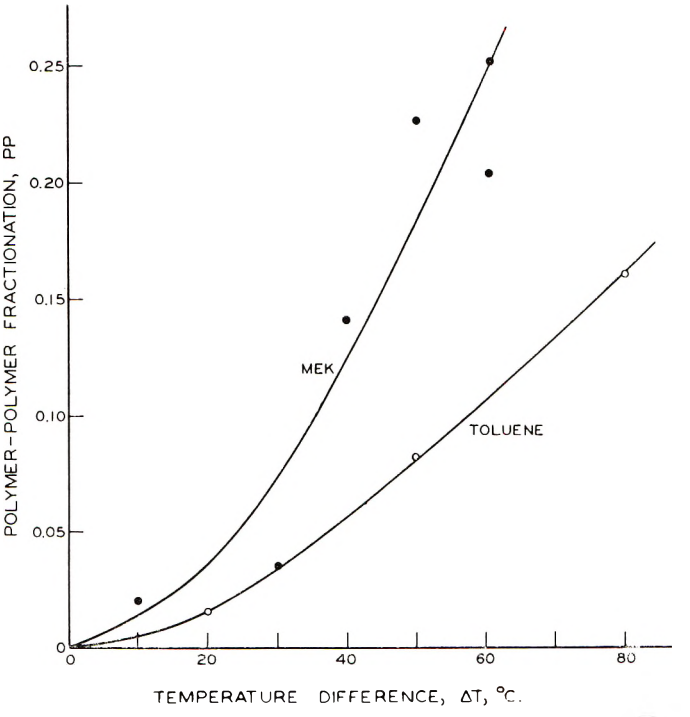

Fig. 2. Effect of temperature gradient on *PP* polymer B6 (c_0 = 0.50%, $\overline{T}$ = 45°C.).

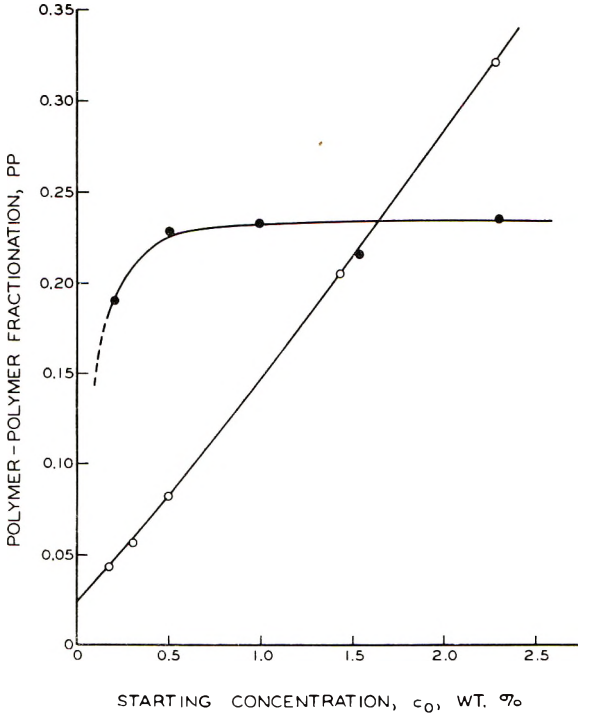

Fig. 3. Effect of concentration on *PP* polymer B6 (ΔT = 50°C., $\overline{T}$ = 45°C.): (O) in toluene; (●) in MEK.

duce the true distribution curve. But, surprisingly, the fractionation does not improve with lower initial concentrations, as seen in Figure 3.

Limited data indicated that PP may increase strongly with decreased mean temperature, PP was 0.14 at 45°C. and 0.20 at 28°C. for MEK solutions at 0.5% concentration with $\Delta T = 40$°C.

Narrow Distribution Polymers

A full 2^4 factorial experiment was completed, with factors used being the two narrow distribution polymers S102 and S111, both solvents, concentrations of 0.4 and 1.0%, and temperature differences across the annulus of 30 and 50°C. The PS responses showed an apparent strong positive molecular weight effect, but simple calculations demonstrated that this effect was completely attributable to the influence of solution viscosity on the convection velocities. Thus, there was no inherent molecular weight effect. Although the data of Figure 2 would suggest a large M–ΔT interaction, only a barely significant effect was found. The other PS responses were in accord with the PS data previously obtained with polymer B6.

In an effort to obtain a direct measure of the effect of molecular weight on PS, independent of hydrodynamic differences, equal portions by weight of polymers S102 and S111 were mixed, dissolved, and subjected to thermal diffusion in toluene at $\Delta T = 50$°C., $\bar{T} = 45$°C., and 1.0% concentration. There resulted no significant variation of intrinsic viscosity along the length of the column, and the PS obtained was exactly the average of PS's obtained separately for the two polymers (0.316 and 0.417).

CALCULATIONS

Data concerning PS for all three polymers in toluene were converted to equivalent γ and extrapolated to zero concentration. The thermal diffusion coefficient of each polymer was then computed from eqs. (4) and (6) by using literature data for the temperature dependence of η, ρ, and D and for the molecular weight dependence of D. The term expressing the temperature dependence of D' was omitted from eq. (6); computed values of D' therefore correspond approximately to the mean annular temperature. The D' for polymer B6 is some undefined average for the polydisperse sample. The results are presented in Table I (for $\Delta T = 50$°C., $\bar{T} = 45$°C.).

TABLE I
Analysis of Data at Infinite Dilution

Polymer	Wt.-av. mol. wt. M_w	Extinction coeff. γ, cm.$^{-1}$	$D \times 10^7$, cm.^{2} sec.$^{-1}$	$D' \times 10^7$, cm.^{2} sec.$^{-1}$ deg.$^{-1}$
S102	82,000	0.0090	7.5	1.07
S111	239,000	0.0093	3.9	0.95
B6	425,000	0.0098	2.8	0.90

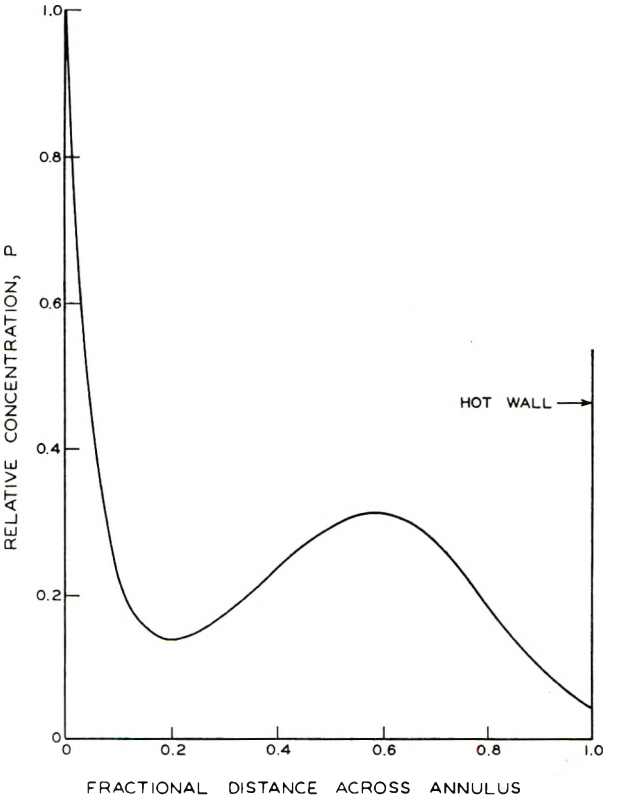

Fig. 4. Radial concentration function in column (polymer S111 in toluene, $\Delta T = 50°C.$, $\overline{T} = 45°C.$).

The radial concentration function P resulting from the computation for polymer S111 is shown in Figure 4 and is similar in shape to those for the other polymers.

To provide a more complete picture of how D and D' determine γ, the computations were extended to wider ranges of the variables. The results are plotted in Figure 5, where both transport coefficients have been assumed independent of temperature.

DISCUSSION OF THE FRACTIONATION EFFECT

The experimental values of the extinction coefficient (Table I) depended very slightly on molecular weight, being somewhat greater for the larger molecules, but the diffusion coefficient D varied significantly over the range studied. Therefore, D did not have a strong influence in determining γ. The relative constancy of D' (compared with D) suggests that D' determines the order of magnitude of γ. However, if D' alone determined γ, then the largest γ would correspond to the largest D', but the data contradict this. Therefore, the ordinary diffusion coefficient D must assume an important

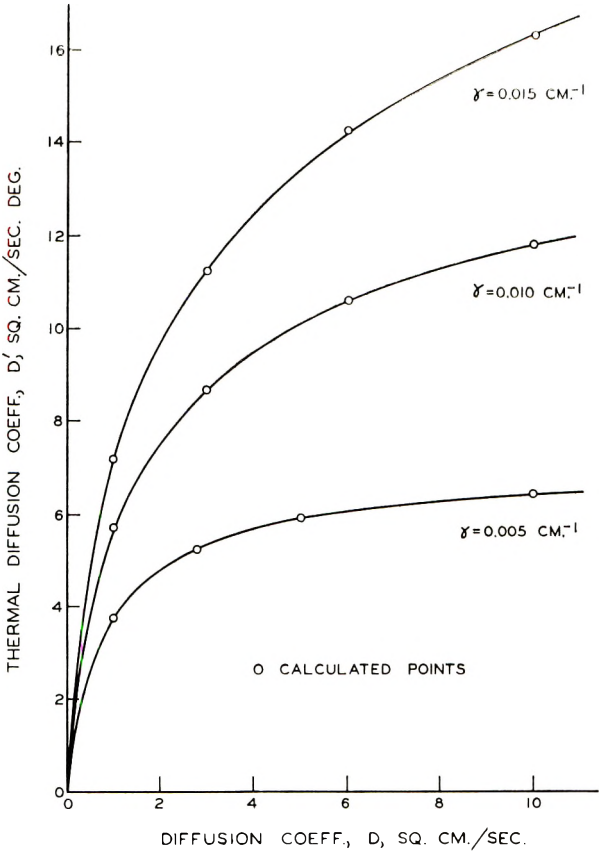

Fig. 5. Column operating characteristics.

secondary role in determining the relative values of γ for different molecular weights. Thus, in the range of molecular weight studied it appears that D' mainly determines the extent of polymer–solvent separation (PS) while differences in D govern the extent of the polymer–polymer fractionation effect (PP). According to the recent theory of Ham,[9] the thermal diffusion coefficient is not a strong function of molecular weight for sufficiently large molecules, and therefore any fractionation effect in a thermal diffusion column should be due primarily to differences in the ordinary diffusion coefficient; the larger molecules would have a greater rate of transport toward the cold wall because of their smaller tendency to diffuse back toward the lower concentrations near the hot wall. The results presented in Table I are therefore in qualitative agreement with Ham's theory.

If the fractionation effect is largely associated with differences in the ordinary diffusion coefficient, a more detailed view of the fractionation mechanism can be developed. Assume that D and D' are both independent of temperature and concentration and that only D is dependent on

molecular weight. Imagine a differential volume element across which exists a temperature gradient $dT/dr = \theta$ and a linear concentration gradient $-\alpha c/\alpha r$. No fractionation can occur as a polydisperse solute diffuses through this element because the rate of transport of each solute species is constant across the element. However, if $\alpha^2 c/\alpha r^2$ is nonzero, then a fractionation effect must occur if there are differences in D among the solute species. Thus, fractionation should occur to the greatest extent where d^2p/dr^2 (or $\alpha^2 c/\alpha r^2$) is greatest. The various concentration dependencies of polymer solutions will modify the above reasoning, but the general correlation of the large second derivative of P with regions producing a strong fractionation effect should be valid.

Examination of Figure 4 reveals that d^2P/dr^2 is several times greater in the region extending from the cold wall to the first zero value of dP/dr than anywhere else across the annulus. The major portion of the fractionation process should therefore occur near the cold wall.

A second item of interest in Figure 4 is the region between zero values of dP/dr, where the concentration gradient and the temperature gradient have the same sign. Any fractionation occurring in this region must be detrimental to the overall fractionation effect. The reversal of sign of dc/dr causes molecules with largest D to have the greatest net velocity toward the cold wall. Hence, a counterfractionation occurs in the central region.

A third observation concerning the fractionation effect is that at steady state conditions the total polymer concentration of any volume element is maintained constant by an exact balance of the three material fluxes through the element due to thermal diffusion, ordinary diffusion, and convection; therefore, it is to be expected that any change of conditions which increases the ratio of the ordinary diffusion flux to the thermal diffusion flux will tend to increase the fractionation effect.

Temperature Gradient Effect

As was shown in Figure 2, the degree of polymer–polymer fractionation (PP) increased markedly with temperature. If differences in the thermal diffusion coefficient were the main source of the fractionation effect, then changes in the temperature gradient should not affect PP to any great extent. This follows from either the Furry-Jones[12,13] or Debye[1] treatment of column operation, where it is shown that the separation factor (PS in the present terminology) of the individual solute species is independent of temperature gradient because the velocity of both the convective flow and the thermal diffusion flux are proportional to the temperature gradient. If, however, PP is governed by differences in the ordinary diffusion coefficient of the solute species, then the observed effect is readily explainable in the following manner.

An increased temperature gradient must cause an increase in the concentration gradient at the cold wall so that eq. (7) is satisfied. Physically, this means that the greater thermal diffusion flux caused by increased temperature gradient must be accompanied by an increased backward dif-

fusion at the wall because there can be no net flow of material through the wall. An increased temperature gradient does not significantly affect the symmetry of the velocity profile, and therefore the location of the first minimum in the radial concentration function (Fig. 4) will not be greatly altered. It follows that $\alpha^2c/\alpha r^2$ must increase in the region near the cold wall, and therefore the PP increases with increased temperature gradient.

Concentration Effect

The increase of PP with increased concentration of toluene solutions (Fig. 3) can also be interpreted in terms of the detailed mechanism of the fractionation process presented above.

The viscosity of polymer solutions increases rapidly with concentration, and therefore the velocity of the convection currents in a thermal diffusion experiment are smaller for higher initial concentrations. The maintenance of a steady-state concentration for any volume element then becomes more of a balance between thermal and ordinary diffusion because of the decreased importance of convective transport. Hence, the fractionation effect tends to increase because the ratio of ordinary diffusion flux to thermal diffusion flux is increased.

A decrease in the convective flow implies a decrease in the deviation of the radical concentration function (Fig. 4) from the smooth logarithmic relation which exists in the absence of any convection. As the convectionless state is approached, the counterfractionation zone described above must vanish and a further increase in PP will result.

An increased initial concentration will contribute to the increase in PP in the same manner as an increased temperature gradient. According to eq. (7) a higher concentration necessitates a larger $\alpha c/\alpha r$ at the walls which in turn leads to greater fractionation.

Increased concentration can adversely affect PP in at least two ways. First, the relative differences in the diffusion coefficients of various size molecules are reduced because of the strong concentration dependence of D for polymers. Second, increased concentration greatly magnifies the variation of solution viscosity across the annulus which in turn distorts the convection velocity profile in such a manner that the cold stream is broadened and the position of maximum downward velocity is shifted away from the cold wall.[13] The position where $\alpha c/\alpha r = 0$ will also be shifted away from the cold wall so that $\alpha^2c/\alpha r^2$ must be reduced in this region resulting in a reduced fractionation effect. Apparently, in the MEK system (Fig. 3) the concentration factors which tend to decrease PP approximately balance those which tend to increase PP so that PP for polystyrene in MEK is largely concentration independent.

The influence of a reduction in mean temperature in increasing PP is probably associated with increased solution viscosity and resultant diminution of convection velocities in parallel with the effects noted above for increased concentration.

Molecular Weight Effect

The data have suggested that fractionation occurs among the higher molecular weight species present in polymer B6 but not among the lower: (*a*) the interaction of molecular weight with temperature gradient in the factorial experiment was small even though the temperature gradient strongly influenced *PP* for the polydisperse polymer B6; (*b*) the molecular

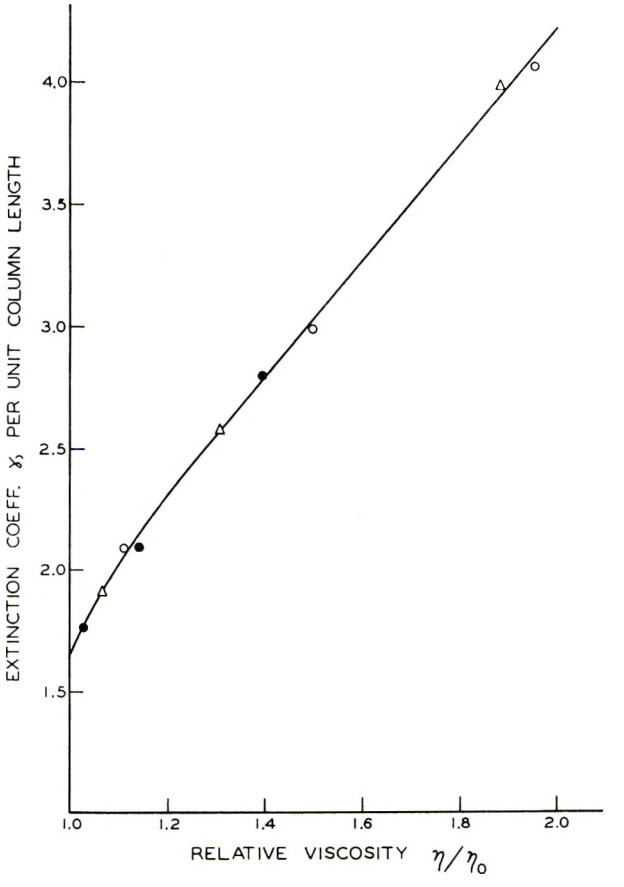

Fig. 6. Effect of solution viscosity on extinction coefficient (toluene solvent, ΔT = 50°C., $\overline{T}$ = 45°C.): (●) polymer S102; (△) polymer S111; (○) polymer B6, from smoothed *PS* data.

weight effect in the factorial experiment was small when differences in solution physical properties were eliminated; (*c*) no fractionation occurred when a mixture of polymers S102 and S111 was subjected to thermal diffusion. If there is no intrinsic molecular weight effect for the smaller polystyrene molecules (those included by polymers S102 and S111 and the lower half of the polymer B6 distribution), then differences in *PS* for the three polymers should be attributable to differences in solution viscosity

over the range studied. The data for the three polymers at identical temperature conditions are plotted in Figure 6 against the relative viscosity of the initial solutions. It is apparent that the equivalent extinction coefficient is independent of molecular weight for the range of molecular weight involved when hydrodynamic differences are removed.

According to Ham's theory, polymer thermal diffusion coefficients are not a strong function of molecular weight.[9] For polystyrene, D' should increase with molecular weights less than 300,000 and then should be relatively constant.[10] If such behavior of D' is superimposed upon the theoretical relations presented in Figure 5, the experimental results become quite plausible. For polystyrene, molecules larger than 300,000 molecular weight have diffusion coefficients of less than 2.5×10^{-7} cm.^{2}/sec. In this region it is seen that small changes of D for constant D' result in large differences of γ. In the region of higher D, the γ curves diverge and also become more nearly parallel to the D axis, differences in D or D' for smaller molecules therefore should not produce large differences in γ. The experimental results, the theoretical calculations, and Ham's theory are therefore in mutual agreement.

Drickamer's theory of polymer thermal diffusion[8] predicts that the thermal diffusion constant, $\alpha = D'T/D$, should be directly proportional to molecular weight. For the polystyrene–toluene system, D is proportional to $M^{-0.56}$ and therefore D' should be proportional to $M^{0.44}$ which is a much stronger relation than predicted by Ham's theory. The experimental results cannot be interpreted in terms of Drickamer's theory as well as in terms of Ham's theory.

The calculated thermal diffusion coefficients presented in Table I are of the same order of magnitude as the few data available in the literature.[10,14,15] A detailed comparison is not possible because of varying conditions of temperature and concentration. All literature values of D', given directly or calculated from values of α, fall in the range from 0.4×10^{-7} to 4.0×10^{-7} cm.^{2}/sec. deg. for the polystyrene–toluene system except for a few data of Whitmore.[16] The small decrease of D' with molecular weight indicated in Table I may not be significant; small experimental errors or temperature nonuniformities can have a strong effect on the calculated D'. Some literature data[14,16] indicate a small inverse dependence of D' on molecular weight in agreement with the present results. However, regardless of the accuracy of the calculations, it is clear that the data suggest D' is not strongly dependent on molecular weight.

The author wishes to thank Dr. R. W. Nelson for his generous assistance in the development of a mathematical description of the column operation and his guidance in the solution of the resulting equations.

References

1. Debye, P., and A. M. Bueche, in *High Polymer Physics*, H. A. Robinson, Ed., Remsen, New York, 1948, p. 497.
2. Kossler, I., and J. Krejsa, *J. Polymer Sci.*, **29**, 69 (1958).
3. Kossler, I., and M. Stolka, *J. Polymer Sci.*, **44**, 213 (1960).
4. Langhammer, G., *Svensk Kem. Tidskr.*, **69**, 328 (1957).
5. Langhammer, G., and H. Forster, *Z. Physik. Chem. (Frankfurt)*, **15**, 212 (1958).
6. Dougherty, E. L., and H. G. Drickamer, *J. Chem. Phys.*, **23**, 295 (1955).
7. Dougherty, E. L., and H. G. Drickamer, *J. Phys. Chem.*, **59**, 443 (1955).
8. Emery, A. H., and H. G. Drickamer, *J. Chem. Phys.*, **23**, 2252 (1955).
9. Ham, J. S., *J. Appl. Phys.*, **31**, 1853 (1960).
10. Herren, C. L., and J. S. Ham, *J. Chem. Phys.*, **35**, 1479 (1961).
11. McCormick, H. J., *J. Polymer Sci.*, **36**, 341 (1959).
12. Jones, R. C., and W. H. Furry, *Revs. Mod. Phys.*, **18**, 151 (1946).
13. Emery, A. H., Jr., *Ind. Eng. Chem.*, **51**, 651 (1959).
14. Hoffman, J. D., and B. H. Zimm, *J. Polymer Sci.*, **15**, 405 (1955).
15. Meyerhoff, V. G., H. Lutje, and B. Rauch, *Makromol. Chem.*, **14–16**, 489 (1961).
16. Whitmore, F. C., *J. Appl. Phys.*, **31**, 1858 (1960).

Résumé

Le mécanisme de fractionnement de polymères dans une colonne à diffusion thermique "Clusius-Dickel" a été élucidé par une étude systématique des effets d'importants facteurs expérimentaux sur les séparations possibles, combinée avec une description analytique du fonctionnement de la colonne et avec les récentes théories de la diffusion thermique des polymères. Plusieurs échantillons de polystyrène de distribution connue du poids moléculaire ont été étudiés dans le toluène et dans la méthyl-éthyl-cétone sous diverses conditions de gradient de température (jusqu'à 1050°C/cm), de température moyenne (20 à 45°C) et de concentration (jusqu'à 2,4% en poids). La colonne de diffusion thermique était du type cylindre concentrique équipée de trente échantillons. Le degré de séparation du polymère à partir de son solvant augmente avec les gradients de température en-dessous de 400°C/cm; il augmente légèrement avec la diminution de la température moyenne, et il augmente fortement avec la concentration de départ et à une concentration donnée, il était plus grand dans le toluène où on trouve que le degré de fractionnement augmente rapidement avec le gradient de température et est en grande partie indépendant de la concentration dans la méthyl-éthyl-cétone, mais augmente fortement avec la concentration dans des solutions de toluène. Ces effets ont été interprêtés à l'aide d'un calcul théorique de l'influence et de la diffusion ordinaire et de la diffusion thermique sur le comportement de la colonne en accord avec une évaluation des gradients radicaux de concentration. Les résultats expérimentaux sont en accord avec une théorie récente de la diffusion thermique des polymères qui prévoit que le coefficient de diffusion thermique ne serait pas une fonction stricte du poids moléculaire. L'effet de fractionnement est apparemment régi par des différences dans les coefficients ordinaires de diffusion. Le fractionnement est plus grand pour des poids moléculaires plus élevés.

Zusammenfassung

Der Mechanismus der Polymerfraktionierung in einer Thermodiffusionssäule nach Clusius-Dickel wurde durch eine systematische Untersuchung des Einflusses wichtiger Versuchsparameter auf die erreichbare Trennung in Kombination mit einer analytischen Beschreibung des Säulenbetriebes und neuerer Theorien der thermischen Polymerdiffusion aufgeklärt. Mehrere Polystyrolproben mit bekannter Molekulargewichtsverteilung wurden in Toluol- und Methyläthylketonlösung bei verschiedenem Temperaturgradienten (bis zu 1050°C/cm), verschiedener mittlerer Temperatur (20 bis 45°C) und Konzen-

tration (bis zu 2,4 Gewichts-%) untersucht. Die Thermodiffusionssäule war vom konzentrischen Zylinder-Typ und mit dreissig Probenöffnungen versehen. Der Trennungsgrad des Polymeren vom Lösungsmittel nahm unterhalb 400°C/cm mit dem Temperaturgradienten zu, verringerte sich etwas bei Herabsetzung der mittleren Temperatur, stieg mit der Ausgangskonzentration merklich an und war bei gegebener Konzentration in Toluol höher. Der Fraktionierungsgrad nahm mit dem Temperaturgradienten rasch zu und war in Methyläthylketon von der Konzentration weitgehend unabhängig, während in Toluollösung eine starke Zunahme mit der Konzentration auftrat. Diese Effekte konnten durch eine theoretische Berechnung des Einflusses der normalen und der Thermo-Diffusion auf das Verhalten in der Säule in Verbindung mit einer Ermittlung der radialen Konzentrationsgradienten gedeutet werden. Die Versuchsergebnisse sind mit einer neueren Theorie der Polymer-Thermodiffusion in Übereinstimmung, welche fordert, dass der Thermodiffusionskoeffizient nicht sehr stark vom Molekulargewicht abhängen sollte. Der Fraktionierungseffekt wird offenbar durch die Unterschiede der normalen Diffusionskoeffizienten bewirkt. Die Fraktionierung war bei höheren Molekulargewichten besser.

Received November 20, 1962

JOURNAL OF POLYMER SCIENCE: PART A VOL. 2, PP. 627–644 (1964)

Crystallographic Study of Xylan from Wood

MASAO HORIO and RIKIZO IMAMURA, *Department of Polymer Chemistry, Faculty of Engineering, Kyoto University, Kyoto, Japan*

Synopsis

Some preparations of xylan in the form of transparent membrane or amorphous powder prepared from deciduous woods such as beech and birch show a number of Debye-Scherrer rings at the irradiation with x-ray. Of special interest from the crystallographic standpoint is the diffraction pattern of the membrane, which shows an indication of a fiber diagram with the beam parallel to the surface, and this is more obvious when the membrane is stretched to an appropriate extent by rolling. The diagram can be neatly interpreted on the basis of an end surface-centered rhombic cell whose two axes of the base plane have exactly the ratio of $\sqrt{3}:1$, within the limit of experimental error. It is assumed that the cell has a trigonal or hexagonal symmetry. The observed reflections are indexed on the base of orthohexagonal unit cell, whose postulated three axes are a = 9.16 A., $b = \sqrt{3}a$., and c = 15.5 A. (fiber axis). The crystalline lattice of xylan is susceptible to mechanical treatment, heat, and moisture. The crystallinity depends greatly upon the uronic acid content. The diffraction pattern becomes less distinct and the interplanar spacings are enlarged with increasing uronic acid content, until at last the pattern diffuses into a single halo.

Introduction

Xylan is the general name given to the polysaccharides consisting mainly of xylose residues which are encountered most frequently in all the lignified plant cell walls next to the glucose residues which are main components of α-cellulose. Before entering into the discussion of the main theme a short survey of chemical aspects of xylan will be made in comparison with cellulose, for this is important to an interpretation of the crystalline nature of xylan.

As is generally accepted, the cellulose molecule consists of a number of β-glucopyranose residues, which are linked in head-to-tail relationship at 1 carbon atoms and 4, forming a long, threadlike macromolecule. This definition of cellulose, idealized as it may be, is on the whole applicable to the cell walls consisting almost entirely of cellulose, as is the case with cotton fibers. Each glucopyranose residue contains three free hydroxyl groups, which serve to line up the molecules in the bundles by hydrogen bonds into an organized structure consisting of regions having different degrees of order. Thus the molecules are in part so highly ordered as to display a fine crystallinity, as can be seen with cotton, ramie, and so forth.

It is more than thirty years ago that the molecule of xylan from esparto was expressed as a polysaccharide consisting of the 1–4′-linked β-xylo-

pyranose residues, in quite a similar manner to cellulose consisting of the 1–4′-linked β-glucopyranose residues.[1] However, the knowledge of hemicelluloses has made rapid strides during these ten years since the chromatographic technique opened up a new stage of chemical researches of sugars, and the structure of xylan has proved more complicated than was formerly presumed. It is true indeed that the main feature of xylan molecules is the 1–4′-linked β-xylopyranosidic chains, but the detailed features are diversely different according to the sources from which the sample was derived and the methods by which the sample was prepared. For instance, the chain of xylopyranose residues of esparto xylan is branched and a linkage of the 1–3′ type is found at the branch point.[2] The arabinose-rich fractions of the same xylan are considered to contain arabofuranose residues attached to the chain by the links of the 1–3′ type.[3] A similar relation is observed with the araboxylan from rye flour.[4] On the other hand, in some of other arabinose-rich xylans, L-arabofuranose residues are attached to the parent polysaccharides by the linkages of both 1–2′ and 1–3′ type.[5,6] The most important point revealed within these several years is that the xylans extracted from various species of woods contain in general an appreciable amount of 4-*O*-methyl-α-D-glucuronic acid residues.[7–10] Strong evidence that the uronic acid residues are directly combined with D-glucose by a 1–2′ link in the xylan macromolecule was provided by the isolation of a aldobiouronic acid which turned out to be 2-(4-*O*-methyl-α-D-glucuronopyranosyl)-D-xylose.[7]

In general, the xylose-base polymers in cell walls of various species of woods are thought to be 4-*O*-methylglucuronoxylan (predominantly hardwood) and 4-*O*-methylglucuronoaraboxylan (predominantly softwood).[9] The content of uronic acid residues differs widely, depending on the species of woods, and generally softwood xylan contains a greater amount of uronic acid than hardwood xylan.[11–13] Further, the content of nonxylosic residues depends greatly upon the chemical treatments to which the xylan has been subjected. It can be easily expected that the crystallinity of xylan might be largely affected by the side chains of 4-*O*-methyl-D-glucuronic acid and L-arabinose residues which are attached to the skeletal chains of xylopyranose residues.

A very close structural analogy between cellulose and xylan has long been emphasized, and the difference between them has been attributed mainly to the absence of —CH_2OH group from each xylopyranose residue. However, when the structural feature of xylan molecules is viewed in the way as mentioned above, its resemblance to cellulose has become less significant than it was formerly anticipated. Especially the bulky side groups such as uronic acid residues which are encountered so frequently along the xylosidic chains are unfavorable for making an ordered arrangement of xylan macromolecules. This may be the reason why there has been no evidence available to show that the xylan is crystallizable. However, following the numerous successful investigations made on the cellulose by the x-ray diffraction method, attention has long been drawn to the

crystallographic analysis of xylan, in order to authenticate the chemical aspect of its constitution in terms of the space pattern and to approach the problem of participation of xylan in cellulose structure, which is important in the field of wood chemistry and in connection with the practical problems of wood cellulose.

Hess and Lüdtke[14] prepared a sample of xylan-rich substance from sulfite pulp of spruce and subjected it to x-ray diffraction analysis. They obtained a pattern, which, however, consisted of a single diffuse halo, as is usually the case with liquid and many organic amorphous materials. According to Astbury, Preston, and Norman,[15] progressive removal of xylan from xylan-rich cellulose of Manilla hemp caused no fundamental change in x-ray diffraction pattern, which led them to the opinion that the incorporation of xylan would be a sort of mixed crystallization.

Yundt[16] succeeded in preparing the crystalline samples of xylan by modifying it through a series of operations involving hydrolysis and repeated autoclaving. The hemicellulose extracted from mature barley straw was selectively hydrolyzed by heating it in the presence of oxalic acid until the susceptible linkages had been hydrolyzed. The water paste of the hydrolyzed material was autoclaved at 120°C. for 3–5 hr., dissolved in alkali, precipitated by acetic acid, and then autoclaved again. Through these operations a fraction of the material was precipitated as fine particles whose uronic acid content was reduced as low as 0.4%. The precipitate was dissolved again in water in an autoclave at 120°C. On cooling to 60–70°C. the xylan crystallized as hexagonal platelets with rounded corners as was observed under an electron microscope. The experiment of Yundt is very important, in that it showed first the crystallinity of xylan, but, on the other hand, it provides an impression that xylan is by nature very hard to crystallize and that drastic modification, involving the elimination of uronic acid residues to an extreme limit and intense degradation of the main chains, is indispensable for obtaining the crystalline particles. Similar experiments to those of Yundt were done later by Bishop[17] and Roelofsen.[18] Of great interest is the recent work done by Marchessault et al.,[19] who succeeded in revealing the morphology of single crystals of esparto xylan by an improved technique and concluded that chain folding very likely occurs in these crystals.

In the course of our studies on wood hemicelluloses, it was found that the preparations of xylan in the form of homogeneous membrane showed very distinct x-ray diffraction patterns which consisted of a number of Debye-Scherrer rings. Of utmost interest is the fact that the diffraction pattern of membrane manifests an indication of fiber diagram, although not so complete, with the x-ray beam parallel to the membrane surface.

X-Ray Crystallographic Analysis of Xylan Membrane from Beech

The membrane obtained by evaporating an aqueous solution of beech and birch xylan manifests a number of Debye-Scherrer rings with x-ray beam perpendicular to the plane, which are approximately as sharp

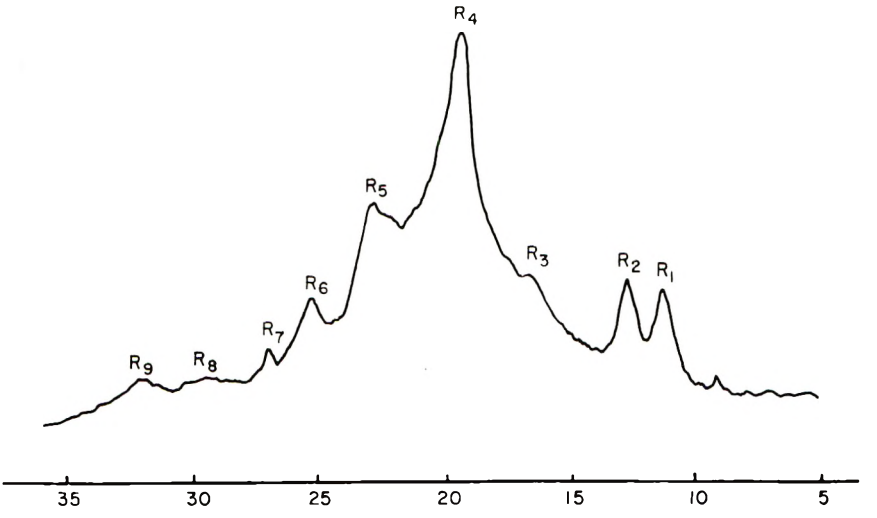

Fig. 1. Diffractometer trace of the x-ray diffraction pattern of xylan membrane prepared from beech.

as those of cellulose patterns of random orientation. The diffraction was measured by the photographic technique as well as a Geiger counter x-ray diffractometer. Figures 1 and 2 show respectively the diffractometer trace and the photograph of the diffraction pattern of membrane of beech xylan with x-ray beam perpendicular to the surface.

The samples of membrane were prepared as follows.[20] Xylan was extracted with caustic solution from the holocellulose of beech under hydrogen atmosphere to minimize the oxidative degradation, and the filtrate was neutralized with acetic acid, and the xylan was precipitated by adding methanol. The precipitate was washed several times with fresh methanol by decantation, centrifuged, and the methanol was replaced by ether. The ether-wet mass was dissolved in hot water, cooled, and subjected to elec-

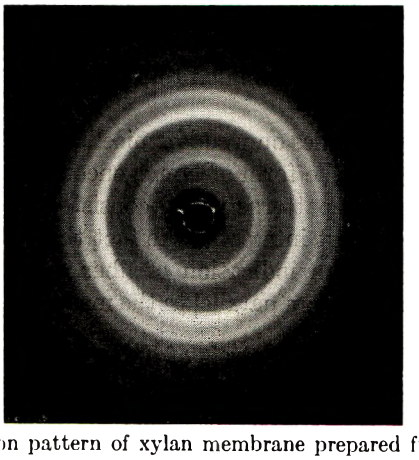

Fig. 2. X-ray diffraction pattern of xylan membrane prepared from beech with x-ray beam perpendicular to the surface.

trodialysis to remove the inorganic impurities. The purified solution was concentrated by heating on a hot water bath until the liquid became suitably viscous. The paste was spread on the surface of a clean glass plate, and water was evaporated further until a transparent dry film was formed. It is worth noticing that xylan becomes more resistant to water by drying, and this suggests that crystalline structure will be produced during the process of drying.

The purity of xylan from beech was estimated at 87–91%, while the uronic acid content was determined to be 3–5% by measurements of carbon dioxide evolution. Thus, the samples contain by far larger amount of uronic acid than the samples of Yundt used for examination of crystalline property. The DP of the sample was estimated at about 80 from the osmotic pressure measurements and shows the sample to be less degraded. If it is reckoned that the original DP of xylan immediately after precipitation is about 150 or greater, the sample may be regarded as considerably degraded, but it has a greater DP than any of the preparations of so-called crystalline xylan. In other words, the sample is less modified and more closely allied to the natural xylan than any of the samples which have been referred to as crystalline xylan.

The sample taking the form of membrane as in this case is macroscopically homogeneous, and there is no indication of crystals even under an optical and an electron microscope. The crystallinity of this sample is of the macromolecular nature like that of cellulose membranes and fibers, and differs from that of isolated crystalline particles of degraded polysaccharides. The x-ray diffraction of this sample must, therefore, be attributed to the micellar structure. This suggests the possibility that the xylan occurring in nature is more or less crystallizable depending on the degree of branching and amount of the side chains.

The linear character of xylan molecules in the samples as used here is evidenced by several properties of membranes. The xylan membrane has a considerable tensile strength in the dry state, which is comparable to that of commercial cellophane, and is of an order of magnitude characteristic of the materials consisting of linear high polymers. The Young's modulus in the dry state also is as large as about 6×10^{10} dynes/cm.^{2}, which is the value to be found ordinarily for the crystalline high polymers. Xylan is, however, more hygroscopic than cellulose, as can be seen in Table I. Another important evidence of linearity is a prominent birefringence which appears when the membrane is stretched, as is shown in Table II. The molecular constant of the viscosity formula is similar to that of cellulose and has the magnitude to be found for linear high polymers.[21] The light-scattering data of the xylan derivative in solution also suggest the stretched-out character of the molecule.[22]

The diffraction data of xylan film from beech are shown in Table III. The diffraction measured by us seems to be that of the hydrate according to Marchessault and Timell,[23] although the spacings are somewhat greater than those reported by them.

TABLE I
Xylan Membrane in Comparison to Cellulose Membrane

	Tensile strength at 65% R.H., kg./mm.^{2}	Elongation at 65% R.H., %	Young's modulus at 65% R.H., dynes/cm.^{2}	Moisture content, %	
				At 50% R.H.	At 78% R.H.
Xylan film	6.0	3.9	5.7×10^{10}	12.0	42.0
Cellophane	12.8	5.0	11.8×10^{10}	7.5	24.0

TABLE II
Birefringence of Xylan Membrane

Extension, %	Birefringence $\times 10^2$
0	0
0.96	1.21
2.90	1.38
3.80	1.40

TABLE III
X-Ray Diffraction of Xylan Membrane from Beech (Cu Kα, λ = 1.54 A.)

	By diffractometer			By photograph		
Reflection	Intensity[a]	Angle of diffraction	Interplanar spacing d, A.	Intensity[a]	Angle of diffraction	Interplanar spacing d, A.
R_1	s	11°12′	7.90	s	10°58′	8.06
R_2	s	12°36′	7.03	m	12°21′	7.15
R_3	w	16°30′	5.37	w	16°03′	5.51
R_4	vs	19°24′	4.58	vs	18°58′	4.67
R_5	m	22°36′	3.93	s	22°36′	3.93
R_6	w	25°18′	3.52	m	25°07′	3.54
R_7	w	27°00′	3.30	—	—	—
R_8	vw	29°09′–51′	3.06–2.99	w	29°05′	3.06
R_9	vw	32°00′	2.80	m	32°00′	2.80
R_{10}	—	—	—	vw	35°46′	2.51
R_{11}	—	—	—	vw	36°05′	2.49
R_{12}	—	—	—	vw	37°09′	2.42
R_{13}	—	—	—	vw	40°52′	2.21

[a] vs = very strong, s = strong, m = medium, w = weak, vw = very weak.

It is of interest to note here that the x-ray diffraction data of crystalline xylan from barley straw, which have been privately communicated from Dr. Yundt by his courtesy, coincide almost completely with our data obtained with xylan membrane from beech, as compared in Table IV.

Yundt's sample differs from ours in the point that, while the former is in the form of isolated crystalline particles consisting of short chain molecules, the latter is a homogeneous membrane. According to Marchessault et al.,[19] it is possible that the crystalline platelets of Yundt also are com-

TABLE IV
Comparison of Diffraction Data

	Xylan membrane from beech		Yundt's sample of xylan from barley straw[a]			
			By diffractometer		By photograph	
Reflection	Intensity	Interplanar spacing d, A.	Intensity	Interplanar spacing d, A.	Intensity	Interplanar spacing d, A.
R_1	s	7.90	s	7.85	s	7.87
R_2	s	7.03	s	7.04	s	7.03
R_3	w	5.37	—	—	vw	5.53
R_4	vs	4.58	vs	4.54	vs	4.54
R_5	m	3.93	m	3.90	m	3.84
R_6	w	3.52	m	3.52	m	3.50

[a] Private communication from Dr. Yundt.

posed of molecules which have their chain axes perpendicular to the plate and are folded over various times, depending on the extended length of the molecule and the thickness of the crystalline layer. Such an arrangement of molecules would not be impossible in the case of a membrane, but we want to deal with the problem, assuming that the xylan membrane has a similar structure to that of cellulose membrane, where the long chain molecules are extended and in part so well ordered as to display crystallinity while in others a more amorphous arrangement is found. At any rate, however, it is very interesting to note that the crystalline particles and the membrane of xylan show similar x-ray diffraction patterns.

When the membrane is irradiated with the x-ray beam parallel to the plane, the pattern exhibits the indication of fiber diagram, as can be seen in Figure 3, showing the sample to possess the tendency of the uniplanar orientation. In this regard, the xylan membrane shows a lower order of orientation than the cellulose membrane, which shows a higher order of

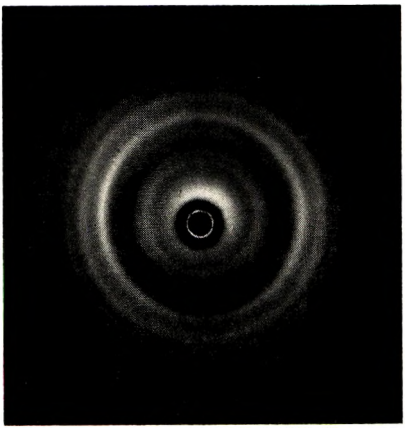

Fig. 3. X-ray diffraction pattern of xylan membrane prepared from beech with x-ray beam parallel to the surface.

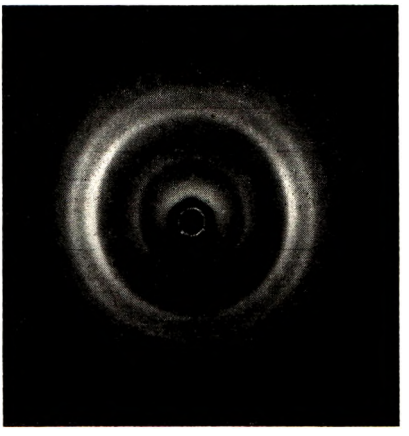

Fig. 4. X-ray diffraction pattern of the rolled membrane of xylan from beech with x-ray beam parallel to the surface and perpendicular to the rolling direction. Extension by rolling is 1.8 times.

orientation such as the selective uniplanar orientation. Next, a strip of a thin membrane was rolled carefully between a pair of similar rolls, both ends of the strip being kept free. This procedure was repeated until an adequate extension in the rolling direction was accomplished. Then the specimen comes to show a tendency for uniaxial orientation.

Figure 4 shows the diffraction pattern of the rolled membrane irradiated with x-ray beam parallel to the plane and perpendicular to the rolling direction. The overall extension of the membrane is 1.8 times in the direction of rolling. The pattern obtained with the beam perpendicular to the plane and to the direction of rolling is similar to this figure in the intensity relation of each interference.

A careful examination of the patterns as shown in Figures 3 and 4 reveals that the intensities of several reflections (R_1, R_4, R_5, and R_8) are not uniform throughout the entire circle, but are stronger at the equator and its vicinity, while the others (R_2, R_3, R_6, R_9, and R_{10}) seem to have greater intensities above and below the equator in symmetry. The intensity relation of each reflection is illustrated schematically in Figure 5.

The reflections (R_1, R_4, R_5, and R_8) which have the intensity maximum at the equator can be assumed to have resulted from the planes parallel to the fiber axis, while the reflections (R_2, R_3, R_6, R_9, and R_{10}) having different intensity relations may have resulted from the planes tilting to the fiber axis or perpendicular to it and might have exhibited layer lines if the orientation were more complete. Thus far, however, attempts to prepare a sample which possesses a higher degree of orientation have had no success.

An astonishing fact now is that the ratio of interplanar spacings of the strong reflections, namely $d_1:d_4$, is exactly equal to $\sqrt{3}:1$ within the limit of experimental error. Although this axial ratio can happen occasionally also for rhombic and monoclinic gratings, the most important point is that the diagrams can be neatly interpreted on the base of end surface-

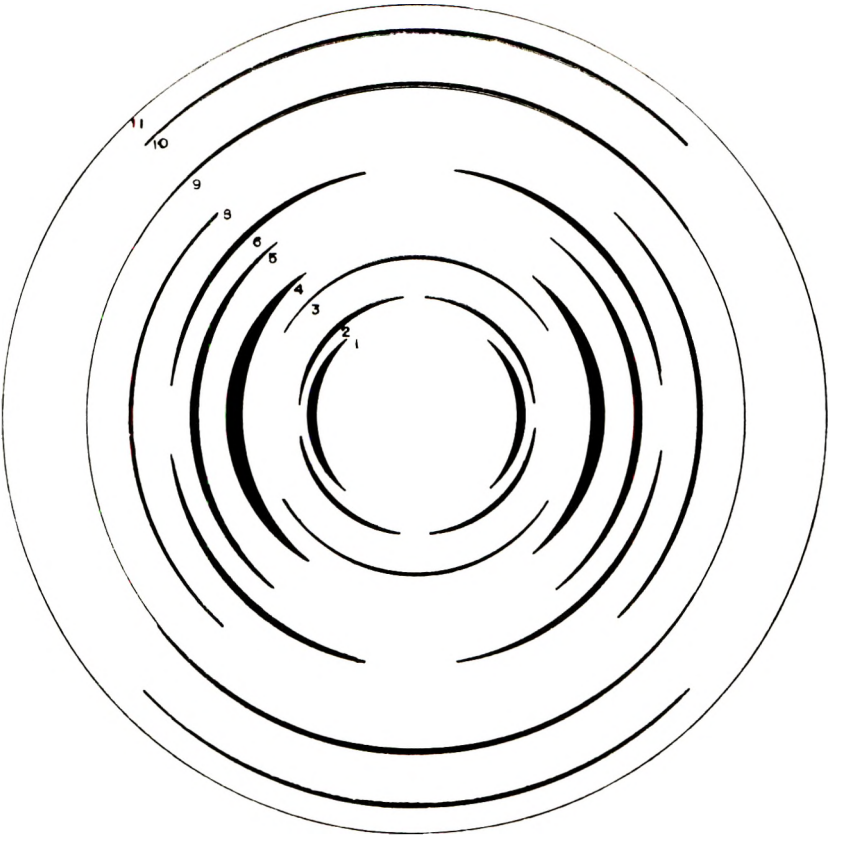

Fig. 5. Schematic representation of the diffraction pattern of xylan membrane with x-ray beam parallel to the surface under special consideration of intensity distribution.

centered rhombic cell whose two axes of the basis plane have exactly the ratio of $\sqrt{3}:1$. This is the relation characteristic to all the cells which have the trigonal or hexagonal symmetry. The ratio of interplanar distances producing the observed equator interferences can be represented by giving respective indices on the base of orthohexagonal cell as follows:

$$d_{1\,(110)}^{(020)} : d_{4\,(130)}^{(200)} : d_{5\,(220)}^{(040)} : d_{8\,(310)}^{(150)\,(240)} = \sqrt{3}:1:\sqrt{3}/2:\sqrt{3}/\sqrt{7}$$

As to the reflections having intensity maximum above and below the equator the following relation is important: the differences $1/d_2^2 - 1/d_1^2$ and $1/d_6^2 - 1/d_5^2$ are equal to 1^2 and 2^2 times 0.00416, respectively, which results in that the fiber period is 15.5 A., equal to three times the length of the pyranose residue. It is interesting, then, to note that the reflections R_3 and R_{10}, each of which has its own intensity maximum at the meridian, can be assigned to (003) and (006), respectively. If these assignments are correct, it is natural to postulate that the fiber axis is a trigonal screw axis.

The quadratic equation for the orthohexagonal cell is

$$1/d^2 = (h^2/a^2) + (k^2/3a^2) + (l^2/c^2)$$

TABLE V
Indices Based on the Orthohexagonal Cell, and Observed and Calculated Spacings of Beech Xylan Diagram

Reflection[a]	Intensity	Indices (orthohexagonal)	Interplanar spacings	
			Observed	Calculated
R_1 (A_1)	s	(020) (110)	7.90	7.93
R_4 (A_2)	vs	(200) (130)	4.58	4.58
R_5 (A_3)	m	(040) (220)	3.93	3.97
R_8 (A_4)	w	(150) (240) (310)	2.99–3.06	3.00
R_2 (I)	s	(021) (111)	7.03	7.07
R_6 (II)	w	(042) (222)	3.52	3.53
R_3 (III)	w	(003)	5.37	5.17
R_9 (IV)	vw	(224) (042)	2.80	2.77
R_{10} (VI)	vw	(006)	2.51	2.58

[a] R_7 is omitted, because it does not appear in the photograph and the intensity relation is unknown.

where a is determined to be 9.16 A. from the interplanar spacing of d_4, and c is 15.5 A. as mentioned above. Then, the quadratic equation can be expressed as follows:

$$1/d^2 = 0.01192h^2 + 0.00397k^2 + 0.00416l^2$$

The probable indices of reflections in the orthohexagonal cell and the values of interplanar spacings calculated from the quadratic equation as given above are shown in Table V in comparison with the values observed.

The volume of the hexagonal elementary cell is 1126 A.^{3}. The density of the xylan membrane measured by the substitution method with toluene as a medium is 1.48–1.52 g./cc. This is an average value covering those of crystalline and amorphous regions. Consequently, the density of the membrane can be smaller than that of the crystallite. In fact, the sample prepared according to the method of Yundt shows a higher density of 1.61 g./cc., although even this is not completely crystalline. By use of this value of density the number n of xylose residues in a unit cell is calculated to be

$$n = (1.61)\ (1126)/(132)\ (1.65) = 8.3$$

Taking a probable integer nearest to the above, we postulate that $n = 9$. Then the x-ray crystallographic density of xylan is

$$d = (9)\ (132)\ (1.65)/\ 1126 = 1.74$$

This value of density is about 12% greater than that of cellulose.

Figure 6 shows the projection of the hexagonal unit cell (hatched) on the base plane. The rectangle shows the base plane projection of the orthohexagonal cell.

As mentioned above, it has not been possible to prepare the sample fit to perform the crystallographic analysis of xylan with a greater certainty. Therefore, the analysis as presented here may be no more than a prelim-

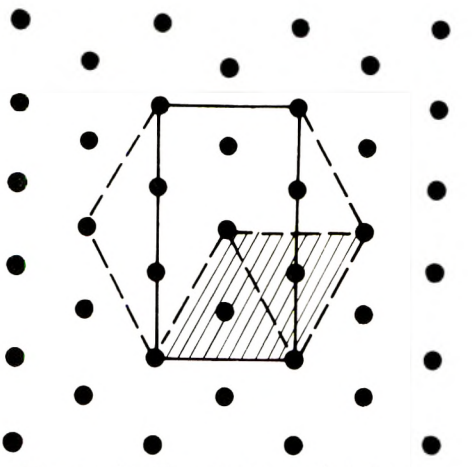

Fig. 6. Hexagonal lattice of xylan projected on the base.

inary attempt. However, it is interesting to mention here the crystallographic similarity of xylan crystals as analyzed above to those of several cellulose derivatives having the fiber period of 3 × 5.1 A., which were studied in detail by Gundermann.[24] According to him, five cellulose derivatives, including Cu-alkali-cellulose II and Na-Cellulose II can be nicely indexed on the base of the end surface-centered rhombic cell whose base plane axes have the ratio of $\sqrt{3}:1$. The crystals have threefold screw symmetry along the fiber axis. There is a surprising resemblance between the x-ray crystallographic data of xylan with those of the cellulose derivatives mentioned above. It is not certain for the present whether or not the resemblance is merely coincidental.

In recent years, a number of examples of polymorphism have been found in synthetic high polymers which show the triclinic or monoclinic structure when the interactions between the neighboring molecules, such as the interchain hydrogen bonds, exert an essential influence upon the crystal arrays, while the hexagonal packing is seen often when the formation of hydrogen bonds is inhibited. For instance, the normal triclinic packing of nylon 66 changes gradually into the hexagonal packing with rising temperature.[25] This transformation is related to the increasing molecular rotation with temperature, which hinders the molecules from forming hydrogen bonds. The hexagonal packing as observed here is, therefore, an intermediate between randomness and full crystalline state, and is usually unstable. This relation may be compared to the relation between cellulose and xylan. The formation of the stable monoclinic lattice of cellulose is due largely to the strong hydrogen bonds between polymer chains. On the other hand, the molecular cohesion of xylan is reckoned to be considerably smaller than that of cellulose, possibly due to the absence of the primary alcohol group which is the origin of hydrogen bond formation. This would result in an unstable lattice of hexagonal packing of xylan. In other words, the lattice of xylan has a degree of order which

is only by one step higher than complete randomness. This is related to the instability of the xylan crystal, which will be mentioned later. If this assumption holds, the cellulose derivatives as studied by Gundermann would have similar properties as xylan with respect to the interaction between neighboring molecules.

Susceptibility of Xylan Crystals

The crystalline lattice of xylan is very sensitive to mechanical treatments and liable to be destroyed. When a xylan membrane is rolled between a pair of rolls, it happens frequently that many minute cracks are produced in the lateral direction and the membrane becomes opaque. This takes place, for instance, when the pressure applied is too great or the membrane is extended too much. Such a cracked membrane no longer shows a distinct diffraction pattern, as shown in Figure 7, indicating that the crystalline arrangements of molecules are considerably disordered.

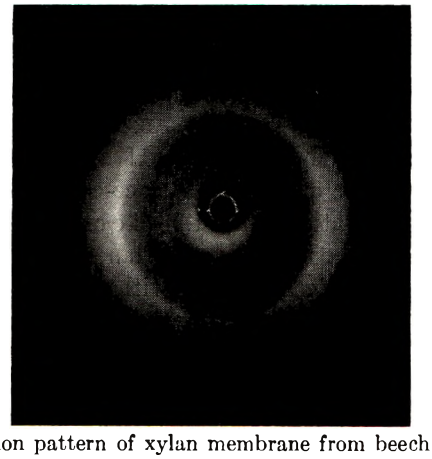

Fig. 7. X-ray diffraction pattern of xylan membrane from beech which was extended about 2 times the original length by rolling and has many minute cracks.

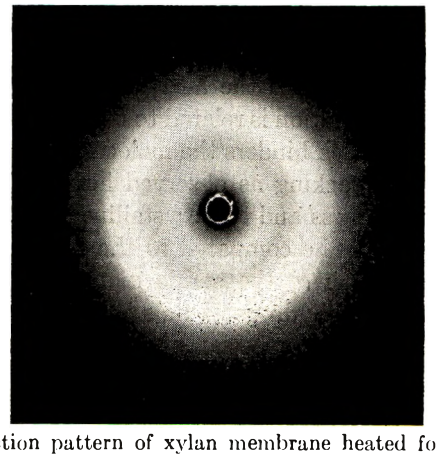

Fig. 8. X-ray diffraction pattern of xylan membrane heated for 2 hr. at 100°C. by immersing into hot glycerol.

Xylan is sensitive to water, as is proved by its marked hygroscopic character. Although the immersion of xylan in cold water does not give rise to the complete destruction of the crystalline structure, the interplanar spacings are enlarged to some extent.

The xylan crystals are susceptible also to heat. A sheet of xylan was heated at 100°C. by immersing it in hot glycerol, and the x-ray diffraction pattern was measured after various lengths of time of immersion. The diffraction pattern diffuses more and more with increasing time of heating. Figure 8 shows the diffraction pattern of xylan membrane immersed for 2 hr. in hot glycerol. It can be seen that the crystalline structure is considerably destroyed.

As explained at the beginning of this paper, the crystalline properties of xylan can be greatly affected by the chemical nature of molecules, such as the content of the side chains and degree of branching. The most important factor in the case of wood xylan is the content of uronic acid residues. Generally, softwood xylan contains a greater amount of uronic acid than hardwood xylan. While the molecular ratio of uronic acid residue to xylose residue of the beech xylan used in the experiments mentioned above is about 1:40, the xylan-rich sample prepared from pine contains by far greater amount of uronic acid, and the molecular ratio is 1:4.6.[20] This sample does not manifest Debye-Scherrer rings but a single blurred halo at x-ray irradiation. The band spreads from 18° to 22° in terms of the deflection angle. The diffuse band observed by Hess and Lüdtke[14] with a xylan sample obtained from sulfite pulp of spruce is supposed to be similar to ours, considering the coincidence of deflection angle. The interplanar spacing corresponding to these reflections results in 4–5 A., a distance which is usually associated with the average distance of closest approach of two neighboring molecules in most organic liquids and amorphous polymers.[26] This indicates that the xylan is hardly crystallizable when the molecules contain too many, up to a limit, uronic acid residues.

A similar effect can be seen also with the hardwood hemicellulose. When the holocellulose of beech is fractionated into α-, β-, and γ-cellulose according to the method widely used in industry, it is found that about 75% of γ-cellulose is xylan, and the molecular ratio of uronic acid residue to xylose residue in the sample is 1:13. This sample, similar to the pine xylan, does not display a crystalline pattern but only a single diffuse halo, as indicated by diffractometer trace *E* in Figure 9. It seems, therefore, that there is an allowable limit, if any, of the uronic acid content in xylan in order to accomplish the crystalline arrangements of molecules.

As mentioned before, the uronic acid content differs widely, depending on the chemical treatments to which the xylan has been subjected. While the γ-cellulose separated from the holocellulose of beech has the molecular ratio of 1:13, as indicated above, the xylan samples extracted from the sulfite and sulfate pulps which were prepared from the same wood have different molecular ratios: about 65% of the β-cellulose of sulfate pulp is xylan, and the molecular ratio of uronic acid to xylose is 1:30. As to the γ-cellulose of

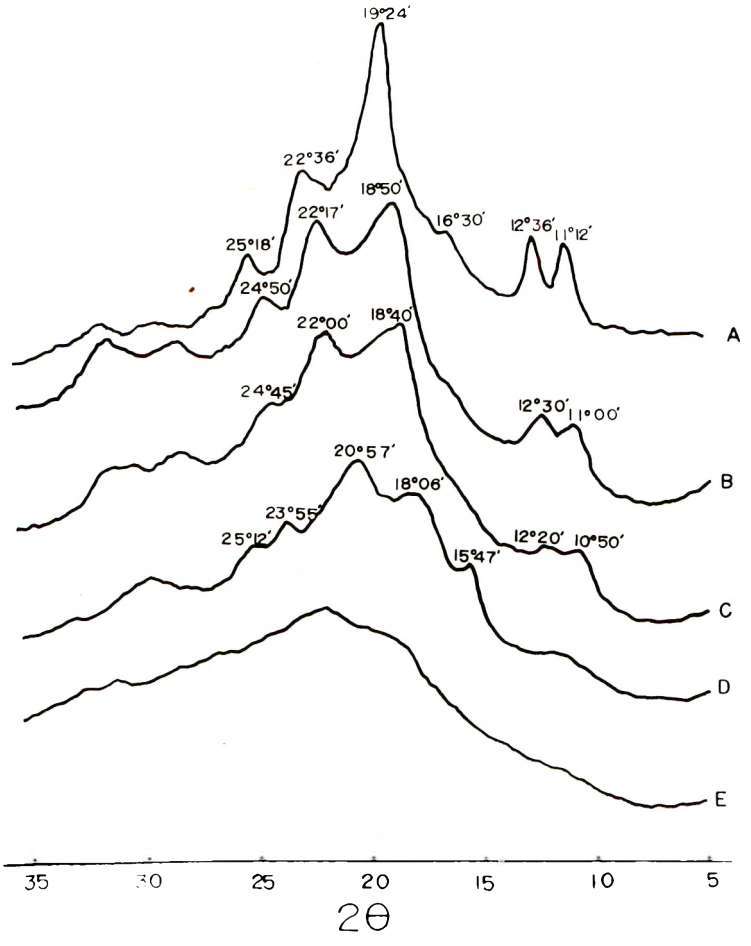

Fig. 9. Diffractometer traces of the x-ray diffraction patterns of various xylan samples originating from the same wood (beech) and differing in uronic acid content: (*A*) purified xylan membrane, uronic acid: xylose = 1:40; (*B*) β-cellulose of sulfate pulp of beech, uronic acid: xylose = 1:30; (*C*) γ-cellulose of the sulfate pulp of beech, uronic acid: xylose = 1:28; (*D*) γ-cellulose of the sulfite pulp of beech, uronic acid: xylose = 1:20; (*E*) γ-cellulose of the hollocellulose of beech, uronic acid: xylose = 1:13.

sulfate pulp, of which about 83% is xylan, the molecular ratio is 1:28. On the other hand, the γ-cellulose of sulfite pulp, of which about 73% is xylan, contains greater amount of uronic acid, and the molecular ratio of uronic acid to xylose is 1:20. In general, the xylan of sulfate pulp contains a smaller amount of uronic acid than that of sulfite pulp, in agreement with the observations of Hamilton et al.,[9] who concluded that during the kraft cook, the 4-*O*-methylglucuronoxylan undergoes a selective alkaline hydrolysis of 4-*O*-methylglucuronic acid from the xylan chain.

The x-ray diffraction patterns of this series of samples originating from the same wood specimen and differing in the uronic acid content are shown

TABLE VI
Dependence of Interplanar Spacings of Xylan upon Uronic Acid Content

Reflection	Interplanar spacing d, A.				
	Xylan membrane, mol. ratio 1:40	β-Cellulose of KP, mol. ratio 1:30	γ-Cellulose of KP, mol. ratio 1:28	γ-Cellulose of SP, mol. ratio 1:20	γ-Cellulose of holocellulose, mol. ratio 1:13
R_1	7.90	8.04	8.16	—	
R_2	7.03	7.08	7.17	—	blurred
R_4	4.58	4.70	4.75	4.90	single
R_5	3.93	3.99	4.04	4.24	halo
R_6	3.52	3.59	3.60	3.72	

in Table VI and Figure 9. It is interesting to note here that with increasing uronic acid content, the pattern becomes less distinct and the interplanar spacings are enlarged until at last the pattern diffuses into a single halo.

The samples of so-called crystalline xylan are characterized by small molecular weights, and generally their DP's are smaller than 50. This is due to the intense degradation of molecules which has taken place during the drastic treatments applied to the original xylan to make it crystallizable. It has been shown in this study that some preparations of xylan, which do not appear crystalline from the macroscopic point of view, as is the case with homogeneous membrane and amorphous powder, can be proved to be crystalline in the light of the x-ray diffraction analysis. This happens also frequently in the cases of many other high polymers. It is now interesting to know the effect of molecular weight upon the crystallinity of xylan, and inquire into the problem whether or not the natural xylan is crystallizable.

Xylan is degraded noticeably in its hot water solution. The degradation occurs very rapidly when the solution is acidic, even if very slightly.[27] As mentioned above, the DP's of the samples of xylan membrane are about 80 and about a half of the original DP. This reduction of DP is thought to have happened during the process of making the membrane by evaporating water from the solution by heating. The sample of xylan which was prepared without subjecting it to heating after precipitation has a greater DP. For instance, the powdery sample prepared as above from the holocellulose of beech has a DP of 132. Its uronic acid content is 8.24%, and the molecular ratio of uronic acid to xylose residue is 1:15. Another sample prepared as above from the wood meal of birch has a DP of 122, and a content of uronic acid of 7.90%. The molecular ratio is about the same as that of the beech xylan. These samples are considered to be modified only to a slight degree, if any, and may be very close to the natural xylan. It is interesting to note here that these samples show characteristic crystalline patterns of x-ray diffraction, as shown in Figures 10 and 11. Therefore, it is not unreasonable to assume that xylan *in vivo* would possibly exist in crystalline state in cell walls, when its uronic acid content is not too great, as is the case with the hardwood xylan.

Fig. 10. X-ray diffraction pattern of xylan from beech having DP of 132.

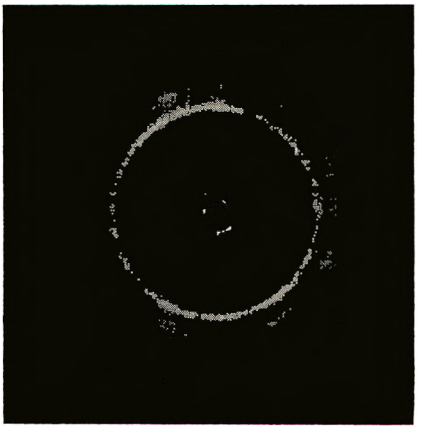

Fig. 11. X-ray diffraction pattern of xylan from birch having DP of 122.

Fig. 12. X-ray diffraction pattern of hemicellulose of sulfate pulp from beech.

Another evidence for the fact that the uronic acid content has a decisive influence upon the crystallinity of xylan is given by the kraft pulp xylan of beech, which, as shown in Figure 12, manifests the most distinct diffraction pattern among all that have been observed in this study. The purity of xylan of this sample is estimated at 98.6% from the amount of furfural produced, and the uronic acid content is smaller than the limiting value of accuracy of measurement by the carbon dioxide method, while the DP is as large as 135.

The authors wish to express their gratitude to Dr. A. P. Yundt for his private communication on the x-ray diffraction data of xylan from barley straw. Thanks are due to Mr. K. Nishida for his valuable help in the measurements of x-ray diffraction.

References

1. Hampton, H. A., W. N. Haworth, and E. L. Hirst, *J. Chem. Soc.*, **1929**, 1739.
2. Chanda, S. K., E. L. Hirst, J. K. N. Jones, and E. G. V. Percival, *J. Chem. Soc.*, **1950**, 1289.
3. Aspinall, G. O., E. L. Hirst, R. W. Moody, and E. G. V. Percival, *J. Chem. Soc.*, **1953**, 1631.
4. Aspinall, G. O., and R. J. Sturgeon, *J. Chem. Soc.*, **1957**, 4469.
5. Perlin, A. S., *Cereal Chem.*, **28**, 370, 382 (1951).
6. Montgomery, R., and F. Smith, *J. Am. Chem. Soc.*, **77**, 2834 (1955).
7. Jones, J. K. N., and L. E. Wise, *J. Chem. Soc.*, **1952**, 3389.
8. Aspinall, G. O., E. L. Hirst, and R. S. Mahomed, *J. Chem. Soc.*, **1954**, 1734.
9. Hamilton, K. J., E. V. Partlow, and N. S. Thompson, *Tappi*, **41**, 803, 811 (1958).
10. Mian, A. J., and T. E. Timell, *Tappi*, **43**, 775 (1960).
11. Aspinall, G. O., and M. E. Carter, *J. Chem. Soc.*, **1956**, 3744.
12. Timell, T. E., *Tappi*, **40**, 568 (1957).
13. Lindberg, A. B., *Svensk Papperstidn.*, **61**, 675 (1958).
14. Hess, K., and M. Lüdtke, *Ann. Chem.*, **466**, 18 (1928).
15. Astbury, W. T., R. D. Preston, and A. G. Norman, *Nature*, **136**, 391 (1935).
16. Yundt, A. P., *Tappi*, **34**, 89 (1951).
17. Bishop, C. T., *Can. J. Chem.*, **31**, 793 (1953).
18. Roelofsen, P. A., *Biochim. Biophys. Acta*, **13**, 592 (1954).
19. Marchessault, R. H., F. F. Morehead, N. M. Walter, C. P. J. Glaudemans, and T. E. Timell, *J. Polymer Sci.*, **51**, 866 (1961).
20. Horio, M., R. Imamura, and K. Tani, *Tappi*, **43**, 769 (1960).
21. Husemann, E., *J. Prakt. Chem.*, **155**, 13 (1940).
22. Horio, M., R. Imamura, and H. Inagaki, *Tappi*, **39**, 216 (1955).
23. Marchessault, R. H., and T. E. Timell, *J. Phys. Chem.*, **64**, 704 (1960).
24. Gundermann, J., *Z. Physik Chem.*, **B37**, 387 (1937).
25. Brill, R., *J. Prakt. Chem.*, **161**, 49 (1942).
26. Klug, H. P., and L. E. Alexander, *X-Ray Diffraction Procedures for Polycrystalline and Amorphous Materials*, Wiley, New York, 1954, p. 586.
27. Thompson, J. O., and L. E. Wise, *Tappi*, **35**, 331 (1952).

Résumé

Un certain nombre de préparations de xylane, préparés au départ de bois divers, tels de hêtre et de Bouleau montrent par irradiation aux rayons-X des diagrammes nettement cristallins. D'intérêt particulier du point de vue du cristallographe est la diffraction de la préparation sous forme de membranes, parce qu'elle manifeste par irradiation Röntgen perpendiculairement à la surface plus de dix anneaux de Debye-Scherrer, tandis

que l'irradiation parallèle à la membrane donne une sorte de diagramme de fibre, et encore plus clairement, lorsque la membrane est calendrée jusqu'à un degré bien déterminé. Étonnant est le fait que les diagrammes se laissent clairement ramener à une cellule élémentaire rhombique à face centrée; endéans la précision des mesures, un rapport déterminé des deux axes formant la base de la cellule s'élève à $\sqrt{3}:1$. On pourrait donc admettre que la cellule a une symétrie trigonale et hexagonale. Les réflexions observées ont été déduites sur la base d'une cellule orthohexagonale, dont les trois axe sont égaux à $a = 9.16$ Å, $b = \sqrt{3}\,a$ et $c = 15.5$ Å (axe de la fibre). Les réseaux cristallins du xylane sont sensibles à un traitement mécanique, la chaleur et l'humidité. La cristallinité du xylane dépend de la teneur en acide uronique, et en effet les diagrammes deviennent moins nets, et les distances entre les plans du réseau augmentent avec une teneur croissante en acide uronique, et les diagrammes se transforment finalement en un anneau élargi.

Zusammenfassung

Eine Anzahl von Xylan-Präparaten, die aus den Laubhölzern, wie z.B. Buche und Birke hergestellt worden sind, wiesen beim Bestrahlen mit Röntgenstrahlen die ausgeprägten kristallinen Beugungsdiagramme auf. Von besonderem Interesse von dem kristallographischen Standpunkt aus ist nun die Beugung des zu Membran geformten Präparates, weil es bei Röntgenbestrahlung senkrecht zur Ebene mehr als zehn Debye-Scherrer Ringe zeigt, während die Bestrahlung parallel zur Membran ein Anzeichen des Faserdiagrammes ergibt, und zwar noch deutlicher wenn die Membran bis zu einem angemessenen Grade ausgewalzt wird. Überraschend ist nun die Tatsache, dass die diagramme sich in sauberer Weise auf die basiszentrierte rhombische Elementarzelle zurückführen lassen, die innerhalb der Messgenauigkeit ein bestimmtes Verhältnis der beiden die Basis der Zelle bildenden Achsen von $\sqrt{3}:1$ besitzt. Demnach liegt die Annahme nahe, dass diese Zelle die trigonale oder hexagonale Symmetrie hat. Die beobachteten Reflexe sind auf Grund der orthohexagonalen Zelle induziert, deren drei Achsen werden wie folgt angenommen: $a = 9.16$ Å., $b = \sqrt{3}a$ und c = 15.5 Å. (Faserachse). Die Kristallgitter des Xylans sind empfindlich gegen die mechanischen Behandlungen, Wärme und Feuchtigkeit. Die Kristallinität des Xylans hängt beträchtlich von dem Uronsäuregehalt ab, und zwar werden die Diagramme weniger ausgeprägt und die Netzebenabstände vergrössert mit zunehmendem Uronsäuregehalt, um schliesslich die Beugungsdiagramme sich in einen verbreiteten Ring zu verwandeln.

Received November 20, 1962

JOURNAL OF POLYMER SCIENCE: PART A VOL. 2, PP. 645–668 (1964)

Estimation of Copolymer Reactivity Ratios: An Example of Nonlinear Estimation

D. W. BEHNKEN, *American Cyanamid Company, Central Research Division, Stamford, Connecticut*

Synopsis

The first portion of the paper consists of a brief statement of the statistical procedures involved in obtaining efficient estimates of parameters from experimental data, determining their precision, and selecting optimum experiments. Emphasis is primarily directed toward models in which the parameters appear in a nonlinear fashion. Some of the difficulties and pitfalls which are encountered are discussed; primary among these are the problems arising from linearization schemes and transformations affecting the error structure. References are given which supplement the necessarily cursory discussion given here. Utilizing this background, the second half applies itself to the problem of estimating the reactivity ratios in the copolymer equation. Approximate and exact estimation schemes are described which both guarantee most efficient use of the data and allow objective probabilistic statements to be made about the reliability of the estimates. A graph is presented which allows the experimenter to select the two initial feed ratios for his experiments which provide the most information for the estimation scheme. Use of the graph presumes that order of magnitude estimates of the reactivity ratios can be made in advance. A sequential scheme can be followed when prior information is lacking or is not very precise. When more than two different initial feed ratios are to be used, the optimum ratios for two-point experiments give a good indication of the proper range to cover.

1. INTRODUCTION

As experimental and theoretical work on a research project proceeds, a point is often reached where it becomes possible to represent the system under study by a mathematical model. While initially the model may be a completely empirical one, as insight improves a more mechanistic model may be developed that embodies the scientist's deeper understanding of the phenomenon under study. Such functions may be obtained, for example, as solutions of differential equations which describe the kinetics of a reaction. Before the model can be of use to predict and describe the mechanism however, it is usually necessary to run experiments which will provide the data necessary to estimate the unknown parameters in the expression. Both the estimation problem and its complement, the determination of the reliability of the estimate, will be discussed for the situation in which the parameters appear in a nonlinear form. Specifically, the problem of estimating the reactivity ratios in the copolymer equation will be treated

in some detail, including some contributions to the problem of choosing experiments to minimize the effect of experimental error on the reliability of the estimates.

Those primarily interested in the reactivity ratio problem will find it in section 4 and sequel. The estimation problem is discussed in section 4, and the design of experiments in section 5. An example illustrating the use of Figure 6, which provides the two-point design feed ratios, appears in section 5.2.

2. ESTIMATION OF PARAMETERS FROM DATA

When experimental data have been obtained, the question then arises of how they can best be used to estimate the parameters of interest. Two general classes of functions arise that must be considered separately for this purpose. In the first the parameters appear linearly in the function. That is, the function is of the form

$$\eta = \sum_{i=1}^{p} \theta_i x_i \tag{1}$$

where η is an observable response variable, $\theta_1, \theta_2, \ldots, \theta_p$ are the unknown parameters, and the x_i are independent variables or functions of independent variables, that can be controlled from experiment to experiment. The second general class effectively includes all other functions, since it is made up of those functions in which the parameters do not appear in a linear manner. Some simple examples of this class are

$$\eta = \theta_1 (1 - e^{-\theta_2 x}) \tag{2}$$

and

$$\eta = x \frac{(\theta_1 x + 1)}{\theta_2 + x} \tag{3}$$

A set of differential equations that can be solved numerically but which involve unknown parameters would also fall in this category.

Before distinguishing between these classes from the standpoint of statistical estimation it will be necessary to establish some notation. In making an experimental observation or measurement it is practically inevitable that we observe not the true value of η but a value $y = \eta + \epsilon$, where ϵ is a random experimental error. In a program of N experiments we will denote the observation obtained under one particular set of experimental conditions by y_u so that we can write

$$y_u = f(\mathbf{x}_u; \boldsymbol{\theta}) + \epsilon_u \qquad u = 1, 2, \ldots, N \tag{4}$$

where $f(\mathbf{x}_u; \boldsymbol{\theta})$ is any function of the k controllable variables set at levels $\mathbf{x}_u' = (x_{1u}\, x_{2u} \ldots x_{ku})$ and the p unknown parameters $\boldsymbol{\theta} = (\theta_1\, \theta_2 \ldots \theta_p)$. We assume for simplicity here that the errors in setting or determining the x values in the experimental procedures are either zero or negligible. The

program of N experiments can be represented by an $N \times k$ matrix $\mathbf{X}$ whose rows specify the experimental conditions, and a vector of observations $\mathbf{y}$, that is, by

$$\mathbf{X} = \begin{bmatrix} x_{11}\ x_{21} \cdots x_{k1} \\ x_{12}\ x_{22} \cdots x_{k2} \\ \cdots \\ x_{1u}\ x_{2u} \cdots x_{ku} \\ \cdots \\ x_{1N}\ x_{2N} \cdots x_{kN} \end{bmatrix}$$

and

$$\mathbf{Y} = \begin{bmatrix} y_1 \\ y_2 \\ \cdots \\ y_u \\ \cdots \\ y_N \end{bmatrix} \tag{5}$$

2.1. Linear Estimation

When the function $\eta = f(\mathbf{x};\boldsymbol{\theta})$ is linear in the parameters [equation (1)] and the random errors ϵ_u are independent with an expected value of zero and common variance σ^2, it was shown by Gauss in the early nineteenth century[1] that the least squares estimates of the parameters are the "best" linear unbiased estimators. This implies that the parameters will be estimated with minimum variance (maximum precision) and that the estimate will, on the average, equal the true value. The least squares estimates are obtained by selecting those values of $\boldsymbol{\theta}$ that minimize

$$S^2(\boldsymbol{\theta}) = \sum_{u=1}^{N} (y_u - f(\mathbf{x}_u;\boldsymbol{\theta}))^2 \tag{6}$$

where $S^2(\boldsymbol{\theta})$ is referred to as the residual sum of squares. By setting the derivatives of eq. (6) with respect to each θ_i equal to zero for these models, linear in the parameters, it can be shown that the least squares estimates are obtained explicitly by solving linear "normal equations,"

$$\mathbf{X}'\mathbf{X}\boldsymbol{\theta} = \mathbf{X}'\mathbf{y} \tag{7}$$

If the model can be assumed adequate an unbiased estimate of the experimental error variance, σ^2, is obtained from $s^2 = S^2(\hat{\boldsymbol{\theta}})/N\text{-}p$, where $S^2(\hat{\boldsymbol{\theta}})$ is the residual sum of squares at the least squares estimate $\hat{\boldsymbol{\theta}}$. The precision of thee stimates, as measured by the variances and covariances, are easily estimated from the inverse of the coefficient matrix of the normal equations $(X'X)$ and s^2, viz.,

$$\text{Estimate of } V(\hat{\boldsymbol{\theta}}) = [\mathbf{X}'\mathbf{X}]^{-1} s^2 \tag{8}$$

Since experimental errors are often the compound effect of a number of random influences that perturb the system under study, it follows from the

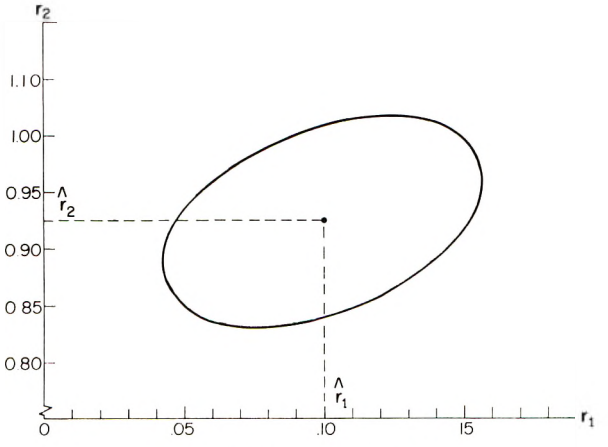

Fig. 1. 95% Confidence region.

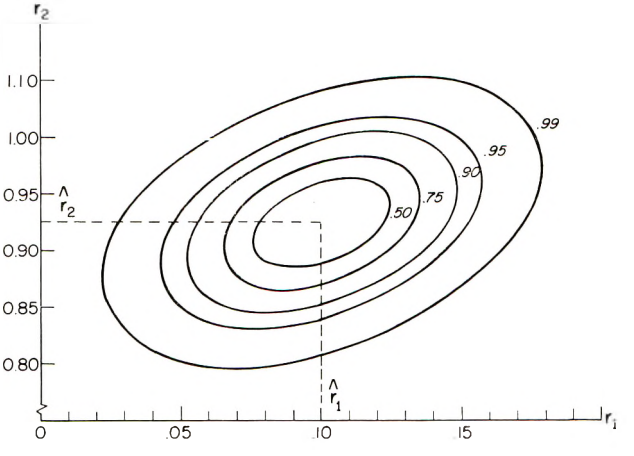

Fig. 2. Confidence regions.

central limit theorem of probability theory that the resultant errors tend to have a normal (Gaussian) distribution. If normality is assumed, quantitative probability statements about the precision of the estimates can be made in the form of confidence intervals, confidence regions, and likelihood functions. That is to say, once the least squares estimates $\hat{\theta}_1, \hat{\theta}_2, \ldots, \hat{\theta}_p$ are determined, a region bounded by an ellipsoid in p dimensions can be defined such that the probability of its including the actual parameter values $\theta_1, \theta_2, \ldots, \theta_p$ is any desired value α. The boundary of a region with confidence coefficient α in the space of the parameters is formed by the values of $\boldsymbol{\theta}$ that satisfy the equation

$$(\boldsymbol{\theta} - \hat{\boldsymbol{\theta}})'[\mathbf{X}'\mathbf{X}](\boldsymbol{\theta} - \hat{\boldsymbol{\theta}}) = ps^2 F_\alpha(p,\nu) \tag{9}$$

where s^2 is an independent estimate of the error variance σ^2 with ν degrees of freedom and $F_\alpha(p,\nu)$ is the α percentage point of the tabulated F dis-

tribution with p and ν degrees of freedom. Figure 1 shows a typical two-parameter example of a 95% confidence region. A more complete picture of the reliability of the estimate is obtained by showing several such contours to approximate the likelihood function which summarizes the information given by the sample about the parameters (Fig. 2). The smaller the experimental error and the better the experimental design, the smaller will be the size of this region of uncertainty. Since σ^2 is usually fixed, the importance of a good choice of experimental runs can be seen. For this linear situation, statisticians have the design problem well in hand and are able to provide the experimenter with efficient designs which will minimize the size of the confidence regions (or likelihood contours) for given fixed values of N and σ^2. For linear models in which the x_i's are all functionally independent and for which the design values are standardized so that

$$\sum_{u=1}^{N} x_{iu}^2 = C \qquad \text{all } i$$

(C is any constant), it has been shown,[2] for example, that the volume of the confidence region is minimized and the standard errors of the estimated parameters are minimized, if the columns of the $\mathbf{X}$ matrix are chosen to be orthogonal, i.e., for any two columns

$$\sum_{u=1}^{N} x_{iu}x_{ju} = 0 \qquad \text{all } i \neq j \qquad (10)$$

Factorial designs and their fractions are examples of orthogonal designs.

Marginal α-level confidence intervals for the individual θ_i's can also be obtained from

$$\theta_i \pm t_\alpha(\nu)s\sqrt{c_{ii}} \qquad (11)$$

where $t_\alpha(\nu)$ is the α percentage point of the two-tailed tabulation of the t-distribution and c_{ii} is the ith diagonal element of the $[\mathbf{X}'\mathbf{X}]^{-1}$ matrix. When the estimates are highly correlated, however, these intervals give an incomplete account of the reliability of the estimates.

2.2. Nonlinear Estimation

When the function is not linear in the parameters the least squares estimation procedure loses its great simplicity and the justification of the procedure on theoretical grounds is not so straightforward. On the latter point it will suffice to say here that as long as the errors can be assumed normally distributed least squares estimators coincide with a class of estimators called maximum likelihood estimators whose usefulness can be justified from several points of view. While the assumption of normality is rarely completely realistic, most of the useful statistical theory based upon it is not too sensitive to the small departures from exact normality we might often expect as a result of the central limit theorem.

Differentiation of the residual sum of squares function [eq. (6)] with respect to the parameters in the case of nonlinear models does not usually produce simultaneous equations of a tractable nature. To find the least squares values of the parameters which minimize this function an iterative scheme based on original guesses is required. It was shown by Gauss[1] that the solution can be approached in most cases by a series of linear approximations which will converge on the solution values. A number of numerical tricks have been added to the basic scheme, most of which are described and incorporated in the IBM 704 nonlinear estimation program listed as reference 3. The procedure basically consists of expanding the function in a Taylor's series about a set of first guesses for the parameters, $\boldsymbol{\theta} = \boldsymbol{\theta}^\circ$, dropping all but the linear terms as shown in eq. (12).

$$f(\mathbf{x}_u;\ \boldsymbol{\theta}) \approx f(\mathbf{x}_u;\ \theta^\circ) + \sum_{i=1}^{p} \left.\frac{\partial f(\mathbf{x}_u;\ \boldsymbol{\theta})}{\partial \theta_i}\right|_{\boldsymbol{\theta}=\boldsymbol{\theta}^\circ} (\theta_i - \theta_i{}^\circ) \tag{12}$$

If we then let

$$z_u{}^\circ = y_u - f(\mathbf{x}_u;\ \boldsymbol{\theta}^\circ)$$

and

$$x_{iu}{}^\circ = \left.\frac{\partial f(\mathbf{x}_u;\ \boldsymbol{\theta})}{\partial \theta_i}\right|_{\boldsymbol{\theta}=\boldsymbol{\theta}^\circ}$$

we have

$$z_u{}^\circ \approx \sum_{i=1}^{p} (\theta_i - \theta_i{}^\circ) x_{iu} \tag{13}$$

Considering the terms $(\theta_i - \theta_i{}^\circ) = h_i$ as p unknowns the problem is now reduced to that discussed under linear estimation [eq. (1)] and least squares estimates of the h_i values lead to improved guesses for the start of the next iteration from

$$\theta_i{}^{(1)} = \theta_i{}^\circ + h_i \tag{14}$$

The sequence is then repeated until the minimum of $S^2(\boldsymbol{\theta})$ is reached. Procedures discussed elsewhere[3,4] will take care of most cases of practical interest which frequently require some additional sophistication to ensure convergence. The method of steepest descents described by Marquardt[5] is often used initially to speed convergence.

Confidence regions for parameters estimated by nonlinear least squares can be given approximately by using linear theory if the errors can be assumed normally distributed. Two orders of approximation are available. The first and by far the simplest to obtain is based upon the matrix of partial derivatives of the function with respect to the parameters evaluated at the least squares estimates, $\hat{\boldsymbol{\theta}}$. That is, if we let $\mathbf{P}$ equal the $N \times p$ matrix with element f_{iu} in row u and column i where

$$f_{iu} = \left.\frac{\partial f(\mathbf{x}_u;\ \boldsymbol{\theta})}{\partial \theta_i}\right|_{\boldsymbol{\theta}=\hat{\boldsymbol{\theta}}} \tag{15}$$

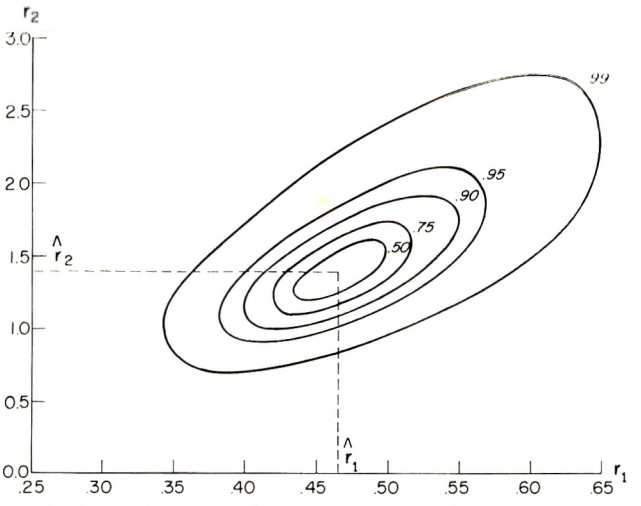

Fig. 3. Confidence regions based on sum of squares contours.

then, as in the linear case, the α confidence region is bounded by those values of $\boldsymbol{\theta}$ that satisfy the quadratic equation

$$(\boldsymbol{\theta} - \boldsymbol{\theta})'[\mathbf{P}'\mathbf{P}](\boldsymbol{\theta} - \hat{\boldsymbol{\theta}}) = ps^2F_\alpha(p,\nu) \tag{16}$$

Such confidence regions are called asymptotic regions and are exact for extremely large samples. For small samples they are equivalent to second-degree approximations, and their accuracy depends upon the degree of nonlinearity of the function. Ideally s^2 is an independent estimate of σ^2, the variance of the experimental errors, but if it can be safely assumed that the model is correct, s^2 can be obtained from the residual sum of squares, i.e.,

$$s^2 = S^2(\hat{\boldsymbol{\theta}})/N - p \tag{17}$$

Although this does not yield an independent estimate in the nonlinear case, it is adequate within the degree of approximation of the overall scheme.[6] Individual confidence intervals for each θ_i can be obtained from eq. (11) where c_{ii} is replaced by the diagonal element of $[\mathbf{P}'\mathbf{P}]^{-1}$.

The second procedure is more satisfactory in that the region is bounded by contours corresponding to those of the likelihood function. It is much more difficult to compute, however, in that we are required to find the locus of all parameter sets $(\theta_1,\theta_2, \ldots, \theta_p)$ that yield the same residual sum of squares. The α confidence region is that bounded by the contour for which

$$S^2(\boldsymbol{\theta}) = S^2(\hat{\boldsymbol{\theta}}) + ps^2F_\alpha(p,\nu) \tag{18}$$

These contours will not be exactly ellipsoidal, but in most practical cases they will not depart too markedly from it. The use of the residual sum of squares to estimate s^2 is again justified here when the function is sufficiently near-linear to insure validity of the whole procedure. A comprehensive discussion of the confidence region problem is given by Beale.[6]

A computer program can be written which will solve for enough coordinates of the contour to allow plotting. Examples of such regions are shown in Figure 3. The difficulty lies in graphing the results when there are more than three or four parameters. The same problem, of course, exists for the first scheme. A general feeling for the region, however, can be obtained by locating the coordinates of the extreme values of the contours. A discussion of such a procedure is given elsewhere.[3,4]

The problem of optimum experimental design for nonlinear functions is also much more involved. Each function must be considered separately so that no panacean design can be prescribed as can, for example, the factorial for models linear in both the parameters and the independent variables. A general formulation of the nonlinear design problem, with a few specific results for exponential models, has been given by Box and Lucas.[7] The approach taken there was to find designs which minimize the size (area or volume) of the asymptotic joint confidence region obtained from linear theory. The same criterion will be adopted here in finding designs for the estimation of reactivity ratios in the copolymer equation, the results of which will be described in some detail later. In most nonlinear designs obtained by this criterion the value of the unknown parameters themselves appear in the expressions for the design coordinates. We are thus in the awkward position of having to know the answer in order to estimate it efficiently. The mitigating feature, however, is that the experimenteres prior information usually allows him to determine "ball park" estimates and the sensitivity of the area or volume of the confidence region to modest departures from the actual parameter values may not be too great.

3. SOME DIFFICULTIES AND PITFALLS IN NONLINEAR ESTIMATION

When confronted with the problem of estimating nonlinear parameters the computational difficulties may be considerable, even when an electronic computer is available to do the arithmetic, and it is tempting to seek a transformation of the function which will "linearize" it. Before discussing the difficulties of nonlinear estimation, therefore, it might be useful to look briefly at the consequences of such linearizations.

We assume we are given a set of observations $y_u = \eta_u + \epsilon_u$ such that the errors (ϵ_u) can at least all be assumed independent samples from the same symmetric population with an expected value of zero. This is summarized by writing $E(\epsilon_u) = 0, V(\epsilon_u) = \sigma^2$, Cov $(\epsilon_u \epsilon_u') = 0$. The expected value of each y_u is then $\eta_u = f(\mathbf{x}_u;\boldsymbol{\theta})$ and each observation is equally reliable in its part in the estimation of the parameters. By using least squares, useful objective estimates are obtained and an approximation to the confidence region for the parameters can be constructed based on normal theory. Even graphical methods such as slope and intercept determinations give quite good estimates with this error structure when the model is linear in

the variables as well. If the model is transformed, however, the original error structure is usually transformed with it. Consider, for example, the function given previously as eq. (3)

$$\eta = \frac{x(\theta_1 x + 1)}{\theta_2 + x}$$

which can be made linear in the parameters by transforming to

$$x\left(\frac{\eta - 1}{\eta}\right) = -\theta_2 + \theta_1 \frac{x^2}{\eta} \tag{19}$$

the equation of a straight line with intercept $-\theta_2$ and slope θ_1 in the variables x^2/η and $x(\eta - 1)/\eta$. Substituting $\eta = y - \epsilon$ and letting $w = x(y - 1)/y$ and $v = x^2/y$, we have

$$w_u = -\theta_2 + \theta_1 v_u + e_u \tag{20}$$

where now

$$e_u = (\theta_2 + x_u)\epsilon_u / y_u \tag{21}$$

As long as the errors ϵ_u, are reasonably small compared to the expected values, η_u, a first approximation to the expected value and variance of e_u is given by

$$E(e_u) \approx -(\theta_2 + x_u)\frac{\sigma^2}{\eta_u^2} \tag{22}$$

and

$$V(e_u) \approx (\theta_2 + x_u)^2 \frac{\sigma^2}{\eta_u^2}\left(1 - \frac{\sigma^2}{\eta_u^2}\right)$$

The transformed errors no longer have an expected value of zero and their magnitude is now a function of x. Equally important, the error term is correlated with the independent variable v, now a random variable, so that the original error structure is replaced by something completely different and one which does not lend itself to simple analysis. Least squares is no longer a suitable estimation procedure and by analogy, graphical subjective schemes tend to suffer. These objections, of course, become less important when the coefficient of variation σ/η_u is small and when $V(e_u)$ is small relative to the change in η over the experimental region. In these experimental situations, however, the contribution of statistical procedures is minimized in any event.

While it is unwise to deal in any but the original measured variables when the error structure is as discussed above, exceptions of course exist. In situations in which the error variance is not constant from observation to observation, transformations can be used to alleviate this. For example, when the error standard deviation is proportional to the expected value, a log transformation will stabilize the variance and may at the same time be

useful in linearizing multiplicative exponential functions. Since a log transformation is essentially linear over short ranges, its use can sometimes be rationalized for the purpose of linearizing the function even when the error variance is constant. This last statement, of course, applies to most transformations over some "suitable range," but care should be taken before resorting to such techniques.

The difficulties encountered in nonlinear estimation itself can be divided into two classes. In the first it will be assumed that the error structure is as originally outlined at the start of section 3. In this case many of the problems fall in the category of numerical analysis. That is, given a certain function and a set of observations, the problem is one of devising a procedure which will converge rapidly on the values of the parameters which minimize the residual sum of squares. When the information contained in the data is not sufficient to allow the parameters to be estimated with some degree of independence, the sum of squares surface tends to become flat and ridgelike in some directions causing slow convergence. The equations to be solved at each iteration may become poorly conditioned and cause rounding errors to further complicate matters. Such situations may arise as a result of poor experimental design in which case supplementary data may cure the ill. In other cases such problems are inherent in the model and can only be alleviated to some degree by estimating less correlated functions of the parameters. Illustrations of this technique can be found in the IBM and Box publications,[3,4] Problems of multiple minima also arise and can only be coped with by seeking approximate methods which give good initial guesses or by starting the iteration procedure from several points.

Another problem that falls in the first category is one in which the dependent variable in the function cannot be solved for explicity. This commonly occurs where the function is a set of differential equations that cannot be integrated explicitly, but may also occur in the form of an implicit function. In any case, this presents no formal difficulty other than a numerical one, perhaps. For any guessed values of the parameters the differential equation can be integrated numerically or, in the case of the implicit function, the roots can be found by a scheme such as Newton's method and the resulting solutions subtracted from the observations to obtain the residuals necessary for the least squares procedure. A possible complication in the latter problem is the existence of multiple roots in the region of the observations. Here, and in fact for most nonlinear problems, good first guesses based on approximate methods tend to reduce difficulties. Numerical approximations to the partial derivatives of the non-explicit dependent variable with respect to the parameters, which are required in the iteration scheme [eq. (12)] are often necessary in these problems.

The second class of difficulties which will be touched upon here are those arising through the error structure. It is not infrequent that the scientist builds his models in terms of variables which are not directly measurable. For example, an equation may be expressible in terms of molar ratios but

in experimental work these are calculated from determinations of weight or weight fractions. Thus, although the analytical errors may be additive and of constant variance over the experimental range, the manufactured molar ratio will not be. This is then the reverse of the situation discussed at the start of this section, since it is now necessary to juggle the equation into a different form to achieve the proper error structure.

Examples of several of the difficulties mentioned above will be seen in the illustrative nonlinear estimation problem which follows.

4. ESTIMATION OF THE REACTIVITY RATIOS IN THE COPOLYMER EQUATION

The differential equation governing the relative rates of consumption of two monomers M_1 and M_2 under steady state conditions in a copolymerization reaction is

$$\frac{d[M_1]}{d[M_2]} = \frac{[M_1]\, r_1[M_1] + [M_2]}{[M_2]\, r_2[M_2] + [M_1]} \tag{23}$$

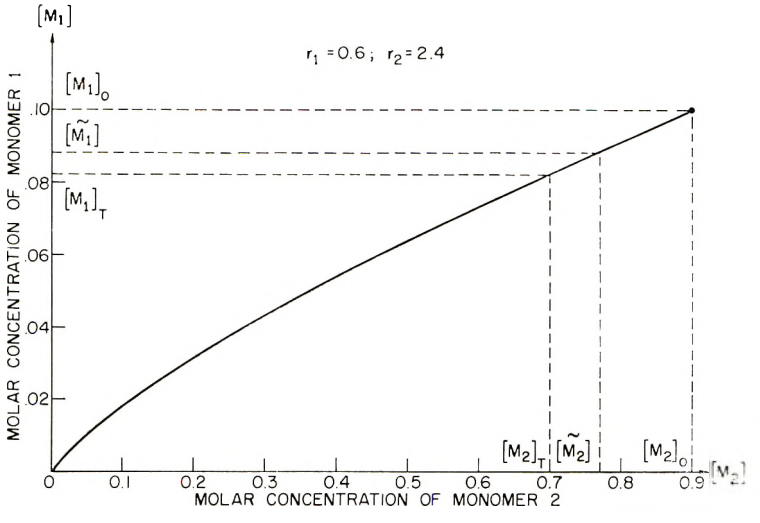

Fig. 4. Molar concentrations in feed during copolymerization.

where the square brackets indicate molar concentrations and the parameters r_1 and r_2 are called the reactivity ratios.[8] Given the initial conditions that $[M_1] = [M_1]_0$ when $[M_2] = [M_2]_0$, the solution of the differential equation determines a curve of the type shown in Figure 4. Since all monomer consumed appears in the copolymer, if the reaction is terminated at the point $[M_1]_T$, $[M_2]_T$ the molar ratio of M_1 to M_2 in the copolymer, denoted by m_1/m_2 is well approximated by

$$\frac{m_1}{m_2} \approx \frac{[M_1]_0 - [M_1]_T}{[M_2]_0 - [M_2]_T} = \frac{\Delta[M_1]}{\Delta[M_2]} = \frac{[\tilde{M}_1]\, r_1[\tilde{M}_1] + [\tilde{M}_2]}{[\tilde{M}_2]\, r_2[\tilde{M}_2] + [\tilde{M}_1]} \tag{24}$$

where the $[\bar{M}_i]$ are mean values lying somewhere in the interval $([M_i]_0, [M_i]_T)$. The degree of approximation depends only upon the volume change in the interval.

4.1. Approximate Estimation Procedure

When the reaction is terminated at low conversions, it is often assumed an adequate approximation for experimental purposes to substitute the initial feed molar concentrations in eq. (24) in place of the unknown mean values, giving the equation

$$\frac{m_1}{m_2} = \frac{[M_1]_0}{[M_2]_0} \cdot \frac{r_1[M_1]_0 + [M_2]_0}{r_2[M_2]_0 + [M_1]_0} \tag{25}$$

The approximation can usually be improved by substituting the average or midvalue $([M_i]_0 + [M_i]_T)/2$ instead of $[M_i]_0$.

In a series of experiments the copolymer molar ratio m_1/m_2 can be determined analytically for each of several initial molar concentrations providing data which, by using eq. (25), allow the reactivity ratios to be estimated.

If we let the ratio $m_1/m_2 = \eta$ and the molar ratio in the feed $[M_1]_0/[M_2]_0 = x$, it is readily seen that we have eq. (3) which was discussed in some detail earlier, i.e.,

$$\eta = x \frac{r_1 x + 1}{r_2 + x} \tag{26}$$

In the application to be considered here, however, the experimental determination of η is not perturbed by an additive random error with constant variance. If we erroneously assume that $y = \eta + \epsilon$ and proceed to estimate r_1 and r_2 by a nonlinear least squares technique minimizing

$$S^2(\mathbf{r}) = \sum_{u=1}^{N} \left(y_u - x_u \frac{\hat{r}_1 x_u + 1}{\hat{r}_2 + x_u} \right)^2 \tag{27}$$

we find that the estimates depart somewhat from what the experimenter's prior knowledge suggests. This was in fact done unwittingly and it was not until the experimenter's skepticism pointed out the discrepancy that the analytical procedure was looked at more carefully and the actual error structure determined. Experimentally the total weight of a sample of each copolymer was determined very precisely and the weight fraction of M_2 in the copolymer determined analytically with an additive error that could be assumed to have a constant variance, σ^2 and expected value of zero. Letting ζ denote the true weight fraction of M_2 in the copolymer and z its measured value we have

$$z = \zeta + \epsilon \tag{28}$$

so that the molar ratio of M_1 to M_2 in the copolymer is

$$\eta = \frac{(1 - \zeta)/\mu_1}{\zeta/\mu_2} \tag{29}$$

where μ_1 and μ_2 are the molecular weights of M_1 and M_2, respectively. When η is estimated by

$$y = \frac{\mu_2}{\mu_1}\left(\frac{1 - z}{z}\right) \tag{30}$$

it can be shown that for small σ/ζ

$$E(y_u) \approx \eta_u \tag{31}$$

but that

$$V(y_u) \approx \left(1 + \frac{\mu_1}{\mu_2}\eta_u\right)^4 \sigma^2 \tag{32}$$

so that the error variance is decidedly not constant since the experimental range of η_u can easily vary by a factor of ten.

Substituting eq. (29) in eq. (26) and solving for ζ we can write

$$z_u = \zeta_u + \epsilon_u = \frac{r_2 + x_u}{(r_2 + x_u) + (\mu_1/\mu_2)x_u(1 + r_1x_u)} + \epsilon_u \tag{33}$$

and a nonlinear least squares estimation scheme can now be used to fit this function to data z_u,x_u. Such a fit is shown in Figure 5 and the confidence regions or likelihood surface calculated from these data is that shown earlier

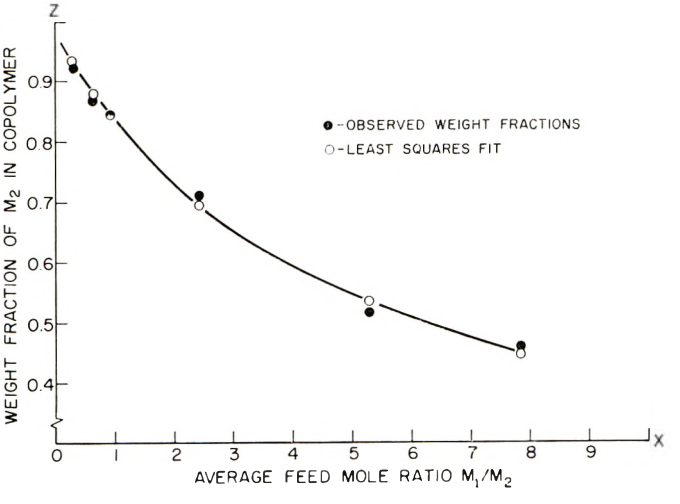

Fig. 5. Experimental data and least squares fit.

in Figure 3. It might be noted here that these contours are similar to those suggested without a probabilistic interpretation by Alfrey, Bohrer, and Mark.[8] They recognized that a means of obtaining more objective and meaningful estimates of the errors than those resulting from the subjective schemes of Mayo and Lewis[9] or Fineman and Ross[10] was needed.

4.2. Estimation Scheme Based on the Exact Solution of the Differential Equation

In the preceding section an approximation was used which related the copolymer composition to the instantaneous rate of monomer disappearance [eq. (25)]. While this should be an excellent approximation for very low conversions (or where the feed ratio changes very slowly) it may be experimentally more convenient at times not to terminate the reaction as quickly. In this case, or if it is felt that an exact expression is needed because of rapidly changing feed molar ratios, it is possible to use the solution of the differential equation itself, in the estimation scheme. The exact relationship between $[M_1]$ and $[M_2]$ at any point in the copolymerization is given by

$$\frac{[M_2]}{[M_2]_0}\left(\frac{[M_1]}{[M_1]_0}\right)^{-r_2}\left(\frac{1 - p[M_1]_0/[M_2]_0}{1 - p[M_1]/[M_2]}\right)^{-(1/p + r_2)} = 1 \qquad (34)$$

where $p = (1 - r_1)/(1 - r_2)$. Since $[M_1]/[M_2]$ cannot be solved for explicitly as a function of $[M_1]_0$, $[M_2]_0$, r_1 and r_2 it follows that we must work with an implicit function in the response variable ζ. Given a first guess for the reactivity ratios and the algebraic relationships between $m_1/m_2,\zeta$, the initial weights of M_1 and M_2 in the feed, the copolymer yield, the volume contraction ratio and the molar concentrations in the feed at the point the reaction was terminated, it is possible, by Newton's method say, to solve for the value of ζ that satisfies eq. (34). For the error structure to remain ideal it is assumed that all determinations except the measurement of ζ, will have negligible errors. The observed values of z are used as first guesses for the Newton iteration. Once ζ is found the residuals $(z_u - \zeta_u)$, $u = 1,2, \ldots, N$ are obtained for each copolymerization and their sum of squares minimized by the Gauss procedure to produce the least squares estimates of r_1 and r_2.

For several sets of experiments where the reaction was terminated after low conversions both computer programs were used to estimate r_1 and r_2. Agreement between the two procedures was good, the estimates varying only in the third or fourth digit. This then offers some confirmation that the simpler approximate scheme can be used with confidence in low conversion copolymerizations in which the feed ratio of $[M_1]$ to $[M_2]$ is not changing too rapidly. Confidence regions for the exact scheme are obtained in the same way as before although it is computationally more time-consuming.

5. EXPERIMENTAL DESIGNS FOR DETERMINING REACTIVITY RATIOS

As mentioned previously, the criterion to be used in selecting optimal experimental designs will be that of finding those initial feed ratios that minimize the area of the confidence region based on the least squares estimates. Since there are two approximate confidence regions, the question

arises as to which one to choose. While the region based on eq. (18) would be preferable, it is mathematically much more difficult to deal with so, for expediency, we choose to minimize the asymptotic confidence region [eq. (16)]. For parameter values of r_1 and r_2 not too close to zero we would expect the area of the elliptical approximation to vary roughly proportionally to the more exact likelihood contours. The design points minimizing one should therefore provide a good approximation to those minimizing the other. For those values of r_1 and r_2 for which the likelihood contours are badly unsymmetrical about the least squares estimate the agreement will not be as good but still should provide rough working estimates.

It was pointed out by Box and Lucas[7] that the area of the asymptotic confidence region is minimized if the determinant of the matrix $\mathbf{P'P}$ is maximized. In order to keep computation to a reasonable level it was decided that the minimum experimental design, that requiring only two different initial feed ratios, would be investigated first as an indication of the experimental range in feed ratios that should be covered. The fact that the optimum two-point (i.e., two-experiment) design can be found only by knowing the reactivity ratios in advance, requires, either reasonably good initial estimates of r_1 and r_2, or the use of a sequential procedure. Some discussion of the consequences of these two alternatives will be given in section 5.4.

5.1. Derivation of Optimum Two-Point Designs

The simplification gained by considering only two point experiments derives from the fact that $|\mathbf{P'P}| = |\mathbf{P}|^2$ and the criterion becomes one of maximizing the absolute value of $|\mathbf{P}|$. Since the initial feed molar ratios are not restricted in any real sense we seek the positive values, x_1 and x_2, which maximize the absolute value of

$$|\mathbf{P}| = \begin{vmatrix} \left.\dfrac{\partial f(x_1;\, r_1,r_2)}{\partial r_1}\right|_{\mathbf{r}=\hat{\mathbf{r}}} & \left.\dfrac{\partial f(x_1;\, r_1,r_2)}{\partial r_2}\right|_{\mathbf{r}=\hat{\mathbf{r}}} \\ \left.\dfrac{\partial f(x_2;\, r_1,r_2)}{\partial r_1}\right|_{\mathbf{r}=\hat{\mathbf{r}}} & \left.\dfrac{\partial f(x_2;\, r_1,r_2)}{\partial r_2}\right|_{\mathbf{r}=\hat{\mathbf{r}}} \end{vmatrix} \tag{35}$$

where $\mathbf{r} = (\hat{r}_1\ \hat{r}_2)$ are, in practice, guesses (or tentative estimates) of the actual values of the reactivity ratios. For the nonlinear function we use the approximation of eq. (33)

$$\zeta_u = f(x_u;\, r_1,r_2) = \frac{r_2 + x_u}{(r_2 + x_u) + (\mu_1/\mu_2)x_u(1 + r_1x_u)}$$

$$u = 1,2 \tag{36}$$

Although in what follows the x_1 and x_2 values are referred to as the initial feed molar ratios, they might equally well be considered as target "average values" during the reaction.

Differentiating eq. (36), substituting into eq. (35), and letting $C = \mu_1/\mu_2$ gives

$$|\mathbf{P}| = \frac{-C^2x_1x_2(x_1 - x_2)(r_2 + x_1 + x_2 + r_1x_1x_2)}{[r_2 + x_1 + Cx_1(1 + r_1x_1)]^2[r_2 + x_2 + Cx_2(1 + r_1x_2)]^2} \tag{37}$$

Thus, for practical design purposes it is necessary to find the x_1, x_2 values that maximize $||\mathbf{P}||$ for all $\mathbf{r} = \hat{\mathbf{r}}$ and C values. The solutions necessary are reduced by two factors, however. First, because of the symmetry of M_1 and M_2 we can always identify the monomer with the higher molecular weight as M_1 and hence need only find solutions for $C \geq 1$. Further, by making the substitutions in eq. (37), $u_i = x_i/r_2$ and $r_1r_2 = \theta$ it is seen that the resulting equation

$$|\mathbf{P}| = \frac{-C^2u_1u_2(u_1 - u_2)(1 + u_1 + u_2 + \theta u_1u_2)}{[1 + u_1 + Cu_1(1 + \theta u_1)]^2[1 + u_2 + Cu_2(1 + \theta u_2)]^2} \tag{38}$$

need only be solved for the range of values of the one additional parameter θ, since it is not a function of r_1 and r_2 independently. It was decided arbitrarily that designs would only be sought for copolymerizations in the range

$$0.02 \leq r_i \leq 50$$
$$0.2 \leq \mu_1/\mu_2 \leq 5 \tag{39}$$

with the added restriction that

$$\theta = r_1r_2 \leq 1$$

It was felt that most copolymerizations of interest would fall within this set. Thus by finding values of u_1 and u_2 maximizing eq. (38) for

$$0.0004 \leq \theta \leq 1$$
$$1 \leq C \leq 5$$

all optimum two-point designs for these copolymerizations could be found by then letting $x_1 = r_2u_1$ and $x_2 = r_2u_2$.

Determining the coordinates of the maximum of eq. (38) proved to be time consuming however. In order to provide a convenient representation of the design points therefore, a number of actual solution pairs were found for selected combinations of θ and C by using an electronic computer. Approximating polynomials were then fitted to these data and contours of constant u_1 and u_2 were plotted against θ and C over the range of interest (Fig. 6).

5.2. Example of Optimum Two-Point Design

To illustrate the use of the graphs in Figure 6 it will be supposed that an experimental copolymerization is to be carried out and that the experimenter's prior knowledge provides rough estimates of the reactivity ratios

$$\hat{r}_1 = 0.2$$
$$\hat{r}_2 = 2.0$$

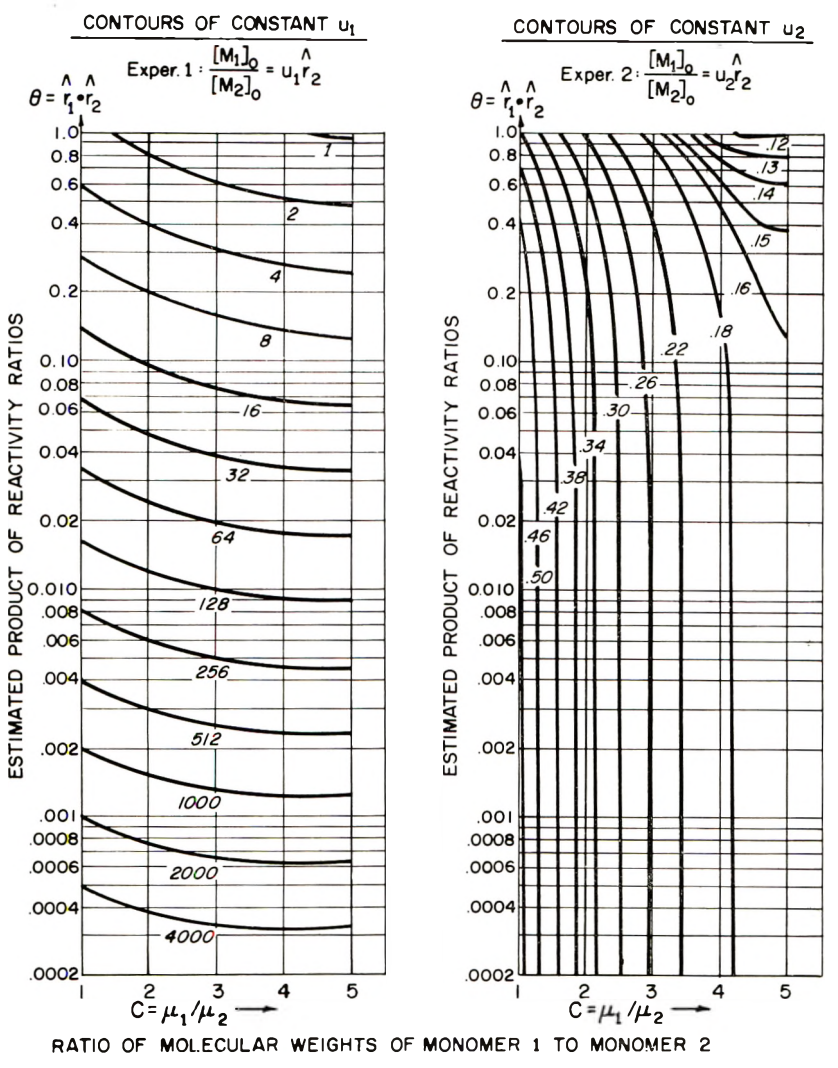

Fig. 6. Graphs for determining optimum feed molar ratios for two-point experiments.

In identifying M_1 and M_2, the monomer with the higher molecular weight is denoted by M_1 according to the convention adopted. In the example, it will be assumed that $\mu_1/\mu_2 = 5$. Entering the graphs with

$$\hat{\theta} = (0.2)(2.0) = 0.4$$

$$C = 5$$

we read approximately

$$u_1 = 2.4 \quad \text{or} \quad x_1 = 2(2.4) = 4.8$$

$$u_2 = 0.15 \quad \text{or} \quad x_2 = 2(0.15) = 0.30$$

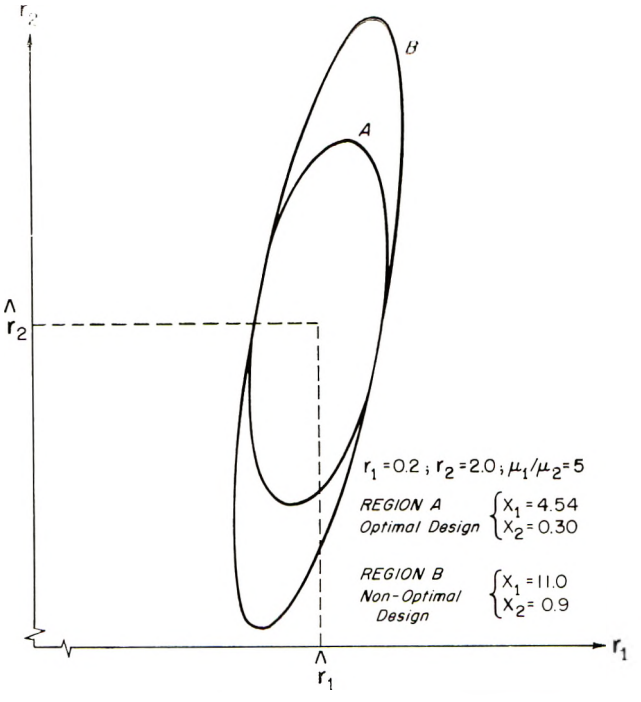

Fig. 7. Effect of nonoptimum design on size of confidence region.

Hence, the initial feed molar ratio of $[M_1]/[M_2]$ is 4.8 for experiment 1 and 0.30 for experiment 2. The exact solutions for these conditions are 4.54 and 0.296; the approximations obtained from the graphs will usually be better than that obtained here for u_1. While the use of log scales for θ and u_1 was convenient for graphing the function it makes visual interpolation a bit difficult. The following procedure is simple and gives adequate accuracy: (*a*) select the vertical line corresponding to $C = \mu_1/\mu_2$; (*b*) note the $\theta = r_1r_2$ coordinates of the contour intersecting this line above $\hat{\theta} = \hat{r}_1\hat{r}_2$, and denote this by θ_a; (*c*) if the contour above r_1r_2 on the vertical C line is called u_a then the interpolated value of u_1 corresponding to $\hat{r}_1 \cdot \hat{r}_2$ is

$$u_1 = (\theta_a/\hat{\theta}) \cdot u_a$$

Using the preceding example as an illustration we have: (*a*) use the vertical line $C = 5$; (*b*) $\hat{r}_1\hat{r}_2 = \hat{\theta} = 0.4$, hence $\theta_a = 0.48$ and $u_a = 2$; (*c*) $u_1 = (0.48/0.4) \times 2 = 2.4$. Visual interpolation for u_2 values will usually be satisfactory.

5.3. Effect of Nonoptimal Two-Point Designs on Confidence Regions

To gain some perspective on the actual effect of poor choices of initial ratios, the copolymerization of the preceding example was assumed to be carried out using initial ratios of $x_1 = 11.0$ and $x_2 = 0.9$ rather than the optimal values obtained in section 5.2. It can be seen from Figure 6 that

TABLE I
Sensitivity to Departures from Optimal Design

	Actual parameters		Optimal design			Non-optimal design			Ratio of confidence region areas
μ_1/μ_2	r_1	r_2	x_1	x_2	$\|\|P\|\|$	x_1	x_2	$\|\|\mathbf{P}\|\|$	
1	0.02	50	130.9	19.1	0.0179	50	10	0.0116	1.5
1	0.02	1	99.6	0.502	0.789	30	0.3	0.525	1.5
1	0.02	0.02	100.0	0.010	39.1	10	0.1	4.27	9.2
1	0.14	7.07	18.5	2.70	0.0179	8	0.125	0.0022	8.1
1	1	1	2.62	0.382	0.0179	5	0.2	0.0128	1.4
1	0.2	2.0	10.78	0.928	0.0436	8	0.125	0.0200	2.2
1	0.8	1.0	3.09	0.405	0.0223	4	0.25	0.0198	1.1
1	0.32	1.0	6.60	0.477	0.0542	8	0.30	0.0503	1.1
5	0.02	50	47.8	6.00	0.0128	50	10	0.0116	1.1
5	0.2	2.0	4.54	0.296	0.0273	6	0.1	0.0195	1.4

these are roughly the optimum design points for $r_1 = 0.2$, $r_2 = 2.0$, but $C = 1$ rather than 5. The effect on the confidence region is shown in Figure 7. The actual regions would be centered about the least squares estimates $\hat{r}_1$ and $\hat{r}_2$ and the scales would depend of course on the value of s^2 and its degrees of freedom. Since, however, the area of the ellipse is given by

$$A = \frac{\pi p s^2 F_\alpha(p,\nu)}{||\mathbf{P}'\mathbf{P}||^{1/2}} \tag{40}$$

the relative areas of any two confidence regions are easily obtained from

$$\frac{A_1}{A_2} = \frac{||\mathbf{P}_2'\mathbf{P}_2||^{1/2}}{||\mathbf{P}_1'\mathbf{P}_1||^{1/2}} \tag{41}$$

which, when $N = p$, becomes

$$\frac{A_1}{A_2} = \frac{||\mathbf{P}_2||}{||\mathbf{P}_1||}. \tag{42}$$

In the illustration given above the ratio of the two determinants is 0.027/0.016 = 1.7.

In Table I a few additional values of $||\mathbf{P}||$ have been listed to give some insight into the amount of precision that is lost by arbitrary departures from optimal designs. It can be seen from these results that small excursions from the optimal values do not cause excessive inflation of the confidence region. Therefore, if reasonably accurate first estimates are obtainable and designs are based on these estimates the resulting confidence regions may be expected to approach an acceptable size.

Additional information on the sensitivity of confidence regions to the design coordinates is obtained from Figures 8, 9, and 10. Contours of constant $||\mathbf{P}||$ have been plotted against the values of x_1 and x_2 for $r_1 = 0.2$, $r_2 = 2.0$ with $\mu_1/\mu_2 = 1$ and $\mu_1/\mu_2 = 5$ to indicate the change in the contours

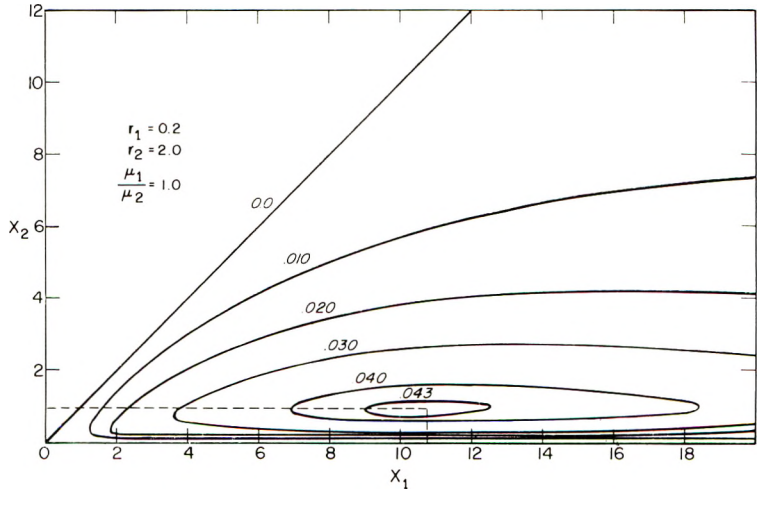

Fig. 8. Contours of constant $|P|$.

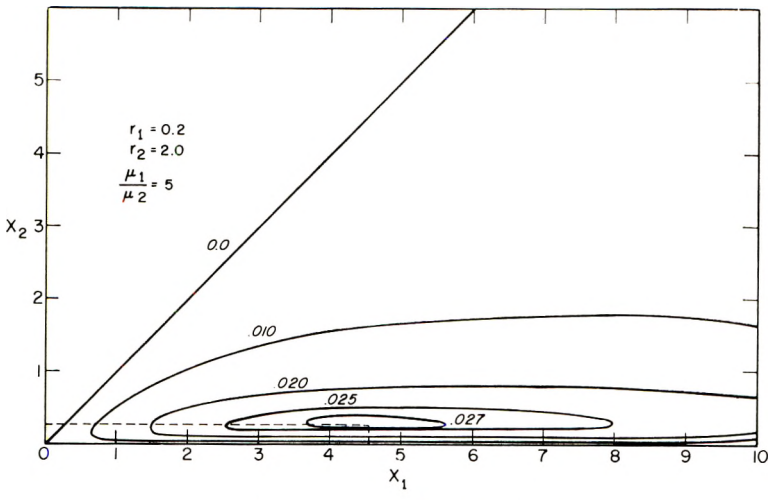

Fig. 9. Contours of constant $|P|$.

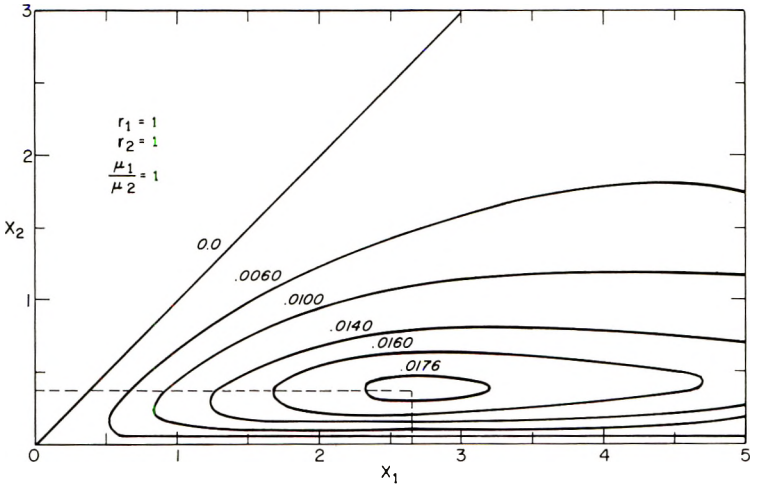

Fig. 10. Contours of constant $|P|$.

for **r** fixed and μ_1/μ_2 changing. The third plot considered with the first indicates the change in $||\mathbf{P}||$ for μ_1/μ_2 fixed at 1 and r_1 changing from 0.2 to 1 and r_2 from 2.0 to 1. The contours above the 45° line are not plotted because of the symmetry about this line.

5.4. Estimation of Reactivity Ratios from Two-Point Designs

While the approach of finding the best two-point designs was adopted initially as an expeditious way of gaining some insight into the design problem, it has proved to be, in fact, the path to optimum experimental designs. It has been demonstrated quite conclusively by computer investigations, that if N experiments are run to determine reactivity ratios, the maximum information is returned per experiment (as reflected in mini-

mized confidence regions) by running half (or approximately half if N is odd) of the points at each of the optimum two-point design levels. This is not surprising by analogy with linear estimation theory where, for example, it is well known that the slope and intercept of a straight line are estimated with maximum precision by choosing two points as far apart as possible and replicating these.

The difficulty which arises from having to know the values of the reactivity ratios before optimum experiments can be chosen to estimate them, are coped with in two ways. In the first we lean heavily on the initial estimates, while in the second, experiments are performed sequentially to provide a feedback of information for determining optimum designs.

5.4.1. Replicated Two-Point Designs

Should the experimenter's prior knowledge allow him to make reasonably dependable initial estimates, it follows from section 5.3 that an acceptable approach would be to run an equal number ($n = N/2$) of replicate experiments at each of the optimum two-point design levels (x_1 and x_2) called for by these initial estimates. Since the function fitted by least squares must pass through the arithmetic means of the two sets of weight fraction data (denoted by z_1 and z_2, respectively), the least squares estimates of the reactivity ratios are easily calculated from the equations

$$\hat{r}_1 = \frac{(\bar{z}_1 - 1)x_2[1 - \bar{z}_2(1 + C)] - (\bar{z}_2 - 1)x_1[1 - \bar{z}_1(1 + C)]}{C[(\bar{z}_1 - 1)\bar{z}_2x_2^2 - (\bar{z}_2 - 1)\bar{z}_1x_1^2]}$$

$$\hat{r}_2 = \frac{x_1\bar{z}_2x_2^2[1 - \bar{z}_1(1 + C)] - x_2\bar{z}_1x_1^2[1 - \bar{z}_2(1 + C)]}{[(\bar{z}_1 - 1)\bar{z}_2x_2^2 - (\bar{z}_2 - 1)\bar{z}_1x_1^2]} \tag{43}$$

The estimate of experimental error which is required in determining the confidence region is given by

$$s^2 = \frac{\sum_{u-1}^{n}(\bar{z}_{1u} - \bar{z}_1)^2 + \sum_{u-1}^{n}(\bar{z}_{2u} - \bar{z}_2)^2}{N - 2} \tag{44}$$

Since it is not usually known beforehand just how closely initial predictions compare with the actual parameter values, the sequential procedure described below is perhaps a better experimental strategy. The strength of the replicated two-point design, however, is its simplicity and the fact that it can be run in a shorter elapsed time.

5.4.2. Sequential Two-Point Designs

A sequential approach can be taken in using the two-point designs which will generally lead to a smaller confidence region for the same number of experiments. Using his experience the experimenter guesses r_1 and r_2, as before, and runs the indicated two experiments. From the resulting two

weight fractions, improved estimates are obtained [from eq. (43), putting $z_1 = z_1$ and $z_2 = z_2$] and the next pair of experiments determined which are optimum for the new tentative estimates. The cycle can then be repeated using all data available at each cycle to obtain improved estimates and then the best approximation to the next "optimum" experiment. Since different feed ratios result at each cycle, nonlinear estimation is required to obtain r_1,r_2 after the first cycle. When the confidence region is small enough to satisfy the experimenter's demands, the procedure is terminated. The better the experimenter's prior information the quicker this will be accomplished. In any event it will lead to a minimum of experimental effort being expended to obtain satisfactory estimates since, at each stage, current information is put to the most efficient use. The sequential nature of the design removes the prime objection to a strictly two-point design, namely, that it provides no check on the fit of the model. Since at each step a somewhat different pair of feed ratios is determined (although hopefully converging into two clusters), the general conformance of the data to the model can be checked. While in general the kinetics of this reaction are not in question, if further confirmation is required a last experiment at a point midway between the final optimum values x_1,x_2 would provide the necessary confirmatory data. Since $x_1 = [M_1]_0/[M_2]_4 =$ constant determines a straight line in the M_1, M_2 plane, a geometric sense of balance in the design is at least satisfied if the midvalue (x_3) is chosen to bisect the angle formed by x_1 and x_2. This is accomplished by taking

$$x_3 = \frac{(x_1x_2 - 1) \pm \sqrt{(x_1^2 + 1)(x_2^2 + 1)}}{x_1 + x_2} \tag{45}$$

the sign being chosen to make x_3 positive. Whenever x_1 and x_2 are reciprocals (i.e., when $C = 1$), $x_3 = 1$.

In summary then, the sequential scheme should provide an extremely efficient procedure for determining reactivity ratios since the tentative estimates of r_1,r_2 should quickly approach the region where $|\mathbf{P}|$ is more or less constant. The sequence of experiments run will therefore approach true optimum experiments which provide the most precise estimates of the reactivity ratios. A compromise between the two procedures could also be considered wherein replicates (perhaps an increasing number of replicates) could be run at each stage.

The author wishes to acknowledge the contribution of Dr. R. Rabinowitz in clarifying the problems of a chemical nature. He is also grateful to R. M. King and K. F. Kolb for useful discussions on the statistical and numerical aspects; to the latter and H. R. Sides for programming and computational assistance.

References

1. Gauss, K. F., *Theory of Least Squares* (Engl. transl. by Hale F. Trotter), Princeton University, S.T.R.G. Tech. Report No. 5, 1957.

2. Hotelling, H., *Ann. Math. Stat.*, **15**, 297 (1943).

3. *Non-Linear Estimation* (Princeton—IBM) 704 Program WLNLI, Math. and Applications Department, I.B.M. Corp., New York, 1959.

4. Box, G. E. P., *Ann. N. Y. Acad. Sci.*, **86**, 792 (1960).
5. Marquardt, D. W., *Chem. Eng. Progr.*, **55**, 65 (1959).
6. Beal, E. M. L., *J. Roy. Stat. Soc.*, **B22**, 41 (1960).
7. Box, G. E. P., and H. L. Lucas, *Biometrika*, **46**, 77 (1959).
8. Alfrey, T., Jr., J. J. Bohrer, and H. Mark, *Copolymerization*, High Polymers, V VIII, Interscience, New York–London, 1952, p. 23.
9. Mayo, F. R., and F. M. Lewis, *J. Am. Chem. Soc.*, **66**, 1594 (1944).
10. Fineman, M., and S. D. Ross, *J. Polymer Sci.*, 5, 259 (1950).

Résumé

La première moitié de l'article décrit brièvement les procédés statistiques intervenant dans l'estimation des paramèters à partir des données expérimentales, déterminant leur précision, et sélectionnant les expériences optimales. On peut d'abord insister sur les modèles dans lesquels les paramètres figurent d'une façon non-linéaire. Certaines difficultés et embûches recontrées sont discutées; parmi celles-ci les problemes provenant des schémas de linèarisation et les transformations affectant le structure des erreurs. Des références sont données qui peuvent suppléer à la discussion donnée ici. Utilisant ces données, la seconde moitié traîte le problème del' estimation des rapports de réactivité dans l'équation des copolymeres. Une estimation approximative et exacte des schémas est décrit, qui a la fois garantit un usage plus efficace des données, et permet de faire des rapports objectifs concernant la valeur des estimations. Un graphique est présenté, permettant à l'expérimentateur de sélectionner les deux rapports initiaux pour les expériences qui donneront le plus d'information pour l'estimation du schéma. L'usage du graphique prévoit que l'ordre et la grandeur des valeurs des rapports de réactivité pourrait être faits à l'avance. Un autre schéma peut etre suivi lorsqu'une primière information n'est pas fort précise. Lorsque plus de deux rapports initiaux différents sont utilisés, les rapports optima pour deux expériences donnent une bonne indication de l'ordre de grandeur.

Zusammenfassung

Der erste Teil der Arbeit enthält eine kurze Zusammenstellung der statistischen Verfahren zur Gewinnung verlässlicher Parameterwerte aus Versuchsdaten, die Bestimmung ihrer Genauigkeit und die Auswahl der optimalen Versuche. Primär werden Modelle betrachtet, in welchen die Parameter in nicht-linearen Beziehungen auftreten. Einige der auftretenden Schwierigkeiten und Fehlermöglichkeiten werden diskutiert; die wichtigsten darunter aind die sich aus dem Linearisierungsschema ergebenden Probleme und die Transformationen, welche die Fehlerstruktur beeinflussen. Literaturhinweise zur Vervollständigung der notwendigerweise kursorischen Diskussion werden gegeben. Auf dieser Grundlage wird im zweiten Teil das Problem der Bestimmung von Reaktivitätsverhältnissen in der Copolymergleichung behandelt. Näherungs- and strenge Bestimmungsschemata werden beschrieben, die die rationellste Auswertung der Daten garantieren und die Angabe objektiver Wahrscheinlichkeitsfestsellungen über die Verlässlichkeit der Bestimmungen gestatten. Es wird ein Diagramm angegeben, das es dem Experimentator ermöglicht, diejenigen beiden Ausgangszusammensetzungen für die Monomerenmischung auszuwählen, welche die grösstmögliche Information für das Bestimmungsschema liefern. Ein Gebrauch des Diagramms setzt voraus, dass von vorneherein die Grössenordnung der Reaktivitätsverhältnisse abgeschätzt werden kann. Bei Fehlen order mangelnder Genauigkeit einer solchen Möglichkeit kann ein Sequenzenschema herangezogen werden. Wenn mehr als zwei verschiedene Ausgangszusammensetzungen verwendet werden müssen, geben die optimalen Verhältnisse für die Zweipunkt-Versuche einen guten Hinweis auf den zu verwendenden Bereich.

Received November 29, 1962

JOURNAL OF POLYMER SCIENCE: PART A VOL. 2, PP. 669–678 (1964)

Infrared Studies of Conformational Changes in Polyvinyl Chloride

S. KRIMM and S. ENOMOTO,* *Harrison M. Randall Laboratory of Physics, University of Michigan, Ann Arbor, Michigan*

Synopsis

Analysis of the infrared spectrum of polyvinyl chloride has permitted the identification, from the frequencies of the several C—Cl stretching bands, of the chain conformations which are associated with particular chlorine pair configurations. These results have made it possible to establish that changes in conformational structure accompany certain changes in physical state of the polymer. Possible interpretations of the origins of these structural changes are considered.

Introduction

The configuration of a polymer chain is an important factor in determining its spatial structure, or conformation, and thereby is significantly correlated with the physical properties of the polymer. Methods for determining chain configuration and conformation are therefore of importance in helping to understand the physical behavior of macromolecules. Infrared spectra should be suited in many cases to such determinations, and several attempts have been made to apply this technique to high polymers. They have usually suffered, however, from ambiguities in spectral interpretation to a greater or lesser degree, and this has affected their utility. It has recently been possible[1] to make what appears to be a secure assignment of certain bands in the spectrum of polyvinyl chloride (PVC), $(CH_2CHCl)_n$, to particular configurations and conformations in the chain. We have observed that this assignment permits an evaluation to be made of changes in conformation which we find to result from certain variations in physical state. While polyvinyl chloride may be an especially favorable case in this respect, these results are nevertheless of interest in showing the kinds of spectral effects which are likely to occur and in demonstrating experimentally the nature of conformational changes in macromolecules which are associated with particular physical changes.

Infrared Determination of Configuration and Conformation

The basis for the infrared method of determining chain configuration and conformation in polyvinyl chloride is the sensitivity of the C—Cl stretch-

* Present address: Kureha Chemical Industry Co., Tokyo Laboratory, Hyakunin-cho, Shinjuku-ku, Tokyo, Japan.

ing frequency, ν(C—Cl), to the rotationally isomeric structure in the vicinity of this bond.[2,3] A detailed study of a series of secondary alkyl chlorides[3] has shown that the ν(C—Cl) frequency depends in particular on the substituents which are *trans* to the Cl atom across both adjacent C—C bonds. For example, for 2-chloropropane, in which both substituents *trans* to the Cl atom must be H, the ν(C—Cl) frequency is located at 611 cm.$^{-1}$. In a series of compounds this mode, designated as S_{HH}, was found in the range of 608–615 cm.$^{-1}$. For 2,2-dimethyl-3-chlorobutane, in which one *trans* substituent is always C and the other is always H, the ν(C—Cl) frequency is located at 667 cm.$^{-1}$. The range observed for this mode, designated as S_{HC}, was 655–674 cm.$^{-1}$. An S_{CC} mode, from a single compound, 3-chloro-2,2,4,4-tetramethylpentane, was observed at 758 cm.$^{-1}$. It was also noted that the ν(C—Cl) frequency range for the case of two *trans* H atoms depended on the structure of the carbon skeleton. The S_{HH} frequency range quoted above referred to a planar zigzag skeletal structure, defined as follows. Let the C atom to which the Cl atom is attached be designated as C_0, the adjacent C atoms as C_1 and C_{-1}, and the next nearest C atoms as C_2 and C_{-2}. Consider the plane formed by C_{-1}, C_0, and C_1. If C_2 is in this plane, i.e., the chain retains a planar zigzag form, then the ν(C—Cl) frequency is S_{HH} as indicated above. If rotation about the C_0—C_1 bond occurs such as to place the other H atom on C_1 *trans* to the Cl atom, thus removing the C_2 atom from the C_{-1}–C_0–C_1 plane, the ν(C—Cl) frequency region is shifted. This mode, designated as S'_{HH}, was found in the range of 627–637 cm.$^{-1}$.

These results, together with an analysis of the spectra of various deuterated PVC's,[1] have permitted a satisfactory interpretation to be made of the bands in the ν(C—Cl) region of the spectrum of this polymer. Studies of a highly crystalline PVC had shown[4] that bands at 604 and 640 cm.$^{-1}$ are to be associated with the fundamentals of the syndiotactic unit in the planar zigzag chain. The spectra of less crystalline polymers show additional bands in this region, attributable to noncrystalline structures. Making allowance for a small frequency shift between the model compounds and the polymer, the band which appears at 615 cm.$^{-1}$ can be assigned to an S_{HH} mode and those at 685 and 693 cm.$^{-1}$ to S_{HC} modes. It was also shown[1] that a band is present at 638 cm.$^{-1}$ associated with the noncrystalline regions of the polymer. On the basis of the above correlations, it is possible to assign this to an S'_{HH} mode.

Because of the dependence of the ν(C—Cl) frequency on the rotation angle about the adjacent C—C bond, it is possible to analyze the infrared bands in terms of the relative configurations of adjacent pairs of Cl atoms. If the carbon skeleton of a PVC chain is confined to a planar zigzag, then two successive Cl atoms are designated as an isotactic (*i*) pair if they are on the same side of this plane and as a syndiotactic (*s*) pair if they are on opposite sides of this plane. Of the three isomers obtained by rotation about a C—C bond, one is most unlikely to occur because of the high

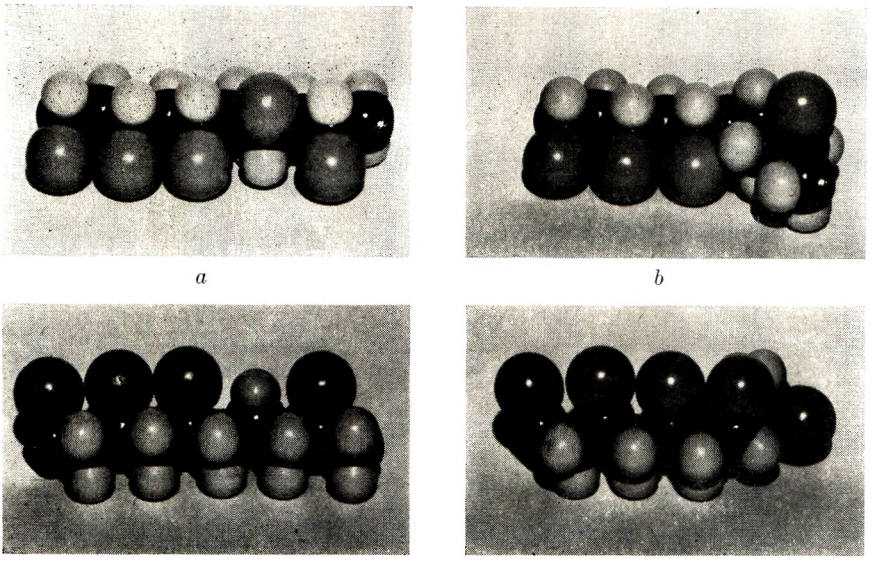

Fig. 1. Portion of an atactic polyvinyl chloride chain, showing conformations obtained by bond rotations in an s pair: (a) and (c) planar zigzag chain; (b) $+120°$ rotation; (d) $-120°$ rotation.

energy associated with it, viz., that in which adjacent Cl atoms are contiguous. Of the other two isomers, studies on model compounds[5] suggest that one is more stable than the other. It is thus possible to specify the possible likely conformations of a PVC chain once the pair configurations are given. To see this more clearly, consider Figure 1. In Figures 1a and 1c are shown two views of a portion of a planar zigzag atactic PVC chain. This portion contains two i pairs and two s pairs. In the s pair region the planar zigzag structure is the most stable, and with it is associated an S_{HH} mode. The structure shown in Figure 1b is produced by rotating $+120°$ about a C—C bond, and is somewhat less stable than that of Figure 1a but will probably be present to some extent. As a result of this rotation one S_{HH} mode is converted to an S_{HC} mode. A rotation of $-120°$ produces the structure shown in Figure 1d, and converts an S_{HH} mode into an S'_{HH} mode. This structure, however, is a very unlikely one since it places adjacent Cl atoms contiguous to each other. We see therefore that s pairs will give rise to S_{HH} (most probable) and S_{HC} (least probable) frequencies. Corresponding effects for the i pair are shown in Figure 2. The planar zigzag chain is shown in Figures 2a and 2c, and we note that its occurrence is most unlikely because of the contiguous adjacent Cl atoms. Of the two likely isomers, the one shown in Figure 2b, and giving rise to an S_{HC} frequency, is most stable, while that shown in Figure 2d, and giving rise to an S'_{HH} frequency, is somewhat less stable. Thus, i pairs are expected to yield S_{HC} and S'_{HH} frequencies, the former being more stable.

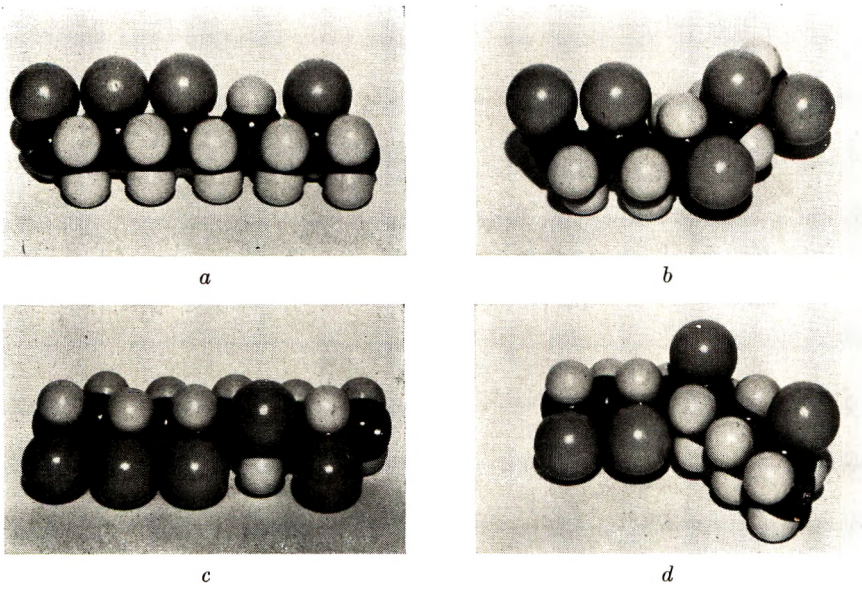

Fig. 2. Portion of an atactic polyvinyl chloride chain, showing conformations obtained by bond rotations in an i pair: (a) and (c) planar zigzag chain; (b) $-120°$ rotation; (d) $+120°$ rotation.

On the basis of these and the previous considerations we can assign the noncrystalline bands of PVC as follows. The 615 cm.$^{-1}$ band, an S_{HH} mode, arises from the s pairs and represents the more stable isomeric form. The 638 cm.$^{-1}$ band, an S'_{HH} mode, arises from the less stable form of the i pairs. The 685 and 693 cm.$^{-1}$ bands, which are assignable to S_{HC} modes, must be associated with the stable i pair and less stable s pair frequencies. A proper correlation can be obtained from a study of the spectrum of a heated PVC.[6] The effect of heating a typical low crystalline PVC to 180°C. is to weaken the 638 cm.$^{-1}$ band markedly and to cause a shift in band maximum from 693 cm.$^{-1}$ to 685 cm.$^{-1}$. If we can assume that heating releases chain constraints that are present at room temperature, and which allow less favorable isomeric structures to exist in measurable quantity, then the decrease in intensity of the 638 cm.$^{-1}$ i band can be accounted for. We would then expect a similar decrease in intensity of the band associated with the less favored s pairs. This suggests the assignment of the 693 cm.$^{-1}$ band to the s pairs and the 685 cm.$^{-1}$ band to the stable i pair frequency. The slight difference between these two S_{HC} frequencies indicates that other than nearest-neighbor effects are not negligible. It might be noted that the above assignment is consistent with the different dichroisms observed for the 685 and 693 cm.$^{-1}$ bands in oriented specimens.[1]

Thus, the intensities of the 615 and 685 cm.$^{-1}$ bands are a measure of the relative number of s and i pairs respectively in a PVC chain. If the extinction coefficients of these bands were known, and if they could be

appropriately separated from overlapping bands, this measure of configuration could be obtained. The latter requirement is best met by measurements on a heated sample or a solution of the polymer, in which case the interfering bands are almost absent. The intensities of the bands at 693 and 638 cm.$^{-1}$ are a measure of the less favored conformations associated with *s* and *i* pairs respectively. From their intensities relative to the previous pair of bands it should be possible to determine, at least qualitatively, the relative proportion of the less favored chain conformation which are present in a specimen of PVC.

Effect of Physical State on Chain Conformation

We have observed that the physical state of a specimen of PVC determines the relative proportion of less favored chain conformations which are present. Samples of Geon 101EP were studied in KBr disks, pressed films, and films cast from solution at room and higher temperatures (tetrahydrofuran, cyclohexanone, and 1:1 volume ratio of acetone and carbon disulfide). In the case of the cast films, residual solvent was removed by extraction with carbon disulfide at room temperature. Orientation in the PVC films was produced by stretching in boiling water or in a glycerine bath. Most spectral measurements were made with a Perkin-Elmer Model 21 spectrophotometer equipped with a KBr prism, although the results were checked on several grating spectrometers.

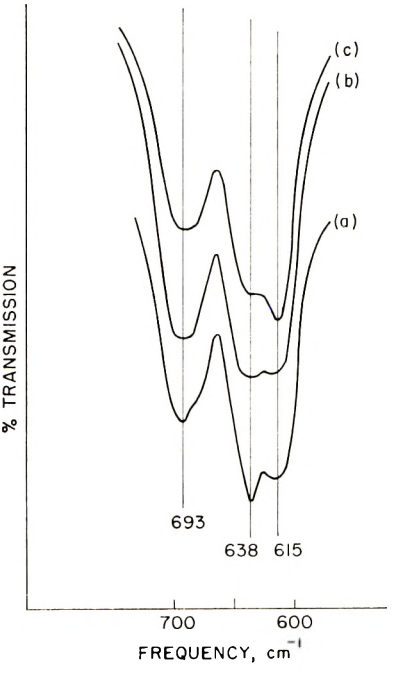

Fig. 3. Infrared spectra of polyvinyl chloride: (*a*) cast film, from tetrahydrofuran; (*b*) pressed film; (*c*) KBr disk.

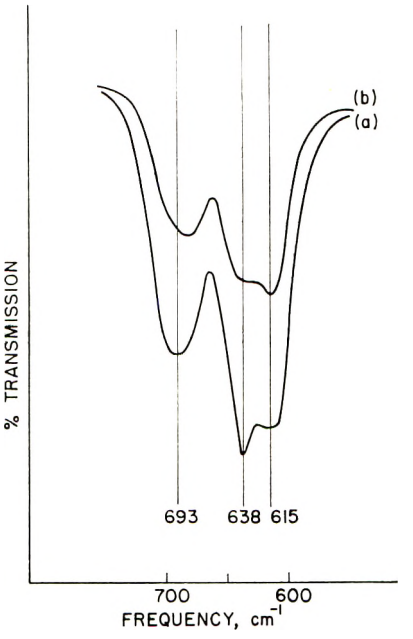

Fig. 4. Infrared spectra of film cast from tetrahydrofuran: (*a*) unoriented; (*b*) stretched 900% at 80°C.

The infrared spectra of various unoriented PVC specimens in the ν(C—Cl) stretching region are shown in Figure 3. The results for the cast film were independent of the solvent used, and thus independent of the temperature of solution. It will be seen that in passing from the cast film to the KBr disk the 638 cm.$^{-1}$ band weakens and the component at 685 cm.$^{-1}$ increases in relative intensity. These samples, which are very poorly crystalline, show little evidence of bands at 604 and 640 cm.$^{-1}$. It might be noted that the observation of a higher intensity at 638 cm.$^{-1}$ than at 615 cm.$^{-1}$ in the cast film depends on operating the spectrometer so that it does not have too slow a response. If the response is too slow, as results, for example, by decreasing the slit width, the 638 cm.$^{-1}$ band will become relatively weaker. This may account for the failure of previous workers to observe spectra such as in Figure 3*a*.

The effect of orientation on the spectrum is shown in Figure 4 for a film cast from tetrahydrofuran. Similar results were obtained for films cast from other solvents. The effects of stretching are seen to be a decrease in relative intensity of the 638 cm.$^{-1}$ band and a shift in band maximum from 693 to 685 cm.$^{-1}$. The latter is most probably a result of the change in relative intensity of two bands, one centered near 693 cm.$^{-1}$ and the other centered near 685 cm.$^{-1}$. The above effects were independent of the orientation of the stretching direction of the sample with respect to the spectrometer slit, so that spectrometer polarization effects are not involved here. If the stretched sample is allowed to shrink back

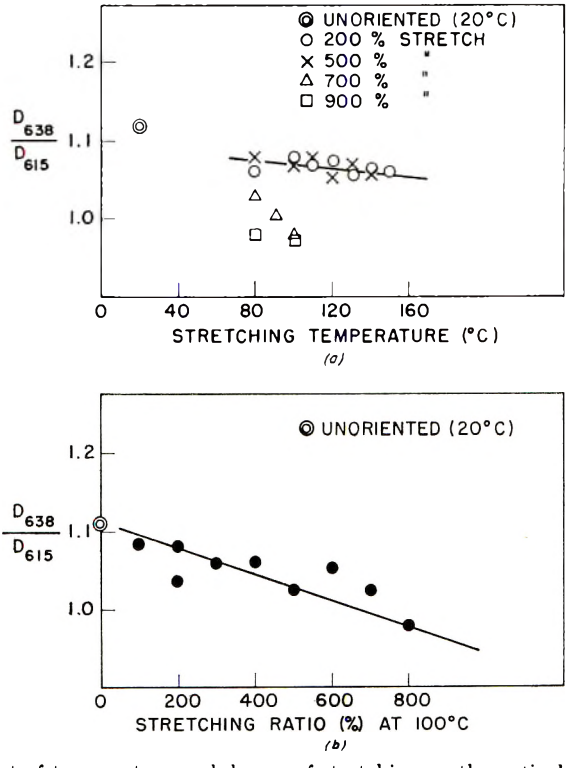

Fig. 5. Effect of temperature and degree of stretching on the optical density ratio of the bands at 638 and 615 cm.$^{-1}$: (*a*) effect of temperature of orientation at fixed elongation; (*b*) effect of stretching ratio at fixed temperature of elongation.

freely in boiling water, the original spectrum is recovered essentially completely.

In order to determine the dependence of these changes on the orientation conditions, samples were stretched by varying amounts at different temperatures. The results are shown in Figure 5. As a measure of the change, the ratio of peak optical densities (above the background) of the 638 and 615 cm.$^{-1}$ bands was used. This is, of course, not a completely satisfactory quantitative determination, since the bands overlap significantly, but it does serve to indicate the direction of the changes. As can be seen, the higher the elongation temperature at fixed stretching ratio and the higher the stretching ratio at fixed temperature of elongation, the lower is the D_{638}/D_{615} ratio.

Several other experiments were performed in order to clarify the nature of the above spectral changes. Pressed films were soaked for brief periods of time (30 sec. and 1 min.) in cyclohexanone and then examined both with and without subsequent carbon disulfide extraction. Another pressed film was soaked in only carbon disulfide for about 15 hr. In all cases the original pressed film spectrum (Fig. 3*b*) changed over to a cast film spectrum (Fig. 3*a*) after the treatment. A pressed film heated in air

or water at 100°C. for 10 min. also showed a conversion to the cast film type of spectrum, although heating at 50°C. produced no spectral change. Cast films, on the other hand, which are formed by evaporation below the second-order transition temperature (a film cast from cyclohexanone at room temperature) have spectra essentially identical to those formed above this temperature (a film cast from cyclohexanone at 150°C.). The spectrum of the original PVC powder in a nujol mull is essentially identical to that of the KBr disk (Fig. 3*c*). Thus, it appears that heat or solvent treatments bring about a spectral change whose main characteristic is a relative enhancement in intensity of the bands at 638 and 693 cm.$^{-1}$.

Discussion

In discussing the meaning of the above spectroscopic observations, one of the important factors to be kept in mind is the different origins of the bands under consideration. The bands at 638 and 685 cm.$^{-1}$ are associated with the *i* pairs, and it is reasonable to expect that a decrease in the intensity of one will be accompanied by an increase in the intensity of the other. A similar inverse intensity relationship should exist between the 615 and 693 cm.$^{-1}$ *s* pair bands. Other intensity ratios, however, are much more difficult to specify since relative extinction coefficients are not known and the contribution of the syndiotactic crystalline bands (at 604 and 640 cm.$^{-1}$) is not always easy to resolve. Thus, it is not perhaps surprising that the spectrum of a solution of PVC (in 1:1 acetone–carbon disulfide) shows very weak absorption at 638 cm.$^{-1}$ (as compared to 615 cm.$^{-1}$), although the maximum of the higher frequency band is near 693 cm.$^{-1}$. Although the *i* pairs are predominantly in the S_{HC} conformation and are absorbing mainly near 685 cm.$^{-1}$, chain bends in the *s* pair regions are undoubtedly more numerous in the solution than in the solid and are contributing to enhanced absorption near 693 cm.$^{-1}$.

Another important factor that is most likely operative in the above experiments is the increase in crystallinity of the sample as a result of heat or solvent treatments, i.e., the tendency to increase the extent of regions of three-dimensional order. Such treatments are known to have this effect on many other high polymers. While carbon disulfide is not a good solvent for PVC, it will extract chains up to about ten monomer units in length and it does penetrate the film (as indicated by spectra of thoroughly surface-dried film); it may therefore act to increase chain mobility and allow further crystallization to occur. The original powder probably has a low degree of crystallinity, most likely associated with the process of precipitation. We find that if the original PVC powder is dissolved (in tetrahydrofuran) and reprecipitated (with methyl alcohol), the spectrum of the powder after such treatment is essentially identical with that before. The process of pressing a film from the powder probably allows some additional crystallization to take place, although the rapid cooling which usually occurs in making such a film is not conducive to optimum crystallization. If, in fact, such a film is left in the press and the temperature of

the latter brought slowly to room temperature, the spectrum of the resulting film is similar to that of a cast film.[7] Finally, the process of forming a cast film by slow evaporation of the solvent from a solution is probably conducive to optimum crystallization of the polymer. This is in agreement with evidence that, under high resolving power, the spectrum of a cast film shows a pronounced shoulder corresponding to 604 cm.$^{-1}$ which is much less prominent in the spectra of the pressed film and the KBr disk.[7] The fact that identical spectra can be obtained from cast films made from different solvents, either with or without carbon disulfide extraction, would indicate that no other kind of specific solvent effect, such as a solvent–polymer interaction, is likely to be involved.

On the basis of these considerations it is possible to suggest what might be occurring concomitant with such increasing crystallization, although the present results by no means establish the process uniquely. More detailed knowledge of the crystalline and noncrystalline morphology would be required in order to do this. However, it is probable that for the relatively poor stereoregularity of the polymers studied here, an increase in crystallinity is accompanied by the more extensive inclusion of i pairs into three-dimensionally ordered regions formed by the s pair portions of chains. (X-ray diffraction studies[8] indicate that the crystalline regions are associated with the latter configuration.) This would favor S_{HH} conformations over S_{HC} for the s pairs, and it is possible that within such ordered regions the i pair "impurities" fit in better in the S'_{HH} conformation than in the (helical) S_{HC} conformation. Molecular models tentatively suggest that this may be the case. It must again be emphasized that our experimental results do not lead uniquely to this conclusion. They only require that the proportion of i pair S'_{HH} conformation be higher in the cast film than in the pressed film. That this may be associated with different crystalline morphologies in these films is not unreasonable. In fact, other data also suggest such structural differences. Thus, the inversion of dichroism in some bands with increasing specimen elongation[9,10] is found to vary with the kind of film. For cast films it occurs at about 200% elongation,[9,10] whereas for pressed films it is found at about 20% elongation.[1]

The crystalline morphology must also govern the effects observed upon stretching a cast film of PVC. In part the spectral differences may be understood in terms of a conversion of less elongated chain conformations into more elongated conformations under the influence of the external stress. For a region of a chain containing a sequence of s pairs the most stable conformation is the planar zigzag, and this is also the most elongated. We anticipate that constraints imposed by chain entanglements, interchain interactions, etc., are responsible for the presence of some unfavored conformations in the noncrystalline regions of an unoriented specimen. When an external stress is applied, a rearrangement of chains can occur such that unfavored conformations are converted into favored ones, with an accompanying increase in chain extension. In the i pair

regions it is possible that helical structures orient more readily under the influence of the stress, and therefore the S_{HC} conformation is favored. However, the changes which occur in the crystalline regions may also be contributing to the spectral differences. Thus, if the crystalline syndiotactic regions consist of folded chain crystals, and if these are unfolded to some extent during elongation, the relative numbers of the different s pair conformations could well alter (on the assumption that the fold regions contain conformations other than those of the planar zigzag chain). Further work is needed in order to establish the relative effect of these various factors on the spectrum, but it is already clear that the infrared spectrum can be a valuable tool in following changes in conformational structure.

We are indebted to Mr. J. J. Shipman of The B. F. Goodrich Company for furnishing us with PVC samples and for making available to us some of his results obtained with a Perkin-Elmer 421 spectrophotometer. We wish to thank Dr. W. J. Potts of the Dow Chemical Company for the opportunity of using their grating spectrometers. This research was supported by National Science Foundation grant G17469.

References

1. Krimm, S., V. L. Folt, J. J. Shipman, and A. R. Berens, *J. Polymer Sci.*, **A1**, 2621 (1963).
2. Mizushima, S., T. Shimanouchi, K. Nakamura, M. Hayashi, and S. Tsuchiya, *J. Chem. Phys.*, **26**, 970 (1957).
3. Shipman, J. J., V. L. Folt, and S. Krimm, *Spectrochim. Acta*, **18**, 1603 (1962).
4. Krimm, S., A. R. Berens, V. L. Folt, and J. J. Shipman, *Chem. Ind. (London)*, **1959**, 433.
5. Shimanouchi, T., and M. Tasumi, *Spectrochim. Acta*, **17**, 755 (1961).
6. Shimanouchi, T., S. Tsuchiya, and S. Mizushima, *Kobunshi*, **8**, 202 (1959).
7. Shipman, J. J., private communication.
8. Natta, G., and P. Corradini, *J. Polymer Sci.*, **20**, 251 (1956).
9. Asahina, M., and S. Enomoto, *Nippon Kagaku Zasshi*, **81**, 1011, 1370 (1960).
10. Tasumi, M., and T. Shimanouchi, *Spectrochim. Acta*, **17**, 731 (1961).

Résumé

L'analyse du spectre infra-rouge du chlorure de polyvinyle a permis d'identifier à partir des fréquences de plusieurs bandes des vibrations C—Cl, des conformations de chaînes liées aux configurations particulières des paires d'atomes de chlore. Ces résultats ont permis d'établir que des changements dans la structure conformationnelle accompagnent certains changements dans l'état physique du polymère. On considère différentes interprétations possibles pour expliquer les origines de ces changements structuraux.

Zusammenfassung

Eine Analyse des Infrarotspektrums von Polyvinylchlorid erlaubte mit Hilfe der Frequenzen der verschiedenen C—Cl-Valenbanden eine Identifizierung der mit besonderen Konfigurationen von Chlorpaaren verknüpften Kettenkonformationen. Die Ergebnisse zeigten, dass gewisse Änderungen im physikalischen Zustand des Polymeren von Änderungen der Konformation begleitet werden. Deutungsmöglichkeiten für die Ursache dieser Strukturänderungen werden diskutiert.

Received November 18, 1962

JOURNAL OF POLYMER SCIENCE: PART A VOL. 2, PP. 679–687 (1964)

Effect of Film Thickness upon the Sorption of Organic Vapors in Polymers Slightly above Their Glass Transition Temperatures

A. KISHIMOTO* and K. MATSUMOTO, *Physical Chemistry Laboratory, Department of Fisheries, University of Kyoto, Maizuru, Japan*

Synopsis

Absorption and desorption of organic vapors in amorphous polymers in the temperature region slightly above T_g were studied as a function of film thickness. The systems chosen for this study were polyvinyl acetate (PVAc)–allyl chloride at 40°C. and polymethyl acrylate (PMA)–methyl acetate at 15 and 35°C. In PVAc studies reduced adsorption curves for different film thicknesses at relatively high equilibrium concentrations were apparently normal, but the initial slopes of the plots increased with increasing film thickness X and appeared to approach certain limiting values at the limit of infinite X. At lower equilibrium concentration two-stage absorption curves appeared, and the variation of absorption curve with film thickness was too complicated to be interpreted in terms of the theory proposed by Crank and Long and Richman. The desorption curve was at all concentrations studied, almost normal and the initial slopes increased with increasing X. By assuming that the hypothetical sorption curve with the initial slope extrapolated to infinite X is controlled by a purely Fickian diffusion mechanism, we calculated the mutual diffusion coefficient D for this system and compared it with that derived by Meares from steady-state permeation measurements. Both results agreed quite well, suggesting that the method presented here is effective for obtaining D. Absorption and desorption of methyl acetate by PMA at 15°C. were entirely similar to those obtained by PVAc in the corresponding region of equilibrium concentration. At 35°C. reduced sorption curves were independent of X and were purely Fickian. Following the analysis in PVAc, we predicted D for PMA at 15°C. as a function of methyl acetate concentration.

INTRODUCTION

In a previous paper,[1] we calculated integral diffusion coefficients for the system allyl chloride–polyvinyl acetate (PVAc) at 40°C. from sorption data and compared them with the values which had been deduced by Meares[2] from steady-state permeation measurements. It was found that the steady-state integral diffusion coefficients increase more rapidly with the penetrant concentration C than do the integral diffusion coefficients for sorption, but both coefficients converge to the same value at the limit of zero penetrant concentration. A similar discrepancy between steady-state

* Present address: The Composite Research & Development Center, Toyo Seikan and Toyo Kohan Companies, Okazawa, Hodogaya, Yokohama, Japan.

and transient diffusion coefficients has recently been observed for PVAc–methanol,[3] for natural rubber–benzene[4] and for polyethylene–benzene[5] above the glass transition temperatures T_g of the respective polymers. The divergence of two sets of diffusion coefficient was interpreted as being due to slow relaxation of the polymer chain involved in nonsteady-state measurements; steady-state measurements are apparently free from such an effect, because they deal with the state of a polymer in which all chain molecules are fully relaxed.

In order to obtain more information about the sorption of organic vapors by amorphous polymers in the temperature region not far above T_g, we made absorption and desorption measurements for the systems PVAc–allyl chloride at 40°C. and for polymethyl acrylate (PMA)–methyl acetate at 15°C. as a function of film thickness.

EXPERIMENTAL

Material

The PVAc sample used in the present study was the same as that employed previously.[1] Its viscosity-average molecular weight was estimated to be 3.5×10^5. The films for the sorption measurements were prepared in exactly the same manner as described previously,[6] and their thicknesses ranged from 1.62×10^{-3} to 1.15×10^{-2} cm.

The PMA used was identical to that used for obtaining the data for concentration and temperature dependence of diffusion coefficients for *n*-alkyl acetates in this polymer.[7] The number-average molecular weight of the PMA, determined osmotically in acetone at 25°C., was 3.1×10^5. Films of 2.15×10^{-3} to 1.20×10^{-2} cm. thickness were prepared.

The allyl chloride used as penetrant was dried over calcium sulfate and fractionally distilled. The methyl acetate was purified by fractional distillation after thorough removal of water by anhydrous potassium carbonate.

Apparatus and Procedure

The sorption apparatus described previously[6] was used throughout this investigation. Integral absorption from and desorption to zero pressure were studied.

Measurements of sorption on PVAc were carried out at 40°C. and at vapor pressures of 43.4, 90, 130, 145, and 196 mm. Hg. Experiments with PMA were performed at 15°C. and at vapor pressures of 17, 43, and 66 mm. Hg. These pressures had been used in our previous study[7] of diffusion of methyl acetate in PMA. Only one experiment was made at 35°C. at a pressure of 43 mm. Hg.

The equilibrium concentrations in films of different thicknesses at a given pressure were constant to within an error of 2%.

Granted the published values[8] of about 28°C. and about 3°C. for T_g of PVAc and PMA, respectively, the systems studied in the present experiments are about 12°C. above the corresponding glass transition points.

RESULTS AND DISCUSSION

PVAc–Allyl Chloride

Figure 1 shows typical absorption data for PVAc–allyl chloride at 40°C. and at 130 mm. Hg. To avoid confusion, only partial data are presented. Here, M is the amount of the penetrant absorbed per gram of dry polymer at time t, M_∞ the value of M at absorption equilibrium, and X the thickness of film. It is seen from the figure that the absorption plots are not reduced to a single curve; the initial slope, I_a, of the plot increases with increasing film thickness. A similar trend was observed for the data at 145 and 196 mm. Hg vapor pressures. These results imply that the absorption of allyl chloride in PVAc at 40°C. and at these high vapor pressures is not controlled by a purely Fickian diffusion mechanism.

Crank[9] discussed the effect of film thickness upon the rate of absorption in a system in which the diffusion coefficient depends not only upon concentration but also upon time. According to his theory, the absorption plot for either very thick or very thin films is linear and those for intermediate films are of a sigmoid type. He showed further that as the film becomes thicker the absorption proceeds faster, and at the limit of infinite thickness the time effect disappears and the absorption rate is governed by the equilibrium diffusion coefficient. Here the equilibrium diffusion coefficient may be identified with the steady-state diffusion coefficient. It is seen from Figure 1 that for films of medium thickness the absorption

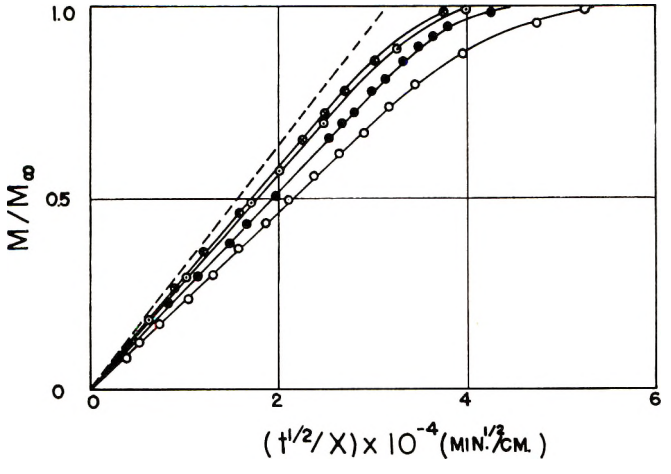

Fig. 1. Absorption curves for allyl chloride in PVAc at 40°C. and 130 mm. Hg vapor pressures (X is the film thickness, t is the time): (○) $X = 1.90 \times 10^{-3}$ cm.; (●) $X = 3.05 \times 10^{-3}$ cm.; (⊙) $X = 4.03 \times 10^{-3}$ cm.; (⊗) $X = 6.30 \times 10^{-3}$ cm.

plots do not show any sigmoid character, and the initial slope of the plot tends to approach a certain limiting value with increasing film thickness indefinitely.

Recently, Long and Richman[10] have shown that anomalous absorption curves of vapors by glassy polymers can be derived from the Fick diffusion equation by assuming a time-dependent approach to the equilibrium surface concentration. Their solution to the diffusion equation involves a parameter $\beta X^2/D$, in which β is a rate parameter and is a measure of the rate of relaxation motion of polymer structure and D is a diffusion coefficient. According to their model, the overall rate of absorption increases with increase of $\beta X^2/D$, and at the limit of infinite thickness the absorption follows a normal curve expected from the condition that an equilibrium concentration is established instantly at the film surfaces. The data shown in Figure 1 appear to be consistent with this theoretical prediction.

At concentrations of 1.45×10^{-2} and 3.00×10^{-2} g./g. corresponding to 43.4 and 90 mm. Hg vapor pressures, respectively, the absorption behavior revealed a feature different from that observed at higher concentrations. Figure 2 shows the absorption data at 43.4 mm. Hg, in which the data for a film 1.62×10^{-3} cm. thick are taken from our previous article.[1] It is seen that for the thinnest film the absorption curve is almost linear up to two-thirds of the total vapor uptake. With increasing film thickness, two-stage absorption curves appear. The sorption starts with an extremely rapid initial uptake followed by a very slow approach to equilibrium. It is of interest that none of the previous studies has reported two-stage absorption behavior at temperatures above T_g. With further increase of film thickness the first-stage portion shifts toward the region of longer time and, at the same time, the second-stage portion shifts toward the

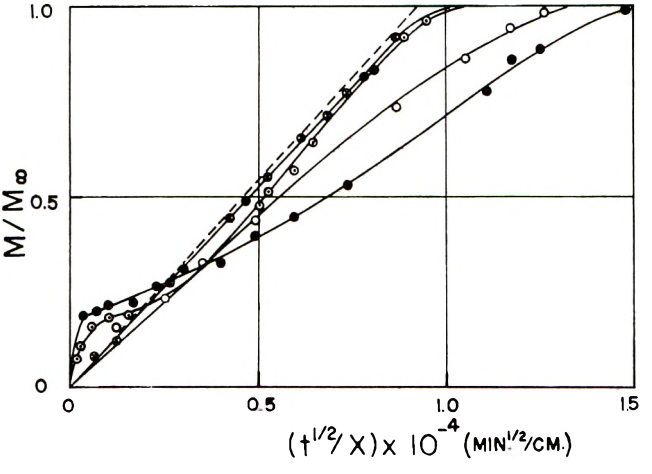

Fig. 2. Absorption curves for allyl chloride in PVAc at 40°C. and 43.4 mm. Hg vapor pressure: (○) $X = 1.62 \times 10^{-3}$ cm.; (●) $X = 3.04 \times 10^{-3}$ cm.; (⊙) $X = 6.75 \times 10^{-3}$ cm.; (⊗) $X = 8.92 \times 10^{-3}$ cm.

shorter time region. Eventually, the two-stage absorption process disappears, and the absorption turns out to be normal. Similar data were obtained at 90 mm. Hg vapor pressure.

The Long-Richman model[10] accounts for the occurrence of anomalous absorption curves of the two-stage type. However, the variation of absorption curve with film thickness cannot be described in terms of this model by merely changing X, because the increase of X results in a monotonous increase of overall rate of absorption.

For all values of film thickness and concentrations studied, the desorption plots were linear up to one-fourth of the total uptake and were

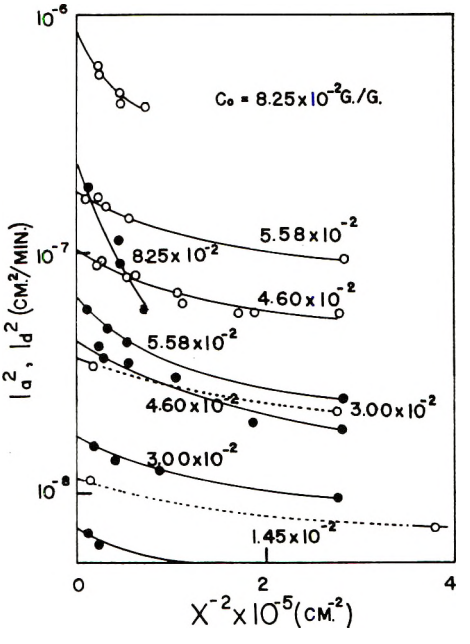

Fig. 3. Plots of I_a^2 and I_d^2 vs. X^{-2} for the system PVAc–allyl chloride at 40°C.: (○) absorption; (●) desorption.

concave against the abscissa for large $(t)^{1/2}/X$. The initial slope, I_d, of the plot increased with increasing X and appeared to tend to a certain limiting value. No evidence of the two-stage behavior was observed at the concentration at which the corresponding absorptions exhibited a marked two-stage behavior.

Except for the plots showing two-stage behavior, the squares of the initial slopes, I_a^2 and I_d^2, of absorption and desorption plots are semilogarithmically plotted against X^{-2} in Figure 3. The open circles refer to absorption and the solid circles refer to desorption. It is seen that I_a^2 and I_d^2 increase with increase of X and converge to certain limiting values at infinite thickness. At a concentration of 8.25×10^{-2} g./g. the dependence of I_a^2 and I_d^2 on film thickness is quite pronounced, but with decreasing

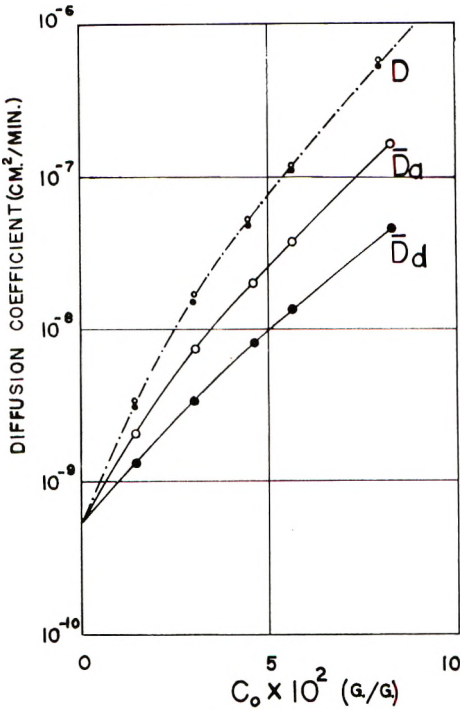

Fig. 4. Plots of various diffusion coefficients against penetrant concentration for the system PVAc–allyl chloride at 40°C. (○) D from $\bar{D}_a$, (●) D from $\bar{D}_d$; (— · —) steady-state-diffusion coefficients derived by Meares.

equilibrium concentration it becomes less marked and appears to vanish at the limit of zero concentration.

The values of I_a and I_d extrapolated to infinite thickness are denoted by I_a^∞ and I_d^∞. If we assume that the hypothetical absorption and desorption curves for a film of infinite thickness are controlled by the purely Fickian diffusion mechanism, we may calculate the mutual diffusion coefficient D from data for I_a^∞ and I_d^∞ as functions of penetrant concentration. To this end we define two apparent diffusion coefficients, $\bar{D}_a$ and $\bar{D}_b$, by

$$\bar{D}_a = (\pi/16)(I_a^\infty)^2$$
$$\bar{D}_d = (\pi/16)(I_d^\infty)^2 \qquad (1)$$

The values of $\bar{D}_a$ and $\bar{D}_d$ deduced from Figure 3 are plotted semilogarithmically against allyl chloride concentration C_0 in Figure 4. It is seen that both $\bar{D}_a$ and $\bar{D}_d$ increase with C_0, and the difference between them becomes larger as C_0 increases but is smaller than the difference obtained previously for thin films.[1] By using the weighted mean method proposed by Crank,[11] the mutual diffusion coefficient D was calculated as a function of C from $\bar{D}_a$ and $\bar{D}_d$, and is shown in Figure 4, where Meares's data[2] for $D(C)$ from

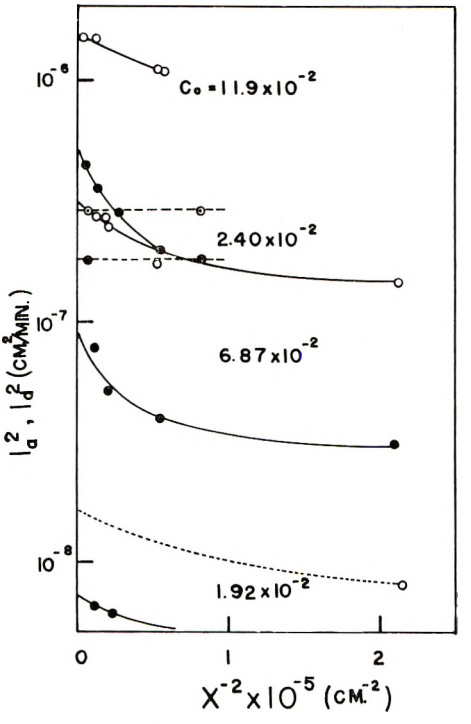

Fig. 5. Plots of I_a^2 and I_d^2 vs. X^{-2} for the system PMA–methyl acetate at 15 and 35°C.: (○, ●) absorption and desorption at 15°C.; (⊖, ⊗) absorption and desorption at 35°C.

steady-state permeation measurements are also indicated. The three sets of $D(C)$ are in good agreement, which indicates that there is the possibility that we can predict the diffusion coefficient from absorption and desorption measurements even when the sorption behavior exhibits non-Fickian features.

PMA–Methyl Acetate

At concentrations of 11.9×10^{-2} and 6.87×10^{-2} g./g., corresponding to 66 and 43 mm. Hg methyl acetate vapor pressure at 15°C., respectively, the absorption behavior is essentially similar to that obtained for PVAc at relatively higher concentrations. Absorption curves obtained from varying thickness experiments are initially linear, and the slope I_a increases with increase of film thickness.

At a lower concentration of 1.92×10^{-2} g./g., the absorption behavior resembles that obtained for PVAc at lower concentrations. For the thinnest film the absorption curve is normal. With increasing film thickness two-stage absorption curves appear as was the case with PVAc at 1.45×10^{-2} g./g. concentration. With increase of X the first-stage portion shifts toward the region of small time and reaches a maximum slope at a certain

film thickness. With further increase of X this stage shifts toward longer time and tends to converge to a limiting slope. The movement of the second stage portion is reverse to that of the first stage portion; first the second stage shifts toward longer time, and above a certain value of X the inverse shift occurs.

The desorption behavior for PMA at 15°C. was entirely similar to that for PVAc at 40°C.; the desorption plots are initially linear and the slope of the plot increases with increasing film thickness.

At 35°C., well above T_g of PMA, and at a concentration of 2.40×10^{-2} g./g. the absorption and desorption curves with films of two different thicknesses were normal. This suggests that at this temperature the sorption process is controlled by a truely Fickian diffusion mechanism and also the diffusion coefficient is purely concentration-dependent.

Values of I_a^2 and I_d^2 for PMA–methyl acetate are plotted against X^{-2} in Figure 5. The trend is similar to that observed in Figure 4; at 15°C. the values of I_a^2 and I_d^2 increase with increase of X and approach some limiting values at infinite X. At 35°C., however, I_a^2 and I_d^2 are constant independent of X. From this figure the values of I_a^∞ and I_d^∞ may be evaluated by graphical extrapolation, but too much reliance should not be placed on the exact value of I_a^∞ at a concentration of 1.92×10^{-2} g./g., since the absorption curves at this concentration showed marked two-stage behavior. By using the procedure described above we evaluated the mutual diffusion coefficient D for the system PMA–methyl acetate at 15°C. as a function of methyl acetate concentration and found that two sets of D derived from absorption and desorption plots agreed with each other but increased more rapidly with C than do the diffusion coefficient obtained in previous studies[7] with thinner films.

The authors wish to thank Professor H. Fujita, Department of Polymer Science, Osaka University, Osaka, for his encouragement and his continued interest in the course of this investigation.

References

1. Kishimoto, A., and K. Matsumoto, *J. Phys. Chem.*, **63**, 1529 (1959).
2. Meares, P., *J. Polymer Sci.*, **27**, 391 (1958).
3. Kishimoto, A., unpublished results.
4. Barrer, R. M., and R. R. Fergusson, *Trans. Faraday Soc.*, **54**, 989 (1958).
5. Rogers, C. E., V. Stannett, and M. Szwarc, *J. Polymer Sci.*, **45**, 61 (1960).
6. Fujita, H., and A. Kishimoto, *J. Polymer Sci.*, **28**, 547 (1958).
7. Fujita, H., A. Kishimoto, and K. Matsumoto, *Trans. Faraday Soc.*, **56**, 424 (1960).
8. Williams, M. L., R. F. Landel, and J. D. Ferry, *J. Am. Chem. Soc.*, **77**, 3701 (1955).
9. Crank, J., *J. Polymer Sci.*, **11**, 151 (1953).
10. Long, F. A., and D. Richman, *J. Am. Chem. Soc.*, **82**, 513 (1960).
11. Crank, J., *Trans. Faraday Soc.*, **51**, 1632 (1955).

Résumé

L'absorption et la désorption des vapeurs organiques dans des polymères amorphes à des températures légèrement au-dessus de T_g ont été étudiées en fonction de l'épaisseur

du film. Le système, choisi pour cette étude était l'acétate de polyvinyle et le chlorure d'allyle à 40°C, les polyméthacrylates et l'acétate de méthyle à 15° et à 35°C. Dans les études des PVAc les courbes d'absorption réduites pour des pellicules d'épaisseurs différentes à des concentrations d'équilibre relativement élevées étaient apparemment normales. Mais la pente initiale des courbes augmentait avec l'épaisseur des pellicules et tendait à une valeur limite pour une valeur infinie de X. Pour des concentrations à l'équilibre plus basses on trouvait des courbes d'absorption à deux phases et la variation des courbes d'absorption en fonction de l'épaisseur des pellicules était trop compliquée pour être interprêtée au moyen de la théorie proposée par Crank, Long et Richman. La courbe de désorption était, dans toutes les concentrations étudiées, normale et les pentes initiales augmentaient en fonction de X. En admettant que la courbe hypothétique de sorption pour une pente initiale extrapolée à X infini, est contrôlée entiérement par le mécanisme de diffusion suivant la loi de Fick, on a calculé la constante de diffusion réciproque D pour ce système. On a comparé cette constante de diffusion avec celle de Meares obtenue par des mesures de l'état stationnaire d'imprégnation. Les deux résultats étaient en accord, ceci veut dire que la méthode présentée ici est valable pour obtenir D. L'absorption et la désorption de PMA à 15°C étaient totalement pareille à celles obtenues avec le PVAc dans des régions de concentration d'équilibre correspondantes. A 35°C des courbes de sorption réduites étaient indépendantes de X et entièrement conformes à la loi de Fickian. Suivant l'analyse de PVAc, on a prédit D pour PMA à 15°C en fonction de la concentration de l'acétate de méthyle.

Zusammenfassung

Absorption und Desorption von organischen Dämpfen durch amorphe Polymere wurde im Temperaturbereich knapp oberhalb T_g in Abhängigkeit von der Filmdicke untersucht. Das System Polyvinylacetat(PVAc)–Allylchlorid wurde bei 40°C und Polymethylacrylat(PMA)–Methylacetat bei 15 und 35°C untersucht. Bei PVAc waren die reduzierten Absorptionskurven bei verschiedener Filmdicke und Verhältnismässig hoher Gleichgewichtskonzentration offenbar normal, die Anfangsneigung der Diagramme nahm jedoch mit wachsender Filmdicke zu und schien sich für $X \rightarrow \infty$ einem bestimmten Grenzwert zu nähern. Bei niedrigerer Gleichgewichtskonzentration traten zweistufige Absorptionskurven auf und die Abhängigkeit der Absorptionskurve von der Filmdicke war für Deutung nach der von Crank und Long und Richman vorgeschlagenen Theorie zu kompliziert. Unter der Annahme, dass die hypothetische Sorptionskurve mit der Anfangsneigung bei der Extrapolation zu $X \rightarrow \infty$ von einem rein Fickschen Diffusionsmechanismus bestimmt wird, wurde der wechselseitige Diffusionskoeffizient, D, für dieses System berechnet und mit dem von Meares aus Permeationsmessungen im stationären Zustand abgeleiteten verglichen. Beide Ergebnisse stimmten gut überein, was zeigt, dass die hier angegebene Methode zur Ermittlung von D brauchbar ist. Absorption und Desorption von Methylacetat durch PMA bei 15°C war den bei PVAc in den entsprechenden Bereichen der Gleichgewichtskonzentration gefundenen Verhältnissen völlig analog. Bei 35°C waren die reduzierten Sorptionskurven unabhängig von X und entsprachen dem Fickschen Gesetz. Aus der Analyse bei PVAc wurde D für PMA bei 15°C als Funktion der Methylacetatkonzentration berechnet.

Received November 27, 1962

JOURNAL OF POLYMER SCIENCE: PART A VOL. 2, PP. 689–704 (1964)

Polymer Degradation. I. Column Elution Fractionation and Thermal Degradation of Polyoxypropylene Glycol–Toluene Diisocyanate (PPG–TDI) Polymers

NEVILLE SUE RAPP and JOHN D. INGHAM, *Jet Propulsion Laboratory, California Institute of Technology, Pasadena, California*

Synopsis

A procedure has been worked out for the column elution fractionation of polyoxypropylene glycol–toluene diisocyanate (PPG–TDI) polymers of molecular weight ~100,000; by decreasing the column temperature from 34 to 7°C. the method was extended to degraded polymer of molecular weight ~25,000. Graphical differentiation of the integral curves was eliminated by using Tung's empirical equations. The results for both degraded and undegraded polymer agreed with the theoretical most probable distributions; therefore, a random scission process of degradation is indicated.

I. INTRODUCTION

A. Column Elution Fractionation

Fractionation and characterization of the molecular weight distribution of a polymer can provide significant information about the mechanisms of polymerization and depolymerization or degradation, since these processes may produce different distributions of molecular weights, depending on the mechanisms involved. Precipitation fractionation was successfully applied to a PPG–TDI polyurethane by Moacanin.[1] The present work was undertaken to establish more rapid and efficient column elution procedures for characterization of molecular weight distributions of this type of polymer before and after thermal degradation.

Moacanin obtained a value of the ratio of weight-average to number-average molecular weight ($\bar{M}_w/\bar{M}_n$) of 1.7 instead of 2.0, the expected value for condensation polymers that usually polymerize by a random mechanism to give the "most probable" molecular weight distribution.[2] Values of $\bar{M}_w/\bar{M}_n$ of 2.0–2.2 were obtained in the present work, indicating that column elution fractionation is more efficient than precipitation from a solvent, presumably as a result of the decreased polymer concentrations. Furthermore, considerably less manipulation and time are required for elution fractionation.

The column elution procedures used here are slight modifications of those developed elsewhere[3–5] in which the polymer fractions are successively

eluted from the column at constant temperature from an inert support by eluent increments of increasing solvent-nonsolvent ratios. The differential distribution curves for the polymers have been constructed from the experimental integral data by using the empirical equation suggested by Tung.[6] This procedure allows mathematical differentiation of the integral curves, thus eliminating the inaccuracies imposed by graphical differentiation. The differential distribution curves are desired because they can be more readily interpreted and compared (by visual inspection) than the integral curves.

B. Thermal Degradation

Comparison of the distributions before and after thermal degradation in a vacuum at 200°C. with theoretical curves for most probable distributions shows that the experimental data give distributions which may be slightly broader than, but can be approximated by, the theoretical most probable curves. Although these results are consistent with a random mechanism of degradation, they do not provide unequivocal proof, because other mechanisms, for example, unzipping at the chain ends, can also give invariant most probable distributions.[7] However, such depolymerizations would be accompanied by much larger extents of volatilization for comparable reductions in molecular weight than are observed for these polymers (<5% volatilization). Furthermore, the results show that invariant most probable distributions occur to give a constant relationship between the weight-average and number-average molecular weights so that the latter may be derived from measurements of intrinsic viscosity. Thus, the number of bonds broken can be easily determined, since it is readily shown that

$$X_{n(t)} = \frac{X_{n(0)}}{S + 1} \tag{1}$$

where $X_{n(t)}$ is the number-average chain length at a given time t, when, on the average, S links per original chain have been ruptured, and $X_{n(0)}$ is the original number-average chain length. The parameter S is a measure of the extent of degradation, from which the chemical kinetics may be calculated, and can therefore be used for the elucidation of mechanisms on the basis of kinetics. Such studies, as well as absolute measurements of number-average molecular weight during the course of degradation, are presently being carried out in our laboratory.

II. EXPERIMENTAL

A. Polymer Preparation

Polyoxypropylene glycol (PPG) was obtained from Union Carbide Chemicals Co. Analyses indicated that it contained: hydroxyl, 9.8×10^{-4} moles/g., unsaturation, 3.2×10^{-5} moles/g., and little or no peroxide or carbonyl. Toluene 2,4-diisocyanate (TDI) from E. I. du Pont de Nemours

and Co. was redistilled before use. The PPG and TDI were polymerized in bulk by the method described previously,[1] except that our dry box relative humidity was somewhat higher, ~2.5 instead of <1.0%. Polymers were obtained with intrinsic viscosities of 0.65–0.75 dl./g. These have higher molecular weights than those obtained in earlier work,[1] perhaps because the polyether used here may have contained less monofunctional PPG contaminant. Furthermore, the molecular weight obtained is strongly dependent on the isocyanate-to-hydroxyl ratio, which is difficult to control exactly.

B. Column Elution Fractionation

Approximately 1 g. of polymer was deposited on 200–300 ml. of column support by evaporation from benzene solution. This was added to the Pyrex column after pouring in an equal volume of uncoated substrate. When glass beads were used as the support, degradation apparently oc-

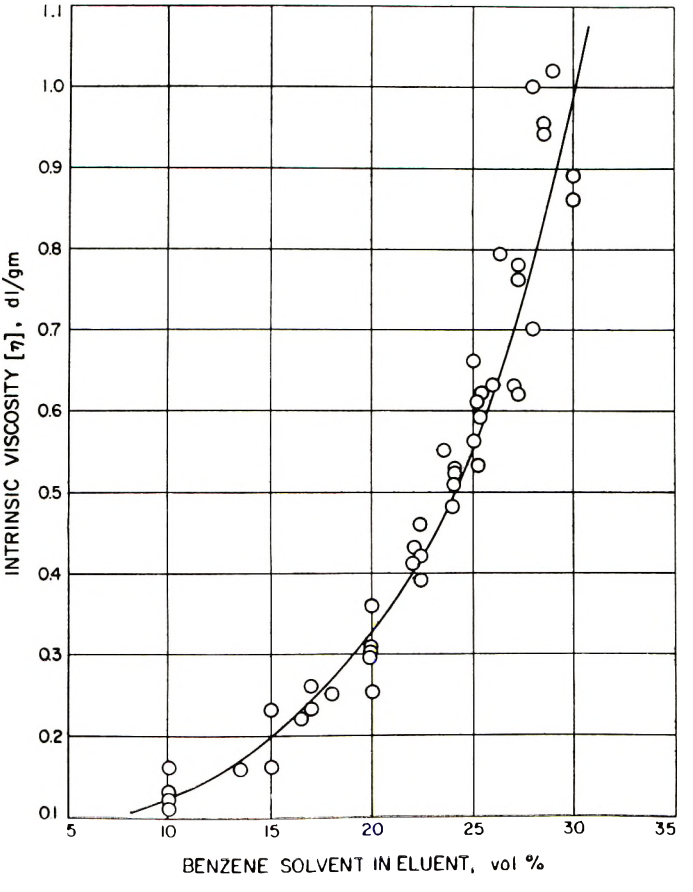

Fig. 1. Intrinsic viscosity of fraction vs. eluent composition; benzene solvent, isooctane nonsolvent at 34°C.

curred, since the intrinsic viscosity $[\eta]$ of the unfractionated polymer invariably was higher than the weighted average $[\eta]$ for all the fractions, calculated from

$$[\eta] = \sum_{1}^{i} W_i[\eta]_i$$

The degradation was believed to have been caused by the inherent high surface pH of glass beads. Neither prior acid washing of the beads nor the use of antioxidants in the polymer solutions prevented degradation during fractionation. Subsequently, Haloport F or Fluoropak 80, which apparently consist of Teflon particles, have been used with improved results. The column jacket temperature was kept at 34°C. with refluxing ether. Eluent increments of ~300 ml., containing increasing ratios of benzene solvent and isooctane nonsolvent, were passed through the column at ~100 ml./hr. The polymers were recovered by solvent evaporation and freeze-drying. This procedure did not work for low molecular weight polymers because they were too soluble in pure isooctane; for these, separation was initially carried out by using Dow Corning 200 fluid (viscosity grade 0.65 cstokes at 25°C.) as the nonsolvent with isooctane as the solvent. However, degradation occurred during these fractionations, so the benzene–isooctane procedure has been used more recently with the temperature reduced from 34 to 7°C. A plot of intrinsic viscosity of the fractions versus eluent composition is shown in Figure 1 for fractionation at 34°C. This graph is useful for choosing appropriate eluent compositions for PPG–TDI polymers of different molecular weights.

For comparison, one polymer was fractionated by conventional precipitation from 4% benzene solution.

C. Intrinsic Viscosity Measurements

Viscosities were determined in benzene with Ubbelohde suspended-level viscometers at 25 ± 0.02°C. at two concentrations. Intrinsic viscosities were calculated from

$$\eta_{sp}/c = [\eta] + k'[\eta]^2 c \tag{2}$$

in which η_{sp} is the specific viscosity and c is the polymer concentration (in grams/deciliter). A value for the constant k' of 0.39 as determined previously[1] was assumed. Since the values of $[\eta]$ calculated from the two concentrations were in good agreement, the use of 0.39 for k' was justified.

Molecular weights were calculated from

$$[\eta] = 4.13 \times 10^{-4} \bar{M}_w^{0.64} \tag{3}$$

Equations (2) and (3) were determined by Moacanin[1] for the range of $[\eta] = 0.05$–0.55; therefore, for $[\eta] > 0.55$ the molecular weights were obtained from an extrapolation of the curve. The fractionation curves are

given in terms of the cumulative weight fraction $W_{[\eta]}$ corresponding to the intrinsic viscosity $[\eta]_i$ of the ith fraction

$$W_{[\eta]} = (W_i/2) + \sum_{j=1}^{i-1} W_j \tag{4}$$

Intrinsic viscosity was used because the relationship between $[\eta]$ and molecular weight has not been firmly established for degraded polymer or polymer of very high molecular weight.

III. RESULTS AND DISCUSSION

A. Fractionation by Precipitation

Large-scale precipitation fractionation of PPG–TDI polymer of intrinsic viscosity 0.33 dl./g. gave a value of $\bar{M}_w/\bar{M}_n = 1.7$,[1] calculated from:

$$\bar{M}_w/\bar{M}_n = \sum_1^i W_i M_i / \sum_1^i (W_i/M_i) \tag{5}$$

Data for a polymer of intrinsic viscosity 0.57 dl./g. that was fractionated by precipitation from benzene are given in Table I and Figure 2. The $\bar{M}_w/\bar{M}_n$ was found to be 1.62, showing that the distributions are similar in the two

TABLE I
Precipitation Fractionation of PPG–TDI Polymer at 25°C.[a]

Fraction	Cumulative weight fraction $W_{[\eta]}$,[b]	Intrinsic viscosity $[\eta]$, dl./g.[c]	Weight-average molecular weight $\bar{M}_w$[d]
1	0.0345	0.151	10,200
2	0.239	0.388	44,400
3	0.559	0.500	65,600
4	0.735	0.588	84,500
5	0.810	0.696	110,000
6	0.930	0.944	177,000
Initial:[e]		0.570	82,000
Combined:[e]		0.550	77,000

[a] Recovery: 99.8%; $\bar{M}_w/\bar{M}_n = 1.62$.

[b] W_η was calculated from $W_{[\eta]} = [(W_i/2) + \Sigma_{j=1}^{i-1} W_j]$.

[c] $[\eta]$ was determined in duplicate and calculated from $\eta_{sp}/c = [\eta] + k'[\eta]^2 c$ for a value of k' of 0.39.[1]

[d] $\bar{M}_w$ was calculated from $[\eta] = KM^a$ for $K = 4.13 \times 10^{-4}$ and $a = 0.64$.[1]

[e] Initial refers to unfractionated polymer; combined are corresponding data calculated from $[\eta] = \Sigma_1^i W_i[\eta]_i$ and $\bar{M}_w = \Sigma_1^i W_i M_i$.

polymers. This is evidence that the broader distributions ($\bar{M}_w/\bar{M}_n \sim 2$) obtained by column elution are the result of more efficient fractionation rather than an increase in polydispersity of these higher molecular weight polymers.

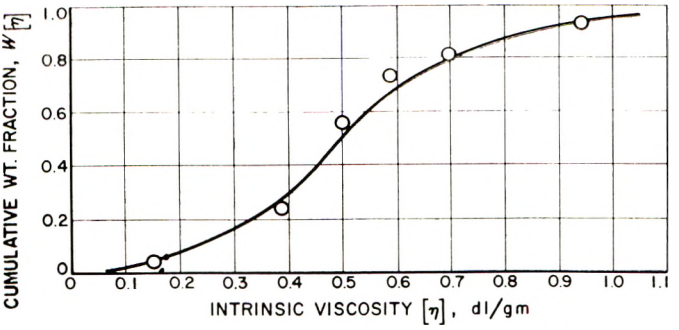

Fig. 2. Integral distribution curve for PPG–TDI polymer fractionated by precipitation.

B. Column Elution Fractionation

The results for column fractionation of four different polymer samples are given in Tables II–V. Although the integral curve may be obtained directly from the experimental results, because of its S-shape and the inherent scatter of fractionation data, determination of the most likely curve is difficult. On graphical differentiation, the uncertainties are increased so that the differential curve is not likely to provide a very unique

TABLE II
Column Fractionation of PPG–TDI: Polymer A[a]

Fraction	Cumulative weight fraction $W_{[\eta]}$	Intrinsic viscosity [η], dl./g.	Weight-average molecular weight $\bar{M}_w$
1	0.055	0.127	7,730
2	0.148	0.259	23,400
3	0.239	0.313	31,600
4	0.351	0.420	49,800
5	0.472	0.477	61,400
6	0.592	0.605	88,500
7	0.715	0.631	94,400
8	0.890	0.867	155,600
Initial:		0.600	87,300
Combined:		0.550	76,300

[a] Recovery: 97.2%; $\bar{M}_w/\bar{M}_n$: 2.24; column packing: glass beads (Minnesota Mining and Manufacturing); column temperature: 34°C.

representation of the distribution. The differential distribution curves are desired because they can be more readily interpreted and compared since asymmetry about the maximum provides an estimate of the relative weights of high and low molecular weight polymer in a most probable distribution, the maximum gives the approximate value of the number-average molecular weight, and the width or aspect ratio provides a relative estimate of polydispersity for polymers of comparable molecular weight.

TABLE III
Column Fractionation of PPG–TDI: Polymer B[a]

Fraction	Cumulative weight fraction $W_{[\eta]}$	Intrinsic viscosity $[\eta]$, dl./g.	Weight-average molecular weight $\bar{M}_w$
1	0.032	0.159	11,000
2	0.106	0.234	20,200
3	0.195	0.360	39,400
4	0.301	0.463	58,200
5	0.423	0.528	71,600
6	0.547	0.619	92,300
7	0.673	0.785	133,000
8	0.793	1.02	200,000
9	0.924	1.12	222,000
Initial:		0.673	104,500
Combined:		0.680	106,100

[a] Recovery: 98.2%; $\bar{M}_w/\bar{M}_n$: 2.14; column packing: Haloport F. (F and M Scientific Co.); column temperature: 34°C.

TABLE IV
Column Fractionation of PPG–TDI: Polymer C[a]

Fraction	Cumulative weight fraction $W_{[\eta]}$	Intrinsic viscosity $[\eta]$, dl./g.	Weight-average molecular weight $\bar{M}_w$
1	0.0365	0.158	10,800
2	0.118	0.294	28,600
3	0.235	0.427	51,300
4	0.373	0.547	75,500
5	0.497	0.662	101,800
6	0.619	0.788	133,600
7	0.761	1.001	194,200
8	0.919	1.266	280,300
Initial:		0.725	120,000
Combined:		0.710	113,300

[a] Recovery: 99.4%; $\bar{M}_w/\bar{M}_n$: 2.03; column packing: Fluoropak 80 (Fluorocarbon Co., Fullerton, Calif.); column temperature: 34°C.

Therefore the equations suggested by Tung,[6] which are applicable to a variety of different polymeric systems by suitable choice of the parameters, were tried. From these equations a linear plot may be obtained, using only the experimental integral data. From the slope and intercept of this straight line, an analytical expression for the integral curve can be calculated and from it the differential curve can be obtained by mathematical differentiation. In Figure 3 the logarithm of $1/[1 - W_{[\eta]}]$ is plotted against $[\eta]$ on log–log paper in conformance with the Tung equations:

$$W_{[\eta]} = 1 - \exp\{-a'[\eta]^b\} \tag{6}$$

$$dW_{[\eta]}/d[\eta] = w_{[\eta]} = a'b(\exp\{-a'[\eta]^b\})[\eta]^{b-1} \tag{7}$$

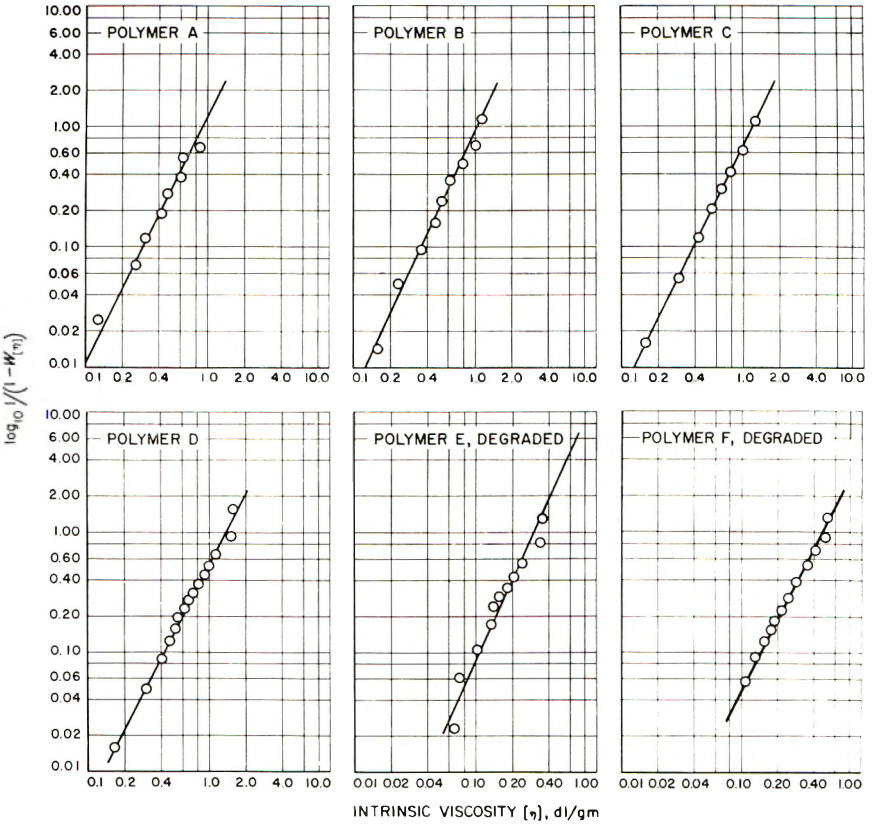

Fig. 3. Column elution fractionation data for PPG–TDI polymers.

in which a' is a constant obtained from the ordinate intercept of the log–log plot at the point where the abscissa equals unity. This intercept is equal to log (a' log e). The constant b is equal to the slope of the log–log plot. The distributions observed can be fitted by straight lines as shown in Figure 3; the values of a' and b are given in Table VI. The least squares fitting of the lines of Figure 3 and all the distributions were calculated by means of programs written for the IBM 1620 computer. From these and eqs. (6) and (7) the integral and differential curves have been calculated and are shown as solid curves in Figure 4 with the circles representing experimental points. It can be seen that experimental data fit the Tung distribution very well. Since the ratio of weight-average to number-average molecular weight was only slightly more than two, theoretical curves have been calculated for the most probable distributions for the values of the fractional extent of polymerization P, corresponding to one-half the weight-average molecular weight of the polymer as determined directly from the experimental data. The equations used to calculate P are:[2]

$$\bar{M}_n = \bar{M}_w/2 \tag{8}$$

$$\bar{M}_n/\bar{M}_u = 1/(1 - P) \tag{9}$$

TABLE V
Column Fractionation of PPG–TDI: Polymer D[a]

Fraction	Cumulative weight fraction $W_{[\eta]}$	Intrinsic viscosity $[\eta]$, dl./g.	Weight-average molecular weight $\bar{M}_w$
1	0.036	0.167	11,800
2	0.107	0.304	30,200
3	0.181	0.403	46,900
4	0.251	0.468	61,200
5	0.308	0.525	70,800
6	0.361	0.557	77,700
7	0.413	0.633	94,900
8	0.466	0.688	108,100
9	0.521	0.747	122,900
10	0.579	0.822	142,700
11	0.639	0.920	170,200
12	0.701	0.999	193,600
13	0.780	1.141	238,300
14	0.888	1.520	373,000
15	0.974	1.536	379,200
Initial:		0.730	121,000
Combined:		0.790	137,400

[a] Recovery: 101%; $\bar{M}_w/_n\bar{M}$: 2.19; column packing: Fluoropak 80 (Fluorocarbon Co., Fullerton, Calif.); column temperature: 34°C.

TABLE VI
Empirical Constants from PPG–TDI Fractionation Data

Sample	a'	b
A	2.628	1.934
B	1.855	2.036
C	1.530	2.019
D	1.251	1.960
E	24.894	2.058
F	10.930	2.015

or

$$P = 1 - (M_u/\bar{M}_n)$$

in which $\bar{M}_u$, the unit-average molecular weight was somewhat arbitrarily taken as 1100, calculated by taking the average for TDI and PPG units. The value of $\bar{M}_u$ chosen does not effect the distributions significantly except at high extents of degradation. This is intuitively apparent and is shown more clearly below. The equations used to calculate the most probable distributions are based on Flory's equation:[2,8,9]

$$dW_X/dX = X(1 - P)^2P^{X-1} \tag{10}$$

in which W_X is the weight fraction of polymer of degree of polymerization X. Since it is necessary to compare distributions in terms of the intrinsic

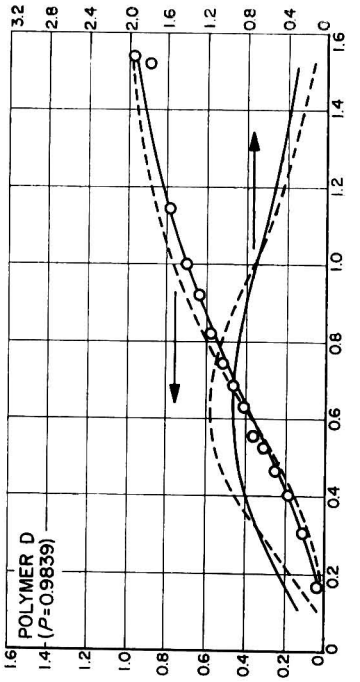
POLYMER D
(P=0.9839)

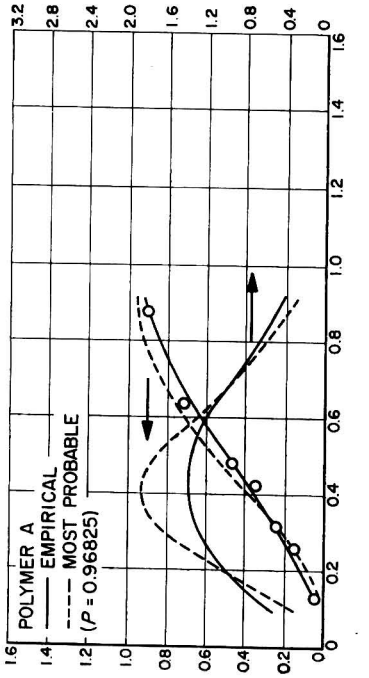
POLYMER A
—— EMPIRICAL
---- MOST PROBABLE
(P=0.96825)

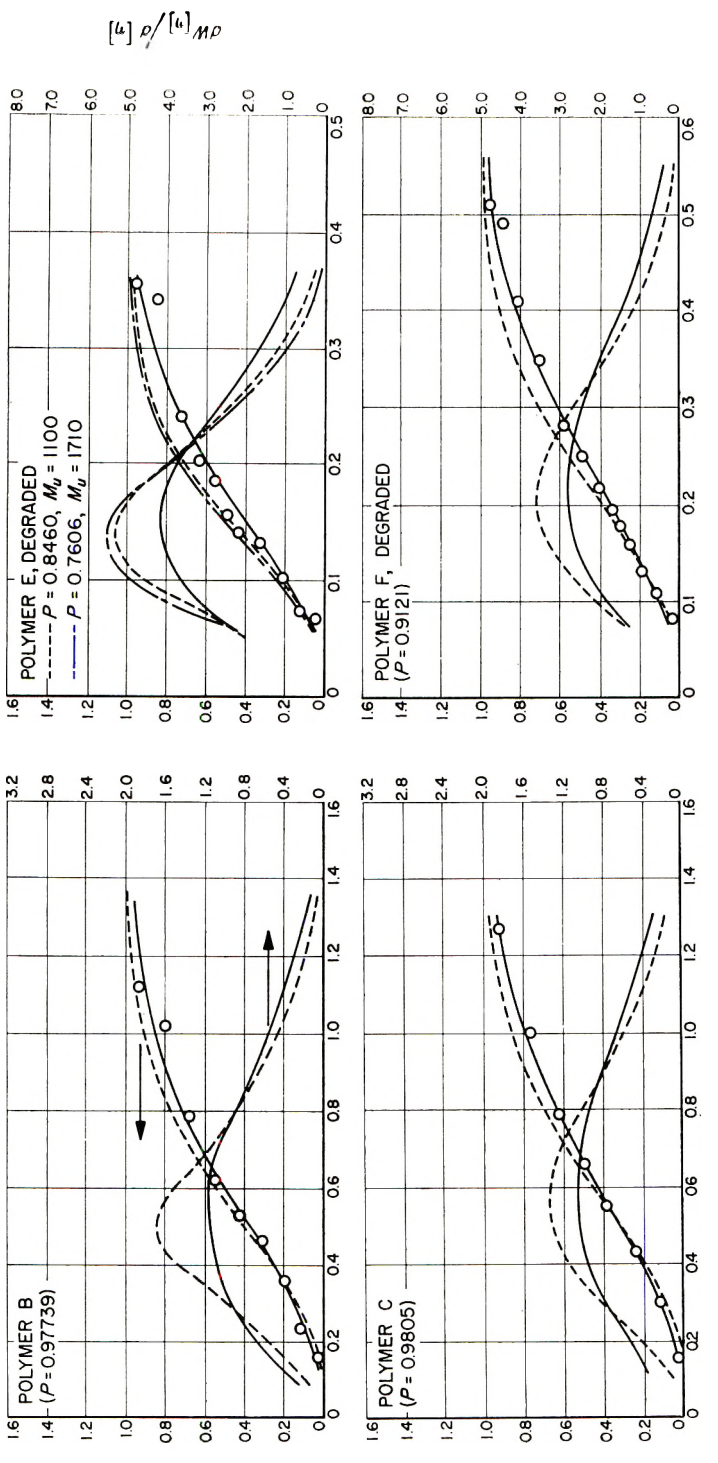

Fig. 4. Integral and differential distribution curves for PPG-TDI polymers fractionated by column elution.

viscosity, because the experimental data and the Tung distributions are given in terms of $W_{[\eta]}$ and $[\eta]$, it is necessary to introduce the relationship:

$$[\eta] = KM^a = K(\bar{M}_u X)^a \tag{11}$$

and use

$$dW_{[\eta]}/d[\eta] = dW_X \, dX/dX \, d[\eta] \tag{12}$$

in which $W_{[\eta]}$ and W_X are numerically equal.

Therefore:

$$\frac{dW_{[\eta]}}{d_{[\eta]}} = \frac{dW_X}{dX}\left(\frac{[\eta]^{(1/a)-1}}{aK^{1/a}\bar{M}_u}\right) \tag{13}$$

Equation (13) was used to calculate the differential most probable distribution curves for values of $\bar{M}_u = 1100$, $K = 4.13 \times 10^{-4}$, and $a = 0.64$.

Integration of eq. (10) gives:

$$W_X = 1 + \left[\frac{X(1-P)^2P^{X-1}}{\ln P}\right] - \left[\frac{(1-P)^2P^{X-1}}{(\ln P)^2}\right] \tag{14}$$

from which the integral curves can be calculated. It can be shown that eq. (14) is strictly valid only when the degree of polymerization is large relative to the unit chain length, i.e., when P is close to one, otherwise the summation equation should be used. From the summation of eq. (10):

$$\begin{aligned} W_X &= (1-P)^2\left(\sum_{i=1}^{X} iP^{i-1}\right) \\ &= (1-P)^2\frac{d}{dP}\left(\sum_{i=1}^{X} P_i\right) \\ &= (1-P)^2\frac{d}{dP}\left[\frac{P(1-P^X)}{1-P}\right] \\ W_X &= 1 + XP^{X+1} - (X+1)P^X \end{aligned} \tag{15}$$

Since $W_X = W_{[\eta]}$ it is only necessary to convert the values of X for which W_X has been calculated to the corresponding $[\eta]$[eq. (11)] to obtain the integral or summed distributions in terms of $W_{[\eta]}$ and $[\eta]$. The most probable distributions calculated from eqs. (13), (14), and (15) by means of the IBM 1620 program are shown in Figure 4 as dashed lines for each polymer. The values of P were sufficiently close to one so that the integral eq. (14) gave the same curves as the summation eq. (15), except for degraded polymers discussed below. As expected from the experimental $\bar{M}_w/\bar{M}_n$ ratios, the calculated distributions are slightly narrower but tend to agree with the experimental curves within the accuracy of the data.

C. Thermal Degradation and Column Elution Fractionation

Tables VII and VIII and Figure 4 (E, F) show the distributions for two polymer samples (from the same preparation as Polymer B) that were

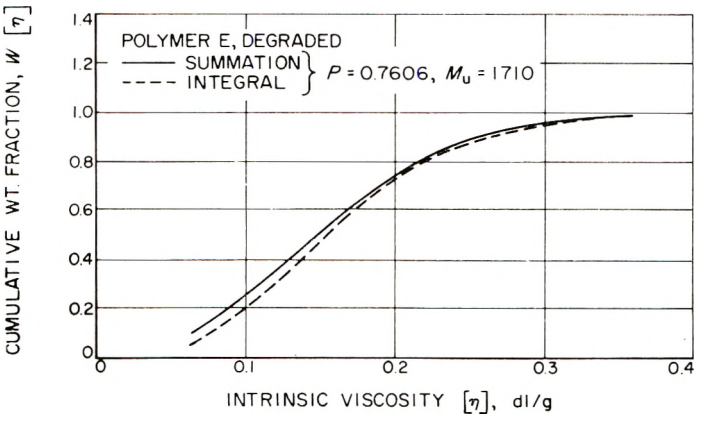

Fig. 5. Comparison of cumulative most probable distributions obtained from the integral and summation equations.

degraded from intrinsic viscosities of ~68 to 0.24 dl./g. by heating in a vacuum (~0.1 mm. Hg pressure) at 200°C. for 24 hr. Figure 5 shows the slight error introduced by using eq. (14) instead of eq. (15) for the lowest value of P used. The curves show that the molecular weight distributions have not changed appreciably. That is, for F, $\bar{M}_w/\bar{M}_n$ was initially 2.14 before and 2.05 after degradation. For E, silicone fluid was used as the nonsolvent and the intrinsic viscosity underwent a further decrease from 0.24 to 0.19 dl./g. during fractionation. This decrease may have been caused by residual active basic centers present in the silicone.[10] Thus this result does not necessarily reflect the distribution obtained for the purely thermal degradation process.

TABLE VII
Column Fractionation of Thermally Degraded PPG–TDI: Polymer E[a]

Fraction	Cumulative weight fraction $W_{[\eta]}$	Intrinsic viscosity $[\eta]$, dl./g.	Weight-average molecular weight $\bar{M}_w$
1	0.052	0.067	2,800
2	0.133	0.073	3,200
3	0.216	0.102	5,500
4	0.330	0.132	8,200
5	0.428	0.140	9,000
6	0.494	0.155	10,500
7	0.554	0.182	13,500
8	0.625	0.202	15,900
9	0.724	0.241	21,000
10	0.844	0.340	35,900
11	0.952	0.355	38,400
Initial:		0.240	21,000
Combined:		0.190	14,600

[a] Recovery: 102.3%; $\bar{M}_w/\bar{M}_n$: 1.79; column packing: Fluoropak 80 (Fluorocarbon Co., Fullerton, Calif.); column temperature: 34°C.

TABLE VIII
Column Fractionation of Thermally Degraded PPG–TDI: Polymer F[a]

Fraction	Cumulative weight fraction $W_{[\eta]}$	Intrinsic viscosity $[\eta]$, dl./g.	Weight-average molecular weight $\bar{M}_w$
1	0.045	0.080	3,700
2	0.124	0.106	5,800
3	0.191	0.130	8,000
4	0.254	0.158	10,900
5	0.303	0.176	12,800
6	0.345	0.194	15,000
7	0.402	0.216	17,700
8	0.488	0.246	21,700
9	0.589	0.281	26,700
10	0.701	0.348	37,300
11	0.806	0.411	48,300
12	0.881	0.492	64,000
13	0.957	0.506	68,000
Initial:		0.27	27,000
Combined:		0.27	27,000

[a] Recovery: 98.07%; $\bar{M}_w/\bar{M}_n$: 2.05; column packing: Fluoropak 80 (Fluorocarbon Co., Fullerton, Calif.); column temperature: 6.8°C.

Although $\bar{M}_w/\bar{M}_n \sim 2$ for the most probable distributions at reasonably high values of X_n, the parameters X_n, $\bar{M}_u$, $\bar{M}_w$, and P are interrelated, as follows:

$$X_n = 1/(1 - P) \tag{16}$$

$$X_w = (1 + P)/(1 - P) \tag{17}$$

where X_n and X_w are the number-average and weight-average degree of polymerization, respectively. Therefore,

$$P = (X_w/X_n) - 1 \tag{18}$$

Since

$$\bar{M}_w = \bar{M}_u X_n$$

and

$$\bar{M}_n = \bar{M}_u X_n$$

from eq. (17)

$$P = (\bar{M}_w/\bar{M}_n) - 1 \tag{19}$$

From eq. (9)

$$P = 1 - (\bar{M}_u/\bar{M}_n) \tag{9}$$

Equating eqs. (19) and (9) gives

$$(\bar{M}_w/\bar{M}_n) = 2 - (\bar{M}_u/\bar{M}_n) \tag{20}$$

or

$$\bar{M}_u = 2\bar{M}_n - \bar{M}_w \tag{21}$$

At high X_n, in practice, the difference expressed in eq. (21) is so small relative to the accuracy of measurements of $\bar{M}_n$ and $\bar{M}_w$ that $\bar{M}_u$ can not be determined uniquely, and it is only at catastrophically high degrees of degradation that $\bar{M}_u$ affects the distributions to give changes outside the limits of error. For example, for polymer E, for $\bar{M}_w/\bar{M}_n = 1.79$ and $\bar{M}_w = 14{,}600$ (as determined from intrinsic viscosity), calculation of $\bar{M}_u$ gives 1710 from eq. (21). The theoretical most probable distribution obtained for $P = 0.7606$ and $\bar{M}_u = 1710$ is shown as the semi-dashed line in Figure 4*E*, and is only slightly different from the previous calculated curve for $P = 0.8460$ and $\bar{M}_u = 1100$. From the limited data available, it is difficult to tell whether $\bar{M}_u$ is actually of the order of one to two thousand; however, preliminary work at very high extents of degradation presently in progress indicates predominant urethane scission, which is consistent with $\bar{M}_u = 2000$–2200, assuming either vaporization of the aromatic degradation product or only one scission per aromatic group.

IV. CONCLUSIONS

Satisfactory experimental column elution fractionation procedures for undegraded and thermally degraded PPG–TDI polymers have been developed. These procedures demonstrate the applicability of column elution fractionation to condensation polymers and should be particularly adaptable to other polyurethanes. Differential distributions were calculated by use of the empirical relations suggested by Tung,[4] thus eliminating the need for graphical differentiation of the integral curves. The molecular weight distributions were found to approximate theoretical most probable distributions calculated from Flory's equation. The results obtained show that, for moderate extents of bond scission, the molecular weight distributions of PPG–TDI are invariant. Thus, the most likely mechanism of thermal degradation in a vacuum is a random scission process.

The authors wish to acknowledge the contributions of Professor R. Simha and Dr. R. F. Landel for many helpful discussions during the course of this work.

References

1. Moacanin, J., *J. Appl. Polymer Sci.*, **1**, 272 (1959).
2. Flory, P. J., *Principles of Polymer Chemistry*, Cornell Univ. Press, Ithaca, N. Y., 1953.
3. Desreux, J., and M. C. Spiegels, *Bull. Soc. Chim. Belg.*, **59**, 476 (1950).
4. Francis, P. S., R. C. Cooke, and J. H. Elliot, *J. Polymer Sci.*, **31**, 453 (1958).
5. Davis, T. E., and R. L. Tobias, *J. Polymer Sci.*, **50**, 227 (1961).
6. Tung, L. H., *J. Polymer Sci.*, **20**, 495 (1956).
7. Gordon, M., in *Thermal Degradation of Polymers*, Macmillan, New York, 1961.
8. Flory, P. J., *J. Am. Chem. Soc.*, **58**, 1877 (1936).
9. Flory, P. J., *Chem. Revs.*, **39**, 137 (1946).
10. Kučera, M., and J. Lanikova, *J. Polymer Sci.*, **54**, 375 (1961).

Résumé

Un procédé a été mis au point pour l'élution fractionnée par colonne des polymères polyoxypropylèneglycol-diisocyanate de toluène (PPG–TDI) de poids moléculaire ~100.000; en diminuant la température de la colonne de 34 à 7°C, la méthode a été étendue au polymère dégradé de poids moléculaire ~25.000. La différentiation graphique des courbes d'intégration a été éliminée en employant les équations empiriques de Tung. Les résultats pour les polymères dégradés et non-dégradés sont en accord avec les distributions théoriques les plus probables; il est donc indiqué de considérer un processus de scission statistique pour la dégradation.

Zusammenfassung

Ein Verfahren zur Säuleneluierungs-Fraktionierung von Polyoxypropylenglykol-Toluoldiisocyanatpolymeren (PPG–TDI) vom Molekulargewicht ~100000 wurde ausgearbeitet; durch Herabsetzung der Säulentemperatur von 34 auf 7°C wurde die Methode auf abgebaute Polymere vom Molekulargewicht ~25000 ausgedehnt. Graphische Differentiation der Integralkurven wurde durch Verwendung der empirischen Gleichungen von Tung vermieden. Die Ergebnisse für abgebaute und nicht abgebaute Polymere stimmten mit der theoretischen wahrscheinlichsten Verteilung überein; der Abbau erfolgt offenbar durch einen statistischen Spaltungsprozess.

Received November 20, 1962

JOURNAL OF POLYMER SCIENCE: PART A VOL. 2, PP. 705–709 (1964)

Detection of Ethylene Homopolymer in Ethylene–Propylene Block Copolymers

JOHN N. LOMONTE, *Research Division, W. R. Grace & Company, Clarksville, Maryland,* and GEORGE A. TIRPAK, *Polymer Chemicals Division, W. R. Grace & Company, Clifton, New Jersey*

Synopsis

A method has been developed for the determination of per cent ethylene incorporation in ethylene–propylene block copolymers by infrared spectroscopy. Standardization is done from mixtures of the homopolymers. Both standards and samples are scanned at 180°C. in a spring-loaded demountable cell. The standardization was confirmed by the analysis of copolymers of known ethylene content prepared with C^{14}-labeled ethylene. By comparison of the infrared results from the analyses performed at 180°C. and also at room temperature, the presence of ethylene homopolymer can be detected. An equation has been derived for the quantitative estimation of per cent ethylene present as copolymer blocks.

Introduction

Since the development of ethylene–propylene block copolymers, it has been desirable not only to know the amount of ethylene incorporated into the material, but also to know if the material were a true copolymer or a physical mixture of the two homopolymers. It has usually been necessary to perform tedious fractionations and subsequent analysis of the fractions to determine the manner in which the ethylene had been incorporated. In this paper we present a rapid method to determine this by means of infrared spectroscopy. A method for the quantitative estimation of per cent ethylene incorporated as a homopolymer is also presented.

This method makes use of a characteristic infrared rocking vibration due to sequences of consecutive methylene groups. Such sequences are found in polyethylene and in the segments of ethylene blocks in ethylene–propylene copolymers. This makes it possible to detect them at 730 and 720 $cm.^{-1}$. There are bands at both these locations in the infrared spectrum of the crystalline phase but only at 720 $cm.^{-1}$ in the amorphous phase. The ratio of these two bands in the infrared spectrum of a polymer film at room temperature is a rough measure of crystallinity. As seen by this ratio, the infrared spectra of the copolymers show varying degrees of polyethylene type crystallinity, dependent on ethylene concentration and method of incorporation. It is this varying degree of crystallinity which allows the qualitative detection of ethylene homopolymer in these materials.

Experimental

All infrared scans were made on a Perkin-Elmer 221G infrared spectrophotometer with the following instrumental conditions: slit program, 964 (415 μ at 750 cm.$^{-1}$); pen response, 3 sec. full scale; chart scale, 12.5 cm.$^{-1}$ per centimeter of chart length; scan speed, 60 cm.$^{-1}$ per minute; scan length, 760–680 cm.$^{-1}$; analytical frequency, 720 cm.$^{-1}$.

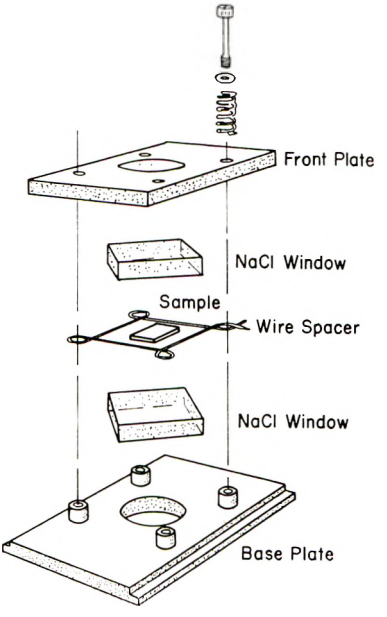

Fig. 1. Spring-loaded demountable cell.

A series of physical mixtures of isotactic polypropylene and linear polyethylene were made in the range 0–25% ethylene. These mixtures were made by weighing portions of polymer films on the analytical balance in the correct weight ratios and molding the films together on a hydraulic press with heated platens. The resulting film was cut into several fragments, stacked and repressed a minimum of five times. The final films were completely homogeneous as evidenced by infrared examination of several areas.

The films were mounted in a spring-loaded demountable cell with wire spacers as shown in Figure 1. The films were measured with a micrometer before assembly to assure their being about 25% thicker than the wire spacer. The films are assumed to acquire the same thickness as the wire under heat and pressure because of the high ratio of wire thickness to surface contact area on the salt plates as compared to standard shim spacers. Micrometer measurements on recovered films show them to be the same thickness as the wire after a slight allowance for shrinkage on cooling.

The cell assembly was placed in a heated cell block and the temperature of the whole apparatus was raised to 180°C. After this temperature was reached, an additional 15 min. was allowed for equilibrium to be established. The assembly was placed in the sample beam and the sample aligned with the aid of a dentist's hand mirror. The sample was scanned according to the given conditions. The slide interrupting the sample beam was closed and the scan rerun, thus obtaining a spectrum of sample emissivity. This latter scan was used as the infinite absorbance line for the measurement of the sample absorbance. The sample was allowed to cool in position and rescanned when the temperature reached ambient.

A calibration curve of absorbance at 720 cm.$^{-1}$ versus ethylene was made from these known mixtures for both the hot and the cold runs. Both plots resulted in straight lines from which the following equations were calculated.

$$\% \text{ Ethylene at } 180°\text{C.} = A/(0.55b)$$

where A = absorbance measured at 720 cm.$^{-1}$ and b = thickness of wire spacer in centimeters and

$$\% \text{ Ethylene at room temperature} = A/(3.0b)$$

where A and b have the same definitions as above.

A series of ethylene–propylene block copolymers was prepared with C^{14}-labeled ethylene. The per cent ethylene incorporation was determined by radiochemical methods. These samples when scanned at 180°C. gave results by the foregoing procedure which checked the radiochemical assay quite well. However, when the cooled samples were scanned, the results from the cold calibration were low in comparison with the known ethylene content. These data are shown in Table I.

TABLE I
C^{14}-Labeled Ethylene–Propylene Copolymers

	Ethylene, %		
Sample No.	Radiochemistry	Hot infrared scan	Cold infrared scan
3401	2.4	2.9	0.9
3402	4.0	3.65	1.3
3403-A	22.4	20.7	14.7
3403-B	24.5	22.2	15.3
3404	12.4	13.0	7.1
3405	14.0	14.1	7.5

A pair of samples were prepared in which the active sites on the growing propylene polymer were eliminated by hydrogen before addition of ethylene. Practically identical values for per cent ethylene incorporation were calculated for both the hot and the cold scans. These data are shown in Table II.

TABLE II
Samples with Hydrogen-Reduced Active Sites

Sample No.	Ethylene, %	
	Hot infrared scan	Cold infrared scan
1487	5.0	5.3
1553	7.1	6.9

Results

Standardization for per cent ethylene incorporation in ethylene–propylene block copolymers can be done by the use of physical mixtures of the homopolymers provided the analysis is done in the amorphous phase at 180°C.

Some of the ethylene present is in the form of ethylene blocks in a copolymer when values for per cent ethylene incorporation calculated from the hot runs are significantly higher than values from the cold runs.

The sample is a mixture of the homopolymers when values from the hot and the cold runs for a given sample are essentially the same.

Discussion

The infrared absorption bands at 730 and 720 cm.$^{-1}$ are greatly influenced by crystallinity, and the different values calculated for mixtures and copolymers at room temperature are obviously caused by the crystallinity of the samples. The samples run at room temperature are always scanned after the annealing process of slowly cooling from 180°C. so as to maximize the effect of crystallinity on the intensity of these bands. The results calculated from the cold runs for the copolymers are probably low in comparison to mixtures of the homopolymers, because the ethylene blocks are not able to produce a crystallinity effect on the intensity of the band as great as the homopolymer. This is caused by the tendency of the polypropylene chains to segregate the ethylene blocks from each other and the possibility of the ethylene blocks not being sufficiently long to bend back on themselves to form large crystalline volumes. Some crystallinity is obviously due to the ethylene blocks but its effect on the intensity of the band is not as great as the homopolyethylene.

The samples prepared by the elimination of the active sites with hydrogen before the addition of ethylene gave the same values for both hot and cold runs. These samples were a deliberate attempt to make a mixture of the homopolymers under conditions similar to the method used to make the copolymers. As these samples gave the same values when compared to melted homopolymer mixtures and also when compared to the same mixtures at room temperature, it was assumed they were actually the desired homopolymer mixture.

An ethylene–propylene copolymer made under carefully controlled conditions gave the largest difference for ethylene content between hot and

cold determinations. The sample calculated 16.2% ethylene in the melt and only 6.5% at room temperature. This sample was assumed to have all the ethylene in blocks with no ethylene homopolymer present. By making theoretical known additions of polyethylene to this copolymer, it is possible to derive an equation of the ratio of cold and hot values as related to the per cent ethylene present as copolymer blocks. This equation is:

$$E = 167(1 - R)$$

where E = per cent ethylene as copolymer and R = ratio of per cent ethylene values, cold/hot. This equation should be valid for the quantitative estimation of per cent ethylene present as copolymer in a sample.

The authors are indebted to Dr. J. D. Moyer of the Research Division for the preparation of the copolymers containing the C^{14}-labeled ethylene and the subsequent radiochemical analyses performed. The authors also wish to thank Dr. R. J. Ehrig of the Research Division for the preparation of the samples in which the active sites on the growing polymer had been eliminated by hydrogen before the addition of ethylene.

Résumé

On a développé une méthode de détermination par spectroscopie infrarouge de la teneur d'éthylene incorporé dans des copolymères a blocs éthylène–propylène. On standardise la méthode a partir de mélanges d'homopolymères. Les échantillons de même que les mélanges étalons sont examinés à 180°C dans une cellule démontable chargée d'un ressort. La standardisation a été confirmée par l'analyse de copolymeres de teneur en éthylene connue préparés avec de l'éthylene refermant du C^{14} marqué. En comparant les résultats de l'infra-rouge a partir dèanalyses effectuées à 180°C. ainsi qu'à température de chambre, on peut décéler la présence d'homopolymère d'éthylène. On a dédui une équation pour l'estimation quantitative du pourcentage d'éthylène présent sous forme de copolymère à blocs.

Zusammenfassung

Eine Methode zur infrarotspektroskopischen Bestimmung des prozenteullen Äthyleneinbaus in Athylene–Propylen-Blockcopolymere wurde entwickelt. Die Standardisierung erfolgt mit Homopolymer-Mischungen. Sowohl Standards als auch Proben werden in einer abnehmbaren Federzelle gemessen. Die Standardisierung wurde durch die Analyse von Copolymeren mit bekanntem Äthylengehalt überprüft, die mit ^{14}C-markiertem Äthylen dargestellt worden waren. Durch Vergleich der Infrarotergebnisse bei 180°C und auch bei Raumtemperatur kann die Anwesenheit von Homopolyäthylen festgestellt werden. Eine Gleichung zur quantitative Bestimmung des als Blockcopolymeres vorhandenen Äthylenes wurde abgeleitet.

Received December 3, 1962

JOURNAL OF POLYMER SCIENCE: PART A VOL. 2, PP. 711–730 (1964)

Emulsion Polymerization of Styrene in Coacervating and Noncoacervating Soap–Electrolyte Systems

J. L. MATEO* and IRVING COHEN, *Department of Chemistry, Polytechnic Institute of Brooklyn, Brooklyn, New York*

Synopsis

An attempt is made here to delineate some of the consequences of the special properties of coacervating soaps when the soaps are used in the emulsion polymerization of styrene. In dilute solutions an essential difference between a coacervating soap and a noncoacervating soap is the critical suppression of the micellar ionization in coacervating systems when relatively small amounts of simple electrolytes are added to the systems. A direct correlation between the polymerization rates and polymer molecular weights with the state of micellar ionization has been demonstrated. The highest polymerization rates and highest polymer molecular weights occur in solutions in which the coacervating soaps show a maximum ionization. In soap solutions in which the micellar ionization is critically suppressed there is evidence of soap desorption from polymer particles, resulting in the generation of an increasing number of particles during the course of the polymerization Two coacervating systems and two noncoacervating systems were used in this investigation. For the anionic noncoacervating K laurate–KCl system, where the micellarsize remains practically constant with the addition of electrolyte, the following relationship between the polymerization rate and KCl concentration, up to 1M KCl, has been found: $R = R_0 + B\sqrt{C}$. The effects of the charge properties of soap micelles on the course of the polymerization of styrene have been associated with two effects. (*a*) For highly ionized micellar systems the micelle periphery presents an open structure due to the coulombic repulsion of the charged polar hydrophilic groups of the soap molecules. This open structure facilitates the diffusion of monomer to the loci of polymerization. (*b*) Where the micellar ionization is suppressed, monomer diffusion to the loci of polymerization is impeded. Extensive suppression of micellar ionization results in micelles of enhanced stability. In the highly stabilized systems when the loci of polymerization are polymer particles there is competition for soap molecules between the adsorption sites on the polymer particle and soap micelles. The influence of soap concentration on the emulsion polymerization for different soaps and electrolyte concentrations has been investigated. For the coacervating Hyamine 1622 soap at zero electrolyte concentration, the rate of polymerization has been found to be proportional to the 0.5 power of the soap concentration. This relationship is not maintained when electrolyte is added to the polymerization system.

INTRODUCTION

Aqueous solutions of some long-chain quaternary ammonium salts at concentrations above the critical micelle concentration separate into two

* Post-Doctoral Fellow on leave from Departamento de Plasticos del Instituto de Quimica Alonso Barba, Madrid, Spain.

solution layers with the addition of small quantities of simple electrolytes, such as NaCl, $NaNO_3$, NaSCN, or Na_2SO_4.[1-3] This phenomenon is classified as a form of simple coacervation.

At a fixed temperature, there is a critical electrolyte concentration above which the system separates into two layers. These layers are well defined: one layer is practically free of the quaternary ammonium salt and the other layer shows the characteristics of an oil. At very high electrolyte concentrations, the colloidal species is precipitated as a solid phase.

A precondition for layering is the tremendous growth of the micellar aggregate in the homogeneous phase under the influence of added electrolyte. The onset of two-phase formation is characterized by a greater than one hundredfold increase in micellar molecular weight as compared to the salt-free micellar system. For example, in the case of the coacervating Hyamine 1622–NaCl-H_2O system,[3] a complicated micelle growth pattern is observed (Fig. 1*B*). Initially there occurs a relatively small micellar growth with the first small additions of NaCl. At 30°C., in a 2% Hyamine 1622 solution which is 0.01*M* in NaCl, the micellar molecular weight is 1.6×10^4. The initial small micellar growth is followed by a relatively sharp rise in micellar molecular weight over a narrow range of NaCl concentration (0.06–0.10*M*) to a near plateau. The micellar molecular weight at the plateau is 4.8×10^4.

For NaCl concentrations of 0–0.1*M*, the latter concentration corresponding to the molecular weight plateau, viscosity and diffusion experiments indicate that the micelles are essentially spherical in shape.[2] Micellar growth may be attributed to a more highly ordered and tightly packed micellar entity. With further addition of NaCl beyond the plateau, a sharp discontinuity is observed in the micellar molecular weights at 0.10*M* NaCl corresponding to a 20% growth of the micelle. The remaining micellar growth to the critical electrolyte concentration (CEC) 0.38*M* NaCl, is an exponential function of the NaCl concentration. The micellar molecular weight at the CEC is 1.98×10^6. In the NaCl concentration region corresponding to the onset of coacervate formation the micelles are cylindrical, rodshaped particles. The micellar molecular weight discontinuity described above may be associated with the transition of a spherical micelle to an insipient rod-shaped micelle. For the Hyamine 1622–NaCl–H_2O system, this transition is rather sharp and resembles a phase transition.

The micellar charge density, expressed as the ratio of the number of charges on the micelle (p) to the aggregation number (m) undergoes striking changes with the addition of electrolyte to the Hyamine 1622 solutions[2] (Fig. 1*A*, *b*). The manner in which the micellar charge properties vary as a function of added electrolyte has a direct bearing on the micellar growth pattern described above.[3] In a coacervating soap system the first small additions of electrolyte produce a relatively sharp rise in the p/m value, as compared to the salt-free system, to a maximum value. For the Hyamine 1622–NaCl–H_2O system this maximum ionization (0.26–0.28) occurs in

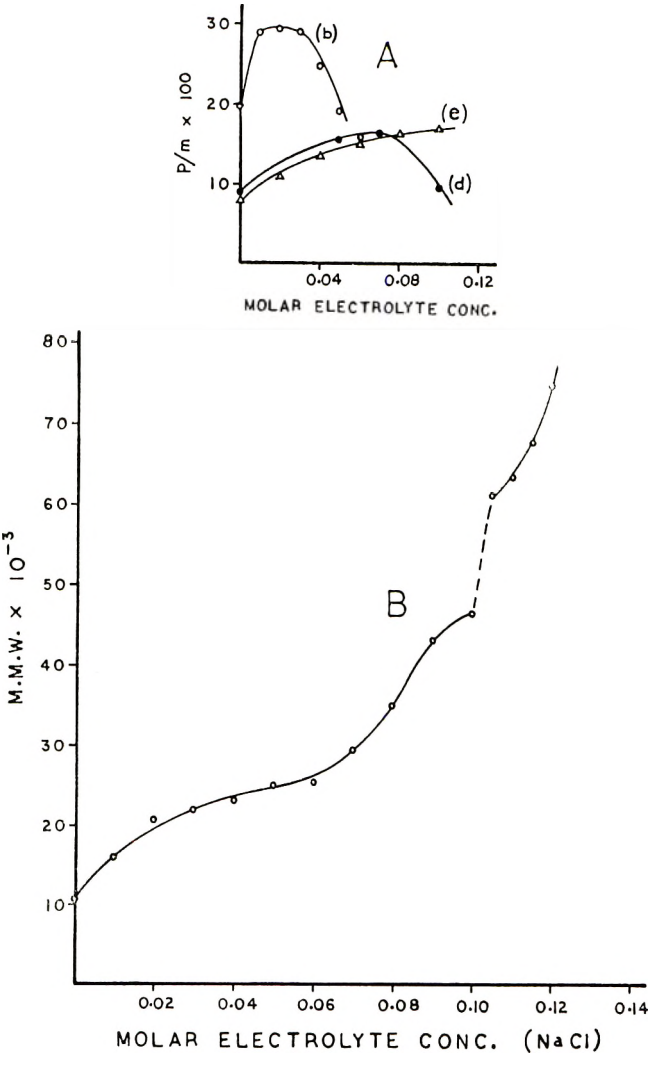

Fig. 1. (*A*) Variation of micellar charge density (p/m) with addition of electrolyte: (*b*) Hyamine 1622–NaCl–H_2O, 30°C.; (*d*) EHDDAB–$NaNO_3$–H_2O, 36°C.; (*e*) HDTAB–KBr, 30°C. (*B*) Micellar weights (M.M.W.) of Hyamine 1622–NaCl–H_2O as a function of NaCl concentration at 30°C.

0.03*M* NaCl solutions. The maximum p/m value is followed by a critical suppression of micellar ionization with further additions of NaCl. In a 0.10*M* NaCl solution corresponding to the observed micellar molecular weight discontinuity the p/m value is estimated to be ~0.06.

In the noncoacervating cationic soap system investigated, the HDTAB–KBr–H_2O system, a markedly different p/m behavior is observed (Fig. 1*A*, *e*). The first additions of KBr produce a rise in p/m to a maximum value of 0.16. With further additions of KBr, the p/m value remains at

0.16. It is of interest to note here that the two noncoacervating soap systems used in this study show very different properties with the addition of electrolyte to dilute aqueous solutions of these soaps. Debye[4] has reported rod-shaped micelles for the HDTAB–KBr–H_2O system, 1312 A. in length in 0.233*M* KBr. In this case the intramicellar coulombic interactions are sufficiently depressed with the addition of KBr to permit a large growth of an anisotropic micellar particle while maintaining a sufficient micellar charge to inhibit coacervation, even in saturated KBr solutions.

The effect of electrolyte addition on the micellar size of fatty acid soap is apparently very small. Data for diffusion coefficients[5] indicate that the micellar molecular weight of laurate solutions is practically unaffected by the addition of up to 1*M* NaCl or KCl to the laurate solution.

This investigation is concerned with the effects on the emulsion polymerization of styrene in soap systems produced by the addition of electrolyte to these systems. In particular, the effects of the changes in the micellar charge and micellar size properties of coacervating soap systems upon the course of the polymerization were studied. Two coacervating soap systems, Hyamine 1622–NaCl–H_2O and EHDDAB–$NaNO_3$–H_2O, and two noncoacervating soap systems, HDTAB–KBr–H_2O and potassium laurate–KCl–H_2O have been used in this investigation.

EXPERIMENTAL

Materials

The following soaps were used in this investigation.

(1) Hyamine 1622, diisobutylphenoxyethoxyethyldimethylbenzylammonium chloride monohydrate:

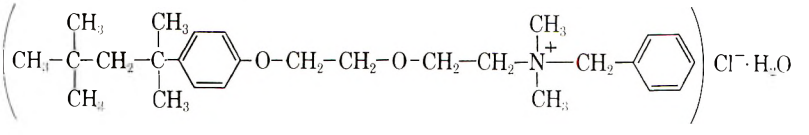

Hyamine 1622 is a commercial bactericide produced by Rohm and Haas.

(2) HDTAB, hexadecyltrimethylammonium bromide:

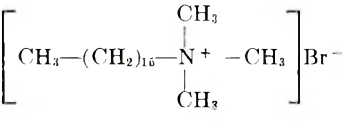

(3) EHDDAB, ethylhexadecyldimethylammonium bromide:

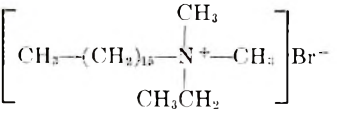

HDTAB and EHDDAB are produced by Eastman Organic Chemicals.

(4) Potassium laurate:

$$[CH_3—(CH_2)_{10}—COO^-]K^+$$

This soap is manufactured by K and K Laboratories.

The three cationic soaps (Hyamine 1622, HDTAB, and EHDDAB) were purified in the following manner. A quantity of the soap was dissolved in boiling acetone. The solution was filtered while hot and left to cool slowly. A crystalline product was formed. The crystals were filtered and the complete cycle was repeated (solution in boiling acetone, cooling, etc.). Finally, the crystals were dried in a vacuum desiccator. All inorganic electrolytes used and the initiator potassium persulfate were of C.P. grade. Potassium laurate was used without further purification.

Apparatus and Experimental Techniques

Polymerizations were carried out in a three-necked flask (1-liter) with two necks used for inlet and outlet of nitrogen. The third neck was closed with a rubber gasket. Magnetic stirring was used and the temperature was controlled and maintained by the immersion of the reaction flask in a thermostated bath. The materials were charged into the flask as solutions in water or liquid monomers, with the addition of aqueous solutions first, and then the liquid monomer. After the temperature was reached and the air removed by continuous passage of nitrogen for 1 hr. the initiator was added to the solution.

Samples of approximately 10 g. were withdrawn during the course of the reaction by insertion of a hypodermic needle through the gasket. The syringe was weighed to the nearest 0.02 g. The emulsion was precipitated in methanol and the syringe reweighed in order to determine the weight of the sample. The precipitated polymer was filtered and washed several times with methanol, and then dried at 75°C. for 24 hr., and weighed on a precision balance.

A total aqueous volume of 150 ml., a concentration of initiator of $6.15 \times 10^{-4}M$, and a weight of styrene of 22.5 g. were used in all experiments.

Viscosity

Viscosity measurements were performed in a Ubbelohde viscometer at 30°C. with toluene as solvent (Tables I and II).

Additional viscosity measurements of solutions in toluene of those polymers obtained using Hyamine 1622 as an emulsifying agent and without addition of electrolyte were performed in a modified Ubbelohde viscometer (Table III) as described by Immergut and Schurz[8] in order to eliminate the effects of shear gradient. The average rate of shear $\bar{G}$ was obtained by use of eq. (1):

$$\bar{G} = 8V / 3\pi r^3 t \tag{1}$$

where r is the radius of the capillary, 0.24 mm. in our case, V is the volume of the bulb, and t is the time of flow through the bulb being considered.

TABLE I
Intrinsic Viscosities of Polymers Obtained with the Hyamine–NaCl System

Experiment	Reaction time, hr.	Conversion, %	$[\eta]$	M.W.[a]
HYSP-0.02–5H	2.5	6.6	6.4	
HYSP–0.02–5H	5.5	16.6	6.7	
HYSP–0.04–5H	3	9.4	6.9	
HYSP–0.04–5H	8	27.9	6.5	
HYSP–0.04–5H	22	55.5	6.4	
HYSP–0.06–5H	4	8.2	6.5	
HYSP-0.06–5H	24	45	6.2	
HYSP-0.03–5H			7.5	
HYSP–0.03–2.5H			6.8	
HYSP–0.03–15H	3.5	31.5	10.8	
HYSP-0.07–5H	15	28.4	7.8	
HYSP–0.08–5H	7	2.6	2.6	1,600,000
HYSP–0.08–5H	25.75	42.84	7.2	
HYSP–0.1–5H	19	2.67	1.5	659,400
HYSP–0.1–5H	135		1.5	659,400
HYSP–0.1–5H	162		1.6	731,000
HYSP–0.18–5H	23	2.64	0.8	239.000

[a] Calculated from the equation of Goldberg et al.:[6] $[\eta] = 3.7 \times 10^{-4} M^{0.62}$.

TABLE II
Intrinsic Viscosities of Polymers Obtained with the HDTAB–KBr and EHDDAB–$NaNO_3$ Systems

Experiment	Reaction time, hr.	Conversion, %	$[\eta]$
HDSP–0–2.5H			11.7
HDSP–0.07–2.5H			18.8
HDSP–0.24–2.5H			10.6
HDSP–1–2.5H			4.45
EHSP–0–5E			8.6
EHSP–0.06–5E			13.9
EHSP–0.09–5E			11.6
EHSP–0.06–2.5E			13.7
EHSP–0.06–0.625E			10.1
EHSP–0.12–5E	2.5	27.5	10.1
EHSP–0.13–5E	2.5	9.75	7.4
EHSP–0.18–5E	7	63.7	11.7

TABLE III
Intrinsic Viscosities at Zero Shear Gradient of Polymers Obtained at Zero Electrolyte Concentration with Hyamine 1622 Soap

Experiment	$[\eta]$	M.W.[a]
HYSP–0–5H	11.45	7,153,000
HYSP–0–2.5H	9.8	5,756,000
HYSP–0–1.25H	8.9	5,036,000
HYSP–0–0.625H	8.05	4,381,000

[a] Calculated from the equation of Hahn et al.:[7] $[\eta] = 1.33 \times 10^{-4} M^{0.72}$.

The volume of each bulb was measured by weighing the amount of mercury which each contained. The plots of reduced viscosities versus shear gradient were extrapolated to zero shear gradient. These values were plotted against polymer concentration to determine the intrinsic viscosity by extrapolation to zero concentration.

RESULTS AND DISCUSSION

Influence of Added Electrolyte on the Polymerization Reaction

Figures 2–5 are conversion-time curves corresponding to polymerizations of styrene for each of the four soaps investigated at fixed electrolyte concentrations. In Figure 6, polymerization rates are plotted against electrolyte concentrations for the four soaps.*

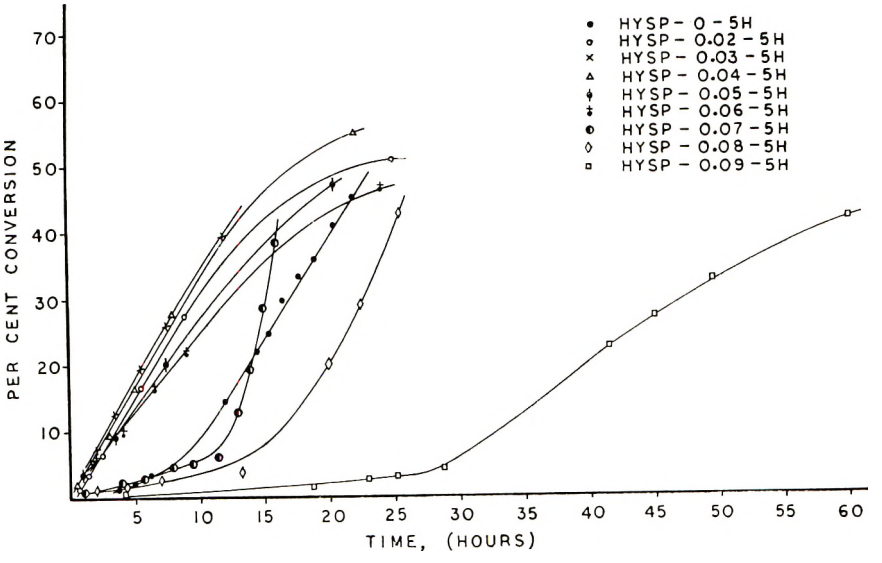

Fig. 2. Conversion–time curves at several electrolyte concentrations. Emulsifying-electrolyte system: Hyamine 1622–NaCl; temperature of reaction: 30°C.

For the noncoacervating systems (HDTAB–KBr–H_2O and K laurate-KCl–H_2O) (Figs. 3 and 5) the time–conversion curves are straight lines for the electrolyte concentrations investigated. In the HDTAB–KBr–H_2O system at low KBr concentrations, the polymerization rate rises to a maximum value at 0.07*M* KBr, decreasing very slowly as the KBr concentration increases (Fig. 6*b*). At 0.5*M* KBr the polymerization rate is reduced to the polymerization rate in the absence of added electrolyte.

* On the graphs and tables the following notation is used: each experiment is labeled with the first two letters of the soap followed by S and P the initial letters of styrene and persulfate. The first number in the label is the molar concentration of the electrolyte and the second number is the weight per cent of the soap.

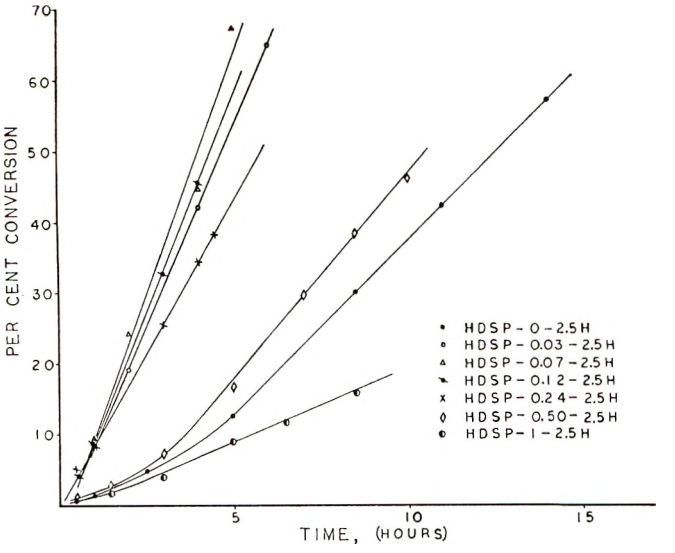

Fig. 3. Conversion–time curves at several electrolyte concentrations. Emulsifying-electrolyte system: HDTAB–KBr; temperature of reaction: 30°C.

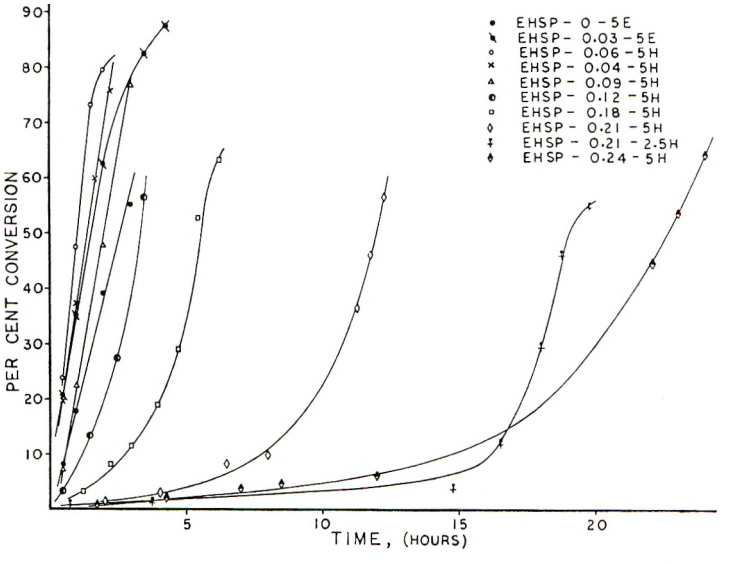

Fig. 4. Conversion–time curves at several electrolyte concentrations. Emulsifying-electrolyte system: EHDDAB–$NaNO_3$; temperature of reaction: 36°C.

The polymerization rate for the K laurate–KCl system increases as the electrolyte concentration increases without showing a maximum rate from 0 to 2*M* KCl (Fig. 6*d*).

The polymerization follows a different course when a coacervating soap system is used. The polymerization rate increases with the electrolyte

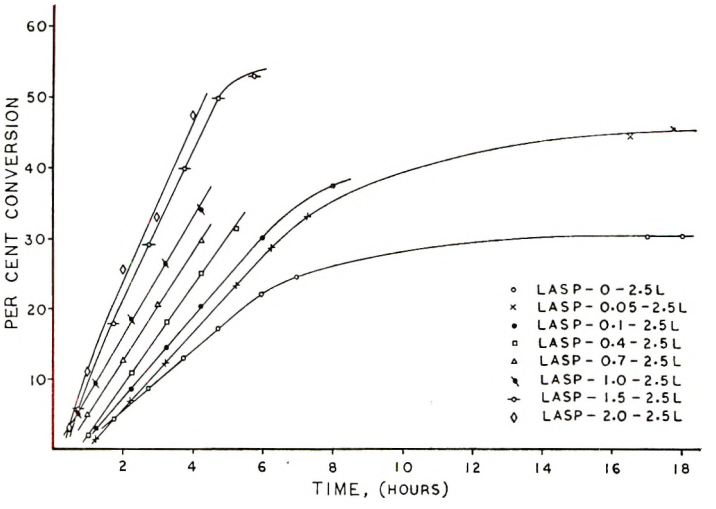

Fig. 5. Conversion–time curves at several electrolyte concentrations. Emulsifying-electrolyte system: K laurate–KCl; temperature of reaction: 30°C.

concentration up to a maximum value in 0.03*M* NaCl solutions for the Hyamine 1622–NaCl–H_2O system, and in 0.06*M* $NaNO_3$ solutions for the EHDDAB–$NaNO_3$–H_2O system, decreasing sharply from these values with further additions of electrolyte (Fig. 6*a*,*c*). In addition, a marked change in the course of the polymerization is observed above a well defined electrolyte concentration for each of the coacervating systems investigated (0.06*M* NaCl for the Hyamine 1622–NaCl–H_2O system, and 0.1*M* $NaNO_3$ for the EHDDAB–$NaNO_3$–H_2O system). For electrolyte concentrations above these values the conversion–time curves are not straight lines, but show a relatively long induction period followed by an accelerated increase in the polymerization rate with the polymerization reaction time. At still higher electrolyte concentrations additional effects are observed. For the coacervating Hyamine 1622–NaCl–H_2O system above 0.09*M* NaCl concentration, it is difficult to follow the course of the reaction accurately because the emulsion becomes unstable, precipitating part of the polymer formed. However, qualitatively an accelerated increase in the polymerization rate after 100 hr. of reaction is observed when an NaCl concentration of 0.1*M* is used.

There is a marked similarity between the p/m versus electrolyte concentration curves for the Hyamine 1622–NaCl–H_2O systems and EHDDAB–$NaNO_3$–H_2O systems (Fig. 1*A*, *b* and *d*) and the polymerization rates versus electrolyte concentration curves (Fig. 6*a*,*c*) of this study. The maxima occur at the same electrolyte concentrations for both sets of curves. The coincidence of these maxima would seem to indicate that micellar ionization is a major controlling factor in the changes observed in the polymerization. Other factors, such as monomer solubility and number of micelles have an influence on the course of the polymerization. However,

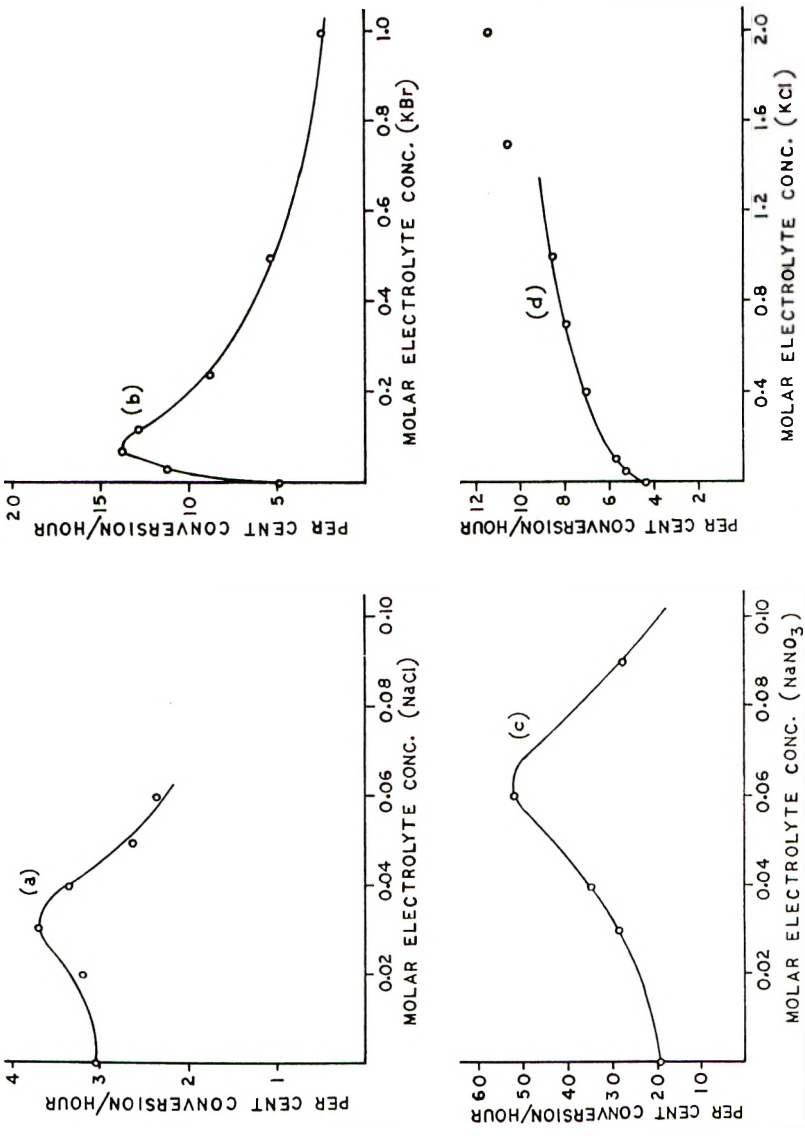

Fig. 6. Effect of electrolyte added on rate of polymerization for the four soaps investigated: (*a*) Hyamine 1622–NaCl system; (b) HDTAB–KBr system; (*c*) EHDDAB–$NaNO_3$ system; (*d*) K laurate–KCl system.

it is the micellar ionization properties which are apparently responsible for the special properties of emulsion polymerization in coacervating soap systems.

In the noncoacervating HDTAB–KBr system, for KBr concentrations from 0 to 0.7M, the p/m versus KBr concentration curve (Fig. 1A, e) and the polymerization rate versus KBr concentration (Fig. 6b) have the same shape. For higher KBr concentrations the polymerization rate curves show a slow decrease while the p/m curves show a fairly constant p/m value. This difference between the p/m versus electrolyte and polymerization rate versus, electrolyte curves at higher KBr concentrations may be associated with two effects. (a) At higher KBr concentrations the micelles undergo a very large growth.[2,4] For the fixed soap monomer concentrations used in this study, there are fewer micelles at these higher KBr concentrations than in solutions containing a lower concentration of KBr. Since the initial polymerization rate is a function of the number of micelles in the system, at higher KBr concentration, with fewer micelles in the system, it is to be expected that the overall rate of polymerization will be depressed. (b) The large micellar growth at higher KBr concentration is accompanied by a corresponding large increase in the viscosity of the medium. The increased viscosity effects the diffusion of monomer to the polymerization loci and a further depression of polymerization rate is to be expected.

By way of contrast, no appreciable micellar growth occurs with the addition of KCl to a dilute potassium laurate solution. Under these circumstances it might be expected that only the micellar charge properties will be responsible for changes in polymerization rate with the addition of KCl.

This is observed to be true (Fig. 6d) and the polymerization rate R may be related to the KCl concentration (Fig. 7) up to 1M KCl, by eq. (2) where

$$R = R_0 + B\sqrt{C} \tag{2}$$

where R_0 is the polymerization rate in an electrolyte free solution, B is a constant, and C is the concentration of KCl.

The Smith and Ewart theoretical estimation of emulsion polymerization[9,12] gives the following expression for the polymerization rate:

$$R = K_p N/2\ [\mathrm{M}] \tag{3}$$

where N is the number of particles of polymer in the emulsion, [M] is the monomer concentration, and K_p is the propagation rate constant. N is determined by eq (4):

$$N = 0.4[\mathrm{S}](a_s)^{3/5}\,(\rho/\mu)^{2/5} \tag{4}$$

where [S] is soap concentration, a_s is the area occupied by an adsorbed soap molecule, ρ is the rate of formation of radicals per milliliter of water and μ is the rate of increase in the volume of a particle.

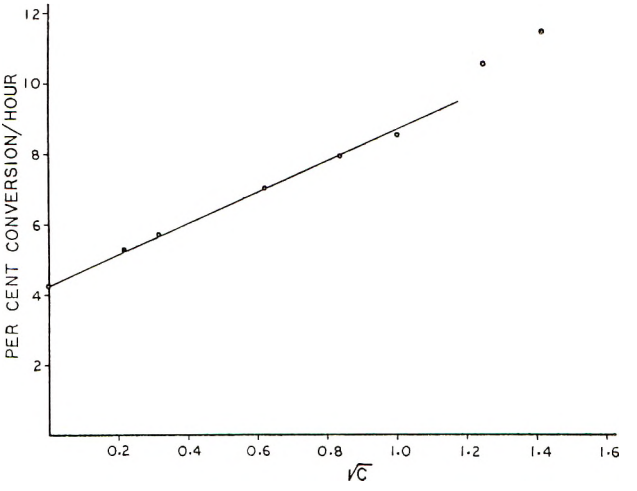

Fig. 7. Rate of polymerization dependence of the square root of electrolyte for the K laurate–KCl system. Temperature of reaction: 30°C.

Each primary radical which enters an inactive particle is presumed to start the growth of a new polymer chain, and this chain is terminated almost immediately following capture of another radical. If it is assumed that chain transfer may be disregarded, the average degree of polymerization X_n under these conditions should equal the ratio of the rate of growth of a chain to the frequency ρ/N of a capture of primary radicals.[9,10]

$$X_n = K_p N [\mathrm{M}]/\rho \tag{5}$$

During the polymerization reaction the steady-state concentration of monomer in the particles or in the micelles is controlled by a dynamic balance between the rate of polymerization on the one hand, and the rate of diffusion of monomer from the droplets to the particles, or to the micelles, on the other hand.

When a relatively high soap concentration is used, it has been found[11] that free soap (micellar) still remains at high conversions, and, since the polymerization rate is observed to be constant during the polymerization reaction, the equations cited above must be valid for the two stages of the polymerization, both in the early stage, where the loci of the propagation are the soap micelles and, later, when the polymer particles become the loci of polymerization.

An increase in the p/m value, i.e., micellar ionization may be related to an increase in monomer diffusion rate in the following manner.

The greater the charge density at the micelle periphery the greater will be the coulombic repulsion of the charged polar groups of the micelle at the micelle-water interface. This effect results in a more open structure at the micelle surface. The open structure facilitates the diffusion of monomer to the interior of the micelles, the loci of the initial polymerization. A

similar argument may be made for the increased monomer diffusion in the later stages of polymerization when the polymer particles are the loci of polymerization. A highly dissociated adsorbed soap would tend to have an open structure and thus facilitate the diffusion of monomers to the polymer particles. The enhanced monomer diffusion to the loci of polymerization should result in a higher polymerization rate.

The interpretation of larger dynamic concentration of monomer at the loci of polymerization with increasing ionization of the soap is buttressed by an examination of polymer intrinsic viscosities and molecular weights for a number of polymers obtained. Higher intrinsic viscosities are observed for those polymer solutions corresponding to higher micellar ionization (Table I). For the Hyamine 1622 system, the highest intrinsic viscosities are observed in 0.03M NaCl solutions. As indicated previously, the 0.03M NaCl solutions exhibit the maximum micellar ionization.

A change in the course of the polymerization is observed in Hyamine 1622–NaCl systems at NaCl concentrations in excess of 0.07M. A comparison of the 0.04M and 0.08M NaCl systems is instructive in this respect. For the 0.04M NaCl systems, for reaction times of 3, 8, and 22 hr., the conversions are 9.4, 27, and 55.5%, respectively, with the intrinsic viscosity ranging between 6.9 and 6.5. For the 0.08M system, a 2.6% conversion is achieved after 7 hr. The polymer intrinsic viscosity is 2.6 (corresponding to a molecular weight of 1.6×10^6). After 25.75 hr., a conversion of 42.25% is achieved and an intrinsic viscosity of 7.2 isobserved. This latter system shows the characteristic long induction period followed by an accelerated rate of polymerization. The long induction period is further illustrated in the 0.1 and 0.18M NaCl system. In the 0.1M system, a 2.67% conversion is achieved after 19 hr. of reaction. The resulting polymer shows an intrinsic viscosity of 1.5 and a corresponding molecular weight of 6.594×10^5. In the latter systems, the micellar ionization ($\sim$0.06) is very much lower than the micellar ionization in salt free systems.

A possible explanation of the accelerated rate of polymerization for coacervating soap systems in a well defined range of concentration of electrolyte is the following. With the suppression of micellar ionization in this electrolyte concentration range the micelles become more stable than the micelles at lower electrolyte concentrations. Debye[12] and Ooshika[13] have developed expressions for the energy per micelle involving a coulombic term related to the repulsive interactions of the charged polar heads of the soap molecules in the micelle and a van der Waals term related to attractive interactions of the hydrophobic tails of the soap molecules. The Ooshika expression contains a term which takes into account the change in surface energy with micelle formation:

$$W = N^{2/3}W_e + N^{1/3}W_s + NW_m \qquad (6)$$

where N is the micellar aggregation number and W_e, W_s, and W_m are the coulombic, surface, and van der Waals' energies per soap monomer.

The major effect of electrolyte addition to a soap system involves the

coulombic term of this expression. For the coacervating soap systems described here, in the electrolyte concentration range corresponding to ionization suppression, both the counterion screening effects and ionization suppression cooperatively decrease the repulsive coulombic term. The net result is a more stable micelle.

The consequences of this enhanced micellar stability in the emulsion polymerization system under investigation may be considered to be the following. When the loci of polymerization are the polymer particles, there is a competition for soap monomers between the adsorption sites on the polymer particles and newly formed micelles. In effect, a portion of the soap desorbs from the polymer particles to form new micelles which are in turn loci for the initiation of the polymerization of additional polymer particles. The process of soap desorption will produce a continuous increase of the number of particles and in accordance with eqs. (3) and (5) an increase in the polymerization rate will occur. That soap desorption from polymer particles does occur at higher electrolyte concentration is indicated by the precipitation of a portion of the polymeric product in systems in which the NaCl concentration is in excess of 0.1*M*.

Influence of the Soap Concentration at Different Electrolyte Concentrations on the Polymerization Reaction Chain Initiation Rate

The conversion–time curves for the emulsion polymerization of styrene in Hyamine 1622–NaCl–H_2O systems for fixed electrolyte concentrations and different soap concentrations show a number of distinctive char-

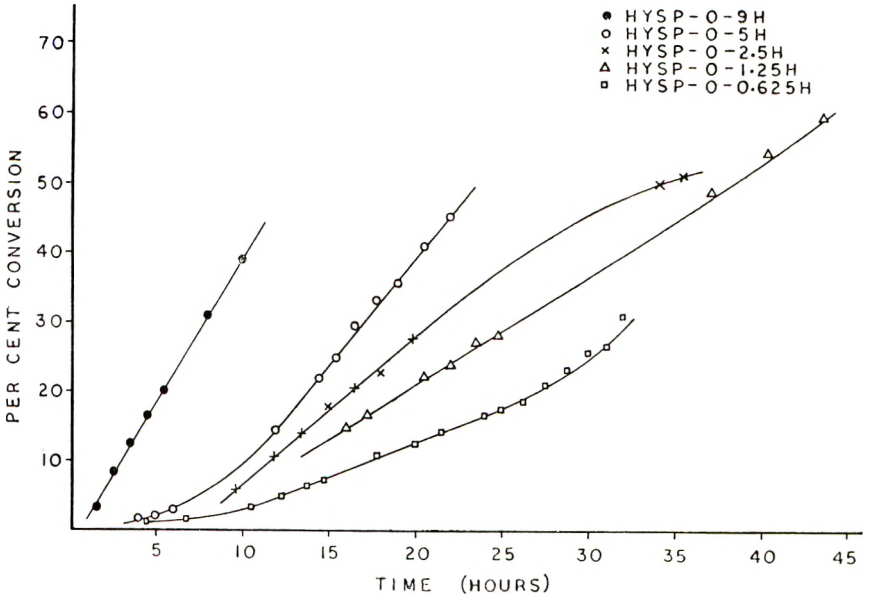

Fig. 8. Conversion–time curves at zero electrolyte concentration at several soap concentrations. Emulsifying soap: Hyamine 1622; temperature of reaction: 30°C.

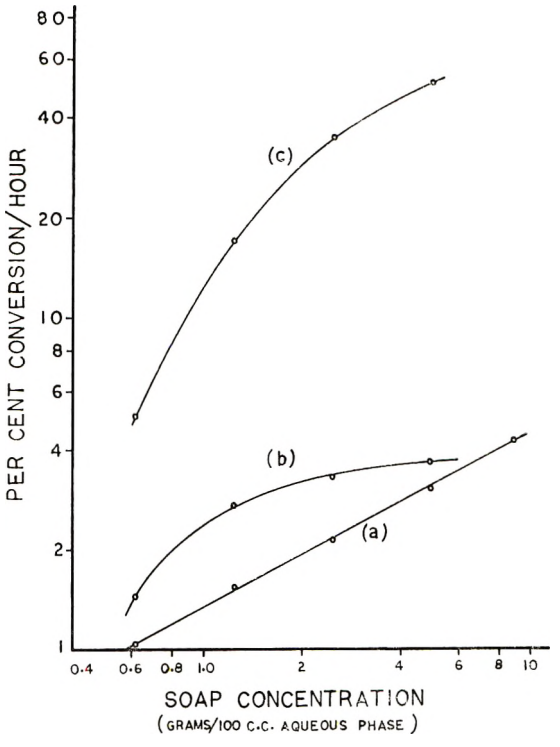

Fig. 9. Rate of styrene polymerization as a function of soap concentration: (*a*) Hyamine 1622, zero electrolyte concentration, 30°C.; (*b*) Hyamine, 1622, 0.03*M* NaCl, 30°C.; (*c*) EHDDAB, 0.06*M* $NaNO_3$, 36°C.

acteristics. Figure 8 represents the zero NaCl concentration system with the Hyamine 1622 concentration ranging from 0.625 to 9 wt.-%. When the polymerization rates versus soap concentrations are plotted on a log–log scale (Fig. 9*a*) the polymerization rate is shown to be proportional to the half-power of the soap concentration with considerable accuracy:

$$R \alpha [S]^{0.5} \tag{7}$$

Measurements of intrinsic viscosities at zero shear gradient of these polymers obtained at zero electrolyte concentration are given in Table III.

Under conditions of constant molecular weight and polymerization rate, the rate of polymer molecule formation can be determined by dividing the rate of polymerization by the degree of polymerization. The rate of polymer molecule formation corresponds to the value $\rho/2$ of eq. (5). For different concentrations of soap the values obtained for rates of polymer molecule formation calculated from the observed polymer molecular weights are given in Table IV. This table indicates that the rate of polymer molecule formation becomes greater for the higher concentration of soap. However, the rate of initiation at constant persulfate concentration, according to the Ewart-Smith theory[9,10] must remain constant for different

concentrations of soap. In the definitive studies of Smith on the emulsion polymerization of styrene, the argument is made that at high concentrations of particles (i.e., high soap concentrations) where the degree of polymerization is roughly in excess of 5×10^4, the apparent deviation from constancy of the rate of polymer molecule formation, calculated from experimentally determined polymer molecular weights may be attributed to chain transfer with styrene monomer.[10] The observed polymer molecular weights are lower than those predicted by theory. The values obtained in this study for rate of polymer molecule formation are in good agreement with those calculated by Smith,[10] both for the absolute values and the changes observed with increasing soap concentration for the emulsion polymerization of styrene where S-F soap flakes were used as the emulsifying agent. The above would indicate that in an electrolyte free solution the Hyamine 1622 soap behaves in a normal fashion in emulsion polymerization processes.

TABLE IV
Effect of Soap Concentration Rate of Polymer Molecule Formation 30°C., K Persulfate = $6.15 \times 10^{-4}M$

Experiment	Polymerization rate, molecule cc.$^{-1}$ sec.$^{-1}$	$\bar{X}$	Rate of polymer molecule formation, molecule cc.$^{-1}$ sec.$^{-1}$
HYSP-0-5H	9.9×10^{15}	68,780	1.43×10^{11}
HYSP-0-2.5H	6.85×10^{15}	55,346	1.05×10^{11}
HYSP-0-1.25H	4.95×10^{15}	48,423	1.02×10^{11}
HYSP-0-0.625H	3.34×10^{15}	42,120	0.80×10^{11}

The relationship, $R \propto [S]^{0.5}$, is not maintained when NaCl is added to the system. Figure 10 represents the $0.03M$ NaCl system. For Hyamine 1622 concentrations of 0.625–5.0% the conversion–time curves are roughly linear. However, the rate of polymerization in this concentration range is not proportional to the half power of the soap concentration as indicated in Figure 9*b*. For higher soap concentrations, 9.6 and 15%, an accelerated polymerization rate is indicated similar to that for the 0.07 and $0.08M$ NaCl solutions (Fig. 2) in which the soap concentration is 5%.

The conversion–time curves for the $0.07M$ NaCl solutions of Hyamine 1622 are represented in Figure 11. A higher initial polymerization rate is observed in 1.25 and 2.5% soap than for the higher soap concentration system, i.e., the 5% soap solution. The apparent anomaly may be explained as follows. The soap contributes to the chloride counterion concentration of the bulk solution so that the chloride concentration is $0.07M$ plus a contribution from the partially dissociated soap. From Figure 1*a*, it may be seen from the shape of the curve that in the region of $0.07M$ NaCl, a small increment of electrolyte (in this case Cl^- counterions) pro-

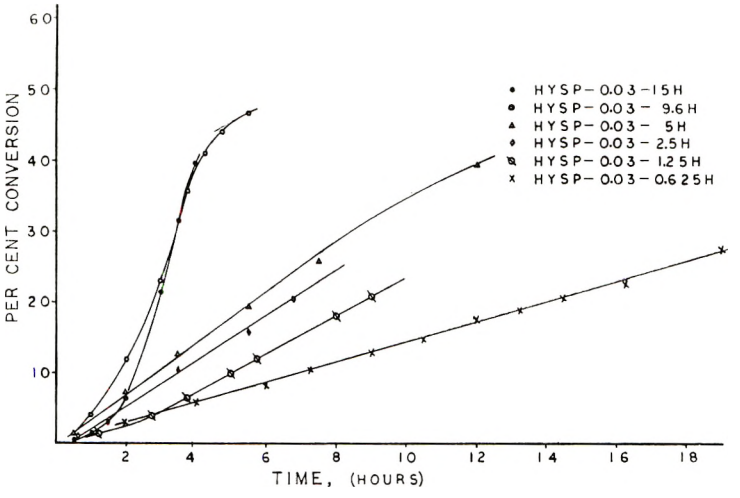

Fig. 10. Conversion–time curves at several soap concentrations for the Hyamine 1622–NaCl system. NaCl concentration 0.03M; temperature of reaction: 30°C.

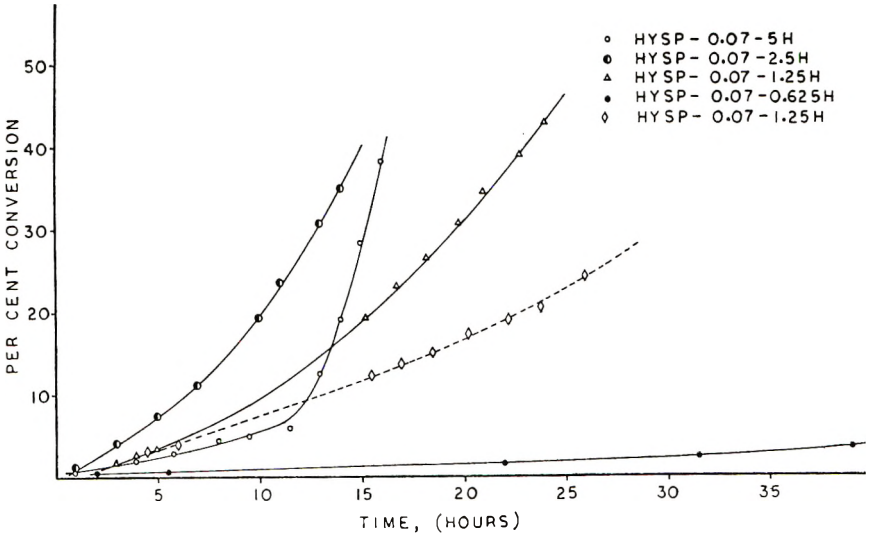

Fig. 11. Conversion–time curves at several soap concentrations for the Hyamine 1622–NaCl system. NaCl concentration: 0.07M; temperature of reaction: 30°C. The run HYSP-0.07-1.25H was carried out with 45 g. of monomer.

duces a large decrease in the micellar ionization. The reduced ionization of the higher soap concentration system, in turn, depresses the monomer diffusion to the interior of the micelle sufficiently so that the overall effect is a lower initial polymerization rate. The comparatively lower initial polymerization rate occurs in the 5% soap concentration solution even though the system contains a larger number of micelles than are present in the 2.5 or 1.5% soap systems. These observations point out the critical

role of micellar ionization in emulsion polymerization systems, for those systems in which large changes in micellar ionization are observed with the addition of electrolyte to the systems.

For the coacervating EHDDAB–$NaNO_3$–H_2O system (Fig. 12), in a 0.06*M* $NaNO_2$ solution the deviation from the half-power relationship of the rate of polymerization to the soap concentration is very pronounced (Fig. 9*e*). In this system, anions of the soap and the added electrolyte are different ionic species. Counterion exchange undoubtedly plays a role in the course of the polymerization reaction in this system.

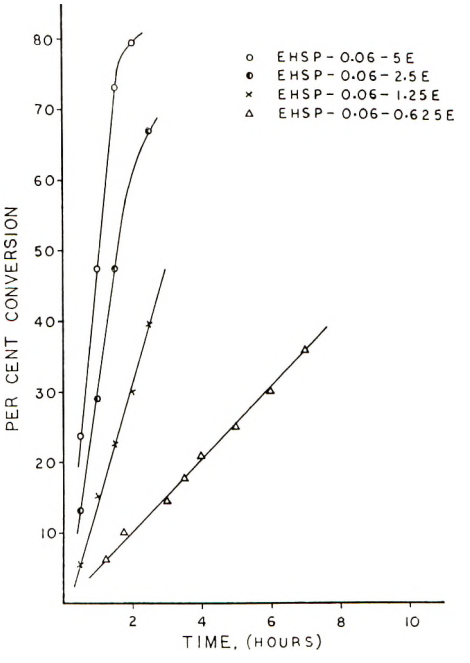

Fig. 12. Conversion–time curves at several soap concentrations for the EHDDAB–$NaNO_3$ system. $NaNO_3$ concentration: 0.06*M*; temperature of reaction: 36°C.

Coacervation phenomena in soap systems and all of the changes observed in the homogeneous phase prior to two phase formation show a high degree of electrolyte specificity.[2] For example, in dilute EHDDAB soap solutions, $NaNO_3$ will induce coacervate formation whereas KBr will not induce coacervate formation.

In all of the experiments of this investigation the electrolyte concentration was maintained constant during the course of the experiment. At the present time we are investigating the effects produced by changing the electrolyte concentration during the course of the polymerization.

References

1. Cohen, L., C. F. Hiskey, and G. Oster, *J. Colloid Sci.*, **9**, 243 (1954).
2. Cohen, L., and T. Vassiliades, *J. Phys. Chem.*, **65**, 1774 (1961).
3. Cohen, L., P. Economou, and A. Libackyj, *J. Phys. Chem.*, **66**, 1829 (1962).
4. Debye, P., and E. W. Anacker, *J. Phys. Colloid Chem.*, **55**, 644 (1951).
5. Graydon, W. F., Ph.D. thesis, University of Minnesota (1949).
6. Goldberg, A. I., W. P. Hohenstein, and H. F. Mark, *J. Polymer Sci.*, **2**, 503 (1947).
7. Hahn, W., W. Muller, and R. V. Webber, *Makromol. Chem.*, **21**, 131 (1956).
8. Immergut, E., and J. Schurz, *J. Polymer Sci.*, **9**, 279 (1952).
9. Smith, W. V., and R. H. Ewart, *J. Chem. Phys.*, **16**, 592 (1948).
10. Smith, W. V., *J. Am. Chem. Soc.*, **70**, 3695 (1948).
11. Harkins, W. D., *J. Am. Chem. Soc.*, **69**, 1428 (1947).
12. Debye, P., *Ann. N. Y. Acad. Sci.*, **51**, 575 (1949); *J. Phys. Chem.*, **53**, 1 (1949).
13. Ooshika, Y., *J. Colloid Sci.*, **9**, 254 (1954); Y. Ooshika and Y. Ikeda, *Kolloid-Z.*, **145**, 3 (1956).

Résumé

Cette étude est essentiellement explorative. On tente ici de délimiter certaines conséquences des propriétés spéciales des coagulats de savons lorsque ces savons sont utilisés lors de la polymérisation en émulsion du styrène. En solution diluée, il existe une différence essentielle entre un savon coagulant ou non, dans la suppression critique de l'ionisation micellaire dans les systèmes coagulants lorsque des quantités relativement faibles d'électrolytes simples sont ajoutées aux systèmes. On démontre une relation directe entre les vitesses de polymérisation et les poids moléculaires avec l'état d'ionisation micellaire. On obtient les vitesses de polymérisation et les poids moléculaires les plus élevés en solutions dans lesquelles les coagulats de savons ont une ionisation maximum. En solution savonneuse dans lesquelles l'ionisation micellaire est supprimée de façon critique, il se fait une désorption du savon des particules de polymère, provoquent la formation d'un nombre croissant de particules durant la polymérisation. On a utilisé lors de cette étude deux systèmes coagulants et deux systèmes non-coagulants. Pour le système anionique non-coagulant K-Laurate-KCl, dans lequel la dimension micellaire demeure pratiquement constante par addition dIélectrolytes, on trouve la relation suivante entre la vitesse de polymérisation et la concentration en KCl, jusqu'à 1M KCl: $R = R_0 + B\sqrt{C}$. On a associé les effets des propriétés de la charge des micelles de savon, durant la polymérisation du styrène avec deux effets: (*a*) Pour les systèmes micellaires fortement ionisés, la surface de la micelle possède une structure ouverte, due à la répulsion de coulomb des groupes hydrophiles polaires chargés des molécules de savon. Cette structure ouverte favorise la diffusion du monomère vers les sites de polymérisation. (*b*) Lorsque l'ionisation micellaire est supprimée, la diffusion du monomère vers les sites de polymérisation est empêchée. La suppression extensive de l'ionisation micellaire produit des micelles de stabilité accrue. Dans des systèmes fortement stabilisés lorsque les sites de polymérisation sont les particules de polymère elles-même, il existe une compétition pour les molécules de savon entre les sites d'adsorption sur les particules de polymères et sur les micelles de savon. On a étudié l'influence de la concentration en savon sur la polymérisation en émulsion pour divers savons et diverses concentrations en électrolytes. Pour le savon coagulant Hyamine 1622 à concentration nulle en électrolyte on a déterminé une vitesse de polymérisation proportionnelle à la puissance $^1/_2$ de la concentration en savon. Cette relation n'est plus valable lorsque un électrolyte est ajouté au système en polymérisation.

Zusammenfassung

Die vorliegende Untersuchung hat orientierenden Charakter. Es wird ein Versuch unternommen, einige Konsequenzen aus den speziellen Eigenschaften koazervierender

Seifen bei ihrer Verwendung bei der Emulsionspolymerisation von Styrol zu skizzieren. In verdünnter Lösung besteht ein wesentlicher Unterschied zwischen einer Koazervierenden und einer nicht koazervierenden Seife in der kritischen Unterdrückung der Mizellionisierung in koazervierenden Systemen beim Zusatz verhältnismässig kleiner Mengen einfacher Elektrolyte. Eine direkte Beziehung zwischen Polymerisationsgeschwindigkeit und Molekulargewicht des Polymeren und der Mizellionisierung wurd nachgewiesen. Die höchste Polymerisationsgeschwindigkeit und die höchsten Molekulargewichte der Polymeren treten in Lösungen mit maximaler Ionisierung der koazervierenden Seifen auf. Bei Seifenlösungen, in welchen die Mizellionisierung kritisch unterdrückt wird, findet offenbar eine Desorption der Seife von den Polymerteilchen statt, die zur Bildung einer steigenden Zahl von Teilchen im Verlauf der Polymerisation führt. Zwei koazervierende und zwei nicht koazervierende Systeme wurden untersucht. Für das anionische nicht koazervierende System K-Laurat-KCl, bei welchem die Mizellgrösse bei Elektrolytzusatz praktisch konstant bleibt, gilt bis zu 1M KCl folgende Beziehung zwischen Polymerisationsgeschwindigkeit und KCl-Konzentration: $R = R_0 + B\sqrt{C}$. Der Einfluss der Ladung der Seifenmizellen auf den Verlauf der Stryolpolymerisation wurde auf zwei Effekte zurückgeführt: (a) Bei hochgradig ionisierten Mizellsystemen bildet die Mizelloberfläche wegen der Coulombschen Abstossung der geladenen, polaren, hydrophilen Gruppen der Seifenmoleküleeine offene Struktur, welche die Diffusion des Monomeren zum eigentlichen Polymerisationsort erleichtert. (b) Bei Unterdrückung der Mizellionisierung wird die Diffusion des Monomeren zum Polymerisationsort erschwert. Extensive Unterdrückung der Mizellionisierung führt zu Mizellen erhöhter Stabilität. Bei hochgradig stabilisierten Systemen, in welchen die Polymerisationsorte Polymerteilchen sind besteht eine Konkurrenz um die Seifenmoleküle zwischen den Adsorptionsstellen an den Polymerteilchen und Seifenmizellen. Der Einfluss der Seifenkonzentration auf die Emulsionspolymerisation wurde bei verschiedenen Seifen und Elektrolytkonzentrationen untersucht. Für die koazervierende Seife Hyamine 1622 war die Polymerisationsgeschwindigkeit bei der Elektrolytkonzentration Null der Wurzel aus der Seifenkonzentration proportional. Diese Beziehung ist bei Elektrolytzusatz zum Polymerisationsansatz nicht mehr gültig.

Received December 3, 1962

JOURNAL OF POLYMER SCIENCE: PART A VOL. 2, PP. 731–753 (1964)

Phase Changes in Fibrous Macromolecular Systems and Associated Elasticity. Model Phase Diagrams

A. CIFERRI and K. J. SMITH, JR., *Chemstrand Research Center, Inc., Durham, North Carolina*

Synopsis

In order to illustrate the concepts of solid–solid and solid–melt first-order transitions and associated elasticity for an ideally homogeneous fiber where different conformational arrangements of the macromolecules in the crystalline state are possible, phase diagrams were arbitrarily constructed on the basis of reasonable estimates of the variables involved. With some limitations, these diagrams illustrate several situations which might be expected to occur in real systems and the conditions under which one crystalline modification can be expected to be stable or metastable and under which a transition to another crystalline form or to the amorphous rubbery state can be observed. The variables which determine the state of the system were considered to be the external tensile force and temperature, pressure being regarded as a constant. Thermodynamic concepts and relationships used under such conditions were only a generalization of those established by Flory and Gee. Large changes of length of the fiber were assumed to occur during the reversible phase changes. A unified schematic picture of the elastic behavior of a fiber in its different physical states (single phase: crystalline or amorphous; two co-existing phases: crystal–crystal or crystal–amorphous) is afforded by the construction, on the basis of the phase diagram, of stress–strain isotherms, length–temperature curves at constant load, and stress–temperature curves at constant length.

INTRODUCTION

In recent years the occurrence of first-order transitions between enantiotropic crystalline modifications in polymers and proteins has been suggested. Noticeable examples are the cases of alkali-treated keratin fibers[1] where the $\alpha \rightleftarrows \beta$ transformation takes place, reversibly, on application of a particular value of the stress, f, which is a function of the temperature, T, (at constant pressure, P); and the case of *trans*-1-4 polybutadiene,[2a] where a crystalline modification with an identity period (along the chain axis) of 4.92 A. turns reversibly into another crystalline modification (characterized by an identity period of 4.65 A.) at about 350°K., under ordinary pressure and $f = 0$. Recently Boye[2b] has reported a similar transition for polyformals of tetramethylcyclobutanediols.

In other cases, notably poly-α-butene[2] and gutta-percha,[3] phenomena of monotropy are observed, i.e., only one crystalline form appears to be stable, and the polymorphic change seems to take place only in the direction from metastable to stable form.

In all cases mentioned, x-ray diffraction studies show that the transformation is accompanied by changes of the identity period along the direction of the chain axis which, in the case of a homogeneous fiber, may correspond to changes of length of the entire system. The possibility thus arises, in case of a reversible transformation, of a long-range elasticity due to first-order solid–solid transition. This has been discussed in detail for the case of keratin fibers.[1]

Long-range elasticity can also result from another type of phase transition, namely, the (reversible[4]) melting of oriented crosslinked fibers, as has been indicated by various authors,[4] notably by Flory.[5]

Conformational changes are, in general, responsible for the elasticity due to both solid–solid and solid–melt transitions.

The additional possibility of conformational changes not accompanied by length changes or of length changes not accompanied by important conformational variations should be considered. In this paper, however, specific reference will be made to the case of fibrous systems where a long-range elasticity arises from the transformation. Because of the great importance assumed by cooperative phenomena in both biological and synthetic macromolecular systems, it seemed desirable to present a unified description of both solid–solid and solid–melt transitions. As originally done by Flory in the case of solid–melt equilibria, this can conveniently be accomplished by the use of phase diagrams where the field of stability of each phase is represented as a function of physical variables such as P, T, and f. Since, according to general thermodynamic principles, transformations accompanied by length changes can be affected by an external tensile force, f–T phase diagrams at constant P are convenient for this representation and, as will be shown below, are an adequate tool for predicting the elastic behavior of the system.

At the present time no systematic experimental study of a complete phase diagram comprising solid–solid and solid–melt equilibrium curves for fibrous, homogeneous, macromolecular systems has been made, although particular cases of phase diagrams for a solid–melt[5] and for a solid–solid[1] transition have been discussed. The purpose of the present paper is that of exploring the features which such phase diagrams should display on the basis of the model of a homogeneous fiber displaying first-order solid–solid as well as solid–melt transitions.

It is believed that the general features and correlations, implied in the model, to be expected for an ideal case, will be of considerable help in both the interpretation of future experimental data and in clarifying the concepts of f–T phase diagrams and elasticity associated with phase changes in fibrous macromolecular systems.

PHASE DIAGRAMS

Model phase diagrams are arbitrarily constructed using the following criteria and approximations.

It will be assumed that a homogeneous, 100% crystalline fiber (except for the presence of chemical crosslinkages, cf. seq.) may exist, depending upon the values of f and T, in one (cases 1a, 2a) or two (cases 3a, 4a, 5a, 6) enantiotropic crystalline modifications and, above the melting point, in an amorphous, rubberlike state.

TABLE I

	α Form	β Form	Amorphous
L_0 at 300°K., cm.	4.00	6.00	1.00
$(1/L)(\Delta L/\Delta T)$, degree^{-1}	1×10^{-4}	1×10^{-4}	2×10^{-4}
E at 300°K., kg./cm.^{2}	2×10^4	3×10^4	—
$(1/E)(\Delta E/\Delta T)$, degree^{-1}	-1×10^{-3}	-1×10^{-3}	—
$\nu KT\langle\alpha\rangle^2/V_0$ at 300°K., kg./cm.^{2}	—	—	10
Stress–strain dependence	$f = E\left(\frac{L}{L_0} - 1\right)$	$f = E\left(\frac{L}{L_0} - 1\right)$	$f = \frac{\nu KT\langle\alpha\rangle^2}{V_0}\left[\frac{L}{L_0} - \left(\frac{L_0}{L}\right)^2\right]$

The reversible first-order transitions from one crystalline form to the other, or to the melt, are accompanied with large, reversible changes in the length of the fiber. The lengths (L_0) that the fiber would have if at 300°K. and $f = 0$ it was to be stable in the α, β, or amorphous form are assumed to be, respectively, 4, 6, and 1 cm. A priori, one can expect solid–solid transitions accompanied by either an increase or decrease in length (with increasing temperatures). We discuss in cases 3a and 5a solid–solid transitions accompanied by an increase in length and in case 6 transitions accompanied by a decrease in length. This latter case appears to be more common (cf. *trans*-1,4-polybutadiene[2] and the polyformals prepared by Boye[2b]). In Table I are collected other data necessary for the construction of the phase diagrams. They have been assumed to have values similar to those expected for real systems.

In the crystalline states the fiber exhibits short-range elasticity described by the equation

$$f = E\,[(L/L_0) - 1]$$

where E is Young's modulus. In the amorphous state the sample exhibits entropy elasticity described by the Gaussian theory of rubber elasticity. Volume changes accompanying the transitions are assumed to be negligible without, however, intending to restrict the treatment to cases where the average intermolecular interaction energy does not change on transition. The phase rule for a homogeneous one-component, two-phase system affected by variations of P, T, and f predicts the degrees of freedom to be equal to two. At constant pressure such a system should therefore be uni-

variant and, according to Le Chatelier's principle, the application of an external tensile force (simple elongation) should increase or decrease the transition temperature, depending upon whether the transformation (on increasing T) is accompanied by a decrease or an increase in length. The thermodynamic relationship governing phase equilibria in these conditions has been derived by Gee and Flory[5] and is the analog of the Clausius-Clapeyron equation governing the more familiar phase equilibria where the only physical variables considered are P and T. The Gee-Flory equation is

$$(\partial f/\partial T)_P = -\Delta S/\Delta L \tag{1}$$

or alternatively

$$(\partial f/\partial T)_P = -(\Delta H - \int \Delta L)/T\Delta L \tag{2}$$

where ΔS and ΔL are the changes of entropy and length, for the entire system, accompanying the transformation, and ΔH is the corresponding enthalpy change. For an $\alpha \rightleftarrows \beta$ transformation,

$$\Delta L = L_\beta - L_\alpha$$

and for an $\alpha \rightleftarrows$ melt (or $\beta \rightleftarrows$ melt) transformation

$$\Delta L = L_a - L_c$$

where $L_c = L_\alpha$ or L_β.

Exact application of these equations requires the appropriate equations of state for both forms of matter under consideration. For the fusion process, Flory[5] obtains approximate results by assuming Gaussian behavior for the amorphous phase and integrating eq. (2) with the condition that both the heat of fusion, ΔH, and the length of the totally crystalline sample, L_c, remain constant. His result,

$$\frac{2\Delta H}{B}\left(\frac{1}{T_m} - \frac{1}{T_m^\circ}\right) = 2(L-L_c)\left(L - \frac{L_0^3}{L^2}\right) - \left(L^2 + \frac{2L_0^3}{L} - 3L_0^2\right) \tag{3}$$

may be put in terms of stress (force referred to the initial cross-sectional area) through use of the relationship

$$f = BT\,[(L/L_0) - (L_0^2/L^2)] \tag{4}$$

where L_0 designates the isotropic amorphous sample length, L is the length of the stretched amorphous sample, T_m and T_m° are the respective melting temperatures of the stretched and unstretched sample, and

$$B = \gamma k \langle\alpha\rangle^2 / V_0$$

where γ represents the total number of chains in the network, k is Boltzmann's constant, $\langle\alpha\rangle$ is the dilation factor,[5] and V_0 the sample volume.

In the case of solid–solid transitions, eq. (2) may be integrated by assuming ΔH and ΔL constant. We obtain

$$f = \frac{\Delta H}{\Delta L}\left[1 - (T_t/T_t^\circ)\right] \tag{5}$$

where T_t° is the transition temperature at zero stress.

Application to any real system might require a more accurate analysis, particularly with respect to the temperature variation of L_c, and ΔH. In general the temperature variation of the L_c is rather small. However, the heat of fusion (or transition) could have considerable temperature variation depending upon the magnitudes of the differences of heat capacities involved.

More exact relationships are obtained by assuming

$$\Delta H = \Delta H_0 + \Delta C_p\, T \tag{6}$$

where C_p, the heat capacity, is regarded as a constant and ΔH_0 is a constant of integration. With the use of eq. (6), eqs. (3) and (5) become:

$$\frac{2}{B}\left[\Delta H_0\left(\frac{1}{T_m} - \frac{1}{T_m^\circ}\right) + \Delta C_p \ln (T_m^\circ/T_m)\right] = 2\,(L - L_c)\left(L - \frac{L_0^3}{L^2}\right) - \left(L^2 + \frac{2L_0^3}{L} - 3L_0^2\right) \tag{7}$$

$$f = \frac{\Delta H_0}{\Delta L}(1 - T_t/T_t^\circ) + \frac{\Delta C_p}{\Delta L}\, T_t \ln (T_t^\circ/T_t) \tag{8}$$

For the determination of our f–T phase diagrams use of the approximate eqs. (3) and (5) was made and the values of ΔH, T_m°, and T_t° are reported, for each case, on the corresponding phase diagrams (Figs. 1, 5, 9, 13, 15, and 18). These values were chosen as to be of the same order of magnitude as those observed for real systems. Values of ΔL were determined, at each f and T pair, from the data in Table I.

It is possible to see that use of the more exact eqs. (7) and (8) would not essentially alter the shape of the diagrams; thus, by regarding enthalpies and entropies of transformations as temperature-independent quantities, simple relationships can be used. In particular

$$\Delta H_{\alpha \rightleftarrows \beta} = \Delta H_{\alpha \rightleftarrows \text{melt}} - \Delta H_{\beta \rightleftarrows \text{melt}}$$

for all T.

From the phase diagrams and the data from Table I, stress–length isotherms, length–temperature curves at constant load, and stress–temperature curves at constant length were constructed as indicated in correspondence to each type of phase diagram (cases 1a, 2a, 3a, 4a, 5a). Values of stresses are referred, in all graphs, to the unit cross-sectional area of the sample in its amorphous state. In the phase diagrams, dotted lines are

lines of transformation of metastable phases. In the other diagrams, broken lines indicate the single rubbery phase.

The presence of a minimum number of chemical crosslinkages, (imposed on the oriented fiber) which is necessary for the stability of the network in the molten state and which also assures to the network a "memory" of the original orientation of the fiber,[4] is assumed. It has been shown[5] that if such crosslinkages are imposed in an already present, homogeneous structure, the heterogeneity thus introduced will not essentially affect the possibility of regarding the melting of the entire fiber as a reversible first-order transition. The further stipulation is necessary here that, likewise, the first-order transition character of solid–solid transformations is not appreciably affected by the presence of (few) chemical crosslinkages.[1]

Case 1a

The phase diagram represented in Figure 1 is of the type described by Flory.[5] The polymer can assume only one crystalline form, the β. The positive slope of the curve of equilibrium $\beta \rightleftarrows$ melt reflects the fact that $\Delta L = L_a - L_\beta$ is negative, although its absolute value is decreasing as f and T simultaneously increase. This is the expected trend if in the β form the molecular chains are in a highly extended conformation, and conditions where $L_a > L_\beta$ cannot be realized because of rupture of the fiber at high stress values. Figure 2 illustrates stress–length isotherms to be expected for a fiber having a phase diagram corresponding to Figure 1.

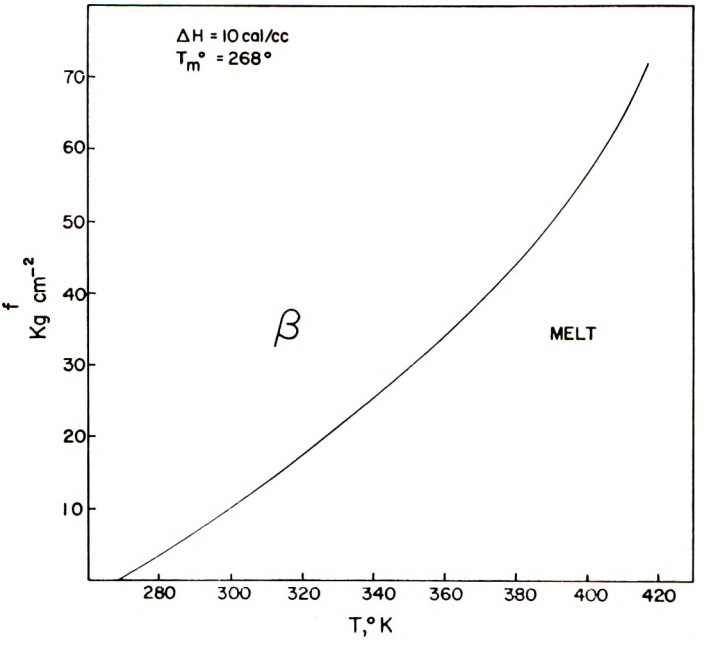

Figure 1.

At 320°K., the $\overline{AB}$ section represents the stretching of the initially amorphous network. When the stress attains the value 17.5 kg./cm.^{2} at 320°K., (a point on the line of biphasic equilibrium on Fig. 1) the system becomes uninvariant and the entire amorphous phase must be converted into crys-

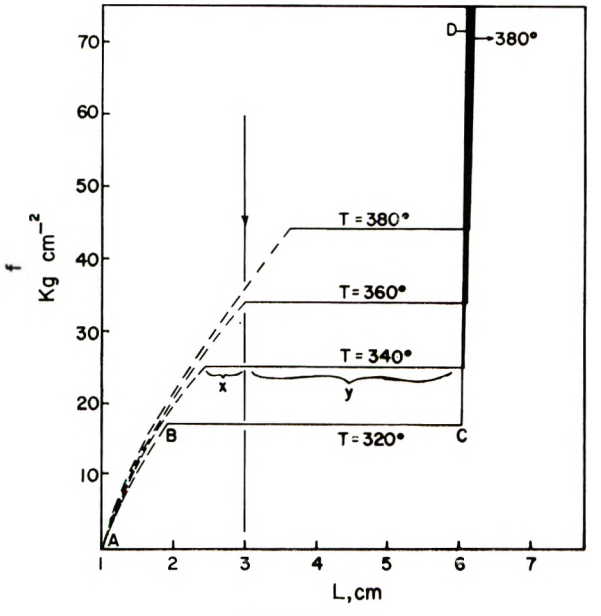

Figure 2.

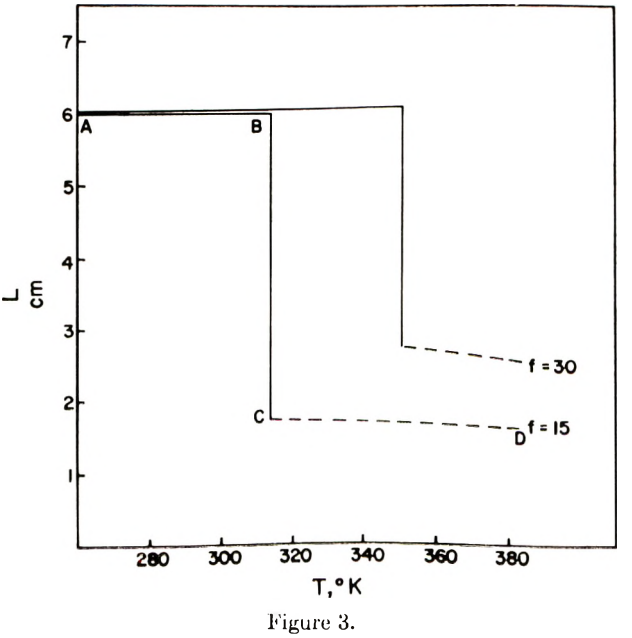

Figure 3.

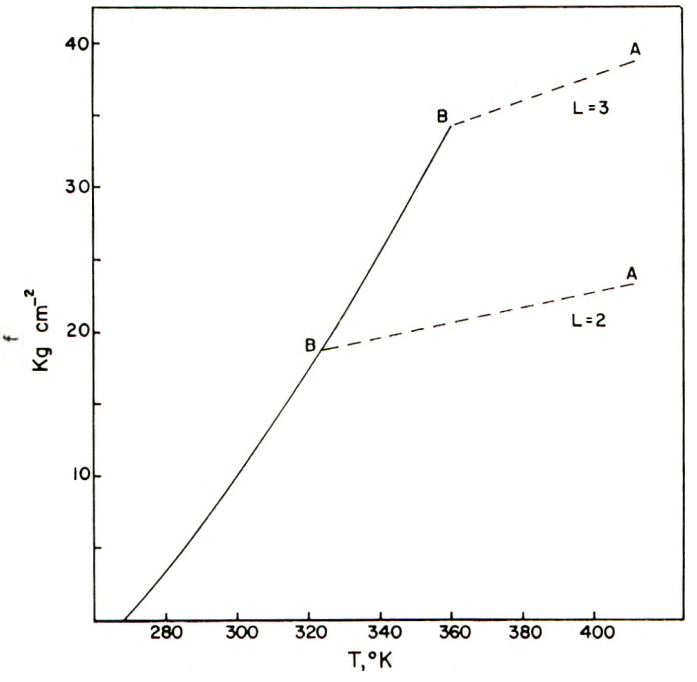

Figure 4.

talline β (section $\overline{BC}$) before the force can increase on further stretching of the high modulus β form (section $\overline{CD}$).

The decrease of ΔL with rising temperature (and with f) is due to the fact that the rubber remains more easily deformable than the fiber in spite of the opposite sign of the temperature coefficient of the modulus. Since in the β form $(\partial f/\partial L)_T > 0$ and $(\partial L/\partial T)_f > 0$ it follows that $(\partial f/\partial T)_L < 0$: in fact, a cross-over of the isotherms for $L > 6$ cm. is observed. Figure 3 illustrates length–temperature curves at constant load corresponding to Figure 1. $\overline{AB}$ represents the small increased deformability of the fiber on increasing T, $\overline{BC}$ the sudden change of length due to fusion, and along $\overline{CD}$ the length decreases on increasing T as required for entropy-elasticity.

Figure 4 illustrates the case in which the length, rather than the load, is kept constant as the temperature is varied (specific reference is made here to the often used experimental technique where the distance between the two clamps holding the stretched fiber is maintained constant, and the force acting on the clamps is recorded). Although the phase diagram in Figure 1 is also a f–T diagram, we wish to emphasize its difference from the corresponding f–T diagram at constant L reported in Figure 4. The ordinate on the phase diagram (Fig. 1) only represents the stress for which two phases (β + melt) coexist at any given temperature. The value of the stress at which, at a given temperature, the transformation takes place is independent of the length, as obvious from the univariance of the equilibrium[5] and as illustrated by the plateau on the stress–length curves of

Figure 2. Therefore, in so far as it represents only the stress for coexistence of two phases, the phase diagram (Fig. 1) is valid independently of any restriction on the length of the fiber.

In the diagram of Figure 4, however, the stress exerted by a sample for a given length and temperature is represented even in the region where only one phase is present. Section $\overline{AB}$ represents the variation of stress with temperature for the stretched network displaying entropy-elasticity. When stress and temperature have attained the values at point B, which is a point represented on the f–T diagram of Figure 1, the crystalline phase appears, but the restriction on L prevents the fiber from transforming completely into β at the point B. Rather, the amount of the crystalline phase can increase only on further decrease of temperature along the line of biphasic equilibrium $\overline{BC}$. The representation of the "cooling line" at $L=3$ in Figure 2 makes this evident and also illustrates the application of the "tie-rule" for the determination of the coexisting amounts of crystalline and amorphous phases. It clearly appears that the length merely determines the relative amounts of the two phases in the transition region.[5] The restriction on L prevents a development of crystallinity above the equilibrium amount dictated by the tie-rule since, if the amount of β were to increase, a decrease of the tension exerted by the remaining amorphous portion of the network would be generated and the system would tend to be, at a given temperature, under a stress smaller than that required for biphasic equilibrium. The excess β would therefore automatically remelt. When the point C is reached the restriction on L is no longer effective, since, according to the model, the fiber at its temperature of transformation when $f = 0$ will spontaneously elongate and attain 100% crystallinity.

Case 2a

In case 2a, similar to case 1a, only one crystalline modification is possible, the α. However, the amorphous rubber can be stretched to an elongation higher than L_α without rupture. This case can be expected if in the α form the molecular chains are in a very compact helical conformation or if they are folded. The slope of the line of univariant equilibrium is positive when, for low f values, $L_a < L_\alpha$ and negative when, at higher stresses, $L_a > L_\alpha$. The most interesting feature of this diagram is that, in correspondence to isotherms between 309 and 340°K., two values of the stress for phase equilibrium are predicted. As a result, in the corresponding force–length isotherms of Figure 6, the crystallization of the α form at a given f value ($\overline{BC}$ plateau) is followed by a remelting ($\overline{DE}$ plateau) at a higher f value which is attained by increasing the strain on the α form (section $\overline{CD}$). When the amorphous (stretched) form has been regenerated the stress–length isotherm will follow the $\overline{EF}$ section, which is a continuation of the $\overline{AB}$ section. An isotherm at 341°K. will not intersect the line of two-phase equilibrium, (Fig. 5), and therefore no transition is observed on the f–L plot. At temperatures below 309°K. (melting point of the α

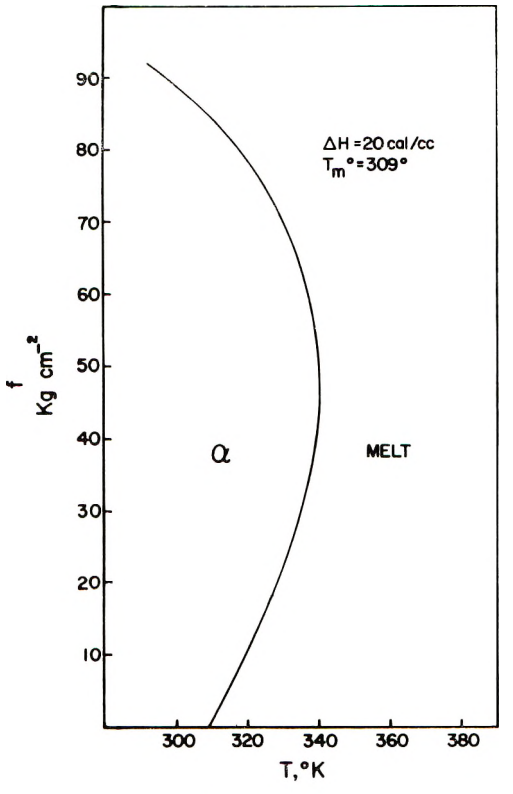

Figure 5.

form at $f = 0$), the stress–length isotherm begins with the stretching of the α form (section $\overline{AB}$ on the isotherm at 300°K., Fig. 6), and when the stress attains the critical value for phase coexistence the fiber will melt (section $\overline{BC}$) and remain in the rubbery state (section $\overline{CD}$). The possibility of a remelting at high stress values was recognized by Flory.[5] The length–temperature diagram at constant load (Fig. 7) clearly illustrates that, on melting, the fiber contracts at low f values and extends at high f values.

In the case of stress–temperature diagrams at constant L (Fig. 8), when an initially amorphous stretched network is cooled (section $\overline{AB}$), the stress may increase or decrease (depending upon the actual value of L) after the point representative of the system has reached the critical value of stress at which the crystalline phase appears. With this limitation, the same considerations made in the case of Figure 4 apply, in particular the degree of crystallinity increases along the lines $\overline{BC}$ (as obvious from cooling lines represented in Fig. 6), irrespective of the fact that the stress may actually increase, as in the case of the stress–temperature diagram for $L = 7$ in Figure 8. The diagrams corresponding to $L = 4$ (Fig. 8) will be discussed in some detail. If the rubbery sample is maintained between clamps 4.00 cm. apart the point representative of the system will descend along the

$\overline{ABC}$ section until, at $T = 309°K.$, the stress will be equal to zero. Under this condition, the sample can crystallize completely and will assume the length of the fully crystalline fiber, 4.003 cm. (cf. expansion coefficient in Table I) at 309°K. On further cooling thermal contraction of the fiber will ensue, but no force will act on the clamps until the temperature has

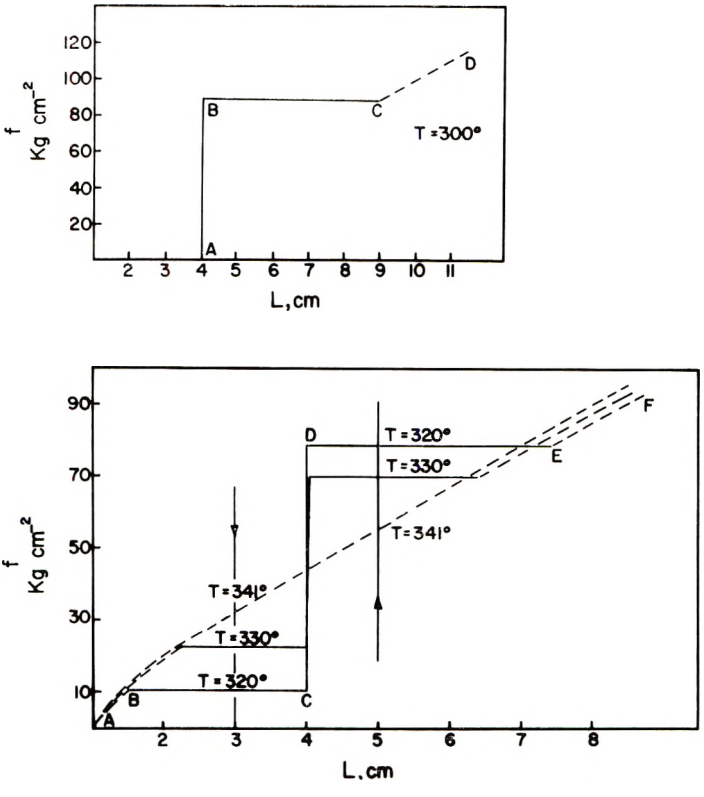

Figure 6.

reached 300°K., at which temperature the fiber is exactly 4.00 cm. long. The $\overline{EF}$ line represents the force acted on the clamps as a result of the subsequent thermal contraction of the fiber.

Case 3a

In the case of the diagram in Figure 9, two crystalline forms, each having its own field of stability, can exist.

Below the melting temperature, the α form will be stable in a given region of the phase diagram if, in that region,

$$(F_\alpha - fL_\alpha) < (F_\beta - fL_\beta)$$

where F is the Gibbs free energy.

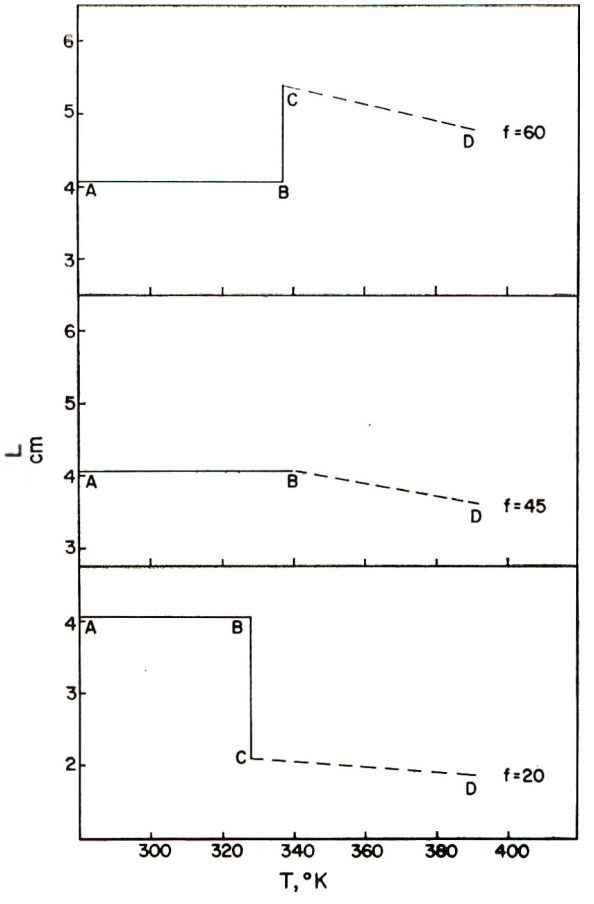

Figure 7.

Neglecting the temperature dependence of ΔH, ΔS, and ΔL we may write:

$$F_\alpha - fL_\alpha \simeq F_a - f\,L_a - \Delta H_{\alpha \rightarrow \text{melt}} + T\Delta S_{\alpha \rightarrow \text{melt}} + f(L_a - L_\alpha)$$

$$F_\beta - fL_\beta \simeq F_a - f\,L_a - \Delta H_{\beta \rightarrow \text{melt}} + T\Delta S_{\beta \rightarrow \text{melt}} + f(L_a - L_\beta)$$

and since the fusion entropies may be approximated by:

$$\Delta S_{\alpha \rightarrow \text{melt}} \simeq [\Delta H_{\alpha \rightarrow \text{melt}} - f(L_a - L_\alpha)]/T_m{}^\alpha$$

$$\Delta S_{\beta \rightarrow \text{melt}} \simeq [\Delta H_{\beta \rightarrow \text{melt}} - f(L_a - L_\beta)]/T_m{}^\beta$$

it follows that:

$$F_\alpha - fL_\alpha \simeq F_a - f\,L_a - (1 - T/T_m{}^\alpha)\,[\Delta H_{\alpha \rightarrow \text{melt}} - f(L_a - L)_\alpha] \quad (9)$$

$$F_\beta - fL_\beta \simeq F_a - f\,L_a - (1 - T/T_m{}^\beta)[\Delta H_{\beta \rightarrow \text{melt}} - f(L_a - L_\beta)] \quad (10)$$

Therefore, eqs. (9) and (10) allow one to determine (within the limit of the approximation) the appropriate modification in each region.

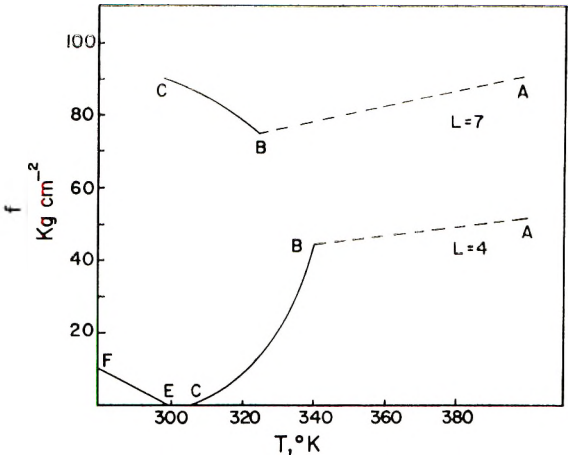

Figure 8.

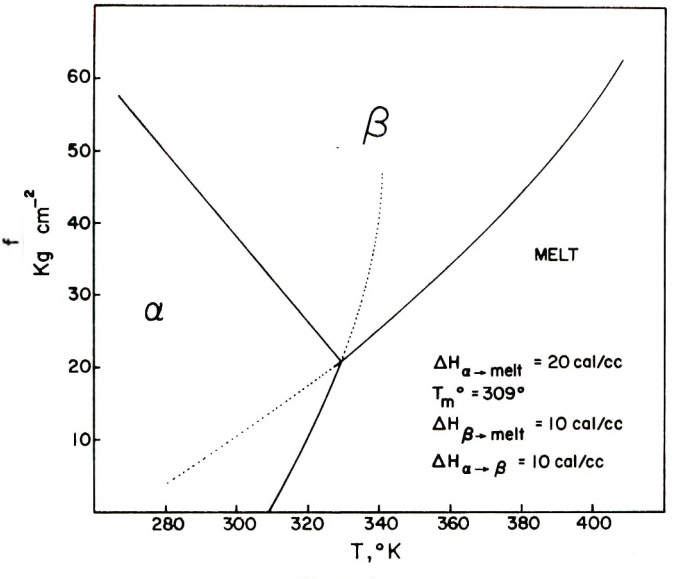

Figure 9.

For the case at hand it is seen that the shorter form, α, is more stable at low temperatures and has a higher value of the melting enthalpy. This is also true in the case of diagrams reported in Figures 13 and 15 which may be considered as particular cases of case 3a (Fig. 9). The difference between the three diagrams is that in case of Figure 13 the β form is stable even at $f=0$ and therefore only the $\alpha \rightleftarrows \beta$ and $\beta \rightleftarrows$ melt transformation can be observed in equilibrium conditions while in the case of Figures 9 and 15 the β form is not stable at $f=0$ and therefore the $\alpha \rightleftarrows$melt transformation can also be observed for low values of the stress. Diagram 9 differs from diagram 15 because in the latter the region of stability of β is

limited to high values of stress. In all cases the field of stability of the long form is increased at high stresses.

Stress–length isotherms below 309°K. (the melting point of the α form at $f=0$) exhibit the stretching of the α form (section $\overline{AB}$), the $\alpha \rightleftarrows \beta$ trans-

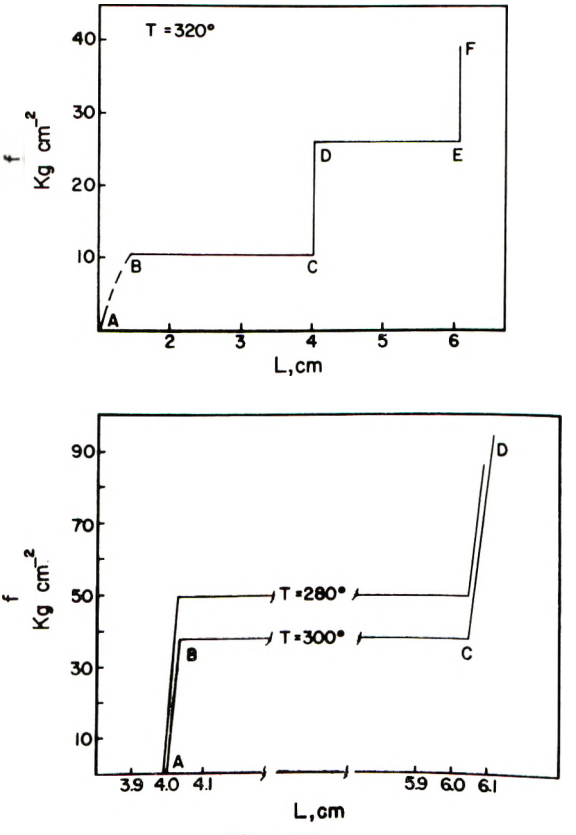

Figure 10.

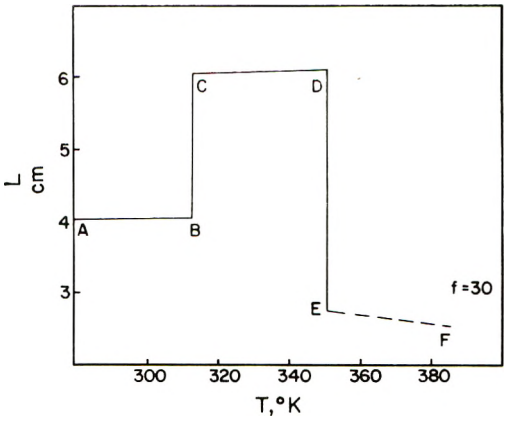

Figure 11.

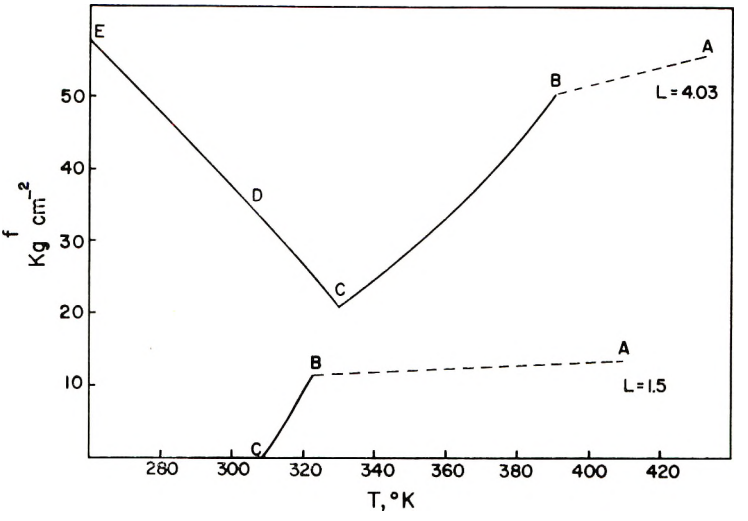

Figure 12.

formation (plateau $\overline{BC}$) and the stretching of the β form (Fig. 10). This case was previously discussed in connection with the $\alpha \rightleftarrows \beta$ transformation in keratin.[1] An isotherm between 309 an 329°K. (the temperature of the triple-point in Fig. 9) is also included in Figure 10. The initially amorphous network is stretched along $\overline{AB}$ until the α form crystallizes along $\overline{BC}$. $\overline{CD}$ corresponds to the stretching of the α form which is transformed into β along $\overline{DE}$. $\overline{EF}$ represents the deformation of the β form.

Isotherms at temperatures higher than 329°K. would exhibit only one transition: the melt $\rightleftarrows \beta$. In Figure 11 the length–temperature diagram at a constant load (exceeding the f value at the triple-point) is shown. Here, $\overline{AB}$ is the thermal expansion of α form; $\overline{BC}$ represents the $\alpha \rightleftarrows \beta$ transformation with increase of length; $\overline{CD}$ is thermal expansion of the β form; $\overline{DE}$ denotes melting of the β form with shrinkage; and $\overline{EF}$ is the length decrease on increasing T as required for entropy-elasticity.

The stress–temperature diagrams at constant L, particularly the case $L = 4.03$, in Figure 12, deserves consideration.

If a fiber in the α form is stretched to a length of 4.03 cm. at 260°K., E will be the point representative of the system. Comparison with Figure 9 reveals that the stress at the point E is less than that required for phase equilibrium, therefore only the α modification is present at E. On heating, the stress decreases along $\overline{ED}$ due to the thermal expansion and variation of the modulus with temperature.

At D, comparison with Figure 9 reveals that the stress has attained the value for phase equilibrium, therefore the β form will appear and on further heating the stress will decrease along $\overline{DC}$ (the line of univariant equilibrium). At the triple point C the amorphous phase appears and the equilibrium is zero-variant: one phase, the α, must disappear before T

can be further increased and, henceforth, the point representative of the system will move along the line of univariant $\beta \rightleftarrows$ melt equilibrium, $\overline{CB}$. At B, β disappears and the stress will increase along $\overline{BA}$ where only the amorphous phase is present. If $L = 1.5$, the field of existence of β is not encountered and the situation is similar to that considered in the simpler cases.

Case 4a

In the case of the stress–temperature diagram at constant length reported in Figure 14 (which corresponds to the phase diagrams of Fig. 13)

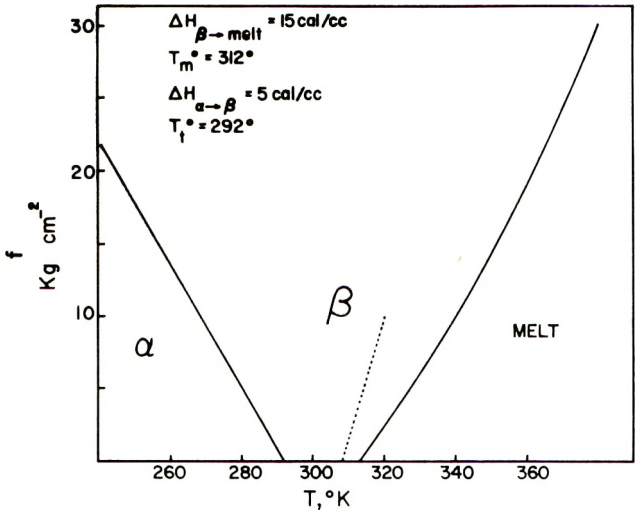

Figure 13.

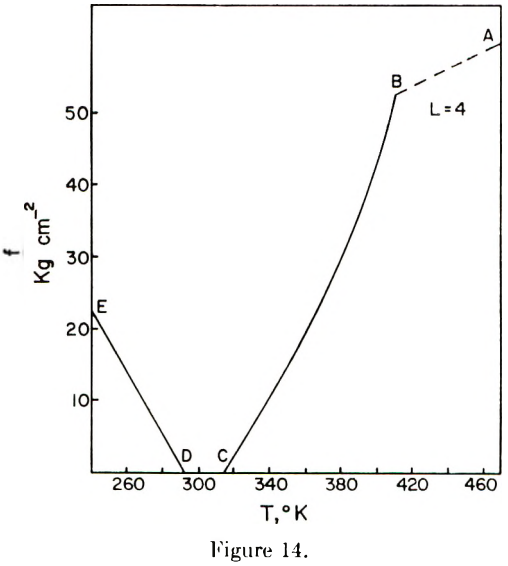

Figure 14.

if a fiber is kept between clamps maintained 4 cm. apart, line $\overline{AB}$ represents the decrease of stress with temperature for the amorphous network, and line $\overline{BC}$ is the line of equilibrium $\beta \rightleftarrows$ melt. Along $\overline{BC}$ the amount of β

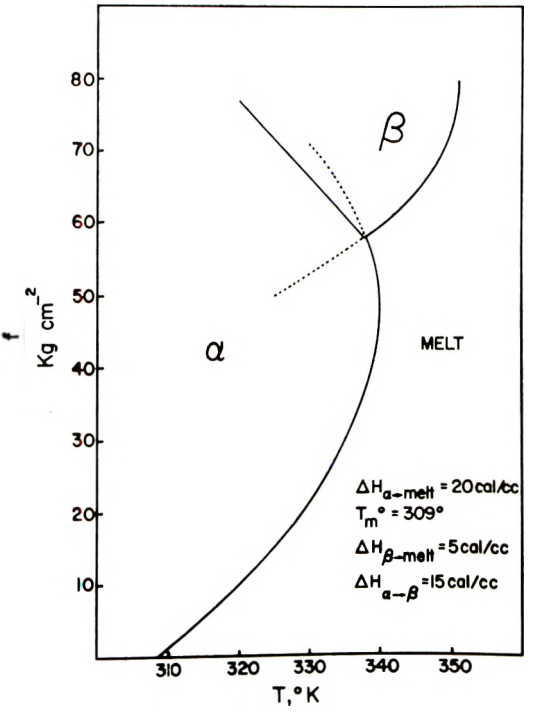

Figure 15.

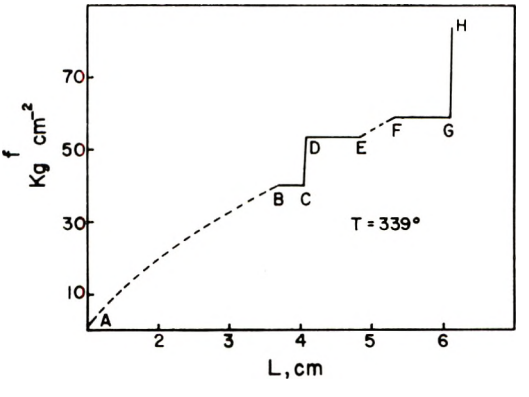

Figure 16.

increases in the direction of temperature decrease. At C, melting point of the β form at $f = 0$, the fiber can elongate and attain 100% crystallinity; no force being effective on the clamps. At D, however (temperature

of transition at $f=0$) β transforms into α and the constriction of the clamps becomes effective once more, and on further cooling, the stress will move along the $\overline{DE}$ line of univariant equilibrium.

Case 5a

The stress–length isotherm of Figure 16 illustrates an interesting feature of the corresponding phase diagram reported in Figure 15. Because of the particular position of the field of stability of the β form, the sample shows a crystallization into the α form ($\overline{BC}$), a melting ($\overline{DE}$) and a subsequent

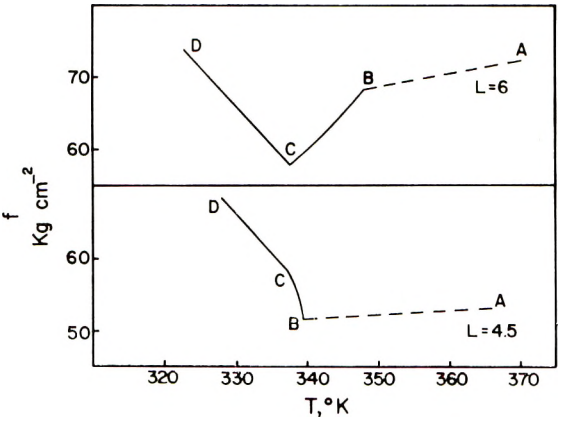

Figure 17.

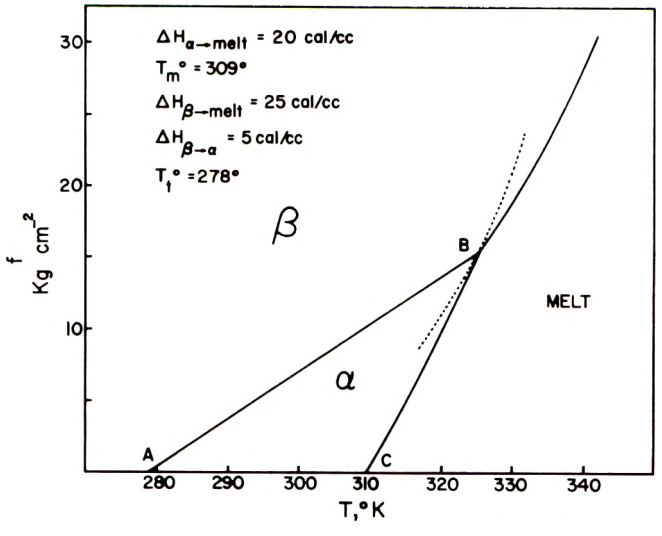

Figure 18.

recrystallization into the β form ($\overline{FG}$). Section $\overline{EF}$ is on the continuation of the $\overline{AB}$ line corresponding to the stretching of the amorphous network.

Corresponding stress–temperature curves at constant length are reported in Figure 17. The case for $L=6$ is reminiscent of the similar curve reported in Figure 12. In the case $L=4.5$, the $\overline{CB}$ section corresponds to the line of univariant $\alpha \rightleftarrows$ melt equilibrium, C is the triple-point (compare with Fig. 15) and $\overline{CD}$ the line of univariant $\alpha \rightleftarrows \beta$ equilibrium.

While it is believed that the cases illustrated in the preceding graphs will serve as a satisfactory description of the concept of phase transitions and associated elasticity, the different possibilities which may arise are clearly more numerous than those described here. For instance, more than one crystalline modification may be present. Also, in all cases described, the shorter α form was supposed to be more stable at low temperatures. Figure 18 illustrates a case where the longer β form is more stable at low temperatures. In this case the field of stability of the α form is limited by the triangle $\overline{ABC}$.

In the extreme (improbable) circumstance where the two forms have identical ΔH_m and T_m° ($\Delta H_T=0$) a unique situation arises, i.e., at $f=0$ either the α or the β form may be stable. However, on extension the β form will be stabilized while compression results in the stabilization of α.

CONCLUSIONS

The above diagrams are presented as an illustration of the assumed model of a 100% crystalline, homogeneous fiber capable of undergoing reversible solid–solid and solid–melt transitions accompanied by rather large length changes.

Since the behavior of real systems can be expected to depart from that of the above idealized model, these diagrams can only, at best, be regarded as a useful guide for the interpretation of experimental data. Among the complications to be expected for real systems, a serious one is the difficulty of attaining equilibrium conditions. Some transformations, for instance the melting, may be completed in relatively short times, others may be very sluggish. Since for many real systems chemical degradation is also effective, when experiments are protracted for long times even at moderate temperatures, equilibrium conditions may, sometimes, never be obtained. Another complication arises from the difficulty of obtaining real systems which fulfill the condition of homogeneity. The possibility of regarding the transformation of the entire system as a result of several phase transitions corresponding to different homogeneous regions of the fiber may have to be considered.[5] The simple "Gaussian" stress–strain dependence for the network, assumed here for simplicity, should also be replaced, especially for high extensions, by the more general expressions derived from non-Gaussian statistics.

A more serious limitation arises from the fact that the reversible changes of length, assumed to occur for our model on phase transition, are not al-

ways observed for real systems. This limitation is particularly serious in the case of molten, unstretched networks where any orientation which the network might have had in the crystalline state is destroyed. It has been shown,[4] however, that, provided the crosslinking occurred in the oriented fiber, the corresponding amorphous network possesses a "memory" of the original orientation which enables it to partly reelongate on crystallization even when $f=0$. A detailed interpretation of this effect has not yet been given, however, results obtained to date[6] indicate that some degree of anisotropy is maintained in these networks above the shrinkage temperature. This is just one reason which indicates that the model system we have used is expected to be a somewhat better approximation to the behavior of systems crosslinked in the oriented state than to the conventional network crosslinked in the disordered state. Other features of crystallization, under stress, of polymer networks will be presented in a forthcoming publication.[8] Reversible changes of length on solid–solid transitions should be more easily obtained for oriented systems since the overall orientation need not be destroyed during the transition. However, also in the case of solid–solid transitions, the particular state in which the crosslinks are formed may have an effect on the transition. It is well known, for instance, that the $\alpha \rightleftarrows \beta$ transformation in keratin is generally reversible. However, if the fiber is stretched in steam, instances are observed where the β form no longer reverts to the α on relieving the stress (permanent set). Substantial evidence indicates[7] that under action of steam important chemical changes take place, and it appears probable that some of the chemical crosslinkages (which were formed in accordance with the naturally occurring α form) are destroyed or displaced thus allowing the formation of a β form which may no longer be converted to α.

In spite of these limitations, the general features exhibited by the model diagrams should find a correspondence in real systems. In fact, in the case of alkali-treated keratin fibers, stress–length isotherms approximately display the plateau ($\overline{BC}$ in Fig. 10) corresponding to the solid–solid transition. Also, rather large changes of length corresponding to the melting of oriented synthetic and natural fibers[4,5] have been observed for small temperature changes, and the stress values for phase equilibrium have been shown to be unaffected by relatively large variations of the length for natural rubber fibers.[5]

As evident from Figures 9 and 15, some crystalline modifications which are never observed (under equilibrium condition) when $f=0$ may be stabilized by application of an external force.

An interesting feature presented by the model stress–temperature curves at constant length is the rapid upturn of the stress which can be observed on crystallization when $L_a > L_\alpha$ (Fig. 5) or when there is a solid–solid transition of the $\beta \rightarrow \alpha$ type. Gent[4] has observed such upturns of the stress on cooling of stretched polyethylene networks (crosslinked in the random state) and has associated these upturns to transitions from an extended to a folded

arrangement of the macromolecules in the crystal. It is not yet clear, however, if such transformations can be regarded as phase transitions. In connection with stress–temperature experiments at constant length, it should be noted also that they are not a very sensitive tool for studying phase transitions accompanied by length changes. The restriction on the length prevents, in fact, the most obvious feature of the transition to be observed. Furthermore, as evident from Figures 5, 12, 14, and 17, thermal contraction can affect the stress in the same manner as can be expected from phase transitions, as discussed above. An independent way of verifying the occurrence of the transition seems in this case necessary. In the construction of the above f–T diagrams at constant length, it has been assumed throughout that when two phases coexist the point representative of the system may be found on the line of univariant equilibrium. In practice, thermal contraction effects may become important even in the presence of two phases, thus accentuating the upturn of the stress on cooling. Because of these considerations, length temperature measurements at constant load appear preferable. The technique used by Oth and Flory[5] appears also very convenient. These authors performed stress–temperature measurements at constant length but, in the region of univariant equilibrium, small length changes were allowed in order to verify the predicted independence of stress on length at constant temperature.

Finally, it should be noted that the possibility of existence, under appropriate conditions of f, P, T, of different crystalline modifications could be predicted on the basis of (*1*) potentials hindering bond rotations for the macromolecule (which indicate which conformations of the macromolecule are possible on the basis of intramolecular forces[10]), (*2*) an evaluation of the elastic modulus of the different modifications,[11] and (*3*) a needed evaluation of intermolecular forces. The latter are expected to be particularly effective in those cases where the conformation of the macromolecules in the crystal does not correspond to the absolute minimum of energy predicted on the basis of intramolecular interactions alone. On the same basis, a molecular description of solid–solid transitions accompanied by conformational changes could be made.

Phase transitions, in particular the solid–melt, can also be affected by action of external variables different from the tensile force considered here. In particular, variations of the chemical environment of the system may result in large elastic dimensional changes or, as they are more often designed, in phenomena of "contractility."[4]

References

1. Ciferri, A., *Trans. Faraday Soc.*, **59**, 515 (1963).

2. (a) Natta, G., *Makromol. Chem.*, **35**, 103 (1960); (b) C. A. Boye, *Bull. Am. Phys. Soc.*, **8**, 241 (1963).

3. Selikhova, V. I., G. S. Markova, and V. A. Kargin, *Vysokomol. Soedin.*, **2**, 1398 (1960).

4. Cf. Mandelkern, L., abstracts from the Conference on Contractility, Pittsburgh, Pa., January 1960.

5. Flory, P. J., *Science*, **124**, 53 (1945); *J. Am. Chem. Soc.*, **78**, 5222 (1956); J. F. M. Oth, and P. J. Flory, *J. Am. Chem. Soc.*, **80**, 1297 (1958); G. Gee, *Quart. Rev.*, **1**, 265 (1947).

6. Greene, A., and A. Ciferri, *Kolloid-Z.*, **186**, 1 (1962).

7. Peters, L., and H. J. Woods, *Mechanical Properties of Textile Fibres*, Meredith Ed., North Holland, 1956, p. 167.

8. Smith, K. J., Jr., A. Greene, and A. Ciferri, to be published.

9. Gent, A. N., paper presented at the 142nd Meeting, American Chemical Society, Atlantic City, September 1962.

10. DeSantis, P., E. Giglio, A. Liquori, and A. Ripamonti, *J. Polymer Sci.*, **A1**, 1383 (1963).

11. Shimanouchi, T., M. Asahina, and S. Enomoto, *J. Polymer Sci.*, **59**, 93, 101 (1962).

Résumé

On a établi arbitrairement des diagrammes de phase en utilisant de valeurs probables des variables en question, afin d'illustrer la notion des transitions du premier ordre de systèmes solide–solide et solide–liquide, et la notion associée de l'élasticité d'une fibre complètement homogène où des arrangements conformationnels différents des macromolécules sont possibles à l'état cristallin. A quelques limitations prés, ces diagrammes montrent diverses situations qui pourraient se produire dans des systèmes réels et les conditions dans lesquelles und modification cristalline peut être stable ou métastable et dans lesquelles on peut observer une transition à une autre forme cristalline ou à l'état amorphe. On a pris comme variables, qui déterminent le système, la force de tension externe et la tempèrature, en considérant la pression comme constante. Les théories thermodynamiques et les relations appliquées dans ces conditions sont seulement und généralisation de celles établies par Flory et Gee. On admet que des modifications considérables de la longueur de la fibre se produisent durant les changements réversibles des phases. Une image schématique unifiée de l'élasticité d'une fibre dans ces différents états physiques (une seule phase: cristalline ou amorphe; deux phases coexistantes: cristal–cristal ou cristal–amorphe) a été fournie par la construction sur la base de daigrammes de phase des isothermes tension–élongation, de courbes longueur–température à charge constante, et des courbes tension–température à longueur constante.

Zusammenfassung

Zur Veranschaulichung des Konzepts der Fest–Fest- und Fest–Flüssig-Umwandlungen erster Ordnung und der damit verknüpften Elastizitätserscheinungen bei einer ideal homogenen Faser, bei welcher verschiedene Konformationen der Makromoleküle im kristallinen Zustand möglich sind, wurden Phasendiagramme mit willkürlich gewählten, vernünftig erscheinenden Werten für die in Frage kommenden Variablen entworfen Mit gewissen Einschrankungen lassen diese Diagramme einige Möglichkeiten erkennen, die in realen Systemen zu erwarten sind, sowie die Bedingungen, uuter welchen die Stabilität oder Metastabilität einer kristallinen Modifikation erwartet und unter welchen eine Umwandlung in eine andere kristalline Form oder in den amorphen Kautschykzustand beobachtet werden kann. Als Variable, von denen der Zustand des Systems abhängt, kommen äussere Zugkraft und Temperatur in Frage; der Druck wird als konstant betrachtet. Die unter diesen Bedingungen verwendeten thermodynamischen Ansätze und Beziehungen waren eine blosse Verallgemeinerung der von Flory und von Gee aufgestellten. Es wurde angenommen, dass grosse Längenänderungen der Faser wäh-

rend der reversiblen Phasenumwandlung der Faser auftreten. Ein einheitliches, schematisches Bild des elastischen Verhaltens einer Faser in ihren verschiedenen physikalischen Zuständen (eine Phase: kristallin oder amorph; zwie koexistierende Phasen: kristallin-kristallin oder kristallin-amorph) wird durch Konstruktion von Spannungs-Dehnungsisothermen, Länge-Tempreatyrkurven bei konstanter Belastung und Spannungs-Temperaturkurven bei konstanter Länge auf Grund des Phasendiagramms erhalten.

Received December 26, 1962

JOURNAL OF POLYMER SCIENCE: PART A VOL. 2, PP. 755–767 (1964)

Synthesis of Crystalline Polyvinylcyclobutane and Polyvinylcycloheptane*

C. G. OVERBERGER, H. KAYE,† and G. WALSH,†
Department of Chemistry, Polytechnic Institute of Brooklyn, Brooklyn, New York

Synopsis

The synthesis of vinylcyclobutane and vinylcycloheptane is described. These compounds were polymerized to crystalline polyvinylcyclobutane and polyvinylcycloheptane with a triisobutyl aluminum–titanium tetrachloride catalyst system.

Crystalline polyvinylcyclopropane, polyvinylcyclopentane and polyvinylcyclohexane have previously been reported.[2] As a continuation of the study of the effect of pendant alicyclic rings on the physical properties of oriented vinyl polymers, the syntheses of crystalline polyvinylcyclobutane and polyvinylcycloheptane are described here.

VINYLCYCLOBUTANE

Vinylcyclobutane has previously been prepared in low yield by 1,2 addition of ketene to butadiene with subsequent Wolf-Kishner reduction of the vinylcyclobutanone.[3] As an improved method of preparation, an alternate synthesis of vinylcyclobutane was carried out as shown in eq. (1):

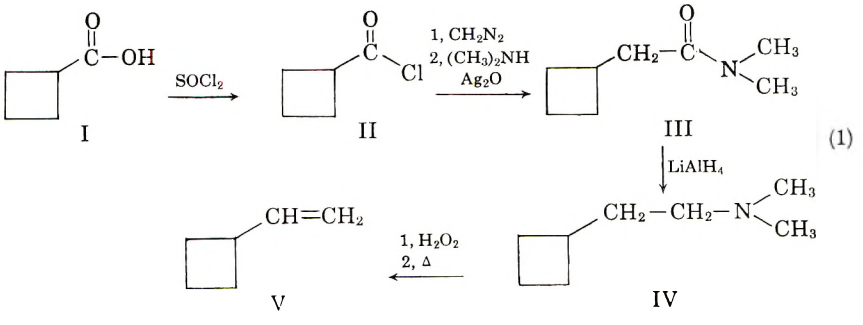

I II III IV V (1)

* This is the 25th in a series of papers on new monomers and polymers. For the previous paper in this series, see Overberger and Davidson.[1]

† Portions of theses submitted by H. Kaye and G. Walsh for the degree of Bachelor of Science, and by H. Kaye in partial fulfillment of the requirements for the degree of Doctor of Philosophy, Polytechnic Institute of Brooklyn.

Cyclobutanecarbonyl chloride (II)[4] obtained from cyclobutanecarboxylic acid (I) and thionyl chloride in 82% yield was converted into *N,N*-dimethylcyclobutylacetamide (III) in 75.5% yield by formation of the diazoketone followed by a modified Wolf rearrangement with dimethylamine and silver oxide. Lithium aluminum hydride reduction of III gave a 65% yield of *N,N*-dimethyl-2-cyclobutylethylamine (IV), which was converted to an amine oxide with 30% hydrogen peroxide and then pyrolyzed by the Cope[5] procedure to give an 85% yield of vinylcyclobutane (V) boiling at 68°C. Vapor-phase chromatography indicated 99.6% vinylcyclobutane and 0.4% of an unidentified compound.

In order to prepare a derivative of III, the synthesis was carried out as shown in eq. (2).

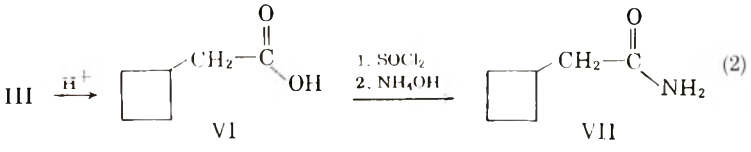

We observed a melting point of 156.5–157.5°C. for cyclobutylacetamide (VII) not in agreement with the work of Zelinski and Kasanski,[6] who reported a melting point of 176–179°C., a melting point identical with that of the isomeric cyclopentanecarboxamide. Zelinski and Kasanski's alleged synthesis of cyclobutylacetamide was carried out by reacting cyclobutylmethanol with phosphorus and iodine to give an iodide followed by a Grignard reaction with carbon dioxide to an acid which subsequently was converted to an amide by the usual procedure.

However, it has been shown that cyclobutylmethanol is converted into cyclopentylbromide when treated with phosphorus tribromide.[7] A nuclear magnetic resonance study of *N,N*-dimethylcyclobutylacetamide (III) indicates the presence of a cyclobutyl ring on the basis of areas of equivalent protons. The infrared spectrum shows the presence of a vinyl group in the vinylcyclobutane we prepared and our physical constants agree with the work of Vogel and Muller.[3] The nuclear magnetic resonance spectrum of vinylcyclobutane is consistent with the structure.

We therefore conclude that Zelinski and Kasanski probably prepared cyclopentanecarboxamide.

VINYLCYCLOHEPTANE

Vinylcycloheptane has been prepared by the synthetic scheme (3) as shown on next page.

Cycloheptanone (VIII) was reduced with lithium aluminum hydride to cycloheptanol (IX) in 87% yield.[8] This was brominated with phosphorus tribromide to give 71.4% yield of cycloheptylbromide (X).[8,9] An alkylation was then carried out with ethyl malonate in the presence of potassium tertiary butoxide to give diethylcycloheptyl malonate, which was then saponified with base and decarboxylated with sulfuric acid to cycloheptylacetic

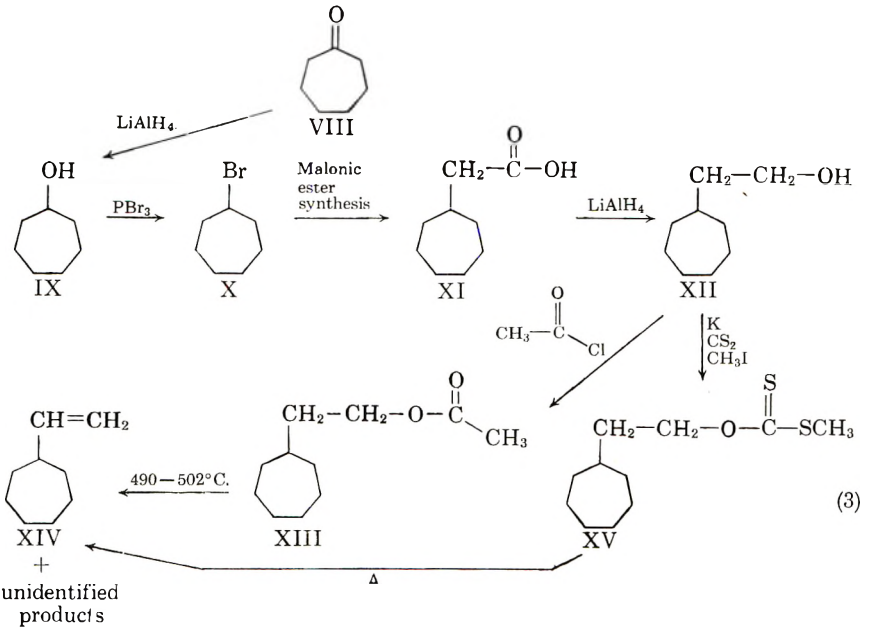

(3)

acid (XI)[10] in 47.2% yield. Reduction of XI with lithium aluminum hydride gave a 95.5% yield of 2-cycloheptylethanol (XII); acetylation with acetyl chloride yielded 2-cycloheptylethyl acetate (XIII) in 98% yield. A mixture of 90% XIII and 10% XII was pyrolyzed at 490–502°C., and vapor-phase chromatography of the product showed the presence of 43.5% vinylcycloheptane (XIV), 48% starting material, and 8.5% of 9 unidentified products. On distillation through a 90-theoretical plate concentric tube column, vinylcycloheptane of 99.9% purity boiling at 160°C. was obtained. After removal of the monomer, the pyrolyzate was repyrolyzed at 530°C., and vapor-phase chromatography indicated the presence of 66% XIV, 3.7% of the starting material, and 30.3% of a mixture of 10 unidentified compounds. Distillation through a 90-theoretical plate concentric tube column yielded a very small amount of pure XIV.

Since the high temperature pyrolysis of the acetate yielded impurities which were difficult to separate, 2-cycloheptylethyl *S*-methylxanthate (XV) was prepared by a general method of Chugaev[11] in 71.2% yield from XII. This was pyrolyzed, giving a 78.5% conversion to olefin which vapor-phase chromatography proved to be 97% XIV and 3% of 6 unidentified components. Rectification through a 90-theoretical plate column yielded pure XIV.

POLYMERS

Initial attempts to polymerize vinylcyclobutane containing 0.4% of an unidentified impurity with triisobutyl aluminum–titanium tetrachloride catalyst system led to low yields of tacky, semisolid polymers. A control polymerization was carried out with vinylcyclohexane under identical con-

TABLE I
d Spacings of Crystalline Polyvinylcyclobutane

d Spacings, A.	Intensity
3.16	Weak
3.42	Very weak
3.92	Medium weak
4.68	Very strong
5.33	Medium
6.48	Very weak
8.50	Strong

TABLE II
d Spacings of Crystalline Polyvinylcycloheptane

d Spacings, A.	Intensity
3.79	Medium
4.60	Strong
5.47	Very strong
6.34	Medium
8.28	Medium
11.84	Strong

ditions. That solid polyvinylcyclohexane was obtained in good yield indicated that the catalyst and polymerization procedure were satisfactory and that the 0.4% impurity in the monomer was inhibiting the polymerization. Distillation through a 90-theoretical plate column failed to remove the impurity, but a successful separation was obtained with a preparatory vapor-phase chromatographic column. Polymerization of the pure vinylcyclobutane gave a 24.5% yield of solid polyvinylcyclobutane, 34% of which was soluble in benzene and 66.0% of which was soluble only in hot decalin. The benzene-insoluble fraction was found to have a softening point of 228°C. (Fisher-Johns melting point apparatus) and to be crystalline by x-ray analysis. The *d* spacings for polyvinylcyclobutane are listed in Table I.

Vinylcycloheptane was polymerized with a triisobutyl aluminum–titanium tetrachloride catalyst system in 9.8% conversion to benzene-soluble polyvinylcycloheptane, 58.8% of which was insoluble in ether. The ether-insoluble fraction exhibited an intrinsic viscosity of 0.39 dl./g. in benzene, melted above 300°C. (Fisher-Johns melting point apparatus), and was highly crystalline by x-ray analysis. Table II lists the *d* spacings.

EXPERIMENTAL*

General

All infrared spectra were obtained with a Perkin-Elmer 21 and an Infracord spectrophotometer. Nuclear magnetic resonance spectra were taken

* All melting points and boiling points are uncorrected. Analyses were determined by Alfred Bernhardt Microanalytische Laboratorium, Mulheim (Ruhr), Germany, and by Schwartzkopf Microanalytical Laboratories, Woodside, N. Y.

on a Varian HR-60 instrument operating at 60 Mcycles/sec. at 25°C., tetramethylsilane set at 10 p.p.m. being used as internal standard. The ratio of peak areas was determined with a planimeter. Analysis by vapor-phase chromatography was carried out on a Perkin-Elmer Model 154-B, and preparative work was carried out on a Model 154-D. Polymerization reagents were purified as follows. The *n*-heptane was refluxed over sulfuric acid, washed with sodium bicarbonate and water, dried over magnesium sulfate, and distilled from and stored over sodium metal; the triisobutyl aluminum was distilled (b.p. 38°C./0.5 mm.); titanium tetrachloride was distilled from copper turnings (b.p. 134–136°C./755 mm.).

Synthesis of Monomers

Cyclobutanecarbonyl Chloride (II). Cyclobutanecarbonyl chloride was prepared according to the procedure of Henze and Taylor.[4] From 104 g. (1.04 moles) of cyclobutane carboxylic acid, there was obtained 100.5 g. (82%) of cyclobutanecarbonyl chloride, b.p. 135°C./750.3 mm., n_D^{25} 1.4515 (by the same method, b.p. 137°C./750 mm., 85%.[4]

N,N-Dimethylcyclobutylacetamide (III). Cyclobutanecarbonyl chloride, 40 g. (0.34 mole), n_D^{25} 1.4515, was added at a rate of 30 drops/min. to 45 g. (1.07 moles) of diazomethane (prepared from *N*-nitrosomethylurea without distillation[12]) in 2 liters of ether at 5°C. with stirring. The mixture was then stirred for 2 hr. at 5°C., at which time all of the ether was removed under reduced pressure. To the residue was added 126 ml. of dioxane, 100 ml. of dimethylamine, 15 ml. of 10% aqueous silver nitrate solution, and 2 g. of freshly prepared silver oxide. A brisk evolution of gas occurred, and it was necessary to cool the flask in an ice bath. Silver oxide was added from time to time to maintain the brisk evolution of nitrogen. After stirring for 1 hr. at 25°C. in the presence of excess silver oxide, the mixture was filtered and the solvent removed under reduced pressure. The crude product was distilled through a 45 cm. packed column yielding 36 g. (75.5%) of *N*,*N*-dimethylcyclobutylacetamide, b.p. 92–93°C./4.9 mm., n_D^{25} 1.4700, d_4^{25} 0.9640. Vapor-phase chromatography on a column of polyglycol (Ucon LB-550-X) indicated 98% purity.

ANAL. Calcd. for $C_8H_{15}NO$: C, 68.04%; H, 10.71%; N, 9.92%; M_D 41.26. Found: C, 68.10%; H, 10.84%; N, 10.00%; M_D 41.26.

Infrared analysis indicated a strong peak at 1650 cm.$^{-1}$ indicative of an amide. The nuclear magnetic resonance spectrum in carbon tetrachloride indicated a doublet centered at 7.19 p.p.m. with a relative area of 6 corresponding to the *N*,*N*-dimethyl protons. Peaks at 7.68 and 7.78 p.p.m. with relative areas of 2 and 1 may correspond to the alpha protons and the tertiary proton, respectively. The spectrum was particularly complicated in this region. A multiplet centered at 8.20 p.p.m. with a relative area of 6 corresponds to the cyclobutyl protons.

The above data are consistent with the structure for *N*,*N*-dimethylcyclobutylacetamide.

Cyclobutylacetic Acid (VI). *N,N*-Dimethylcyclobutylacetamide, 15 g. (0.106 mole), n_D^{25} 1.4700, was refluxed with 350 ml. of 15% hydrochloric acid for 48 hr. After cooling the reaction mixture, extracting with three 50-ml. portions of ether, drying the ether solution over anhydrous sodium sulfate, removing the ether, and distilling the crude acid, cyclobutylacetic acid, b.p. 78°C./2 mm., (209.4°C./752.4 mm.) (micro), n_D^{25} 1.4424, d_4^{25} 1.0202, 10.0 g. (82%), was obtained.

ANAL. Calcd. for $C_6H_{10}O_2$: C, 63.13%; H, 8.83%; M_D 29.73. Found: C, 63.33%; H, 9.01%; M_D 29.64.

Cyclobutylacetamide (VII). Cyclobutylacetic acid, 8 g. (0.07 mole) n_D^{25} 1.4424, was heated to 60°C., and 9 g. (0.076 mole) of thionyl chloride was added slowly with stirring. After stirring the reaction mixture for 24 hr. at 60°C., cyclobutylacetyl chloride was distilled out of the reaction vessel, b.p. 153°C./747.4 mm. The acid chloride was then slowly added to 250 ml. of 30% ammonium hydroxide at 0°C. with stirring. A white precipitate immediately formed which was collected and recrystallized three times from carbon tetrachloride, yielding fine white needles of cyclobutylacetamide, m.p. 156.5–157.5°C., 1.0 g., (12.7%).

ANAL. Calcd. for $C_6H_{10}NO$: C, 63.68%; H, 9.80%; N, 12.38%. Found: C, 63.77%; H, 9.67%; N, 12.31%.

Infared analysis exhibited peaks at 3390, 3180, 1667, 1640, and 1409 $cm.^{-1}$, indicative of a primary amide.

N,N-Dimethyl-2-cyclobutylethylamine (IV). *N,N*-Dimethylcyclobutylacetamide, 34 g. (0.241 mole), n_D^{25} 1.4700, in 100 ml. of ether was added to 9.5 g. (0.248 mole) of lithium aluminum hydride in 125 ml. of ether at a rate sufficient to maintain reflux. After the addition, the mixture was refluxed for 2 days, after which time the excess lithium aluminum hydride was destroyed by dropwise addition of 35 ml. of water. The mixture was filtered and the remaining white residue washed with two 50-ml. portions of ether which were then combined with the filtrate and dried over anhydrous sodium sulfate. The ether was removed and the crude amine distilled under reduced pressure through a 45-cm. packed column to yield *N,N*-dimethyl-2-cyclobutylethylamine, b.p. 60°C./30 mm., 152°C./759.4 mm., n_D^{25} 1.4320, d_4^{25} 0.8014, 19.8 g. (65%). Vapor-phase chromatography on a column of diisodecyl phthalate indicated 100% purity.

ANAL. Calcd. for $C_8H_{17}N$: C, 75.52%; H, 13.47%; N, 11.00%; M_D 41.38. Found: C, 75.41%; H, 13.37%; N, 10.81%; M_D 41.07.

A picrate was prepared by adding 0.8 g. (0.006 mole) of *N,N*-dimethyl-2-cyclobutylethylamine to 50 ml. of a saturated ether solution of picric acid at 20°C. A yellow flocculant compound crystallized out immediately. After three recrystallizations from ethanol the picrate of *N,N*-dimethyl-2-cyclobutylethylamine had a melting point of 146–147.5°C.

ANAL. Calcd. for $C_{14}H_{20}N_4O_7$: C, 47.17%; H, 5.66%; N, 15.72%. Found: C, 47.10%; H, 5.99%; N, 15.60%.

A trimethylammonium iodide was prepared by the general procedure described by Shriner and Fuson.[13] From 0.2 g. (0.0016 mole) of *N,N*-dimethyl-2-cyclobutylethylamine and 5 ml. of methyl iodide white crystals melting at 217–219.5°C. were obtained.

ANAL. Calcd. for $C_9H_{20}NI$: C, 40.15%; H, 7.48%; N, 5.20%. Found: C, 40.42%; H, 7.69%; N, 5.00%.

Vinylcyclobutane (V). To 10 g. (0.078 mole) of *N,N*-dimethyl-2-cyclobutylethylamine in 26 ml. of methanol at 0°C. was added 26.5 g. of 30% hydrogen peroxide at a rate of one drop every 2 sec. with stirring. After the addition the mixture was stirred for 12 hr. at 25°C., at which time 0.6 g. of platinum black was added as an aqueous suspension and stirring was continued for an additional 6 hr. At the end of this time, the solvent was removed under reduced pressure with a rotatory evaporator leaving a thick viscous oil. This amine oxide was then cracked according to the method of Cope[5] with pyrolysis taking place at 118°C./40 mm. to give 5.5 g. (85%) of vinylcyclobutane which vapor-phase chromatography on a column of diisodecyl phthalate showed to be 99.6% vinylcyclobutane and 0.4% of some unidentified compound. Distillation through a 90-theoretical plate concentric tube column failed to remove the 0.4% of impurity, b.p. 68°C./753 mm., n_D^{25} 1.4210, d_4^{25} 0.7467. (The product obtained by a Wolf-Kishner reduction of vinylcyclobutanone had b.p. 68–68.5°C., n_D^{20} 1.4241.[3])

ANAL. Calcd. for C_6H_{10}: C, 87.73%; H, 12.27%; M_D 27.73. Found: C, 87.89%; H, 12.32%; M_D 27.89.

Infrared analysis showed peaks at 1820, 1640, 1420, 990, and 910 cm.$^{-1}$ indicative of a vinyl group. The nuclear magnetic resonance spectrum exhibited an octet centered at 4.30 p.p.m. and two quartets centered at 5.20 and 5.41 p.p.m. each with a relative area of 1 corresponding to the vinyl protons. A broad peak at 7.24 p.p.m. with a relative area of 1 corresponds to the tertiary proton and a multiplet at 8.17 p.p.m. with a relative area of 6 corresponds to the cyclobutyl protons. The above data are consistent with the structure for vinylcyclobutane.

A 2,4-dinitrobenzenesulfenyl chloride derivative of vinylcyclobutane was prepared by the general procedure of Kharasch,[14] except that the reactants were sealed in a Pyrex tube and rotated in an oil bath for 48 hr. at 80°C. After two recrystallizations from ethanol, 2-chloro-2-cyclobutylethyl 2,4-dinitrobenzene sulfide melting at 85–87°C. was obtained.

ANAL. Calcd. for $C_{12}H_{13}ClN_2O_4S$: C, 45.50%; H, 4.14%; S, 10.12%. Found: C, 46.00%; H, 4.12%; S, 10.61%.

Cycloheptanol (IX). A solution of 89.5 g. (0.80 mole) of cycloheptanone in 500 ml. of ether was added to 32 g. (0.84 mole) of lithium aluminum hydride in 1900 ml. of ether under a nitrogen atmosphere at a rate sufficient to maintain reflux. After the addition the reaction was refluxed for 12 hr. at which time 125 ml. of water was added dropwise followed by 630 ml. of

6*N* hydrochloric acid. The ethereal solution was washed with 300 ml. of water, 100 ml. of saturated sodium chloride and dried over anhydrous sodium sulfate. The ether was removed and the crude product distilled through a 45 cm. packed column to yield cycloheptanol, b.p. 73.5°C./8 mm., n_D^{25} 1.4750, 79 g. (87%). (The product obtained by reduction with sodium in moist ether had b.p. 185°C./761 mm., n_D^{20} 1.4747, d_4^{20} 0.9478.[9])

Cycloheptyl Bromide (X). Cycloheptyl bromide was prepared according to the procedure of Vogel,[8] except that the reaction was carried out under a nitrogen atmosphere and kept under ice for 12 hr. followed by stirring for an additional 5 hr. at room temperature. From 78 g. (0.68 mole) of cycloheptanol, n_D^{25} 1.4750 and 99 g. (0.37 mole) of phosphorus tribromide there was obtained 85.7 g. (71.4%) of cycloheptyl bromide, b.p. 61–63°C./6 mm., n_D^{20} 1.5045. (A product obtained by the same method had b.p. 63–63°C./6 mm., n_D^{20} 1.4991, $d_4^{15.7}$ 1.2597, (65%);[8] by a similar method, b.p. 64.3–64.5°C./7 mm., n_D^{20} 1.5049, d_4^{20} 1.3090 was reported.[9])

Cycloheptylacetic Acid (XI). Ethylmalonate, 164 g. (1.03 moles), n_D^{25} 1.4116, in 63 ml. of benzene was added over a period of 1 hr. to 23.2 g. (0.59 g. atom) of potassium metal dissolved in 625 ml. of *tert*-butyl alcohol (distilled from sodium wire), n_D^{24} 1.3851. After refluxing for 30 min., 100 g. (0.57 mole) of cycloheptyl bromide, n_D^{20} 1.5045 was added over a 45-min. interval. The reaction mixture was refluxed for 12 hr., at the end of which time 4 ml. of glacial acetic acid was added and 660 ml. of solvent was removed by distillation. The residue was extracted with 380 ml. of water followed by extraction of the aqueous phase with two 100-ml. portions of benzene. After combining the organic residue with the organic washings, the benzene was removed by distillation, and the remaining residue saponified with 1000 ml. of 2*N* sodium hydroxide for 24 hr. Ethanol was removed by distillation and then the basic solution was extracted with two 100-ml. portions of benzene, followed by addition of 500 ml. of concentrated sulfuric acid. The resulting mixture was refluxed for 24 hr., whereupon a brown oil formed on the surface. This was taken up in 100 ml. of benzene, washed with two 50-ml. portions of water, and then dried over anhydrous sodium sulfate. The benzene was removed by distillation, and the crude product distilled through a 45-cm. packed column yielding cycloheptylacetic acid, b.p. 137°C./2 mm., m.p. 14–15°C., $n_D^{24.6}$ 1.4709, 41.9 g. (47.2%). (Product obtained by hydrogenation of cycloheptenylacetic acid over Raney nickel,[10] b.p. 159–161°C./15 mm., n_D^{25} 1.4743, d_{25}^{25} 1.023.)

In an alternate procedure cycloheptylmalonic acid was first prepared by the above procedure with the use of 250 ml. of *tert*-butyl alcohol, 9.35 g. (0.24 g.-atom) of potassium metal, 65.5 g. (0.41 mole) of ethyl malonate, and 40 g. (0.23 mole) of cycloheptyl bromide, except that the saponified solution was diluted to 3 liters with methanol and passed through a large column of Dowex 50 ion exchange resin followed by elution with 2 liters of methanol. The methanolic eluates were evaporated to dryness on a rotary

evaporator to give 33 g. (71%) of cycloheptyl malonic acid, m.p. 153–154°C. (For the product obtained by reduction of cycloheptylidene cyanoacetate with moist aluminum amalgam followed by hydrolysis with base, m.p. 164.5°C. with decomposition was reported.[15])

ANAL. Calcd. for $C_{10}H_{16}O_4$: C, 59.98%; H, 8.06%; N.E. 200.2. Found: C, 59.87%; H, 8.00%; N.E. 203.3.

The cycloheptylmalonic acid, 31.0 g. (0.16 mole) was then decarboxylated by heating for 2 hr. at 175–180°C. The product was dissolved in 50 ml. of methylene chloride and treated with 1 g. of Darco G-60. The methylene chloride was removed and the remaining solution cooled in a refrigerator for 14 hr. to give 19.8 g. (82%) of white crystals of cycloheptylacetic acid, m.p. 15.0–15.2°C., n_D^{22} 1.4709, d_4^{20} 1.0225.

ANAL. Calcd. for $C_9H_{16}O_2$: C, 69.16%; H, 10.32%; M_D 43.11; N.E. 156.2. Found: C, 69.11%; H, 10.28%; M_D 42.76; N.E. 155.6.

2-Cycloheptylethanol (XII). A solution of 13.2 g. (0.085 mole) of cycloheptylacetic acid, n_D^{22} 1.4709, in 100 ml. of anhydrous ether was added dropwise to 8.0 g. (0.21 mole) of lithium aluminum hydride in 600 ml. of anhydrous ether. When the addition was complete (1.5 hr.), the reaction was refluxed an additional 2 hr., cooled, and then the excess lithium aluminum hydride was destroyed by slowly adding 150 ml. of 6*N* hydrochloric acid. After washing the organic layer with 300 ml. of water, drying with anhydrous sodium sulfate, removing the ether, and distilling the crude product there was obtained 11.0 g. (91.5%) of 2-cycloheptylethanol, b.p. 103°C./6 mm., n_D^{20} 1.4729, d_4^{20} 0.9348.

ANAL. Calcd. for $C_9H_{18}O$: C, 75.99%; H, 12.76%; M_D 43.10. Found: C, 75.98%; H, 12.74%; M_D 42.68.

The infrared spectrum exhibited strong absorption peaks at 3275 and 1050 cm.$^{-1}$, indicative of a hydroxyl group.

From 41.5 g. (0.27 mole) of cycloheptylacetic acid, $n_D^{24.6}$ 1.4709, and 25 g. (0.66 mole) of lithium aluminum hydride under a nitrogen atmosphere and a reflux period of 12 hrs., there was obtained 36 g. (95.5%) of 2-cycloheptylethanol, b.p. 103°C./6 mm., n_D^{25} 1.3743, M_D 42.94.

2-Cycloheptylethyl Acetate (XIII). 2-Cycloheptylethanol 5.3 g. (0.037 mole), n_D^{20} 1.4729, was added dropwise to 25 ml. of acetyl chloride, and the reaction mixture was refluxed for 13 hr. The excess acetyl chloride was distilled, the remaining material dissolved in 50 ml. methylene chloride, washed successively with 50 ml. of water, 50 ml. of 1% sodium carbonate solution, 50 ml. of water, dried over anhydrous sodium sulfate, treated with 1 g. Darco G-60, and filtered. Subsequent distillation of the crude product through a small packed column gave 6.77 g. (98%) of 2-cycloheptylethyl acetate, b.p. 77.5–78°C./0.75 mm., n_D^{25} 1.4576, d_4^{20} 0.9578.

ANAL. Calcd. for $C_{11}H_{20}O_2$: C, 71.69%; H, 10.94%; M_D 52.47; sap. equiv. 184. Found: C, 72.00%; H, 11.01%; M_D 52.66; sap. equiv. 183.

The infrared spectrum exhibited strong absorption peaks at 1740 and 1250 cm.$^{-1}$, indicative of an acetate.

Pyrolysis of 2-Cycloheptylethyl acetate. A mixture of 90% 2-cycloheptylethyl acetate and 10% 2-cycloheptylethanol 31.2 g. was pyrolyzed[16] by being passed at a flow rate of 1 drop/10 sec. into a 30 cm. Pyrex glass tube packed with 7 × 7 mm. Pyrex glass Raschig rings which was inserted in a vertically-mounted furnace at a temperature of 490–502°C. in a stream of nitrogen. The pyrolyzate was washed with 150 ml. of 5% sodium bicarbonate solution, 100 ml. of water, and then dried over anhydrous sodium sulfate. Vapor-phase chromatography on a column of diisodecyl phthalate indicated 43.5% vinylcycloheptane, 48% starting material and 8.5% of 9 unidentified products. On distillation through a 90-theoretical plate concentric tube column, 2 g. (9.3%) of constant-boiling vinylcycloheptane was obtained, b.p. 160°C./759 mm., n_D^{25} 1.4586, d_4^{25} 0.8305. Vapor-phase chromatography on a column of D.C. 200 silicone oil indicated 99.9% purity.

ANAL. Calcd. for C_9H_{16}: C, 87.01%; H, 12.99%; M_D 41.11. Found: C, 87.01%; H, 12.96%; M_D 40.86.

The infrared spectrum showed absorption peaks at 1820, 1640, 1420, 992, and 910 cm.$^{-1}$, indicating a vinyl group.

After removal of the olefinic impurities by distillation, 16.2 g. of starting material remained. Fifteen grams of this was then repyrolyzed at 530°C. at a flow rate of 1 drop/10–15 sec. The resulting dark green solution on treatment with 5% sodium bicarbonate turned brown. After washing with water and drying over anhydrous sodium sulfate, vapor-phase chromatography on a column of di-isodecylphthalate indicated a mixture consisting of 66% vinylcycloheptane, 3.7% starting material, and 30.3% of 10 unidentified components. Distillation of the mixture through a 90-theoretical plate concentric tube column yielded 0.7 g. of vinylcycloheptane, b.p. 160°C./761 mm., n_D^{25} 1.4584.

A 2,4-dinitrobenzenesulfenyl chloride derivative of vinylcycloheptane was prepared by the general procedure of Kharasch,[14] except that the reactants were stirred for 2 days at 70°C. After being recrystallized from 50% petroleum ether–ethanol and twice from ethanol, 2-chloro-2-cycloheptylethyl 2,4-dinitrobenzene sulfide, melting at 99.6–100.6°C. was obtained.

ANAL. Calcd. for $C_{15}H_{19}ClN_2O_4S$: C, 50.20%; H, 5.34%; S, 8.94%. Found: C, 50.87%; H, 5.49%; S, 9.45%.

2-Cycloheptylethyl *S*-Methylxanthate (XV). 2-Cycloheptylethyl *S*-methylxanthate was prepared by the general method of Chugaev.[11] To 5 g. (0.13 mole) of potassium dispersed in 200 ml. of dry toluene at 60–80°C. was slowly added 13 g. (0.092 mole) of 2-cycloheptylethanol, n_D^{25} 1.4739, in 40 ml. of dry toluene. The mixture was stirred for 12 hr. at 70°C. After cooling the yellow viscous alcoholate mixture, 10 g. (0.13 mole) of

reagent grade carbon disulfide in 16 ml. of ether was added, and the stirring was then continued for 24 hr. at room temperature, at which time 16.5 g. (0.12 mole) of purified methyl iodide,[17] n_D^{25} 1.5274, in 40 ml. of ether was added. Stirring was continued for four days at room temperature. The mixture was filtered and the residue of potassium iodide collected and washed with 100 ml. of ethanol followed by 100 ml. of water. The washings were extracted with two 75-ml. portions of ether which were then combined with the filtrate. Solvent was removed and 2-cycloheptylethyl *S*-methylxanthate was then distilled through a 45-cm. packed column. Three fractions were collected, boiling from 84–113°C./0.24 mm. Physical measurements were taken on the middle fraction, b.p. 111.5°C./0.24 mm., 15.1 g., 71.2%, n_D^{25} 1.5458, d_4^{25} 1.0766.

ANAL. Calcd. for $C_{11}H_{20}OS_2$: C, 56.85%; H, 8.67%; S, 27.60%. Found: C, 57.03%; H, 8.71%; S, 27.50%.

Infrared analysis showed strong absorbance at 1210 and 1058 cm.$^{-1}$, which is characteristic of a xanthate.

Pyrolysis of 2-Cycloheptylethyl *S*-Methylxanthate. 2-Cycloheptylethyl *S*-methylxanthate, 15.1 g. (0.065 mole) was pyrolyzed by refluxing in a 100-ml. round-bottomed flask attached to a 13-cm. packed column with a distillation head at a mantle temperature of 250°C. for 12 hr., at which time the mantle temperature was raised to 450°C. and crude vinylcycloheptane distilled over. This was washed six times with 50-ml. portions of 5% aqueous sodium hydroxide, once with 100 ml. of water, and then dried over anhydrous sodium sulfate. According to vapor-phase chromatography on a column of D.C. 200 silicone oil, the crude yield, 3.5 g., contained 97% vinylcycloheptane and 3% of six unidentified components. Distillation of the yellow liquid through a 90-theoretical plate concentric tube column yielded a colorless fraction of vinylcycloheptane, b.p. 160°C./762 mm., n_D^{25} 1.4589, 2.3 g. (28.5%). A residue of 3.25 g. in the pyrolysis flask indicated a 78.5% conversion of xanthate to olefin.

Polymers

Polyvinylcyclobutane. Vinylcyclobutane, 0.57 g. (0.069 mole), n_D^{25} 1.4210, containing 0.4% of an unknown impurity was passed through a Perkin-Elmer Model 154D vapor fractometer using a preparative polyglycol (Ucon LB-550-X) column. The pure vinylcyclobutane was then condensed at −78°C. in a Pyrex polymerization tube containing 4 ml. of purified *n*-heptane and fitted with a self-sealing rubber serum cap along with a side arm and calcium chloride drying tube. Triisobutyl aluminum 0.40 g. (0.002 mole) and titanium tetrachloride, 0.21 g. (0.0011 mole), were injected under a nitrogen atmosphere and the tube sealed. After 7 days in a rotating oil bath at 75°C. the tube was opened and its contents digested in 10% hydrochloric acid methanol for 7 days. After washing with isopropyl alcohol for 4 days, 0.14 g. (24.5%) of polyvinylcyclobutane was obtained. Upon fractionation with 25 ml. of benzene in a semimicro-

Soxhlet extractor for 48 hr., 0.092 g. (66%) of polymer remained insoluble. This polymer was found to be soluble in hot decalin. After drying the polymer at 100°C./0.1 mm. for 48 hr., it was found to have a softening point of 228°C. on the Fisher-Johns melting point block and to be highly crystalline by x-ray analysis (see Table I).

ANAL. Calcd. for $(C_6H_{10})_n$: C, 87.73%; H, 12.27%. Found: C, 87.03%; H, 11.96%; ash, 0.78%. After subtracting the ash: C, 87.66%; H, 11.97%.

Polyvinylcycloheptane. To a 10 × 2 cm. dry Pyrex glass tube, whose constricted neck held a side arm with a calcium chloride drying tube and a glass crown, bearing a self-sealing rubber plug, immersed in a Dry Ice–acetone bath, was added 0.53 g. (0.0028 mole) of titanium tetrachloride, 2 ml. of *n*-heptane, 0.37 g. (0.0030 mole) of vinylcycloheptane, n_D^{25} 1.4589, and 0.82 g. (0.0041 mole) of triisobutyl aluminum. The tube was then sealed under a nitrogen atmosphere and placed in a rotating oil bath at 72°C. for 7 days after which time the tube was cooled in Dry Ice–acetone, opened, and its contents poured into 200 ml. of a 1% hydrochloric acid–methanol solution. A dark viscous semisolid was obtained which was dissolved in 25 ml. of benzene and poured into 250 ml. of acetone, whereupon a flocculant white precipitate formed which was collected and digested in a 5% hydrochloric acid–methanol solution for 24 hr. Pure polyvinylcycloheptane was obtained by reprecipitation from a benzene–acetone system as mentioned above. After drying for 24 hr. at 25°C./0.25 mm., 0.036 g. (9.77%) of polyvinylcycloheptane melting above 300°C. (Fisher-Johns melting point apparatus) was obtained.

ANAL. Calcd. for $(C_9H_{16})_n$: C, 87.01%; H, 12.99%. Found: C, 87.01%; H, 12.96%.

Upon fractionation with 25 ml. of ether in a semimicro-Soxhlet extractor for 48 hr., 0.022 g. (58.8%) of polymer remained insoluble. The ether insoluble fraction was found to be highly crystalline by x-ray analysis (see Table II) and to have an intrinsic viscosity of 0.39 dl./g. in benzene at 30°C.

References

1. Overberger, C. G., and E. B. Davidson, *J. Polymer Sci.*, **62**, 23 (1962).
2. Overberger, C. G., A. E. Borchert, and A. Katchman, *J. Polymer Sci.*, **44**, 491 (1960).
3. Vogel, E., and K. Muller, *Ann.*, **615**, 29 (1958).
4. Henze, H. W., and C. W. Taylor, *J. Am. Chem. Soc.*, **74**, 3616 (1952).
5. Cope, A. C., R. A. Pike, and C. E. Spencer, *J. Am. Chem. Soc.*, **75**, 3212 (1953).
6. Zelinski, W. D., and B. A. Kasanski, *Ber.*, **60B**, 711 (1927).
7. Kuivila, H. G., and W. L. Masterson, *J. Am. Chem. Soc.*, **74**, 4953 (1952).
8. Vogel, A. J., *J. Chem. Soc.*, **1938**, 1323.
9. Fierens, P. F., and P. Verschalden, *Bull. Soc. Chim. Belg.*, **61**, 427 (1952).
10. McCarthy, W. C., and T. H. Brown, *J. Am. Pharm. Assoc.*, **43**, 661 (1954).
11. Chugaev, L. A., *Ber.*, **32**, 332 (1899).

12. Eistert, B., in *Newer Methods of Preparative Organic Chemistry*, Interscience, New York, 1948, p. 564.

13. Shriner, R., R. Fuson and D. Curtin, *The Systematic Identification of Organic Compounds*, Wiley, New York, 1958, p. 228.

14. Kharasch, N., and C. M. Buess, *J. Am. Chem. Soc.*, **71**, 2742 (1949).

15. Vogel, I., *J. Chem. Soc.*, **1928**, 2010.

16. Overberger, C. G., A. Fischman, C. W. Roberts, L. H. Arond, and J. Lal, *J. Am. Chem. Soc.*, **73**, 2540 (1951).

17. Fieser, L. F., *Experiments in Organic Chemistry*, Heath, New York, 1955, p. 282.

Résumé

On a décrit la synthèse du vinylcyclobutane et du vinylcycloheptane. La polymérisation de ces composés, en présence de catalyseurs tri-isobutyl-aluminium tétrachlorure de titane, donne lieu à la formation de polyvinylcyclobutane et polyvinylcycloheptane cristallins.

Zusammenfassung

Die Synthese von Vinylcyclobutan und Vinylcycloheptan wird beschrieben. Diese Verbindungen wurden mit einem Triisobutylaluminium–Titantetrachlorid-Katalysatorsystem zu kristallinem Polyvinylcyclobutan und Polyvinylcycloheptan polymerisiert.

Received December 27, 1962

JOURNAL OF POLYMER SCIENCE: PART A VOL. 2, PP. 769–781 (1964)

Photoelastic Properties of Tightly Crosslinked Networks

ALEXANDRE BLUMSTEIN,* *Instruments Division, Budd Company, Phoenixville, Pennsylvania*

Synopsis

The photoelastic properties of tightly crosslinked networks formed from epoxy resins were investigated in the rubbery and in the glassy states. The following resins were used: bisphenol–diepoxy, resorcinol–diepoxy, and trisphenol–triepoxy resins. The anisotropy Δa of the links, the degree of crosslinking N, and the rigidity of the network were varied independently and the variation of the stress-optical constant with these parameters measured at different temperatures. The results indicate the strong influence of a parameter g depending upon the interactions between the links of the network. g and Δa contribute to the value of the stress-optical constant in opposite directions and can partially compensate each other. If this parameter is introduced in order to account for the interchain interactions, the theory of rubber photoelasticity can account qualitatively for the photoelastic behavior of these networks.

The measurement of photoelastic properties of polymers, besides its widespread applications in stress analysis, is, in combination with other techniques, an excellent tool for the interpretation of the mechanical properties of polymers in terms of their molecular structure. This is particularly important in the case of thermosetting resins, where so few methods of investigation are available. The basis of the method is the fact that when a uniaxial stress is applied to a solid polymer, the material becomes birefringent and behaves as a uniaxial crystal with its optical axis parallel to the direction of the stress. Birefringence measurements can be made in both the rubbery and the glassy states, but only in the former does the theory permit a simple calculation of the birefringence as a function of molecular parameters.

The theory of rubber photoelasticity was developed by Kuhn and Grün,[1] who used as a model an amorphous network containing N links per unit volume, each link behaving as a freely jointed Gaussian chain. The mean anisotropy of the chain (link) was calculated as a function of the difference between the principal polarizabilities α_1 and α_2 of the statistical segment. For a homothetic and small deformation of the network characterized by an extension ratio λ (final length/initial length):

* Present address: Department of Chemistry, University of Delaware, Newark, Delaware.

$$\Delta n = \frac{2\pi}{45} \frac{(\bar{n}^2 + 2)^2}{\bar{n}} (\alpha_1 - \alpha_2) \left(\lambda^2 - \frac{1}{\lambda}\right) \tag{1}$$

where the mean of the refractive indexes is $\bar{n} = (n_1 + n_2)/2$. On the other hand, James and Guth[2] calculated for perfectly elastic networks the relationship between stress and strain:

$$\sigma = NkT[\lambda^2 - (1/\lambda)] \tag{2}$$

where σ is the stress (in kilograms per square centimeter), k the Boltzmann constant, and T the absolute temperature. Combining eqs. (1) and (2) yields:

$$\Delta n = \frac{2\pi}{45} \frac{(\bar{n}^2 + 2)^2}{\bar{n}} (\alpha_1 - \alpha_2) \frac{\sigma}{kT} \tag{3}$$

The stress-optical and strain-optical coefficients are:

$$C = \frac{\Delta n}{\sigma} = \frac{2\pi}{45} \frac{(\bar{n}^2 + 2)^2}{\bar{n}} (\alpha_1 - \alpha_2) \frac{1}{kT} \tag{4a}$$

$$K = \frac{\Delta n}{[\lambda^2 - (1/\lambda)]} = \frac{2\pi}{45} \frac{(\bar{n}^2 + 2)^2}{\bar{n}} (\alpha_1 - \alpha_2)N \tag{4b}$$

Gotlib[3] extended the theory of rubber photoelasticity to chains with Gaussian distribution, restricted rotation of segments, and fixed bond angles. He showed that in the case of a chain composed of segments with symmetrical distribution of polarizabilities around the principal axis of the segment, the relations (4a) and (4b) can be written:

$$C = \frac{2\pi}{27} \frac{(\bar{n}^2 + 2)^2}{\bar{n}} \frac{1}{kT} \overline{\Delta a} \tag{5a}$$

$$K = \frac{2\pi}{27} \frac{(\bar{n}^2 + 2)^2}{\bar{n}} N \overline{\Delta a} \tag{5b}$$

where $\overline{\Delta a}$ is the polarizability of the link:

$$\overline{\Delta a} = \chi(\alpha_1 - \alpha_2)$$

with χ a coefficient accounting for the difference in behavior between a freely jointed and a real chain.

In the present work we have studied the photoelastic properties of three different resins belonging to the family of epoxides, currently used in the photoelastic analysis of stresses. The variations of C and K were studied in both the rubbery and the glassy states by varying $\alpha_1 - \alpha_2$, T, N, and the flexibility of the network.

The epoxy resins permit a variation of these parameters and are thus a good material for this kind of experiments. The resins used were a resorcinol diglycidyl ether, a bisphenol diglycidyl ether, and a trisphenol triglycidyl ether. An attempt was made to interpret the differences in their

behavior at a given concentration of anisotropic groups in terms of differences in their structures.

EXPERIMENTAL

Five different resin systems were used.

A. Variation of Degree of Crosslinking

In order to vary the degree of crosslinking, bisphenolic diepoxy resins with increasing molecular weights, varying from 390 to 2000, were reacted with stoichiometric amounts of hexanediamine. The solid resins were dissolved in methyl ethyl ketone and cast from this solvent. The curing was done after evaporation of the solvent for several days in a dry box at room temperature, followed by 3 hr. of post cure at 150°C. A set of variably crosslinked resins was thus obtained. The extent of the crosslinking was controlled in the following way.

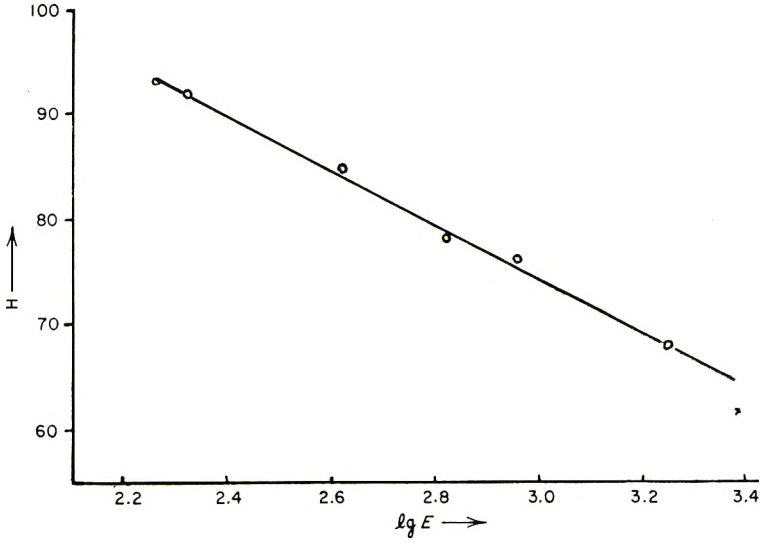

Fig. 1. Shore hardness H as a function of the epoxy equivalent E.

The hardness (Shore) of the resin was taken at different temperatures in the rubbery state. The magnitude of the final hardness at temperatures above that of the transition state gave a rough value of the degree of crosslinking. Figure 1, which gives the variation of the final hardness with the logarithm of the epoxy equivalent, shows that there is indeed a definite relationship between hardness and degree of crosslinking. (The epoxy equivalent can be considered to be equal to $^1/_2 M_c$, M_c being the average molecular weight of a link.)

On the other hand, the extent of crosslinking was checked by direct measurement of the modulus of elasticity E in the rubbery state.

B. Variation of Network Flexibility

In order to vary the flexibility of the network, a bisphenolic diepoxy resin with a molecular weight of 390 was crosslinked successively with stoichiometric amounts of maleic anhydride, succinic, adipic, and sebacic acids, the extent of the crosslinking being kept approximately constant.

C. Variation of Concentration of Anisotropic Groups

In order to vary the concentration of groups with high anisotropy within the links of the network, an aromatic and a cycloaliphatic diepoxy monomer were copolymerized in various proportions using stoichiometric amounts of adipic acid. Three aromatic epoxy monomers were used: resorcinol diglycidyl ether(I), bisphenol diglycidyl ether(II), and trisphenol triglycidyl ether(III).

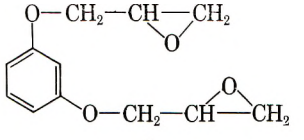

I

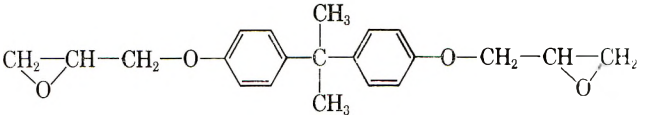

II

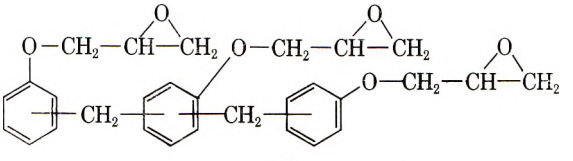

III

III is a mixture of *ortho* and *meta* isomers, as indicated symbolically by the above formula.

I, II, and III were separately copolymerized with increasing amounts of 3,4 - epoxy - 6 - methylcyclohexylmethyl - 3,4 - epoxy - 6 - methylcyclohexanecarboxylate(IV):

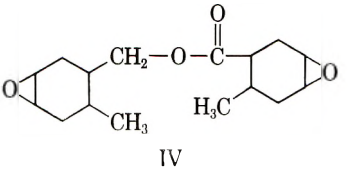

IV

The contribution of IV and of the adipic acid to the anisotropy of the network is small when compared to that of the aromatic units: the anisotropy δ^2 of benzene is 7.3, while it is 0.8 for cyclohexane and 1.5 for butyric acid (measured from the depolarization of light in vapor molecules[4a]). The

difference of anisotropies measured on condensed systems is even higher:[4b] $\delta^2_{benzene} = 38$; $\delta^2_{cyclohexane} = 2.9$.

C and K have been studied for varying values of the concentration in benzene rings. The concentration is denoted as c' if expressed as the weight of molecules of benzene per gram of the resin, and c if expressed as the ratio of the number of molecules of the aromatic epoxy over the total number of epoxy molecules in the resin.

The resins described under sections B and C above were cast and cured for 2 hr. at 150°C. and postcured for 4 hr. at 200°C. A trace of benzyldimethylamine was added in order to accelerate the cure of the maleic anhydride system, which was somewhat sluggish to react.

The resins were cast on glass plates and coated with silicon varnish, using frames made of epoxy resins. The plates were leveled, the resin poured into the mold and cured. Sheets of an average thickness of 0.08 in. were obtained. The experiments were carried out on tensile specimens 0.5 in. wide and 5 in. long.

The specimens were coated on one side with a special reflective coating, placed in an air thermostat between two grips of an external loading device represented in Figure 2*a*. The specimens were centered, and the applied stress was determined by means of a load-cell device. The birefringence was measured with a large field polariscope such as the one described by Zandman[5] and schematically represented in Figure 2*b*, by following the displacement of the fringe corresponding to the "tint of passage" $\lambda = 5.706 \times 10^{-1}$ cm., with the load applied to the specimen, the thermal expansion of the plastic being taken into account. The average indexes of refraction were measured with an Abbé refractometer on films of materials at 25°C.

RESULTS AND DISCUSSION

Figure 3 gives the variation of the stress-optical coefficient C with the temperature for four different resins. In accordance with previous qualitative observations made for different networks,[6,7] we notice a sharp increase of the photoelastic constant at the transition temperature and a linear decline in the rubbery state, according to eqs. (4a) and (5a). (One can see

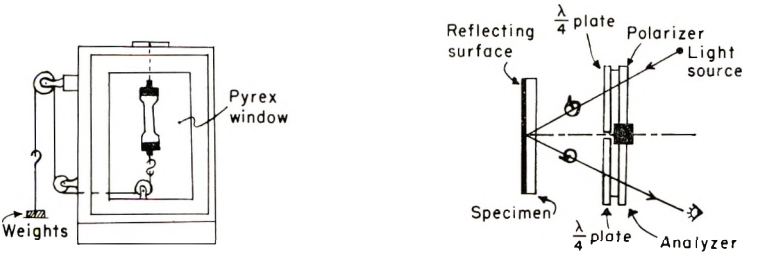

Fig. 2. Schematic diagrams of (*a*) the testing chamber; (*b*) top view of the experimental installation.

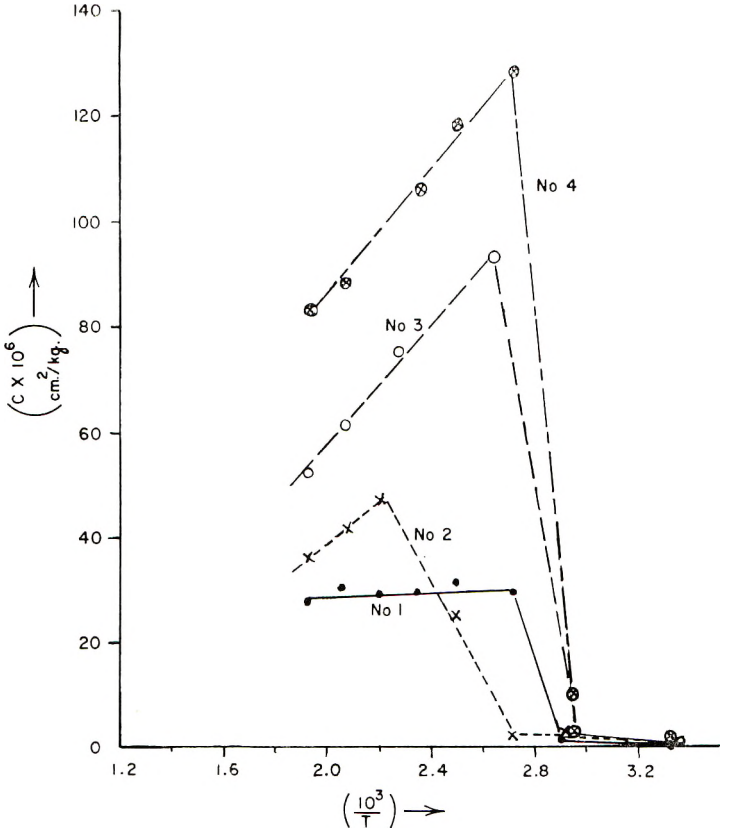

Fig. 3. Variation of the stress-optical coefficient C with the temperature $(1/T)$: (*1*) IV cured with adipic acid; (*2*) novolac epoxide cured with adipic acid; (*3*) resorcinol diepoxide cured with adipic acid; (*4*) bisphenol diepoxide cured with adipic acid.

that the measure of the photoelastic constant is a very sensitive means for the determination of the transition point.)

It is interesting to note that the sign of the constant does not change in the vicinity of the transition point for these resins. This is because the anisotropic groups are built into the link itself and orient similarly with respect to the direction of the stress in both the glassy and the rubbery states. In polymers such as polystyrene or poly(methyl methacrylate), where the anisotropic groups are attached to the side of the main chain, a change in the sign of the constant occurs.[7]

Figure 3 furthermore shows that the transition temperature increases significantly for the trisphenolic triepoxy network, suggesting that it is considerably more rigid than the bisphenolics or the resorcinol diepoxide.

According to eqs. (5) the slope $[dC/d(1/T)]_c$ permits the calculation of $\overline{\Delta a}$ in the rubbery state, as shown in Table I (the variation of n with the temperature is very small as compared to the experimental error on the measurement of C, and is neglected). The small value of $\overline{\Delta a}$ for resin IV

is due to the small value of the anisotropy of its cyclohexane units, as stated previously. On the other hand the unusually small value of $\overline{\Delta a}$ of resin III, as compared to that of resins I and II, is difficult to explain on the basis of eq. (5), since all three resins contain similar anisotropic units and equal proportions of benzene rings. An intuitive explanation of this fact can, however, be given if one takes into account the peculiar structure of the novolacs, whose benzene rings are not entirely built into the main chain forming the network and thus do not respond fully to the constraints imposed upon the latter. The bulky glycidyl groups, particularly when situated *ortho* to the —CH_2— bridges, furthermore, pull the benzene rings apart. When under stress, the three benzene rings forming a novolac molecule take different orientations, and their anisotropies partially compensate each other.

TABLE I

Resin	T_c, °C.	$CT_c \times 10^6$, cm.²/kg.	$dC/d(1/T)$, $\times 10^7$, c.g.s.	$\overline{\Delta a} \times 10^{25}$ cm.³
Resorcinol diepoxide	115	92	0.55	26.8
Bisphenol diepoxide	98	127	0.59	27.5
Trisphenol triepoxide	175	48	0.42	19.0
Epoxide IV	98	29	0.06	7–8

Figures 4 through 7 show the variation of C versus c for the copolymers of IV with I, II, or III. The concentrations range from zero (pure IV plus adipic acid) to 1 (pure aromatic resin plus adipic acid). The measurements were made at 178, 210, and 243°C. in the rubbery state and at room temperature in the glassy state. In both states the stress-optical coefficient increases with c, as is expected. But the form of the C versus c relation varies from one resin to the next. C is proportional to c in the case of

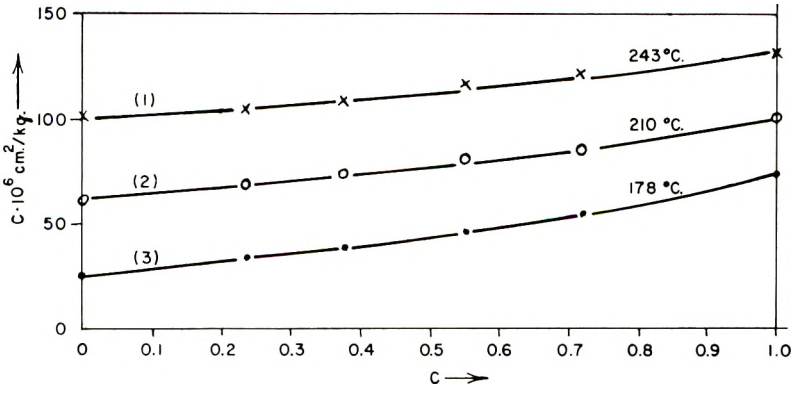

Fig. 4. Variation of the stress-optical coefficient C with the concentration for the resorcinol diepoxide resins in the rubbery state. (Curve *2* displaced 40 units up; curve *1* displaced 80 units up.)

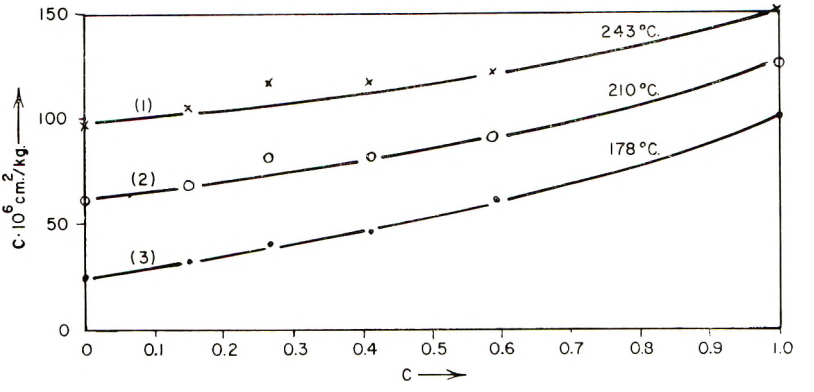

Fig. 5. Variation of the stress-optical coefficient C with the concentration for the bisphenol diepoxide resins in the rubbery state. (Curve *2* displaced 40 units up; curve *1* displaced 80 units up.)

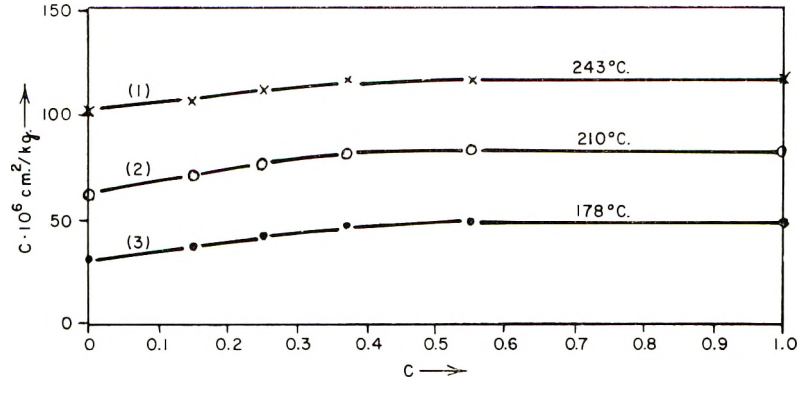

Fig. 6. Variation of the stress-optical coefficient C with the concentration for the; trisphenol triepoxide resins in the rubbery state. (Curve *2* displaced 40 units up; curve *1* displaced 80 units up.)

resorcinol diepoxide resins (Fig. 4). For the bisphenol diepoxide resin C is at first proportional to c. The slope dC/dc continuously increases at higher concentrations (Fig. 5). The triepoxy resins display still different behavior, since a leveling off of the curve occurs at higher concentrations (Fig. 6).

The three resins thus differ in their photoelastic behavior, although they are all three aromatic epoxides, copolymerized with the same monomer, using the same hardener, and are expected to behave in a similar fashion.

In order to account qualitatively for these differences in behavior a relationship between $(dC/dc)_T$ and $[dC/d(1/T)]_c$ can be derived from eq. (5).

If we call A the curing agent (adipic acid), M_1 the aromatic monomer (I, II, or III), M_2 the monomer (IV), we can see that the overall network is built up of two different types of units, A-M_1 and A-M_2, whose respective

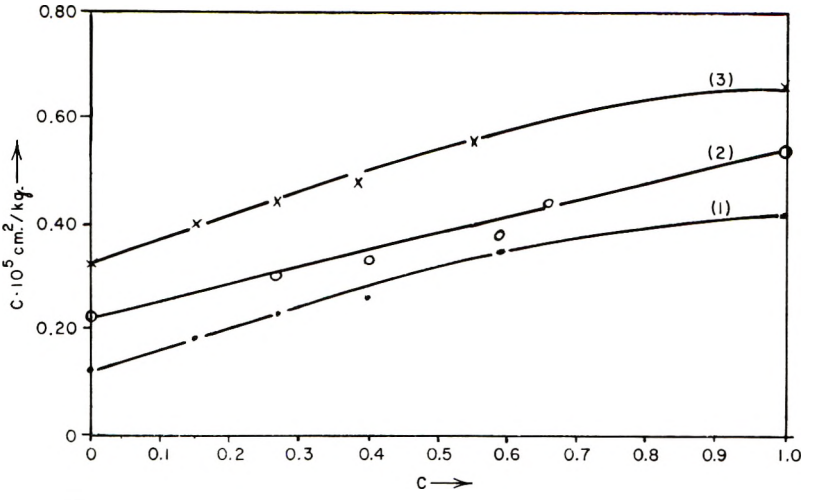

Fig. 7. Variation of the stress-optical coefficient C with the concentration: (1) bisphenol diepoxide resin system; (2) resorcinol diepoxide resin system; (3) trisphenol triepoxide resin system in the glassy state. (Curve *2* displaced 10 units up; curve *3* displaced 20 units up.)

contributions to the stress-optical constant are C_1 and C_2. Assuming that the anisotropy is an additive property:

$$C = cC_1 + (1 - c)C_2$$

where c is the concentration in units of the A-M_1 type. On this basis eq. (5) can be written as:

$$C = \frac{(\bar{n}^2 + 2)^2}{\bar{n}} \frac{2\pi}{27} \frac{1}{kT} [c\Delta a_1 + (1 - c)\Delta a_2] \tag{6}$$

$\bar{n}$ is taken to be $(\bar{n}_1 + \bar{n}_2)/2$, which introduces an approximation similar to the experimental error on the measurement of C. Equation (6) can be taken as the basis for the interpretation of the differences of behavior observed. It shows that C is proportional to $c(\overline{\Delta a_1} - \overline{\Delta a_2})$ as long as $\overline{\Delta a_1}$ and $\overline{\Delta a_2}$ are independent of c. This can be assumed to be the case at low concentrations, where the stiff benzene molecules are diluted in a more flexible matrix, composed mostly of molecules of resin IV and adipic acid.

$$T\left(\frac{\partial C}{\partial c}\right)_T = \frac{2\pi}{27} \frac{(\bar{n}^2 + 2)^2}{\bar{n}} \frac{1}{k} (\overline{\Delta a_1} - \overline{\Delta a_2}) \tag{6a}$$

and

$$T\left(\frac{\partial C}{\partial c}\right)_T = \frac{1}{c}\left[\frac{\partial C}{\partial (1/T)}\right]_c \left[1 - \frac{\overline{\Delta a_2}}{c(\overline{\Delta a_1} - \overline{\Delta a_2}) + \overline{\Delta a_2}}\right] \tag{6b}$$

Indeed Figures 4, 5, and 6 show that for low concentrations the variation of C with c is linear. Furthermore the slope dC/dc decreases with increasing temperatures.

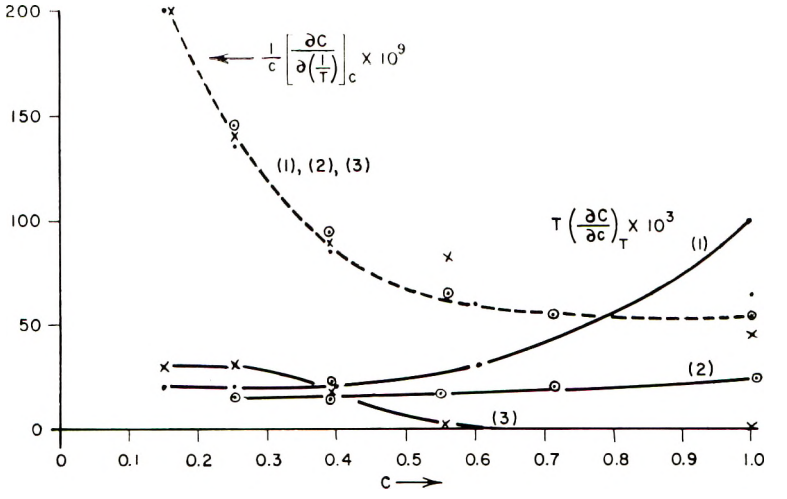

Fig. 8. Plots of (——)$(1/c)[\partial C/\partial(1/T)]_c \times 10^9$ and (——)$T(\partial C/\partial c)_1$ as a function of the concentration: (1) bisphenol diepoxide resin system; (2) resorcinol diepoxide resin system; (3) trisphenol triepoxide resin system.

For high concentrations, remembering that $\overline{\Delta a_1} > \overline{\Delta a_2}$ (see Table I) $c\overline{\Delta a_1} \gg (1 - c)\overline{\Delta a_2}$. One can thus write:

$$C = \frac{(\bar{n}^2 + 2)^2}{\bar{n}} \frac{2\pi}{27} \frac{1}{kT} [c\overline{\Delta a_1}] \tag{6c}$$

$$T \frac{\partial C}{\partial c} = \frac{1}{c}\left[\frac{\partial C}{\partial(1/T)}\right]_c \left[1 + \frac{c^2}{\overline{\Delta a_1}} \frac{\partial \overline{\Delta a_1}}{\partial c}\right] \tag{6d}$$

For a freely jointed chain, $\partial\overline{\Delta a_1}/\partial c = 0$ for all concentrations and thus

$$T\left(\frac{\partial C}{\partial c}\right)_T = \frac{1}{c}\left[\frac{\partial C}{\partial(1/T)}\right]_c$$

One should not expect this to hold in the case of our resins, because of the important steric effects taking place. Figure 8, which records the experimental values of $T(\partial C/\partial c)_T$ and $(1/c)[\partial C/\partial(1/T)]_c$ versus c, shows that this is indeed not so.

However it is expected from eq. (6d) that, since $\partial\Delta a_1/\partial c$ is positive, $T(\partial C/\partial c)_T > (1/c)[\partial C/\partial(1/T)]_c$. But even this is not satisfied, except for resin II at very high concentrations. In the case of I and II, $T(\partial C/\partial c)_T < (1/c)[\partial C/\partial(1/T)]_c$, which is impossible to explain in terms of eq. (6d); furthermore the value of dC/dc is particularly small in the case of the novolacs.

Thus at high concentrations in benzene rings the resins I and III behave in a manner which cannot be explained in terms of eq. (6d).

For a given intrinsic anisotropy the observed birefringence increases with increasing orientation of the anisotropic groups in the direction of the

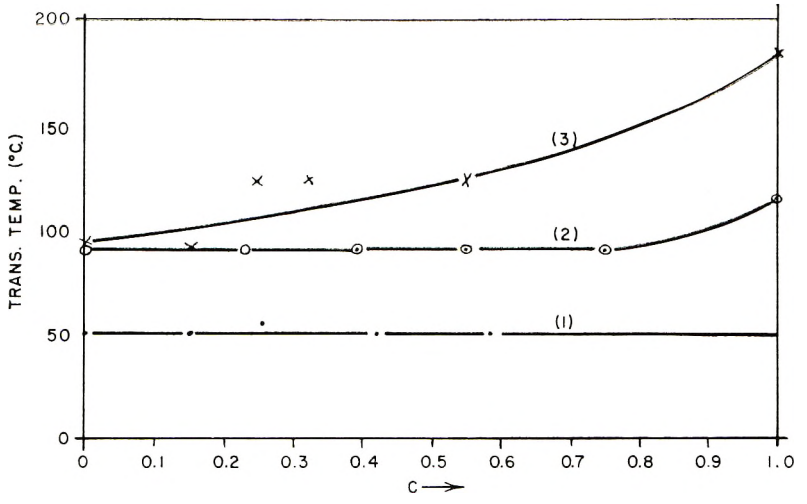

Fig. 9. Transition temperature as a function of the concentration: (*1*) bisphenol diepoxide resin system; (*2*) resorcinol diepoxide resin system; (*3*) trisphenol triepoxide resin system. (Curve *1* displaced 50 units down.)

applied stress. A rigid network resists the deformation; a flexible network yields more easily.

The rigidity of the network depends on chain interactions and network defects such as polar forces acting between the segments, chain entanglements, and the presence of side groups fastening the entanglement points between the chains through steric effects (interchain interactions). On the other hand, the rigidity of the network depends on the rigidity of the individual links (intrachain effects). The interchain interactions will lower the degree of orientation of the anisotropic groups, because of nonuniform transmission of strains, thus leading to low values of dC/dc. The "intrachain" rigidity has an opposite effect on the birefringence stress sensitivity of the network. In this case the anisotropic groups are "preoriented" in the chain, due to restricted rotations and fixed bond angles between the segments. It is easy to see that resin III gives a good example of a network with predominant interchain interactions. The bisphenolics are an example of a network with predominant intrachain effects. They contain the rigid and highly hindered dimethyl diphenylmethane $(CH_3)_2C(C_6H_5)_2$ units. As their concentration increases, there is severe restriction to the rotation of the segments. The links are less coiled than if they were freely jointed and thus more anisotropic. One can expect high values of dC/dc at high concentrations, which is indeed observed.

A macroscopic measure of the "rigidity" of the network is given by the value of the transition temperature T_c, which is a function of the combined effects of the various interchain interactions and restrictions to motion. Figure 9 shows the variation of T_c versus c for the three resins. In the case of resin II, T_c is entirely independent of c. A noticeable increase of T_c takes place at high c for resin I. The T_c of resin III increases continuously

with the concentration with a sharp increase of the slope at high values of c.

Another illustration of the influence of the interchain interactions in tightly crosslinked networks is given by Figure 10, in which the values of C and K of the bisphenolic diepoxy resin are plotted against the degree of crosslinking in the rubbery state. C, although decreasing slightly for high degrees of crosslinking, does not vary significantly with N, as might indeed be expected from eq. (5); K is expected to vary linearly with N, but this is only true for small degrees of crosslinking. At high values of N, K rises sharply. Since $K = EC/1 + \nu$, considering C and the Poisson's coefficient ν as independent of N, this traduces an abnormal rise of the modulus of elasticity E at high N.

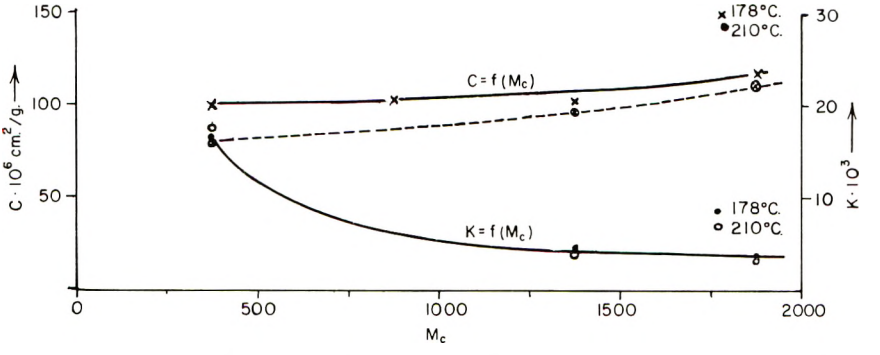

Fig. 10. Variation of the stress-optical coefficient C and of the strain-optical coefficient K with molecular weight of the resin M_c.

A third set of measurements, also effected on resin II, shows once more the effect of the intermolecular interactions. This time, the concentration of benzene rings and the degree of crosslinking were kept constant and different hardeners were used. The moduli of elasticity of the resins measured at 178°C. are: $E_{\text{maleic anh.}} = 170$ kg./cm.^{2}; $E_{\text{adipic}} = 164$ kg./cm.^{2}; $E_{\text{sebacic}} = 140$ kg./cm.^{2}, which indicates that the degree of crosslinking does not vary very much by varying the hardener.

The longer the molecule of the hardener, the more the rigid epoxy chains are pulled apart, the weaker are the interchain interactions, as can be seen from the measurement of the variation of T_c versus length of the hardener molecule (Fig. 11*a*).

Figure 11*b* gives the value of C at different temperatures with different hardeners and, for each isotherm, it can be seen that C decreases with increasing rigidity of the network, although c' increases slightly in the same interval.

The measurements of C and T_c versus c, of E versus N, and of T_c and C for different hardeners, all indicate that an experimental corrective factor must be introduced in order to account for the intermolecular forces of various origins in a tightly crosslinked network.

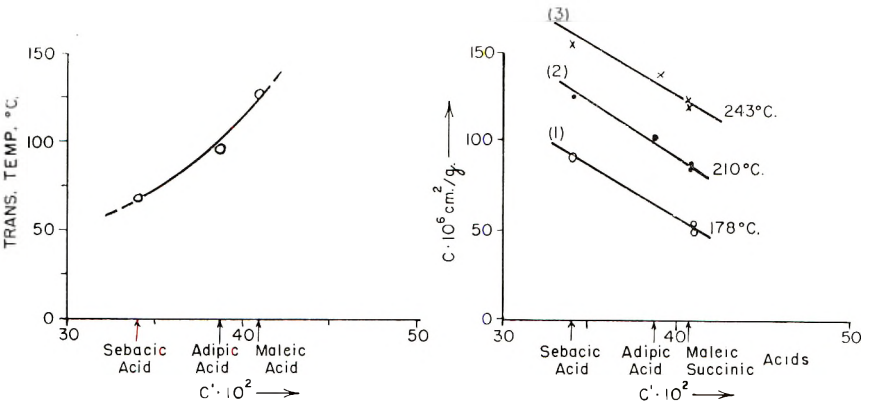

Fig. 11. Plots of (*a*) transition temperature for bisphenol diepoxides cured with diacids of increasing chain length; (*b*) variation of the stress-optical coefficient C with the flexibility of the network. (Curve *2* displaced 40 units up; curve *3* displaced 80 units up.)

A similar factor has already been used by Flory[8] to explain the abnormal rise of E at high degrees of crosslinking in vulcanized rubber networks, transforming the James and Guth relation,[2] eq. (2), for rubbers into:

$$\sigma = gNkT(1 - 2M_c/M)\varphi(\lambda) \tag{2a}$$

where M_c is the molecular weight of the crosslink, M the molecular weight of the main chain, g an experimental factor varying with N and the nature of the network. For high N, $M_c/M \ll 1$, and

$$\sigma = gNkT\vartheta(\lambda) \tag{2b}$$

Taking eq. (2b) into account, eq. (6) can be written in the more general form:

$$C = \frac{(\bar{n} + 2)^2}{\bar{n}} \frac{2\pi}{27} \frac{1}{kT} \frac{1}{g} [c\overline{\Delta a}_1 + (1 - c)\overline{\Delta a}_2] \tag{7}$$

$$T\left(\frac{\partial C'}{\partial c}\right)_T = \left[\frac{\partial C}{\partial (1/T)_c}\right] \frac{1}{c} \left\{1 + \frac{c^2}{\overline{\Delta a}_1}\left(\frac{\partial \overline{\Delta a}_1}{\partial c}\right) - \left[\frac{\overline{\Delta a}_2}{c(\overline{\Delta a}_1 - \overline{\Delta a}_2) + \overline{\Delta a}_2} + \frac{c^2}{g^2}\left(\frac{\partial g}{\partial c}\right)\right]\right\} \tag{7a}$$

Since T_c and g are closely related, Figure 9 can give an idea of the manner in which g varies with the concentration for the different types of networks; for resin III systems dg/dc is large, except at very low concentrations, and it is particularly large at high values of c. On the other hand dg/dc is negligible for the bisphenolic diepoxides. For the resorcinol diepoxides it has a significant value only at high concentrations.

The corrective term, which has been introduced between braces in eq. (7a), can be simplified in the two particular cases of low and high concen-

trations. In the former case it is possible to neglect $\partial g/\partial c$ and $\partial\overline{\Delta a_1}/\partial c$. Hence:

$$T\left(\frac{\partial C}{\partial c}\right)_T = \frac{1}{c}\left[\frac{\partial C}{\partial(1/T)}\right]_c\left[1 - \frac{\overline{\Delta a_2}}{c(\overline{\Delta a_1} - \overline{\Delta a_2}) + \overline{\Delta a_2}}\right] \qquad (7b)$$

The symbols in this relation were replaced by their numerical value for concentrations up to 0.01 and a quantitative agreement was obtained, within the limit of the experimental error, on the determination of $\overline{\Delta a_2}$.

On the other hand it was already seen that at high concentrations $c\overline{\Delta a_1} \gg (1 - c)\overline{\Delta a_2}$. Hence:

$$T\left(\frac{\partial C}{\partial c}\right)_T = \left[\frac{\partial C}{\partial(1/T)}\right]_c \frac{1}{c}\left[1 + \frac{c^2}{\overline{\Delta a_1}}\left(\frac{\partial \Delta a_1}{\partial c}\right) - \frac{c^2}{g}\left(\frac{\partial g}{\partial c}\right)\right] \qquad (7c)$$

The values of g and dg/dc could not be determined at this stage, but the above relations are in qualitative agreement with the observed facts, which could not be explained on the basis of eq. (6) alone. The two terms $c^2\partial\overline{\Delta a_1}/\overline{\Delta a_1}\partial c$ and $c^2\partial g/g\partial c$, the first expressing the rigidity of the individual chain (intrachain interactions) and the second the rigidity of the whole network (interchain interactions) contribute in opposite directions to the value of C. According to the nature of the network, either one of these two positive terms may be the dominant one.

In a network such as III, for which the values of dC/dc are given on curve *3*, Figure 8, the interchain interactions dominate at higher concentrations, dg/dc rising much more rapidly with c than $\partial\overline{\Delta a_1}/\partial c$. Figure 11*a* shows that for flexibilized systems dg/dc is particularly high. Thus, as

$$\frac{1}{g}\left(\frac{dg}{dc}\right) > \frac{1}{\overline{\Delta a_1}}\left(\frac{\partial\overline{\Delta a_1}}{\partial c}\right)$$

and $\partial\overline{\Delta a_1}/\partial c$ is low, the sign of $T(dC/dc)$ is inverted, as can be seen on Figure 11*b*.

Figure 12 shows that interchain steric hindrances also play a part in the glassy state. C does not depend significantly on N, except at very high degrees of crosslinking, where it decreases. Since in the glassy state the network is "frozen," the mobility of large chain segments is excessively small. The effect of the intersegment interactions can therefore be eliminated, and the measure of the variation of C at high degrees of crosslinking could be used to evaluate the contribution of some intermolecular forces to the restriction of the movements of smaller anisotropic groups under strain.

In summary we can say that the theory of rubber photoelasticity, as given by eqs. (3) or (4) cannot be applied to the tightly crosslinked networks which have been studied here. The experiments suggest a strong influence of an interchain parameter, restricting the movements of molecular groups and depending largely upon the degree of crosslinking and the structure of the network. Measurement of the transition temperature can give an idea of the extent of the effect of this factor g. The parameters

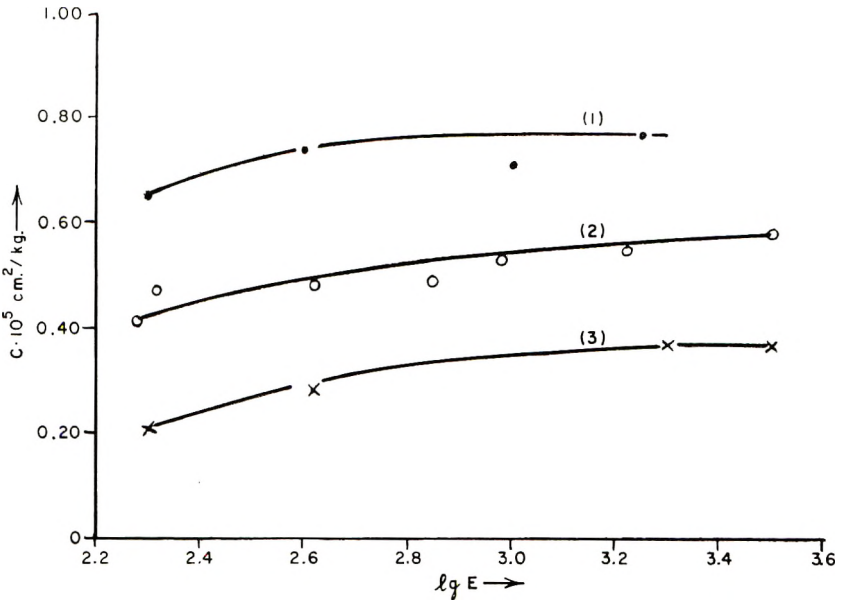

Fig. 12. Stress-optical constant as a function of epoxy equivalent of resins in the glassy state: (*1*) epoxy resin cured with adipic acid; (*2*) epoxy resin cured with hexanediamine; (*3*) epoxy resin cured with sebacic acid. (Curve *1* displaced 20 units up; curve *3* displaced 20 units down.)

g and $\overline{\Delta a}$ contribute to the value of C in opposite directions and can partially compensate each other.

The introduction of the corrective factor g in the relations giving C and K for gaussian chains with restricted rotations of segments and fixed bond angles permits a qualitative explanation of the differences between the behavior of the actual network and the behavior predicted by the theory of the rubber photoelasticity. In order to express the properties of a network in a more quantitative way a study of simpler molecular models would be of great interest.

I wish to thank Dr. John H. Buck for encouraging this work and its publication. I also wish to express my thanks to Bela Nagy and Robert Kiehl for their skillful technical assistance.

References

1. Kuhn, W., and F. Grün, *Kolloid-Z.*, **101**, 248 (1942).
2. James, H., and E. Guth, *J. Polymer Sci.*, **4**, 153 (1949).
3. Gotlib, Yu. Ya., *Dokl. Akad. Nauk SSSR*, **114**, 57 (1957).
4. Stuart, H. A., *Die Struktur des freien Moleküls*, Springer, Berlin, (a), p. 452; (b) *ibid.*, p. 462.
5. Zandman, F., *The Nondestructive Testing Handbook*, Ronald Press, New York.
6. Kawata, K., *J. Polymer Sci.*, **19**, 359 (1956); *J. Polymer Sci.*, **32**, 27 (1958).
7. Andrews, R. D., MCA-MIT Plastics Research Project Progress Report, July 15, 1959; R. S. Stein, in *Die Physik der Hochpolymeren*, H. A. Stuart, Ed., Vol. IV, Springer, Berlin, p. 110.
8. Flory, P. J., *Chem. Revs.*, **35**, 51 (1944).

Résumé

Les propriétés photoélastiques de réseaux fortement pontés et formés de résines époxy ont été envisagées dans les états caoutchouteux et vitreux. Les résines suivantes ont été employées: résines bisphénol–diépoxy, résorcinol–diépoxy et triphénol–triépoxy. L'anisotropie Δa des liaisons, le degré de pontage N et la rigidité du réseau ont été variés indépendamment et la variation de grandeur de la constante optique en fonction de ces paramètres a été mesurée à différentes températures. Les résultats montrent la forte influence d'un paramètre g dépendant des interactions entre les mailles du réseau. g et Δa apportent une contribution en sens opposé à la valeur de la grandeur de la constante optique et peuvent se compenser partiellement. Si ce paramètre est introduit pour expliquer les interactions intercaténaires, la théorie de la photoélasticité du caoutchouc peut expliquer qualitativement le comportement photoélastique de ces réseaux.

Zusammenfassung

Die photoelastischen Eigenschaften stark vernetzter, aus Epoxyharzen gebildeter Substanzen wurden im Kautschuk- und Glaszustand untersucht. Zur Untersuchung kamen Bisphenol–Diepoxy-, Resorcin–Diepoxy- und Trisphenol–Triepoxyharze. Die Anisotropie Δa der Bindeglieder, der Vernetzungsgrad N und die Starrheit des Netzwerkes wurden unabhängig variiert und die Abhängigkeit der spannungs-optischen Konstanten von diesen Parametern bei verschiedenen Temperaturen gemessen. Die Ergebnisse zeigen den starken Einfluss eines von der Wechselwirkung zwischen den Bindegliedern des Netzwerks abhängigen Parameters g. g und Δa beeinflussen den Wert der spannungs-optischen Konstanten im entgegengesetzten Sinn und können sich zum Teil gegenseitig kompensieren. Bei Einführung dieses Parameters für die Wechselwirkung zwischen den Ketten liefert die Theorie der Kautschuk-Photoelastizität eine qualitative Erklärung des photoelastischen Verhaltens dieser Netzwerke.

Received November 15, 1962

JOURNAL OF POLYMER SCIENCE: PART A VOL. 2, PP. 785–796 (1964)

Mechanism of Film Formation From Latices. Phenomenon of Flocculation*

JESSE C. H. HWA, *Rohm and Haas Company, Research Laboratories, Philadelphia, Pennsylvania*

Synopsis

The mechanism of film formation was studied with respect to the flocculation phenomenon. It was observed that almost all latices would air-dry to a point at which coagulation of the latex particles had just occurred and beyond which the wet film was no longer redispersible in water. This flocculation point was sharp and could be detected visually or by immersing the film in water. Two methods have been devised to measure the solids at which incipient flocculation occurred: cross-section method, and cone method. The floc point was found to be about 50–60% for a model acrylic latex depending on the soap present in the dispersion. After flocculation had occurred, further drying would lead to different film properties depending on the hardness of the particles, the rate of drying, the substrate, and the degree of crosslinking.

INTRODUCTION

The mechanism of film formation from latices has been studied earlier by several workers.[1–3] It was postulated that in essence a dry film is formed by loss of water to a point of irreversible contact of the polymer particles and then by a fusion of the particles effected by surface tension and capillary pressure. Undoubtedly this qualitative picture is very useful but there are many details that need clarification.

This work describes additional findings on the film-forming process with particular emphasis on the flocculation step.

EXPERIMENTAL RESULTS

Materials

Acrylic latices representing soft, borderline, and hard polymers were used in most cases. The compositions were respectively: (A) poly(ethyl acrylate); (B) 66:34 poly(ethyl acrylate-*co*-methyl methacrylate); and (C) 10:89.5:0.5 poly(ethyl acrylate-*co*-methyl methacrylate-*co*-methacrylic acid). These polymers were prepared by conventional emulsion polymerization techniques. Latices A and B contained only a very small amount of soap. A crosslinked 90:10 poly(ethyl acrylate-*co*-divinylben-

* Paper presented at the 142nd National Meeting of the American Chemical Society, Atlantic City, September 1962.

zene) latex (D) and a poly(methyl methacrylate) latex were also used in some instances.

A custom-made Petri dish having a conical bottom was obtained from the Kontes Glass Co., Vineland, N. J. The diameter of the dish was 14 cm. and the slope of the cone was about 2°.

Observations of the Flocculation Phenomenon

When an acrylic latex was air-dried on a flat glass disk, three circular areas were invariably observed, independent of the hardness of the polymer. The top and side views of a partially dried latex are illustrated in Figure 1. Since the latex was in the form of a lens, the drying appeared to proceed from the outside inward. When viewed under normal illumination, or especially between crossed Polaroids, one could observe distinctly the respective dry, flocculated, and wet regions. Figure 2 shows the appearance of a partially dried acrylic latex on a convex Petri dish. These observations seemed to be general for all latices, since polystyrene, poly(vinylidene chloride), and poly(vinyl acetate) latices also behaved similarly.

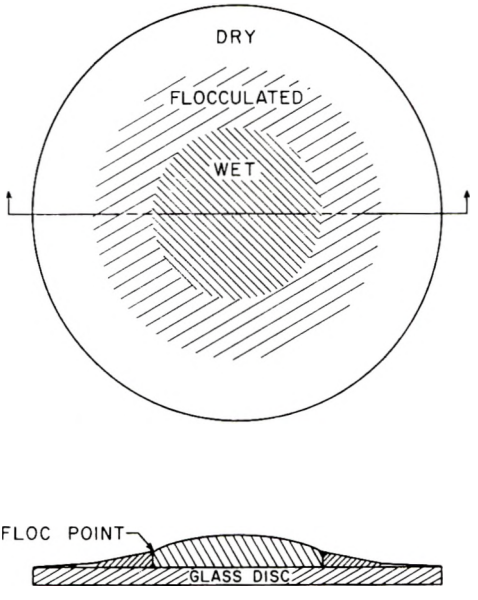

Fig. 1. The occurrence of dry, flocculated and wet regions accompanying the drying of a typical latex on a flat glass disk.

A direct way of distinguishing the wet and flocculated areas was to immerse the partially dried specimen in water. The wet material, being concentrated latex, freely and spontaneously dispersed in water. The flocculated material did not. In fact, after washing away the liquid latex, a sharp boundary bordering the flocculated zone appeared. This boundary was also identical to that observed optically before washing. Figure 3

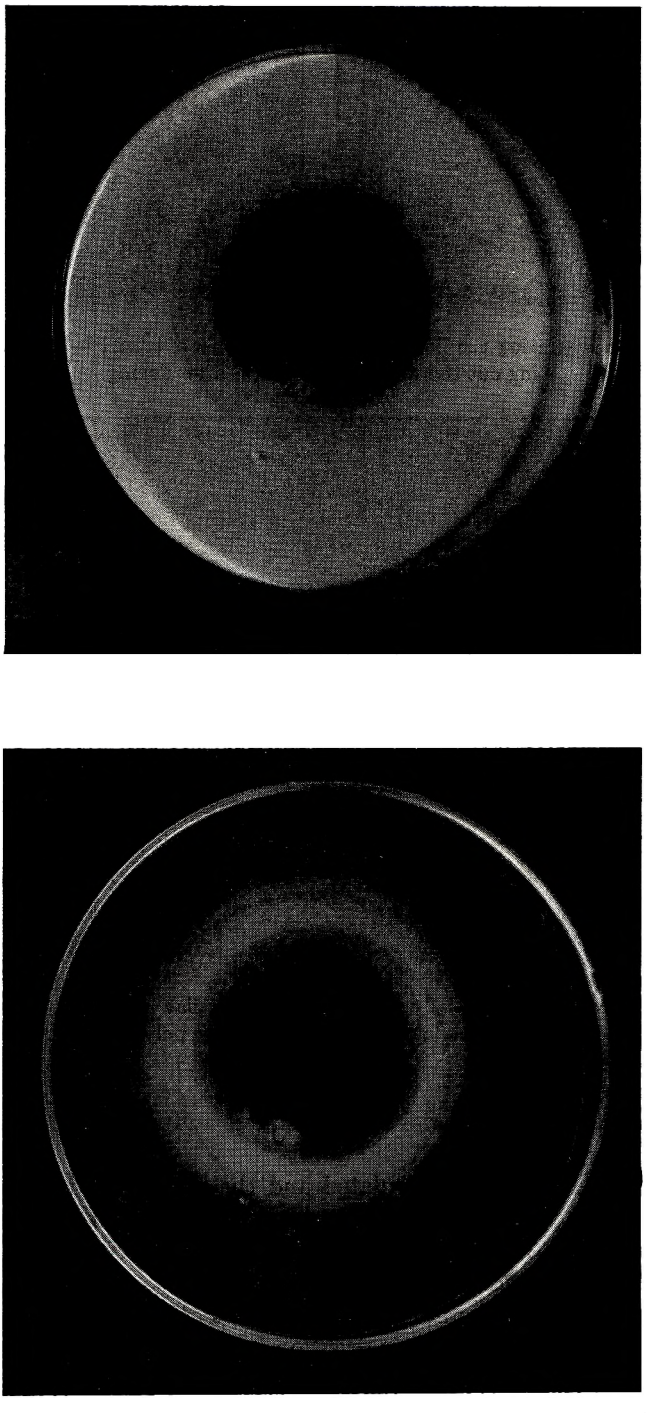

Fig. 2. Appearance of partially dried latex B on a conical Petri dish: (*a*) by reflected light; (*b*) under crossed Polaroids. Outer zone is wet latex; inner circle is transparent dry film; narrow band in between is the flocculated zone.

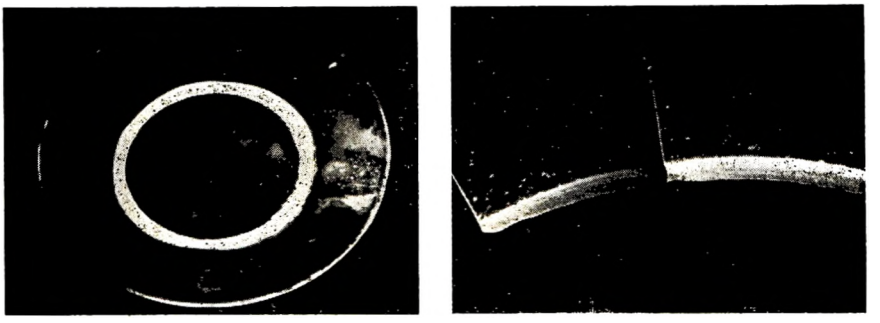

Fig. 3. Border separating the flocculated and wet zones of latex B: left (*a*) after washing out the wet zone; right (*b*) after drying.

Fig. 4. Appearance of partially dried latex C on a flat glass disk between crossed Polaroids. Inner zone is wet latex; outer ring is dry polymer; middle band is the flocculated zone.

shows the flocculated material after wash-out and after wash-out and drying.

The appearance of the flocculated and the dry zones depended on the hardness of the polymer and the nature of the substrate. For a latex of film-forming type (soft polymer), both zones appeared continuous. For a polymer of intermediate hardness, the flocculated zone was continuous, but the dry zone would crack if the film was thick (see Fig. 3*b*). When a latex of a hard polymer was air-dried on a flat disk, the flocculation zone now had fine radiant cracks extending all the way to its edge (Figs. 4 and 5). The outer zone representing the dry polymer was more opaque than the flocculated zone next to it. All latices, regardless of polymer hardness, air-dried on mercury to give continuous "films." [A dry poly(methyl meth-

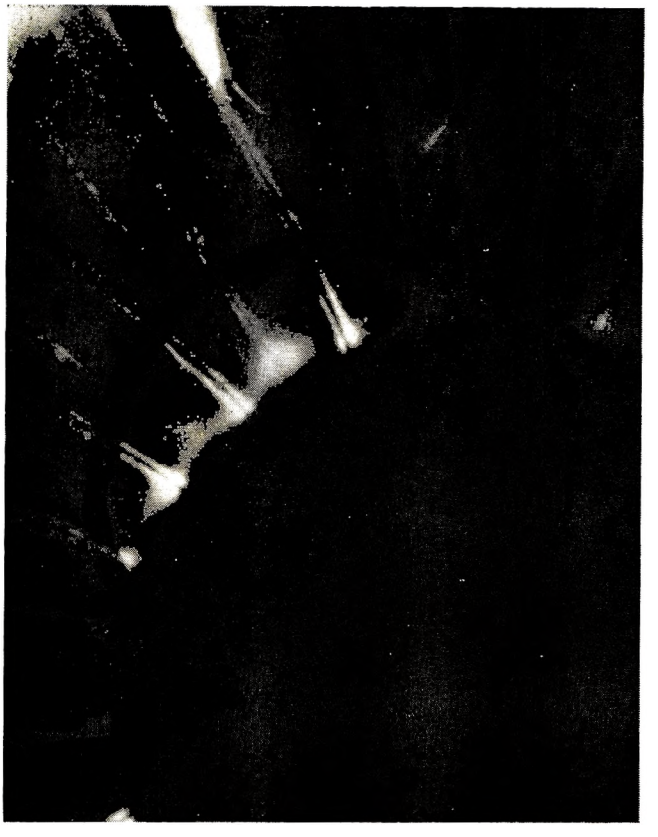

Fig. 5. Close-up of latex C at floc point.

acrylate) film was found to have 13.9 ± 0.5 m.²/g. of surface area (by BET method) which was of the same order of magnitude as that of the original latex.]

The drying behavior of crosslinked and uncrosslinked latices of poly(ethyl acrylate) appeared similar, but their dry film properties were different. The former polymer creeped badly, showed no photoelastic effect when stretched, and redispersed to an emulsion when mixed with common organic solvents.

Determination of the Flocculation Point

Two techniques were developed to determine the volume fraction of the polymer at which flocculation occurs. Both methods met these three requirements: (*a*) detection of the floc point, (*b*) reasonable accuracy and reproducibility, and (*c*) rapidity of the experiment.

Cone Method. This method consists of measuring zone changes that accompany the drying of a latex. The apparatus was a specially made Petri dish with a conical bottom. By recording the area change of the flocculated and dry zones (Fig. 2), one could calculate the floc point.

If one assumes that the rates of evaporation in the wet and flocculated areas at any instant are equal, it can be shown that the volume fraction of the polymer at floc point ϕ is related to the initial latex solids s_0 and to the specific volume of the polymer $\bar{v}$ by eq. (1) (see Appendix):

$$\phi^{-1} = (1 - r)(s_0^{-1} - 1)\bar{v}^{-1} + 1 \tag{1}$$

$$r = (r'_c - r_c)(r'_f - r_f)^{-1} \qquad r_c > 0 \tag{2}$$

here r_c and r_f denote the radii of the clear and flocculated zones, respectively, and r'_c and r'_f are the respective values at another instant of observation. Hence r is the slope of a plot of r_c versus r_f accompanying film formation. Equation (1) allows for the calculation of the floc point from simple experimental observations and initial solids. Interestingly the calculation of ϕ is independent of the solid angle of the cone or the amount of the latex used in drying.

There was some evidence to support the assumption that the rates of drying before and after flocculation remained the same, at least for a hard polymer. A drop of a poly(methyl methacrylate) latex was air-dried in a recording microbalance. No break in the linear drying curve was observed.

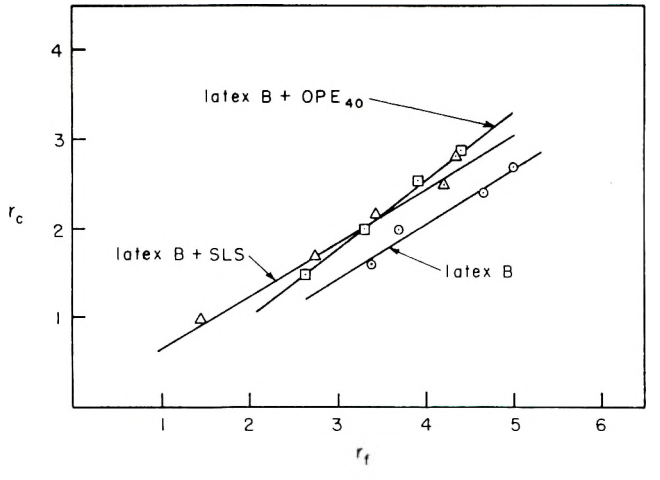

Fig. 6. Relationship between the radii of clear and flocculated zones, in arbitrary units, when latex B is dried on a conical Petri dish: (O) as is; (△) 3% sodium lauryl sulfate post-added; (□) 3% OPE_{40} post-added.

The floc points of latex B (intermediate hardness), and of the same latex to which 3% each (based on polymer) of sodium lauryl sulfate (SLS) and Triton X-405 [OPE_{40}, a poly(ethylene oxide)-type nonionic soap] were post-added, were determined by the cone method. The relationships of the radii that accompanied air-drying are shown in Figure 6. The calculated floc points are listed in Table I.

TABLE I
Floc Point Determinations of Latex B by Optical Methods

Latex	Cone method			Cross-section method	
	s_0	r^a	ϕ^b	ϕ (5 min.)	ϕ (3 hr.)
B	0.324	0.63	0.53	0.69	0.78
B + 3% SLS	0.304	0.60	0.49	0.65	—
B + 3% OPE_{40}	0.300	0.77	0.62	0.75	—

[a] From Fig. 6.
[b] From eq. (1), $\bar{v} = 0.910$.

Cross-Section Method. This is a direct photographic method of measuring the cross-sectional area of a specimen at floc point and after drying. A latex diluted to ca. 15% solids was allowed to air-dry in a 2–3 in. watchglass until a distinct ring of flocculated zone was observed. The partially dried latex was carefully immersed in water and the fluid was rinsed away thoroughly. The specimen now looked like that shown in Figure 3A. While submerged in water, a small section of the ring was sliced off and mounted between two plastic strips held together by a clamp. The wet flocculated cross section faced upward. In an assembly shown in Figure 7, the cross-sectional area while wet (excess surface water still present) and after dry-down was measured photographically at a tenfold magnification. Typical photographs are shown in Figure 8. The floc point is the ratio of the dry and wet (at floc point) areas. The results for the same latex B with

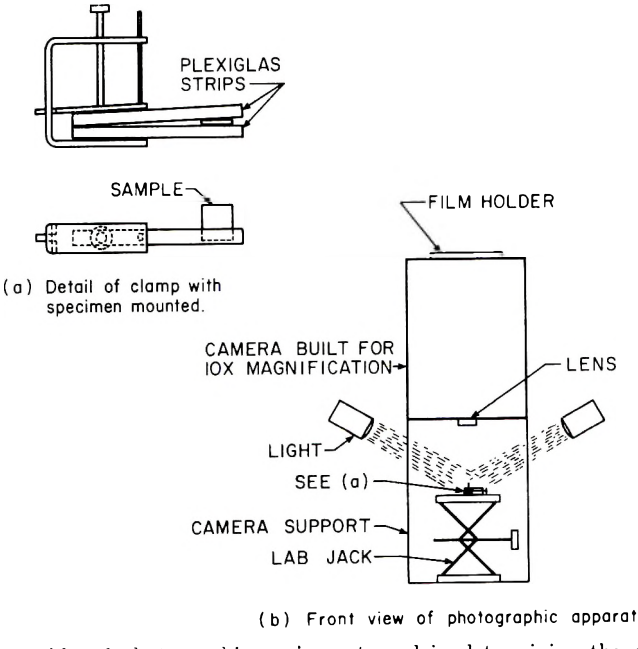

Fig. 7. Assembly of photographic equipment used in determining the cross-sectional area of a flocculated specimen.

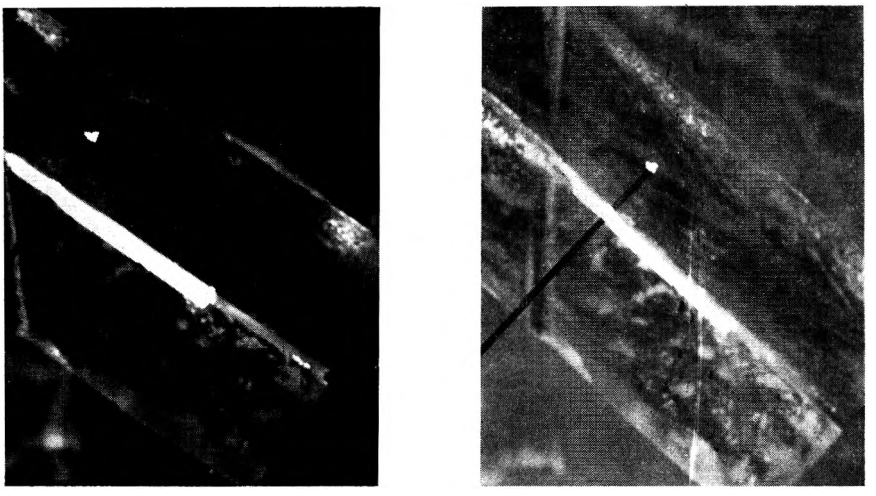

Fig. 8. Typical appearance of the cross-sectional area of latex B: (*a*) at floc point; (*b*) after drying.

and without post-added soaps are shown in Table I. The effect of time elapsed between the immersion of the partially dried latex in water and the actual photographing of the flocculated material is also indicated in the table.

DISCUSSION

The flocculation phenomenon is believed to be a characteristic that accompanies film formation. Apparently at floc point, the latex particles just touch each other to form a giant flocculated network. Such a network is porous and is glued together by van der Waals' forces. This force, effective only at the very small areas of particle/particle contact, nevertheless is great enough to remain unbroken when the network comes in contact with excess water.

At floc point, the polymer particles are far from being close-packed. One knows that the volume fractions of rigid spheres acquiring loose random, dense random, and close-packed arrangements are 0.60, 0.64, and 0.74, respectively, for a monodisperse,[4] and probably larger for a polydisperse system. The results in Table I show that by the cone method the volume fraction of polymer B (a polydisperse) at floc point ranged from 0.49 to 0.62. Hence the initial flocculated state has a fairly open structure.

It was found that the position of the floc point depended on the surface characteristics of the latex particles and on the method by which it was determined. Whereas the floc point of latex B itself was 0.53 (cone method), the presence of sodium lauryl sulfate caused it to occur slightly sooner at 0.49, and that of OPE_{40} delayed it to 0.62. The desorptive nature of these soaps on the polymer surface could account for these observations. Possibly the role of soaps in a latex undergoing a slow concentration process

may be different from that in latex stability (constant solids) and in latex rheology (short-time phenomenon). Sodium lauryl sulfate is known to be able to adsorb on and desorb from the particle surface.[5] While present on the surface originally, these soap molecules would escape from the points of contact as the particles are forced together slowly.[5] The "squeezed out" molecules would form solvated micelles which occupy space and induce the flocculation to occur sooner. OPE_{40}, on the other hand, is not too readily desorbed.[5] The polymer particles are more effectively solvated under the drying conditions and hence delay the floc point.

Similar effects of the soaps on floc point were observed when the cross-section method was used. These effects apparently are real, since this method is independent of theory. However, the floc points are now significantly higher than the corresponding ones determined by the cone method (see Table I). One interpretation is that the floc point may indeed have occurred earlier than that found by the cross-section method, but the 5 min. of time elapsed between the flocculation and the photography allowed the flocculated network to shrink under polymer–water interfacial tension. This view was supported by conducting an identical experiment but immersing the flocculated specimen in water for three hours before photography; the apparent floc point had increased further.

After the onset of the floc point further changes during the film forming process would depend on (a) the hardness of the particles, (b) the rate of drying, and (c) interaction of the film with the substrate.

As it was pointed out earlier, after floc point, soft or borderline polymers will continue to coalesce by the interfacial tension of the flocculated particles, even though the rate of drying is zero. But under normal conditions, where the rate of drying is more rapid than the rate of coalescence due to surface forces, further coalescence of the particles is controlled by the compressive capillary pressure. Polymers of various deformability respond differently to this pressure.

For most hard polymers, such as polystyrene latex or latex C, further loss of water after floc point apparently involves an isotropic contraction of the flocculated state by particle–particle slippage to a more compact form. On a movable substrate such as mercury, this isotropic contraction can be accomplished with no film cracking. On a fixed substrate, such as glass or steel, where there is some interaction between the particles and the substrate, most of the stress developed can be relieved by film cracking at periodic intervals. After the maximum compact state has been achieved, further drying involves loss of capillary water from the fixed interstices. The residue is a cracked, friable cake wherein the particles are held together by weak van der Waals' forces at contact points.

For polymers of borderline hardness, volume shrinkage of the film after floc point can be accomplished by not only interparticulate slippage but also anisotropic deformation of the semisoft particles, driven by capillary pressure and interfacial tension. Under some conditions microscopic imperfections resulting from incomplete coalescence could develop. The final

film hence becomes slightly hazy and cracked if the film is thick; it is also moderately strong with some whitening on stretch.

For a soft polymer such as poly(ethyl acrylate), the anisotropic deformation mechanism probably dominates. In the final film the original particles would lose their identity; the polymer chain segments belonging to different particles would interpenetrate by diffusion resulting in a significant degree of chain entanglement. Hence the film becomes elastic and shows photoelastic effect when stretched. Should the soft particles be crosslinked initially, little chain entanglement between the particles would result. The particles, retaining their identities, are now compressed to close-packed polyhedra. When such a dry film is subjected to a strain, the stress could be readily relieved, not by further deformation of each elastic particle, but by particle–particle slippage in the dry state. Hence the film creeps badly, shows no photoelasticity, and redisperses to an emulsion in organic solvents.

APPENDIX

Derivation of Equation (1)

Consider the drying of a sample of latex originally at level l in a modified Petri dish of an exaggerated design shown in Figure 9. After some degree of drying to level m the radii of the flocculation and clear (dry) zones are r_f and r_c respectively. The same two radii at another instant of drying to level n are r'_f and r'_c. The distances f and f' indicate the film thickness at the positions shown.

By definition:

$$\phi = f/(f + h) = f'/(f' + h') \tag{A-1}$$

The following relations (A-2) to (A-6) are obtainable by considering the simple geometry of the system.

$$\begin{aligned} H' - H &= x + f' - f + h' - h \\ &= x + \phi^{-1}(f' - f) \end{aligned} \tag{A-2}$$

$$\begin{aligned} H' - H &= (c + r'_f)\tan\theta - (c + r_f)\tan\theta \\ &= (r'_f - r_f)H_0/c \end{aligned} \tag{A-3}$$

$$\begin{aligned} x &= (r'_c - r_c)\tan\theta' \\ &= (r'_c - r_c)(1 - \phi_0)H_0/c \end{aligned} \tag{A-4}$$

where ϕ_0 is the volume fraction of the polymer in the original latex. Combining eqs. (A-2), (A-3), and (A-4), one gets

$$\phi^{-1}(f' - f) = [(r'_f - r_f)H_0/c] - [(r'_c - r_c)(1 - \phi_0)H_0/c] \tag{A-5}$$

Since

$$f' - f = [(c + r'_f)\phi_0 H_0/c] - [(c + r_f)\phi_0 H_0/c]$$
$$= (r'_f - r_f)\phi_0 H_0/c \qquad \text{(A-6)}$$

by combining eqs. (A-5) and (A-6) and simplifying one gets:

$$\phi^{-1} = (1 - r + r\phi_0)/\phi_0 \qquad \text{(A-7)}$$

where

$$r = (r'_c - r_c)/(r'_f - r_f) \qquad (2)$$

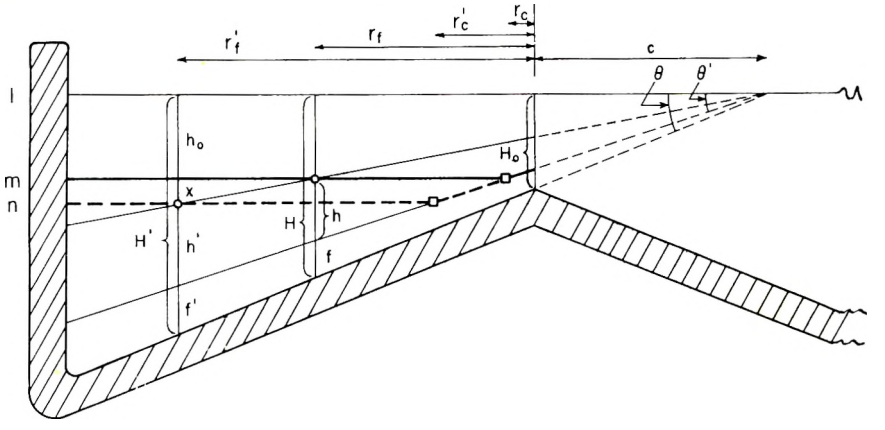

Fig. 9. Relationship between the radii of clear and flocculated zones when a latex is dried on a conical Petri dish of exaggerated design.

The relationship between volume fraction ϕ_0 and weight fraction (per cent solids) s_0 of the polymer in the initial latex is governed by:

$$s_0^{-1} = 1 + \bar{v}(\phi_0^{-1} - 1) \qquad \text{(A-8)}$$

where $\bar{v}$ is the specific volume of the polymer. Combination of eqs. (A-7) and (A-8) gives eq. (1).

The latices were kindly furnished by Messrs. B. B. Kine and A. Kowalski. Mr. W. R. Weber assisted skillfully and enthusiastically in this work. He and Mr. S. Chmielewski also did the photography. Their contributions are gratefully acknowledged.

References

1. Dillon, R. E., L. A. Metheson, and E. B. Bradford, *J. Colloid Sci.*, **6**, 108 (1951).
2. Henson, W. A., D. A. Taber, and E. B. Bradford, *Ind. Eng. Chem.*, **45**, 735 (1953).
3. Brown, G. L., *J. Polymer Sci.*, **22**, 423 (1956).
4. Scott, G. D., *Nature*, **187**, 930 (1960); *ibid.*, **188**, 908 (1960); J. D. Bernal and J. Mason, *Nature*, **188**, 910 (1960).
5. Hwa, J. C. H., unpublished information.

Résumé

On a étudié le mécanisme de la formation de films, en tenant compte du phénomène de la floculation. On a observé que les gommes sèchent généralement à l'air jusqu'au point ou la coagulation des particules de latex a tout juste eu lieu. Passé ce point, le film humide ne peut plus être redispersé dans l'eau. Ce point de floculation est net et peut être déterminé visuellement ou en immergeant le film dans l'eau. On développe deux méthodes pour mesurer les moments où débute la floculation, la méthode de section transversale et la méthode du cône. On trouve que le point de floculation se situe aux environs de 50 à 60% pour un modèle de gomme acrylique, ceci dépend de la quantité de savon dans la dispersion. Si on continue à tourner, après floculation, on obtient des films possédant des propriétés différentes, dépendant de (a) la dureté des particules, (b) la vitesse d'agitation, (c) la substrat, et (d) le degré de pontage.

Zusammenfassung

Der Filmbildungsmechanismus wurde in Hinblick auf Flokkulierungserscheinungen untersucht. Faste alle Latices trockneten an Luft bis zu einem Punkt, bei welchem die Koagulation der Latexteilchen gerade eingesetzt hatte und über welchen hinaus der feuchte Film nicht mehr in Wasser redispergiert werden konnte. Dieser Flokkulierungspunkt war scharf definiert und konnte. Dieser Flokkulierungspunkt war scharf definiert und konnte visuell odor durch Einbringen des Films in Wasser bestimmt werden. Zwei Methoden zur Bestimmung des Festkörpergehaltes, bei welchem beginnende Flokkulierung auftrat, wurden angegeben: die Querschnittsmethode und die Kegelmethode. Der Flok-Punkt lag bei einem Modell-Acryllatex in Abhängigkeit von der in der Dispersion vorhandenen Seife bei 50–60%. Nach Eintritt der Flokkulierung führt weiteres Trocknen je nach Härte der Partikel, Trocknungsgeschwindigkeit, Substrat und Vernetzungsgrad zu verschiedenen Filmeigenschaften.

Received October 1, 1962
Revised November 20, 1962

JOURNAL OF POLYMER SCIENCE: PART A VOL. 2, PP. 797–810 (1964)

Rheological Properties of Polybutadienes Prepared by *n*-Butyllithium Initiation

J. T. GRUVER and GERARD KRAUS, *Research and Development Department Phillips Petroleum Company, Bartlesville, Oklahoma*

Synopsis

The flow behavior of *n*-butyllithium-polymerized polybutadienes was investigated as a function of molecular weight, temperature, and shear rate. At low shear rates these polymers exhibit Newtonian flow up to molecular weights of several hundred thousand so that "zero shear" Newtonian viscosities can readily be determined without the risk of long extrapolation. Above 10,000 molecular weight the Newtonian viscosities obey the well-known 3.4 power dependence on weight-average molecular weight. The entanglement spacing molecular weight is estimated at 5600. The temperature dependence of viscosity is substantially independent of molecular weight and shear stress and can be represented analytically by functions proposed in the literature. The apparent activation energy for viscous flow is not constant, but decreases with rising temperature. The flow of the polymers becomes increasingly non-Newtonian with the product of shear rate, molecular weight and Newtonian viscosity. However, the departure from Newtonian behavior is apparently less than for any polymer system whose flow behavior has been described in the literature. The indications are, therefore, that sharp molecular weight distribution and freedom from long chain branching favor Newtonian flow and that the *n*-butyllithium initiated polybutadienes represent some of the most perfectly linear, narrow distribution polymers known.

I. INTRODUCTION

Most of the rheological investigations of raw elastomers reported in the literature have been concerned with natural rubber and emulsion polymers and copolymers of butadiene. The flow behavior of these rubbers unfortunately does not lend itself readily to molecular interpretation. This is because molecular weight distributions are relatively broad and subject to poorly controlled changes by scission and recombination reactions, and because they are generally not free from long chain branching. The preparation of sharp molecular weight fractions of these rubbers in sufficient quantity for rheological studies is often prohibitively laborious and difficult. The development of polymerization techniques employing organolithium initiators has made possible the preparation of unbranched linear polybutadienes of narrow molecular weight distribution which, in addition, are relatively resistant to degradation. In the present report we describe a detailed study of the rheological behavior of polybutadienes prepared with *n*-butyllithium.

II. EXPERIMENTAL

A. Polybutadienes

The polymers were prepared in hydrocarbon solution by the well-known bottle technique. Number-average molecular weights were calculated from the amount of initiator consumed in the polymerization, after correction for initiator destroyed by impurities. These values, along with intrinsic viscosities measured at 25°C. in toluene and light-scattering weight-average molecular weights are shown in Table I. The intrinsic viscosity-molecular weight relation found was

$$[\eta] = 1.56 \times 10^{-4} \bar{M}_w^{0.78} \quad (1)$$

in fair agreement with the work of Cooper and associates.[1] All polymers contained 0.5% of a phenolic antioxidant.

TABLE I
Molecular Weight of Polymers Investigated

Polymer identification	$\bar{M}_n$	$\bar{M}_w$	$[\eta]$, dl./g.
A	52,000	61,000	0.85
B	131,000	145,000	1.57
C	230,000	238,000	2.35
D	282,000	278,000	2.65
E	298,000	298,000	2.75
F	360,000[a]	334,000	3.10
G	520,000[a]	447,000	3.85
H	740,000[a]	524,000	4.39
I	1,200	2,300[b]	—
J	2,350	3,900[b]	—
K	4,550	6,800[b]	—
L	6,700	9,700	—
M	15,700	20,600	—

[a] Estimates of $\bar{M}_n$ from initiator level become increasingly uncertain as initiator levels decrease, i.e., $\bar{M}_n$ increases. It is believed that $\bar{M}_w/\bar{M}_n$ in reality is close to unity for these polymers.

[b] Estimated by extrapolation of $\bar{M}_w/\bar{M}_n$ ratio to lower molecular weights.

B. Viscosity

Three different methods were employed for the determination of viscosity, depending on the magnitude of the viscosity to be measured. Viscosities of liquid polymers (<2000 poise) were determined with an Ostwald-Cannon-Fenske viscometer. In the range 2000–5,000,000 poise a capillary extrusion rheometer was used. Viscosities in excess of 10 megapoise were calculated from tensile creep data.

The extrusion rheometer was of the CIL (Canadian Industries, Ltd.) type. In this viscometer polymer is extruded under nitrogen pressure from a barrel through a capillary. The shear stress is calculated from the driving pressure and the shear rate from the weight of extrudate collected

under steady state conditions. It is necessary to correct the observed pressure drop for energy losses at the capillary entrance. In addition, for non-Newtonian materials the so-called Rabinowitsch correction[2] must be applied to obtain the maximum shear rate (at the wall) from the average shear rate. Details of these calculations are reviewed in a recent paper by Philippoff and Gaskins.[3] In the present work the entrance correction was uniformly small for all polymers, never exceeding 6% of the total pressure drop. As a consequence of close approach to Newtonian behavior at low shear rates of all the elastomers studied, the Rabinowitsch correction was negligible at the lowest shear rates and did not exceed 31% for any of the polymers at the highest shear rates measured. The data were obtained by using two capillaries of the different dimensions: capillary 1 was 0.447 cm. long and 0.0489 cm. in diameter; capillary 2 was 0.061 cm. in length and 0.210 cm. in diameter. Capillary 2 was used mainly to determine the entrance correction. In all experimental runs measurements were taken both at increasing and decreasing pressures. No evidence of thixotropy or degradation was observed except at the highest temperature (152°C.). Consequently, only few experimental points were obtained at 152°C., and these were determined as rapidly as possible to minimize residence time in the rheometer. In spite of this the data taken at this temperature exhibited some anomalies attributable to degradation which will be discussed at a later point in this paper.

Creep data were obtained by two methods. The first was essentially that described by F. Bueche.[4] Polymer films were prepared by casting from solution and the creep measurement was confined to elongations less than 10% to minimize complications due to change in cross section. These measurements showed the steady-state elastic compliance to be of the order of 10^{-6} cm.^{2}/dyne for the polymers studied. Attainment of steady state was quite rapid and recovery was small. The viscoelastic behavior of the polymers was linear. Viscosities calculated from the steady-state slope of the creep curve, from the permanent set, and from the difference between creep and recovery in the manner described by Bueche[4] all agreed within about ± 10%. The accuracy of this method, though probably satisfactory for measurements of this type, is limited by the low elongations employed.

The second method used to obtain viscosities from creep data utilized higher elongations, with a gain in experimental precision. The data were corrected for the change in cross section by basing the compliance on the instantaneous sample dimensions. The success of this scheme relies on the small magnitude of the elastic compliance and the rapid attainment of steady state. At steady state the sample is, in effect, regarded as a purely viscous liquid. If the sample elongates from length L to $L + dL$ between times t and $t + dt$

$$\frac{dL/L}{F/A} = \frac{dt}{3\eta} \tag{2}$$

TABLE II. Rheological Data

Polymer	$\bar{M}_w$	300°K. f, dynes/cm.^{2} × 10^{-6}	300°K. $\dot{s}$, sec.$^{-1}$	339°K. f, dynes/cm.^{2} × 10^{-6}	339°K. $\dot{s}$, sec.$^{-1}$	380°K. f, dynes/cm.^{2} × 10^{-6}	380°K. $\dot{s}$, sec.$^{-1}$	425°K. f, dynes/cm.^{2} × 10^{-6}	425°K. $\dot{s}$, sec.$^{-1}$
A	61,000	0.18	2.53	0.55	35.9	0.090	16.3	0.051	24.3
		0.35	5.10	0.89	62.3	0.125	24.4	0.081	32.2
		0.57	8.23	1.20	87.8	0.183	31.4	0.125	54.9
		0.77	10.53	1.41	106.7	0.253	46.8	0.172	74.1
		0.81	13.1			0.350	65.8		
		0.94	13.4						
		1.16	18.7						
		1.28	22.0						
		1.46	23.5						
		1.73	31.3						
		1.81	35.1						
B	145,000	0.55	0.48	0.18	0.77	0.19	1.79	0.20	4.19
		0.78	0.89	0.42	1.74	0.31	2.75	0.38	7.03
		0.90	0.89	0.52	2.20	0.56	5.32	0.55	13.2
		1.07	1.17	0.75	3.12	0.71	7.06	0.69	15.9
		1.26	1.35	0.92	4.05	0.92	9.73	1.07	28.4
		1.64	1.86	1.07	4.56	1.32	13.90	1.23	35.1
		2.04	2.45	1.27	5.73	1.44	15.3	1.39	39.1
		2.14	2.84	1.46	6.85	1.63	17.5	1.54	45.9
		2.54	3.36	1.81	8.65	1.89	20.8	1.74	53.1
		3.64	6.11	2.17	11.0	2.08	24.6	1.90	60.2
		5.40	14.2	2.35	12.1	2.39	29.0	2.08	68.5
				2.74	15.2	2.56	31.1	2.31	81.8
				3.11	18.9	2.77	36.3		
				3.63	25.7	3.05	42.5[a]		
						3.88	59.8		
C	238,000	0.72	0.13	0.70	0.52	0.37	0.68	0.58	2.03
		0.91	0.19	0.73	0.66	0.74	1.41	0.89	3.20
		1.24	0.26	1.06	0.88	0.91	1.71	1.27	5.08
		1.76	0.34	1.19	0.93	1.11	2.25	1.62	6.82[a]
		2.03	0.40[a]	1.27	0.99	1.27	2.60	1.93	8.66
		2.13	0.45	1.45	1.23	1.46	3.03[a]	2.43	11.0
		2.25	0.51	1.80	1.51[a]	1.63	3.50	3.30	17.0
		2.46	0.55	2.01	1.74	1.82	4.01	4.27	28.1
		3.02	0.72	2.16	1.91	1.99	4.45	5.99	46.9
		4.36	1.50	2.34	2.11	2.16	4.98		
				2.53	2.42	2.31	5.32		
				2.86	2.85	2.50	5.96		
				3.62	4.27	2.72	6.68		
				5.69	10.3	2.90	7.27		
						3.53	9.35		
D	278,000	—	—	0.72	0.29	0.54	0.56	0.36	0.68
				0.91	0.35	0.71	0.74	0.75	1.45
				1.15	0.45	0.94	0.99	1.06	2.00
				1.28	0.52	1.09	1.17	1.71	3.04[a]
				1.46	0.57	1.26	1.38		
				1.81	0.73[a]	1.44	1.59		
				2.00	0.83	1.55	1.70[a]		
				2.35	1.04	1.64	1.87		

(*continued*)

TABLE II (*continued*)

Polymer	$\bar{M}_w$	300°K. f, dynes/cm.² × 10^{-6}	300°K. $\dot{s}$, sec.$^{-1}$	339°K. f, dynes/cm.² × 10^{-6}	339°K. $\dot{s}$, sec.$^{-1}$	380°K. f, dynes/cm.² × 10^{-6}	380°K. $\dot{s}$, sec.$^{-1}$	425°K. f, dynes/cm.² × 10^{-6}	425°K. $\dot{s}$, sec.$^{-1}$
D	278,000	—	—	2.52	1.18	2.00	2.35		
				2.68	1.24	2.14	2.59		
				2.87	1.43	2.34	2.83		
				3.09	1.55	2.50	3.07		
				4.44	3.07	2.74	3.58		
				5.85	5.30	2.88	3.76		
						4.22	7.35		
						5.00	10.2		
E	298,000	—	—	0.70	0.26	0.74	0.67	—	—
				0.97	0.33	1.01	0.94		
				1.08	0.36	1.07	0.99		
				1.31	0.49	1.23	1.14		
				1.42	0.52	1.42	1.36		
				1.65	0.61[a]	1.62	1.61[a]		
				1.82	0.66	1.97	2.03		
				1.99	0.73	2.13	2.32		
				2.40	0.90	2.35	2.61		
				2.70	1.07	2.48	2.78		
				2.99	1.23	2.69	3.10		
				3.46	1.51	2.86	3.40		
						3.74	5.62		
F	334,000	—	—	—	—	0.89	0.54	0.36	0.40
						1.08	0.67	0.71	0.78
						1.21	0.71	1.07	1.13
						1.30	0.82	1.45	1.57
						1.45	0.92	3.11	3.42[a]
						1.66	1.08[a]		
						1.81	1.18		
						1.98	1.34		
						2.12	1.41		
						2.48	1.74		
						2.72	2.05		
						2.94	2.26		
						3.41	2.64		
						5.89	7.08		
G	447,000	—	—	—	—	0.73	0.16	0.72	0.24
						0.93	0.20	1.07	0.34
						1.25	0.27	1.28	0.42
						1.36	0.31	1.44	0.53
						2.35	0.62[a]	2.44	0.90[a]
						3.04	0.91	3.81	1.76
						4.25	1.48		
H	524,000	—	—	—	—	—	—	0.62	0.130
								0.71	0.148
								1.02	0.234
								1.34	0.30
								1.44	0.37
								2.22	0.90[a]

[a] First appearance of extrudate roughness.

where F is the tensile force, A the cross section of the sample, and η the shear viscosity. Since $AL = V$, the volume of the specimen (which remains constant), we find:

$$\frac{d}{dt}\left(\frac{1}{L}\right) = -\frac{F}{3\eta V} \tag{3}$$

The slope of a plot of the reciprocal length versus time thus immediately yields the viscosity. Excellent linear plots of L^{-1} versus t were obtained, and the viscosities calculated in this manner were in satisfactory agreement with those obtained by the Bueche method, as well as with the capillary viscometer data in the overlap region. The mechanical procedure employed to obtain these measurements was as follows. The polymers were pressed out to a thickness of about 1 mm. between Holland cloth (no advantage could be demonstrated for solution casting), and strips 0.317 cm. in width were died out through the cloth. Upon removal of the Holland cloth backing and the placing of gauge marks on the sample, the strip was clamped into the upper jaw of an Instron table model tester equipped with an air thermostat. Small weights were clamped to the lower end of the strip and allowed to rest on the crosshead with some slack in the strip. The crosshead was lowered manually until the load cell (100 g. full scale deflection) barely recorded a force (ca. 0.2 g.). At this point the crosshead was lowered at 50 in./min., rapidly disengaging the support. The creep was measured with a cathetometer reading to 0.01 cm. No attempt was made to analyze the creep curve for any parameter except viscosity.

III. RESULTS AND DISCUSSION

Table II shows the capillary extrusion data obtained at the various shear rates and temperatures. Table III lists the "zero" shear (Newtonian) viscosities calculated from these data along with the viscosities of the liquid polymers and the creep viscosities.

A. Molecular Weight Dependence

Figure 1 shows the data of Table III as a function of $\bar{M}_w$. Above $\bar{M}_w = 5600$ the well-known 3.4 power relation[5] is observed at all temperatures.

The values of $\bar{M}_w$ for the lowest molecular weight samples were obtained by an extrapolation of the relation between $\bar{M}_w$ and $\bar{M}_n$ for this family of polymers to lower values of $\bar{M}_n$, as reliable light-scattering molecular weights for polymers below 5000 molecular weight could not be obtained.

The break point in the viscosity–molecular weight relation has been identified with the entanglement molecular weight M_e.[6] Its value from Figure 1 is about 5600. The same quantity can also be obtained from the quasiequilibrium modulus of a polymer of high molecular weight. Figure 2 shows the longitudinal creep compliance for polymer H ($\bar{M}_w = 524{,}000$). This curve represents the composite data obtained at six temperatures and

TABLE III
Newtonian (Zero Shear) Viscosities[a]

	Viscosity, Mpoises					
$\bar{M}_w$/1000	235°K.	267°K.	300°K.	339°K.	380°K.	425°K.
2.3			0.0000052		0.00000065[b]	—
3.9			0.0000103	—	0.0000012[b]	—
6.8			0.000037	—	0.0000039[b]	—
9.7			0.000096	—	0.0000098[b]	—
20.6			0.001156	0.000280	0.000137[b]	0.0000424
61			0.070	0.0165	0.0055	0.0022
145			1.00	0.235	0.106	0.049
238			5.2	1.24	0.54	0.29
278	*1210*	*50*	9.4, *10.2*	2.50	0.97	0.525
298	*1120*	*66*	*12.5*	2.77	1.14	—
334	*1750*	*95*	*18.2*	—	1.67	0.92
447	*4150*	*264*	*46*	—	4.5	3.0?
524[c]	*7750*	*386*[d]	*76*	—	—	5.0?

[a] Values in italics determined by creep.
[b] At 372°K.
[c] Also *1710* Mpoise at 248°K., *890* at 253°K., *252* at 277°K., *148* at 287°K.
[d] At 265°K.

shifted to coincidence by time–temperature superposition. The plateau allows calculation of M_e by the kinetic theory of rubber elasticity.[7] This procedure leads to $M_e \approx 3000$, which leaves much to be desired as to agree-

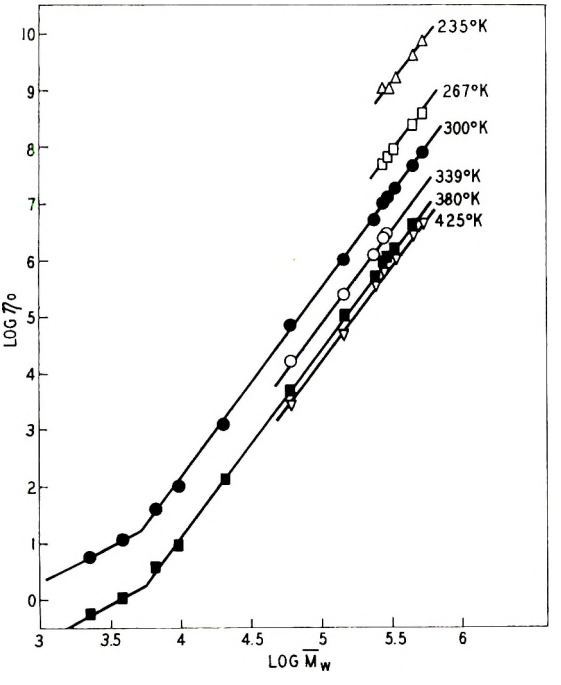

Fig. 1. Dependence of Newtonian viscosity on molecular weight.

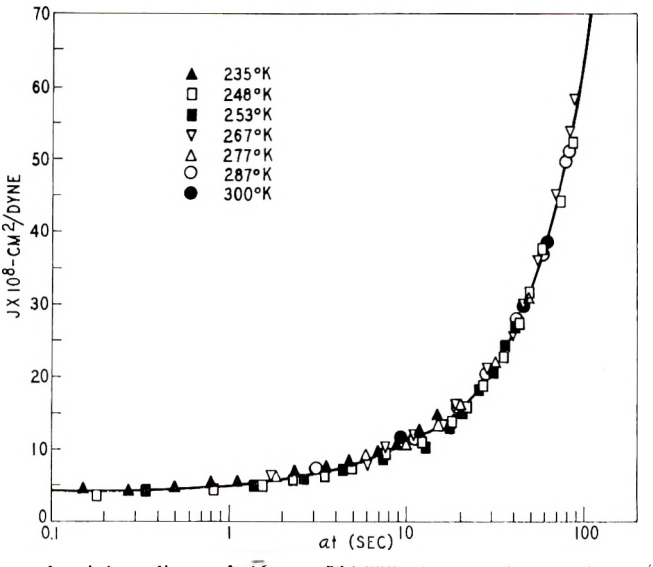

Fig. 2. Creep of polybutadiene of $\bar{M}_w$ = 524,000 at seven temperatures (shifted to 300°K.).

ment. Still another method, based on the maximum number of entanglements which can be trapped by chemical crosslinks in vulcanization[11] yields the value of 6000. For this reason, it is felt that 5600 represents a more reasonable estimate of M_e.

The molecular weight dependence below the critical entanglement molecular weight has been variously reported[5] as a power law with exponent ranging from 0.84 to 1.76; different theories give $^4/_3$ and 1, respectively.[6,8] The best fit of the present data gives a value closer to $^4/_3$, but does not permit a clear distinction between the two theories.

B. Dependence of Viscosity on Temperature

Figures 3 and 4 illustrate the effect of temperature on rheological properties. Figure 3 shows the data of Table II superimposed by the temperature shift factors plotted against T^{-3} in Figure 4. Also included in the latter plot are shift factors for the Newtonian viscosities obtained from creep and for the liquid polymers.

There are two empirical relationships which have enjoyed considerable success in representing viscosity–temperature relationships for polymers. The Fox and Loshaek[5,9] equation gives

$$\log \eta_2 - \log \eta_1 = B\, e^{-\beta/Z_n}\left(\frac{1}{T_2^{\,a+1}} - \frac{1}{T_1^{\,a+1}}\right) \tag{4}$$

where η_2 and η_1 are the viscosities at absolute temperatures T_2 and T_1, respectively, Z_n is the number-average chain length (skeletal carbon/molecule), and β, B, and a are empirical constants. Our data show no obvious dependence on Z_n. We conclude that throughout the range

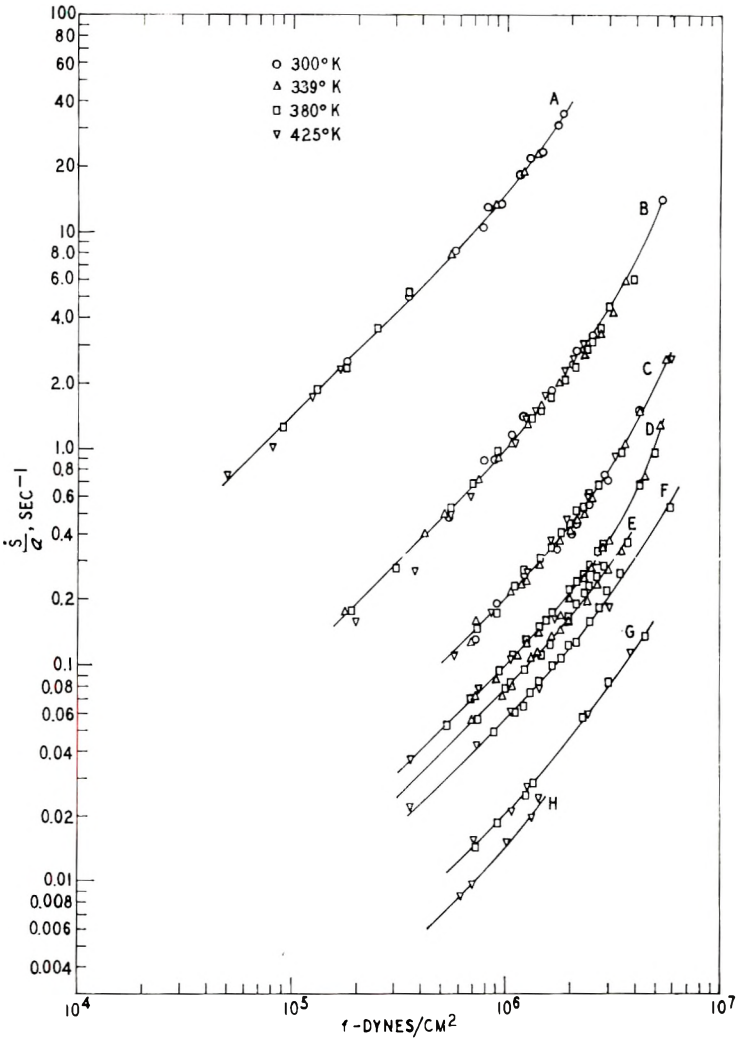

Fig. 3. Rheological properties of polybutadiene prepared by butyllithium initiation (shifted to 300°K.).

investigated β/Z_n is negligibly small. This means that β itself must be small, as it is for polyisobutylene,[5] and the exponential is essentially unity. The best fit of the high temperature data is obtained with $a = 2$. With 300°K. as reference temperature:

$$\log (\eta_{300}/\eta_T) = 2 - (54 \times 10^6/T^3) \tag{5}$$

The quality of the fit is seen in Figure 4. With $a = {}^3/_2$ the entire curve can be fitted by

$$\log (\eta_{300}/\eta_T) = 2.302 - (35.9 \times 10^5/T^{5/2}) \tag{6}$$

with some loss in agreement above room temperature.

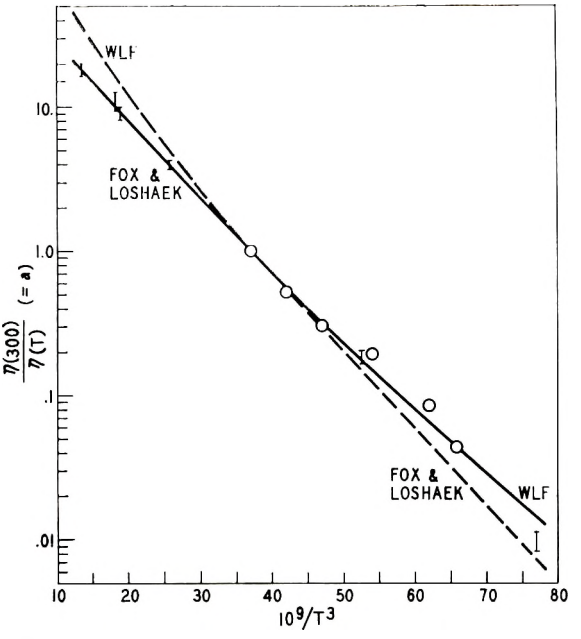

Fig. 4. Temperature dependence of viscosity. Bars represent range of values for all polymers measured at indicated temperature.

Another method of representing viscosity-temperature has been proposed by Williams, Landel, and Ferry (WLF). The WLF equation is:[10]

$$\log \frac{\eta_T T_s \rho_s}{\eta_s T \rho} = \frac{-8.86(T - T_s)}{101.6 + T - T_s} \approx \log \frac{\eta_T}{\eta_s} \tag{7}$$

where T_s is a suitably chosen reference temperature, usually within 50 degrees of the glass transition T_g, but most frequently above T_g. The validity of this formula is confined to a 100 degree range above T_g.* The glass transition of *n*-butyllithium-initiated polybutadiene, as determined in these laboratories, is ca. 180°K. Hence, one would expect conformance with the WLF equation only below room temperature. The agreement with T_s = 190°K. is indicated in Figure 4. In general, the Fox and Loshaek equation is capable of producing a better fit of all the data (with $a = {}^3/_2$), which is not surprising since it lacks the universal character of the WLF equation and, besides, contains one more parameter.

In examining Figure 4 it should also be kept in mind that the method of representation chosen forces agreement at 300°K. The range of the observed viscosity ratios therefore increases in going to both higher and lower temperatures. At the highest temperature this range is larger than indicated on Figure 4, but part of this spread can be attributed to degradation (see Experimental Section). This degradation was in the direction

* The small variation in the ρT factor has been neglected (see Reference 5).

of scission (lower viscosity) in the low molecular weight polymers, but at the higher molecular weights toughening due to crosslinking occurred. For this reason only the polymers in the 145,000–334,000 molecular weight range, in which some cancellation of these effects is probable, are represented by the bar in Figure 4 corresponding to 425°K.

The observed temperature dependence of viscosity indicates a variable activation energy for flow, which changes from about 8 kcal./mole at 300°K. to 4.7 kcal./mole at 425°K.

C. Non-Newtonian Flow

One of the most striking features of the results obtained in the remarkably Newtonian character of even the high molecular weight members of this series of polymers. This is believed to be the result of the strict linearity of the molecules and narrowness of the molecular weight distribution. It was also observed by Arnett and Hughes[12] on a series of hydrogenated polybutadienes serving as model polymers for monodisperse polyethylene. Another observation of Arnett and Hughes was that roughness of the extrudate emerging from the capillary viscometer was not necessarily accompanied by anomalies in the flow curve (such as the increased flow which often accompanies melt fracture) and could occur even in the Newtonian flow regime. The present work confirms these observations. Since the appearance of extrudate roughness is not accompanied by a discontinuity in the shear rate–shear stress relation or its derivative, it is felt that the data collected on rough extrudates (see Table II) are substantially correct. We have used these data in the following analysis of our results in terms of current theories of non-Newtonian flow. It should be emphasized, however, that the conclusions drawn do not depend on the use of these data; the same conclusions would be reached on the basis of the more limited data on smooth extrudates.

The Ree-Eyring theory of generalized viscosity yields[13]

$$\eta = \sum_{n=1}^{N} \frac{x_n \beta_n}{\alpha_n} \frac{\sinh^{-1} \beta_n \dot{s}}{\beta_n \dot{s}} \tag{8}$$

where $\dot{s}$ is the shear rate, x_n is the fraction of the area on a shear surface occupied by flow units of the nth kind, $\alpha = \lambda\lambda_2\lambda_3/2kT$, $\beta = \{(\lambda/\lambda_1)2k'\}^{-1}$, k' the rate constant for the flow process at zero stress, and λ_1, λ_2, λ_3, and λ are the molecular distances in the Eyring theory of viscosity.[14] The parameters β_n are the relaxation times characteristic of the N types of flow units. The present data can be fitted to an equation of this type by using a single non-Newtonian flow element. More logically, since the viscosity should not approach zero in the limit of high shear:

$$\eta = \eta_{00} + \eta_0 (\sinh^{-1} \beta\dot{s})/\beta\dot{s} \tag{9}$$

wherein $\eta_{00} \ll \eta_0$ so that the fit of experimental data is incapable of distinguishing between η_0 and the true zero shear viscosity ($\eta_{00} + \eta_0$). Values

TABLE IV
Values of Relaxation Time β, Eyring Theory

Polymer	$M_w \times 10^{-3}$	β, sec.	$\beta/M_w^{3.4} \times 10^{18}$
A	61	0.055	3
B	145	0.55	1.6
C	238	2.2	1.2
D	278	4.6	1.4
E	298	5.1	1.4
F	334	6.3	1.1
G	447	20.5	1.2
H	524	46	1.7

of β at 300°K. are shown in Table IV. It will be noted that the relaxation time β is evidently proportional to $\bar{M}_w^{3.4}$.

In the theory of F. Bueche,[15] the non-Newtonian viscosity η is given by

$$\frac{\eta}{\eta_0} = 1 - \frac{6}{\pi^2} \sum_{n=1}^{N} \frac{\dot{s}^2\tau^2}{n^2(n^4 + \dot{s}^2\tau^2)} \left(2 - \frac{\dot{s}^2\tau^2}{n^4 + \dot{s}^2\tau^2}\right) \tag{10}$$

where η_0 is the viscosity at zero shear and τ is a characteristic relaxation time, the other symbols having already been defined. The relaxation time is

$$\tau = 12\, v\, \eta_0 M/\pi^2 RT \tag{11}$$

where v is the specific volume and M the molecular weight.

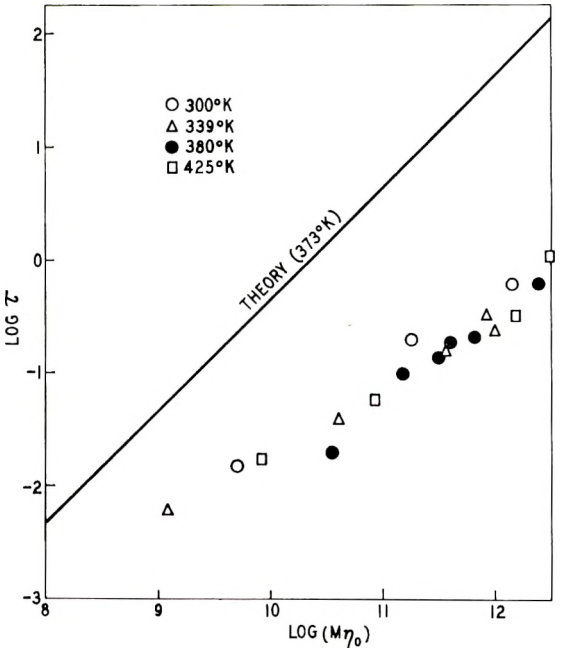

Fig. 5. Test of Bueche's theory of non-Newtonian flow.

Through suitable choice of τ, it is generally possible to obtain a reasonably close fit of the data of Table II to eq. (10) for any one polymer at a particular temperature. In Figure 5 the τ's so obtained are plotted against the product $M\eta_0$. It is apparent that the data follow the trend required by eq. (10) but differ from it quantitatively by one to two orders of magnitude. The theory calls for the ratio η/η_0 to fall much too rapidly with shear rate, unless the τ's are chosen with complete disregard of eq. (11). In other words, the polymers exhibit considerably more Newtonian character than indicated by the Bueche theory.

IV. CONCLUSIONS

Compared with polymers described in the literature, the *n*-butyllithium-initiated polybutadienes exhibit Newtonian behavior to higher molecular weights, higher shear rates and lower temperatures than any known polymer system.

The Newtonian viscosities follow the well-known 3.4 power relation with weight-average molecular weight. Departure from this relation occurs at molecular weights below 6000. The molecular weight between entanglements is estimated to be about 5600.

The temperature dependence of viscosity is substantially independent of shear stress. It follows functional relationships similar to those found applicable to other polymers.

Of the two principal current theories of non-Newtonian viscosity, the one of Eyring and Ree formally fits the experimental data best.

The authors are indebted to Dr. R. P. Zelinski for the preparation of the polymers, to Dr. C. J. Stacy for the light-scattering molecular weights, and to Mr. K. W. Rollmann for the creep determinations.

References

1. Cooper, W., Dunlop Rubber Co., private communication.
2. Rabinowitsch, B., *Z. Physik. Chem.*, **A145**, 1 (1929).
3. Philippoff, W., and F. H. Gaskins, *Trans. Soc. Rheol.*, **2**, 263 (1958).
4. Bueche, F., *J. Appl. Phys.*, **26**, 738 (1955).
5. Fox, T. G, S. Gratch, and S. Loshaek, *Rheology*, Vol. I, F. R. Eirich, Ed., Academic Press, New York, 1956, pp. 431.
6. Eyring, H., T. Ree, and N. Hirai, *Proc. Natl. Acad. Sci., U. S.*, **44**, 1213 (1958).
7. Bueche, F., *J. Polymer Sci.*, **25**, 305 (1957).
8. Bueche, F., *J. Chem. Phys.*, **25**, 599 (1956).
9. Fox, T. G, and S. Loshaek, *J. Polymer Sci.*, **15**, 371 (1955).
10. Williams, M. L., R. F. Landel, and J. D. Ferry, *J. Am. Chem. Soc.*, **77**, 3701 (1955).
11. Kraus, G., *J. Appl. Polymer Sci.*, **7**, 1257 (1963).
12. Arnett, R. L., and J. K. Hughes, Phillips Petroleum Company, unpublished work.
13. Ree, T., and H. Eyring, *J. Appl. Phys.*, **26**, 793 (1955); *ibid.*, **26**, 800 (1955).
14. Eyring, H., *J. Chem. Phys.*, **4**, 283 (1936).
15. Bueche, F., *J. Chem. Phys.*, **22**, 1570 (1954).

Résumé

On a examiné le comportement d'écoulement de polybutadiènes initiés par la *n*-butyllithium, en fonction du poids moléculaire, de la température et de la tension de cisaillement. À des vitesses basses, ces polymères montrent un écoulement Newtonien jusqu'à des poids moléculaires de plusieurs centaines de mille, et on peut donc déterminer les viscosités Newtoniennes à cisaillement nel en évitant ainsi les risques d'une extrapolation lointaine. Au-dessus du poids moléculaire 10.000 les viscosités Newtoniennes dépendent, comme connu, du poids moléculaire en poids à la puissance 3,4. Le poids moléculaire entre les pontages successifs est estimé à 6.000. La variation de la viscosité en fonction de la température est indépendante du poids moléculaire et de la tension d'écoulement, et on peut la représenter analytiquement par des fonctions proposées dans la littérature. L'énergie d'activation apparente de l'écoulement visqueux n'est pas constante, mais elle diminue avec une augmentation de la température. L'écart entre le comportement d'écoulement des polymères et le comportement Newtonien augmente avec le produit du poids moléculaire et de le viscosité Newtonienne. Cependant, la différence avec le comportement Newtonien est apparemment plus petite qu'avec n'importe quel système polymérique dont l'écoulement est décrit dans la littérature. Ceci indique qu'une étroite distribution du poids moléculaire et l'absence de ramifications en longues chaînes favorisent l'écoulement Newtonien et que les polybutadiènes initiés par le *n*-butyllithium représentent quelques-uns des polymères les plus parfaitement linéaires dans un étroit domaine de distribution.

Zusammenfassung

Das Fliessverhalten *n*-butyllithium-polymerisierter Polybutadiene wurde in Abhängigkeit von Molekulargewicht, Temperatur und Schergeschwindigkeit untersucht. Bei niedriger Schergeschwindigkeit zeigen diese Polymeren bis zu Molekulargewichten von mehreren hunderttausend Newtonsches Fliessen, so dass die Newtonsche Viskosität für den "Schub Null" ohne das Risiko einer weiten Extrapolation leicht bestimmt werden kann. Oberhalb eines Molekulargewichts von 10000 gehorcht die Newtonsche Viskosität der wohlbekannten Abhängigkeit von der Potenz 3,4 des Gewichtsmittels des Molekulargewichts. Das Molekulargewicht für Verschlingungsabstände wird zu 6000 geschätzt. Die Temperaturabhängigkeit der Viskosität ist von Molekulargewicht und Schubspannung im wesentlichen unabhängig und kann durch in der Literatur angegebene Funktionen dargestellt werden. Die scheinbare Aktivierungsenergie des viskösen Fliessens ist nicht konstant, sondern nimmt mit steigender Temperatur ab. Das Fliessverhalten der Polymeren erhält mit steigenden Werten des Produkts aus Molekulargewicht und Newtonscher Viskosität zunehmend nicht-Newtonschen Charakter. Die abweichung von Newtonschen Verhalten ist jedoch geringer als für irgend ein in der Literatur beschriebenes Polymersystem. Man kann daraus schliesson, dass enge Molekulargewichtsverteilung und Fehlen von Langkettenverzweigungen das Newtonsche Fliessben begünstigen und dass die *n*-butyllithium-gestarteten Polybutadiene zu den am vollkommensten linearen, eng verteilten bekannten Polymeren gehören.

Received December 4, 1962
Revised April 22, 1963

JOURNAL OF POLYMER SCIENCE: PART A VOL. 2, PP. 811–822 (1964)

Polymer–Solvent Interaction Parameters and Creep Behavior of Ethylene–Propylene Rubbers*

T. J. DUDEK† and F. BUECHE,‡ *Aeronautical Systems Division, Wright-Patterson AFB, Ohio, and University of Dayton, Dayton, Ohio*

Synopsis

The polymer–solvent interaction parameter for an ethylene–propylene terpolymer containing 53 mole-% ethylene was determined as a function of degree of crosslinking in *n*-heptane and benzene. A well characterized EPR gum vulcanizate was used to obtain the polymer–solvent interaction parameter in fourteen solvents, and the cohesive energy density of the terpolymer was evaluated. The composite tensile creep curves for gum and filled EPR vulcanizates were obtained and compared with SBR creep curves.

INTRODUCTION

This work was undertaken to provide data to characterize ethylene–propylene rubber (EPR) vulcanizates by equilibrium swelling methods and to investigate the dynamics of network response in EPR networks by creep experiments.

BACKGROUND THEORY

Swelling and Polymer–Solvent Interaction Parameter

The modified Flory-Rehner equation[1] relates the number of elastically effective network chains in a swollen vulcanizate to the volume fraction of rubber in the swollen sample at equilibrium, V_r.

For a network constructed from tetrafunctional crosslinks, the equation takes the form

$$\nu'_e = -\frac{1}{V_1}\left[\frac{\ln(1 - V_r) + V_r + \mu V_r^2}{g^{2/3} V_r^{1/3} - V_r/2}\right] \tag{1}$$

where ν'_e is the number of elastically effective network chains per unit volume of gel rubber, V_1 is the molar volume of the swelling solvent at the temperature of the measurement, g is the volume fraction of gel rubber in

* This paper was presented before the Division of Rubber Chemistry, American Chemical Society, Cleveland Meeting, October 17–19, 1962.

† Present address: Materials Sciences Laboratory, Aerospace Corporation, El Segundo, California.

‡ Aided by a grant from The Goodyear Tire and Rubber Company.

the sample at the time of crosslinking, and μ is the polymer–solvent interaction parameter.

One way to determine μ for use in this equation is through the use of equilibrium stress–strain data. According to the kinetic theory of rubber elasticity for a swollen vulcanizate[2] the stress is related to the strain in a simple extension experiment by the equation

$$f/A_0 = \nu'_e RTV_r^{-1/3} (\alpha - \alpha^{-2}) \quad (2)$$

where f is the tensile force, A_0 is the original unstrained cross-sectional area of the sample, R is the gas constant, T is the absolute temperature, α is the extension ratio, defined as the ratio of the extended length to the unstrained swollen length of the vulcanizate, and ν'_e and V_r have already been defined. The value of ν'_e obtained for eq. (2) can be used in eq. (1) to solve for μ.

Cohesive Energy Density

For the swelling of nonpolar polymers in nonpolar solvents the polymer–solvent interaction parameter μ depends on the difference in the square roots of the cohesive energy densities for the solvent and the polymer and is given by[3]

$$\mu = \mu_s + (V_1/RT) (\delta_1 - \delta_p)^2 \quad (3)$$

where μ_s is usually a constant with a value between 0.3 and 0.5 depending on the system, V_1 is the molar volume of the swelling liquids, R is the gas constant, T is the absolute temperature, and δ_1 and δ_p are the solubility parameters for the solvent and polymer, respectively. The solubility parameters are related to cohesive energy density, c.e.d., by the equation

$$\delta = (\text{c.e.d.})^{1/2} = (\Delta E_v/V_1)^{1/2}$$

where ΔE_v is the molar energy of vaporization at the temperature of interest and V_1 is the molar volume at the same temperature.

The solubility parameters of solvents are readily computed from thermodynamic data. For polymers, however, the solubility parameters can only be obtained from swelling measurements on well characterized networks in solvents of varying cohesive energy densities. Bristow and Watson[4] have suggested using eq. (3) in a form more suitable for obtaining δ_p. Rearrangement of eq. (3) gives

$$(\delta_1^2/RT) - (\mu/V_1) = (2\,\delta_p/RT)\,\delta_1 - (\delta_p^2/RT) - (\mu_s/V_1) \quad (4)$$

A plot of the left side of the eq. (4) against δ_1 should give a straight line. From both the slope and the intercept of this line δ_p can be computed.

EXPERIMENTAL

Materials

Ethylene–Propylene Terpolymer (EPR). Du Pont's ECD-330 (now called Nordel) was used in this investigation. ECD-330 is an amorphous

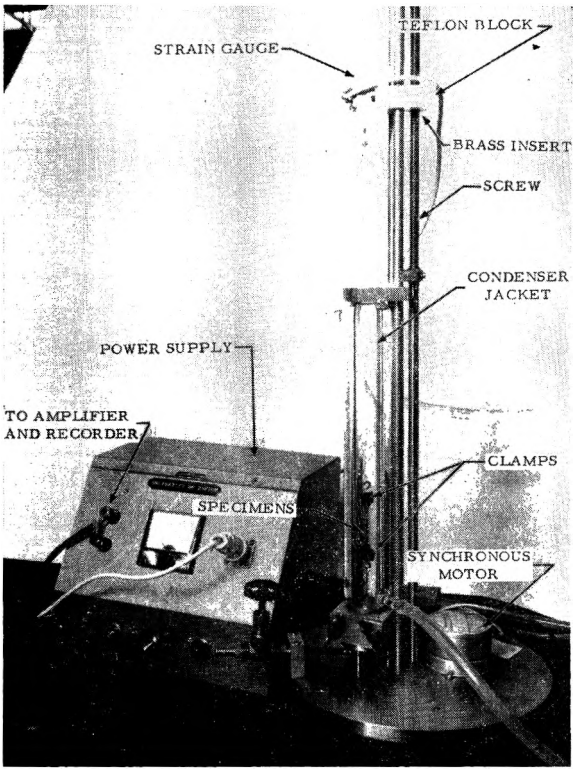

Fig. 1. Apparatus for tension measurements.

terpolymer of ethylene, propylene, and a nonconjugated diene. The unsaturation present in the polymer allows the elastomer to be vulcanized by conventional curing systems.[5]

The ECD-330 contained about 19% gel, and 5.8% of the rubber was extractable by acetone. The polymer unsaturation could not be determined by infrared analysis. Analysis of solutions of an acetone-extracted ECD-330 sample (soluble portion) in CCl_4 with the use of a Varian Associates Model A60 high resolution NMR spectrometer gave a copolymer composition of 53 ± 1 mole-% ethylene. The proton resonances occurred in their normal positions relative to tetramethylsilane.[6] It was not possible to completely resolve the methine protons from the methylene protons. Hence, the ratio of the area under the absorption curve of the methyl protons to the area under the absorption curve of the methylene plus methine protons was determined. Mole per cent ethylene in the copolymer was obtained by comparing this result to a theoretical curve obtained by assuming the material to contain only ethylene and propylene.

Solvents used were reagent grade with the exception of *n*-hexadecane which was technical grade.

Stress-Strain Apparatus. The apparatus shown in Figure 1, which was patterned after a similar device described by Oth and Flory,[7] was used for

equilibrium tension measurements. The apparatus consisted of a strain gauge (Model G-1, Statham Instruments, Inc.) mounted on a Teflon block which slid easily over the steel rods shown. The strain gauge was driven up or down at constant speed by a reversible Hurst synchronous motor. The gears used to drive the threaded rod are located under the bottom plate of the instrument. By changing gear ratios and using two interchangeable motors (1 and 6 rpm) the strain gauge could be moved at rates between 0.03 and 1.5 in./min. Water or silicone oil from a thermostat was circulated through the condenser jacket to control the temperature of the test specimen. The specimen and clamps are shown in the figure. Bench marks on the sample were monitored with a cathetometer. Measurements on swollen samples were easily made, since solvent could be poured into the condenser into intimate contact with the sample.

A Zener diode was used in the power supply to stabilize the voltage delivered to the transducer. The output from the transducer was delivered through a DC amplifier to a recorder. The amplifier was used to provide adequate sensitivity to the system for low force measurements. The voltage to the strain gauge and the amplification factor were chosen to give full scale recorder deflection for a force close to the maximum force expected in an experiment. The strain gauge was calibrated before and after each experiment with standard weights. The transducer response was linear and a precision of 1 to 2 per cent was obtained in the force measurements. The zero point and the calibration remained constant during the time taken for an experiment.

Procedures

Compounding. The EPR stocks were compounded on a rubber mill according to the formula given in Table I.

TABLE I

Component	Parts by weight
ECD-330	100
Philblack O	0 or 30
Zinc Oxide	5
Methyl Tuads	4
Altax	1

Vulcanization. Vulcanization was carried out in a mold under 1500 psi pressure for the times and temperatures specified in the report. Sheets 3 × 6 in. were obtained of thickness 0.010 or 0.020 in. Vulcanizates were stored in a refrigerator to preclude further curing.

Stress–Strain Measurements. Dumbbell specimens of gauge length 1.59 cm. and width 0.320 cm. were cut from vulcanized sheets with a die and the average thickness determined. For swollen measurements the specimen was allowed to swell for about 36 hr. with three solvent changes

in the solvent of interest. It was placed in a set of small clamps and into the tension apparatus shown in Figure 1. Solvent was poured into the condenser as soon as possible after the sample was positioned. Increments of elongation chosen to give an accurate stress-strain plot were added to the sample. After each elongation increment a wait of 5 min. was standard procedure before the force was recorded. During this waiting time the distance between bench marks on the sample was measured with a cathetometer. For swollen specimens, stress relaxation during this period was negligible. The unstrained length of the sample was obtained by extrapolation of a force versus length plot to zero force.

Swelling Measurements. The following technique was used for all equilibrium swelling measurements. Samples (3 × 0.5 cm.) were cut from vulcanized sheets and weighed on an analytical balance. They were placed in about 75 ml. of solvent and allowed to swell for about 24 hr. at 50°C. The solvent was changed once during this interval. After 24 hr. the solvent was changed a second time and the samples allowed to remain for 24 hr. at 25°C. The swollen samples were blotted quickly with a hard filter paper and weighed in tared, stoppered bottles. The samples were dried in a vacuum oven to constant weight. The volume of solvent present at equilibrium was obtained by dividing the difference between the weight of the swollen sample and the dry, extracted sample by the density of the solvent. The density of extracted samples was determined by the hydrostatic weighing technique in methanol. The volume of the extracted rubber was corrected for the volume of insoluble compounding material present prior to computing the volume fraction of rubber in the swollen sample.

Creep Experiments. The techniques used in the creep experiments have been described in detail elsewhere.[8] A fixed load was applied to the end of the sample and the elongation was observed as a function of time with a cathetometer. Elongations were always kept below about 5%. The sample temperature was maintained constant to within ±0.2°C.

By making use of the equivalence of temperature and time it was possible to obtain a composite curve showing the tensile creep behavior of the sample over many decades of time.

RESULTS AND DISCUSSION

Equilibrium Stress–Strain Measurements and Determination of μ

Equilibrium stress–strain curves were determined at 25°C. on EPR gum vulcanizates of different crosslink densities, prepared by varying the temperature and time of cure, swollen to their equilibrium volume in *n*-heptane and benzene. Figures 2 and 3 give typical plots obtained when the data are plotted according to the kinetic theory of rubber elasticity [eq. (2)]. Good straight lines which pass through the origin are obtained indicating that the theory is obeyed in the region of low elongations. The values of

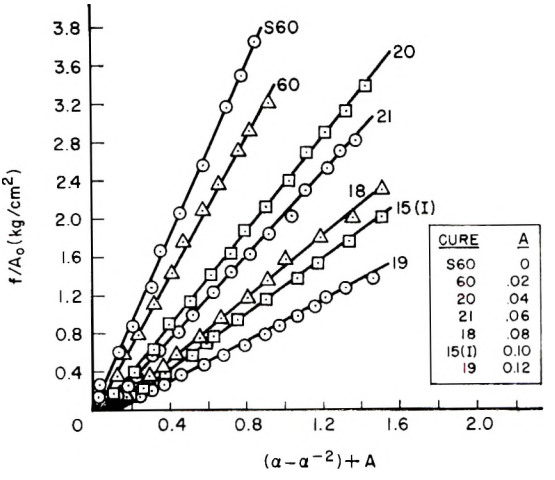

Fig. 2. Kinetic theory plots at 25°C. for ethylene–propylene vulcanizates swollen in *n*-heptane.

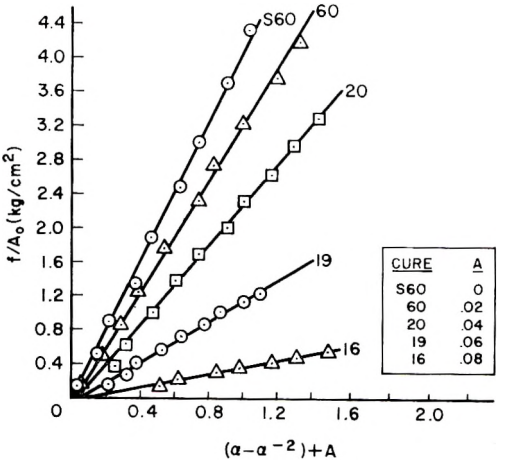

Fig. 3. Kinetic theory plots at 25°C. for ethylene–propylene vulcanizates swollen in benzene

ν'_e obtained from the slopes of the lines and of μ computed from the Flory-Rehner equation are given in Table II. Chain densities obtained for samples of the same cure swollen in heptane or benzene are in agreement within experimental error.

A plot of μ as a function V_r is given in Figure 4 for the two solvents. For *n*-heptane, μ was constant within experimental error with the value 0.44. For benzene, the parameter μ was found to be a linear function of V_r, $\mu = 0.49 + 0.33\ V_r$.

This linear dependence has been observed for many other elastomer–solvent systems,[9] particularly with poor solvents.

TABLE II
Chain Densities of ECD-330 Gum Vulcanizates and Polymer–Solvent Interaction Parameters in *n*-Heptane and Benzene at 25°C.

Solvent	Cure[a]	V_r	g	$\nu'_e \times 10^5$, mole/cm.^{3}	$\nu_e \times 10^5$, mole/cm.^{3}	μ
n-Heptane	S60[b]	0.217	0.875	10.8	9.45	0.44
	60*	0.193	0.850	8.31	7.06	0.44
	20*	0.165	0.821	5.30	4.35	0.45
	21	0.153	0.810	4.63	3.75	0.45
	18	0.132	0.784	3.30	2.59	0.45
	15II	0.127	0.778	3.02	2.35	0.45
	15I	0.116	0.765	2.78	2.13	0.44
	19	0.110	0.765	1.97	1.51	0.46
Benzene	S60[b]	0.290	0.847	10.8	9.15	0.57
	60*	0.271	0.830	8.39	6.96	0.57
	20*	0.240	0.799	5.74	4.59	0.56
	19	0.173	0.745	2.69	2.00	0.54
	16	0.108	0.636	0.74	0.47	0.52

[a] Unstarred samples cured at 305°F. for the indicated number of minutes; starred samples cured at 320°F.

[b] Compound S60 had 0.5 parts of sulfur added to the recipe.

Table II also gives the number of effective network chains based on the total unextracted volume of the rubber, ν_e.

$$\nu_e = g\nu'_e$$

Values of ν_e obtained from a Mooney-Rivlin treatment[10] of unswollen stress–strain data did not agree with values obtained from swollen measurements especially at low crosslink densities. The constant C_2 obtained for the EPR system was found to be abnormally high. This result might be

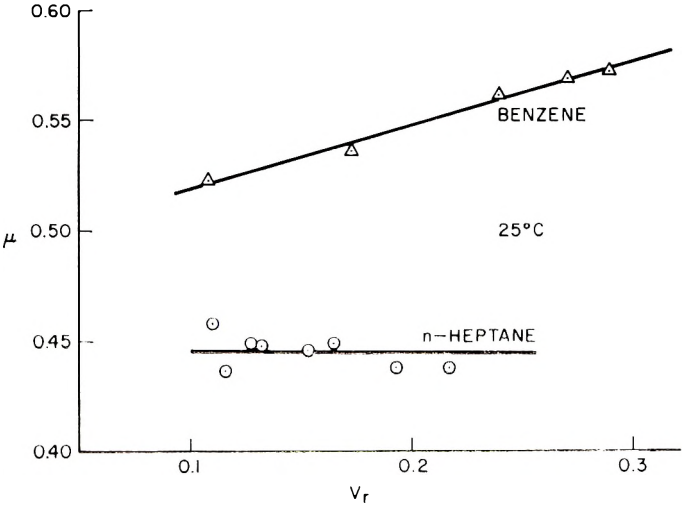

Fig. 4. Polymer-solvent interaction parameter as a function of V_r.

due to the greater number of chain entanglements which are found in EPR elastomer.

Cohesive Energy Density of Ethylene–Propylene Elastomer and μ for Various Solvents

The equilibrium swelling volume of samples of the 60 min. EPR gum cure was determined in fourteen different solvents at 25°C. Since the effective number of network chains was known for this vulcanizate, μ for

TABLE III
Polymer–Solvent Interaction Parameter for an Ethylene–Propylene Vulcanizate in Various Solvents at 25°C.

Solvent	δ_1, (cal./cm.^{3})$^{1/2}$ [a]	V_1, cm.^{3}/mole	V_r	μ
Pentane	7.01	114.2	0.226	0.53
n-Heptane	7.42	147.5	0.193	0.44
Methyl cyclohexane	7.82	128.4	0.145	0.35
n-Hexadecane	7.93	294.2	0.205	0.33$_5$
Cyclopentane	8.10	94.9	0.138	0.39
Cyclohexane	8.18	108.7	0.145	0.35
Decalin	8.30	157.0	0.134	0.27
Tetralin	8.40	136.8	0.191	0.44$_6$
Dipentene	8.50	161.0	0.168	0.37
n-Propylbenzene	8.65	140.1	0.192	0.44
Carbon tetrachloride	8.58	97.1	0.156	0.43
Ethylbenzene	8.80	123.1	0.202	0.49
Toluene	8.91	106.9	0.205	0.49
Benzene	8.15	89.4	0.271	0.58

[a] Data of Hildebrand and Scott[3] and Bristow and Watson.[4]

these solvent–polymer systems could be computed from the Flory-Rehner equation. The results are given in Table III, together with data needed to construct the Bristow and Watson plot shown in Figure 5.

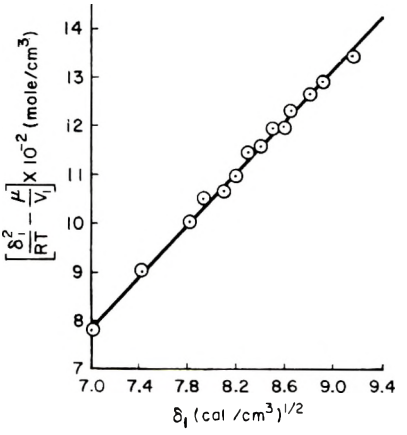

Fig. 5. Plot to determine the solubility parameter of ethylene–propylene elastomer.

A good straight line was obtained when the data were plotted as suggested by eq. (4). From the slope of the line the solubility parameter of ethylene–propylene elastomer was found to be 7.85 $(cal./cm.^3)^{1/2}$. From the y-intercept, δ_p was found to be between 7.89 and 7.92 $(cal./cm.^3)^{1/2}$. This compares well with the value of 7.9 reported for the solubility parameter of polyethylene[11] and 7.8 for polyisobutylene.[4]

Composite Tensile Creep Curve for EPR Gum and Black-Filled Vulcanizates

The composite tensile creep curves reduced to 0°C. for two gum vulcanizates of EPR elastomer and a vulcanizate containing 30 parts of HAF black are given in Figure 6. The creep compliance, $D(t)$, which is defined as $(\Delta L/L)(F/A)$ is plotted against log time in minutes. Also plotted in Figure 6 for comparison are curves reported earlier[12] for a gum and a filled styrene–butadiene vulcanizate. Each composite curve represents data taken at nine temperatures. Since the curves have about one hundred experimental points, the actual points have not been included.

The creep curves for the gum vulcanizates indicate that both SBR and EPR have about the same glass transition temperature. The plateau in the curves due to the entanglement network occurs at a lower compliance for the EPR gum vulcanizate. This means that the entanglement network is tighter for EPR than for SBR. From the compliance in the plateau region[12] the average molecular weight between entanglement points, M_e, in ethylene–propylene elastomer was found to be about 1200 g./mole. This corresponds to about 70 chain backbone atoms between entanglement points and is in good agreement with the value of $M_e = M_b/2 \cong 1150$ g./mole determined for polyethylene from viscosity data.[13] For SBR the value of M_e was found to be about 3000 g./mole which corresponds to about 170 chain backbone atoms between entanglement points. Since the

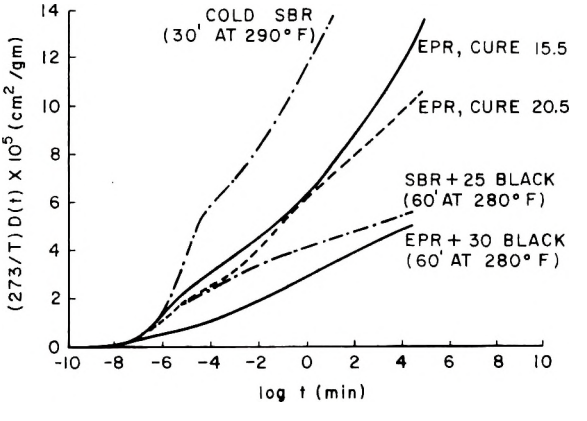

Fig. 6. Tensile creep compliance curves for ethylene–propylene and styrene–butadiene vulcanizates reduced to 0°C. Cure times and black loadings are indicated on the curves. SBR data taken from Bueche.[12]

average molecular weight per chain backbone atom is essentially the same for both EPR and SBR and the densities of the polymers are very close, it would be expected that both polymers would have nearly the same M_e. However, these results show that EPR elastomer has more than twice as many entanglements as SBR elastomer.

Only a fraction of a second is required for chain uncoiling to occur in EPR at 0°C. This is determined from the time required to reach the plateau region of the creep curve. The difference in the entanglement networks between EPR and SBR will lead to a higher nonequilibrium modulus for EPR vulcanizates at low degrees of crosslinking.

It has been pointed out[12] that the shape of the creep curve for SBR shows that the molecules have not been tied into a stable network, because the rubber never reaches an equilibrium extension under an applied load but

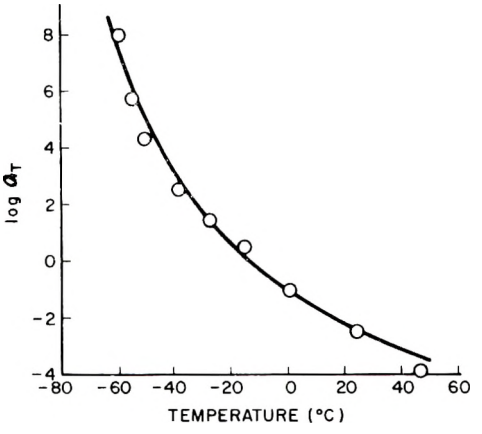

Fig. 7. Temperature dependence of the rate constant (shift factor) for the creep process. Experimental data are for EPR gum vulcanizate 20.5; the curve was computed from the WLF equation using $T_s = 260$°K.

continues to elongate indefinitely. This same behavior is evident for the EPR vulcanizates and could be attributed to a relatively low value of $\bar{M}_n$ for the polymer as in the case of SBR. Also, a low number of unsaturated curing sites in the terpolymer molecules could make it impossible to form a satisfactory network with this polymer.

The chain density of the 15.5-min. EPR cure was found from swelling measurements to be 0.5×10^{-5} mole/cm.^{3} and the chain density of the 20.5-min. cure was 3.12×10^{-5} mole/cm.^{3}. It is evident from the creep curves in Figure 6 that a more stable network has been attained in the more highly crosslinked sample. It is interesting to note that a ν_e of about 12.5×10^{-5} mole/cm.^{3} is computed for the 20.5-min. EPR cure from the compliance at long time. This is four times the equilibrium value obtained by swelling. Hence, EPR requires an extremely long time to reach equilibrium at 0°C. because of the long times required for the greater number of

chain entanglement points and network junction points to move to equilibrium positions.

The vulcanizates containing carbon black show a more satisfactory network response compared to the unfilled samples. This is readily seen by comparing the slopes of the creep curves at long times. The heat build-up to be expected in a rubber subjected to a periodic force has been shown to be directly proportional to the slope of the long time portion of the creep curve.[12] Comparison of the slope of the filled EPR with the slope of the filled SBR curve shows that for these particular compounds SBR would be expected to have better heat build-up properties.

The shift factors, a_T, have been obtained as a result of using the time–temperature superposition procedure to reduce the data for the EPR vulcanizates. The plot of log α_T versus T is given in Figure 7 for EPR cure 20.5. The curve in Figure 7 was obtained from the WLF equation[14] using $T_s = 260°K.$ and the standard constants. The shift factors for cure 15.5 and the black-filled vulcanizate also fit this equation within experimental error. Since, $T_s = T_g + 50$, the glass temperature, T_g, for this EPR rubber is about $-63°C.$ This checks well with the value of $-60°C.$ reported[15] for a terpolymer of the same ethylene content.

CONCLUSION

The polymer–solvent interaction parameters for ethylene–propylene terpolymer and *n*-heptane and benzene have been determined as a function of crosslink density at 25°C. With *n*-heptane as solvent, μ was independent of crosslink density. With benzene μ was found to be a linear function of V_r.

The solubility parameter of the ethylene–propylene terpolymer studied was determined to be 7.9 $(cal./cm.^3)^{1/2}$.

The composite tensile creep curves for EPR gum vulcanizates revealed the presence of a tight entanglement network. The molecular weight between entanglement points in EPR was close to that observed for polyethylene. The low M_e in EPR leads to a higher modulus at low degrees of crosslinking than would be observed for SBR and is probably responsible for higher hysteresis in EPR gum vulcanizates. The rate constants for the creep process for the gum and black filled vulcanizates followed the WLF equation. The glass temperature estimated from T_s in the WLF equation was $-63°C.$

The authors gratefully acknowledge the assistance of Mr. William Powers of the University of Dayton Research Institute who helped with design and construction of the stress–strain instrument and of Miss Mary Ryan of the Physics Laboratory, Aeronautical Systems Division, Wright-Patterson AFB, Ohio, who ran the NMR spectrum of EPR and helped in the interpretation.

References

1. Flory, P. J., *J. Chem. Phys.*, **18**, 108 (1950).
2. Flory, P. J., *Principles of Polymer Chemistry*, Cornell Univ. Press, Ithaca, N. Y., 1953, p. 492.
3. Hildebrand, J. H., and R. L. Scott, *The Solubility of Nonelectrolytes*, Reinhold Publishing Corp., New York, 1950, p. 366.
4. Bristow, G. M., and W. F. Watson, *Trans. Faraday Soc.*, **54**, 1731 (1954).
5. Gladding, E. K., B. S. Fisher, and J. W. Collette, *Ind. Eng. Chem. Prod. Res. Develop.*, **1**, 65 (1962).
6. Jackman, L. M., *Applications of Nuclear Magnetic Resonance Spectroscopy in Organic Chemistry*, Pergamon Press, New York, 1959, p. 52.
7. Oth, J. F. M., and P. J. Flory, *J. Am. Chem. Soc.*, **80**, 1297 (1958).
8. Bueche, F., *J. Appl. Phys.*, **26**, 738 (1955).
9. Kraus, G., *Rubber World*, **135**, 67 (1956).
10. Bueche, F., *Physical Properties of Polymers*, Interscience, New York, 1962, p. 54.
11. Tobolsky, A. V., *Properties and Structure of Polymers*, Wiley, New York, 1960, p. 66.
12. Bueche, F., *J. Polymer Sci.*, **25**, 305 (1957).
13. Porter, R. S., and J. F. Johnson, *J. Appl. Phys.*, **32**, 2326 (1961).
14. Ferry, J. D., *Viscoelastic Properties of Polymers*, Wiley, New York, 1961, p. 228.
15. Verbanc, J. J., M. S. Fawcett, and E. J. Goldberg, *Ind. Eng. Chem. Prod. Res. Develop.*, **1**, 70 (1962).

Résumé

On a déterminé paramètre d'interaction polymère-solvant pour un terpolymère éthylène-propylène, contenant 53 moles pourcent d'éthylène, en fonction du degré de pontage dans le *n*-heptane et le benzène. On a utilisé une gomme EPR vulcanisée bien caractérisée pour obtenir le paramètre d'interaction polymère-solvant dans quatorze solvants et la densité d'énergie cohésive du terpolymère a été évaluée. Les courbes composées du fluage sous traction pour la gomme et les EPR vulcanisés contenant des charges ont été obtenues et comparées avec les courbes de fluage de l'SBR.

Zusammenfassung

Der Polymer-Lösungsmittel-Wechselwirkungsparameter wurde für ein Äthylen-Propylenterpolymeres mit 53 Mol% Äthylen in Abhängigkeit vom Vernetzungsgrad in *n*-Heptan und Benzol bestimmt. Ein gut charakterisiertes ungefülltes EPR-Vulkanisat wurde zur Ermittlung der Polymer-Lösungsmittel-Wechselwirkungsparameter in vierzehn Lösungsmitteln verwendet und die Kohäsionsenergiedichte für das Terpolymere bestimmt. Zusammengesetzte Kriechkurven bei Zugbeanspruchung wurden für ungefüllte und gefüllte EPR-Vulkanisate erhalten und mit SBR-Kriechkurven verglichen.

Received December 4, 1962

JOURNAL OF POLYMER SCIENCE: PART A VOL. 2, PP. 823–834 (1964)

Some Reactions of *p*-Vinylacetophenone–Styrene Copolymers*

RICHARD BECKERBAUER and HENRY E. BAUMGARTEN, *Avery Laboratory, University of Nebraska, Lincoln, Nebraska*

Synopsis

A new synthesis of *p*-vinylacetophenone was developed. Copolymers of *p*-vinylacetophenone and styrene were prepared by copolymerization and by partial Friedel-Crafts acetylation of polystyrene. The copolymers were converted into the oximes, but subsequent reduction was unsuccessful. Beckman rearrangement of the oximes led to insoluble resins. The acetyl copolymers were partially brominated to give an α-bromo-*p*-vinylacetophenone/*p*-vinylacetophenone/styrene terpolymers. Nucleophilic displacement of the bromine of these terpolymers with secondary amines yielded α-piperidino- and α-morpholino-*p*-vinylacetophenone terpolymers. The Delepine reaction of the brominated copolymer produced an α-amino-*p*-vinylacetophenone terpolymer. The piperidino and amino ketone terpolymers were reduced to the corresponding alcohol derivatives with lithium-aluminum hydride. The amino ketone and amino alcohol terpolymers had moderate solubility characteristics in acidic alcohols and water. The α-amino ketone terpolymer was very sensitive to base and afforded a facile crosslinking of the acetyl copolymer.

INTRODUCTION

Poly(*p*-vinylacetophenone) has been prepared by Friedel-Crafts acetylation of polystyrene.[1–3] The oxime of the polymer has been prepared and in one case, with polymers of 5,000–10,000 molecular weight, the oxime has been reduced to the amine polymer.[2] The hypohalite oxidation of the acetyl group has also been described.[3] As part of a study of the limitations placed upon some characteristic reactions of functional groups when these groups are part of a polymer, we have investigated several reactions of the acetyl group of poly-*p*-vinylacetophenone and of copolymers of *p*-vinylacetophenone and styrene prepared by copolymerization of the appropriate monomers and by partial acetylation of polystyrene. A second objective was the preparation of water- or acid-soluble polymers derived from the above polymer species. To this end the synthesis of α-amino ketone and α-amino alcohol polymers was investigated.

* This work was supported in part by grants G-11339 and G-21405 of the National Science Foundation.

EXPERIMENTAL RESULTS

Preparation of Polystyrene

Freshly distilled styrene monomer was polymerized at 50°C. for 3 hr. with 1% potassium persulfate initiator in an emulsion system.[4] Dodecyl mercaptan (0.75%) was added to control the molecular weight. The emulsion was broken with a dilute sulfuric acid and sodium chloride solution, and the crude polymer was collected by filtration. Two precipitations from 2-butanone into methanol yielded polystyrene (I) in 76% yield.

ANAL. Calcd. for $(C_8H_8)_n$: C, 92.26%; H, 7.74%. Found: C, 92.00%; H, 7.95%.

Preparation of Poly-*p*-vinylacetophenone

The above polystyrene (I) was acetylated in carbon disulfide solution with acetyl chloride and aluminum chloride according to the procedure of Kenyon and Waugh.[1] The yield of dry polymer (II) was 89.5%.

ANAL. Calcd. for $(C_{10}H_{10}O)_n$: C, 82.20%; H, 6.90%. Found: C, 82.06%; H, 7.05%.

Preparation of *p*-Vinylacetophenone

To 39.25 g. (0.50 mole) of freshly distilled acetyl chloride and 106.75 g. (0.80 mole) of anhydrous, sublimed aluminum chloride in 100 ml. of methylene chloride was added a solution of 50 g. (0.30 mole) of 2-phenylethyl acetate (III) in 125 ml. of methylene chloride. The solution was refluxed for 1 hr., cooled, and poured into 100 ml. of hydrochloric acid in 800 ml. of ice water. The resulting mixture was heated on the steam bath to remove the organic solvent, and the resulting mixture was extracted three times with 100-ml. portions of ether. The ether extracts were dried over calcium sulfate for 24 hr., filtered, and concentrated in a rotating evaporator to a dark yellow oil. Distillation of the oil yielded 24.3 g. (49%) of 2-phenylethyl acetate (III) (b.p. 90–110°C./1.2 mm.) and 28 g. of a light yellow oil (b.p. 146–148°C./0.75 mm.). Redistillation of this oil yielded 26.7 g. (45%) of 2-(*p*-acetylphenyl)ethyl acetate (IV) as a colorless oil (b.p. 147–147.5°C./0.8 mm.).

ANAL. Calcd. for $C_{12}H_{14}O_3$: C, 69.88%; H, 6.84%. Found: C, 69.17%; H, 6.81%.

A solution of 15 g. (0.073 mole) of the keto ester (IV) in 20 ml. of benzene was dropped (1 drop/sec.) in a nitrogen stream through a 1-in. Pyrex tube packed with $^1/_{16}$-in. Pyrex helices and heated to 555°C. The pyrolyzate was washed with water and the organic layer was separated and dried over calcium sulfate. The oil was stabilized with 1% to *t*-butylcatechol and distilled at 104–106°C./1.5 mm. (lit.[4] 75–80°C./0.3 mm.). The product was solid at room temperature and was recrystallized from 6 ml. of *n*-heptane to yield 8.4 g. (79%) of *p*-vinylacetophenone (V). The overall yield was 36% (67% based on recovered III).

Preparation of *p*-Vinylacetophenone–Styrene Copolymers

By Suspension Copolymerization. A mixture of 10.8 g. of *p*-vinylacetophenone (V), 30 g. of styrene, 210 ml. of water, 1.5 g. of starch, and 0.3 g. (0.75%) of benzoyl peroxide was stirred for 30 min. while nitrogen was bubbled into the mixture. The mixture was heated on a steam bath and stirred with a high speed stirrer for 6 hr. The resulting suspension was cooled and broken with, first, dilute hydrochloric acid solution and then methanol. The crude product was collected by filtration and reprecipitated from chloroform into methanol. This treatment yielded 23.1 g. (55%) of a white copolymer (VI).

ANAL. Calcd. for $C_{10}H_{10}O(30\%)$–$C_8H_8(70\%)$: C, 88.42%; H, 7.41%. Found: C, 88.47%; H, 7.37%.

By Bulk Copolymerization. Five grams (0.04 mole) of styrene 1 g. (0.0068 mole) of *p*-vinylacetophenone (V), 0.12 g. (2%) of bromotrichloromethane, and 0.0012 g. (0.02%) of benzoyl peroxide were combined in a Pyrex test tube which was chilled to −70°C. and sealed. The tube was heated at 90°C. for 24 hr. and then at 190°C. for 4 hr. The tube was chilled and opened, and the polymer plug was dissolved in 2-butanone and precipitated into methanol. From five such runs 14 g. of a white copolymer (VII) was obtained.

ANAL. Calcd. for $C_{10}H_{10}O(32\%)$–$C_8H_8(68\%)$: C, 88.22%; H, 7.40%. Found: C, 88.22%; H, 7.39%.

By Partial Friedel-Crafts Acetylation. To a flask flamed under dry nitrogen were added, in order, 10.4 g. (0.1 mole) of polystyrene (I), 100 ml. of carbon disulfide, and a solution of 2.7 g. (0.021 mole) of aluminum chloride and 1.57 g. (0.02 mole) of acetyl chloride in 60 ml. of carbon disulfide. The solution was refluxed for 1 hr., cooled, and poured into a solution of 100 ml. of hydrochloric acid in 400 ml. of ice and water. The resulting mixture was heated on the steam bath to remove the organic solvent. The liquid was decanted from the solid polymer and the crude polymer was precipitated from tetrahydrofuran into methanol. The solid product was collected by filtration, washed with methanol in a home blender, filtered, and dried under vacuum at 50°. The yield of white copolymer (VIII) was 9.25 g.

ANAL. Calcd. for $C_{10}H_{10}O(40\%)$–$C_8H_8(60\%)$: C, 87.41%; H, 7.35%. Found: C, 87.60%; H, 7.36%.

Preparation of a *p*-Vinylacetophenone Oxime–Styrene Copolymer

To 5 g. (0.02 mole) of the ketone polymer VIII in 50 ml. of pyridine was added 1.2 g. (0.017 mole) of hydroxylamine hydrochloride and 15 ml. of ethanol. This solution was refluxed for 3 hr., cooled, and added to 400 ml. of methanol. The polymer was collected and reprecipitated from tetrahydrofuran into methanol to yield 4.6 g. of white copolymer (IX). The

infrared spectrum had no detectable band at 1675 cm.$^{-1}$ corresponding to unaltered ketone.

ANAL. Calcd. for $C_{10}H_{11}NO(35\%)$-$C_{10}H_{10}O(5\%)$-$C_8H_8(60\%)$: C, 84.62%; H, 7.30%; N, 3.81%. Found: C, 84.69%; H, 7.33%; N, 3.96%.

Attempted Reduction of the Oxime

The oxime copolymer IX was subjected to reduction with W-2 Raney nickel in tetrahydrofuran under 45 psig of hydrogen but was recovered unchanged. Attempted reduction with lithium aluminum hydride in tetrahydrofuran resulted in the formation of an insoluble white solid that appeared to contain a large amount of inorganic material, presumably aluminum salts. The weight of this solid was about four times that of the starting weight of the polymer. When refluxed with concentrated hydrochloric acid, this solid was converted into a yellow, insoluble polymer which gave only a trace of ash on burning. This process was accompanied by a weight loss of about 75%. The infrared spectrum of the product was similar to that of products from attempted Beckman rearrangements of the oxime. The use of tartrate solutions in the isolation of the polymer gave the same results. When 8-hydroxyquinoline was used to complex with the aluminum in the isolation procedure, the inorganic complex was decomposed; but the isolated product proved to be unaltered oxime polymer (82%).

Attempted Beckman Rearrangement of the Oxime Copolymer

The oxime copolymer IX was treated with *p*-toluenesulfonyl chloride in pyridine at 25° and with phosphorus pentachloride in chloroform–pyridine at 0–5°C. Both reactions yielded an insoluble resin which showed no softening up to 270°C., but became rubbery at 200°C. The infrared spectra of these polymers were poorly resolved, but showed a strong band at 1672 cm.$^{-1}$. The solid obtained from the *p*-toluenesulfonyl chloride gave a positive qualitative test for sulfur.

Attempted Leuckart Reaction of the Acetyl Polymer

Poly-*p*-vinyl-acetophenone (II) was dissolved in hot 90% formic acid. Upon the addition of ammonium formate to this solution, a light yellow, insoluble resin formed. The solution was refluxed for 20 hr. with no visible effect on the solid. A similar product formed on the addition of solid acetyl polymer to a hot solution of ammonium formate in formic acid or dimethylacetamide. The solid product did not soften up to 280°C. and was not affected by refluxing with concentrated hydrochloric acid.

Bromination of the Acetyl Copolymer

To 1 g. (0.0028 mole) of the 32% ketone copolymer VII in 20 ml. of chloroform in a 100-ml. flask was added a solution of 0.24 g. (0.0014 mole) of bromine in 10 ml. of chloroform. This addition was carried out only as fast as the bromine color faded from the solution. The solution was stirred

for 30 min. and poured into methanol. The white polymer (X) was filtered from the solution.

ANAL. Calcd. for $C_{16}H_9Br$(16%) $C_{10}H_{10}O$(16%) C_8H_8(68%): C, 79.78%; H, 6.56%; Br, 8.81%. Found: C, 79.54%; H, 6.44%; Br, 9.81%.

When more than this amount of bromine was added, the color no longer faded rapidly and remained even after two days' stirring. The products isolated when equimolar amount of bromine was used were light yellow in color and had reduced solubility properties. The other copolymers gave 50% or more gel formation in this reaction.

Reactions of the α-Bromo Terpolymer

With Piperidine. One gram of the 32% ketone copolymer VII was brominated as above in chloroform solution and the solution treated with a solution of 0.34 g. (0.004 mole) of piperidine in 15 ml. of chloroform and stirred for 1 hr. The solution was poured into 250 ml. of methanol. After 2 hrs. the liquid was decanted. Reprecipitation of the solid from chloroform into methanol yielded 1.1 g. of white polymer (XI). The polymer was soluble in neutral or slightly acidic methanol–chloroform solutions and the addition of a few drops of dilute potassium hydroxide solution was necessary to effect precipitation.

ANAL. Calcd. for $C_{15}H_{19}NO$(16%)–$C_{10}H_{10}O$(16%)–C_8H_8(68%): C, 86.60%; H, 7.76%; N, 1.69%. Found: C, 86.56%; H, 7.55%; N, 1.44%. (Results adjusted for 0.62% ash.)

With Morpholine. The reaction was carried out as above with the substitution of 0.35 g. (0.004 mole) of morpholine for the piperidine. The product (XII) showed the same solubility properties and infrared spectrum (with the exception of a band at 1100 cm.$^{-1}$) as that of the α-piperidino polymer (XI).

With Aniline. The reaction was carried out with aniline but no substitution occurred, and only the α-bromo polymer could be isolated.

With Hexamethylenetetramine (Delepine Reaction). To a solution of 1 g. of the brominated 32% copolymer (VII) in chloroform was added a solution of 0.6 g. (0.004 mole) of hexamethylenetetramine in 10 ml. of chloroform. A white solid formed during the addition. After the mixture was stirred for 6 hr., the white solid (0.27 g.) was filtered off and the filtrate was concentrated in a rotating evaporator to a light pink solid. This product was dissolved in a solution of 100 ml. of tetrahydrofuran and 10 ml. of conc. hydrochloric acid, and the solution was refluxed for 1 hr. An unidentified white solid (0.21 g.) was removed by filtration and the filtrate was poured into 200 ml. of methanol. This solution was concentrated in the evaporator to 0.78 g. of a light yellow polymer. A tetrahydrofuran–water solution of this product was dialyzed against distilled water for 18 hr. The solution was evaporated and the solid remaining was washed with methanol. This mixture was evaporated and the solid product was washed with ether. The solid was dissolved in chloroform and the solution was

saturated with dry hydrogen chloride and then poured into ether. The precipitate (XIII) was collected and dried.

Solutions of XIII, when treated with base, yielded an insoluble orange resin which became tan in the presence of atmospheric oxygen. Treatment with base and hydrogen peroxide gave a tan, insoluble resin directly.

ANAL. Calcd. for $C_{10}H_{12}ClNO(16\%)$–$C_{10}H_{10}O(16\%)$–$C_8H_8(68\%)$: C, 82.15%; H, 7.15%. Found: C, 81.58%; H, 7.12%.

Reduction of the α-Piperidino Terpolymer

A solution of 0.2 g. of the α-piperidino terpolymer (XI) in 15 ml. of tetrahydrofuran was treated with 0.05 g. of lithium aluminum hydride. The reaction mixture was stirred for 2 hr. and then a few drops of ethanol and wet tetrahydrofuran were added to decompose the excess hydride. The mixture was poured into water and the product was collected by filtration and washed well with methanol. The solid product was added to 50 ml. of tetrahydrofuran and the solution was stirred for 30 min. and filtered. The filtrate was concentrated to 10 ml. and poured into methanol. This clear solution was made basic with a drop of dilute potassium hydroxide solution and the white solid (XIV) (0.07 g.) was collected. This product was also soluble in acidic aqueous tetrahydrofuran solutions.

ANAL. Calcd. for $C_{15}H_{21}NO(16\%)$–$C_{10}H_{12}O(16\%)$–$C_8H_8(68\%)$: C, 86.22%; H, 8.21%; N, 1.69%. Found: C, 86.90%; 87.93%; H, 8.11, 8.18%; N, 1.30%; ash, 1.0, 1.22%.

Reduction of the α-Aminohydrochloride Terpolymer

A 0.75-g. sample of the polymer XIII from the Delepine reaction was dissolved in 20 ml. of tetrahydrofuran and reduced with 0.5 g. of lithium aluminum hydride. The solution was stirred for 6 hr. and then treated with ethyl acetate and a few drops of water. The mixture was poured into 200 ml. of a 4% tartrate solution and the solid was filtered off. The product was extracted with hot tetrahydrofuran and this solution was poured into methanol. The resulting clear solution was made basic with one drop of dilute potassium hydroxide solution and 0.5 g. of white polymer (XV) was removed by filtration and dried.

ANAL. Calcd. for $C_{10}H_{13}NO(16\%)$–$C_{10}H_{12}O(16\%)$–$C_8H_8(68\%)$: C, 86.05%; H, 7.89%. Found: C, 86.95%; H, 9.41%.

Analyses were performed by Micro-Tech Laboratories, Skokie, Illinois, and by Alfred Bernhart, Mikroanalytisches Laboratorium, Mulheim (Ruhr), West Germany.

DISCUSSION

There are, of course, a number of factors that make it difficult to translate those reactions that are so successful with low molecular weight compounds to their high molecular weight analogs. Polymers often have low

solubility in the solvent of choice; yet, even though the resulting solutions are dilute, reactive groups are held in close proximity to each other permitting intramolecular crosslinking reactions to further diminish the solubility and complicate the already complex stereochemistry. For these and other reasons the present study was carried out largely with low molecular weight copolymers in which the amount of reactive monomer was adjusted to the maximum that would permit some useful reaction in the ordinary chemical sense. Thus, although the composition and molecular weight of the various copolymers and terpolymers described herein may appear to be arbitrary, in most instances the composition was determined empirically by the success or failure of the various reactions studied.

For example, initially, the homopolymer, poly-*p*-vinylacetophenone (II) was prepared by Friedel-Crafts acetylation of a low molecular weight polystyrene (I), the polystyrene having been prepared by an emulsion polymerization with a dodecyl mercaptan telemer. The molecular weight of II was roughly 100,000. The oxime of II was easily prepared, but in our hands was not readily reduced with lithium aluminum hydride. Since Blanchette and Cotman[2] have successfully reduced the oxime of poly-*p*-vinylacetophenone of molecular weight 7,000 under essentially the same conditions, the failure with II may have been due to its considerably greater molecular weight. Similarly, an attempted Leuckart reaction on II resulted in gel formation, possibly due to crosslinking involving a ketol condensation between acetyl groups.

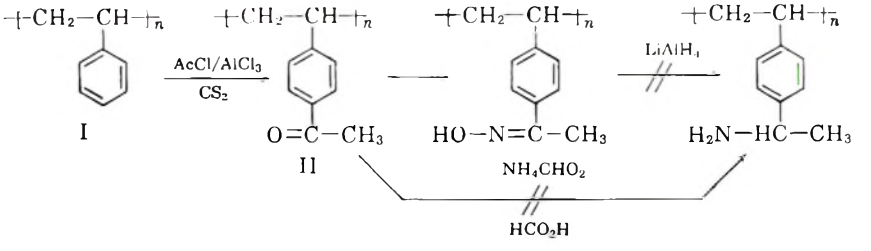

Thus, to avoid some of the interactions caused by the juxtaposition of reactive groups, various copolymers of *p*-vinylacetophenone and styrene were prepared and studied. The copolymers were prepared by copolymerization of the appropriate monomers and by partial Friedel-Crafts acetylation on preformed polystyrene.

The monomer, *p*-vinylacetophenone (V), had been prepared previously from *p*-diacetylbenzene by reduction to the keto alcohol with subsequent preparation and pyrolysis of the acetate;[6] acetylation of polystyrene and subsequent pyrolysis;[5] and from 2-chloroethylbenzene by acetylation and dehydrochlorination,[7] but these procedures seemed unnecessarily involved. In a new synthesis devised for the present study 2-phenylethyl acetate was acetylated under Friedel-Crafts conditions to give 2-(*p*-acetylphenyl)ethyl acetate (IV) in 45% yield and a 47% recovery of unaltered III. The keto ester IV was pyrolyzed in a benzene solution at 555° to *p*-vinylacetophenone

(V) in 79% yield. The overall yield was 37% (67% based on the recovered ester III).

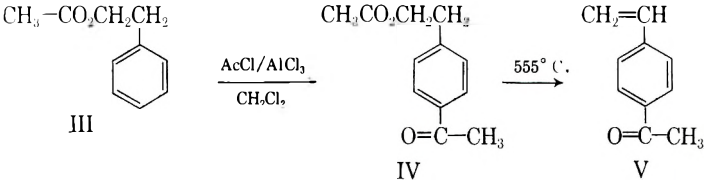

III IV V

A copolymer (VI) containing 30% ketone was prepared by suspension copolymerization with styrene with the use of benzoyl peroxide as initiator. This copolymer had a viscosity-average molecular weight of roughly 70,000. A 32% ketone copolymer (VII) was prepared by bulk copolymerization in the presence of bromotrichloromethane and the peroxide initiator. The polymerization was started at 90°C. and completed at 190°C. to yield a copolymer in the molecular weight range of 8,000.

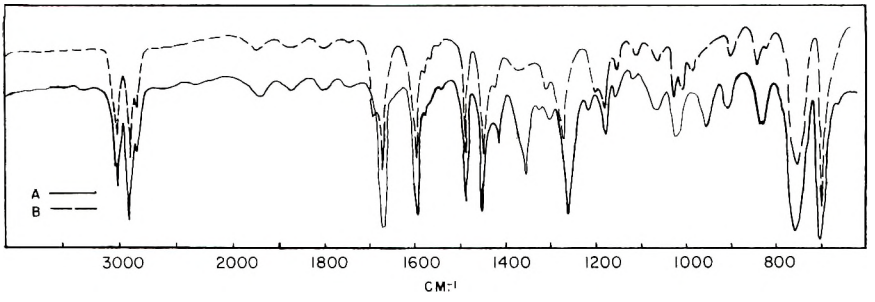

Fig. 1. Infrared spectra of (*A*) polymer VII (32% *p*-acetylstyrene units) and (*B*) polymer X [16% *p*-(α-bromoacetyl)styrene and 16% *p*-acetylstyrene units].

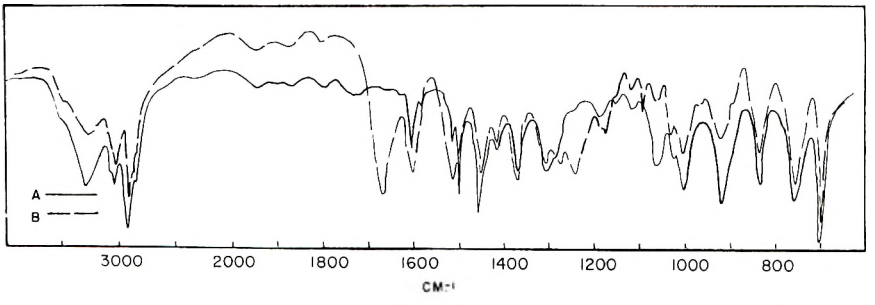

Fig. 2. Infrared spectra of (*A*) polymer IX (40% methyl *p*-styryl ketoxime units) and (*B*) polymer obtained from the attempted Beckman rearrangement of polymer IX.

A 40% *p*-vinylacetophenone copolymer (VIII) was prepared by partial Friedel-Crafts acetylation of polystyrene (I). This copolymer was converted to the oxime (IX), but the subsequent catalytic or chemical reduction of the oxime was unsuccessful. Lithium aluminum hydride reacted with the oxime copolymer (IX) to give an insoluble complex which, upon

decomposition with a solution of 8-hydroxyquinoline, yielded unchanged oxime copolymer. Attempted Beckman rearrangements on IX produced an insoluble resin. The infrared spectrum of this resin had a strong band at 1672 cm.$^{-1}$, which indicated that some rearrangement to the acetanide derivative may have occurred. The resin formation under the Beckman rearrangement conditions is consistent with results obtained by Blanchette and Cotman[2] on a low molecular weight poly-*p*-vinylacetophenone oxime. When the insoluble complex obtained from the attempted reduction of the oxime copolymer was treated with concentrated hydrochloric acid, a product similar to the resin obtained from the Beckman rearrangement was obtained. The reduction of *p*-alkylacetophenone oximes under identical conditions has been investigated[8] previously, and appreciable amounts of products formed from a Beckman-type rearrangement have been found.

Kenyon and Waugh[1] reported that the bromination of the homopolymer of *p*-vinylacetophenone resulted in the formation of insoluble resins containing 30–70% of the calculated amount of bromine. The copolymers VI, VII, and VIII were treated with bromine in chloroform solution to produce the α-bromo derivative. The higher molecular weight copolymers VI and VIII gave 50% or more gel formation in this reaction, but up to 50% of the theoretical amount of bromine could be introduced into the 32% copolymer VII very easily without gel formation. Attempts to introduce more bromine into VII gave a polymer which was yellow and showed a tendency to form gels during isolation steps. The terpolymer (X) obtained from the 50% bromination of VII was easily isolated and was not a lachry-

TABLE I
Physical Properties of the Polymers

Polymer				Softening
No.	Description	$[\eta]^a$	$\eta_{inh}{}^b$	point, °C.[c]
I	Polystyrene	0.54	0.45	130–140
II	Poly-*p*-vinylacetophenone	—	0.61	165–170
VI	Suspension copolymer(30% ketone)	0.48	0.47	140–150
VII	Bulk copolymer (32% ketone)	0.09	0.078	100–110
VIII	Friedel-Crafts copolymer (40% ketone)	0.67	0.63	140–150
IX	Oxime of VIII	—	0.28[d]	160–165
X	α-Bromoketone(16%) from VII	—	0.071	115–125
XI	α-Piperidinoketone (16%) from X	—	0.18	160(120° dec.)
XII	α-Morpholinoketone (16%) from X	—	—	140–145
XIII	α-Amino·HCl ketone (16%) from X	—	0.065	190(160° dec.)
XIV	Reduction product of XI	—	—	125–130
XV	Reduction product of XIII	—	—	120–125

[a] All viscosity measurements were at 25°C. and in chloroform solution except as noted.

[b] Inherent viscosity is at a concentration of 0.5 g./100 ml.

[c] Softening points were recorded on a Kofler hot bench.

[d] Viscosity in 2-butanone solution.

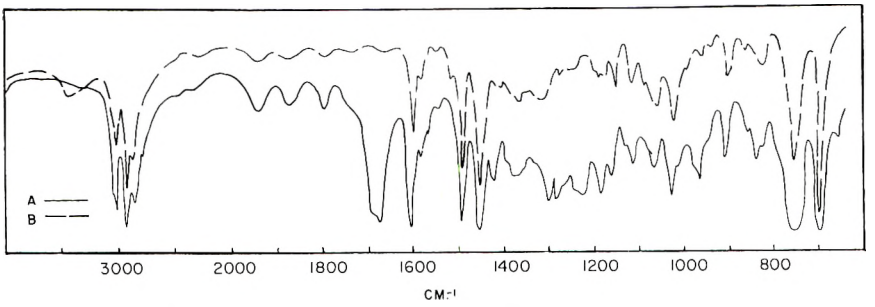

Fig. 3. Infrared spectra of (*A*) polymer XI [16% *p*-(α-piperidinoacetyl)styrene and 16% *p*-acetylstyrene units] and (*B*) polymer XIV, the amino alcohol obtained upon reduction of polymer XI.

mator. Elemental analysis showed it to contain 16% α-bromo-*p*-vinylacetophenone units.

The terpolymer X underwent facile nucleophilic replacement with piperidine and morpholine in solution to form the α-piperidino and α-morpholino terpolymers XI and XII; however, the more weakly basic aniline did not react with X at room temperature.

The terpolymer X was also treated with hexamethylenetetramine (Delepine reaction), and the resultant salt was hydrolyzed with hydrochloric acid to form the α-aminoketone hydrochloride terpolymer (XIII).

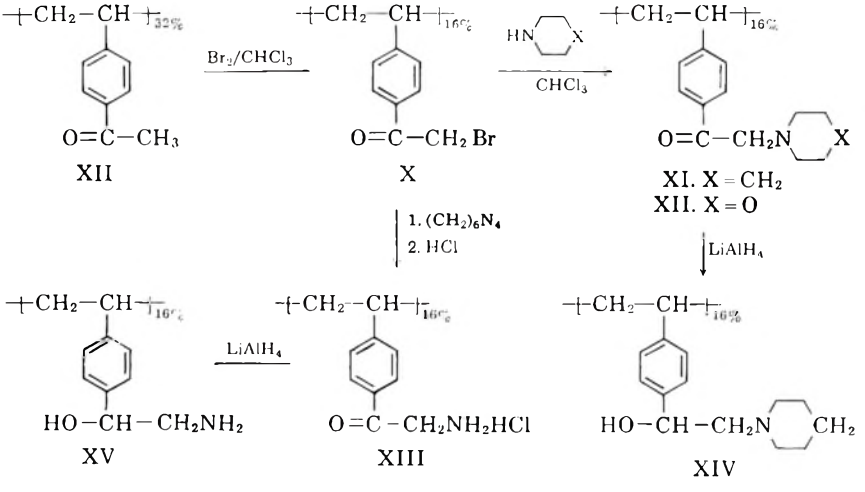

The terpolymers XI and XIII were reduced with lithium aluminum hydride to the corresponding 2-piperidinoethanol (XIV) and 2-aminoethanol (XV) derivatives. The elemental analyses of these amino ketone and amino alcohol terpolymers were complicated by ash formation. In general it was found difficult to remove all traces of lithium and aluminum salts from such reduction products.

The amino terpolymers XI, XII, XIII, XIV, and XV were soluble in acidic methanol–chloroform solutions, from which they could be precipi-

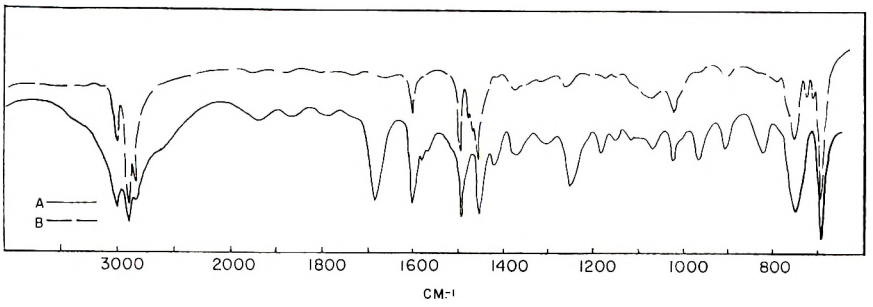

Fig. 4. Infrared spectra of (*A*) polymer XIII [16% *p*-(α-aminoacetyl) styrene hydrochloride and 16% *p*-acetylstyrene units] and (*B*) polymer XV, the amino alcohol obtained upon reduction of polymer XIII.

tated by addition of base. In addition, the reduced products XIV and XV were soluble in acidic aqueous tetrahydrofuran solutions.

Further indication of the formation of the aminoketone terpolymer XIII was the sensitivity of this product to base. Neutralization of acidic solutions of this polymer yielded a bright orange, insoluble resin which lost the orange coloration upon standing in air. Neutralization with a basic solution containing hydrogen peroxide produced a light tan, insoluble resin directly. These results are consistent with the reaction of aminoketone groups to form colored intermediates leading to dihydropyrazine rings accompanied by crosslinking of the polymer chains. Oxidation of these derivatives would yield colorless pyrazine derivatives. It should be noted that this reaction affords a novel method of crosslinking poly-*p*-vinylacetophenone. When a relatively dilute solution of the homopolymer (II) in chloroform was treated with a few drops of bromine and then saturated with ammonia, a gel was formed of such consistency that the vessel could be inverted without loss of any of its contents. Although this reaction has not been studied extensively, it would appear to be useful as a means of crosslinking polymers or copolymers containing the *p*-vinylacetophenone unit.

References

1. Kenyon, W. O., and G. P. Waugh, *J. Polymer Sci.*, **32**, 83 (1958).
2. Blanchette, J. A., and J. D. Cotman, *J. Org. Chem.*, **23**, 1117 (1958).
3. Merrill, S. H., *J. Polymer Sci.*, **61**, 223 (1962).
4. Price, C. C., and C. E. Adams, *J. Am. Chem. Soc.*, **67**, 1674 (1945).
5. Merrill, S. H., *J. Org. Chem.*, **26**, 1300 (1961).
6. Williams, J. L. R., *J. Am. Chem. Soc.*, **75**, 2779 (1953).
7. Baddely, G., E. Wrench, and R. Williamson, *J. Chem. Soc.*, **1953**, 2110.
8. Lyle, R. E., and H. J. Troscianec, *J. Org. Chem.*, **20**, 1757 (1955).

Résumé

On a développé une nouvelle synthèse de la *p*-vinylacétophénone. Ces copolymères de *p*-vinylacétophénone et styrène ont été préparés par copolymérisation et par acétylation partielle Friedel-Crafts du polystyrène. On a converti les copolymères en oximes mais la réduction subséquente était sans succés. Le réarrangement dex oximes a donné des résines insolubles. Les copolymères acétylés ont été bromés partiellement

pour donner des terpolymères α-bromo-*p*-vinylacétophénone/*p*-vinylacétophénone/styrène. Le déplacement nucléophile de l'atome de brome de ces terpolymères avec des amines secondaires produisait des terpolymères de l'α-pipéridine et α-morpholino-*p*-vinylacétophénone. La réaction de Délépine du polymère bromé produisait un terpolymère. On a reduct les piperidino et amino cétones des terpolymères en dérivés alcools correspondants avec l'hydrure de lithium-aluminium. Les terpolymères d'aminoacétones et aminoalcools ont des caractéristiques de solubilité modérée dans des alcools acides et l'eau. Les terpolymères d'α-aminocétones étaient très sensibles à une base et donnaient très facilement une liaison transversale du polymère acétylé.

Zusammenfassung

p-Vinylacetophenon wurde auf einem neuen Wege synthetisiert. Copolymere aus *p*-Vinylacetophenon und Styrol wurden durch Copolymerisation sowie durch partielle Friedel-Crafts-Acetylierung von Polystyrol dargestellt. Die Copolymeren wurden zu den Oximen umgesetzt, die darauffolgende Reduktion hatte aber keinen Erfolg. Beckmann-Umlagerung der Oxime führte zu unlöslichen Harzen. Die Acetylcopolymeren wurden partiell zu einem α-Brom-*p*-vinylacetopheuon/*p*-Vinylacetophenon/Styrolterpolymeren bromiert. Nukleophiler Ersatz des Broms eines dieser Terpolymeren mit sekundären Aminen lieferte α-Piperidin- und α-Morpholin-*p*-vinylacetophenonterpolymere. Die Delepine-Reaktion des bromierten Copolymeren führte zu einem α-Amino-*p*-vinylacetophenon-Terpolymeren. Die Piperidin- und Aminoketonterpolymeren wurden mit Lithiumaluminiumhydrid zu den entsprechenden Alkoholderivaten reduziert. Die Aminoketon- und Aminoalkoholterpolymeren besassen mässige Löslichkeit in saurem Alkohol und Wasser. Die α-Aminoketonterpolymeren waren gegen Basen sehr empfindlich und gestatteten eine leichte Vernetzung des Acetylcopolymeren.

Received December 12, 1962

JOURNAL OF POLYMER SCIENCE: PART A VOL. 2, PP. 835–843 (1964)

Gel Permeation Chromatography. I. A New Method for Molecular Weight Distribution of High Polymers

J. C. MOORE, *Texas Basic Research Department, The Dow Chemical Company, Freeport, Texas*

Synopsis

Polystyrene gels crosslinked in the presence of diluents have been made in fine-mesh bead form suitable for packing into chromatographic columns. A series of narrow molecular weight range polymer fractions was eluted through such columns with aromatic and chlorinated solvents. Effluent concentrations were detected and recorded by a continuous differential refractometer. The fractions were shown to be efficiently separated. Columns capable of separating adjacent polymeric samples of high molecular weight were prepared from gels crosslinked in the presence of large amounts of diluents having little or no solvent action on polystyrene. Smaller proportions of diluents and those with more solvent action yielded columns with lower molecular weight permeability limits. Such studies provided a unique quantitative view of the topology of the gels. They also demonstrated that rapid repetitive molecular weight distribution data can be obtained in this way on polymers for which solvents compatible with the gels are available.

Introduction

Early in their work on ion-exclusion, Wheaton and Bauman[1] found that many nonionic substances of low molecular weight were separated by elution with water through a column packed with ion-exchange resin particles. Since that time the techniques of column chromatography on crosslinked gels have become broadly applicable to separations of large from small molecules in aqueous solutions. Lathe and Ruthven[2] showed that the separating range could be greatly extended by using swollen starch grains as column packing, differentiating between a globulin and hemoglobin, for example, of molecular weights 150,000 and 67,000, respectively. Porath and Flodin[3,4] have made available a series of hydrophilic gel column packings and have introduced the term "gel filtration" for the process, which has achieved considerable usefulness. Lea and Sehon[5] have recently described other hydrophilic gels of this nature. However, being swellable only in aqueous media, their use is limited to the separation of water-soluble substances.

Hydrophobic gels of high permeability have not been available. Several interesting separations were reported by Cortis-Jones[6] on columns packed with crosslinked polystyrene. His investigation did not, however, extend to large molecules. Vaughan[7] showed that some separation of low molec-

ular weight polystyrenes did occur when they were eluted with benzene through polystyrene beads so lightly crosslinked that they had swollen in benzene to 51 times the volume of the dry polymer. However, all these gels were crosslinked in the absence of diluents, while the hydrophilic gels referred to were crosslinked in aqueous solution. This is a significant difference. Lloyd and Alfrey[8,9] have pointed out that gel networks of altered structure are produced by crosslinking in the presence of a diluent which is a solvent for the monomer. If the diluent is a nonsolvent for the resulting polymer, the gel may be still further altered by precipitation to give a rugged internal structure, and outstanding properties of stability and permeability are claimed for ion exchange resins based on such polymers.[10-12] The properties of gels prepared in the presence of various diluents have been investigated by Lloyd and Alfrey,[13] and diluents of intermediate solvent power were shown to give gels of intermediate properties.

Samples and Experimental Method

From the foregoing considerations, it appeared likely that we could prepare polystyrene beads with sufficient crosslinking to confer a desirable amount of rigidity, and still regulate the permeability of the network over a wide range by varying the amount and nature of the diluent present at the time of crosslinking. The permeabilities of the resulting gel networks were revealed by eluting a series of very similar compounds covering a wide range of molecular weights through a column packed with the gel. The properties of these marker materials are shown in Table I. In the low to medium molecular weight range the commercially available polypropylene glycols served as standards. A series of anionically polymerized polystyrenes covered the range from medium to high molecular weights.[14] In both cases the samples, while not monodisperse, gave well defined peaks. Aromatic or chlorinated eluting solvents chemically similar to the polystyrene gel were used to suppress adsorption and partition effects as much as pos-

TABLE I
Sample Materials

Polymer	Mol. Wt., $\bar{M}_w$	$\bar{M}_w/\bar{M}_n$
Anionic polystyrenes:		
S1	13,850	1.50
S102	82,000	1.05
S105	154,000	1.04
S108	267,000	1.08
S1159	570,000	1.05
S12	1,197,000	1.19
S114	3,500,000	1.24
Polypropylene glycols: The Dow Chemical Co.[a]		

[a] Average molecular weight by endgroup analysis as indicated in the identifying number, as: P-2000.

sible, and tailing was not evident with these samples. Eluent composition was followed by a Waters continuous differential refractometer, with a Rinco fraction collector adapted to mark the recorder chart at each volume increment.

Experimental Results and Discussion

A series of polystyrene gels with toluene as diluent in increasing proportions showed several significant changes. To avoid a soft compressible gel with resulting poor flow properties in the packed column, an increase in the proportion of diluent required a corresponding increase in the degree of crosslinking. With diluent and crosslinker increasing together, the permeability limit rose gradually at first, then rapidly at high dilution. With a rigidly crosslinked gel, the packed column became easier to pack and to use, less affected in volume by changes of eluting solvent. The compositions of these gels are shown in Table II. The permeability of each gel was then visualized by plotting the elution volume of each sample peak against the logarithm of the average molecular weight of the sample. These plots showed slanting lines, often quite straight for a considerable range, from an upper limit of permeability sharply defined at the interstitial volume, down to a nebulous lower limit around the total liquid

TABLE II
Permeabilities of Styrene Gels with Varying Proportions of Toluene

	Gel composition				
Gel	Styrene, wt.-%	Divinylbenzene, wt.-%	Toluene, wt.-%	M.W. permeability limit	Notes
PSX8	92	8	0	1,000	
PSX4	96	4	0	1,700	
PSX1	99	1	0	3,500	Rubbery
PSX0.1	99.9	0.1	0		Too soft to pack
A	79.1	4.2	16.7	2,500	
B	65.7	5.7	28.6	c.a. 7,000	
C	30	10	60	7,000	
D	24.8	2.5	72.7		Too soft to pack
E	9	11	80	250,000	

volume of the column, in which region the elution volume was determined more by polarity factors than by molecular size. Examples of the elution tracings obtained and the resulting permeability curves are shown in Figures 1 and 2.

Great increases in permeability were found when the nature of the diluent was changed. In this series the gels were made by polymerizing a mixture of 21.8% styrene, 18.2% commercial (55%) divinylbenzene, and 60% diluent by weight. Varying the diluent by progressively replacing toluene with *n*-dodecane caused regular increases in permeability, but a limit was

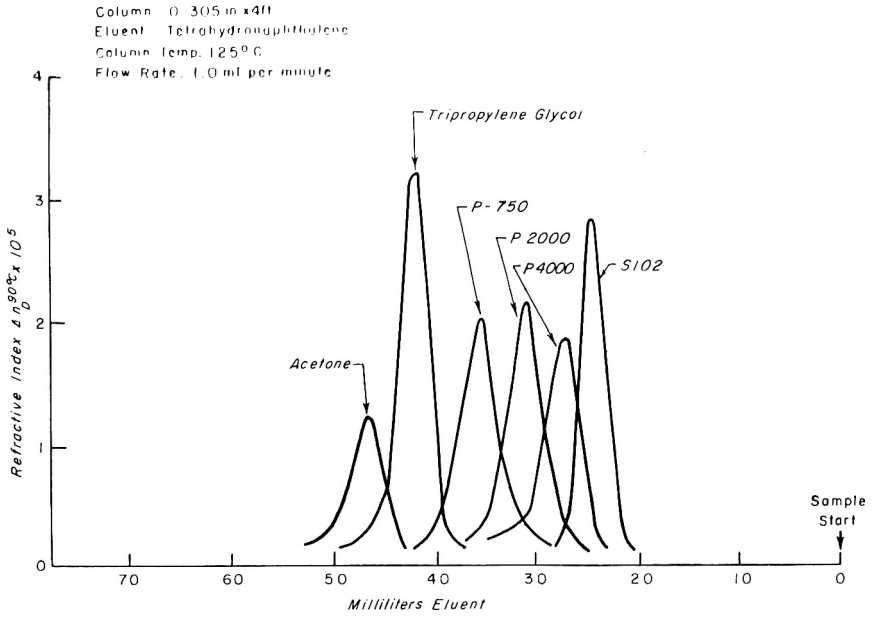

Fig. 1. Superimposed traces of elution peaks obtained with gel C.

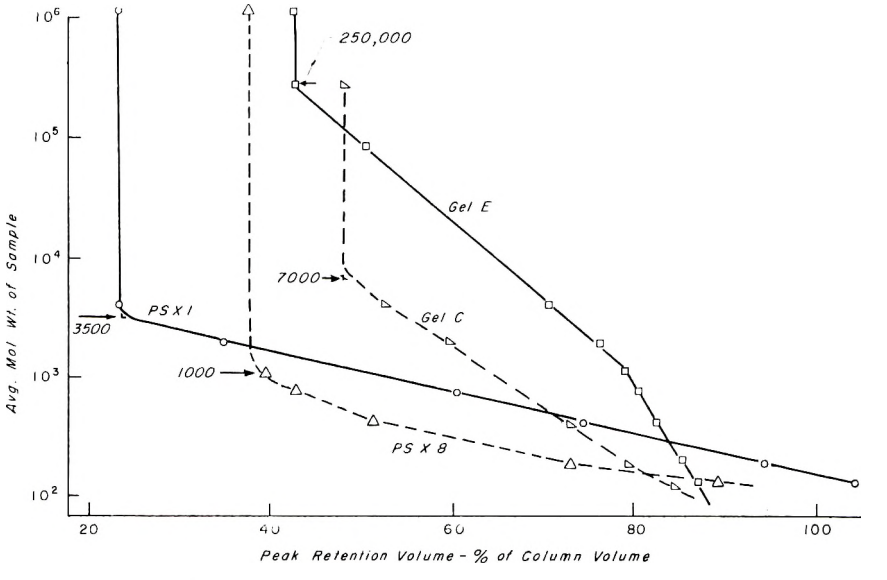

Fig. 2. Representative permeability curves for gels in Table II and determination of permeability limits.

reached when the diluent was 75% dodecane. Above that point the porous-structured beads were coated with a thin but impermeable skin. A non-solvent on the more polar side, isoamyl alcohol, progressively replacing diethylbenzene as diluent, showed very little increase in permeability at

TABLE III
Permeabilities of Gels with Various Diluents, All Made from 30% Styrene, 10% Divinylbenzene, 60% Diluent[a]

Gel	Diluents, parts/100 parts of gel	M.W. permeability limit
C	60 Toluene	7×10^3
F	30 Toluene, 30 diethylbenzene	1.5×10^4
G	60 Diethylbenzene	1.2×10^4
H	45 Toluene, 15 *n*-dodecane	1×10^5
I	30 Toluene, 30 *n*-dodecane	3×10^5
J	15 Toluene, 45 *n*-dodecane	2×10^6
K	10 Toluene, 50 *n*-dodecane	$<2 \times 10^3$
L	40 Diethylbenzene, 20 isoamyl alcohol	ca. 3.6×10^3
M	20 Diethylbenzene, 40 isoamyl alcohol	ca. 8×10^6
N	13.3 Diethylbenzene, 46.7 isoamyl alcohol	ca. 10^{10}
O	60 Isoamyl alcohol	Extremely high

[a] "Styrene" is a mixture of styrene and ethylvinylbenzene.

first, probably because of loss of some of the isoamyl alcohol to the aqueous continuous phase in which the beads were polymerized. With larger proportions of isoamyl alcohol in the diluent during polymerization, the permeability increased rapidly, far beyond the molecular sizes of the test materials used. This series of tests is summarized in Table III and Figures 3 and 4. The changes of gel structure indicated by the permeability curves were further shown in electron micrographs prepared by Dr. E. B. Bradford (Fig. 5). To preserve the swollen gel structure for electron microscopy, the porous polymer beads were soaked in a mixture of acrylate monomers, potted by polymerizing in a small gelatin capsule, and sectioned.

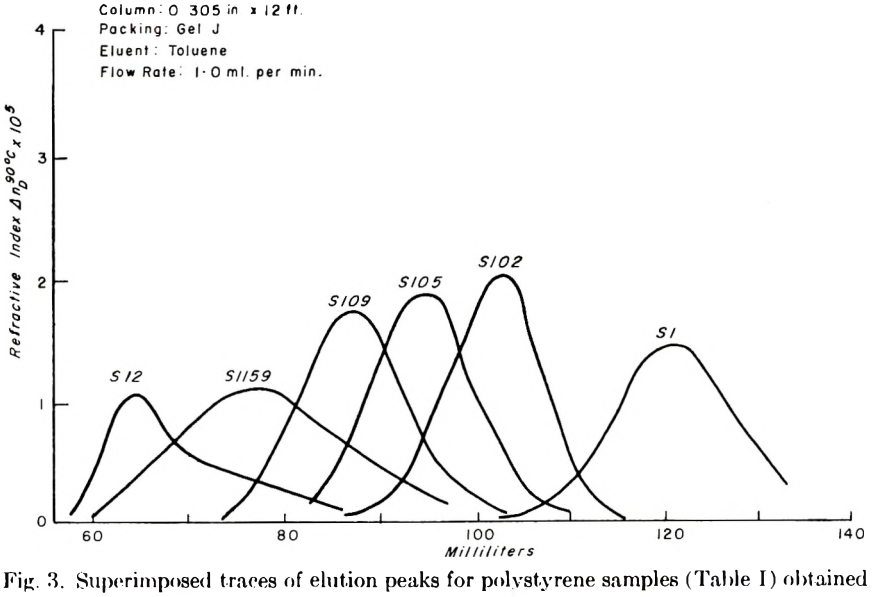

Fig. 3. Superimposed traces of elution peaks for polystyrene samples (Table I) obtained with gel J.

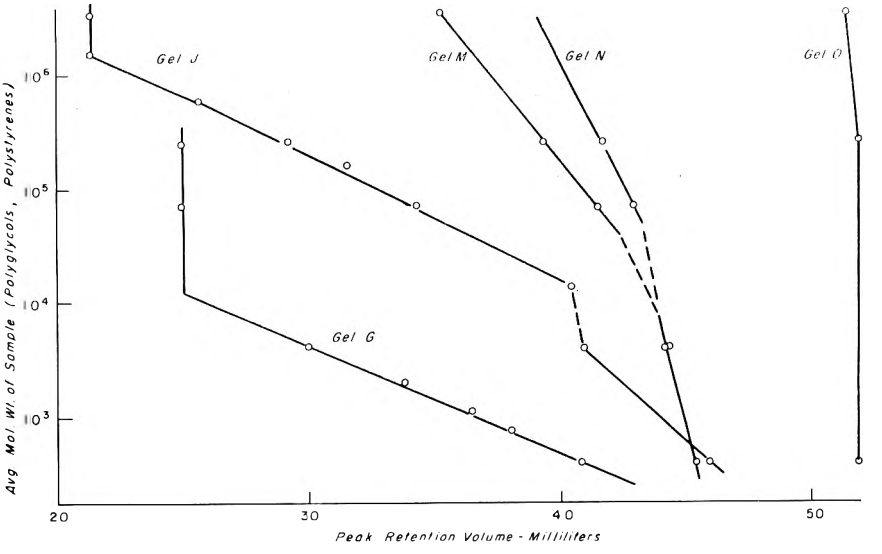

Fig. 4. Representative permeability curves for gels from Table III.

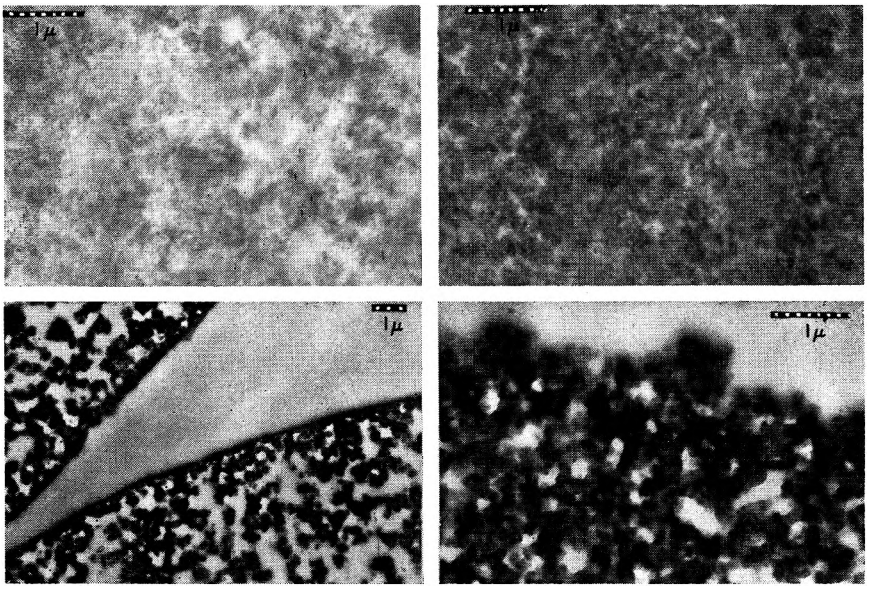

Fig. 5. Electron micrographs of thin sections of gels from Table III: (*a*) gel C; (*b*) ge G; (c) gel K; (*d*) gel M.

The chromatographic separation appears to be close to an equilibrium process, in which the solute molecules very rapidly diffuse into all parts of the gel network not mechanically barred to them. With small samples at slow flow rates, very sharp peaks can be obtained. With larger samples or with faster flow rates, the peaks are broader, but not earlier as would be expected if diffusion rates were the basis of separation. Even large mole-

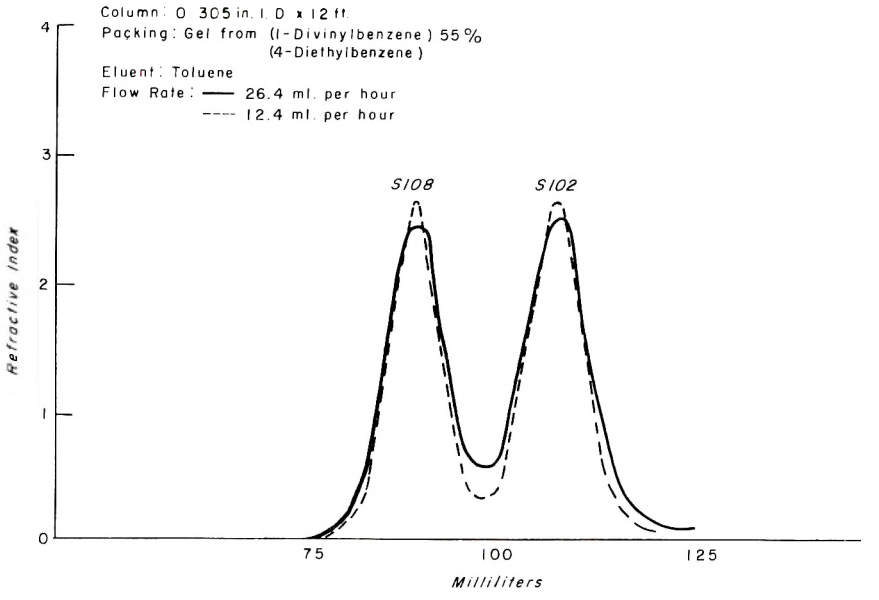

Fig. 6. Separation of two narrow-distribution styrenes at two flow rates.

cules do not appear to affect the permeability of the gel to small molecules, so that the elution pattern of a mixture can be expected to match the sum of the elution patterns of the components, as long as overloads are avoided. These effects were shown in the separation of two polystyrenes by elution with toluene through a column of 0.305 in. i.d. and 12 ft. long. The column was packed with a 200–325 mesh fraction of a bead polymer made from a mixture of one part commercial 55% divinylbenzene and four parts diethylbenzene. The 1.0 ml. sample contained 6.7 mg. each of styrene polymers S108 and S102 (Table I) in toluene. Figure 6 shows the tracings of effluent refractive index at two flow rates, 26.4 ml./hr. and again at 12.4 ml./hr. At the slower rate the resolution was improved, but the peaks were not shifted. Samples of the effluent were evaporated and examined by ultracentrifugation, and the separation was shown to be complete.

While the separation of the different polymeric species from the same monomer can be correlated quite well with molecular weight, nonhomologous compounds do not always correlate so simply. With larger molecules, the molecular size seems to be the prime factor with polarity becoming more important at lower molecular weights. These factors were demonstrated with a gel column of lower permeability, 1.3 cm. diameter and 109 cm. long. The packing was 100–200 mesh PSX4 polystyrene (Table II) swollen in methylene chloride, packed and eluted with the same solvent. Four compounds were sampled, using 0.25 ml. of 1% solution. The elution volumes of the resulting peaks show the expected inverse relationship to molecular model dimensions, with some deviation probably due to polarity, and no correlation with molecular weight, as shown in Table IV.

TABLE IV
Inverse Correlation of Peak Elution Volume with Molecular Size

Substance	Elution volume, ml.	Molecular size, A.	M.W.
Bis (glycidyl ether) of Bisphenol A $(CH_3)_2C(C_6H_4OCH_2CHCH_2O)_2$	75	18.5	340
Dibromotetrachloroxylene m-$(CH_2Br)_2C_6Cl_4$	108	13.5	402
Mixed xylenes, $(CH_3)_2C_6H_4$	109	8.9	106
Perchloroethylene, C_2Cl_4	122	7.7	166

It is apparent that polystyrene gels, crosslinked in the presence of appropriate diluents, can be used in column chromatography to make molecular size fractionations over an extremely wide range. The term "gel permeation chromatography" is proposed for this technique. It suggests and describes a mechanism of fractionation in which solute molecules are separated by their permeation into a gel which offers different internal volumes to molecules of different sizes over an extended range. This mechanism is prominent in the separation of small nonionic hydrophilic molecules by water elution through beds of ion-exchange resins, as noted much earlier by Wheaton and Bauman,[1] and in the "gel filtration" fractionation of hydrophilic molecules on Sephadex.[3,4] However, to us the term "gel filtration" has not seemed apt for a fractionation of extended range. It did seem apt for the short-column, sievelike separations with which the Sephadex gels were first reported.

This work has shown that structurally modified polystyrene gels, eluted with compatible solvents, have utility in making molecular size fractionations of hydrophobic macromolecules. It seems quite possible that suitable copolymer-diluent systems may be found to yield gels of adequate strength and rigidity with any desired combination of solvent compatibility and permeability. This would indeed open a broad field of usefulness to gel permeation chromatography.

Important contributions of many other persons to this study are gratefully acknowledged. Thanks are particularly due to W. G. Lloyd and T. Alfrey for consultations on the control of permeability in crosslinked gels, to D. R. Asher and D. B. Parrish for some of the fine-mesh bead preparations, to H. W. McCormick for the anionically polymerized styrenes and the ultracentrifuge work, to E. B. Bradford for the electron microscopy, and to M. C. Arrington for technical assistance.

References

1. Wheaton, R. M., and W. C. Bauman, *Ann. N. Y. Acad. Sci.*, **57**, 159 (1953).
2. Lathe, G. H., and C. R. Ruthven, *Biochem. J.*, **62**, 665 (1956).
3. Porath, J., and P. Flodin, *Nature*, **183**, 1657 (1959).
4. Flodin, J., and J. Porath, U. S. Pat. 3,002,823 (October 3, 1961).
5. Lea, D. J., and A. H. Sehon, *Can. J. Chem.*, **40**, 159 (1962).
6. Cortis-Jones, B., *Nature*, **191**, 272 (1961).
7. Vaughan, M. F., *Nature*, **188**, 55 (1960).

8. Lloyd, W. G., and T. Alfrey, papers presented at 139th Meeting, American Chemical Society, St. Louis, March 1961, Division of Polymer Chemistry, papers 6 and 7.
9. Lloyd, W. G., and T. Alfrey, *J. Polymer Sci.*, **62**, 301 (1962).
10. Meitzner, E. F., and J. A. Oline, Union S. Africa Pat. Appl. 59/2393 (May 19, 1959), to Rohm and Haas.
11. Bortnick, N. M., U. S. Pat. 3,037,052 (May 29, 1962).
12. Kressman, T., and J. Miller, Brit. Pat. 889,304 (to Permutit).
13. Lloyd, W. G., private communication.
14. McCormick, H. W., *J. Polymer Sci.*, **36**, 341 (1959).

Résumé

On the préparé des gels de polystyrène pontés en présence de diluants sous forme de fines perles convenant à l'entassement dans les colonnes chromatographiques. Une série de fractions polymériques de poids moléculaires voisins est éluée a travers de telles colonnes avec des solvants aromatiques et chlorés. On détermine et enrégistre les concentrations sortante à l'aide d'un réfractomètre continu différentiel. Les fractions sont ainsi efficacement séparées. On prépare des colonnes capables de séparer des échantillons de polymères de poids moléculaires voisins élevés à partir de gels pontés en présence de grandes quantités de diluants possédant une action solvatante faible ou nulle sur le polystyrene. Des proportions plus faibles de diluants et ceux possédant une plus forte action solvatante fournissent des colonnes présentant des limites de perméabilité des moléculaires plus faibles. De telles études donnent une vue quantitative unique de la topologie des gels. Elles démontrent également que des résultats rapides et reproductibles de distributions de poids moléculaires peuvent être obtenus de cette façon sur des polymères pour lesquels des solvants compatibles avec les gels sont existants.

Zusammenfassung

In Gegenwart von Verdünnungsmitteln vernetzte Polystyrolgele wurden in Feinsieb-Kugelform zur Verwendung in chromatographischen Säulen erzeugt. Eine Reihe engverteilter Polymerfraktionen wurde durch solche Säulen mit aromatischen und chlorierten Lösungsmitteln eluiert. Die Effluentkonzentrationen wurden mit einem kontinuierlich arbeitenden Differentialrefraktometer bestimmt und registriert. Es trat eine wirksame Trennung der Fraktionen ein. Zur Trennung von hochmolekularen Polymerproben mit benachbartem Molekulargewicht wurden Säulen mit Gelen gebaut, die in Gegenwart grosser Mengen von Verdünnungsmitteln mit geringer oder fehlender Lösungswirkung für Polystyrol vernetzt worden waren. Kleinerer Gehalt an Verdünnungsmittel und Verdünnungsmittel mit grösserer Lösungswirkung für Polystyrol lieferten Säulen mit niedrigeren Molekulargewichtspermeabilitätsgrenzen. Diese Untersuchungen ergaben einzigartige Aufschlüsse über die Topologie der Gele. Sie zeigten ferner, dass auf diese Weise für Polymere, für welche mit den Gelen verträgliche Lösungsmittel vorhanden sind, rasche und reproduzierbare Ergebnisse für die Molekulargewichtsverteilung zugänglich sind.

Received December 14, 1962

JOURNAL OF POLYMER SCIENCE: PART A VOL. 2, PP. 845–851 (1964)

Some Factors Affecting the Molecular Association of Poly(ethylene Oxide) and Poly(acrylic Acid) In Aqueous Solution*

F. E. BAILEY, JR., R. D. LUNDBERG, and R. W. CALLARD, *Research and Development Department, Union Carbide Chemicals Company, South Charleston, West Virginia*

Synopsis

Investigations of the properties of very high molecular weight polymers of ethylene oxide have shown that, while this polymer structure is relatively nonpolar, it displays a high degree of polymer solvent interaction in aqueous systems. A unique application of the hydrogen bonding affinity of the ether oxygens in the poly (ethylene oxide) chain has been found in the molecular association complexes formed between this polyether and polymeric acids such as poly(acrylic acid). Interest in the properties of these complexes has prompted a more detailed study of the mechanism of association which occurs in solution. In this study the effects of pH, of composition and concentration, and of temperature on solution viscosity are examined in order to define the stoichiometry of the intermolecular association. A wide range of polymer molecular weights has been studied, ranging in the case of poly(ethylene oxide) from low molecular weight waxes to very high molecular weight polymers. The molecular complex of poly(ethylene oxide) and poly(acrylic acid) appears to be an association between ether oxygens and carboxyl groups through hydrogen bonding which approaches 1:1 stoichiometry. While at low pH this association is sufficient to cause phase separation, at higher pH the complex exists in solution. In neutral solution there also appears to be an interaction between the two polymer species.

Introduction

Investigations of the properties of very high molecular weight polymers of ethylene oxide[1,2] have shown that, while this polymer structure is relatively nonpolar, it displays an extraordinary degree of polymer–solvent interaction in aqueous systems. A unique application of the strong hydrogen bonding affinity of the ether oxygens of the poly(ethylene oxide) chains was found in the molecular association complexes of this polyether with polymeric acids such as poly(acrylic acid).[3] It was found that when aqueous solutions of poly(ethylene oxide) and poly(acrylic acid) were mixed in approximately equal proportions, a precipitate formed immediately which could be recovered by filtration, dried and pressed out to form clear, water-insoluble, flexible films. The precipitate was found to be an intermolecular associa-

* Paper presented at 138th Meeting of the American Chemical Society, Division of Polymer Chemistry, New York, N. Y., September 13, 1960.

tion product of poly(ethylene oxide) and poly(acrylic acid), presumably resulting from a multiplicity of hydrogen bonds between ether oxygens and carboxyl groups, with physical properties quite different from those which might be predicted on the basis of either component alone.

Interest in the unusual properties of the molecular association complexes of poly(ethylene oxide) and poly(acrylic acid) has prompted a more detailed study of the mechanism of association which occurs in aqueous solution. This investigation has examined the effect of pH and composition on solution viscosity in order to elucidate some of the factors affecting the intermolecular association reactions.

Experimental

Poly(ethylene oxide) examined in this study has covered a wide range in molecular weight from about 5500 for samples of Carbowax 6000 (lower molecular weight, waxy polymers of ethylene oxide manufactured by Union Carbide Chemicals Co.) to some Polyox poly(ethylene oxide) resins (water-soluble resins manufactured by Union Carbide Chemicals Co.) with viscosity-average molecular weights of about 1,000,000. While the lower molecular weight poly(ethylene oxide) dissolves almost immediately in water, solutions of the higher molecular weight polymers have generally been prepared by mixing the resin thoroughly with water in a glass bottle and then gently agitating by rolling overnight (ca. 16 hr.). The poly(acrylic acid) polymers employed in the experiments reported in this paper were either an Acrysol A-1 (a 25% solution of poly(acrylic acid) in water, available from Rohm and Haas Co.) sample or a much higher molecular weight poly(acrylic acid) prepared in our laboratories for this study. Mixed solutions of poly(ethylene oxide) and poly(acrylic acid) were made by first dissolving the poly(acrylic acid) in water, neutralizing to the desired pH with sodium hydroxide, and then mixing in a poly(ethylene oxide) solution of the required concentration and pH with gentle agitation.

Dilute solution viscosities were determined in a conventional Ubbelohde capillary viscometer. The viscosities of more concentrated, and hence more viscous, solutions were measured with a modified Bergen type[4] viscometer. The Bergen viscometer is a translational viscometer for which an analytical balance is employed to achieve very small shearing stresses. The modified form employed in these studies was equipped with an open-ended cylinder and hence was closely related to a Pochettino instrument similar to that used in previous studies.[1] However, in this work an all-glass cylindrical bob was employed. The all-glass system was found necessary in order to achieve reproducible measurement at low pH, at which considerable interference from trace quantities of heavy metal ions was observed. From this viscometer, data were obtained in the form of a flow curve which, for non-Newtonian systems such as those examined in this study, was symmetrical about the shear stress axis. The slope of the curve, at a particular shear rate, was, by definition, the viscosity at that rate of shear.

Results and Conclusions

The molecular association product of poly(ethylene oxide) and poly(acrylic acid) forms as a precipitate from water solution below pH 3.8. At higher pH, the two resins coexist in aqueous solution. Depending upon the pH of the solution, that is, the relative quantity of poly(acrylic acid) to sodium polyacrylate present, and upon the ratio of polyacrylate to poly(ethylene oxide), the rheology of the solution of mixed polymers displays varying degrees of association between carboxyl and ether groups and of apparent interaction between carboxylate and ether groups. These degrees of association and interaction are observed in the variation of solution viscosity.

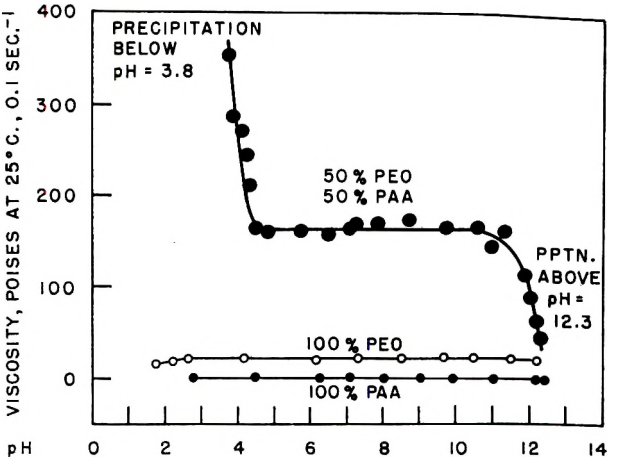

Fig. 1. The dependence of viscosity on pH for aqueous solutions of high molecular weight poly(ethylene oxide) (PEO) and poly(acrylic acid) (PAA). Total polymer concentration is 2 g./100 ml.

The viscosities of poly(ethylene oxide) solutions in water over a range of pH have been determined[1] and found to be almost invariant from pH 2 to 12 as seen in Figure 1. The increase in viscosity of aqueous poly(acrylic acid) solutions with increasing pH, as the ionized polyacrylate is formed, is widely known; however, the viscosity level of the sample used in these studies is too low to permit the effect to be observed on the scale of Figure 1. The viscosity of the poly(acrylic acid)–poly(ethylene oxide) solutions decreases sharply over the pH range of 4 to 6, and then remains essentially constant from pH 7 to about 12 as shown in Figure 1. At higher pH, a decrease in solution viscosity together with polymer precipitation is observed. To ascertain the stoichiometry of these associations in solution, reduced viscosities have been determined of solutions containing a range of ratios of poly(acrylic acid) to poly(ethylene oxide) as a function of both total resin concentration and pH.

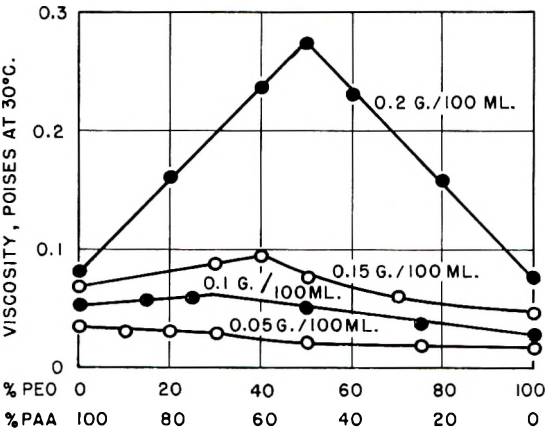

Fig. 2. The dependence of viscosity on composition for aqueous solutions of high molecular weight poly(ethylene oxide)–poly(acrylic acid) at pH = 4.

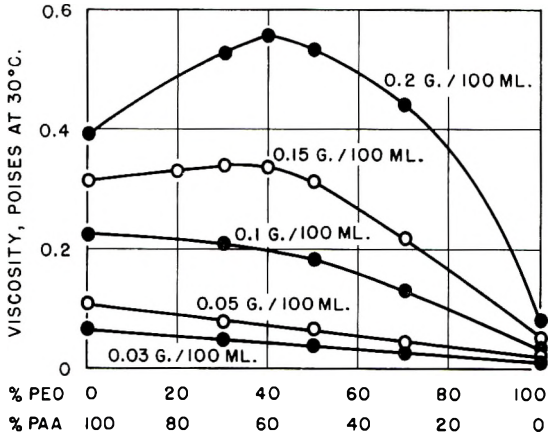

Fig. 3. The dependence of viscosity on composition for aqueous solutions of high molecular weight poly(ethylene oxide)–poly(acrylic acid) at pH = 7.

At pH 4, a sharp maximum is found at 0.5 weight fraction of poly(ethylene oxide) in a plot of reduced viscosity (at constant total polymer concentration) versus weight fraction as shown in Figure 2. This value represents essentially a two to three molar ratio of carboxylic to ether oxygen groups, which is essentially the stoichiometry found for the precipitate polymer below pH 4. At a higher pH of 7, shown in Figure 3, a maximum near same weight fraction is also obtained although it is not as sharply defined. The same behavior is found at pH of 10.0. The degree of these maxima is a function of total resin concentration and decreases as the concentration is decreased. Thus no maximum is observed for the *intrinsic* viscosity at pH of 4.0 or 7.0. This dependence on concentration may be interpreted as due to dissociation of the complexes at high dilution. The association there-

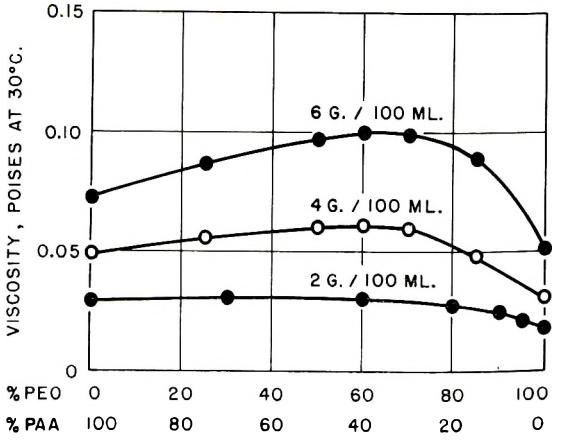

Fig. 4. The dependence of viscosity on composition for aqueous solutions of low molecular weight poly(ethylene oxide)–poly(acrylic acid) at pH = 4.

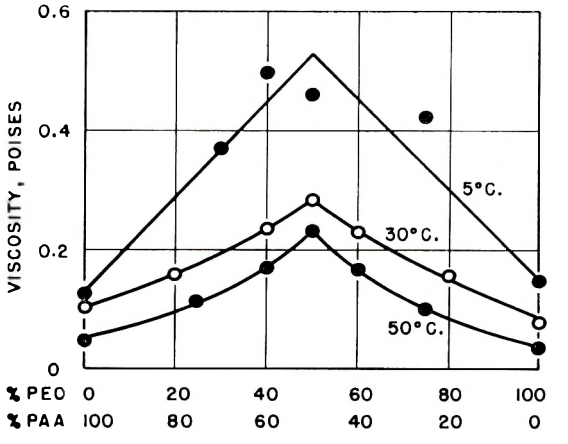

Fig. 5. Dependence of viscosity on composition for aqueous solutions of poly(ethylene oxide)–poly(acrylic acid) at pH = 4 for various temperatures.

fore is a function of polymer concentration. Similar behavior is observed for low molecular weight samples of poly(ethylene oxide) and poly(acrylic acid), but higher concentrations are required to observe a maximum (Fig. 4).

The effect of temperature upon the association reaction has been investigated briefly by studying solution viscosity of the complex as a function of composition at several temperatures (Fig. 5). The magnitude of solution viscosity decreases with increasing temperature; however, the maximum appears more pronounced at the higher temperature. Although the addition of urea is known to break weak hydrogen bonds in other systems, and has been shown to form solid complexes with high polymers of ethylene oxide such as Polyox,[5] the addition of urea, up to 1*M*, to these systems has little effect on solution viscosity at pH 4 or 7. It appears that neither the

addition of urea nor application of heat over the observed temperature range is effective in breaking up the complex.

These studies have been largely concerned with the association of poly(ethylene oxide) with poly(acrylic acid). The association of other polymeric acids is similar to that observed with poly(acrylic acid), and in some cases more pronounced. The association of poly(methacrylic acid) with poly(ethylene oxide) is shown in Figure 6. Two factors differentiate this complex from the one observed with poly(acrylic acid). The magnitude of the viscosity increase as a function of composition is considerably greater than in the latter case, indicating a stronger association. Also the maximum is located at 60 wt.-% poly(methacrylic acid), indicating an apparent stoichiometric ratio of about three ethylene oxide units per methacrylic acid unit.

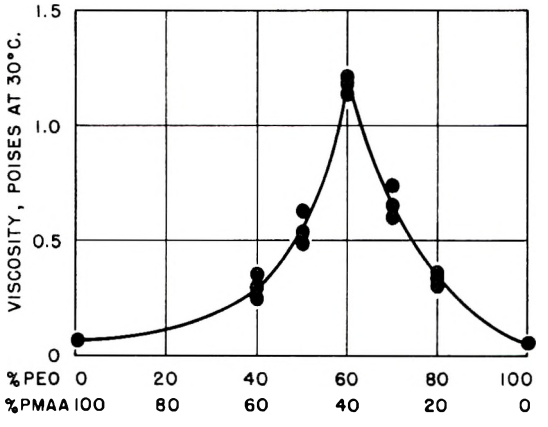

Fig. 6. Dependence of viscosity on composition for aqueous solution of poly(ethylene oxide)–poly(methacrylic acid) at pH = 5.3.

These results strongly support the conclusion that the association between poly(acrylic acid) and poly(ethylene oxide) at lower pH's is due to hydrogen bonding of the carboxyl group with the ether oxygen. The stoichiometry of this association is not yet clear. A few preliminary experiments have indicated that the stereoregularity of the polymer acid greatly affects the observed stoichiometry of the association. Further experiments are in progress to elucidate this point.

The mechanism of association at higher pH's, where the concentration of the acid form of poly(acrylic acid) is extremely small, is attributed to an ion–dipole interaction between the ether oxygen and the poly(acrylate anion). As expected, the addition of salts such as NaCl to the complex at pH's greater than 7 essentially eliminate any association of this type with a consequent reduction in viscosity. Dialysis of the solution containing complex and salt, however, restores the viscosity of the association product to its original value, showing that the phenomenon is indeed reversible.

References

1. Bailey, F. E., Jr., G. M. Powell, and K. L. Smith, *Ind. Eng. Chem.*, **50**, 6 (1958).
2. Bailey, F. E., Jr., and R. W. Callard, *J. Appl. Polymer Sci.*, **1**, 56 (1959); *J. Appl. Polymer Sci.*, **1**, 373 (1959).
3. Smith, K. L., A. E. Winslow, and D. E. Petersen, *Ind. Eng. Chem.*, **51**, 1361 (1959).
4. Bergen, J. T., and W. Patterson, Jr., *J. Appl. Phys.*, **24**, 712 (1953).
5. Bailey, F. E., Jr., and H. G. France, *J. Polymer Sci.*, **49**, 397 (1961).

Résumé

L'étude des propriétés des polymères d'oxyde d'éthylène d'un poids moléculaire très élevé, a démontré que, lorsque la structure du polymère est relativement apolaire, celui-ci laisse apparaître un haut degré d'interaction polymère-solvant dans des systèmes aqueux. On a trouvé une application unique de la tendance à fixer l'hydrogène des atomes d'oxygène des éthers se trouvant sur la chaîne d'oxyde de polyéthylène, dans les complexes d'association moléculaire formés entre ce polyéther et des acides polymériques tels que les acides polyacryliques. L'intérêt des propriétés de ces complexes a poussé à une étude plus détaillée du mécanisme d'association en solution. Dans cette étude, les effects du pH, de la composition et concentration, et de la température sur la viscosité de la solution ont été examinés pour définir la stoechiométrie de l'association intermoléculaire. Une gamme très vaste des poids moléculaires a été étudiée allant dans ce cas-ci de l'oxyde de polyéthylène, de cires de bas poids moléculaire à des polymères d'un poids moléculaire très élevé. Le complexe moléculaire de l'oxyde de polyéthylène et l'acide polyacrylique semble être une association entre les oxygènes de l'éther et les groupes carboxyliques par des ponts hydrogène avec rapport stoechiométrique d'environ 1:1. Si à de faibles valeurs de pH cette association suffit à causer la séparation de phase, aux valeurs de pH plus élevées par contre le complexe existe en solution. En solution neutre, il semble également qu'il existe une interaction entre les deux espèces de polymères.

Zusammenfassung

Untersuchungen der Eigenschaften sehr hochmolekularer Äthylenoxydpolymerer zeigten, dass diese Polymerstruktur trotz ihres verhältnismässig unpolaren Charakters in wässrigen Systemen eine starke Polymer-Lösungsmittel-Wechselwirkung zeigt. Eine besondere Anwendung der Wasserstoffbindungsaffinität der Äthersauerstoffe in der Polyäthylenoxydkette wurde in den zwischen diesem Polyäther und polymeren Säuren, wie Polyacrylsäure, gebildeten Molekülassoziationskomplexen gefunden. Die interssanten Eigenschaften dieser Komplexe liessen eine eingehendere Untersuchung des Mechanismus der in Lösung auftretenden Assoziation als wichtig erscheinen. Bei dieser Untersuchung wurden der Einfluss des pH, der Zusammensetzung und Konzentration sowie der Temperatur auf die Lösungsviskosität überprüft, um die Stöchiometrie der intermolekularen Assoziation festzulegen. Ein weiter Molekulargewichtsbereich wurde untersucht, der sich im Falle des Polyäthylenoxyds von niedermolekularen Wachsen bis zu sehr hochmolekularen Polymeren erstreckte. Der Molekülkomplex zwischen Polyäthylenoxyd und Polyacrylsäure scheint in einer Assoziation zwischen Äthersauerstoffen und Karboxylgruppen durch Wasserstoffbindungen mit einer Stöchiometrie von angenähert 1:1 zu bestehen. Während die Assoziation bei niedrigem pH zu einer Phasentrennung führt, bleibt der Komplex bei höherem pH in Lösung. Auch in neutraler Lösung scheint eine Wechselwirkung zwischen den beiden Polymeren zu bestehen.

Received December 19, 1962

JOURNAL OF POLYMER SCIENCE: PART A VOL. 2, PP. 853–864 (1964)

Instrument for the Studies of Differential Flow Dichroism of Polymer Solutions

AKIYOSHI WADA, *Department of Physics, Faculty of Science, University of Tokyo, Bunkyo-ku Tokyo, Japan,* and SHICHIBEI KOZAWA, *Shimadzu Co., Nakakyo-ku, Kyoto, Japan*

Synopsis

A concentric cylinder apparatus for the studies of flow dichroism in polymer solutions is described in detail. The outer and inner cylinders are both made of fused quartz which is transparent in visible and ultraviolet region down to 220 mμ. The velocity gradient is produced in solution in the gap between the cylinders by rotating the inner one. The light path is designed to be perpendicular to the axis of rotation of the quartz cylinder. A differential device makes it possible to measure the difference in absorption coefficients, $\epsilon_{\parallel}$ and $\epsilon_{\perp}$, which are the absorption coefficients measured by plane-polarized light having parallel and perpendicular electric vector with the stream line. The apparatus is found to be useful for studying the regularity of orientation of chromophores in both synthetic and biological polymer chains.

I. INTRODUCTION

In the studies of biological macromolecules such as proteins and nucleic acids, and related synthetic polymers such as polypeptides and polynucleotides, the chain regularity in the main chain and the ordered orientation in side-chain groups seems to be one of the important subjects to be solved in connection with the specific biological character of these materials. These studies are also important for the stereoregularities of isotactic and syndiotactic polymer chains, of course.

For the observation of the internal configuration of polymers such information can be obtained by orienting the polymers and measuring the properties separately parallel with and perpendicular to the orienting axis. Measurements of the birefringence and the dichroic ratio are useful methods for this purpose, and the latter may have some advantage because so much information is obtained from the many spectral lines. Many of the instruments for measurement of dichroism described previously involve the use of either a capillary tube or an optical cell of parallel walls through which the solution is forced to flow to produce the velocity gradient.[1-3] It is evident, however, the method of producing a velocity gradient with a rotating coaxial cylinder[4-6] gives a quantitative result especially in regards to the hydrodynamic properties of macromolecules.

The instrument to be described here shows that the method involving a transparent coaxial cylinder with the light path perpendicular to the rotat-

ing axis is useful for quantitative measurements, especially in the ultraviolet and visible region. The construction of the apparatus for measurements in the infrared region is also possible in principle, though the mechanical weakness of the transparent material for the rotating cell in this region poses some difficulties in processing.

II. APPARATUS

The present apparatus was designed as an attachment for a manual ultraviolet spectrophotometer. Its external appearance is shown in Figure 1, and its optical system is shown in Figure 2.

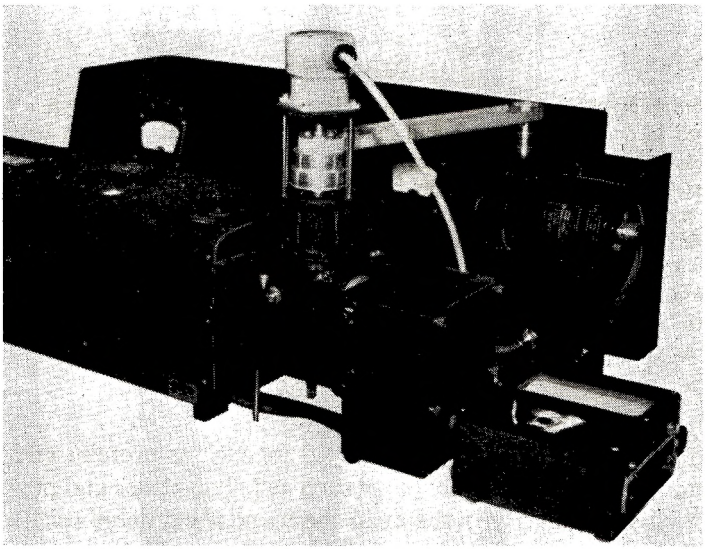

Fig. 1. Photograph of the apparatus equipped with the manual ultraviolet spectrophotometer.

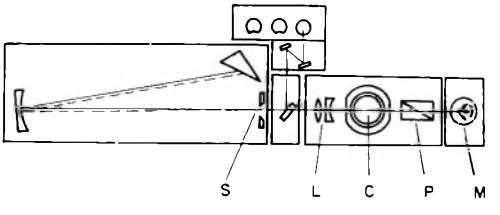

Fig. 2. Diagram of the optical system: (S) exit slit: (L) collimating lens; (C) coaxial cylinder cell; (P) polarizer; (M) photomultiplier.

The monochromatic light beam which exits from the exit slit, S, of the monochrometer is collimated by the quartz lens, L, and enters into the quartz cell of the rotation-type inner cylinder. Then, it passes through the polarizer, P, and enters the photomultiplier, M. The polarizer, P, is made of calcite which is built to Glan-Thompson type by using ultraviolet-

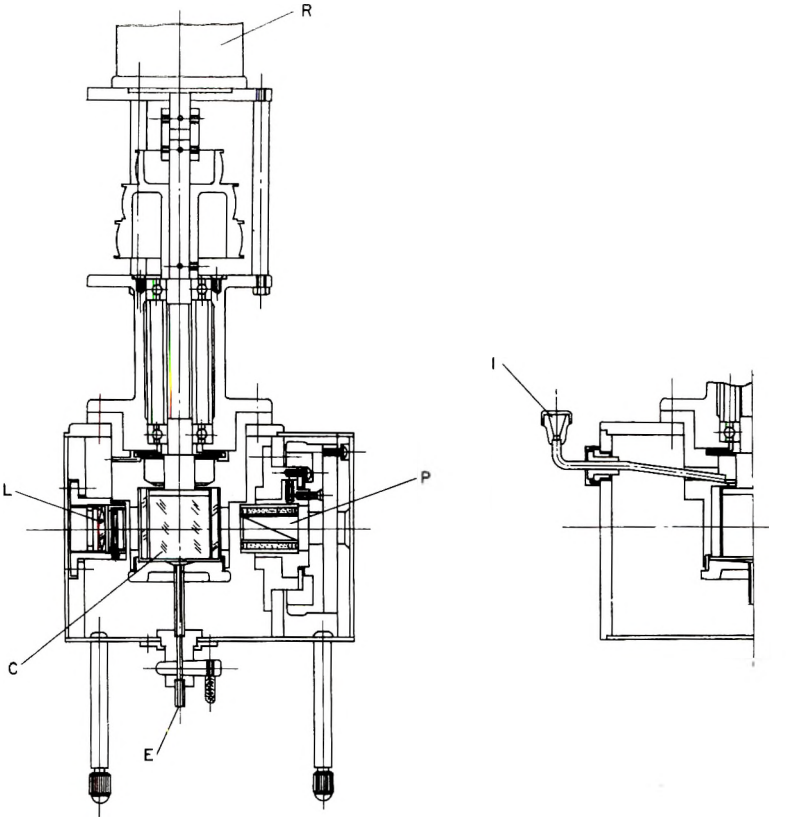

Fig. 3. A cross section of the concentric cylinder apparatus: (L) collimating lens; (C) inner cylinder; (P) polarizer.

transparent adhesive. It can pass the light of wavelengths below 220 mμ. The direction of the electric vector of the plane-polarized light can be changed either to vertical or horizontal plane by a rotating handle.

The cross section of the rotating cell is shown in Figure 3. The inner and the outer cylinders of the cell are both made of fused quartz which is transparent both in visible and ultraviolet region. The outside and inside diameters of the outer cylinder are 40 and 30 mm., respectively. The gap between the outer and inner cylinder is 0.7 mm. The sample solution needed is about 2.6 ml.

The rotation of the inner cylinder of the cell is produced by a variable speed motor. The revolution of the inner cylinder, which can be changed from 0 to about 1500 rpm, that is, 0 to about 4500 sec.$^{-1}$ in velocity gradient, can be measured by an electric tachometer, R, which is directly connected to the axis of the inner cylinder. Eccentricity of the rotating mechanism is less than $^{2}/_{100}$ mm. and the vibration which gives an undesirable influence on a measurement is very small. This is achieved by using ball bearings for the mechanism and by rotating the axis by a pully and a

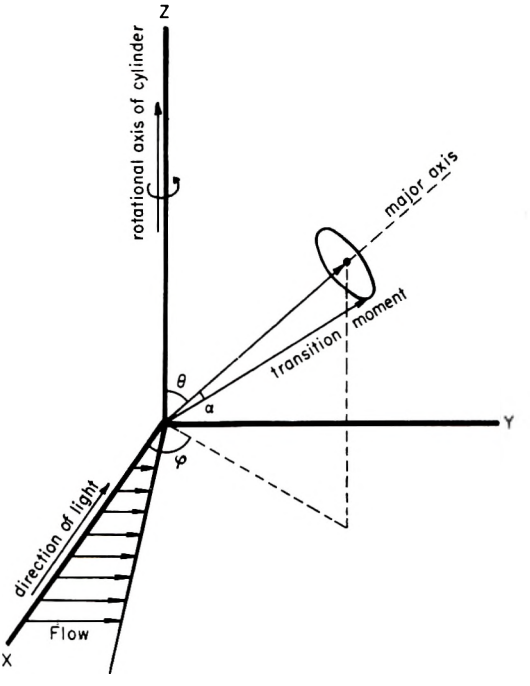

Fig. 4. Diagram of the coordinate system showing the direction of flow, major axis of ellipsoid, and transition moment.

rubber belt from the motor which is set apart from the apparatus. The reason why we used such direction of the optical beam in the optical system mentioned above is as follows. There are several ways to observe flow dichroism of solution by taking different direction of the incident light beam to the flow line, namely, the dichroism can be observed by incident light of either x- or z-direction for a lamellar flow in the y-direction having a velocity gradient in the x-direction as shown in Figure 4. The present apparatus has the light beam in the x-direction rather than in the z-direction, because (*1*) it is possible to use an incident beam of large cross section, (*2*) the undesirable reflections at the cylindrical cell surface are absent, (*3*) the length of liquid in the light beam is constant even if there is a small eccentricity in the rotating mechanism, and (*4*) there is a moderate path length for the measurement of ultraviolet and visible region. In addition, the direction of the electric vector of the incident polarized light must be matched with the axis of double refraction in the measurement of dichroism. If the measurement is done with the incident beam of z-direction, the direction of the axis of double refraction will depend upon the hydrodynamic shape of the molecule and the velocity gradient, but it should be fixed independently of the velocity gradient in the y- and z-direction when an incident beam parallel to the x-direction is used. Of course, the former way will permit measurement of the extinction angle just as the measurement of flow birefringence has been done, but is not neces-

sary otherwise and may be troublesome in the measurement of the dichroism.

III. MEASUREMENT OF DIFFERENTIAL DICHROISM

The apparatus is designed to measure the differential dichroism by which device the small change in dichroic ratio can easily be detected. The measurement of dichroic ratio in the usual sense is also possible by this apparatus.

By referring to the well-known Lambert-law of absorption separately for the plane-polarized light with the electric vector in y- and z-axis, respectively, we have

$$I_y(\lambda,G) = I_{y_0}(\lambda) \exp \{-\epsilon_y(\lambda,G)lc\} \tag{1a}$$

$$I_z(\lambda,G) = I_{z_0}(\lambda) \exp (-\epsilon_z(\lambda,G)lc) \tag{1b}$$

where I_0 and I are the incident and transmitted light intensities, respectively, l is thickness of solution in the light path, c is the concentration of the solution in units of moles/1000 ml. unit, and $\epsilon_y(\lambda,G)$ and $\epsilon_z(\lambda,G)$ are molar extinction coefficient for the different polarizations. The ϵ_y and ϵ_z are functions of velocity gradient G and wavelength λ. These directions, y and z, are parallel and perpendicular with the flow line, respectively, so it may be convenient to rewrite $\epsilon_y = \epsilon_\parallel$, and $\epsilon_z = \epsilon_\perp$. The $\epsilon_\parallel$ and $\epsilon_\perp$ are related to the molar extinction coefficient, ϵ by

$$\epsilon = (\epsilon_\parallel + 2\epsilon_\perp)/3 \tag{2}$$

and

$$\lim_{G\to 0} \epsilon_\parallel = \lim_{G\to 0} \epsilon_\perp = \epsilon \tag{3}$$

If the molecule has only one origin of absorption, $\epsilon_\parallel$, $\epsilon_\perp$, and ϵ will show the same dependence on the wavelength λ, and will not otherwise. This is useful sometimes to separate and assign the absorption bands overlapping each other. Several examples of such use will appear in a subsequent report.

The differential method is the direct measurement of ratios (I_z/I_y), that is, from eqs. (1a) and (1b),

$$(I_z/I_y) = (I_{z_0}/I_{y_0}) \exp \{(\epsilon_\parallel - \epsilon_\perp)lc\} \tag{4}$$

After measuring the ratios in solvent, (I_{z_0}/I_{y_0}), in which usually no dichroism is observed, the differential dichroism spectrum can be given by taking logarithms of eq. (4) as follows:

$$\Delta\epsilon = \epsilon_\parallel - \epsilon_\perp = \log(I_z/I_{z_0})/(I_y/I_{y^0})/lc \tag{5}$$

$\epsilon_{\parallel}$, $\epsilon_{\perp}$ and the dichroic ratio, D, can be derived, if necessary, in terms of $\Delta\epsilon$ and ϵ:

$$\begin{aligned} \epsilon_{\parallel} &= (3\epsilon + 2\Delta\epsilon)/3 \\ \epsilon_{\perp} &= (3\epsilon - \Delta\epsilon)/3 \\ D &= (3 + 2\mathrm{R})/(3 - \mathrm{R}) \end{aligned}$$

where $\mathrm{R} = \Delta\epsilon/\epsilon$.

IV. RELATION BETWEEN $\epsilon_{\parallel}$, $\epsilon_{\perp}$, AND THE INTERNAL ORIENTATION OF CHROMOPHORES

The dichroism is dependent upon the average orientation of chromophores in a coordinate system referred to the incident light and direction of the flow. So, it may be better here to express $\epsilon_{\parallel}$ and $\epsilon_{\perp}$ in terms of the internal coordinates of chromophores in a macromolecule, and of the external coordinates of that macromolecule in the system fixed on the optical and flow system, separately. The latter coordinate, that is, the average orientation angle of the macromolecule, is easily obtained after getting the so-called orientation factor $f(\theta,\varphi)$, such that the fraction of the major axis between θ and $\theta + d\theta$, and φ and $\varphi + d\varphi$, is $f(\theta,\varphi) \sin\theta\, d\theta\, d\varphi$, as follows.

Let us consider the macromolecule as a hydrodynamically equivalent ellipsoid of revolution, and a vector of the electronic transition of a chromophore, which is responsible for the absorption spectrum, has an angle α with its major axis (Fig. 4). The angular distribution function $f(\theta,\varphi)$, the orientation factor of the major axis, can be given by angles of θ and φ in a polar coordinate system as the function of the velocity gradient G sec.$^{-1}$ and some numerical factor defining the molecular shape such as axial ratio ρ.

Putting the **i**, **j**, and **k** as the unit vectors of the major axis and of two minor axes of the ellipsoid of revolution, the anisotropic tensor of absorption, **G**, can be written,

$$\mathbf{G} = \epsilon_{\parallel_0}\mathbf{ii} + \epsilon_{\perp_0}(\mathbf{jj} + \mathbf{kk}) = \epsilon_{\perp_0}\mathbf{I} + (\epsilon_{\parallel_0} - \epsilon_{\perp_0})\mathbf{T} \tag{7}$$

where

$$\mathbf{T} = \begin{bmatrix} \sin^2\theta\cos^2\varphi & \sin^2\theta\sin\varphi\cos\varphi & \sin\epsilon\cos\theta\cos\varphi \\ \sin^2\theta\sin\varphi\cos\varphi & \sin^2\theta\sin^2\varphi & \sin\theta\cos\theta\sin\varphi \\ \sin\theta\cos\theta\cos\varphi & \sin\theta\cos\theta\sin\varphi & \cos^2\theta \end{bmatrix}$$

I = unit tensor and $\epsilon_{\parallel_0}$ and $\epsilon_{\perp_0}$ are the absorption coefficients in the direction of the major and minor axis, respectively. These coefficients can be expressed by the given angle α and the maximum absorption coefficients ϵ_0, which is the absorption coefficient for the incident light with the electric vector is coincident with the direction of the transition moment of chromophores;

$$\begin{aligned} \epsilon_{\parallel_0} &= \epsilon_0\cos^2\alpha \\ \epsilon_{\perp_0} &= (\epsilon_0/2)\sin^2\alpha \end{aligned} \tag{8}$$

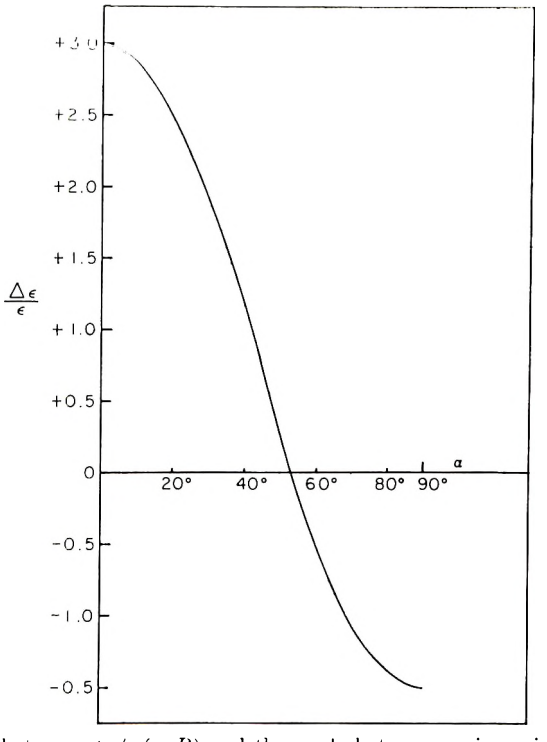

Fig. 5. Relation between $\Delta\epsilon/\epsilon$ ($= R$) and the angle between major axis and transition moment, α.

After averaging the tensor $\mathbf{T}$ by $\mathbf{f}(\theta,\varphi)$

$$\bar{\mathbf{T}} = (1/2)\begin{bmatrix} K_1 + K_3 & K_3 & 0 \\ K_3 & K_1 - K_2 & 0 \\ 0 & 0 & 2 - 2K_1 \end{bmatrix} \tag{9}$$

where

$$K_1 = \int\int \sin^2\theta f(\theta,\varphi)d\Omega \tag{9a}$$

$$K_2 = \int\int \sin^2\theta \cos 2\theta\, f(\theta,\varphi)d\Omega \tag{9b}$$

$$K_3 = \int\int \sin^2\theta \sin 2\theta\, f(\theta,\varphi)d\Omega \tag{9c}$$

the absorption coefficient for the incident light of the electric vector $\mathbf{E}_s$,) (where $s = x, y,$ or z) can be given as follows;

$$\epsilon_s = \mathbf{E}_s\mathbf{G}\mathbf{E}_s \tag{10}$$

And finally, from eqs. (2) and (8)–(10), $\Delta\epsilon$ is given,

$$\Delta\epsilon = \epsilon_y - \epsilon_z = (\epsilon_0/4)(3K_1 - K_2 - 2)(3\cos^2\alpha - 1) \tag{11a}$$

or

$$\Delta\epsilon/\epsilon = (3/4)(3K_1 - K_2 - 2)(3\cos^2\alpha - 1). \tag{11b}$$

when G becomes zero, that is the case of random orientation of the macromolecule, $K_1 = {}^2/_3$, $K_2 = 0$, and $\Delta\epsilon/\epsilon = 0$: On the other hand, when $G \rightarrow \infty$ that is, the case of perfect orientation, $K_1 = 1$, $K_2 = -1$, and $\Delta\epsilon/\epsilon = ({}^3/_2)(3\cos^2\alpha - 1)$. In the latter case, the perfect orientation, the dichroism comes only from the internal factor and the angle α can be given from the measured $\Delta\epsilon/\epsilon$ as shown in Figure 5.

In general, the differential dichroic spectrum of a rigid macromolecule having n origins of absorption is given by eq. (12):*

$$\Delta\epsilon = ({}^3/_4)(3K_1 - K_2 - 2)\sum_{i=1}^{n}\epsilon_i(3\cos^2\alpha_i - 1)/n \qquad (12)$$

K_1, K_2, and K_3 can be expanded as a power series in R, a geometrical parameter related to the axial ratio

$$K_1 = {}^2/_3 - (4\pi/15)\sum_i a_{10i}R^i$$

$$K_2 = (16\pi/5)\sum_i a_{11i}R^i$$

$$K_3 = (16\pi/5)\sum_i b_{11i}R^i$$

$$R = (\rho^2 - 1)/(\rho^2 + 1)$$

where $a_{n,m,i}$ and $b_{n,m,i}$ are coefficients which are functions only of a reduced gradient, G/Θ, the ratio of the velocity gradient in sec.$^{-1}$ to the rotatory diffusion constant of the ellipsoid, Θ.[9]

V. EXPERIMENTAL RESULTS AS AN EXAMPLE

1. Water

Distilled water exhibits a slight dichroic behavior though negligibly small, as shown in Figure 6 where $I_\parallel/I_\perp$ measured at the velocity gradient $G = 4500$ sec.$^{-1}$ is compared with that measured at G = 0. It is still not clear whether this dichroism originates in the water itself or came from some mechanical distortion of the apparatus.

2. Deoxyribonucleic Acid (DNA)

Deoxyribonucleic acid, prepared from calf thymus, in water solution of no added salt shows dichroism as shown in Figure 7. The relation between $\Delta\epsilon/\epsilon$ and the velocity gradient is shown in Figure 8. Although the perpendicular absorption is larger than the parallel absorption as could be expected, the $\Delta\epsilon/\epsilon$ of this DNA ($= 0.13$) is rather smaller than that expected from the ideal case of the Watson-Crick model, in which the planes of purine and pyrimidine bases are almost perpendicular to the helical axis. The result obtained here is, however, of just the same order as Cavalieli's[2]

* A similar calculation for the subject taken in section IV has been done by several authors.[7,8]

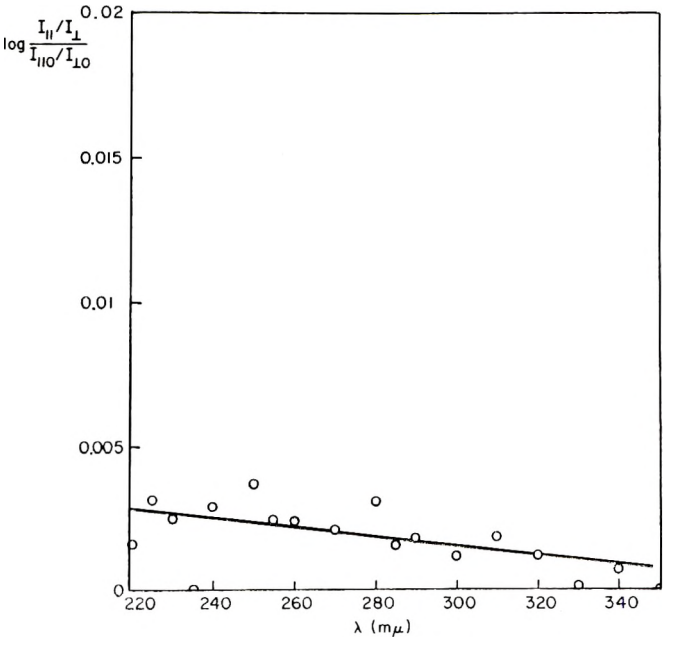

Fig. 6. Logarithmic plot of ratios of $I_{II}/I_{\perp}$ measured at $G = 0$ and $G = 4200$ sec.$^{-1}$ in water.

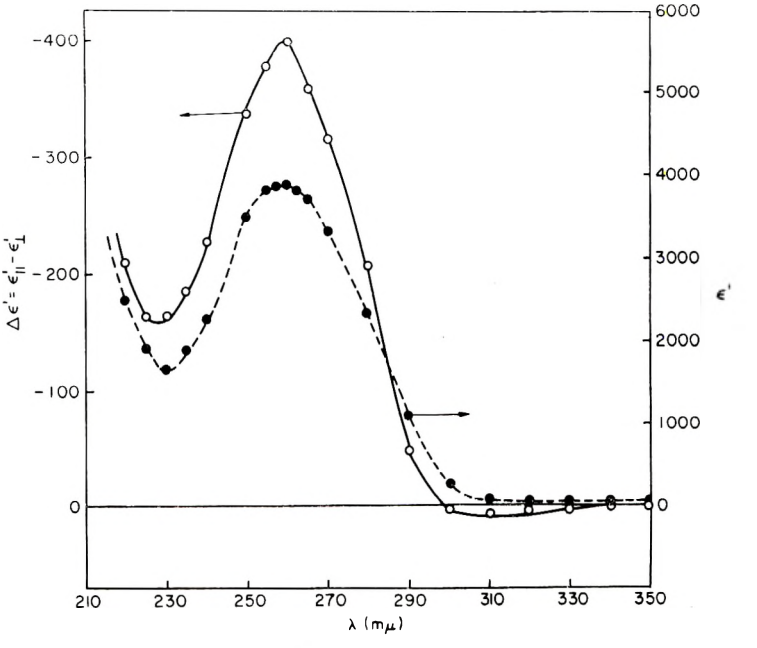

Fig. 7. Plots of (●) $\Delta\epsilon'$ and (○) ϵ' of calf thymus DNA in aqueous solution against wavelength at $G = 2300$ sec.$^{-1}$. Both $\Delta\epsilon'$ and ϵ' are calculated using the residual concentration, so the units of these are residues/l.

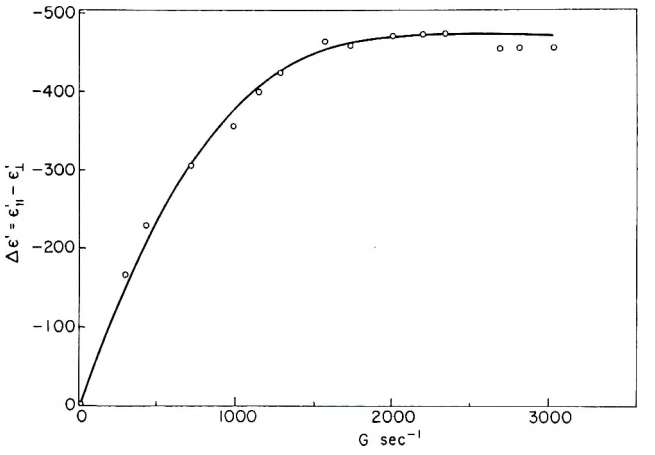

Fig. 8. Velocity-gradient dependence of $\Delta\epsilon'$ of calf thymus DNA in aqueous solution (concn. = 1.28×10^{-3} residues/l.) measured at 260 mμ.

result for the calf thymus DNA. Recent measurements of $\Delta\epsilon/\epsilon$ for the DNA from *Diplococcus pneumoniae* and that from T_2-phage have given the results $\Delta\epsilon/\epsilon = 0.24$ and $\Delta\epsilon/\epsilon = 0.80$, respectively. The results, at the same salt concentration, are quite reproducible for DNAs from the same species by different preparations. This might be one of the typical examples showing the usefulness of this method for studies of the chain regularity of biological polymers. A detailed description of this subject will be reported elsewhere.[10]

3. Globular and Fibrous Actin

Globular (G) and fibrous (F) actin are good examples for demonstrating the merit of this apparatus.* The G-actin is known to be reversibly converted to F-actin, in the so-called F–G transition. Both of these forms give almost the same curve in the ultraviolet region, as shown by the broken lines in Figures 9*a* and 9*b*. The differential dichroic spectrum, however, gives an entirely different picture for G- and F-actin as plotted by the solid lines in these figures. G-actin shows no dichroism at all over the whole region of wavelength measured. A nice contrast is the case of F-actin, which shows negative dichroism in the region of 250–270 mμ, and positive dichroism in the region of 270–295 mμ. Leaving detailed discussion to the forthcoming report,[11] it must be mentioned that the direction of the absorption of adenine base and several aromatic amino acid groups in F-actin should be different, as the former is perpendicular and the latter is parallel with the flow line.

* The dichroic measurements on G- and F-actin described here are a part of the joint research of Dr. Fumio Oosawa and present authors. A detailed report on this subject will appear soon.[11] We wish to thank Dr. Fumio Oosawa for permission to reproduce Figures 9*a* and 9*b*.

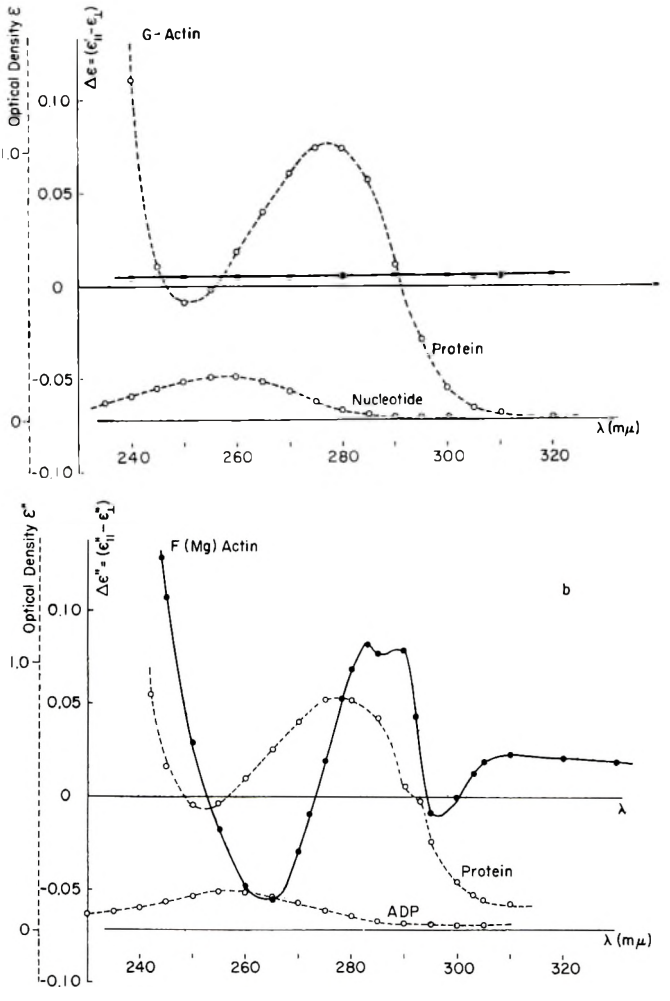

Fig. 9a. Plots of (●) $\Delta\epsilon''$ and (○) ϵ'' of (*a*) G-actin in aqueous solution (protein concn. = 0.78 mg./ml.); (*b*) F-actin in aqueous solution (protein concn. = 0.69 mg./ml.). ϵ'' is optical density and $\Delta\epsilon''$ is corresponding dichroism for l = 10.0 mm.

We wish to thank Miss Norie Kojima for carrying out the measurement of dichroic and absorption spectrum reported here.

References

1. Butenandt, A., H. Friedrich-Freska, S. Hartwig, and G. Scheibe, *Z. Physiol. Chem.*, **274**, 276 (1942).

2. Cavalieli, L. F., M. Rosoff, and B. H. Rosenberg, *J. Am. Chem. Soc.*, **78**, 5235 (1956).

3. Bird, G. R., M. Parrish, and E. R. Blout, *Rev. Sci. Instr.*, **29**, 305 (1958).

4. Rundle, R. F., and R. R. Baldwin, *J. Am. Chem. Soc.*, **65**, 554 (1943).

5. Zucker, D., J. F. Foster, and G. H. Miller, *J. Phys. Chem.*, **56**, 166 (1952).

6. Foster, J. F., and D. Zucker, *J. Phys. Chem.*, **56**, 170 (1952).

7. Fraser, R. D. B., *J. Chem. Phys.*, **21**, 1511 (1953); *ibid.*, **24**, 89 (1956).

8. Bird, G. R., *J. Chem. Phys.*, **28**, 1155 (1958).
9. Peterlin, A., *Z. Physik*, **111**, 232 (1938): A Peterlin and H. A. Stuart, *Z. Physik*, **112**, 1, 129 (1939).
10. Wada, A., *J. Mol. Biol.*, unpublished results.
11. Oosawa, F., S. Higashi, M. Kasai, and A. Wada, *J. Mol. Biol.*, **7** (1963).

Résumé

On décrit en détail un appareil cylindrique et concentrique destiné à l'étude du dichroïsme d'écoulement des polymères en solution. Les cylindres intérieur et extérieur sont tous les deux en quartz fondu transparent dans le visible et dans l'ultraviolet jusqu'à une région inférieure à 220 mμ. Le gradient de vitesses est produit en solution dans l'espace séparant les deux cylindres par rotation du cylindre intérieur. Le chemin optique est placé perpendiculairement à l'axe de rotation du cylindre en quartz. Un dispositif différentiel rend possible la mesure des différences des coefficients d'absorption $\epsilon_\parallel$ et $\epsilon_\perp$ qui sont les coefficients d'absorption mesurée en lumière polarisée plane ayant un vecteur parallèle et perpendiculaire aux lignes d'écoulement. Cet appareil est utilisable pour l'étude de la régularité d'orientation des chromophores dans les chaines polymériques synthétique et biologique.

Zusammenfassung

Ein auf dem Prinzip der konzentrischen Zylinder beruhender Apparat zur Untersuchung des Strömungsdichroismus von Polymerlösungen wird eingehend beschrieben. Äusserer und innerer Zylinder bestehen aus geschmolzenem Quarz, der im sichtbaren und ultravioletten Bereich bis zu 220 mμ durchlässig ist. Der Geschwindigkeitsgradient wird in Lösung im Zwischenraum zwischen den Zylindern durch Rotation des inneren Zylinders erzeugt. Der Lichtweg verläuft senkrecht zur Rotationsachse des Quarzzylinders. Eine Differentialeinrichtung ermöglicht die Messung des Unterschiedes der Absorptionskoeffizienteu, $\epsilon_\parallel$ und $\epsilon_\perp$, für linear polarisiertes Licht mit elektrischem Vektor parallel bzw. senkrecht zu den Strömungslinien. Der Apparat ist zur Untersuchung der Orientierungsregelmässigkeit von Chromophoren in synthetischen und biologischen Kettenpolymeren geeignet.

Received December 20, 1962

JOURNAL OF POLYMER SCIENCE: PART A VOL. 2, PP. 865–880 (1964)

Electroinitiated Anionic Polymerization of Acrylonitrile*

B. LIONEL FUNT and FREDRICK D. WILLIAMS,† *Parker Chemistry Laboratory, Department of Chemistry, University of Manitoba, Winnipeg, Canada*

Synopsis

Polymer was formed by an electrolytically initiated reaction in solutions of acrylonitrile and other monomers in dimethylformamide saturated with sodium nitrate. From analysis of copolymer compositions it was established that the polymer was formed at the cathode by an anionic propagation mechanism. The nature of the chain initiating step was investigated through polarographic measurements. These clearly suggest that chain initiation proceeds via direct electron addition to the double bond. A close correlation between the tendency to form anionic polymer and the polarographic potentials is indicated. The effects of current, time, and monomer concentration on the production of polymer were delineated. The yield of polymer increased linearly with time at fixed current density and showed first order dependence on monomer concentration. The absolute current efficiencies were extremely high and ranged to over 3 polymer molecules formed per electron transferred at the electrode. The molecular weights of the polymers are remarkably independent of monomer concentration, rate, and current density. A reaction scheme is proposed which postulates chain transfer to monomer. A kinetic analysis confirms the consistence of the scheme with experimental findings. Coloration and crosslinking found in some of the polymers are interpreted, and a mechanism is proposed.

Polymerization of various monomers can be electrically activated in a homogeneous organic medium. We have recently reported the free-radical polymerization of methyl methacrylate initiated by the electrolytic discharge of acetate ions at the anode.[1] In this paper we report our investigations of ionic polymerizations initiated electrically. In all of this work we have been impressed with the additional control of the polymerization process that is associated with electroinitiated polymerization. The production of initiating species is directly influenced by the current, which in turn can be easily measured, controlled, or programmed.

The cationic polymerization of styrene resulting from the anodic discharge of BF_4^- was reported by Breitenbach.[2] The polymerization

* Based on a Ph.D. thesis submitted by F. D. Williams in September 1962 to the University of Manitoba. Presented at the 11th Canadian High Polymer Forum in Windsor, Ontario, September 1962.

† Present address: Istituto di Chimica Industriale del Politecnico di Milano, Milan, Italy.

reported by Yang and McEwen[3] and Murphy et al.[4] were both probably ionic in character. Similarly the polymerization of acrylonitrile initiated by cathodic discharge of tetraethylammonium perchlorate, originally assumed to be free radical,[5] was later shown to be anionic in character.[2]

EXPERIMENTAL

Materials

Monomeric acrylonitrile (AcN) (Eastman Organic Chemicals) was fractionally distilled at reduced pressure and the middle portion stored over $CaSO_4$ and BaO for several days before redistillation.

Methyl methacrylate (MMA) was freed of phenolic inhibitors by repeated washings with 5% NaOH solutions containing NaCl. After mixing with distilled water, the monomer was dried over $CaSO_4$ for 24 hr. and then fractionally distilled at reduced pressures.

N,*N*-Dimethylformamide (DMF) (Matheson, Coleman and Bell) was purified by fractional distillation, stored over $CaSO_4$ and BaO for several days, and redistilled before use.

Polarographic grade tetramethylammonium iodide (TMAI) (Southwestern Analytical Chemicals) was used without further purification.

Polymerizations

Polymerizations were initiated electrochemically in cells which had two basic designs. For reactions which require the anode and cathode polymer to be analyzed individually, a cell separated by a sintered glass disk of medium porosity was employed. Circular platinum electrodes of diameter 2.5 cm. were sealed into the glass as close as possible to the glass disk in order that the IR drop be a minimum. The total volume of the cell was approximately 80 ml.

Reaction cells used in all kinetic runs had a total volume of approximately 150 ml. and were cylindrical in shape with side arms for the admission of nitrogen and the withdrawal of samples. The platinum electrodes had a surface area of 1 in.^{2} and were sealed into a removable top of the cell.

The cell and electrodes were dried and flamed before each polymerization.

RESULTS

Locus and Type of Polymerization

Before the reaction mechanism can be understood it is necessary to determine the electrode at which polymer is formed and whether an ionic or radical type of polymerization is taking place.

From Table I it is evident that with acrylonitrile, polymerization is primarily at the cathode and that with other monomers the relative yields at the electrodes parallel the tendencies to anionic polymerization.[6]

TABLE I
Relative Amounts of Anode and Cathode Polymer Formed by Electrolysis in Divided Cells

Monomer	Monomer concn. in DMF, mole-%	Weight cathode polymer, g.	Weight anode polymer, g.
Styrene	25.2	2.583	1.067
Methyl methacrylate	26.8	9.509	1.765
Acrylonitrile	37.0	12.102	<0.200
Vinyl acetate	29.4	No polymerization	

The propagation mechanism can be determined conveniently from analysis of copolymer compositions. When an equimolar mixture of acrylonitrile and methyl methacrylate is polymerized by a free radical mechanism the resulting polymer contains both species in approximately equal amounts. If anionically polymerized, however, the mixture will contain predominantly acrylonitrile,[6,7] whereas if it is cationically initiated, polymer will not form readily.[8]

Mixtures containing 54.1 wt.-% methyl methacrylate and 45.9 wt.-% acrylonitrile were copolymerized in dimethyl-formamide solutions saturated with the salt under investigation.

TABLE II
Analysis of Copolymers from MMA–AcN Feed in DMF Saturated with Various Salts

Salt	N, wt.-%	AcN in copolymer, %
$LiNO_3$	21.5	74.3
$KClO_4$	24.5	92.6
$KC_2H_3O_2$	23.4	88.4
$SrCl_2$	16.9	58.0
NaCl	22.4	84.9
$NaNO_3$	30.7	100
$MgCl_2$	23.1	78.3
$ZnCl_2$	24.9	94.3
$Zn(NO_3)$	25.3	95.7
$TlNO_3$	21.8	82.5
$CoCl_2$	17.3	65.3
$CuSO_4$	13.4	50.8

The analysis for acrylonitrile content was based on Kjeldahl nitrogen determinations of the copolymers formed with methyl methacrylate. Although the data are considered preliminary in character they are of qualitative interest and are tabulated in Table II. For completely anionic polymerization the polymer is calculated to be over 98% AcN. The analyses indicate the simultaneous occurrence of free radical and ionic polymerization at the same electrode in some systems, but a pattern of

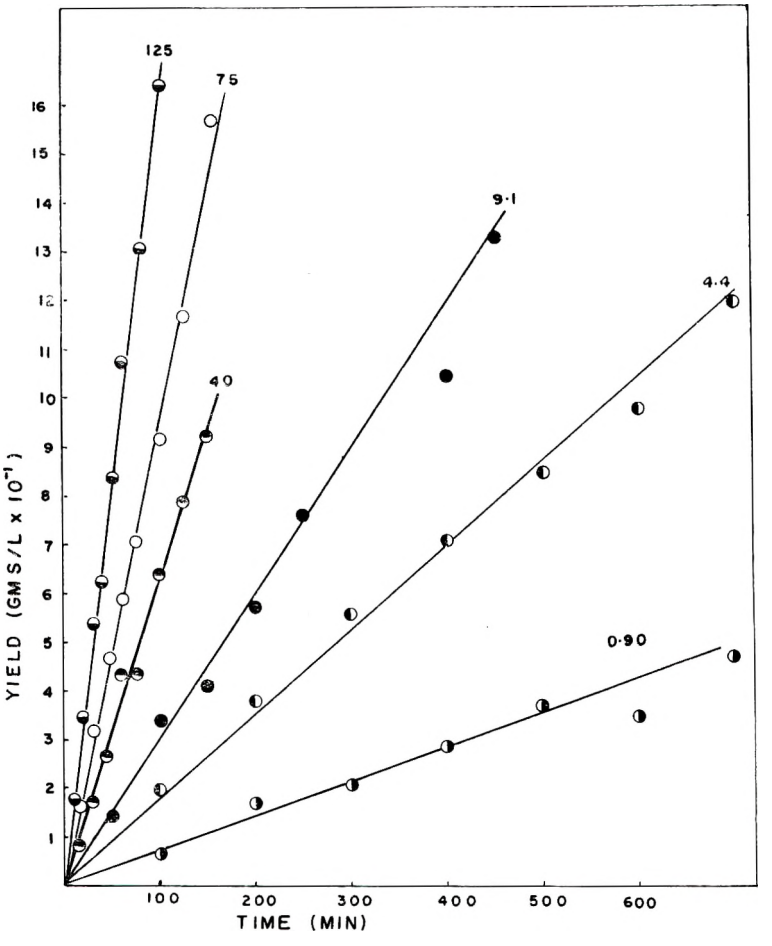

Fig. 1. Formation of polymer as a function of inscribed current (ma.) and time.

correlation must await a more intensive study of this aspect of the polymerization.

For the remainder of this work DMF saturated with $NaNO_3$ and containing 37 mole-% AcN was used. This system was chosen on the basis of the lack of concurrent anodic polymerization, and for its completely anionic character at the cathode, as determined by triplicate analyses of the copolymer.

In this system the degree of conversion per unit volume increased linearly with time at various current densities, as shown in Figure 1.

In these experiments the cell initially contained 100 ml. of the monomer solution thermostatted at 30.0°C. At fixed intervals during the reaction 5-ml. samples were withdrawn for analysis of their polymer content.

At a constant current the rate of initiation per unit volume will be a function of the total volume. If there are initially n_0 moles of monomer

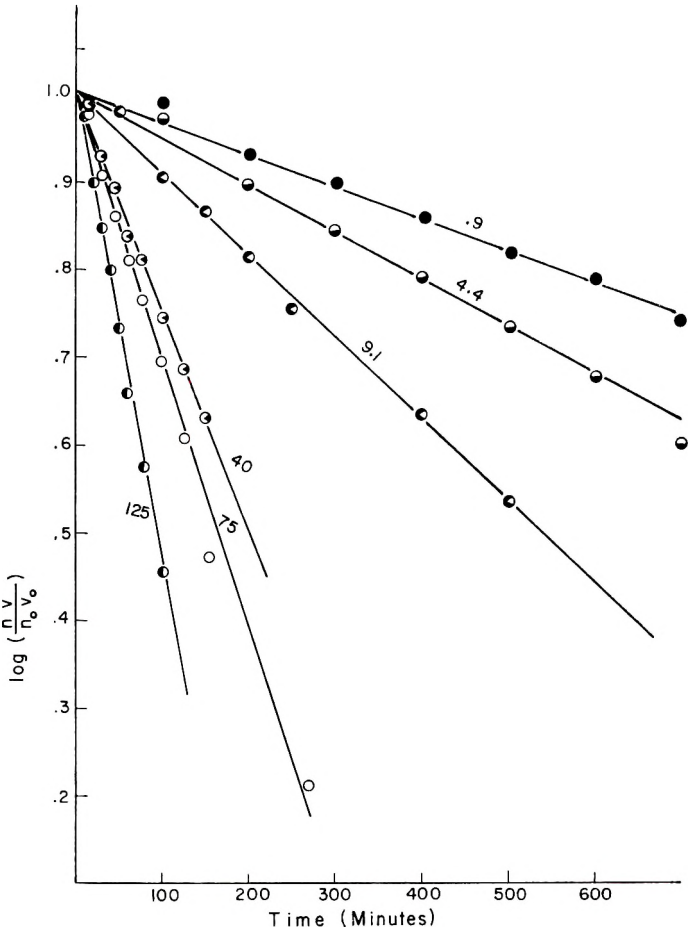

Fig. 2. Dependence of logarithm of monomer concentration (log nv) on time.

per milliliter, then the total monomer content is n_0v_0, where v_0 is the initial volume. If N is the total number of moles, and I the current then

$$-dN/dt = kIN$$

Then

$$[\ln N]\frac{n_1v_1}{n_0v_0} = k(t_0 - t_1)$$

If we sum the integrals for successive intervals corresponding to n_1v_1 $n_2v_2, \ldots, n_nv_n$, we have

$$\ln\left[\frac{n_0v_0}{n_1v_1}\frac{n_1v_1}{n_2v_2}\cdots\frac{n_{n-1}v_{n-1}}{n_nv_n}\right] = k[(t_0 - t_1) + (t_1 - t_2) + \ldots + (t_{n-1} - t_n)]$$

Hence:

$$\ln\left(\frac{n_0v_0}{n_nv_n}\right) = k(t_0 - t_n)$$

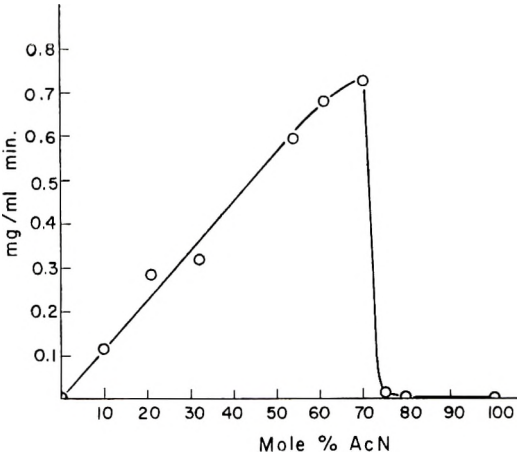

Fig. 3. Influence of monomer concentration on the initial rate of polymerization at a steady current of 15 ma.

Thus the logarithm of the product of the monomer concentration ratio and the volume ratio is expected to be linear with time for a first-order reaction under these experimental conditions.

The data are plotted in Figure 2 and good linearity is observed. Although a cursory examination of the data of Figure 1 could suggest a zero-order dependence, it is seen that first-order dependence on monomer concentration is indeed obtained.

TABLE III

Influence of Current and Monomer Concentration on Initial Rate of Formation and Molecular Weight in the System AcN in DMF at 30.0°C.

Current, ma.	Initial monomer concn., mole-%	Rate, mg./ml. min.	Intrinsic viscosity, dl./g.
0.90	37.0	0.076	0.059
4.4	37.0	0.174	0.053
9.1	37.0	0.303	0.054
15	37.0	0.343	0.052
40	37.0	0.618	0.055
75	37.0	0.954	0.054
125	37.0	1.620	0.050
15	12.4	0.101	0.054
15	20.8	0.194	0.051
15	32.0	0.317	0.050
15	54.0	0.606	0.053
15	62.3	0.704	0.051
15	70.0	0.729	0.053
15	75.1	0.157	0.055
15	79.5	0.065	0.155
15	100.0	0.000	—

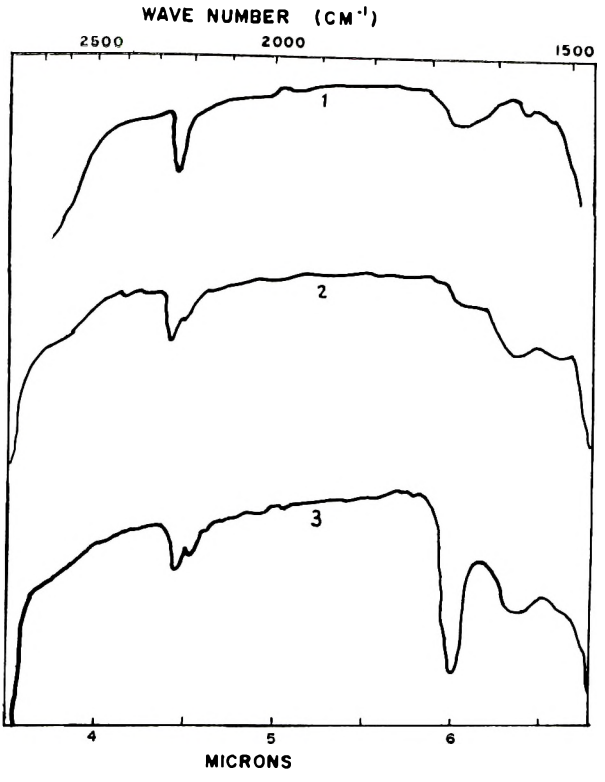

Fig. 4. Infrared spectra of (*1*) colorless polyacrylonitrile; (*2*) soluble cathodic polymer; (*3*) insoluble cathodic polymer.

This aspect of the kinetics was confirmed by the results of experiments performed at a fixed current, but at various initial monomer concentrations. The influence of monomer concentration on the initial rate of the reaction is shown in Figure 3 and on the molecular weight in Table III. The initial rate of reaction per unit volume is proportional to the initial monomer concentration at a fixed current, in accord with expectations for first-order kinetics. The sharp drop in rate at high initial monomer concentrations is perhaps related to a drop in degree of ionization at these concentrations.

The influence of current on the reactions is also tabulated in Table III. Although the rate increases with current the results are ambiguous and apparently show a drift from half-order to first-order dependence with increasing current density. This is probably associated with diffusion of active species but the details of this process have not as yet been elucidated.

The intrinsic viscosities were remarkably independent of both current and monomer content over a wide range of values as shown in Table III. This contrasts with the definite and regular dependence reported for our electroinitiated reactions which proceeded by a free-radical mechanism.[1] However, Zilkha's anionic polymerizations,[15] which were not electrically

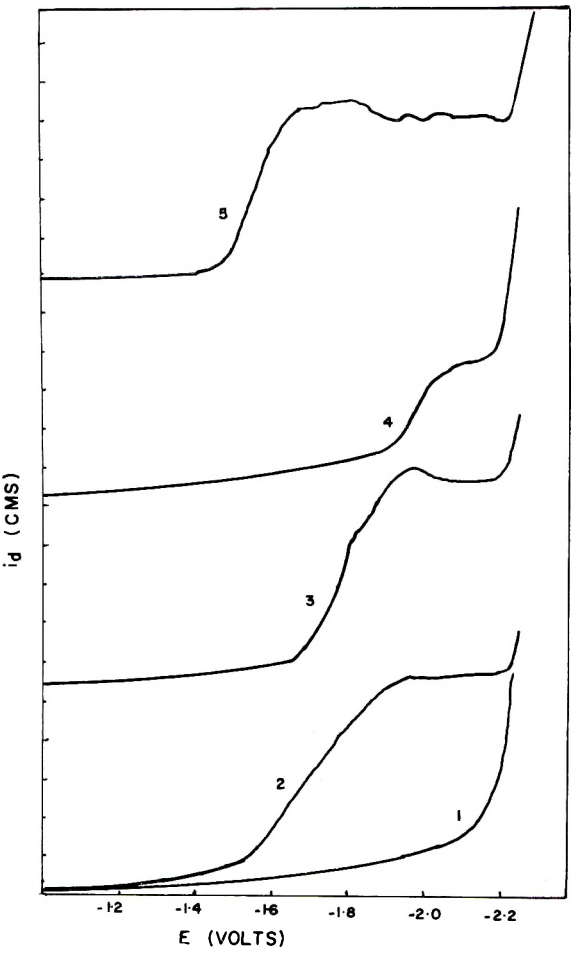

Fig. 5. Diffusion current using a mercury anode for (*1*) vinyl acetate; (*2*) acrylonitrile; (*3*) methyl methacrylate; (*4*) styrene; (*5*) sodium nitrate.

initiated, also showed independence of monomer concentration and yielded molecular weights quite comparable to ours.

The physical appearance of the polymers merits some comment. Polyacrylonitrile samples from the anode and cathode compartments of a divided reaction cell could be distinguished. The anode material was colorless in the reaction solution and precipitated as a white polymer. At the cathode however, the solution was dark orange and the polymer, when precipitated, exhibited various shades of yellow. Moreover, small amounts of insoluble polyacrylonitrile were formed on the cathode and were darker yellow than the soluble polymer.

Infrared spectra of cathodic and anodic polymer are shown in Figure 4, and their significance will be discussed below.

X-ray analysis did not indicate stereoregularity in the polymer.

Polarographic measurements were used to elucidate the mechanism of the electroinitiation. Figure 5 illustrates the distinct waves obtained. These are remarkably similar to those from reductions of unsaturated hydrocarbons[9-11] and lead us to the interpretation that they indicate direct electron addition to the double bond.

The half-wave potentials of the monomer and a number of salts are listed in Table IV.

TABLE IV
Half-Wave Potentials in DMF Saturated with TMAI

Compound	$E_{1/2}$ vs. Hg pool, v.	Polymer formation in DMF–AcN
Acrylonitrile	−1.69	—
$LiNO_3$	−1.95	yes
$KClO_4$	−1.58	yes
$NaNO_3$	−1.55	yes
NaCl	−1.57	yes
$MgCl_2$	−1.90	yes
$Zn(NO_3)_2$	−0.55	no
$CoCl_2$	−0.64	no
$SnCl_2$	+0.21	no

DISCUSSION

Initiation

Values of n from the general polarographic equation[12] indicate that the initiation step is irreversible for acrylonitrile but is reversible for styrene and methyl methacrylate. Our determination of $n = 0.32$ for acrylonitrile is in good agreement with values between 0.36 and 0.18 recently reported.[4] The distinct character of the polarographic waves supports the view that the initiation step involves direct electron addition to the double bond of the monomer.

An inspection of Table IV indicates that no polymer formed when the half-wave potential of the cation was less negative than −1.55 v. It appears, therefore, that when the reduction potential is sufficiently low, the inorganic cations will be discharged to the exclusion of electron addition to the double bond. At higher negative potentials there will be competition for electrons from the double bonds resulting in the activation and subsequent polymerization of the monomer.

Similarly, the polarographic potentials define the tendency of a monomer to undergo initiation in a particular system. Thus it was found that for the monomers acrylonitrile, methyl methacrylate, and styrene the corresponding half-wave potentials were −1.69, −1.79, and −1.99 v., respectively. With vinyl acetate no wave was obtained. From Table I it is seen that the formation of anionic polymer at the cathode followed in the same order as the polarographic potentials.

Qualitative confirmation of the view that initiation is due to a direct electron transfer independent of cations present in solution has been obtained. Electrolysis of acrylonitrile solutions in DMF and dimethyl sulfoxide in the absence of salts still produced polymer at the cathode.

Direct electron addition to monomer is the initiation mechanism postulated by Szwarc for anionic polymerization through adducts of sodium metal with aromatic hydrocarbons. The present work furnishes direct support for this postulate.

The initiation step probably produces a radical ion of the type:

$$\cdot CH_2\overset{\overset{H}{|}}{\underset{\underset{R}{|}}{C}}:^- \longleftrightarrow {}^-:CH_2\overset{\overset{H}{|}}{\underset{\underset{R}{|}}{C}}\cdot$$

which dimerizes to

$$^-:CHR - CH_2 - CH_2 - \ddot{C}HR^-$$

Pure anionic polymerization results when this latter ion propagates at both ends. We expect that this is the usual mechanism for electroinitiated anionic polymerization. It is possible that under conditions where dimerization does not occur, anionic polymerization will take place from one end of the chain and free-radical reaction from the other. Indications of this phenomenon have been reported,[13,14] and it is a possible explanation of the deviation from anionic polymerization found in the copolymerization data from the solutions of different salts.

Propagation and Chain Transfer

The electrical efficiency was calculated from the number of faradays passed through the solution and the number of polymer molecules produced. The molecular weight was essentially constant (Table III) and for the present calculation is assumed to be 4000. From the rate data we find that over 3 polymer molecules may be formed per electron, giving nominal efficiencies over 300%. The efficiency is linear with concentration as shown in Figure 6, and indeed this is predictable from the observation that the molecular weight is independent of rate and the rate is approximately first-order with monomer. Hence, more molecules of the same size are formed at higher rates. These observations point to the dominance of chain transfer in the reaction mechanism. The efficiency as a function of current is shown in Figure 7.

Kinetic Scheme

The accompanying series of reaction steps is proposed to account for the course of the reaction.

Electroinitiation:

$$M + I \rightarrow M\cdot^- \qquad k_1$$

where I is the current.

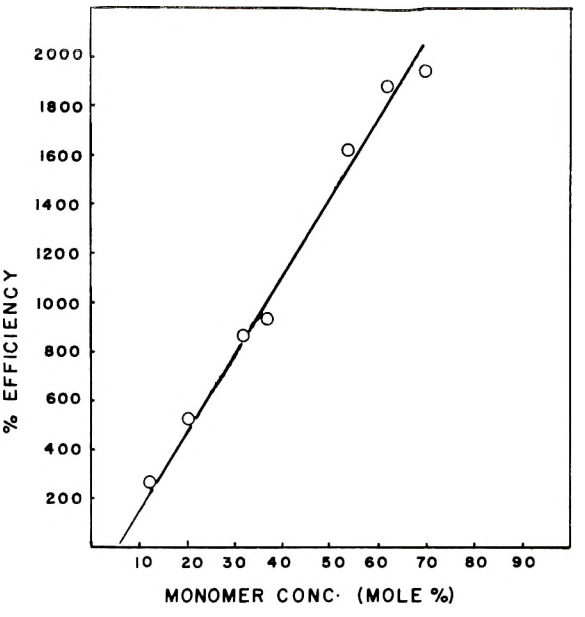

Fig. 6. Dependence of initiation efficiency on monomer concentration.

Dimerization of the radical ion to dianion:

$$2M\cdot^{-} \rightarrow {}^{-}M - M^{-} \qquad k_2$$

Propagation of dianion:

$${}^{-}M - M_{n-1} - M^{-} + M \rightarrow {}^{-}M_n - M^{-} \qquad k_3$$

Chain transfer of dianion:

$${}^{-}M - M_n - M^{-} + M \rightarrow M_{(n+1)}M^{-} + M^{-} \qquad k_4$$

Propagation of anion:

$$M^{-}{}_{(n-1)} + M \rightarrow M_n{}^{-} \qquad k_5$$

Transfer of anion:

$$M_n{}^{-} + M \rightarrow P_n + M^{-} \qquad k_6$$

The rate of propagation is

$$R_p = k_3[{}^{-}M - M_{n-1} - M^{-}][M] + k_5[M_{n-1}][M]$$

or

$$R_p = k_3[\text{dianion}][M] + k_5[\text{monoanion}][M]$$

or

$$R_p = k_3[\text{ion site}][M]$$

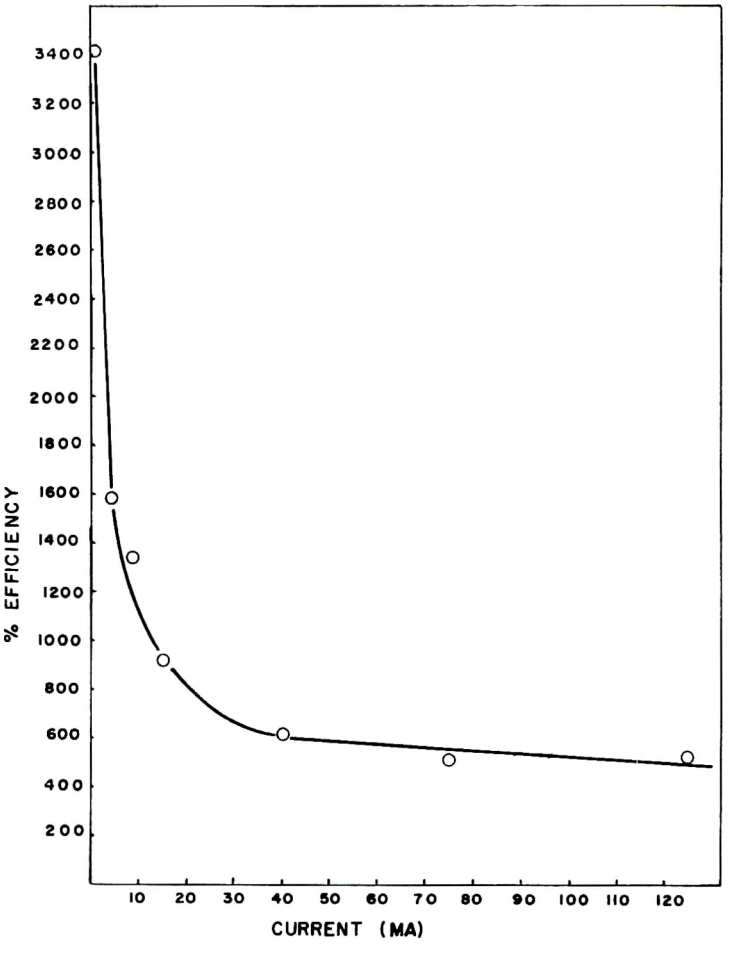

Fig. 7. Dependence of initiation efficiency on current.

where [ion site] refers to the concentration of polymeric negative ions assuming a dianion affords two sites and a monoanion one.

The rate of termination or chain transfer is given by

$$R_t = k_6[\text{ion sites}][\text{M}]$$

and the degree of polymerization is

$$\text{D.P.} = \frac{R_p/R_t = k_3[\text{ion site}][\text{M}]}{k_6[\text{ion site}][\text{M}]}$$

$$= \text{constant}$$

If transfer only with solvent occurred then the D.P. should be a function of the ratio of monomer to solvent concentration.

If the assumption that the reactivity of the anion is independent of the length of the chain is made, then for kinetic purposes

$$[M^-_{n-1}] = [M^-_n] \text{ and } \overline{D.P.} = k_3/k_6, \text{ a constant.}$$

Chain transfer to monomer is the critical reaction. At a constant rate of initiation, the rate of propagation increases but the R_p/R_i ratio remains constant, in agreement with the experimental results.

If transfer with solvent only took place

$$M^-_n + SH \rightarrow P_n + S^- \qquad k_7$$

the expression

$$\overline{D.P.} = k_3[M]/k_7[SH]$$

may be derived. The molecular weight in this case would be a function of the ratio of monomer to solvent concentration.

The independence of molecular weight on initiator and monomer concentration for acrylonitrile has been reported due to chain transfer to monomer in a previous publication.[15] The authors were able to demonstrate that the tertiary hydrogen was responsible for the transfer by repeating experiments with methacrylonitrile. In this case no tertiary hydrogen is available, and a direct dependence of molecular weight on monomer concentration was obtained.

In our opinion the rate-determining step is the dimerization of radical-ions to form dianions. The stabilization of the radical-ions by resonance forms corroborates this assumption although unequivocal justification is not available.

This premise leads to

$$\text{Rate} = {}^1/_2k_2[M\cdot^-]^2$$

and from steady-state condition

$$dM\cdot^-/dt = k_1[M][I] - {}^1/_2k_2[M\cdot]^2 = 0$$

Hence

$$\text{Rate} = k_1[M][I]$$

in general agreement with our experimental findings.

Colors and Spectra

The infrared spectra of the insoluble cathodic polymer show a sharp absorption at 1670 cm.$^{-1}$, as shown in Figure 3. This corresponds to —C=N— absorption,[16] whereas a broad absorption at 1570 cm.$^{-1}$ may be due to the existence of —(C=N)$_n$— chains.[16,17] Grassie and Hay further propose that insolubilization is a result of "propagation crosslinks" arising from the successive combination of nitrile groups.

In the present experiments coloration and insolubilization were at least in part a direct result of an electrode process. This was confirmed by dissolving white soluble polyacrylonitrile in DMF saturated with $NaNO_3$ and electrolyzing. The solution turned red, and insoluble polymer formed at the cathode.

We believe coloration may be catalyzed by an electron:

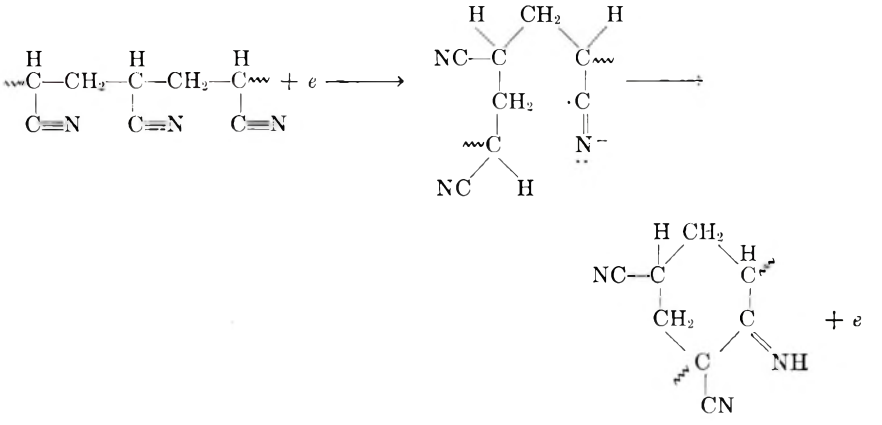

The crosslinking is attributed to an intermolecular reaction:

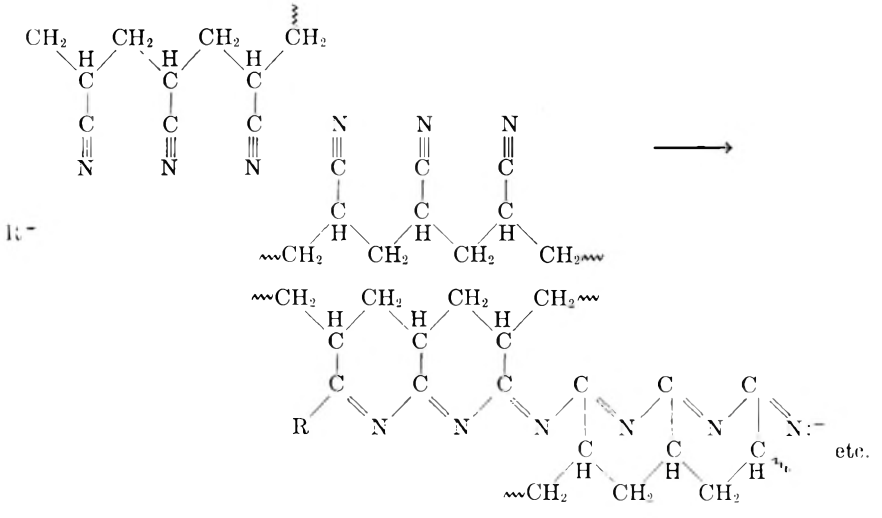

The high-current efficiencies, low molecular weights, and independence of molecular weight of current density and monomer concentration are all in sharp contrast to the behavior of electroinitiated polymerizations which proceed by free-radical mechanisms.[1]

Conversely, these features are not in general typical of anionic polymerization. Although such polymerization had been found in aqueous systems,[15] the electroinitiation of the polymerization profoundly alters the course and character of the reaction. We believe that under the conditions

described here it is possible to obtain new evidence for the simultaneous ion and radical polymerizations suggested by Szwarc[18] and for the influence of gegen ions on the ease of polymerization. The relatively greater control of the reaction and measurable rate may provide means for a more intimate study of ionic polymerization quite apart from the inherent interest in electrically initiated reactions.

We gratefully acknowledge the financial assistance of the National Research Council of Canada in the support of this work.

References

1. Funt, B. L., and K. C. Yu, *J. Polymer Sci.*, **62**, 359 (1962).
2. Breitenbach, J. W., Ch. Srna, and O. F. Alaj, *Makromol. Chem.*, **42**, 171 (1960).
3. Yang, J. Y., W. E. McEwen, and J. Kleinberg, *J. Am. Chem. Soc.*, **79**, 5833 (1957).
4. Murphy, M., M. G. Carangelo, M. B. Ginaine, and M. C. Markham, *J. Polymer Sci.*, **54**, 107 (1961).
5. Breitenbach, J. W., and H. Gabler, *Monatsh.*, **91**, 202 (1960).
6. Walling, C., E. R. Briggs, W. Cummings, and F. R. Mayo, *J. Am. Chem. Soc.*, **72**, 48 (1950).
7. Foster, F. C., *J. Am. Chem. Soc.*, **74**, 2299 (1952).
8. Landler, Y., *J. Polymer Sci.*, **8**, 63 (1952).
9. Laitinen, H. A., and S. Wawzonek, *J. Am. Chem. Soc.*, **64**, 1765, 2365 (1942).
10. Wawzonek, S., E. W. Blaha, R. Berkey, and M. E. Runner, *J. Electrochem. Soc.*, **102**, 235 (1955).
11. Wawzonek, S., and D. Wearring, *J. Am. Chem. Soc.*, **81**, 2067 (1959).
12. Kolthoff, I. M., and J. J. Lingane, *Polarography*, Interscience, New York, 1952, p. 192.
13. O'Driscoll, K. F., R. J. Boudreau, and A. V. Tobolsky, *J. Polymer Sci.*, **31**, 115 (1958).
14. O'Driscoll, K. F., and A. V. Tobolsky, *J. Polymer Sci.*, **31**, 123 (1958).
15. Zilkha, A., B. A. Flit, and M. Frankel, *J. Polymer Sci.*, **49**, 231 (1961).
16. Grassie, N., and J. N. Hay, *J. Polymer Sci.*, **56**, 189 (1962).
17. Overberger, C. G., H. Yuki, and N. Urakawa, *J. Polymer Sci.*, **45**, 127 (1960).
18. Szwarc, M., *Advan. Chem. Phys.*, **2**, 147 (1959).

Résumé

On a formé du polymère par une réaction initié électrolytiquement au départ de solutions d'acrylonitrile et d'autres monomères dans le diméthylformamide saturé par du nitrate de sodium. A partir d'analyse de composition du copolymère on peut établir que le polymère est formé à la cathode par un mécanisme de propagation anionique. On a étudié la nature de l'étape d'initiation de chaîne par des mesures polarographiques. Celles-ci montrent clairement que l'initiation de chaîne a lieu par une addition directe d'électron à la double liaison. On indique une corrélation entre la tendance à former un polymère anionique et les potentiels polarographiques. On esquisse les effets du temps d'électrolyse et de la concentration en monomère sur la formation de polymère. Le taux de polymère augmente linéairement avec le temps à une densité de courant constante et montre une dépendance du premier ordre par rapport à la concentration en monomère. L'efficacité absolue du courant est extrèmement élevée et se situe vers 34 molécules de polymère, formées par électron transférée à l'électrode. Les poids moléculaires des polymères sont remarquablement indépendants de la concentration en monomère, de la vitesse et de la densité de courant. On propose un schéma de réaction qui postule un transfert de chaîne sur monomère. Une analyse cinétique confirme le schéma avec les

données expérimentales. On interprète la coloration et la ramification trouvées dans certains polymères et on propose un mécanisme.

Zusammenfassung

Durch eine elektrolytisch gestartete Reaktion in Lösungen von Acrylnitril und anderen Monomeren in Natriumnitrat-gesättigtem Dimethylformamid wurde Polymeres gebildet. Aus der Analyse der Copolymerzusammensetzung ergab sich, dass das Polymere an der Kathode durch einen anionischen Wachstumsmechanismus gebildet wird. Die Natur des Startvorganges wurde polarographisch untersucht. Es zeigte sich, dass der Kettenstart durch direkte Elektronenaddition an die Doppelbindung erfolgt. Es besteht eine enge Beziehung zwischen der Tendenz zur anionischen Polymerisation und den polarographischen Potentialen. Der Einfluss von Stromstärke, Dauer und Monomerkonzentration auf die Polymerbildung wurde beschrieben. Bei einer bestimmten Stromdichte nahm die Polymerausbeute mit der Zeit linear zu und zeigte eine Abhängigkeit erster Ordnung von der Monomerkonzentration. Die absoluten Stromausbeuten lagen extrem hoch und erstreckten sich bis zu einer Bildung von über 3 Polymermolekülen pro Elektronentransfer an der Elektrode. Das Molekulargewicht der Polymeren ist bemerkenswert unabhängig von Monomerkonzentration, Geschwindigkeit und Stromdichte. Ein Reaktionsschema mit Kettenübertragung zum Monomeren wird aufgestellt. Eine kinetische Analyse bestätigt die Übereinstimmung des Schemas mit den experimentellen Befunden. Eine Erklärung der bei einigen Polymeren gefundenen Verfärbung und Vernetzung wird gegeben und eine Mechanismus vorgeschlagen.

Received October 9, 1962
Revised December 21, 1962

JOURNAL OF POLYMER SCIENCE: PART A VOL. 2, PP. 881–893 (1964)

Polyurethane Sulfides Containing Cyclohexane Ring in the Polymer Chain

YOSHIO IWAKURA, MUNENORI SAKAMOTO,* and YASUHIRA AWATA,† *Research Laboratory of Resources Utilization, Tokyo Institute of Technology, Meguro-ku, Tokyo, Japan*

Synopsis

Polyurethane sulfides of high molecular weight containing *trans*-1,4-cyclohexylene groups were successfully obtained by both methods of polymerization, polyaddition of *trans*-1,4-cyclohexylenebis(N,N-ethyleneurethane) or *trans*-hexahydro-*p*-xylylenebis-(*N*,*N*-ethyleneurethane) with polymethylene dimercaptans and polycondensation of bis(chloroformates) with polymethylenebis(β-aminoethyl thioethers) prepared by reaction of ethylenimine with polymethylene dimercaptans. Comparison of physical properties of the polymers prepared by both methods of preparation indicated that (*1*) polymer repeating units of polyaddition and polycondensation products were quite equivalent; (*2*) polycondensation polymers had chloroformyl groups as terminal groups.

INTRODUCTION

As a part of a study on polyaddition reactions, linear polyurethane sulfide (I) has been obtained by intermolecular addition of polymethylenebis(*N*,*N*-ethyleneurethane) (II) and polymethylene dimercaptan.[1]

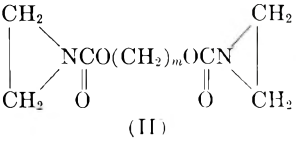

(II)

$$+\ HS(CH_2)_nSH \longrightarrow$$

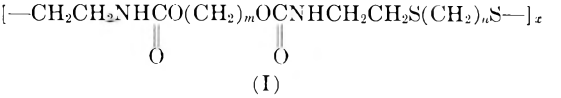

(I)

The above polyaddition was successfully conducted with the aid of triethylamine under mild conditions in order to avoid any competitive self-polymerization of polymethylenebis(*N*,*N*-ethyleneurethane) which would lead to formation of reaction product with a crosslinked structure. The polyurethane sulfides thus obtained were considered to be linear in structure. This conclusion was based on the basis of (a) nitrogen analyses;

* Present address: Oji Paper Co. Ltd. Shinonome-cho, Koto-ku, Tokyo, Japan.

† Present address: Department of Textile Engineering, Tokyo Institute of Technology, Meguro-Ku, Tokyo, Japan.

(b) solubilities; (c) Huggins' constants; and (d) characteristic dependence of the molecular weights on molar ratio of the two components.

In this report an investigation is presented to extend this polyaddition reaction to two bis(*N*,*N*-ethyleneurethanes) containing a 1,4-*trans*-cyclohexylene group. Interfacial polycondensation of polymethylenebis(β-aminoethyl thioethers) (III) and bis(chloroformates) was also investigated. The reaction was expected to give an authentic linear polyurethane-sulfide specimen.

$$NH_2(CH_2)_2S(CH_2)_nS(CH_2)_2NH_2 + ClCO{-}R{-}OCCl \longrightarrow$$

(III)

$$[{-}NH(CH_2)_2S(CH_2)_nS(CH_2)_2NHCO{-}R{-}OC{-}]_x \quad \text{(IV)}$$

When it is necessary to discriminate among various kinds of polyurethane sulfides and to simplify the description, the following abbreviations are used: 2U2 [IV, where $n = 2$ and R = $(CH_2)_2$], 4UC (IV, where $n = 4$ and R = trans-C_6H_{10}), 5UH (IV, where $n = 5$, and R = *trans*-$CH_2C_6H_{10}$-CH_2), and similar abbreviations.

Polyurethane sulfides having cyclohexane rings in the polymer chain were easily obtained by both polyaddition and polycondensation. Comparison between polyurethane sulfides prepared by the above two types of polymerization confirmed again the proposed structure of the polyaddition polymers.

EXPERIMENTAL

Materials

trans-1,4-Cyclohexylenebis(*N*,*N*-ethyleneurethane) was prepared from the corresponding bis(chloroformate) as described in a preceding paper.[2]

trans-Hexahydro-*p*-xylylenebis(chloroformate) was obtained as a solid part of the phosgenation products of commercial cyclohexanedimethanol (*cis*/*trans* = 30/70) in 57% yield. Recrystallization from *n*-hexane + ether gave a pure sample, m.p. 65.5–68°C.

ANAL. Calcd. for $C_{10}H_{14}O_4Cl_2$: C, 44.6%; H, 5.2%. Found: C, 44.3%; H, 5.4%.

The liquid part of the products was apt to decompose and could not be purified by distillation.

trans-Hexahydro-*p*-xylylenebis(*N*,*N*-ethyleneurethane), m.p. 97–98°C., was analogously synthesized and purified by recrystallization from acetone; yield 61%.

ANAL. Calcd. for $C_{14}H_{22}O_4N_2$: C, 59.6%; H, 8.9%; N, 9.9%. Found: C, 59.5%; H, 7.5%; N, 9.5%.

Polymethylenebis(chloroformates) were prepared by the usual procedure.[2]

Polymethylene dimercaptans were prepared from polymethylene dibromides.[3]

Reaction of Ethylenimine with Polymethylene Dimercaptan

A patent[4] claimed the production of polymethylenebis(β-aminoethyl thioether) by reaction of ethylenimine with dimercaptan, but no experimental details nor any physical properties of the products were given. In our preliminary experiments, a marked solvent effect was observed on the reaction of ethylenimine and tetramethylene dimercaptan: The reaction

TABLE I
Effect of Solvent on Reaction of Ethylenimine with Tetramethylene Dimercaptan[a]

Solvent	Solvent b.p., °C.	Yield, %		
		Monoamine	Diamine	Total
Hexane	69	40	41	81
Benzene	80	39	40	79
Acetone	56	12	70	82
Methanol	65	12	77	89
Ethanol	78	11	81	92
Acetonitrile	82	21	70	91

[a] A mixture of 0.20 mole of ethylenimine, 0.10 mole of tetramethylene dimercaptan, and 10 ml. of solvent was refluxed for 6 hr.

TABLE II
Monoamines and Diamines Prepared by Reaction of Ethylenimine with Polymethylene Dimercaptans

	Monoamine or diamine			
n	b.p., °C./mm. Hg	Acid value		Derivative
		Found	Calc.	
Monoamine:	$HS(CH_2)_nS(CH_2)_2NH_2$ (IR: S—H stretching vibration at 2550 cm.$^{-1}$)			
2	70–73/0.10	139	137	
4	88/0.04	165	165	
5	102–104/0.18	179	179	
6	114–116/0.26	193	193	
Diamine:	$H_2N(CH_2)_2S(CH_2)_nS(CH_2)_2NH_2$ (III)			
2	130/0.10	91	90	Phenylthiourea[a]
4	144/0.06	103	104	Phenylthiourea[b]
5	155–160/0.03	111	111	Benzamide[c]
6	160–165/0.2	119	118	Benzamide[d]

[a] M.p. 142.5–143.0°C. Anal. Calc. for $C_{20}H_{26}N_4S_4$: C, 53.3%; H, 5.8%; N, 12.4%. Found: C, 53.8%; H, 6.0%; N, 11.9%.

[b] M.p. 122.5–123.5°C. Anal. Calc. for $C_{22}H_{30}N_4S_4$: C, 55.2%; H, 6.3%; N, 11.7%. Found: C, 55.3%; H, 6.4%; N, 12.0%.

[c] M.p. 89.5–91°C. Anal. Calc. for $C_{23}H_{30}N_2O_2S_2$: C, 64.2%; H, 7.0%; N, 6.5%. Found: C, 64.7%; H, 7.5 %; N, 6.4%.

[d] M.p. 115.5–116.0°C. Anal. Calc. for $C_{24}H_{32}N_2O_2S_2$: C, 66.8%; H, 7.3%; N, 6.3%. Found: C, 64.9%; H, 7.6%; N, 7.2%.

TABLE III
Polyaddition Reaction of Bis(*N*,*N*-ethyleneurethane) and Polymethylene Dimercaptan

Polymer structure	Reaction conditions[a]					Results					Nitrogen, %	
	Reactant, mmole	Catalyst[b]	Solvent, ml.[c]	Temperature, °C.	Time, hr.	Appearance	Yield, %	$[\eta]^d$	M.p., °C.	Melt-spinnability[e]	Found	Calc.
2UC	5.0	TED	F/A, 10	120	6	Precipitated	83	0.43	204–205	+	7.7	8.0
3UC	5.0	TEA	DMF, 10	100	24	Solution	73	0.20	199–202	−	7.2	7.7
4UC	4.0	TEA	DMF, 5	75–120	6	Precipitated at 75°C., solution at 120°C.	67	0.54	212–214	++	7.0	7.4
4UC	3.0	TED	F/B, 10	120	6	Precipitated	88	0.55	211–212.5	++	7.4	7.4
5UC	5.0	TED	F/A, 15	120	6	Solution	78	0.42	185–189	++	7.5	7.2
6UC	5.0	TED	F/A, 15	120	6	Solution		0.4	200–204	++	6.3	6.9
3UH	5.0	TEA	DMF, 15	100	24	Solution	57	0.61	104–105	+	6.9	7.2
4UH	5.0	TEA	DMF, 10	100	24	Solution	56	0.35	125–128	++	6.6	6.9
5UH	5.0	TEA	DMF, 10	100	24	Solution	65	0.39	99–101.5	+	6.4	6.7
6UH	5.0	TEA	DMF, 10	100	24	Solution	63	0.59	ca. 124	++	6.2	6.5

[a] An equimolar mixture of bis(*N*,*N*-ethyleneurethane) and polymethylene dimercaptan was brought to reaction in solution.

[b] TED: Triethylenediamine; TEA: Triethylamine. In every run, 1.0 mmole of catalyst was used.

[c] DMF: Dimethylformamide; F/A: A mixture of equivolume of DMF and dimethylacetamide; F/B: A mixture of equivolume of DMF and *o*-dichlorobenzene.

[d] Measured in *m*-cresol at 30.0°C.

[e] Code: (−) cannot be drawn from the melt; (±) can be drawn into filament, which cannot be stretched; (+) filament can be stretched after cooling; (++) can be stretched with necking, strong fibers are obtained.

proceeded slowly in nonpolar solvent such as benzene and *n*-hexane where lower boiling 7-amino-5-thiaheptyl mercaptan and high boiling tetramethylenebis(β-aminoethyl thioether) (III, where $n=4$) were obtained, while in polar solvent such as methanol and ethanol it proceeded fast to give diamine as a major product (Table I). This solvent effect is consistent with that observed in the polyaddition reaction of tetramethylene dimercaptan and hexamethylenebis(*N*,*N*-ethyleneurethane).[1]

Ethylene, pentamethylene, and hexamethylene dimercaptans were also caused to react with ethylenimine to yield the corresponding mono- and diamines. A typical procedure is as follows. To 10 ml. of ethanol were added 8.6 g. (0.20 mole) of ethylenimine and 12.2 g. (0.10 mole) of tetramethylene dimercaptan. The mixture was refluxed for 6 hr., then the solvent was evaporated. The residue was distilled under reduced pressure to give colorless material, b.p. 144°C./0.06 mm. Hg, in 81% yield. The exothermic reaction proceeded very vigorously in some experiments. No polymerization of ethylenimine was encountered through the preparations.

Identification and physical properties of amines thus prepared are listed in Table II.

Polyaddition Reaction

Polyaddition reactions were carried out at temperatures below 120°C. Triethylamine or triethylenediamine was used as a catalyst; the latter did not differ significantly from the former amine in catalytic activity. Introducing cyclohexane rings in the polymer chain lessened the solubility of polyurethane sulfide in dimethylformamide at 75°C. Mixed solvent systems, such as dimethylformamide–dimethylacetamide and dimethylformamide–*o*-dichlorobenzene were examined but expected improvement in solubility was not achieved. A typical procedure is as follows.

A solution of 1.21 g. of *trans*-1,4-cyclohexylenebis(*N*,*N*-ethyleneurethane), 0.61 g. of tetramethylene dimercaptan, and 0.10 g. of triethylamine in 10 ml. of dimethylformamide was placed in a 20-ml. glass tube and sealed under an atmosphere of nitrogen. The polymerization tube was kept at a scheduled temperature for 6 hr., then opened. The resulting hot, viscous solution was poured dropwise with stirring into 500 ml. of methanol. White powders were precipitated, which were collected by filtration and dried *in vacuo* at 50°C. for about 40 hr. Complete homogeneous conditions were necessary at the beginning stage of the polyaddition reaction, otherwise, a gel was precipitated.

Results obtained are summarized in Table III.

Polycondensation Reaction

Interfacial polycondensation of bis(chloroformates) and polymethylenebis(β-aminoethyl thioethers) (III) was effected under conditions similar to those in the literature.[5] Polycondensation of polymethylenebis(chloroformates) and III was also carried out to yield samples useful for

TABLE IV
Polycondensation of Bis(chloroformate) and Polymethylenebis(β-aminoethyl thioether)

Polymer structure	Method[a]	Yield, %	$[\eta]$[b]	M.p., °C.	Melt-spinnability[c]	Nitrogen, % Found	Nitrogen, % Calc.
2UC	A	47	0.20	210–214	−	7.2	8.0
4UC	A	71	0.54	207–209	±	6.7	7.4
2UH	A	54	0.24	121	±	6.5	7.4
4UH	A	63	0.92	126–129	+	6.6	6.9
2U2	B	61	0.69	166–168	++	9.1	9.5
4U2	B	76	Insol.	124–126.5	+	8.2	8.7
5U2	B	64	Insol.	121–126.5	+	8.4	8.3
6U2	B	69	Insol.	127–129.5	±	7.6	8.0
2U3	B	55	0.32	154–157	±	8.6	9.1
4U3	B	61	0.69	110–113	+	7.8	8.3
5U3	B	57	0.60	100–112	±	7.4	8.0
6U3	B	52	Insol.	114–115	++	7.3	7.7
2U4	B	60	0.36	150–177	++	8.3	8.7
4U4	B	59	0.83	117–119	++	7.6	8.0
5U4	B	55	0.54	101–113	++	7.0	7.7
6U4	B	52	0.70	112–117	+	6.9	7.4
2U5	B	54	0.40	126–130	±	7.7	8.3
4U5	B	55	0.68	82	+	7.7	7.7
5U5	B	58	0.60	85–87	±	6.8	7.4
6U5	B	49	Insol.	90–94	+	6.5	7.1
2U6	B	58	0.39	140	++	7.5	8.0
4U6	B	56	0.70	111–113	+	6.8	7.4
5U6	B	57	0.74	95–98	++	6.8	7.1
6U6	B	54	0.83	105–106	++	6.2	6.9

[a] (A) a solution of diamine hydrochloride was used; (B) an alkaline solution of diamine was used. Details are given in the Experimental Section.

[b] Measured in *m*-cresol at 30.0°C.

[c] See footnote e in Table III.

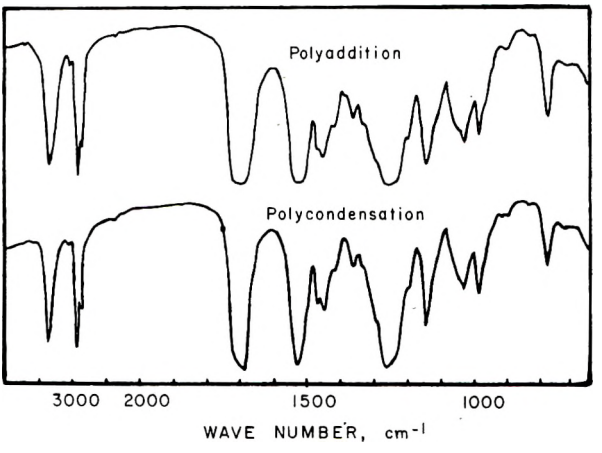

Fig. 1. Infrared absorption spectra of 4UH prepared by polyaddition and polycondensation.

comparison with polyurethane sulfides containing cyclohexylene groups. The resulting polymers were generally white powders of high molecular weight; however, in some runs, crosslinked products were obtained, contrary to our aim of obtaining samples of polyurethane sulfides. Several attempts were made to find favorable condition under which linear high molecular weight polymer might be produced without fail. No conclusive result was obtained on the effect of reaction temperature, concentration of the reagents, purification of III, and so on. Compared with polymethylenediamines, III seemed to have more tendency towards crosslinking. It seems possible that crosslinks might come from the condensation of bis(chloroformates) and *sec*-urethane groups (—NHCOO—) in the polymer chains, which would result in the formation of *tert*-urethane linkages (—NCOO—) or branching.

Typical procedures are as follows. (*A*) A mixture of 1 ml. of concentrated HCl, 0.006 mole of diamine, and 12 ml. of water was placed in a blender with a solution of 0.006 mole of bis(chloroformate) and 0.1 g. of sodium lauryl sulfate in 4 ml. of benzene. With vigorous stirring, a solution of Na_2CO_3 (0.024 mole/13 ml. water) was added dropwise to the emulsion.

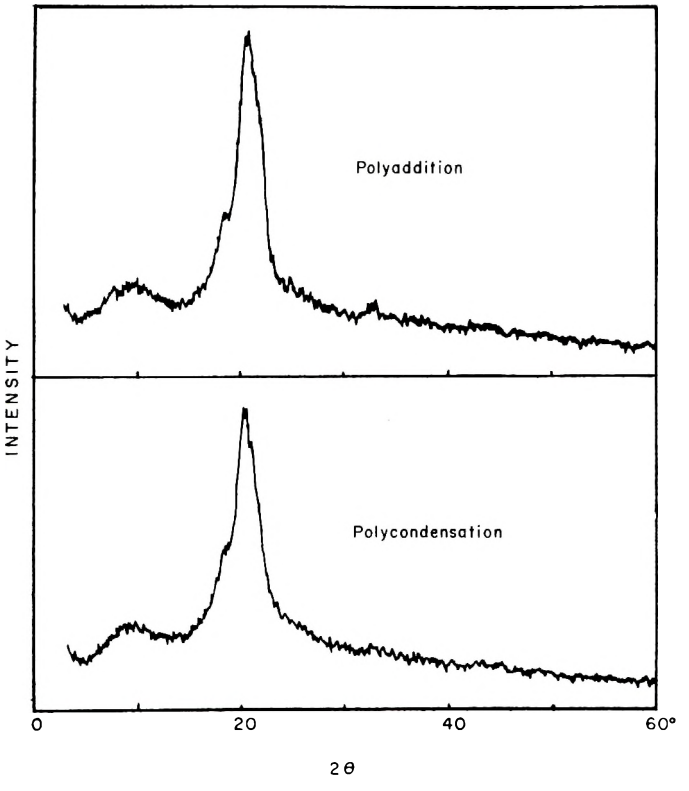

Fig. 2. X-ray diffraction diagrams of 4UC prepared by polyaddition and polycondensation.

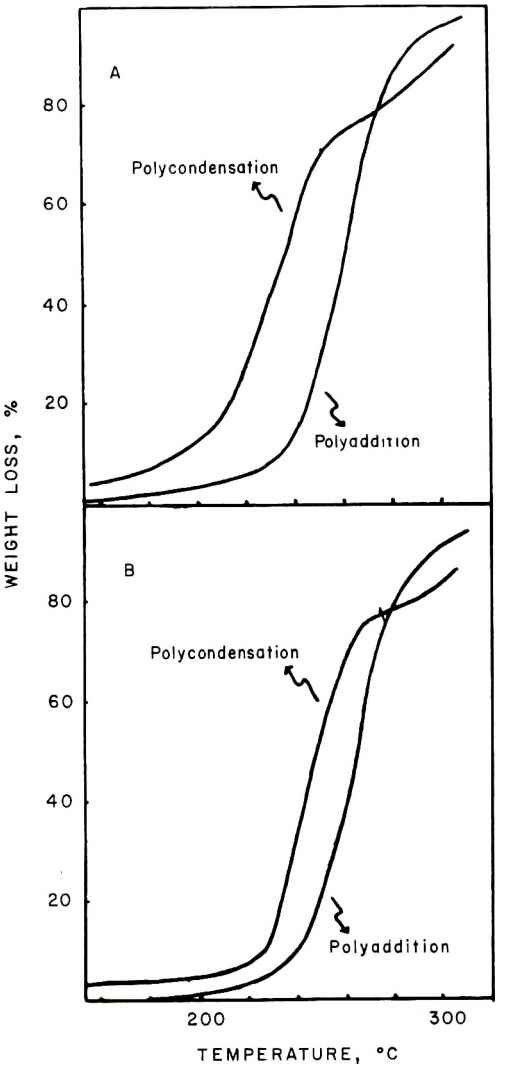

Fig. 3. Thermal degradation curves of (*A*) 2UC and (*B*) 4UC prepared by polyaddition and polycondensation.

Stirring was continued for 30 min. after the completion of the addition. After about 20 ml. of acetone was added to the reaction mixture, the polymer powders were filtered and washed well with methanol and water, then dried *in vacuo* at 50°C. for about 40 hr. (B) A mixture of 0.012 mole of Na_2CO_3, 0.006 mole of diamine, 26 ml. of water, 2 ml. of benzene, and 0.1 g. of sodium lauryl sulfate was placed in a blender. With vigorous stirring a solution of 0.006 mole of bis (chloroformate) in 4 ml. of benzene was added dropwise to the emulsion. The products were treated analogously as described in the above procedure.

Results obtained are summarized in Table IV.

Properties of the Product

Melting Point. A small amount of polymer was placed between two sheets of cover glass on a metal block and was observed through a microscope with crossed polarizers, and the melting point was determined.

Solubility. Solubilities were observed in sixteen common solvents. About 10 mg. of polymer was mixed with 2 ml. of solvent in a test tube, and the solubility was determined. The result was expressed in number from 0 to 6 according to a slightly modified expression of Beaman and Cramer.[6]

Infrared Absorption. Thin films were prepared from dimethylformamide or *m*-cresol solutions of polymers by evaporating the solvent and afterwards washing with water and methanol, and infrared absorption spectra were recorded with a Hitachi infrared spectrometer, Model EPI-S2. The absorption charts of the polyurethane sulfide prepared by polyaddition and polycondensation agreed well, which showed N—H stretching at 3420 $cm.^{-1}$, C=O stretching at 1685 $cm.^{-1}$, and C—O stretching mode of absorption in the 1300–1200 $cm.^{-1}$ region. An example is demonstrated in Figure 1.

X-Ray Diffraction. Samples of 3,8-dithiadecamethylene *trans*-1,4-cyclohexylene polyurethane (4UC) prepared by polyaddition or by polycondensation, were finely pulverized, and x-ray diffractions were recorded without any crystallization process such as annealing by use of Philips X-ray-diffractometer, employing CuKα radiation ($\lambda = 1.541$ A.) (Ni-filtered). Diffraction diagrams thus obtained are shown in Figure 2.

Thermal Degradation. Thermal degradation was observed with a Shimazu Thermano thermobalance. A powdered sample of 100 mg. of polymer was placed on a platinum boat which was connected to a torsion balance. The apparatus was evacuated (0.3 mm. Hg), and the temperature was raised at a constant rate (2°C./min.). At appropriate intervals the temperatures and the weight losses were recorded, which were plotted as a thermal degradation curve.

Results obtained are demonstrated in Figure 3.

RESULTS AND DISCUSSION

Polyurethane sulfides prepared by polyaddition and polycondensation afforded the identical infrared spectra (Fig. 1) and x-ray diffraction diagrams (Fig. 2) to justify that their polymer repeating units were quite equivalent. The similar melting points (Table V) and solubilities (Table VI) also verified the above conclusion.

Kinetic features of thermal degradation of polyurethane sulfides, on the other hand, indicated that there exists an appreciable difference between polyaddition and polycondensation polymers; the latter were less thermostable than the former (Fig. 3). Samples of 6,4-polyurethane prepared by interfacial polycondensation were reported to be less thermostable; treatment with hot methanol or other reagents, which would convert terminal groups, supposedly chloroformyl groups, to more thermosta-

TABLE V
Physical Properties of Polyurethane Sulfides Prepared by Polyaddition and Polycondensation

Polymer structure	Method of preparation[a]	$[\eta]$	M.p., °C.	Melt-spinnability
2UC	A	0.43	204–5	+
2UC	C	0.20	210–4	−
4UC	A	0.55	211–2.5	+
4UC	C	0.54	207–9	±
4UH	A	0.35	125–8	++
4UH	C	0.92	126–9	+

[a] (A) polyaddition; (C) polycondensation.

TABLE VI
Solubilities of Polyurethane Sulfides Prepared by Polyaddition and Polycondensation

Solvent	Solubility of polyurethane sulfides[a]					
	2UC[b]	2UC[c]	4UC[b]	4UC[c]	4UH[b]	4UH[c]
Acetic acid	0	3	3	3	4	2
Carbon disulfide	0	0	0	0	0	0
Carbon tetrachloride	0	0	0	0	0	0
Chloroform	0	0	0	0	5	5
Dioxane	0	0	0	0	4	2
Dimethylacetamide	3	3	3	3	5	4
Dimethylformamide	3	3	3	3	4	4
Dimethylsulfoxide	3	3	3	3	4	4
Ethyl acetate	0	0	0	0	1	0
Formic acid	3	3	2	0	0	0
Methylene chloride	0	0	0	0	4	2
Nitrobenzene	3	3	3	3	3	3
Pyridine	2	3	3	3	5	5
Sulfuric acid	5	5	5	4	5	5
Tetrachlorethane	4	3	3	3	5	5
Tetralin	1	1	1	1	1	3

[a] Code: 0 = unaffected by hot solvent; 1 = melted, sticky, or swollen in hot solvent; 2 = slightly soluble in hot solvent; 3 = soluble in hot solvent, precipitated in cold; 4 = soluble in hot solvent, remains soluble in cold; 5 = soluble in cold solvent.
[b] Polyaddition product.
[c] Polycondensation product.

ble groups, improved the thermal stability of the polymer.[7,8] Therefore, this thermal instability of polyurethane sulfides prepared interfacially seems to demonstrate the presence of chloroformyl groups in the polycondensation products. Infrared spectra of polycondensation polymer samples used for the thermal degradation study showed new absorption at 1760, 1168, and 840 cm.$^{-1}$ (in KBr disks or Nujol mulls) which were located at positions very similar to those of the three strong absorptions (1770, 1165, and 827 cm.$^{-1}$) of *trans*-1,4-cyclohexylenebis(chloroformate). These three absorptions observed in the polyurethane sulfides may be attributed

to the presence of chloroformyl groups as terminal groups of low molecular weight oligomers, although it seems unreasonable that washed and dried polymer powders would contain chloroformyl groups, while washed and dried films made from the above powders would not contain the chloroformyl groups. Polymers prepared by polycondensation are reported to have various molecular weight distributions, depending on the reaction conditions.[9] Results of fractionation of 6,4-polyurethane made by interfacial polycondensation by Nishide and Sera[10] indicate that the polyurethane is of broader distribution, with two peaks in the distribution curve. Therefore, the polyurethane sulfides under discussion may be expected to contain an appreciable amount of lower molecular weight materials, enough for the detection of terminal groups in infrared absorption.

Effect of Cyclohexane Ring on the Polymer Properties

Melting points of polyurethane sulfides containing cyclohexane groups were plotted against number of chain atoms in the polymer repeating unit. This number is the sum of the number of atoms which constitute the main chain in the polymer repeating unit (formula IV): for 2U2, this is 16; for 4U2, 18; for 2U4, 18. The number of chain atoms of the cyclohexane ring is 4, and not 6; thus for 2UC, the number is 18; for 2UH, 20, respectively.

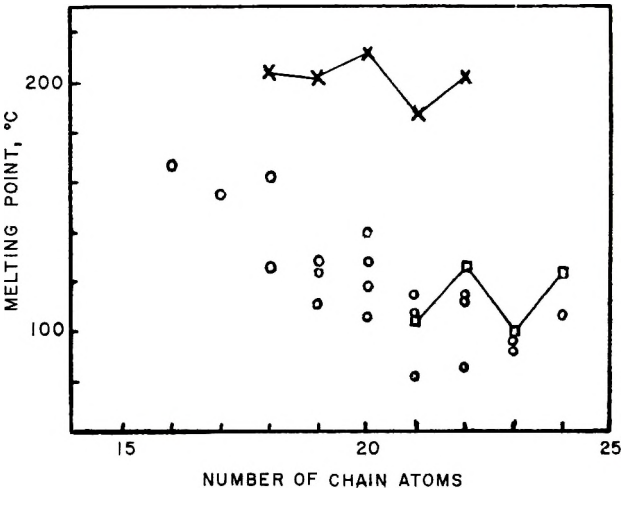

Fig. 4. Melting points of polyurethane sulfides: (×) polyurethane sulfides containing *trans*-1,4-cyclohexylene groups; (□) polyurethane sulfides containing *trans*-hexahydro-*p*-xylylene groups; (○) polyurethane sulfides without any ring in the polymer chain.

The plots of melting points and number of chain atoms make it possible to elucidate the rigid ring effect on the melting point by eliminating the effect of urethane concentration in the polymer chain (Fig. 4). Rigid *trans*-cyclohexylene groups of good symmetry markedly increased the melting

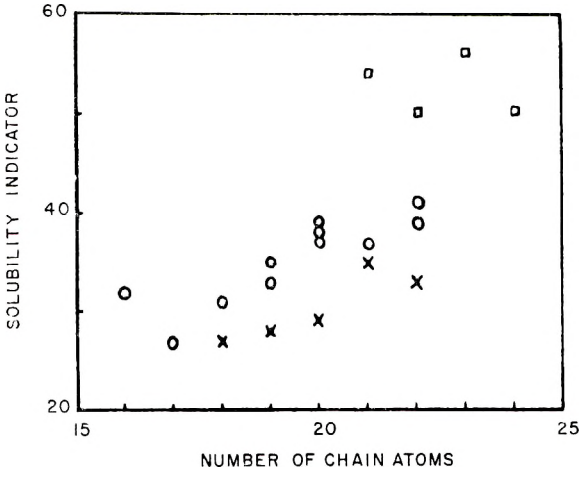

Fig. 5. Solubilities of polyurethane sulfides: (×) polyurethane sulfides containing *trans*-1,4-cyclohexylene groups; (□) polyurethane sulfides containing *trans*-hexahydro-*p*-xylylene groups; (O) polyurethane sulfides without any ring in the polymer chain.

points, as expected. When cyclohexylene groups were not linked directly but separated by methylene groups, however, the increase was small. Sulfide linkages seemed to lower the melting point. Usual odd-even alternations of melting points of polymeric homologous series were observed.

As mentioned in the Experimental section, cyclohexane groups appeared to lessen the solubilities. An attempt was made to obtain a more precise evaluation of the polymer solubility. The effect on solubilities was considered in terms of solubility indicator; this was defined as a sum of solubilities observed in sixteen solvents. Solubility indicators were plotted again against number of chain atoms of the polymer repeating unit (Fig. 5). Solubility indicators of some polycondensation samples which seemed to be slightly crosslinked gave anomalously low values, and were omitted in plotting in the figure. This indicator failed to clearly distinguish the difference in solubilities, but it might well be said that polyurethane sulfides with *trans*-cyclohexane groups directly connected to urethane linkages showed poorer solubilities, while those with cyclohexane groups separated by methylene linkages had larger solubilities.

We wish to thank the personnel of the Microanalytical Laboratory, Tokyo Institute of Technology for the elemental analyses. We also wish to acknowledge Mr. M. Kato for measurement of x-ray diffraction.

References

1. Iwakura, Y., and M. Sakamoto, *J. Polymer Sci.*, **47**, 277 (1960).
2. Iwakura, Y., M. Sakamoto, and H. Yasuda, *Nippon Kagaku Zasshi*, **82**, 606 (1961).
3. Marvel, C. S., and H. E. Baumgarten, *J. Polymer Sci.*, **6**, 127 (1957).
4. Berchet, G. J., U. S. Pat. 2,304,623 (1943).
5. Wittbecker, E. L., and M. Katz, *J. Polymer Sci.*, **40**, 367 (1959).

6. Beaman, R. G., and F. B. Cramer, *J. Polymer Sci.*, **21**, 223 (1956).
7. Nishide, M., and M. Sera, *Kogyo Kagaku Zasshi*, **64**, 1148 (1961).
8. Nishide, M., and M. Sera, *Kogyo Kagaku Zasshi*, **64**, 1151 (1961).
9. Wittbecker, E. L., and P. W. Morgan, *J. Polymer Sci.*, **40**, 289 (1959).
10. Nishide, M., and M. Sera, *Kogyo Kagaku Zasshi*, **63**, 1467 (1960).

Résumé

On a bien obtenu un sulfure de polyuréthanne macromoléculaire contenant des groupes de *trans*-1,4-cyclohexylène par deux méthodes de polymérisation, l'une la polyaddition de *trans*-1,4-cyclohexylène-bis-N,N-éthylène-uréthannes ou de *trans*-hexahydro-*p*-xylène-bis-*N*,*N*-éthylène-uréthannes avec les polyméthylène-dithiols, l'autre la polycondensation des bis-chloroformiates avec les polyméthylène-bis-β-aminoéthylthioéthers, préparés eux-mêmes par réaction des éthylène-imines avec les polyméthylènedimercaptans. La comparaison des propriétés physiques des polymères préparés par les deux méthodes a fourni les informations suivantes: (*1*) les unités périodiques des polymères obtenus par polyaddition et par polycondensation contiennent des groupes chloroformiques et sont équivalents entre eux; (*2*) les polymères de polycondensation portent des groupes chloroformiques comme groupes terminaux.

Zusammenfassung

Makromolekulare Polyurethansulfide mit *trans*-1,4-Cyclohexylengruppen in der Kette wurden nach zwei Polymerisationsmethoden, nämlich Polyaddition von *trans*-1,4-Cyclohexylenbis(*N*,*N*-äthylenurethan) oder von *trans*-Hexahydro-*p*-xylylenbis(*N*,*N*-äthylenurethan) mit Polymethylendimercaptanen und Polymethylenebis(β-aminoäthyl-thioäthern), die aus Äthylenimin und Polymethylendimercaptanen synthetisiert wurden, dargestellt. Ein Vergleich der physikalischen Eigenschaften der Polyadditionsprodukte mit denen der Polykondensationsprodukte spricht dafür, dass (*1*) die chemische Struktur der Kette der Polyadditionsprodukte und der Polykondensationsprodukte völlig gleichartig war; (*2*) die Polykondensationsprodukte Chloroformylgruppen als Endgruppen besassen.

Received November 8, 1962
Revised January 2, 1963

JOURNAL OF POLYMER SCIENCE: PART A VOL. 2, PP. 895–905 (1964)

High Resolution NMR Study of Vinylidene Chloride–Vinyl Chloride Copolymer

RIICHIRO CHÛJÔ, SHIROH SATOH, and EIICHI NAGAI, *The Research Institute, Kureha Spinning Co., Ltd., Takatsuki, Osaka, Japan*

Synopsis

The presence of head-to-head structure in vinylidene chloride sequence in copolymer of vinylidene chloride and vinyl chloride with various feed ratios was demonstrated by the high resolution NMR study. The ratio of head-to-head structure in vinylidene chloride sequence was evaluated from measurement of the intensities of NMR spectra. The quantities of local regularity of copolymer were used in the theoretical treatment based on the virtual boundary energy and combinatory method. The experimental results were compared with the theoretical calculations.

INTRODUCTION

High resolution nuclear magnetic resonance (NMR) spectroscopy has been applied to polymers in solution to obtain the informations on local regularity of the molecules. Tacticity in stereospecific polymers from the splitting of spectra by chemical shift[1–6] and by I·I coupling,[7] sequence length of constituent monomers in copolymers from the splitting by chemical shift[7–9] and head-to-tail and head-to-head structures in vinyl and vinylidene polymers[8,9] were successfully studied.

A copolymer of vinylidene chloride (VDC) and vinyl chloride (VC) was studied in this work by the same procedure to obtain information on local regularity, and head-to-tail and head-to-head structure. The sequence length was not considered in the present study, because this involves a large ambiguity for reasons which will be described under results and discussion.

It is generally accepted that the molecule of this copolymer would be exclusively composed of head-to-tail arrangement of the constituent monomers like —$CH_2CCl_2CH_2CCl_2$—, —$CH_2CCl_2CH_2CHCl$—, or —CH_2-$CHClCH_2CHCl$—. In order to confirm that this copolymer is arranged in a different manner, the high resolution NMR spectra of several kinds of copolymer prepared under different monomer feed ratio were measured together with the relevant polymers as follows: polyvinylidene chloride (PVDC); poly-2,3-dichlorobutadiene (PDCB, [—CH_2CCl=$CClCH_2$—]$_n$); and partially chlorinated poly-2,3-dichlorobutadiene (PCPDCB).

The mole fraction of head-to-head structure in the VDC sequence in the

copolymer was evaluated quantitatively from the intensity of peaks in NMR spectra.

The amounts of local regularity of the copolymer were obtained theoretically by means of the method of virtual boundary energy and the combinatory method as an extension of the theory[10] developed by one of the authors.

Finally, the experimental data were compared with our theory.

EXPERIMENTAL

Samples

All samples used in the present experiment, which are listed in Table I, were presented by the Kureha Chemical Industry Co., Ltd.

TABLE I
Samples Used

Sample	VDC/VC feed ratio, weight of fraction	Conversion, %
Low conversion copolymer 1	5/95	2.0
Low conversion copolymer 2	25/75	4.8
Low conversion copolymer 3	30/70	4.0
Low conversion copolymer 4	50/50	1.2
Low conversion copolymer 5	80/20	2.4
Low conversion copolymer 6	85/15	1.8
PVD		
PDCB		
PCPDCB[a]		

[a] The content of $-CH_2CCl_2CCl_2CH_2-$ to the whole molecule is about 35%.

After the specimen was dissolved in *o*-dichlorobenzene (about 10% concentration), small amount of methyl benzyl ether was added to the solution in order to prevent thermal degradation. After being put into the test tube (5 mm. o.d.) the tube was degassed at −70°C. and sealed.

Instrument and Measurement of Spectra

The Proton magnetic resonance of these samples was measured on a Varian Associates Model V-4311 high resolution NMR spectrometer equipped with a variable temperature probe accessory, Model V-4340, operating at fixed frequency (60 Mcycles/sec.) at high temperature (about 100°C.) to get better solubility of the polymers and to get better resolution of the spectra. Chemical shifts were determined by the conventional side band method, cyclohexane being used as interval standard.

RESULTS AND DISCUSSION

Spectra are shown in Figure 1 for the copolymer, PVDC, PDCB, and PCPDCB.

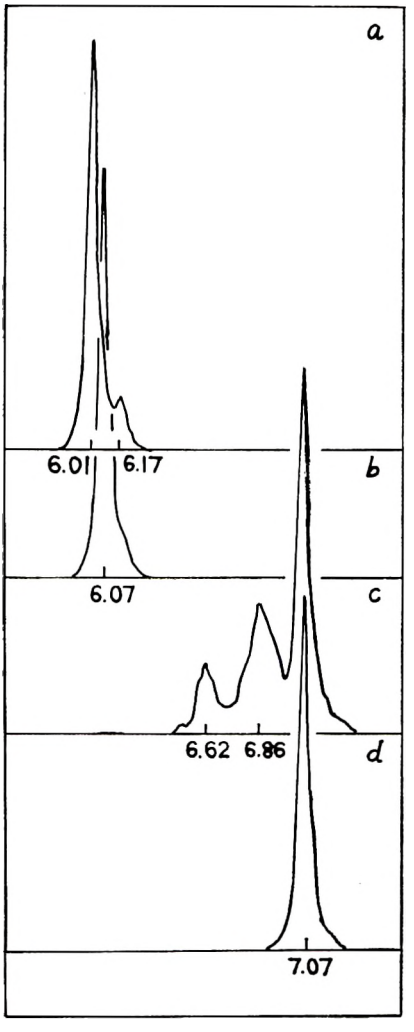

Fig. 1. NMR absorption spectra in *o*-dichlorobenzene solution of (*a*) 85/15 VDC–VC copolymer (only the thermally stable peaks shown); (*b*) PVDC; (*c*) PCPDCB; (*d*) PDCB.

Throughout every spectrum of the copolymers, some peaks (e.g., $\tau \approx 6.2$) were observed only when the sample contained methylbenzyl ether. This means that the structures giving these peaks in the copolymers are easily lost by thermal degradation. Some peaks (e.g., $\tau = 6.7$) have a complicated structure due to the splitting through I·I coupling with the nearest neighbor protons. Exclusive of these peaks, only two peaks ($\tau =$ 6.01 and 6.17) remain. As they are thermally stable, and also do not suffer any I·I coupling, they can be used with accuracy for the analysis (only these peaks are shown in Fig. 1*a*). Possible structures for them will be —$CCl_2CH_2CCl_2$— and —$CCl_2CH_2CH_2CCl_2$—, corresponding to head-to-

tail and head-to-head structures in VDC sequences, respectively. The diamagnetic screening of the protons in the former is larger than in the latter because of large electronegativity of chlorine atom, so that the assignment that

$$\tau = 6.01 \text{ —}CCl_2CH_2CCl_2\text{—}$$

$$\tau = 6.17 \text{ —}CCl_2CH_2CH_2CCl_2\text{—}$$

may be adopted. This assignment suggests the existence of head-to-head structure in the VDC sequences in VDC–VC copolymers.

On the contrary, only one peak ($\tau = 6.07$) is observed in the spectrum of PVDC (Fig. 1*b*), suggesting a structure like —$CCl_2CH_2CCl_2$—.

Three peaks are observed in the spectrum of PCPDCB ($\tau = 6.62$, 6.86, and 7.07), but only one peak for PDCB ($\tau = 7.07$). By comparison between these two spectra with consideration of large electronegativity of chlorine atom the peaks at 6.62, 6.86, and 7.07 may be assigned to the structures of —CCl_2—CH_2—CH_2—CCl_2—, =CCl—CH_2—CH_2—CCl_2—, and =CCl—CH_2—CH_2—CCl=, respectively. This fact also supports the presence of head-to-head structure in the VDC sequences in the VDC–VC copolymer. The τ value corresponding to the structure of —CCl_2CH_2-CCl_2— of PCPDCB is different from that of the copolymer. This may be due to the diamagnetic screening of protons by π-electrons in the former. For the purpose of comparison of NMR spectra of the copolymers, chlorinated poly-2,3-dichlorobutadiene would be more suitable than PCPDCB, but it could not be used since no solvent for this polymer was available. On consideration of these facts, it is certain that the two thermally stable peaks at $\tau = 6.01$ and 6.17 may be assigned as noted above. Then it follows that the number (or mole) fractions of the protons contained by the head-to-tail and head-to-head structure in VDC sequence can be directly obtained from the evaluation of the ratios of intensities of the two peaks at $\tau = 6.01$ and 6.17. The existence of tail-to-tail structure, —CCl_2CCl_2—, which, of course, give no peak in NMR spectra, would be neglected except for the extreme case of the copolymerization. (Perhaps, tail-to-tail bonds may be constructed in the boundary regions of the two kinds of constituent

TABLE II
Number (or Mole) Fraction of Skeletal Head-to-Head Structures in VDC–VC Copolymers

Sample	VDC/VC feed ratio	Fraction, %
1	5/95	—
2	25/75	45.5
3	30/70	34.8
4	50/50	24.7
5	80/20	12.6
6	85/15	10.1
PVDC	100/0	0.0

monomers.) Then, the number (or mole) fractions of the skeletal structures (head-to-tail or head-to-head) are obtained from the ratio of intensity of the peak at $\tau = 6.01$ or a half of that at $\tau = 6.17$ to the sum of these two, because the peaks at $\tau = 6.01$ and 6.17 are results of contributions from the structural units with two and four protons, respectively. The obtained result is shown in Table II and Figure 2. In the copolymer 1, these peaks could not be observed. This would mean that in this sample every VDC unit was always bonded with a VC unit.

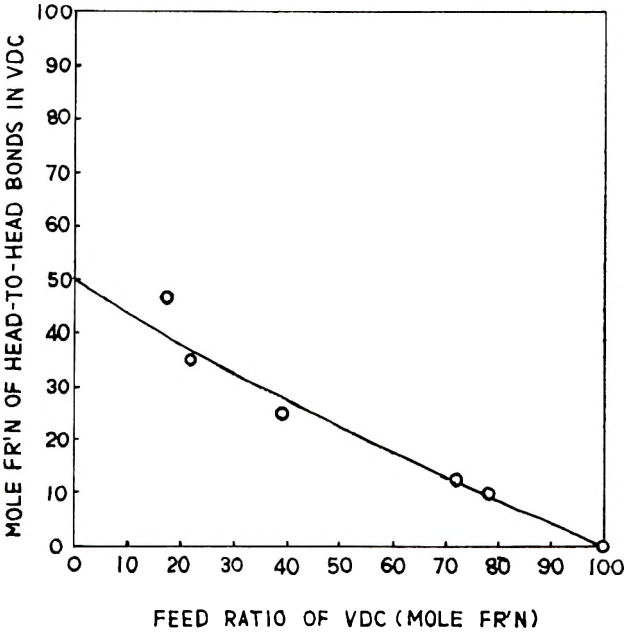

Fig. 2. Mole fraction of head-to-head bonds in VDC portions of VDC–VC copolymers determined from NMR spectra vs. feed ratio of VDC (mole fraction). The curve is obtained theoretically by eq. (21) for $B = 2.5$.

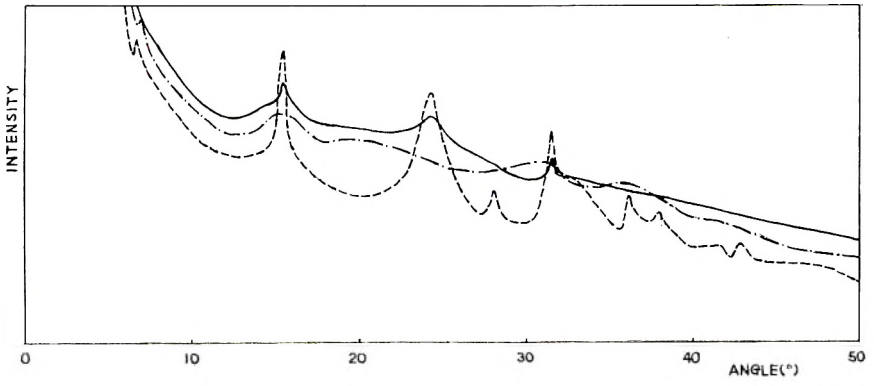

Fig. 3. X-ray diffraction patterns of (——) 25/75 VDC–VC copolymer; (- -) PVDC; (-·-) PCPDCB.

It is quite a new information that a head-to-head structure can exist in VDC–VC copolymers. (Similar information has been obtained for other polymers., e.g., polyvinyl alcohol[11] from the degradation with periodic acid, polyvinylidene fluoride,[8] and the copolymer of vinylidene fluoride and hexafluoropropylene[9] from high resolution NMR, etc.) It is of interest to compare with the result from other techniques.

It has been shown on the other hand that the x-ray diffraction patterns of these copolymers, except copolymer 1, are similar to that of PVDC, but not to that of CPDCB[2] (Fig. 3). This means that the head-to-head structure cannot enter the crystalline regions; in other words, the crystallinity of the copolymer is reduced also by the occurrence of head-to-head structure of the same specie.

Theoretical Considerations

The information on the local regularity of copolymers, such as the number fractions of head-to-head structure in VDC sequences in the copolymers, can be obtained theoretically with the aid of the method of the eigenvalue problem which has been successfully applied to the Ising model.[10,13]

Suppose that copolymer is constructed of two types of monomers, L and H, in which L polymerizes with a lower energy than H different by J. In the sample of low conversion the numbers (N_L and N_H) of constituent monomers in the copolymer are much smaller than those (M_L and M_H) of the original.

Assuming that there is a virtual energy $-I$ at each boundary between the L- and H-monomer constituents in copolymers, neglecting the effect from the ends of polymer chains, we can express the total energy E of the copolymer system as

$$E = \sum_{i=1}^{N} \epsilon_i = -J \sum_{i=1}^{N} \mu_i - I \sum_{i=1}^{N} (\mu_i - \mu_{i+1})^2 \tag{1}$$

where $\mu_i = 1$ if the ith monomer is L, and $\mu_i = 0$, if the ith monomer is H, and

$$N = N_L + N_H \tag{2}$$

Then, the partition function in the ensemble of low conversion copolymer system is given by

$$Z = \sum_{\mu_1} \sum_{\mu_2} \cdots \sum_{\mu_N} \prod_i \rho_i \exp\{-\epsilon_i/kT\} = \text{Trace } (\mathbf{A}^N) \tag{3}$$

where $\rho_i = M_L/M_H$ ($\equiv \rho_0$), if the ith monomer is L, and $\rho_i = 1$ if the ith monomer is H; the transition matrix is:

$$\mathbf{A} = (\rho_i \rho_{i+1})^{1/2} [\exp\{(J/2kT)(\mu_i + \mu_{i+1}) + (I/kT)(\mu_i - \mu_{i+1})^2\}] \tag{4}$$

and the matrix elements are

μ_i \ μ_{i+1}	1	0
1	$\rho_0 B$	$\rho_0^{1/2} B^{1/2} D$
0	$\rho_0^{1/2} B^{1/2} D$	1

(5)

with

$$\mathrm{B} = \exp\{J/kT\} \tag{6}$$

and

$$D = \exp\{I/kT\} \tag{7}$$

where k is the Boltzmann constant and T is the polymerization temperature in degrees Kelvin). Since $N \gg 1$, we have

$$Z = \lambda^N \tag{8}$$

where λ is the largest eigenvalue of the matrix A:

$$\lambda = {}^1/_2 \{\rho_0 B + 1 + [(\rho_0 B - 1)^2 + 4\rho_0 B D^2]^{1/2}\} \tag{9}$$

The quantities of local regularity of copolymers as are obtained from eq. (8). Since eq. (9) is obtained by substitution of B's in eq. (I.7) in the previous paper for $\rho_0 B$'s, the following formulae are given by the substitution of B's in eqs. (I.8), (I.9), and (I.10) in the previous paper for $\rho_0 B$'s.

$$N_{\mathrm{L}} = N\rho_0 B/(\rho_0 B + 1) \tag{10}$$

$$N_{\mathrm{H}} = N/(\rho_0 B + 1) \tag{11}$$

$$n = N\rho_0 B/(\rho_0 B + 1)^2 \tag{12}$$

$$\langle l \rangle = \rho_0 B + 1 \tag{13}$$

$$\langle h \rangle = (\rho_0 B + 1)/(\rho_0 B) \tag{14}$$

where n is the average number of the blocks composed of L-monomers, and $\langle l \rangle$ and $\langle h \rangle$ are the average number of elements per block with L- and H-monomers, respectively.

These quantities can be obtained by the same combinatory method as adopted in the previous paper.[2] The number of the blocks composed of l L-monomers and h H-monomers are given by

$$\begin{aligned} x_l &= (\sum_l x_l)(e^{-\beta} - 1)\, e^{\beta l} \\ y_h &= (\sum_h y_h)(e^{-\gamma} - 1)\, e^{\gamma h} \end{aligned} \tag{15}$$

respectively, where β and γ are undeterminate multipliers [see eq. (I.15) in the previous paper]. Thus,

$$n = \sum_l x_l = \sum_h y_h = N_L(1 - e^{\beta}) = N_H[1 - e^{\gamma}) \tag{16}$$

is also obtained. From the comparison of eqs. (10), (11), and (12) with eq. (16), β and γ are determined as

$$e^{\beta} = \rho_0 B/(\rho_0 B + 1)$$

$$e^{\gamma} = 1/(\rho_0 B + 1) \tag{17}$$

and eqs. (15) are rewritten as

$$x_l = \frac{N}{(\rho_0 B + 1)^2}\left(\frac{\rho_0 B}{\rho_0 B + 1}\right)^l$$

$$y_h = \frac{N(\rho_0 B)^2}{(\rho_0 B + 1)^2}\left(\frac{1}{\rho_0 B + 1}\right)^h \tag{18}$$

Comparison of Theory with Experiment

If the head-to-head structure in the VDC sequence in VDC–VC copolymer is exclusively constructed by the existence of boundary regions of VDC and VC monomer constituents, the number (or mole) fraction, r, of the former is given by

$$r = (n - x_1)/(N_L - x_1) \tag{19}$$

where VDC monomers are denoted as L. The term $-x_1$ in the denominator is inserted since head-to-head and head-to-tail structure cannot be made with only one monomer, and the same term in the numerator was used because of the impossibility of head-to-head structure in blocks with only one monomer. Under the above assumption, all protons in VDC parts are observed in NMR experiment as the peaks corresponding to VDC, not boundary, so that the $-n$ term does not appear in the denominator of eq. (19). Substituting n, x_1 and N_L in eq. (19) in eqs. (10), (11), and (18), we have

$$r = 1/(\rho_0 B + 2) \tag{20}$$

If the feed ratio,

$$f = \rho_0/(\rho_0 + 1) \tag{21}$$

of L- or VDC monomers is introduced, we have

$$r = (1 - f)/\{2 + (B - 2)f\} \tag{22}$$

The curve in Figure 2 is obtained by using the value of $B = 2.5$ in eq. (22). This shows good agreement with the experiment in $f > 0.5$ (50%). (The discrepancy between both curves in $f < 0.5$ perhaps resulted from experimental inaccuracy due to low intensity of NMR peaks in this region.) Using the value $B = 2.5$ in eq. (6), the difference between the two polymerization energies is given as $J = 600$ cal./mole for $T = 328°K$.

Common terms for local regularity of the copolymers are monomer reactivity ratios, r_L and r_H,[14] defined by

$$r_L = k_{LL}/k_{LH} \tag{23}$$

and

$$r_H = k_{HH}/k_{HL}$$

where k_{ij} is a rate constant in which j monomer adds to the copolymer radical terminating with i monomer end. Such ratios are related in our formulae as follows with the aid of Goldfinger and Kane's work:[15]

$$\langle l \rangle = r_L (M_L/M_H) + 1$$

$$\langle h_H \rangle r_H (M_H/M_L) + 1 \tag{24}$$

Thus, we have

$$r_L = 1/r_H = B \tag{25}$$

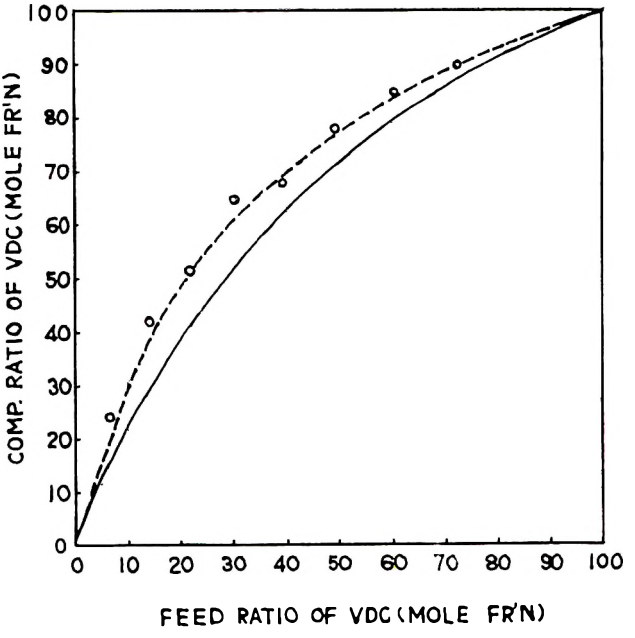

Fig. 4. Composition ratio of VDC vs. feed ratio of VDC with calculated value of monomer reactivity ratio obtained from (——) NMR spectra and (- -) infrared absorption data;[16] (○) experimentally obtained values in infrared absorption study.[16]

Two quantities, r_L and $1/r_H$, are not equal in general but are equal in our single parameter theory. Substituting $B = 2.5$ in eq. (25) for B we have

$$r_L = 2.5 \tag{26}$$

and

$$r_H = 0.4$$

These values show fairly good consistency with those obtained from infrared absorption:[16]

$$r_L = 3.15 \tag{27}$$

and

$$r_H = 0.23$$

The relation between N_L, N_H and M_L, M_H and r_L, r_H is given by eq. (28):[14]

$$N_L/N_H = (M_L/M_H)\,(r_L M_L + M_H)/(r_H M_H + M_L) \tag{28}$$

Equation (28) is identical with eq. (10), if $r_L = 1/r_H$.

Substituted formulae of eqs. (26) and (27) for eq. (28) are plotted in Figure 4 with the experimental data of infrared absorption. The small discrepancy between the two curves in Figure 4 is apparently caused by neglecting the presence of head-to-head bonds in infrared absorption experiment.

The authors would like to express their sincere thanks to Drs. M Asahina, K. Okuda, M. Onozuka, and Y. Amagi for their kind preparation of the samples and their helpful discussions.

References

1. Bovey, F. A., G. V. D. Tiers, and G. Filipovich, *J. Polymer Sci.*, **38**, 73 (1959); F. A. Bovey and G. V. D. Tiers, *J. Polymer Sci.*, **44**, 173 (1960); F. A. Bovey, *J. Polymer Sci.*, **46**, 59 (1960).
2. Nishioka, A., H. Watanabe, I. Yamaguchi, and H. Shimizu, *J. Polymer Sci.*, **45**, 232 (1960); A. Nishioka, H. Watanabe, K. Abe, and Y. Sono, *J. Polymer Sci.*, **48**, 241 (1960).
3. Johnsen, U., and K. Tessmar, *Kolloid. Z.*, **168**, 160 (1960); U. Johnsen, *Kolloid-Z.*, **178**, 161 (1961).
4. Brownstein, S., S. Bywater, and D. J. Worsfold, *Makromol. Chem.*, **48**, 127 (1961).
5. Miller, W. L., W. S. Brey, Jr., and G. B. Butler, *J. Polymer Sci.*, **54**, 329 (1961).
6. Johnsen, U., *J. Polymer Sci.*, **54**, S6 (1961).
7. Chûjô, R., S. Satoh, T. Ozeki, and E. Nagai, *J. Polymer Sci.*, **61**, S12 (1962); S. Satoh, R. Chûjô, T. Ozeki, and E. Nagai, *Rept. Progr. Polymer Phys. Japan*, **5**, 251 (1962); S. Satoh, R. Chûjô, T. Ozeki, and E. Nagai, *J. Polymer Sci.*, **62**, S101 (1962).
8. Naylor, R. E., Jr., and S. W. Lasoski, Jr., *J. Polymer Sci.*, **44**, 1 (1961).
9. Ferguson, R. C., *J. Am. Chem. Soc.*, **82**, 2416 (1960).
10. Miyake, A., and R. Chûjô, *J. Polymer Sci.*, **46**, 163 (1960).
11. Flory, P. J., and F. S. Leutner, *J. Polymer Sci.*, **3**, 880 (1948).
12. Okuda, K., unpublished work.
13. Kramers, H. A., and G. H. Wannier, *Phys. Rev.*, **60**, 252 (1941).
14. Mayo, F. R., and R. M. Lewis, *J. Am. Chem. Soc.*, **66**, 1954 (1944).
15. Goldfinger, G., and T. Kane, *J. Polymer Sci.*, **3**, 462 (1948).
16. Enomoto, S., *J. Polymer Sci.*, **55**, 95 (1961)

Résumé

La présence de structures du type tête-à-tête de séquences de chlorure de vinylidène dans des copolymères chlorure de vinylidène-chlorure de vinyle en rapports différents a été démontrée par une étude de NMR en haute résolution. On a évalué le rapport de la structure tête-à-tête dans les séquences de chlorure de vinylidène par la mesure des intensités du spectre NMR L'importance des séquences régulières locales dans le copolymère a été utilisée dans le traitement théorique basé sur l'énergie de liaison virtuelle et la méthode combinatoire. Les résultats expérimentaux ont été comparés aux calculs théoriques.

Zusammenfassung

Die Anwesenheit einer Kofp-zu-Kopf-Struktur in der Vinylidenchloridsequenz von Vinylidenchlorid-Vinylchloridcopolymeren bei verschiedenen Monomerverhältnissen im Ansatz wurde durch eine Hochauflösungs-NMR-Untersuchung festgestellt. Der Anteil an Kopf-zu-Kopf-Struktur in der Vinylidenchloridsequenz wurde aus Intensitätsmessungen am NMR-Spektrum bestimmt. Die auf die lokale Regelmässigkeit des Copolymeren bezüglichen Grössen wurden in einer theoretischen Behandlung auf Grundlage der virtuellen Grenzenergie und der kombinatorischen Methode verwendet. Ein Vergleich zwischen Versuchsergebnissen und theoretischen Berechnungen wurde durchgeführt.

Received January 2, 1963

JOURNAL OF POLYMER SCIENCE: PART A VOL. 2, PP. 907–921 (1964)

Hydration and Ion Binding of Polyelectrolytes

AKIRA IKEGAMI, *Department of Physics, Faculty of Science, Nagoya University, Nagoya, Japan*

Synopsis

The counterion binding of polyelectrolytes has been investigated with special attention to the change of the structure of water in the neighborhood of charged polymer skeleton induced by the binding. The molar volume change due to this structural change of water was obtained by the method of refractivity measurement. Systems employed were polyacrylic acids neutralized to varying degrees by tetra-*n*-butyl-ammonium hydroxide or sodium hydroxide in the presence and absence of simple low molecular salts such as NaCl and $BaCl_2$. The results indicate that there are two regions of water around the polyion. In the first "intrinsic" hydration region, water molecules are oriented to individual charged groups. In the second region, water molecules are rearranged by the cooperative action of two or more charged groups on the polyion. The binding of Ba^{++} or La^{+++} to the polyion destroys not only the second region but also the first intrinsic region. On the other hand, Na^+ ions are bound only in the second region without effect on the first region. The amount of bound Na^+ ions estimated by refractivity measurement changes with the charge density of the polyion, showing the characteristic feature as a condensation phenomenon.

INTRODUCTION

Various experimental results on the activity of counterions, osmotic pressure of polyelectrolyte solutions, and translational motion of polyions have shown that many counterions are associated with polyions.[1–5] Several kinds of models such as the ion pair, site binding, and domain binding have been proposed on the mechanism of this counterion association phenomenon.[6–11] The purpose of the present work is to investigate experimentally what kind of model is most appropriate.

Absorption spectra measurement,[12] is one of the most useful methods giving direct information on interactions between polyions and low molecular ions at the molecular level, but the applicability of this method is limited to special cases.

As discussed in a previous paper,[13] the state of counterions bound to polyions is closely related not only to the charge or the species of polyions and counterions, but also to the structure of water around the polyion. It is important, therefore, to analyze the counterion–polyion binding with special attention to the change in the structure of water associated with the binding. For such an analysis we applied the method of the refractivity measurement.

Refractivity, Volume Change, and Hydration

Recently it has been shown that the equation of Lorentz and Lorenz is applicable to a multicomponent system;[14,15] that is, the refractive index n of a solution is related to polarizabilities of components in the form

$$\frac{n^2 - 1}{n^2 + 2} = \frac{4\pi}{3 \times 10^3} \sum_{i=0}^{i} C_i P_i \tag{1}$$

where C_i and P_i are the concentrations in moles/liter and the molar polarizability of component i, respectively, and subscript zero indicates solvent.

Let us consider an aqueous solution A containing solute components a_i, the concentrations of which are C_{a_i}. When each solute molecule (ion) changes the structure of water in its neighborhood, the contribution to the refractivity of water molecules in this region (the hydrated water) must be taken into account separately from the usual water. If water in the solution is classified into two kinds (the hydrated water and the usual water), the difference between the refractive index of the solution and that of the pure water is given by

$$\Delta n = \frac{2\pi}{9 \times 10^3} \frac{(n_0^2 + 2)^2}{n_0^2} \left\{ \left[\sum_{i=1}^{i} C_{a_i} P_{a_i} + C_h P_h + C_0 P_0 \right] - C_{00} P_0 \right\} \tag{2}$$

at low solute concentrations where the higher order interaction between solutes can be neglected; P_h and C_h are the polarizability and the concentration in moles/l., respectively, of the hydrated water molecules, C_0 and C_{00} are the concentrations in mole/liter of the usual water in solution A and pure water, respectively.

If the number of hydrated water molecules per solute molecule a_i is denoted by H_{a_i} then

$$C_h = \sum_{i=1}^{i} H_{a_i} C_{a_i}$$

The concentration difference of the usual water in pure solvent and solution $C_{00} - C_0$ is given by

$$C_{00} - C_0 = v_h C_h + \sum v_{a_i} C_{a_i}$$

where v_a and v_h are volume ratios of the solute component and the hydrated water to the usual water, respectively.

Then the increment of refractivity of the solution is expressed as follows:

$$\Delta n = \frac{2\pi}{9 \times 10^3} \frac{(n_0^2 + 2)^2}{n_0} \sum_{i=1}^{i} [(1 - v_h) H_{a_i} C_{a_i} P_0 - v_{a_i} C_{a_i} P_0 + H_{a_i} C_{a_i} (P_h - P_0) + C_{a_i} P_{a_i}] \tag{3}$$

Now, we consider a mixture of two solutions A and B. If there is neither interaction between solute components a_i and b_j nor volume change

upon mixing, the refractive index increment of the solution A + B is equal to the sum of those of A and B. When components a_i and b_j interact with each other and make a complex a_ib_j, the difference in the refractive index due to mixing must be written as

$$\begin{aligned}\Delta n &\equiv \Delta n(\mathrm{A}+\mathrm{B}) - \Delta n_{\mathrm{A}} - \Delta n_{\mathrm{B}} \\ &= \frac{2\pi}{9\times 10^3}\frac{(n_0^2+2)^2}{n_0}\left[(H_{(a_ib_j)} - H_{a_i} - H_{b_j})(1-v_h)P_0\right. \\ &\quad -(v_{(a_ib_j)} - v_{a_i} - v_{b_j})P_0 + (H_{(a_ib_j)} - H_{a_i} - H_{b_j})(P_h - P_0) \\ &\quad \left. + (P_{(a_ib_j)} - P_{a_i} - P_{b_j})\right]C_{(a_ib_j)} \qquad (4)\end{aligned}$$

because polarizability $P_{(a_ib_j)}$, volume ratio $v_{(a_ib_j)}$, number of the hydrated water molecules $H_{(a_ib_j)}$ of complex a_ib_j must be different from either a_i or b_j.

In eq. (4) the first and second terms come from the volume change of water and solutes due to the complex formation. The last two terms come from the polarizability change of the components. Experimentally, however, the polarizabilities of low molecular weight solutes and water have been found not to be much influenced by the interaction among them, so that the contribution of the last two terms can be neglected as compared with the first two terms. Then, the volume change associated with the complex formation $a_i + b_j - a_ib_j$ is directly related to the refractivity change as shown in eq. (5):

$$\begin{aligned}\Delta V &\equiv \bar{V}_{(a_ib_j)} - \bar{V}_{a_i} - \bar{V}_{b_j} \\ &= \frac{-M_0}{\rho_0}\left[(H_{(a_ib_j)} - H_{a_i} - H_{b_j})(1-v_h) - (v_{(a_ib_j)} - v_{a_i} - v_{b_j})\right] \qquad (5) \\ &= \frac{-6n_0\times 10^3}{(n_0^2+2)(n_0^2-1)}\frac{d\Delta n}{dC_{(a_ib_j)}}\end{aligned}$$

where $\bar{V}_a$ is the apparent partial molar volume of component a.

Unfortunately we have few data on the volume change of solute molecules (ions) due to the complex formation. In usual electrolyte solutions, however, the volume change $v_{(a_ib_j)} - v_{a_i} - v_{b_j}$ directly due to the complex formation is very much smaller than that due to the change of the hydration. In this case the change of the number of hydrated water molecules can be related to the refractivity change. Then, if we put v_h equal to 0.89 as estimated by ultrasonic measurements,[16] we have

$$\Delta H = \frac{6}{11}\left[\frac{n_0\times 10^5}{(n_0^2-1)(n_0^2+2)}\right]\frac{d\Delta n}{dC_{(a_ib_j)}} \qquad (6)$$

EXPERIMENTAL

Polyacrylic acid having a degree of polymerization of 3750, was supplied by Towa Gosei Company as a laboratory sample. Other chemicals were reagent grade.

A solution of polyacrylic acid of neutralization degree zero was obtained after dialysis against redistilled water for two weeks. The concentration of polyion of this solution was determined by titration with a standard base in the presence of a sufficient concentration of NaCl. By adding to this polyacrylic acid solution a calculated amount of solutions of pure hydroxides (tetrabutylammonium hydroxide or sodium hydroxide), we obtained solutions of various degrees of neutralization. By mixing these solutions with low molecular salt solutions of different concentrations at an exactly constant volume ratio we made various sample solutions, the refractivities of which were measured. All of the original solutions of polyacrylic acid and low molecular salts and all sample solutions were stored in tightly sealed polyethylene bottles to avoid contamination with sodium or calcium ion.

A differential refractometer was employed for refractivity measurements. The apparatus constant was determined with simple salt solutions for which the concentrations were determined by conductivity measurements. All measurements were made at 25°C. by the use of a temperature-controlled water bath.

RESULTS

A. Low Molecular Weight Electrolyte Systems

Refractivities of solutions of strong acid HCl partially neutralized by strong base sodium hydroxide (NaOH) or tetra-*n*-butylammonium hydroxide, (Bu_4NOH) were measured. Results are shown in Figure 1, where the difference of refractive index

$$\Delta n = \Delta n_{(\text{acid+base})} - \Delta n_{\text{acid}} - \Delta n_{\text{base}}$$

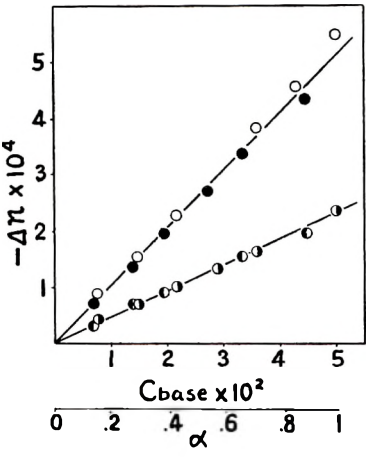

Fig. 1. The relation between the decrement of refractivity of acid solutions and the degree of neutralization α: 0.05N HCl solutions neutralized by (○) Bu_4NOH and (●) by NaOH; 0.05N CH_3COOH solutions neutralized by (◑) Bu_4NOH and (◐) by NaOH.

is plotted against the degree of neutralization α = [base]/[acid]. In this case the difference Δn is caused by the neutralization process;

$$\alpha(H^+ + OH^-) \rightarrow \alpha H_2O \quad (7)$$

In the case of the neutralization of weak acid (CH_3COOH) by strong base (NaOH or Bu_4NOH) (Fig. 1), the refractive index difference is caused by the reaction

$$CH_3COOH + OH^- \rightarrow CH_3COO^- + H_2O \quad (8)$$

By combining reactions (7) and (8), ΔV and ΔH associated with the reaction

$$CH_3COOH \rightarrow CH_3COO^- + H^+ \quad (9)$$

are calculated by the use of eqs. (5) and (6) and given in Table I. For this reaction (9) ΔV is negative, which means that the hydration of COO^- and H^+ is stronger than that of COOH. The results also show that ΔV and ΔH are independent of α and the species of base.

TABLE I
Volume Change Accompanying Various Ionic Reactions

Reaction	ΔV at 25°C., ml./mole: Present results	Literature results	Reference	$-\Delta H$
$H^+ + OH^- \rightarrow H_2O$	28.2	23.4	22	15.6
$CH_3COO^- + H^+ \rightarrow CH_3COOH$	15.5	9.2	22	8.6
		11.47	23	
		12.5	24	
$RCOO^- + H^+ \rightarrow RCOOH$ (α = 1)	18.8	17.7	25	10.4
$RCOO^- + H^+ \rightarrow RCOOH$ (α = 1)	32.5			18.0
$RCOO^- + Na^+ \rightarrow RCOONa$($\alpha$ = 1)	12.5			6.9
$RCOO^- + {}^1/_2Ba^{++} \rightarrow RCOO({}^1/_2)Ba$ (α = 1)	30.8			17.0
$RCOO^- + {}^1/_3La^{+++} \rightarrow RCOO({}^1/_3)La$ (α = 1)	23.3			12.9

B. Partially Neutralized PAA

The difference of refractivity of polyacrylic acid solutions partially neutralized by tetra-*n*-butylammonium hydroxide

$$\Delta n = \Delta n_{(PAA+Bu_4NOH)} - \Delta n_{PAA} - \Delta n_{Bu_4NOH}$$

was measured. The result is shown in Figure 2. The tetrabutylammonium ion Bu_4N^+ can be assumed not to be bound to polyions on account of its large size.[17,18] Then the difference of refractivity Δn is caused by the reaction

$$\alpha RCOOH + \alpha OH^- \rightarrow \alpha RCOO^- + H_2O \quad (10)$$

where RCOOH indicates the monomeric unit of PAA.

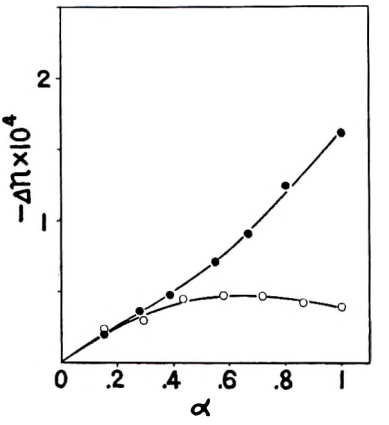

Fig. 2. The relation between the decrement of refractivity of PAA solutions and the degree of neutralization α; 0.05N PAA solutions neutralized by (○) Bu_4NOH and (●) by NaOH.

By combining with the result for the reaction (7), ΔV caused by the reaction $RCOO^- + H^+ \rightarrow RCOOH$ is plotted against α in Figure 4. In this case ΔV is not independent of α but increases in proportion to the increase of α.

Refractivity of solutions of PAA partially neutralized by NaOH was measured and the results are shown in Figure 2, where

$$\Delta n = \Delta n_{(PAA+NaOH)} - \Delta n_{PAA} - \Delta n_{NaOH}$$

is plotted against α.

A remarkable difference is found between the neutralization of carboxyl groups of PAA by Bu_4NOH and that by NaOH.

C. Bu_4NPA and NaPA with Strongly Bound Cations

The refractivities of mixtures of tetra-*n*-butylammonium polyacrylate Bu_4NPA solution with various solutions of HCl, $BaCl_2$, and $LaCl_3$ were measured. The refractivity difference due to the mixing is shown in Figure 3. As reported in the previous paper,[13] the cations H^+, Ba^{++}, and La^{+++} are almost completely bound to Bu_4NPA, so that the refractivity differences are caused by the reactions

$$\begin{aligned} RCOO^- + H^+ &\rightarrow RCOOH \\ RCOO^- + {}^1/_2Ba^{++} &\rightarrow RCOO\ {}^1/_2Ba \\ RCOO^- + {}^1/_3La^{+++} &\rightarrow RCOO\ {}^1/_3La \end{aligned} \qquad (11)$$

In Figure 4, ΔV caused by these reactions is plotted against α or the fraction of complexes to the total carboxyl group F. In these three cases ΔV increases in proportion to the increase of concentration of the complex, and as seen in the figure, the gradients of increase of ΔV are always independent of the species of bound cations being the same as that in the

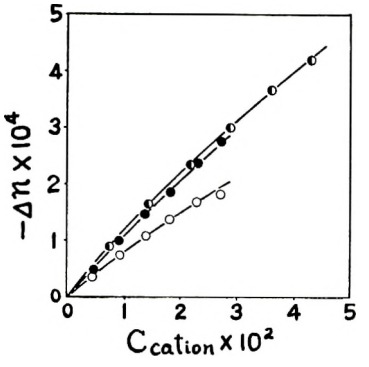

Fig. 3. The relation between the decrement of refractivity of Bu_4NPA solutions accompanying the binding of various cations and the concentration of added cations ($Cp = 0.05N$): (◐) HCl; (○) $BaCl_2$; (●) $LaCl_3$.

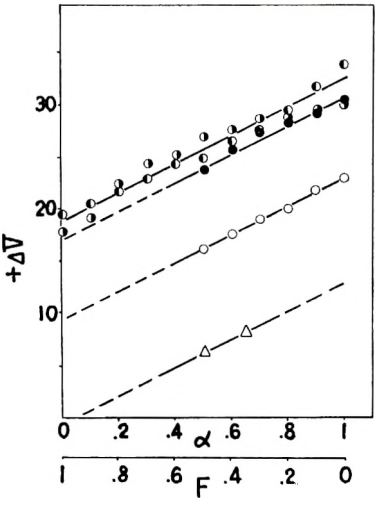

Fig. 4. The relation between the change in partial molar volume ΔV accompanying binding of various cations to Bu_4NPA and α or the fraction of bound cations to the total amount of carboxyl groups F: (◑), (◐)H^+; (△) Na^+; (○) Ba^{++}; (●) La^{+++}.

neutralization of PAA by Bu_4NOH. This suggests that the increase of ΔV with α is due to the increase of interaction between $RCOO^-$ groups on PAA. Referring to the expression of ΔV as shown in eq. (5), it is reasonable to consider that only the contribution from the hydration of $RCOO^-$ groups changes with α, because the hydration of a $RCOO^-$ group is affected by the neighboring COO^- groups. Thus, we interpret that the data in Figure 4 means that

$$\bar{V}_{RCOO^-}(\alpha) = \bar{V}_{RCOO^-}(0) - 13.7\alpha \qquad (12)$$

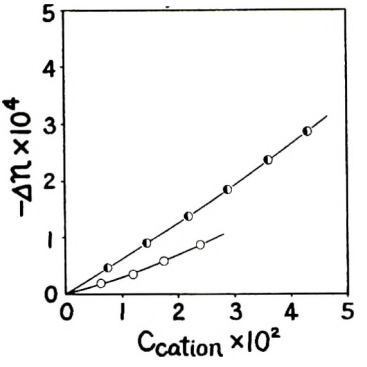

Fig. 5. The relation between the decrement of refractivity of NaPA solutions accompanying the bindng of various cations and the concentration of added cations ($Cp = 0.05N$): (◑), (◐)H^+; (○)Ba^{++}.

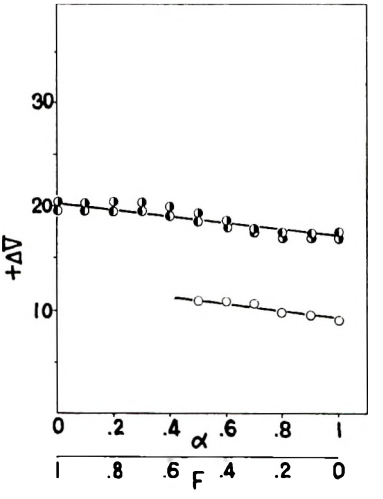

Fig. 6. The relation between the change in partial molar volume ΔV accompanying binding of various cations to NaPA and α or the fraction of bound cations to total amount of carboxyl groups F: (◑), (◐) H^+; (○) Ba^{++}.

or

$$H_{RCOO^-}(\alpha) = H_{RCOO^-}(0) + 7.6\alpha \qquad (13)$$

The numerical value of H_{RCOO^-} is difficult to be estimated because the values of H_{H^+} and H_{RCOOH} are unknown. If we assume that $H_{CH_3COOH} = H_{RCOOH}$, then $H_{RCOO^-}(0)$ is found to be greater than H for carboxyl groups of small molecules, as seen in Table I.

The results of similar experiments on the mixture of sodium polyacrylate NaPA solutions and HCl or $BaCl_2$ solutions are shown in Figures 5 and 6. In this case ΔV is almost constant or a little decreasing with increasing α. Such behavior is similar to the case of the neutralization by NaOH and

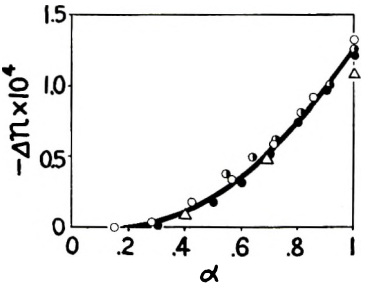

Fig. 7. The decrements of refractivities accompanying Na^+ binding to PAA at various α: (●) obtained by neutralization of PAA by Bu_4NOH and NaOH; (○) obtained by binding of H^+ to Bu_4NPA and NaPA; (◑) obtained by binding of Ba^{++} to Bu_4NPA and NaPA; (△) obtained by binding of Na^+ to PAA partially neutralized by Bu_4NOH (see Fig. 8).

very different from the case of Bu_4NOH. The numerical value of ΔV in the NaPA system is found to be nearly equal to the value of ΔV at $\alpha = 0$ of the Bu_4NPA system.

The difference in the behaviors of ΔV between the NaPA and the Bu_4NPA is attributable to the fact that some fraction f of Na^+ counterions is bound to polyions by the process

$$f\ RCOO^- + f\ Na^+ \rightarrow f\ RCOONa \tag{14}$$

From the difference between two curves in Figures 3 and 5, the refractivity change due to the process (14) can be obtained. The result is shown in Figure 7.

D. Binding of Na^+

To analyze the detailed process of the binding of Na^+ ions to polyions, we examined the effect of the addition of Na^+ to the PAA solutions at various degrees of partial neutralization by Bu_4NOH. The result is shown in Figure 8. The refractivity Δn greatly increases in proportion to the increase of the concentration of added NaCl up to a certain critical concentration of NaCl which depends on the degree of neutralization. Above this critical concentration, the increase of Δn becomes very small and independent of α. It can be assumed that the first steep increase of Δn is due to the binding of added Na^+ to polyions and this binding is saturated at the critical concentration of Na^+ above which the increase of Δn is caused by a simple salt effect.

This assumption is supported by the fact that the value of Δn at critical points as a function of α is in good agreement with the value of Δn due to the binding estimated by the previous method, as shown in Figure 7.

On the basis of this assumption the fraction f of bound Na^+ at saturation can be obtained at various degrees of neutralization α. The result in Figure 9 shows that the binding of Na^+ occurs like a condensation phenomenon. When the degree of neutralization or the density of ionized

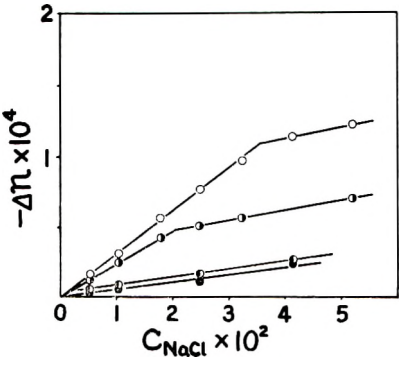

Fig. 8. The relation between the decrement of refractivities accompanying the binding of added Na to PAA partially neutralized by Bu_4NOH and the concentration of added NaCl ($Cp = 0.05$): (○) $\alpha = 1$, (◑) $\alpha = 0.69$; (◐) $\alpha = 0.40$; (●) $\alpha =$ 1 neutralized by NaOH (NaPA).

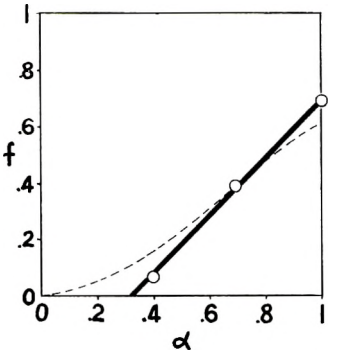

Fig. 9. The relation between the fraction f of bound Na^+ and α: (——) this work; (- -) data of Huizenga et al.[6]

carboxyl groups on polyions reaches a certain critical value ($\alpha = 0.3$), the further increase of ionization is covered by the binding of Na^+. The mean values of ΔV resulting from the Na^+ binding within the range of α of 1–0.3 and that within the range of 0.69–0.3 are calculated and given in Figure 4. The gradient of the change of ΔV with α in this case also is the same as those obtained by other cations.

DISCUSSION

In this paper we neglected the change of the atomic or ionic polarizability due to association or hydration and assumed the additivity law of polarizability. This assumption is supported by the experimental facts that the polarizability of electrolytes including weak acids is not changed within a wide range of concentration in spite of depression of proton dissociation,[19,20] and that the polarizability of water molecules is not changed within a wide range of temperature[21] in spite of the change of hydrogen bonds between

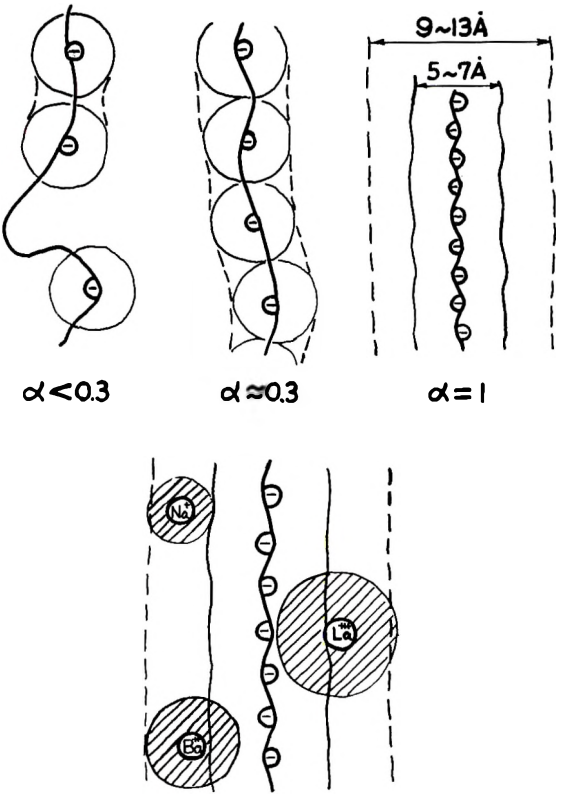

Fig. 10. Schematic representation of (*a*) skelton and hydration regions and (*b*) binding of various cations.

them. Under this assumption the change in refractivity of electrolyte solutions is caused mainly by the volume change resulting from ion binding and dehydration. Thus, the direct measurement of volume or density is equivalent to the refractivity measurement. Actually, the volume change estimated from the present method is almost the same as that by the direct measurement,[22–25] as seen in Table I. In practice, the measurement of a small difference of refractivity is easier than that of volume or density.

In the present system of polyelectrolytes, whether the volume change may be caused by ion binding itself or associated dehydration, it must be related to the structural change in the neighborhood of the polymer skeleton.

At low degrees of neutralization, the structure change due to the ionization of carboxyl groups is independent of each other because the average distance between charged groups is long enough. The ionization of a group increases the density of water in its neighborhood. If we assume a spherical region around each charged group in which the average density of water is about 1.1, then the radius of this region is estimated to be about 3.1 A. when v_H is put equal to − 5 ml.

As the average distance between charged groups becomes short with increasing α, the volume change associated with dissociation of a carboxyl group is affected by charged groups in the neighborhood. Actually, the spheres of radius 3.1 A. around carboxyl groups begin to overlap at $\alpha \approx 0.3$. Therefore, it is reasonable to suppose that at α higher than 0.3, the region of water structurally changed around the polyion becomes rather cylindrical than spherical. If we assume a cylindrical region around the polyion, the radius of this cylinder is estimated to be about A. at $\alpha = 15.6$.

Here, in order to explain the behavior of the change of ΔV with α, we assume two regions of water around a polyion, as shown in Figure 10. The first region is an "intrinsic" hydration region in which water molecules are oriented to individual charged groups. With increasing α, a second region appears in which water molecules are rearranged by the cooperative action of two or more charged groups on the polyion. If the ionization of neighboring carboxyl groups produces the second region in excess of individual first regions around the groups, it can be expected that the excess volume change is proportional to α, because the probability of ionization of a group neighboring to a charged group is proportional to α. The elongation of polyion with increasing α also may favor the increase of ΔV by the formation of special structures of water such as "icebergs" or "hydrates."

At high α, we can apply a rigid rod model having a continuous charge density $\alpha e/l$ around which a cylindrical second layer is formed. If we regard the layer as a continuous dielectric having dielectric constant $\epsilon(E)$ dependent on electric field E, we have the following relation between the electric field and distance r from the rod;

$$E = 2\alpha e/\epsilon(E)lr$$

By the use of the relation between $\epsilon(E)$ and E calculated by Booth,[26] we can get the function $E(r)$. If the outer boundary of the layer is defined by the condition that the potential energy of a water molecule in the field E is equal to kT, then the radius of the cylindrical layer becomes about 4.3 A. at $\alpha = 1$. If we apply a similar method to a spherical region around a point charge, the radius of the sphere becomes about 2.3 A. This means that the cylindrical model produces an excess region of water rearrangement by cooperative action of charge on the rod. The radius of the cylindrical layer is proportional to α, and therefore the total volume of the layer is proportional to α^2. This can explain the increase of ΔV in proportion to α at high α.

The formation of the cylindrical layer increases the stiffness of the polyion. This may be one of the causes of the difference in viscosity of Bu_4NPA and NaPA because in the latter the layer is partly destroyed by Na counterions.

As seen in Figure 4, the binding of La^{+++}, Ba^{++}, and Na^+ counterions to the polyion is associated with a volume increase of the order of 10 ml./mole. If the binding of these counterions causes a complete dehydration of carboxyl groups and bound counterions as in the case of H^+ ion, it is ex-

pected that the volume increase due to Na^+ binding is of the same order as in H^+, and the volume increase due to Ba^{++} or La^{+++} is larger than for H^+. Figure 4 means that the binding does not cause complete dehydration, although the volume change increases with increasing valency of counterions. The same gradient of decrease of ΔV with decreasing α or increasing counterion binding F for four cases suggests that the second region of water rearrangement around the polyion is similarly influenced by binding of four kinds of counterions H^+, Ba^{++}, La^{+++}, and Na^+. However, the difference of the height of ΔV among various kinds of counterions indicates a difference in the manner of binding in the intrinsic region. The lowest value of ΔV is realized in the case of Na^+, where ΔV extrapolated to $F = 1$ becomes nearly zero or negative. This suggests that the binding of Na^+ has no effect on the first "intrinsic" region of water around individual charged groups. Na^+ ions enter only into the second region. On the other hand, in the case of Ba^{++} and La^{+++}, the high extrapolated value of ΔV means that these ions destroy the first region, by local binding with carboxyl groups.

The remarkable character of Na^+ binding is also found in experimental results of Figure 6, where it is shown that ΔV associated with binding of H^+ or Ba^{++} to NaPA is almost constant independently of the amount of added ions. In the case of NaPA of high α, most of the second region was already destroyed by Na^+ counterions. With the addition of H^+ or Ba^{++}, Na^+ ions in the second region are displaced by H^+ or Ba^{++} which destroy the intrinsic hydration region. Therefore, ΔV at $\alpha = 1$ for NaPA is nearly equal to ΔV at $\alpha = 0$ for Bu_4NPA. The small negative gradient of ΔV in Figure 6 may be due to the decrease of fraction f of bound Na^+ with decreasing α.

The fraction of bound Na^+ obtained from transference measurements[5] is shown by the broken line in Figure 9. The characteristic feature of Na^+ binding as a condensation phenomenon is found in our experiments more clearly than in transference experiments. The mobility of Na^+ bound in the second region is smaller than that in water outside because the movement of bound Na must be associated with the change of the stiff structure of water in the second region. The transference experiment shows the decrease of the mobility of counterions even at low α where the refractivity measurements show no binding. It is not strange that the mobility of counterions begins to be lost even when they are not in the hydration region.

The author wishes to thank Prof. F. Oosawa and Dr. N. Imai of this laboratory for their useful advice.

References

1. Kern, W., *Z. Physik. Chem.*, **A181**, 240, 283 (1938); *ibid.*, **A184**, 201 (1939).
2. Kern, W., *Makromol. Chem.*, **2**, 279 (1948).
3. Nagasawa, M., and I. Kagawa, *J. Polymer Sci.*, **25**, 61 (1957); *ibid.*, **31**, 256 (1958).
4. Nagasawa, M., M. Izumi, and I. Kagawa, *J. Polymer Sci.*, **37**, 375 (1959).
5. Huizenga, J., P. F. Grieger, and F. T. Wall, *J. Am. Chem. Soc.*, **72**, 2638, 4228 (1950).
6. Harris, F., and S. A. Rice, *J. Phys. Chem.*, **58**, 725, **733** (1954).
7. Strauss, U. P., and P. D. Ross, *J. Am. Chem. Soc.*, **81**, 5292, 5295, 5299 (1959).
8. Morawetz, H., A. M. Kotliar, and H. Mark, *J. Phys. Chem.*, **58**, 619 (1954).
9. Fuoss, R. M., *J. Polymer Sci.*, **12**, 185 (1954).
10. Oosawa, F., N. Imai, and I. Kawawa, *J. Polymer Sci.*, **13**, 93 (1954).
11. Wall, F. T., *J. Phys. Chem.*, **61**, 1344 (1957).
12. Morawetz, H., *J. Polymer Sci.*, **17**, 442 (1955).
13. Ikegami, A., and N. Imai, *J. Polymer Sci.*, **56**, 133 (1962).
14. J. R. Tessman, A. H. Karn, and W. Schockley, *Phys. Rev.*, **92**, 890 (1953).
15. Roberts, S., *Phys. Rev.*, **76**, 1215 (1949).
16. Yasunaga, T., and T. Sasaki, *Nippon Kagaku Zasshi*, **72**, 87 (1951).
17. Gregor, H. P., and M. Frederick, *J. Polymer Sci.*, **23**, 451 (1957).
18. Gregor, H. P., D. H. Gold, and M. Frederick, *J. Polymer Sci.*, **23**, 467 (1957).
19. Fajans, H. F., H. Kohner, and W. Geffcken, *Z. Elektrochem.*, **34**, 1 (1928).
20. Kohner, H., and M. L. Gressmann, *Z. Physik. Chem.*, **A144**, 137 (1930).
21. *International Critical Tables of Numerical Data, Physics, Chemistry and Technology*, Vol. VII, McGraw-Hill Book Company, London, 1930.
22. Owen, B. B., and S. R. Brinkley, *Chem. Revs.*, **29**, 461 (1941).
23. Redlich, O., and J. Bigeleisen, *Chem. Revs.*, **30**, 171 (1942).
24. Hammann, S. D., and S. C. Lim, *Australian J. Chem.*, **7**, 329 (1954).
25. Wall, F. T., and S. J. Gill, *J. Phys. Chem.*, **58**, 740 (1954).
26. Booth, F., *J. Chem. Phys.*, **19**, 391, 1327, 1615 (1951).

Résumé

La liaison de l'ion de signe contraire des polyélectrolytes a été étudiée avec une attention tout spéciale et reliée au changement, provoquée par cette liaison, dans la structure de l'eau au voisinage du spuelette polymérique chargé. Le changement du volume molaire du à ce changement dans la structure de l'eau a été obtenu par des mesures de réfraction. Les systèmes utilisés sont des acides polyacryliques neutralisés à des taux différents par de l'hydroxyde de tétra-*n*-butyl ammonium en présénce et en absence de sels de faible poids moléculaires tels que NaCl et $BaCl_2$. Les résultats montrent qu'il y a deux régions d'eau autour du polyon. Dans la première région d'hydration "intrinsèque," les molécules d'eau sont orientées par rapport aux groupes chargés pris individuellement. Dans la seconde région, les molécules d'eau sont réarrangées par l'action coopérative de deux groupes chargés ou plus sur le polyion. La liaison de Ba^{++} ou La^{+++} au polyion détruit non seulement la seconde région mais également la première région intrinsèque. D'un autre côté, les ions Na^+ sont liés uniquement dans la seconde région sans effet sur la première région. La quantité des ions Na^+ liés, estimée par mesure de réfraction, change avec la densité de charge du polyion, et présente la marque caractéristique qu'un phénomène de condensation.

Zusammenfassung

Die Bindung von Gegenionen durch Polyelektrolyte wurde mit besonderer Berücksichtigung der in der Nachbarschaft des geladenen Polymerskeletts durch die Bindung induzierte Änderung der Wasserstruktur untersucht. Die Änderrung des Molvolumens

auf Grund dieser Strukturänderung des Wassers wurde durch Refraktionsmessung bestimmt. Untersurcht wurde Polyacrylsäure bei verschiedenem Neutralisationsgrad durch Tetra-*n*-butylammoniumhydroxyd oder Natriumhydroxyd mit und ohne Zusatz einfacher, niedrigmolekularer Salze wie NaCl und $BaCl_2$. Die Ergebnisse lassen die Anwesenheit von zwei Wasserbereichen in der Umgebung des Polyions erkennen. Im ersten Bereich der "inneren" Hydratation werden die Wassermoleküle zu individuellen gelandenen Gruppen orientiert. Im zweiten Bereich stehen die Wassermoleküle unter der kooperativen Wirkung zweier oder mehrerer geladener Gruppen am Polyion. Die Bindung von Ba^{2+} oder La^{3+} an das Polyion zerstört nicht nur den zweiten Bereich sondern auch den ersten, inneren Bereich. Andrerseits werden Na^+-Ionen nur im zweiten Bereich, ohne Einfluss auf den ersten Bereich, gebunden. Die Menge der gebundenen Na^+-Ionen wird durch Refraktionsmessungen bestimmt; sie ändert sich mit der Ladungsdichte des Polyions und zeigt das charakteristische Verhalten einer Kondensationserscheinung.

Received January 7, 1963

JOURNAL OF POLYMER SCIENCE: PART A VOL. 2, PP. 923–930 (1964)

Rheo-Optical Properties of Polymers. V

D. G. LEGRAND, *General Electric Research Laboratory, Schenectady, New York*

Synopsis

A theory of the rheo-optical properties of polycrystalline polymers has been developed. It is based on a model similar to that used by Debye for his theory of dielectric relaxation. Using the theory, sizes of crystals in various types of polyethylene are calculated from rheo-optical data and compared with results obtained by x-ray techniques.

INTRODUCTION

The problem of relating mechanical properties to molecular structure represents one of the most basic problems in the polymer field.

In a previous paper, which we refer to as part I, the rheo-optical properties of polyethylene and polypropylene were studied as functions of frequency and temperature. By using the birefringence technique, it was observed that if one measured the strain-optical coefficient as a function of frequency, that a relaxation dispersion was found. Assuming the system to consist of particles embedded in viscous or viscoelastic medium, a preliminary theory was proposed using the Debye diffusion equation.[1] In this paper, we attempt to give more detail to the theory and examine its relationship with respect to a distribution of relaxation times, and type of stresses imposed on particles.

THEORY

The system, assumed to consist of optically anisotropic particles, which might be segments of chains on a molecular scale or microcrystals on a macromolecular scale is defined in three dimensions by three orientational distribution functions, F_1, F_2, and F_3. These orientation distribution functions represent the density of orientation in space of the optically anisotropic elements.

In order to define the changes in the orientational distribution functions, it is necessary to define the mechanisms by which elements move.

Assuming that any optical anisotropy which occurs is a result of orientation, it follows that the optical elements must rotate through some angle in order to produce an optically anisotropic system. This angular rotation is assumed to be controlled by a diffusion type equation, similar to the one

proposed by Debye for dielectric dispersion. We will consider in detail only the two dimensional case.

The following equation is used:

$$D\frac{\partial f}{\partial t} = \frac{1}{\sin\theta}\frac{\partial}{\partial\theta}\left[\sin\theta\left(\frac{\partial f}{\partial\theta} - \frac{Mf}{kT}\right)\right] \tag{1}$$

where f is the orientation distribution function, θ is the angle between particle optic axis and force, M is torque, $D_{(\theta)}$ is the rotary diffusion constant, k is Boltzman's constant, and T is absolute temperature.

The significance of eq. (1), as used here, is the following. M represents the torque on a segment or particle in the medium and is defined by eq. (2)

$$M = FL\sin\theta \tag{2}$$

where θ represents the angle between the axis of the particle and the force F, and L is the distance from rotation center to the point of focus. The force on a segment or particle does not necessarily possess the same magnitude, direction or phase as the macroscopic force, and, as we will show, is related to the strain of the surrounding medium.

D has physical significance in that it represents a rotary diffusion constant and is defined as:

$$D = (6\pi\eta_0 a^3/8kT)(\chi) \tag{3}$$

where η_0 is the viscosity of the matrix surrounding the particle, a is a linear dimension of the particle, and χ is a shape factor for the particle.

Under the influence of a stress, the orientation distribution function f will change, and we must determine the solution for f as a function of angle and time. If the orientation function f is expanded in terms of even spherical harmonics, i.e.,

$$f(\theta) = f_0(1 + A_2P_2 + A_4P_4 + \ldots) \tag{4}$$

where f_0 is a normalizing constant, A_2, A_4 are parameters characterizing time variables, and P_2, P_4, ..., are the second, fourth, etc., spherical harmonics, then using eqs. (2) and (4), in conjunction with

$$M = FLe^{i\omega t}\sin\theta, \tag{5}$$

where $e^{i\omega t}$ is a periodic time function of angular frequency ω, and performing the prescribed operation, one arrives at

$$A_2 = \frac{1}{1 + i\omega\tau_1}e^{i\omega t}\left(\frac{FL}{kT}\right)$$

where τ is relaxation time. Substitution of the orientation function in the equation for birefringence, i.e.,

$$\Delta_1 = \frac{\pi(n^2 + 2)^2}{9n}(\alpha_1 - \alpha_2)\int_0^{\pi/2} f(\theta)(3\cos^2\theta - 1)d\theta \tag{6}$$

where n is the average refractive index and α_1 and α_2 are the principal polarizabilities per unit volume, results in eq. (7):

$$\Delta_1^* = \frac{\pi(n^2 + 2)^2}{9n}(\alpha_1 - \alpha_2)\left(\frac{FL}{kT}\right)\left(\frac{1}{1 + i\omega\tau_1}\right)e^{i\omega t} \tag{7}$$

which predicts that the birefringence will vary as the field varies.

Equation (7) may be written as

$$\Delta_1(\tau_1) = C_1 F\left(\frac{1}{1 + i\omega\tau_1}\right)e^{i\omega t}$$

where

$$C_1 = \frac{\pi(n^2 + 2)^2}{9n}(\alpha_1 - \alpha_2)\frac{L}{kT} \tag{8}$$

If we multiply and divide the right-hand side of eq. (8) by $(1 - i\omega\tau_1)$, expand $e^{i\omega t}$ in its cosine and sine terms, and retain only the real parts, we obtain

$$\Delta_1(\tau_1) = C_1 F\left(\frac{1}{1 + \omega^2\tau_1^2}\cos\omega t - \frac{\omega\tau_1}{1 + \omega^2\tau_1}\sin\omega t\right) \tag{9}$$

At $\omega\tau \to 0$, we obtain

$$\Delta_1(\tau_1) = C_1 F\cos\omega t \tag{10}$$

while at $\omega\tau \to \infty$,

$$\Delta_1(\tau_1) = 0 \tag{11}$$

It is evident from eqs. (7) or (8) that a phase difference, ϕ, exists between $\Delta_1(\tau_1)$ and F. If we write $\Delta_1(\tau_1)$ as

$$\Delta_1(\tau_1) = \Delta_{10}(\tau_1)\cos(\omega t - \phi) \tag{12}$$

where $\Delta_{10}(\tau_1)$ is the amplitude of the birefringence, then on expanding eq. (12), we obtain

$$\Delta_1(\tau_1) = [\Delta_{10}(\tau_1)\cos\alpha]\cos\omega t + [\Delta_{10}(\tau_1)\sin\alpha]\sin\omega t \tag{13}$$

Comparing eqs. (9) and (13), then

$$\Delta_{10}(\tau_1)\cos\phi = C_1(\tau_1)F\left(\frac{1}{1 + \omega^2\tau_1^2}\right) \tag{14}$$

and

$$\Delta_{10}(\tau_1)\sin\phi = C_1(\tau_1)F\left(\frac{\omega\tau_1}{1 + \omega^2\tau_1^2}\right) \tag{15}$$

Therefore,

$$\tan\phi = \omega\tau_1 \tag{16}$$

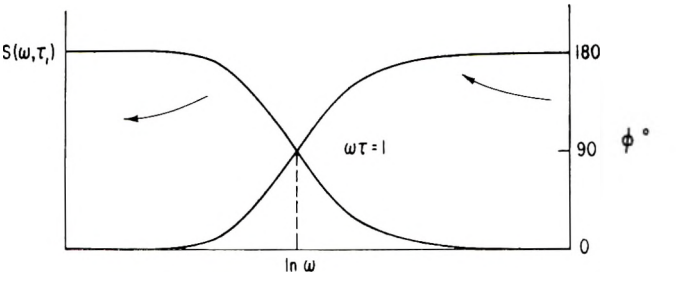

Figure 1.

The torque or internal force on the particle arises as a result of the strain in the medium surrounding the particle. Therefore, we replace the force on the particle by the macroscopic strain, i.e.

$$F = P\epsilon_0 \tag{17}$$

where P is a constant of proportionality between the internal force and the strain.

The dynamic strain-optical coefficient, $S(\omega,\tau_1)$, can be obtained from eqs. (14), (15), and (17), i.e.

$$S(\omega,\tau_1) = \frac{\Delta_{10}(\tau_1)}{\epsilon_0} = \frac{C_1(\tau_1)P}{(1 + \omega^2\tau_1^2)^{1/2}} \tag{18}$$

Plots of $S(\omega,\tau_1)$ and ϕ versus ln ω are shown in Figure 1.

For the most general case where rotation may take place about three different axes of the particle, one would obtain the following equation:

$$\Delta_1 = \epsilon_0\left[Q_1\left(\frac{1}{1 + i\omega\tau_1}\right) + Q_2\left(\frac{1}{1 + i\omega\tau_2}\right) + Q_3\left(\frac{1}{1 + i\omega\tau_3}\right)\right]e^{i\omega t} \tag{19}$$

where the τ's are the relaxation times for rotation about different axes, and the Q's are proportionality constants between the strain and optical properties. This would lead to an equation of the following form for the dynamic strain-optical coefficient:

$$S(\omega) = S_1(\omega,\tau_1) + S_2(\omega,\tau_2) + S_3(\omega,\tau_3) \tag{20}$$

$$S(\omega) = \frac{Q_1(\tau_1)}{1 + \omega^2\tau_1^2} + \frac{Q_2(\tau_2)}{1 + \omega^2\tau_2^2} + \frac{Q_3(\tau_3)}{1 + \omega^2\tau_3^2} \tag{21}$$

In the derivation of the equation we have assumed all the particles to be of the same size. One should use a distribution of sizes to be more correct. However, if one uses the size of the crystal as determined by x-ray diffraction techniques, then the size determined will represent the average of the distribution of sizes. If one determines the size by low angle x-ray scattering, it is found to be approximately the same.[2]

In applying our ideas to the amorphous parts of the material we can follow the same line of reasoning except that we must extend it further.

In terms of a simple chain in the medium, the differences in the principal polarizabilities parallel and perpendicular to the chain are given by:

$$\pi_{\parallel} - \pi_{\perp} = {}^{3}/_{5} N_S (b_1 - b_2)(T''/kT)^2 e^{i\omega t} \tag{22}$$

where π is the principal polarizability of the chain, N_S is the number of segments in the chain, b is the principal polarizability of a segment of the chain, $b_1 - b_2$ is the difference in polarizability of a segment of the chain, T'' is the torque on a segment, k is Boltzman's constant, and T' is absolute temperature.

The polarizability difference in the medium will be the sum of the polarizabilities of all of the chains parallel and perpendicular to the stress axis. This would be defined as

$$P_{\parallel} - P_{\perp} = \sum_i (\pi_{\parallel} - \pi_{\perp})_i \cos^2 \theta_i + (\pi_{\perp})_i - \sum_i (\pi_{\parallel} - \pi_{\perp})_i \sin^2 \theta_i + (\pi_{\parallel})_i \tag{23}$$

where θ_i is the angle between the displacement vector of the ends of the ith chain and the stretching axis.

If we assume all chains to have the same end-to-end length in the undeformed state, then we only need to know the number of chains $N(\theta)$ in an angular interval, θ, $\theta + d\theta$ with respect to the stressing direction. Such calculations have been carried out previously[3] under static conditions, and we will only indicate the results for dynamic conditions.

$$\Delta_2 = \frac{\sigma_0}{kT}\left[\frac{2}{45}\pi\frac{(n^2+2)}{n}(b_1 - b_2)\frac{e^{i\omega t}}{(1 + i\omega\tau_3)}\right] \tag{24}$$

where Δ_2 is the birefringence due to amorphous material, σ_0 is the stress amplitude in the sample, n is the average refractive index, b_1 and b_2 are average polarizability parallel and perpendicular to the chain, respectively, ω is frequency, and τ_3 is relaxation time for a segment.

If we assume the relationship between stress and strain in the amorphous medium is governed by an equation for a viscoelastic medium, then

$$\sigma = \sigma_0 e^{i\omega t} = R\epsilon_0 e^{i\omega t - \delta} \tag{25}$$

where R is a mechanical modulus and δ is the phase difference between the applied stress σ and resulting strain ϵ. Substitution of eq. (25) into eq. (24) gives

$$\Delta_3 = H\left(\frac{1}{1 + i\omega\tau_3}\right)\epsilon_0 e^{-i\delta} e^{i\omega t} \tag{26}$$

where

$$H = \frac{2}{45}\pi\left(\frac{n^2+2}{n}\right)(b_1 - b_2) \tag{27}$$

Under static conditions of uniaxial elongation, we would predict that as the sample is stretched, the crystals in the material would both rotate and translate in a complex manner. The birefringence would thus increase very rapidly and the axis of the crystals would very quickly turn into the direction of stretch. The amorphous material would not, however, contribute much to the birefringence since most of the deformations would be taken up by the rotations of the crystals as a result of the stress imposed on them. However, as the crystals rotate, the force required to further orient them will increase because the angle between the particle axis and force will approach 0°. This will result in a slowing down of the rate of rotations of a particle and an increase in the rate of elongations of amorphous chains.

The foregoing thoughts would appear to be confirmed by the work of Stein and LeGrand.[4]

For the case of stress relaxation, it follows that the birefringence change at constant strain due to crystallites will be zero, except at very short times during the process of obtaining some strain level, ϵ_0, where the crystallites have not had time to respond, thus

$$\Delta_3 = \sigma_0 e^{-t/\tau_\sigma}(B')e^{-t/\tau_3} \tag{28}$$

where τ_σ is the mechanical relaxation time for stress and τ_3 is optical relaxation time for amorphous chains, and thus

$$\Delta_3/\sigma_0 = B'(e^{t/\tau_3 - t/\tau_\sigma}) \tag{29}$$

Therefore, if $\tau_3 = \tau_0$, then $\Delta_3/\sigma_0 = B'$ is constant as a function of time.

If $\tau_3 > \tau_\sigma$, then Δ_3/σ_0 will increase as a function of time, and if $\tau_3 < \tau_\sigma$, then Δ_3/σ_0 will decrease as a function of time.

In terms of the total birefringence of the system, we would have

$$\Delta(\text{total}) = \Delta_{10} + \Delta_{30}(\sigma_0 B')(e^{+t/\tau_3 - t/\tau_\sigma}), \tag{30}$$

where Δ_{10} is due to the crystalline material and Δ_{30} is due to the amorphous material; and if $\Delta_{10} \gg \Delta_{30}$, then Δ (total) would not appear to change although σ might. This appears to be the case for polyethylene as observed by Stein and Tobolsky.[5]

For creep experiments, where constant stress is imposed, the rate of change of birefringence will be governed by the rotations of the crystallites initially which will be followed by a slow diffusion of the chains which will result in slow change in the birefringence.

In terms of the stress and strain with respect of birefringence, we can impose the necessary condition as follows:

$$\Delta_{(\text{total})} = \sigma_0(C') + \epsilon_0 e^{t/\tau_\epsilon}(B'e^{-t/\tau_1}) \tag{31}$$

where τ_1 is the optical relaxation time for crystals and τ_ϵ is the mechanical relaxation time for strain. As before, when $\tau_\epsilon = \tau_1$, $\Delta_1/\epsilon_0 = B'$ is constant as a function of time; when $\tau_1 > \tau_\epsilon$, Δ_1/ϵ_0 will decrease as a function of time; when $\tau_\epsilon \gg \tau_1$, Δ_1/ϵ will increase as a function of time.

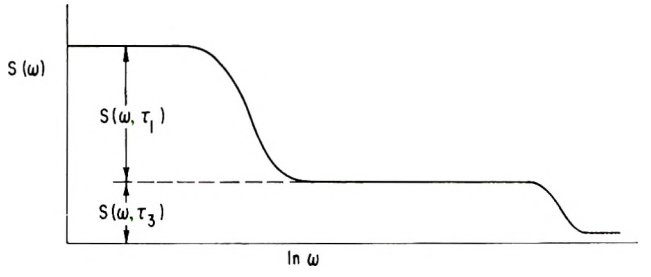

Figure 2.

However, again, the total birefringence will be the sum of a constant plus a time dependent quantity. In terms of actual experiments, it is difficult to perform the measurements, which approach the theory as given, since for stress relaxation experiments, it always takes some finite time to attain some strain level ϵ_0, and this will affect the initial measurements. Similarly, for creep experiments, the actual stress on the specimen changes due to changes in sample dimensions as the sample elongates.

For sinusoidal conditions:

$$\Delta = X_1\Delta_1 + (1 - X_1)\Delta_3 \tag{32}$$

$$= \left[C_1 P \epsilon_0 \left(\frac{1}{1 + i\omega\tau_1}\right) + H\epsilon_0 e^{-\delta}\left(\frac{1}{1 + i\omega\tau_3}\right)\right] e^{i\omega t} \tag{33}$$

where X_1 is the percentage of crystalline material, and $1 - X_1$ is the percentage of amorphous material.

The dynamic strain-optical coefficient will be given by:

$$S(\omega) = S(\omega,\tau_1) + S(\omega,\tau_3) \tag{34}$$

$$= \frac{C_1(\tau_1)PX_1}{(1 + \omega^2\tau_1^2)^{1/2}} + \frac{H(\tau_3)e^{-i\delta}(1 - X_1)}{(1 + \omega^2\tau_3^2)^{1/2}} \tag{35}$$

In Figure 2, a plot is shown of the type of response expected for eq. (35) where $\tau_1 \gg \tau_3$.

Using the theory proposed here with dynamic strain-optical data of Stein et al.[6] and LeGrand et al.,[1] the sizes of crystals in various samples have been calculated and are shown in Table I.

TABLE I

Sample	a_0, A. Calculated	a_0, A. X-ray data	References
Alathon-10	95	90–100	6
Alathon-14	180	180–200	1,9
Marlex-50 120	450	—	6,9
Marlex-50 160	400	380–400	6,9
Profax	350	—	1

Thus, having the strain-optical coefficient at low and intermediate frequencies and the degree of crystallinity, we are able to calculate sizes of the crystals from this approach. The agreement between values calculated from x-ray and dynamic strain-optical data may be fortuitous, but it appears very encouraging.

While the treatment involved here gives a more fundamental approach to the problem of rheo-optical properties in polycrystalline polymers, it is to be noted that one may not be able to describe all rheo-optical properties in terms of our approach. More general approaches based on optical models similar to the Voigt model and generalized Maxwell model of mechanical properties have been presented by Filon and Stein,[7,8] respectively. However, these are phenomenological in nature and thus, although able to adequately describe an experiment, results are not capable of molecular interpretations due to the combinations of processes involved.

The foregoing theory of rheo-optical properties of polycrystalline materials can be expanded to include distribution of relaxation times as have been done in the field of the viscoelastic properties.

References

1. LeGrand, D. G., and P. F. Erhardt, *Trans. Soc. Rheol.*, in press.

2. LeGrand, D. G., Ph.D. Thesis, University of Massachusetts, Amherst, Massachusetts, 1959.

3. Müller, F. H., *Kolloid Z.*, **103**, 210 (1943).

4. Stein, R. S., and D. G. LeGrand, "The Relative Orientation of Crystalline and Amorphous Areas in Polyethylene," ONR Rept. No. 25, University of Massachusetts, Sept. 1, 1960, Contract 2151(00), Proj. NR356-378.

5. Stein, R. S., and A. V. Tobolsky, *Textile Res. J.*, **18**, 302 (1948).

6. Stein, R. S., et al., *J. Polymer Sci.*, **50**, 153 (1961).

7. Filon, L. N. G., and H. T. Jessop, *Phil Trans. Roy. Soc. London*, **A223**, 89 (1923).

8. Stein, R. S., et al., *J. Polymer Sci.*, **57**, 801 (1962).

9. Stein, R. S., et al., Dynamic Optical Symposiun, Polymer Research Institute, University of Massachusetts, January 1962.

Résumé

On étudié les propriétés optiques d'écoulement des polymères polycristallins. On se base sur un modèle semblable à celui utilisé par Debye pour sa théorie de la rélaxation diélectrique. Par cette méthode, on calcule les grandeurs des cristaux de divers types de polyéthylènes au départ de données optiques d'écoulement et on les compare avec les résultats obtenus par la technique des Rayons-X.

Zusammenfassung

Eine Theorie der rheo-optischen Eigenschaften polykristalliner Polymerer wurde entwickelt. Sie beruht auf einem ähnlichen Modell, wie es von Debye für seine Theorie der dielektrischen Relaxation benützt wurde. Mit dieser Theorie wird die Grüsse der Kristalle in verschiedenen Polyäthylentypen aus rheo-optischen Daten berechnet und mit Röntgenergebnissen verglichen.

Received January 8, 1963

JOURNAL OF POLYMER SCIENCE: PART A VOL. 2, PP. 931–942 (1964)

Rheo-Optical Properties of Polymers. VI. Dynamic Birefringence*

D. G. LEGRAND, *General Electric Research Laboratory, Schenectady, New York*

Synopsis

In previous papers we have presented data on the dynamic birefringence and light scattering from polyethylene. New studies of the dynamic birefringence of polytetrafluoroethylene, silicone rubber, polycarbonate, polymethyl methacrylate, and polyethylene as a function of frequency and temperature have been made. The results are presented and interpreted in terms of various proposed theories. The relationships between the mechanical and optical relaxation spectrum are discussed.

INTRODUCTION

Within the realm of present-day knowledge, we are familiar with various manifestations of relaxation phenomena in polymers. Results have been obtained for mechanical, dielectric, and nuclear magnetic relaxation.[1,2] Although these reflect definite types of molecular or macromolecular properties, they do not necessarily possess the same kinetic micromechanism by which the relaxation takes place. Relaxation may occur by: (*a*) side chain relaxation in crystalline as well as amorphous regions; (*b*) intrachain relaxation in amorphous regions; (*c*) interchain relaxation in amorphous regions; (*d*) orientation of crystalline regions. The degree to which these mechanisms affect a particular type of measurement is dependent upon a number of factors. Mechanical measurements reflect mainly the translational motion of molecules or parts of molecules, while dielectric measurements reflect reorientation of dipoles and nuclear magnetic resonance measurements the reorientation of specific internuclear vectors.

Recent measurements of the rheo-optical properties of bulk polyethylene and polypropylene samples have indicated that information can be obtained which is related to the time-dependent changes in polymer morphology.[3–8] Such changes in polymer morphology reflect simultaneous changes in mechanical properties.

We have previously presented data which showed that a relaxation dispersion existed in the dynamic strain-optical coefficient for polyethylene and polypropylene.[4] However, it has also been noted that some discrepancy exists between the data for samples from the same materials.[4,5] In

* Paper presented at the Society of Rheology Meeting, Baltimore, Md., October 1962

this paper, we would like to examine possible reasons for this discrepancy as well as new data for other polymers.

EXPERIMENTAL

Straining Systems

In Figures 1*a* and 1*b* are shown schematic drawings of the two different types of straining mechanisms. In using the system shown in Figure 1*a*, a slight static stress, σ_0, is imposed on the sample. When the eccentric wheel, Q, is rotated, the stress on the sample rises to a maximum value, σ_{max}, and then decreases to some new minimum value, σ_{min}. After a period of time, t, the stress limits are σ^1_{min} and σ^1_{max}. However, a transducer, D, measures the change in the position of the clamp, B, which is related to the strain in the sample. If the initial length of the sample is L_0, and the transducer measurement is made, then when the initial static stress, σ_0, is put on the sample, a static strain, ϵ_0, is also measured. Similarly strains ϵ^1_{min} and ϵ^1_{max} are recorded under dynamic conditions. The strain differential used here is with respect to the position of the sample during the test.

For system 1*b*, a slight static strain ϵ_0, is put on the sample. However, when the eccentric cylinder, Q, is rotated, the end clamps E and F are pushed apart, causing a strain ϵ_{max} to be imposed on the sample. However, when Q is rotated to its initial position, clamps E and F come back to their initial position, but the sample does not come back to strain, ϵ_0, but a value

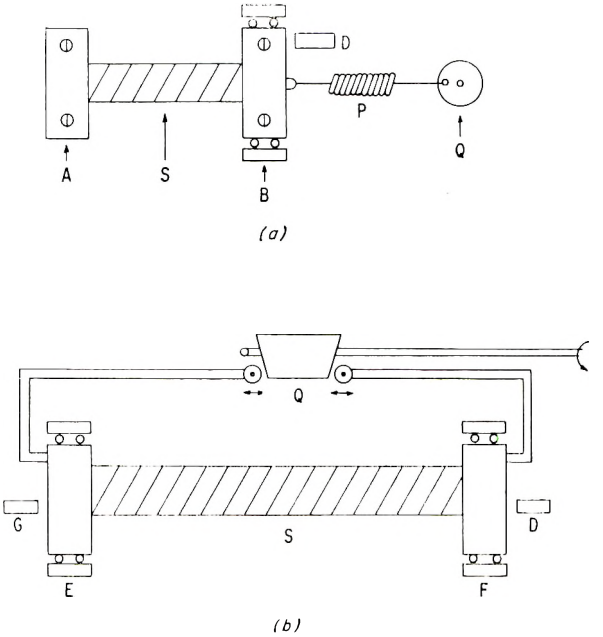

Fig. 1. Deformation system.

slightly greater than this, ϵ_{min}, due to an elastic aftereffect. This causes a slight buckling of the sample, which is easily noted in reflected light. However, transducers, D + G, which measure the position of clamps, E + F, cannot measure this buckling effect and thus the strain limits used are ϵ_0 and ϵ_{max}. Thus, the differential strain used experimentally with this particular setup is $\epsilon_{max} - \epsilon_0$, while in the former type of experiment it is $\epsilon_{max} - \epsilon_{min}$. This effect gives rise to some difference in magnitude of the measured strain-optical coefficient.

Optical Techniques

The optical techniques which were previously used to measure the change in birefringence under dynamic straining were the use of a Babinet compensator and crossed Nicols, using either circular or elliptically polarized light.[4,5]

The crossed Nicol technique was calibrated against a Babinet compensator under static conditions.[4,5]

A major difficulty with the Babinet compensator technique was the inability to detect small changes in the motion of the fringe system at high frequencies (10 cycles/sec.) visually.

It can be shown that for a Babinet compensator between crossed Nicols with a sample in the system the intensity of the fringe system is given by

$$I = I_0[e^{-\tau_1 d} + e^{-\tau_2 d} + e^{-1/2(\tau_1+\tau_2)d}(e^{-i(\delta+\Delta)} + e^{i(\delta+\Delta)})] + T \qquad (1)$$

where τ_1 and τ_2 are turbidities of the sample along axis 1 and axis 2, respectively, d is the thickness of the sample, δ is the phase retardation due to the sample, Δ is phase retardation due to the quartz wedges in the compensator, and T is transmission due to low-angle light scattering.

If this equation is differentiated with respect to Δ and set equal to zero, then a minimum will occur when $\delta = -\Delta$, or

$$\delta = -\Delta \pm (\pi/2) \qquad (2)$$

and maxima occur at $\Delta = 0, \pi, 2\pi$, etc.

Substituting eq. (2) into eq. (1), then, yields

$$I_{min} = I_0(e^{-\tau_1 d} + e^{-\tau_2 d} - 2e^{-1/2(\tau_1+\tau_2)d} + T) \qquad (3)$$

$$I_{max} = I_0(e^{-\tau_1 d} + e^{-\tau_2 d} + 2e^{-1/2(\tau_1+\tau_2)d} + T) \qquad (4)$$

Thus, if the intensity of the minimum is measured as a function of strain, and if τ_1, τ_2, and T are constant as a function of strain, then I_{min} should be constant.

In Figure 2, we show the change in the Babinet compensator reading (which is related to the birefringence) and I_{min} as a function of strain. Under static conditions, a linear relationship exists between the Babinet compensator reading and the strain as well as I_{min} and strain. However, the time dependency of these quantities is not necessarily the same.

Results of dynamic studies by this technique are shown in Figure 3. The top curve was obtained by using the crossed Nicol technique, while the bottom curve was obtained with the new Babinet compensator technique.

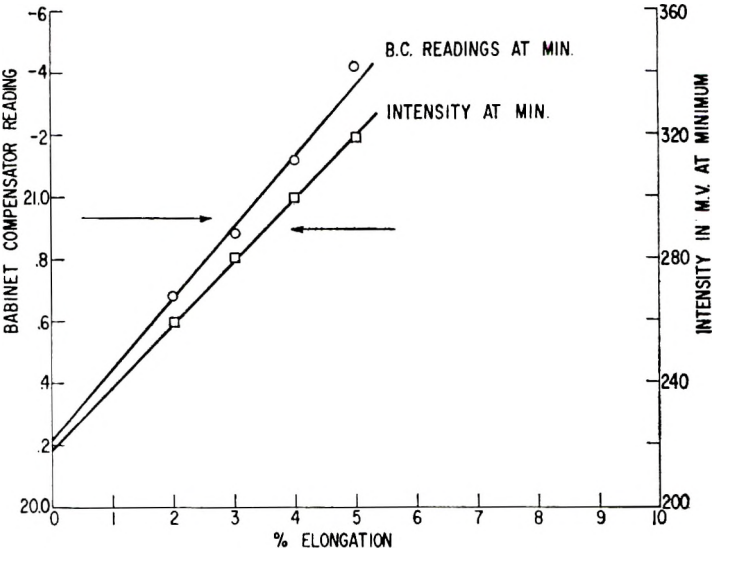

Fig. 2. Babinet compensator (BC) and I_{min}) vs. deformation.

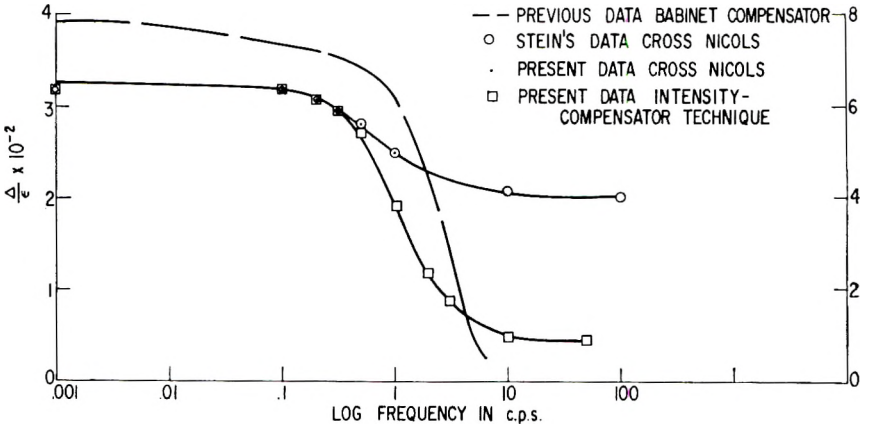

Fig. 3. Strain-optical coefficient vs. log frequency using different techniques of measurement for polyethylene.

These results, as well as previous studies by LeGrand, et al. of the dynamic scattering strain-optical coefficient, indicate the τ's are time-dependent.[5,7]

Stein, Onogi, and Keedy, in a recent paper, refer to the usage of the Babinet compensator for calibration with the transmission crossed Nicols

technique.[8] Their calibration under static conditions is excellent, while their results under dynamic conditions indicate an experimental error as high as 20% in regions where no difficulty is encountered in following the fringe system. Thus, their comment that excellent agreement is obtained between the two techniques is not completely justified. Thus, it becomes quite apparent that for samples which are either absorbent or scattering, it is not correct to use crossed polaroids, as suggested by Stein et al.[8]

In order to verify these results with another technique, the following system was used. If a birefringent sample is put between crossed polaroids, then the intensity transmitted is given by

$$I = I_0\{[e^{-\tau_1 d} + e^{-\tau_2 d} + e^{-1/2(\tau_1+\tau_2)d}(\cos\delta)] + T\} \tag{5}$$

If small amounts of retardation δ_i are added to the system by the insertion of elements, which do not change I_0, then a system of equations, I_i can be written for each δ_i, i.e.,

$$I_i = I_0[e^{-\tau_1 d} + e^{-\tau_2 d} + e^{-1/2(\tau_1+\tau_2)d}\cos(\delta + \delta_i) + T] \tag{6}$$

It can be shown that by a solution of simultaneous equation that

$$\frac{I_i - I}{I_j - I} = \frac{\cos(\delta_i + \delta) - \cos\delta}{\cos(\delta_j + \delta) - \cos\delta} \tag{7}$$

from which values of δ can be solved knowing δ_i, δ_j, I_i, I_j, and I, where I is the intensity when $\delta_i = 0$.

However, an alternate technique is to use a variable retardation plate, such as a Berek or Erhenhous compensator between the crossed polaroids and measure the intensity of transmission when compensation is equivalent. This is similar in principle to the Babinet compensator. However, this technique is much easier to use due to the fact that the compensator at any setting produces only an amount of retardation, δ_i, and is constant over the plate.

A comparison of results obtained with these techniques under dynamic conditions is shown in Figure 3.

Temperature

In order to study the effect of temperature on the dynamic strain-optical coefficient, a copper lined box, which had both a cooling coil as well as electrical heaters, was placed over the stressing system. Small circular openings at the top and bottom of the box, fitted with glass windows, allowed the light beam to pass through the optical system, which for these studies was vertical. Temperature was measured by placing calibrated thermometers and thermocouples near the sample. In addition, it was found necessary to clamp the sample ends in asbestos in order to avoid thermal gradients in the sample, due to the heat transfer at the metal clamps.

Samples

The polyethylene, Al-2-300 (du Pont), was formed in 6-mil-thick sheets. Previous studies of this material have been made under static conditions.[9,10]

The polytetrafluoroethylene (PTFE) was obtained from a $1^1/_2$-in. wide roll and was approximately 2.5 mils thick. The sample density was 2.11 g./cc. and was approximately 40% crystalline.

The silicone rubber was prepared by mixing 100 parts SE-20 (General Electric silicone gum), 10 parts Cab-o-sil, and 1.65 parts benzoyl peroxide. It was cured 20 min. at 125°C. and then 3 hrs. at 150°C. in an air oven.

The polycarbonate samples were obtained from Dr. K. Goldblum, General Electric, Pittsfield, and had been prepared by solvent casting into a thin film.

The poly(methyl methacrylate) was prepared by compression molding into thin sheets.

Theories

Various theories have been proposed to explain the rheo-optical phenomena of polymers in the bulk state.

Filon and Coker proposed that the birefringence developed in a sample is proportional to the stress and strain through two optical coefficients, C_1, C_2.[11]

Their equation is written in the following form:

$$\Delta = C_1\sigma + C_2\epsilon \tag{8}$$

where Δ is birefringence, C_1 is the stress-optical coefficient, σ is stress, C_2 is the strain-optical coefficient, and ϵ = strain.

Stein, Onogi, and Keedy have presented a linear phenomenological theory, which is based on a model similar to that used for mechanical properties in which the strain-optical coefficient is divided into elastic and viscous elements.[5] The theory is expanded to take into account a distribution of elements. The expression for the strain-optical coefficient obtained for an elastic and viscous element connected in series under oscillatory conditions is

$$S(\omega,\tau) = \frac{A(\tau)^2\omega^2\tau^2 + B(\tau)^2}{[1 + \omega^2\tau^2]^{1/2}} \tag{9}$$

where $S(\omega,\tau)$ is the strain-optical coefficient, $A(\tau)$ is the strain-optical coefficient for spring, $B(\tau)$ is the strain-optical coefficient for dashpot, ω is the angular frequency in radians, and τ is relaxation time.

Read has presented the theory of the time and frequency dependence of the birefringence of a linear amorphous polymer.[12] The theory involves an extension of Mooney's theory of the viscoelasticity to the optical properties.[13]

The expression obtained for the strain-optical coefficient under oscillatory conditions is

$$R(\omega,\tau) = K \sum_{n=1}^{\nu} \frac{\omega^2\tau_n^2}{1 + \omega^2\tau\delta_n^2} + K \sum_{n=1}^{\nu} \frac{\omega\tau_n}{1 + \omega^2\tau_n^2} \tag{10}$$

where K is the constant characterizing optical properties of material, and τ_n is the relaxation time for the nth mode.

LeGrand and Erhardt previously interpreted the strain-optical frequency dispersion in polyethylene as being due to a relaxation orientation effect.[4] LeGrand has presented a molecular theory to account for the strain-optical phenomena in polycrystalline polymers.[14] The strain-optical coefficient under oscillatory conditions can be written as

$$L(\omega,\tau) = \frac{C_1(\tau_1)PX_1}{(1 + \omega^2\tau_1^2)^{1/2}} + \frac{H(\tau_3)e^{-i\delta}(1 - X_1)}{(1 + \omega^2\tau_3^2)^{1/2}} \tag{11}$$

where $C_1(\tau_1)$ is the strain-optical coefficient for crystalline regions, P is a proportionality factor relating macroscopic strain to molecular stress, X_1 is the per cent of crystalline material, τ_1 is the relaxation time for crystalline material, $H(\tau_3)$ is the strain-optical coefficient for amorphous material, δ is the phase angle between mechanical stress and strain, and τ_3 is relaxation time for amorphous material.

RESULTS

Rubber and Glasses

In Figure 4, we show the effect of frequency on the strain-optical coefficient for silicone rubber, polymethyl methacrylate, and polycarbonate at

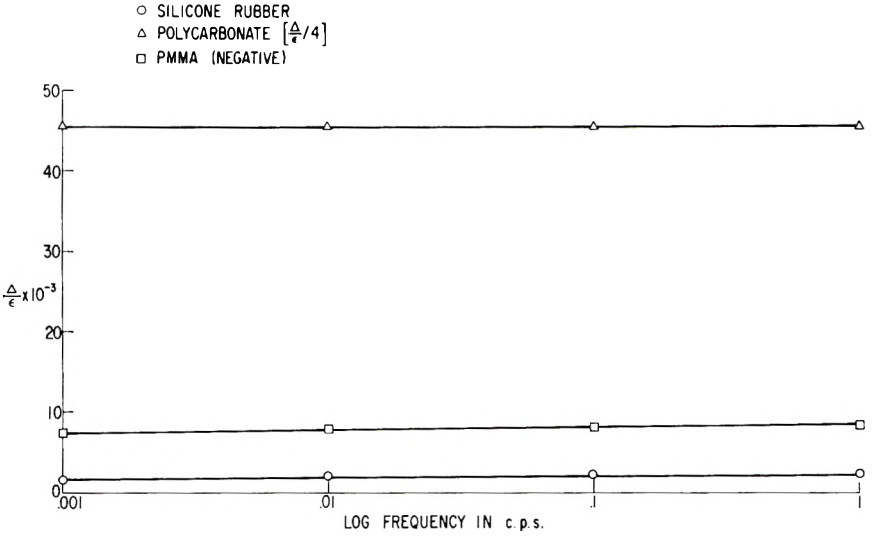

Fig. 4. Strain-optical coefficient vs. log frequency for (○) silicone rubber, (□) polymethyl methacrylate, and (△) polycarbonate.

constant temperature, and in Figure 5 the effect of temperature at constant frequency. Mechanical loss data for these materials are shown in Figure 6.[15] Between 20 and 70°C. the strain-optical and mechanical loss data are relatively constant. PMMA shows the start of a change in the region of the T_g (~90°C.) for the optical and mechanical data. Polycarbonate shows a transition between 20°C. and 0°C. which has not been observed mechanically.

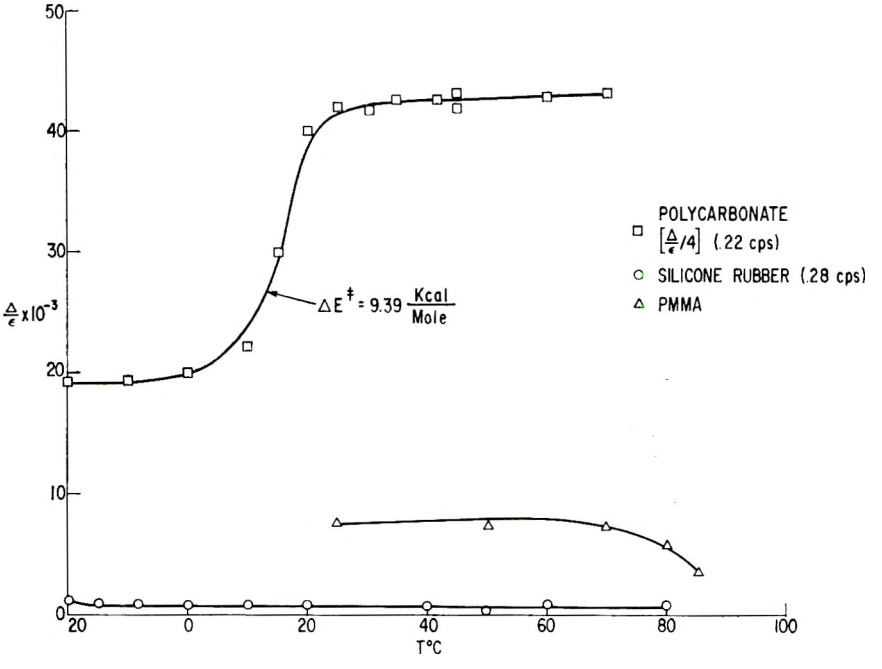

Fig. 5. Strain-optical coefficient vs. temperature for (O) silicone rubber, (△) polymethyl methacrylate, and (□) polycarbonate at constant frequency.

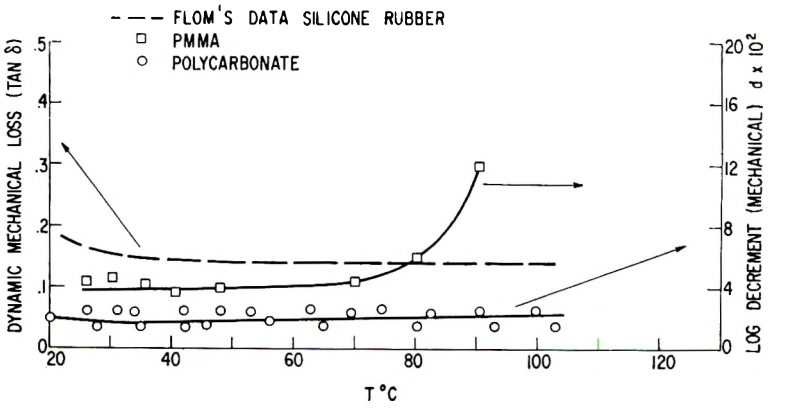

Fig. 6. Mechanical loss vs. temperature for (--) silicone rubber, (□) polymethyl methacrylate, and (O) polycarbonate.

Polycrystalline Polymers

In Figures 3 and 7 we show the strain-optical coefficient as a function of frequency for polyethylene and polytetrafluoroethylene at constant temperature. The effect of temperature at constant frequency is shown in

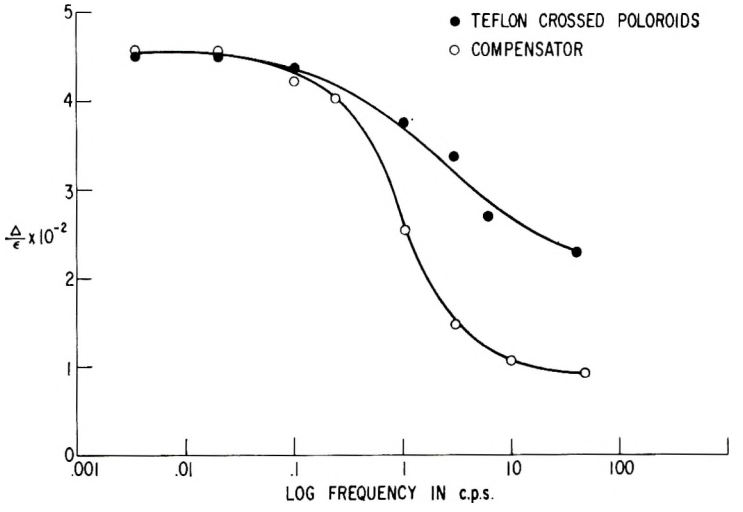

Fig. 7. Strain-optical coefficient for polytetrafluoroethylene vs. log frequency.

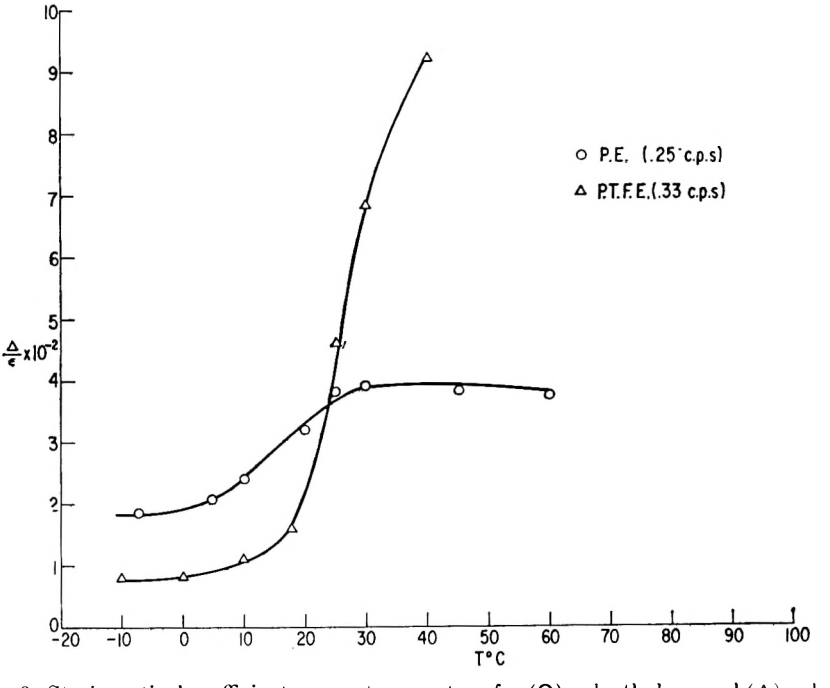

Fig. 8. Strain-optical coefficient versus temperature for (O) polyethylene and (△) polytetrafluoroethylene at constant frequency.

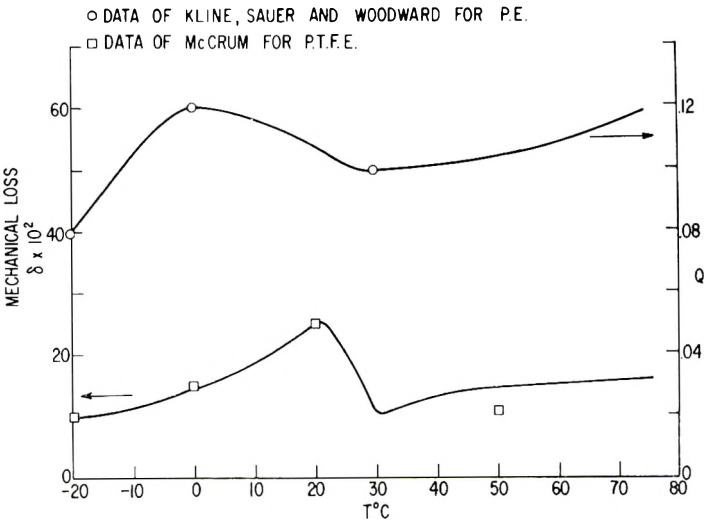

Fig. 9. Mechanical loss vs. temperature for (○) polyethylene and (□) polytetrafluoroethylene.

Figure 8. The mechanical data for similar materials are shown in Figure 9.[16,17]

DISCUSSION AND CONCLUSIONS

In comparing the mechanical loss and strain-optical data for silicone rubber (Figs. 5 and 6), it is apparent that the relaxation time involved in the measurements must be nearly the same as predicted by Read's theory.

Similarly, the data for the glassy polymers (Figs. 5 and 6), indicate that between room temperature and 100°C. the mechanism of relaxations are similar. However, it is to be noted that polycarbonate exhibits a strain-optical dispersion at 0–20°C., while the mechanical data is relatively constant in this region.[18] The activation energy is approximately 9.47 kcal./mole.

The strain-optical data obtained for polyethylene and polytetrafluoroethylene (Figs. 3, 7, and 8), are quite similar both as a function of frequency and temperature. This suggests that the phenomena which are occurring might be the same. The mechanical loss data as a function of temperature are not the same (Fig. 9). Tobolsky has suggested that the glass transition in PTFE should occur around 20°C. while a crystal–crystal transition has actually been observed by Bunn and Howell.[19,20] The strain-optical data might result from either. However, if a statically strained birefringent sample is cooled through the transition region, no change is observed in the birefringence. If the stress is removed from the sample at 0°C., no change is observed in the birefringence while the strain on the sample partially recovers. Similar phenomena are observed in the case of polyethylene.

Thus, the data support the previous interpretation that the orientation of crystals in the amorphous matrix is inhibited by the viscosity of the matrix.[4] McCrum had suggested that part of the mechanical loss peak in this region was associated with the mobility of material surrounding the crystalline regions. A similar mechanism for the β-mechanical dispersion in polyethylene has been postulated and has been observed in strain optical data for polyethylene.

It is to be noted that the magnitude of the change in strain-optical coefficients is more directly relatable to molecular optical properties of the material than in the case of the mechanical loss data.

Thus, from such rheo-optical studies, we can not only gain new information but a better understanding of the molecular properties of polymers.

I would like to acknowledge discussions with many of my colleagues and, in particular, Dr. F. P. Price, and to acknowledge the aid of Mr. P. F. Erhardt in obtaining some of the mechanical loss data.

References

1. Ferry, J. D., *Viscoelastic Properties of Polymers*, Wiley, New York, 1961.
2. Slichter, W. P., *Adv. Polymer Sci.*, **1**, 35 (1958).
3. Onogi, S., D. A. Keedy, and R. S. Stein, *J. Polymer Sci.*, **50**, 153 (1961).
4. LeGrand, D. G., and P. F. Erhardt, Trans. Soc. Rheol., **6**, 301 (1962).
5. Stein, R. S., S. Onogi, and D. A. Keedy, *J. Polymer Sci.*, **57**, 801 (1962).
6. Erhardt, P. F., and D. G. LeGrand, *J. Polymer Sci.*, **62**, S47 (1962).
7. LeGrand, D. G., and Erhardt, P. F., *J. Appl. Phys.*, to be published.
8. Stein, R. S., S. Onogi, K. Sasaguri, and D. A. Keedy, *J. Appl. Phys.*, to be published.
9. LeGrand, D. G., Ph.D. Thesis, University of Massachusetts, Amherst, Mass. (1959).
10. Hoshino, S., J. Powers, D. G. LeGrand, A. Kawai, and R. S. Stein, *J. Polymer Sci.*, **58**, 185 (1962).
11. Fillon, L. N. G., and H. T. Jessop, *Phil. Trans. Roy. Soc., London*, **A223**, 89 (1923).
12. Read, B. E., *Polymer*, **3**, 143 (1962).
13. Mooney, M., *J. Polymer Sci.*, **34**, 599 (1959).
14. LeGrand, D. G., to be published.
15. Flom, D. G., *J. Appl. Phys.*, **31**, 306 (1960).
16. McCrum, N. G., *J. Polymer Sci.*, **34**, 355 (1959).
17. Kline, D. E., J. A. Sauer, and A. E. Woodward, *J. Polymer Sci.*, **22**, 455 (1956).
18. LeGrand, D. G., and P. F. Erhardt, unpublished results.
19. Tobolsky, A. V., *Properties and Structure of Polymers*, Wiley, New York, 1960.
20. Brunn, C. W., and Howell, E. R., *Nature*, **174**, 549 (1954).

Résumé

Dans un article précédent nous avons présenté des données concernant la biréfringence dynamique et la diffusion de lumière du polyéthylène. Nous avons effectué de nouvelles études de la biréfringence dynamique du polytétrafluoroéthylène, de caoutchouc de silicone, du polycarbonate, du polyméthacrylate de méthyle, en fonction de la fréquence et la température. Les résultats sont présentés et interprêtés suivant les différents théories proposées. Les relations entre les relaxations mécanique et optique sont discutées.

Zusammenfassung

In früheren Arbeiten wurden Ergebnisse bezüglich der dynamischen Doppelbrechung und Lichtstreuung von Polyäthylen mitgeteilt. Eine neue Untersuchung der dynamischen Doppelbrechung von Polytetrafluoräthylen, Silikonkautschuk, Polykarbonat, Polymethylmethacrylat und Polyäthylen in Abhängigkeit von Frequenz und Temperatur wurde durchgeführt. Die Ergebnisse werden mit Hilfe der verschiedenen bestehenden Theorien interpretiert. Die Beziehungen zwischen dem mechanischen und dem optischen Relaxationsspektrum werden diskutiert.

Received January 8, 1963

JOURNAL OF POLYMER SCIENCE: PART A VOL. 2, PP. 943–955 (1964)

Studies in the Kinetics of Removal of Water from Cellulosic Fibers

E. H. DARUWALLA and R. T. SHET, *Department of Chemical Technology University of Bombay, Bombay, India*

Synopsis

A study has been made of the kinetics of the removal of water from native, alkali-swollen, and regenerated cellulosic fibers under well defined conditions of experiment. In all cases, the rate of evaporation curve appears to be made up of five distinct and separate portions, and there are four points on each curve at which sudden changes of direction take place. From the changes in the rates of removal of water, attempts have been made to determine the amounts of water present in cellulosic fibers with different degrees of association with the fiber substance and to compare these values with those recorded by other workers employing different techniques. Removal of primary adsorbed water from different cellulosic fibers could be best represented by three distinct phases, the first two of which obey kinetics of reaction of first order and with apparent activation energy of the order of 8–9 kcal./mole. An attempt has also been made to calculate the radii of capillaries present in water-swollen cellulosic fibers.

INTRODUCTION

Water has been found to be held in assemblies of moist fibers in different ways and with varying degrees of tenacity. The main three modes by which water can be held in cellulosic fibers are as chemically bound, i.e., as hydrates of molecules of cellulose; as capillary bound in the capillaries formed in between the spaces as well as in the surface serrations and lumina of fibers; and as dissolved water. For the sake of convenience the sum of chemically bound water and dissolved water has been termed as imbibed water and this imbibed water has been found to influence the intrinsic properties and structure of cellulosic fibers. Different techniques, such as sorption of water,[1–4] electrical conductivity,[5] application of hydrostatic tension[6] or centrifugal force,[7,8] desiccation,[9] depression of freezing point,[10] and drying,[11] have been used to determine the proportion of water held in assemblies of moist textile fibers under different conditions of pretreatment and temperature. As compared with the considerable data available on the sorption of water by cellulosic fiber substances, little information is available on the removal of water from water-soaked cellulosic fibers under critical conditions except for the work of Welo et al.[9] and Ayer.[11] In the present work, a study has been made of the kinetics of the removal of water from native, alkali-swollen, and regenerated cellulosic fibers under well defined conditions of experiment. From the changes in the rates of re-

moval of water attempts have been made to determine the amounts of water present in cellulosic fibers with different degrees of association with the fiber substance and to compare these values with those recorded by other workers employing different techniques. Attempt is also made to calculate the radii of the capillaries present in water-swollen cellulosic fibers.

EXPERIMENTAL

Materials Used

Cotton. 20's single yarn prepared from good quality Indian cotton was used. Removal of impurities was carried out by a standard procedure recommended by the Division of Cellulose Chemistry of the American Chemical Society.[12]

Alkali-Swollen Cotton. High grade Sudanese cotton was freed of noncellulosic components by the standard procedure above and the purified cotton cellulose was then treated with 17.5% aqueous solution of sodium hydroxide at 20°C. for 1 hr. The fiber substance was washed several times with distilled water, steeped in 1% acetic acid for 10–15 min., kept in contact with 0.01*N* hydrochloric acid overnight, washed completely free from acid, and conditioned.

Regenerated Cellulosic Fibers. Commercial samples of viscose (120/40) and cuprammonium rayon (40/30) supplied by National Rayon Corporation, India, and Ashi Kasei Kogya K. K., Japan, respectively, were used after washing repeatedly with distilled water to remove the glycerol present.

All the fiber substances were conditioned in an atmosphere of 75% R.H. at 30°C.

Experimental Procedure

The technique consisted in exposing water-soaked cellulose fiber substance to phosphorus pentoxide in a closed chamber at constant temperature. The technique was so designed that the drying material could be weighed at short intervals without removing it from the drying vessel or in any way disturbing the drying process or drying conditions. For this purpose, a Mettler single-pan balance designed for measuring changes in weight of the order of 0.0001 g. was selected and was kept in an air thermostat where temperature could be maintained with an accuracy of ±0.1°C. The desiccant used was phosphorus pentoxide and it was kept in the enclosed chamber of the balance as well as in the air thermostat. The moist sample was hung on a loop made from stainless steel wire which in turn was attached to the central hook of the balance.

The method of wetting of the sample, in order to establish uniform distribution of moisture throughout the mass of the fiber substance, was found to be one of the most important experimental considerations; un-

less a uniform distribution of moisture was ensured, erratic results were obtained. Different methods of preliminary treatments and wetting were tried and the most successful technique was the one in which sample conditioned at 75% R.H. and 30°C. was soaked in air-free boiled distilled water for 18 hr. at a temperature corresponding to the one at which evapora-

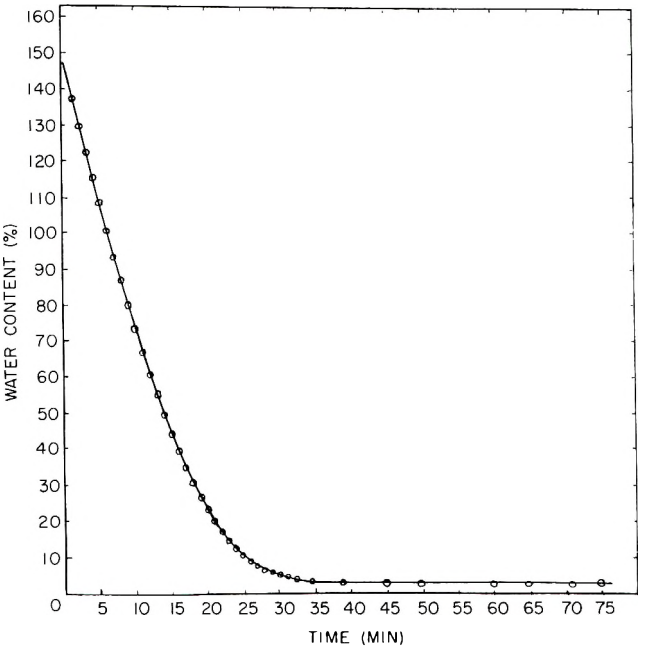

Fig. 1. Relation between water content and time of drying for alkali-swollen cotton at 45°C.

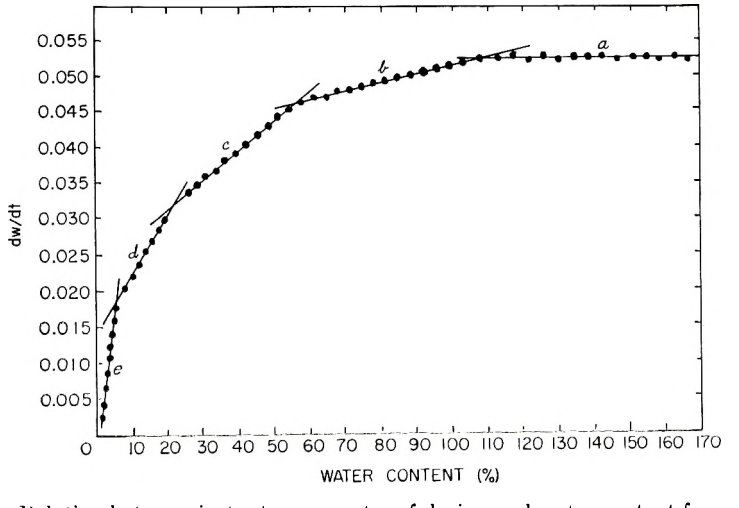

Fig. 2. Relation between instantaneous rates of drying and water content for cotton at 45°C.

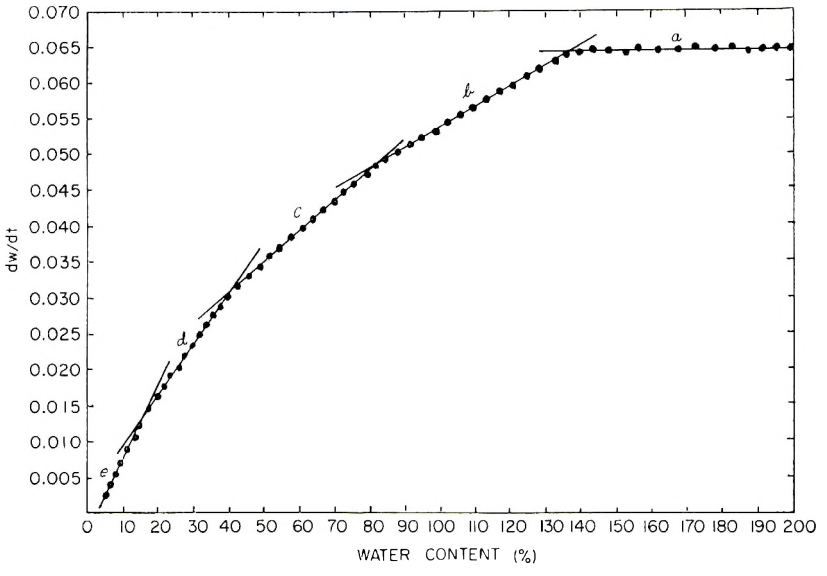

Fig. 3. Relation between instantaneous rates of drying and water content for viscose at 45°C.

tion rates were to be measured, followed by gentle squeezing, opening out, and immediate introduction in the drying chamber of the balance. Weights of moist sample were determined in the beginning at an interval of 1 min. and subsequently at intervals of 2, 5, or more minutes as the rate of drying decreased. At the end of the experiment, the sample was removed, heated in a weighing bottle at 106–108°C. to constant weight and water content (percentage calculated on dry weight) was determined at each stage of drying. Reproducibility was checked by the agreement between triplicate determinations. Experimental time curves for all the fiber substances studied which represented variation in water content with time of drying were of the type shown in Figure 1. Rates of evaporation (dw/dt) were determined at an interval of 1 min. and when these values of the rates of evaporation were plotted against water content at each specific stage, plots of the type shown in Figures 2 and 3 were obtained. These curves represent variation in the rates of evaporation as the water content of the sample falls off.

RESULTS AND DISCUSSION

Moisture can exist in textile fibers in at least two distinct forms, viz., as free moisture adhering to the material and with a vapor pressure equal to that in the bulk, and as sorbed moisture, the vapor pressure of which is always less than that of water in bulk. The rate of evaporation of water under constant drying conditions at any instant per unit of surface would therefore, be proportional to the difference between the vapor pressure of

the evaporating water and the pressure of water vapor in the adjacent atmosphere. With sorbed water, vapor pressure is always less than that of free water and this lowering of vapor pressure is greater, the smaller the amount of sorbed water present. For hygroscopic fibers containing sorbed water to be in equilibrium with moist atmosphere, the vapor pressure of water in the material must be the same as that of the moisture in the atmosphere, and thus moisture content of the fiber substance would depend on the temperature and relative humidity of the surrounding air. This definite relationship is true for any given fiber substance but varies widely for different fibers.

With all the fiber substances investigated and at all the different temperatures studied, the rate of evaporation curve appears to be made up of five distinct and separate portions, and there are four points on each curve at which sudden changes of direction take place (Figs. 2 and 3). The difference observed in the rates of removal of water from cellulosic fibers studied can arise from several factors, viz., water held in pores formed in between fibers, water present in capillaries of different diameters in the fiber, water present in fiber substance adsorbed on cellulose chain molecules in a state of mono- or multilayer adsorption, and water which has been chemically bound to accessible hydrophilic groups in the cellulose chain molecules. It is not possible to attribute the removal of water associated in a specific fashion with the fiber substance to the different clear stages observed in the rates of removal curves because in many cases there is a likelihood of simultaneous removal of water associated with cellulose with different tenacity and in some cases overlapping of removal of water held by different forces is very likely to take place. Furthermore, different samples of similar types of cellulosic material show different types of behavior, depending on the origin; also the treatment which a sample has received prior to desorption has been known to have considerable effect on the rates of removal as well as on the amounts of water retained in different states of association.[11] The analysis of the rate curves in the present study can, therefore, be done in very general terms and with certain approximations.

Along the horizontal portion *a* of the curve, the rate of evaporation is constant. In this region, evaporation is taking place from a free water surface, and the mechanically adhering water is being removed during this initial stage of drying. After this stage, a sudden change of direction occurs, and during the portion of the curve represented by *b*, the curve is straight and on extrapolation cuts the vertical axis at some point above the origin. This is followed by another sharp break in the rate of evaporation curve, and a change of direction occurs represented by portion *c*. Values for water contents at the points of intersection between *b* and c are 57, 72, 80, and 116% for cotton, alkali-swollen cotton, viscose, and cuprammonium rayon, respectively (Table I), which may be compared with the values for water retention obtained by Preston and Nimkar[6] after the application of centrifugal field of 1000 G and of hydrostatic tension

TABLE I
Amounts of Water Present in Cellulosic Fibers at 45°C. in Different States of Association

	Water content, g./100 g. dry fiber							
	Intersection of *b* and *c*		Intersection of *c* and *d*		Intersection of *d* and *e*		Intersection of *x* and *y*	
Fiber	This work	Literature values	This work	Literature values	This work	Literature values	This work	Literature value
Cotton	57	48,[6] 52,[6] 50[13]	21	20–23,[9] 17.5,[10] 21,[14] 26,[15] 28,[16] 21,[17] 21[18]	6	5.8,[11] 5–6.7,[20] 5.6,[21] 5.6[22] 4.3–6.4[24]	2.2	2.0[21]
Alkali-swollen cotton	72	—	33–34	33–35,[10] 30–36[14]	12–13	12,[11] 11.1,[22] 11,[23] 12[24]	4.0	—
Viscose	80	86–103,[6] 86–106[6]	40	39–42,[9] 38,[10] 41,[14] 38,[15] 40,[16] 40,[17] 42[19]	15	19[24]	5.2	—
Cuprammonium rayon	116	89,[6] 100[6]	41	40,[10] 45[16]	15	—	5.0	—

of −30 cm. Hg (for cotton 48%(centrifugal field) and 52%(suction) and for viscose 66–103%(centrifugal field) and 103 (suction)) and with the value of 50% for water retained by cotton after centrifuging as recorded by Coward and Spencer.[13] Thus, during the stage *b*, it is likely that most of the water removed is that retained by fiber assemblies through the agencies of surface tension. After the conclusion of the stage represented by *c*, there is a sudden change in direction, and another phase of drying represented by *d* commences. The points of intersection between *c* and *d* correspond to values of water content of 21, 33, 40, and 41% for cotton, alkali-swollen cotton, viscose, and cuprammonium rayon, respectively; these are comparable with the values of moisture content obtained by Preston and Tawde[10] for bound water which does not freeze (17.5% for cotton, 33–35% for mercerized cotton without tension, 38% for viscose, and 40% for cuprammonium rayon) and with the values for nonfreezing water obtained by Magne and Skau[14] (21% for cotton, 30–36% for swollen cottons, and 41% for viscose). The values of water content for different cellulosic fibers at the points of intersection between *c* and *d* are also in fairly good agreement with critical moisture content of fibers during infrared heating as observed by Preston and Chen[15] (26% for cotton and 38% for viscose), with the values for water content at "break points" in the rate-of-drying curves observed by Alexander and Meek[16] (28% for cotton, 40% for viscose, and 45% for cuprammonium rayon), with the values of water content where cessation of migration during drying takes place as recorded by Preston and Bennett[17] (21 ± 2% for cotton and 40 ± 1% for viscose), and with the values of saturation regain recorded by Urquhart et al.[18,19] (21% for cotton and 42% for viscose). In case of alkali-swollen cellulose and viscose, the values of moisture content at the points of intersection of *c* and *d* are nearly half of those at the points of intersection of *b* and *c*, which is in agreement with the results of Preston and Tawde,[10] who found that about half of the water retained after centrifuging or suction drying did not effect the conductivity and was too loosely bound not to freeze. It appears that most of the water removed during the stage represented by *c* is from the capillaries of smaller diameter, while during stage *d*, most of the water removed is present in cellulose with a tenacity lower than that required for chemical combination or hydrate formation but higher than that of the water which is capable of being frozen. On conclusion of the stage represented by *d*, a sharp change in the direction takes place, and another stage of drying represented by *e* commences. Values for water content at the points of intersection between *d* and *e* are 6, 12, 15, and 15% for cotton, alkali-swollen cotton, and for the two regenerated cellulosic fibers, respectively. These values are close enough to the values of primary adsorbed water or water bound chemically to the hydroxyl group in cellulose, also termed as hydrated water, as determined by several other workers employing different techniques of measurement, viz., adsorption of water vapor,[2,14] contraction in the volume of cellulose phase with increase in the amount of sorbed water,[20] thallous ethylation,[21]

study of ternary system of cellulose–water–sodium thiosulfate and cellulose–water–pyridine,[22,23] drying at 110°C.,[11] and calorimetry[24] (Table I).

The experimental time curves for the stage of removal of water present as primary adsorbed water in different cellulosic fibers at different temperatures have been analyzed in detail. For the resolution of these experimental time curves, the initial moisture content at the start as well as the moisture content at each specific time of drying was that which was equivalent to the moisture content obtained experimentally from the drying experiments minus that below which desorption could not be carried out even after long periods of drying. It was found that the rate of removal of primary adsorbed water in different cellulosic fibers could be best represented by three distinct phases, the first two of which represented by

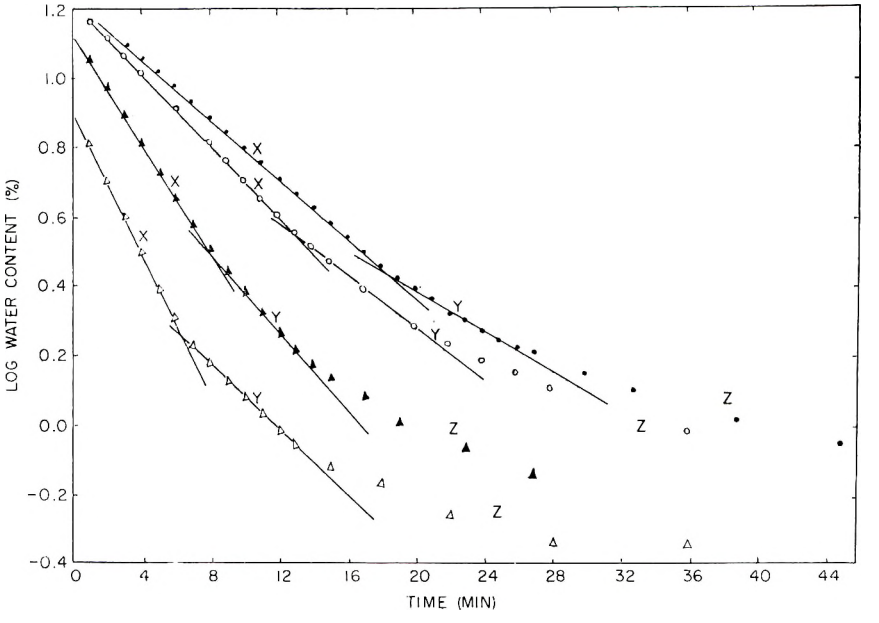

Fig. 4. Relation between log water content and time of drying at 45°C. for primary adsorbed water in different cellulosic fibers: (△) cotton; (▲) alkali-swollen cotton; (○) viscose; (●) cuprammonium rayon.

x and y obey the kinetics of a first-order reaction, in that plots correlating log water content with time of drying are linear (Fig. 4). The apparent rate constants K_1 and K_2 for the two phases for different fibers are given in Table II. The apparent energy of activation for the removal of water in case of these two phases have been calculated from the slopes of the linear curves correlating logarithm of apparent rate constants with reciprocal of temperature. The values for water content for the different fibers at the points of intersection of the two stages represented by x and y are 2.2, 3.96, 5.2, and 5.1% in case of cotton, alkali-swollen cotton, viscose, and cuprammonium rayon, respectively (Table I). These values

correspond to about one third of the values of water content for the total primary adsorbed water in the respective fiber substances.

Each glucose residue in cellulose chain molecule contains three hydroxyl groups which differ markedly in chemical reactivity. Those in the primary or 6 position, have been known to react more rapidly during esterification, etherification, nitration, etc. than the secondary alcoholic groups in the 2 and 3 position in the glucose unit.[25] The primary alcoholic groups are also likely to form bonds with molecules of water which are stronger than those for the secondary alcoholic groups, with the result that the removal of water molecules attached to the primary alcoholic groups would be more difficult during drying than those attached to the secondary alcoholic

TABLE II
Apparent Rate Constants and Activation Energy for the Removal of Primary Adsorbed Water from Cellulosic Fibers

Fiber	Temperature, °C.	K_1, 10^{-4} sec.$^{-1}$	Activation energy, kcal./mole	K_2, 10^{-4} sec.$^{-1}$	Activation energy, kcal./mol.
Cotton	45	39.45	—	16.31	—
Alkali-swollen cotton	15	8.49		—	
	25	14.40		9.60	
	30	20.30	9.0	12.05	8.3
	35	24.40		13.19	
	40	29.10		15.50	
	45	—		21.67	
Viscose	15	5.38		—	
	25	6.98		4.26	
	30	7.04	8.4	4.68	
	35	9.45		6.58	
	40	—		9.24	8.8
	45	16.80		11.31	
Cuprammonium rayon	45	19.75	—	14.26	—

groups. This is borne out by the results of the present study, where there are two distinct stages for the removal of primary adsorbed water in the different cellulosic fibers at all temperatures studied, and the apparent rate constants K_2 for the removal of moisture during the second stage, y, are always lower (approximately 0.6 to 0.7 times) than the rate constants K_1 for the removal of water during the first stage represented by x. Furthermore, the water contents corresponding to the points of intersection of these two rates for different fibers correspond to about one third the values for the total primary adsorbed water. The apparent activation energy for the removal of water during both the first and the second stages are nearly the same, indicating that the same kinetics are operative, irrespective of the cellulosic fibers studied. The values for the apparent activation energy

for the removal of water in both these phases lie between 8 and 9 kcal./mole, values which are much less than the activation energy required for a normal chemical process involving first order kinetics.

The rate of removal of primary adsorbed water during the last stage represented by z is very slow, and the results could not be fitted to kinetics of a first-order reaction. This is in conformity with the observed fact that the differential heat of sorption varies considerably and decreases rapidly with increasing moisture content. Hermans[26] has observed that at not too high a moisture content, water molecules in cellulose gel are bound by chemical forces, and these molecules must apparently overcome a potential barrier of considerable height before they can diffuse through cellulose structure. This barrier is higher, the lower the regain at which the experiment is carried out. This goes to show why the last few per cent of adsorbed material can be removed from the system only with extreme difficulty. In addition to the energetic point of view, steric factors also play an important role in this phenomenon. At low moisture content, cellulose chains are very densely packed, and the molecules of water which occur between cellulose chains may remain enclosed as in a cage with a grating too narrow to let them pass. Only those molecules which have sufficient energy will be able to pass from cage to cage and push their way through by forces of chemical interaction. In this connection, the results of Hermans[26] that molecules of benzene or ether introduced in swollen cellulose gel were not able to escape even after prolonged heating at high temperatures, are of considerable significance. Thus, both kinetic as well as steric factors appear to play a role in the desorption of the last traces of water from cellulose structure. Similar to these observations, Daruwalla and D'Silva,[27] during their studies in the heats of dyeing of direct dyes on cellulose observed considerably high heats of dyeing at low amounts of dye in different cellulosic fibers and noted that the desorption of the last traces of dye from the fiber substance could only be carried out with great difficulty.

Water-swollen cellulose contains water-filled capillaries of different sizes and shape. During evaporation of water, there is a movement of the molecules of water from the interior to the surface to replace the water lost by evaporation. This movement becomes slower as larger pores are emptied and smaller and smaller pores give off their water content. At some point on the drying rate curve, i.e., at a certain definite water content, the rate of a capillary movement would tend to be equal to the rate of evaporation and at this point there would occur a sudden change in direction in the rate of evaporation curve. In the present study, such a sudden break actually occurs in the drying rate curve for each of the cellulosic fibers and the water contents at these break points correspond to 6, 12, and 15% for cotton, alkali-swollen cotton, and regenerated cellulosic fibers, respectively, at 45°C. (intersection of d and e). Anderson,[28] during his studies of vapor pressure relationships of silica gels with water, alcohol, and benzene, established the following relationship connecting vapor pres-

sure with size of pores assuming the capillaries present in the gel to be cylindrical in shape:

$$r = 2TS_0 \times 0.4343/\sigma p_0 \log p_0/p_1 \quad (1)$$

where r is the radius of the pore, T the surface tension of the liquid at a given temperature, S_0 the density of the vapor, σ the density of the liquid, p_0 the saturated vapor pressure of liquid, and p_1 the vapor pressure on the surface of the meniscus. It is strictly not correct to apply eq. (1) to the determination of capillary radius in water-swollen cellulosic fibers because, firstly, the system contains pores of a variety of sizes and shapes and, secondly, eq. (1) is not truly valid for systems where the dimensions of the capillaries are close enough to those of the molecules of water. However, an attempt has been made to calculate the pore radius from the values of vapor pressure obtained from moisture content at the point where there is a sudden change in the rate of evaporation (point at which evaporation from the capillaries has been more or less completed and that of primary adsorbed water commences). The values of p_1 in the present study were obtained from the relative humidity corresponding to the per cent moisture content at the break, from the data given by Jaffries[29] who has determined moisture regain for a variety of cellulosic fibers at different relative humidities and temperatures. The values of the radii of capillaries thus calculated for cotton, viscose and cuprammonium rayon have been given in Table III and compared with the values reported in literature by different

TABLE III
Pore Radii in Different Cellulosic Fibers

Fiber	Pore radius, A.	
	Present study	Literature values
Cotton	17	16[30]
Viscose	33	20–30,[31] 50,[32] 47[33]
Cuprammonium rayon	42	—

workers employing a variety of methods of measurement.[30–33] It can be seen that the values obtained by the above treatment are of the same order as those recorded by others, and agreement between the two sets of values is fairly good.

References

1. Urquhart, A. R., *J. Textile Inst.*, **29**, T125 (1929).
2. Pierce, F. T., *J. Textile Inst.*, **20**, T133 (1929).
3. Sheppard, S. E., *Trans. Faraday Soc.*, **29**, 77 (1933).
4. Hailwood, A. J., and S. Horrobin, *Trans. Faraday Soc.*, **42B**, 84 (1946).
5. Slater, F. P., *Proc. Roy. Soc. (London)*, **B96**, 181 (1924).
6. Preston, J. M., and M. V. Nimkar, *J. Textile Inst.*, **43**, T402 (1952).
7. Preston, J. M., M. V. Nimkar, and S. P. Gundavda, *J. Textile Inst.*, **42**, T79 (1951).

8. Welo, L. A., H. M. Ziifle, and A. W. McDonald, *Textile Res. J.*, **22**, 261 (1952).
9. Welo, L. A., H. M. Ziifle, and L. Loeb, *Textile Res. J.*, **22**, 254 (1952)
10. Preston, J. M., and G. P. Tawde, *J. Textile Inst.*, **47**, T154 (1956).
11. Ayer, J. E., *J. Polymer Sci.*, **21**, 455 (1956).
12. Committee of the Division of the Cellulose Chemistry of American Chemical Society, *Ind. Eng. Chem.*, **15**, 748 (1923).
13. Coward, H. F., and L. Spencer, *J. Textile Inst.*, **14**, T28 (1923).
14. Magne, F. C., and E. L. Skau, *Textile Res. J.*, **22**, 748 (1952).
15. Preston, J. M., and J. C. Chen, *J. Soc. Dyers Colourists*, **62**, 361 (1946).
16. Alexander, P., and G. A. Meek, *J. Soc. Dyers Colourists*, **66**, 530 (1950).
17. Preston, J. M., and A. Bennett, *J. Soc. Dyers Colourists*, **67**, 101 (1951).
18. Urquhart, A. R., and A. M. Williams, *J. Textile Inst.*, **15**, T138 (1924); *ibid.*, **17**, T38 (1926).
19. Urquhart, A. R., and N. Eckersall, *J. Textile Inst.*, **23**, T163 (1932).
20. Hermans, P. H., *Contributions to the Physics of Cellulose Fibers*, Elsevier, Amsterdam, 1946, p. 106.
21. Assaf, A. G., R. H. Haas, and C. B. Purves, *J. Am. Chem. Soc.*, **66**, 66 (1944).
22. Champetier, G., *Compt. Rend.*, **195**, 280 (1932).
23. Tankard, J., *J. Textile Inst.*, **28**, T263 (1937).
24. Magne, F. C., H. J. Portas, and H. Wakeham, *J. Am. Chem. Soc.*, **69**, 1896 (1947).
25. Cramer, F. B., and C. B. Purves, *J. Am. Chem. Soc.*, **61**, 3458 (1939); G. E. Murray, and C. B. Purves, *ibid.*, **62**, 3194 (1940).
26. Hermans, P. H., *Contributions to the Physics of Cellulosic Fibers*, Elsevier, Amsterdam, 1946, p. 31.
27. Daruwalla, E. H., and A. P. D'Silva, *Textile Res. J.*, **33**, 40 (1963).
28. Anderson, J. S., *Z. Physik. Chem.*, **88**, 191 (1914).
29. Jaffries, R., *J. Textile Inst.*, **51**, T339 (1960).
30. Hunt, C. M., R. L. Blaine, and J. W. Rowen, *Textile Res. J.*, **20**, 43 (1950).
31. Morton, F., *Trans. Faraday Soc.*, **31**, 262 (1935).
32. Frey-Wyssling, A., *Protoplasma*, **27**, 372 (1937).
33. Tawde, G. P., Ph.D. Thesis, Manchester University, 1955, p. 106.

Résumé

On a étudié, des conditions bien définies, la cinétique d'élimination d'eau des fibres de cellulose natives, gonflées par des alcalis et régénérées. Dans tous les cas, la vitesse de la courbe d'évaporation semble être faite de cinq parties distinctes et séparées. Il y a quatre points dans chaque courbe où des variations subites de direction ont lieu. On a essayé de déterminer, par les variations de vitesse d'élimination d'eau, les quantités d'eau présentes dans les fibres de cellulose ayant des degrés différents d'association avec la substance de la fibre. On a également essayé de comparer ces valeurs à celles trouvées par d'autres chercheurs par des techniques différentes. L'élimination de l'eau absorbée primairement par des fibres de cellulose peut être représentée par trois phases distinctes, dont les deux premières ont une cinétique de premier ordre avec une énergie d'activation apparente de 8 à 9 Kcal/mole. On a essayé également de calculer les rayons des capillaires présents dans les fibres de cellulose, gonflés lar l'eau.

Zusammenfassung

Eine Untersuchung der Kinetik der Entwässerung nativer, alkaligequollener und regenerierter Cellulosefasern unter wohldefinierten Versuchsbedingungen wurde durchgeführt. In allen Fällen scheint die Kurve der Verdampfungsgeschwindigkeit aus fünf verschiedenen und getrennten Teilen aufgebaut zu sein und auf jeder Kurve befinden sich vier Punkte, bei welchen eine plötzliche Richtungsänderung stattfindet. Aus der Änderung der Entwässerungsgeschwindigkeit wurde versucht die in Cellulosefasern

mit verschiedenem Assoziationsgrad der Fasersubstanz vorhandene Wassermenge zu bestimmen und diese Werte mit den von anderen Autoren nach anderen Methoden erhaltenen zu vergleichen. Die Entfernung des primär adsorbierten Wassers aus verschiedenen Cellulosefasern konnte am besten durch drei unterscheidbare Phasen wiedergegeben werden, von denen die ersten beiden einer Kinetik erster Ordnung mit einer scheinbaren Aktivierungsenergie von etwa 8–9 kcal/Mol gehorchen. Weiters wurde versucht, die Radien der in den wasser-gequollenen Cellulosefasern vorhandenen Kapillaren zu berechnen.

Received January 10, 1963

JOURNAL OF POLYMER SCIENCE: PART A VOL. 2, PP. 957–963 (1964)

Linear Free Energy Relationship in the Diffusion of Gases Through Polymer Films

T. K. KWEI and W. M. ARNHEIM, *Central Research Laboratory, Interchemical Corporation, New York, New York*

Synopsis

The general correlation between $\Delta H^{\ddagger}/T$ and log D_0 in the diffusion of gases through polymers is discussed in terms of a linear free energy relationship. It is shown that the diffusion constant D can be expressed as $\log D = k\alpha +$ constant, where k is a parameter characteristic of the diffusing gas and α is a parameter characteristic of the polymer. The relationships between structural characteristics of gases and polymers and the respective parameters k and α are discussed. The possible application of similar linear free energy relationships for the purpose of expressing the permeability constant (P) and the solubility coefficient (S) is also suggested.

I. Introduction

In a previous publication,[1] the general correlation between $\Delta H^{\ddagger}/T$ and log D_0 in the diffusion of gases through polymers was discussed in terms of a linear free energy relationship. The mathematical representation of the correlation between $\Delta H^{\ddagger}/T$ and $\log D_0$ is:

$$\Delta H^{\ddagger}/T = 6.75 \log D_0 + 25.80 \tag{1}$$

where

$$D = D_0 \exp \{-\Delta E/RT\} \tag{2}$$

$$\Delta H^{\ddagger} = \Delta E - RT \tag{3}$$

$$D_0 = e(kT/h)\lambda^2 \exp \{\Delta S^{\ddagger}/R\} \text{ (transition state theory)} \tag{4}$$

and where D is the diffusion constant, (in square centimeters/second), λ is the jump distance, and ΔE is activation energy.

Combination of eqs. (1)–(4) results in:[2]

$$\log D = -0.14(\Delta H^{\ddagger}/RT) - 4.26 = -0.14(\Delta E/RT) - 3.82 \tag{5}$$

As a consequence of the linear free energy relationship, it is possible to express the diffusion constant of any gas–polymer pair in the following form:[1]

$$\log D = k(\text{gas})\ \alpha(\text{polymer}) + \text{constant} \tag{6}$$

The parameters k and α are characteristic of the gas and of the polymer, respectively. We now wish to discuss the theoretical derivation of eq. (6)

and the procedure of calculating k and α. The discussion will be limited to diffusion data above the glass transition temperature (T_g) of the polymers, as the diffusion of many organic vapors through polymers at temperatures below T_g does not seem to obey the same linear free energy relationship.[1]

II. Theoretical Considerations

The enthalpy of activation, $\Delta H^{\ddagger}$, consists of (1) an "interchain" contribution $P_i \Delta V^{\ddagger}$, and (2) an "intrachain" contribution due to change in chain conformation.[3] (Here P_i is the internal pressure and $\Delta V^{\ddagger}$ is the volume of activation.)

$$\Delta H^{\ddagger} = P_i \Delta V^{\ddagger} + \Delta H^{\ddagger}_{\text{intra}} \tag{7}$$

The volume of activation is related to the size of the diffusing gas.[4] A careful re-examination of the literature data on the dependence of the activation energy of diffusion on the diameter of the diffusing gas, d, suggests that the following relation is applicable to almost all the experimental data:

$$\Delta H^{\ddagger} = J d^2 + \Delta H^{\ddagger}_{\text{intra}} \tag{8}$$

where J is a proportionality constant. (The above correlation, though not always used by previous authors, is a fair representation of the literature data according to the method of linear regression.) For polyvinyl acetate and for many rubbers, $\Delta H^{\ddagger}$ is directly proportional to d^2 and hence $\Delta H^{\ddagger}_{\text{intra}}$ is negligible.[2,5-8] For polyethylenes, extrapolation of the $\Delta H^{\ddagger}$ versus d^2 plot to the ordinate axis gives 5750 cal./mole as $\Delta H^{\ddagger}_{\text{intra}}$;[9] the pronounced intrachain contribution in PE due to change in chain conformation is also found in the elastic behavior[10] and vapor sorption characteristics of polyolefins.[11] We shall now discuss these two cases separately.

For case 1, $\Delta H^{\ddagger} = J d^2$. The volume of activation $\Delta V^{\ddagger}$ may be pictured in terms of an equivalent cylinder with a cross-sectional area $1/4\pi d^2$ and an effective length l,[5] i.e.,

$$\Delta V^{\ddagger} = 1/4\pi d^2 l$$

It follows therefore, that,

$$\Delta H^{\ddagger}_{h,m} = P_i \Delta V^{\ddagger} = N_{\text{av}} (1/4\pi d_m^2) (P_i l)_h \tag{9}$$

The two subscripts h and m refer to the polymer and the gas, respectively. Upon substitution of eq. (9) into eq. (5) there is obtained:

$$\log D_{h,m} = (0.14/RT) (1/4\pi d_m^2) (P_i l)_h = k\alpha - 4.26 \tag{10}$$

The parameter k is not only characteristic of the gas but is also related to the diameter of the gas; the parameter α is characteristic of the polymer and is related to $P_i l/T$. Equation (10) can be cast in the form of a conventional Hammett-type equation.[1]

III. Method of Calculation

With the use of eq. (10), the parameters k and α can be calculated from experimental diffusion data as follows. Selecting oxygen as a reference gas, for convenience in calculation, k_m is taken as $1.614 \times 10^{-9} N_{av} (1/4\pi d_m^2)$ so that $k_{O_2} = 1.0$. The parameter α is then calculated from the oxygen diffusion data for the various polymers. Since the diameters of various gases

TABLE I
k Parameters for Gases

Gas	No. of data points	k	d, A.[a]	$1.614 \times 10^{-9} N_{av} \times (1/4\pi d^2)$	Reference
Hydrogen	13	0.50	2.54–2.72	0.49–0.56	2,5,7,8
Neon	1	0.51	2.60	0.52	2,5,7,8
Oxygen	13	1.0	3.62	1.00	2,5,7,8,9
Argon	7	1.01	3.66	1.02	3,5,8,9
Carbon monoxide	4	1.05	3.7	1.05	9
Nitrogen	14	1.10	3.80	1.10	2,5,7,8,9
Carbon dioxide	13	1.15	3.9	1.16	2,7,9
Water	5	1.0	2.72–4.66	—	6,12
Methanol	6	1.57	~4.6	~1.62	6
Ethanol	6	2.11	~5.4	~2.23	6
n-Propanol	1	2.45	~5.8	~2.56	6
n-Butanol	1	2.72	—	—	6
sec-Butanol	1	2.81	—	—	6
tert-Butanol	1	2.88	—	—	6
Acetone	1	2.40	—	—	6
Benzene	3	2.76	—	—	6
Pyridine	2	2.58	—	—	6
Cyclohexane	1	2.90	—	—	6
Methylene chloride	2	2.27	~5.5	~2.31	6
Chloroform	1	2.59	~5.8	~2.57	6
Carbon tetrachloride	1	2.72	~6.1	~2.68	6
Ethyl chloride	1	2.38	~5.7	~2.48	6
Ethyl bromide	2	2.64	~5.9	~2.63	6
Ethyl iodide	1	2.65	~6.1	~2.68	6
Methane	4	1.39	4.1	1.28	9,13
Ethane	4	2.08	5.2	2.06	9,13
Propene	4	2.24	5.4	2.23	9
Methyl acetylene	4	1.80	4.9	1.83	9
Propane	4	2.63	5.8	2.57	9,13
SF_6	4	3.21	6.4	3.13	9
n-Butane	1	2.70	—	—	13
n-Pentane	1	2.81	—	—	13

[a] Diameters of gases are estimated from viscosity data.[5,9,14] The increase in viscosity diameter as a result of the substitution of C—Cl for C—H bond is assumed to be 1.0 A. (difference in covalent radii of Cl and H is about 0.62 A.); thus d_{CCl_4} is estimated to be 6.1 A. compared with d_{CH_4} of 4.1 A. Where the substitution is unsymmetrical, such as in C_2H_5Cl, appropriate correction is made. The size of the OH group is believed to be slightly less than that of the Cl group; 0.8 A. is used as an estimate of the change in viscosity diameter upon substitution of C—OH for C—H.

and vapors are not always known with great accuracy, the k parameter for any other gas is obtained as the slope of log D versus α plot, using the method of least squares. The k values obtained by the above procedure are in excellent agreement with $1.614 \times 10^{-9} N_{av} \times (1/4\pi d_m^2)$, wherever a

TABLE II
Parameters for Polymers

Polymer	No. of data points	$\alpha_{25°C.}$	$\alpha_{100°C.}$	Reference
Natural rubber	4	−1.49	—	7
Buna S	4	−1.53	—	7
Buna N	4	−2.17	—	7
Neoprene G	4	−2.14	—	7
Oppanol B200	4	−2.83	—	7
Polybutadiene	4	−1.51	—	7
Polyisoprene	4	−2.25	—	7
Mipolam MP	3	−2.71	—	7
Thiokol B	3	−2.89	—	7
Neoprene (S)	3	−2.74	—	8
Neoprene (S)	1	−2.80	—	8
Butadiene–acrylonitrile rubber	2	−2.61	—	8
Polyvinyl acetate	21	−3.19[a]	—	5,6
Butadiene–methyl methacrylate copolymer	1	−2.35	—	8
Butadiene–styrene copolymer	1	−2.06	—	8
Butadiene–styrene copolymer	1	−2.02	—	8
Polymethyl acrylate	4	−2.61	—	6
Poly-*n*-butyl methacrylate	2	−1.64	—	6
Rubber HCl	1	−5.10	—	12
Ethyl cellulose (1)	1	−2.22	—	12
Polystyrene	4	—	−1.63	6
Polyethyl methacrylate	5	—	−1.68	6
Polymethyl methacrylate	3	—	−2.20	6
Polyethylene terephthalate	1	—	−2.61	12

[a] The glass transition temperature of PVAc lies near 25°C. In the calculation of $\alpha_{25°C.}$, extrapolated $D_{25°C.}$ values from high temperature data rather than actual experimental diffusion constants at 25°C. were used.

reasonable estimate of d_m is possible (Table I). From these k values, a set of α parameters can be calculated from the diffusion data of a given gas. The α parameters from the diffusion data of various gases are usually in good agreement with each other; typical variation is 5–10%. Representative values of α are listed in Table II.

For case 2, $\Delta H = Jd^2 + \Delta H_{intra}$.

$$\log D_{h,m} = \frac{-0.14}{RT}\left(\frac{1}{4}\pi d_m^2\right)(P_i l)_h - \frac{0.14\Delta H^{\ddagger}_{intra}}{RT} - 4.26 \qquad (11)$$

$$= k\alpha - \beta - 4.26$$

For the polyethylenes, hydrogenated polybutadiene, and unvulcanized Hevea,[9] $\Delta H^{\ddagger}_{\text{intra}} = 5750$ cal./mole and β can be calculated accordingly. The α parameter of the polymer can be obtained readily from the diffusion data with known k parameters. The results of these calculations are summarized in Table III.

TABLE III
Parameter α for Case 2 Polymers

Polymer	No. of data points	$\alpha_{25°C.}$	$\beta_{25°C.}$	Reference
Polyethylene (high density)	10	−1.15	1.35	9
Polyethylene (low density)	10	−0.77	1.35	9
Polyethylene (medium-high density)	4	−1.05	1.35[a]	13
Polyethylene (low density)	1	−1.04	1.35[a]	12
Polypropylene (isotactic)	1	−0.95	1.35[a]	12
Hydrogenated polybutadiene	10	−0.40	1.35	9
Unvulcanized Hevea	10	−0.25	1.35[b]	9

[a] No $\Delta H^{\ddagger}_{\text{intra}}$ value is available; assume β is also equal to 1.35.
[b] It is not clear why unvulcanized Hevea is so different from the other rubbers.

IV. Discussion

The parameters k, α, and β listed in Tables I, II, and III facilitate the estimation of the diffusion constant of any gas-polymer pair. The accuracy of the prediction is usually within 20% of the experimental value. Considering the divergent sources of experimental data, the agreement can be viewed as satisfactory. Isolated cases do exist, however, where the discrepancies between the experimental and predicted diffusion constants reach as high as 300%. Helium diffusion data do not conform to the above representation.

Several other interesting corollaries immediately follow from the linear free energy relationship. It can be shown that, for case 1,

$$\log \left(\frac{D_{h,m}/D_{j,m}}{D_{h,n}/D_{j,n}} \right) = (k_m - k_n)(\alpha_h - \alpha_j) \tag{12}$$

In as much as the k values for inert gases are close in magnitude, the term $(k_m - k_n)(\alpha_h - \alpha_j)$ is often less than 0.1. Consequently

$$\frac{D_{h,m}}{D_{j,m}} \cong \frac{D_{h,n}}{D_{j,n}} 10^{0.1} \cong \frac{D_{h,n}}{D_{j,n}} \cong \text{approximately constant} \tag{13}$$

and

$$\frac{D_{h,m}}{D_{h,n}} \cong \frac{D_{i,m}}{D_{j,n}} \cong \text{approximately constant} \tag{14}$$

Similar conclusions can be drawn for polymers of case 2.

The constancy of the ratios of the diffusion constants has not been pointed out previously, while the constancy of the ratios of the permeability constants P has been discussed by many authors.[15,16]

It has been pointed out in the previous paper[1] that the diffusion of He, H_2, Ne, O_2, and A through polyvinyl acetate[5] obeys the isokinetic relationship of eq. (1) at temperatures above and below T_g of the polymer. The application of eq. (9) to the activation energy of gas diffusion above and below T_g results in:

$$\frac{(\Delta H^{\ddagger})T < T_g}{(\Delta H^{\ddagger})T > T_g} = \frac{(P_i l)T < T_g}{(P_i l)T > T_g} \tag{15}$$

The ratios of $\Delta H^{\ddagger}$ values below and above the T_g of PVAc are 0.75, 0.67, 0.86, 0.76, and 0.68 for He, H_2, Ne, O_2, and A, respectively. The ratio of the internal pressure[17] below and above the T_g is about 0.6 for PVAc. It appears that, in the above case, the difference in activation energies below and above T_g is due mainly to the difference in the internal pressures of the polymer at the respective temperatures.

Finally, it may be mentioned that in the derivation of eqs. (9) and (11), it has been assumed tacitly that l is a parameter characeristic of the polymer. The justification of this assumption is based on the findings of Meares[5] and Kambour[18] that, l is a length characteristic of the polymer but independent of the diffusant and varies inversely with the size of the pendant group on the polymer chain. The success of our correlation lends further support to their findings. It remains to be seen, of course, whether l is a characteristic of the polymer alone when the size of the diffusant is very large.

The authors wish to thank the management of Interchemical Corporation for permission to publish this article. They also wish to thank Mr. Charles A. Kumins for his constant encouragement and advice. The helpful suggestions of Professor Marvin Charton of Pratt Institute is gratefully acknowledged.

References

1. Kwei, T. K., and W. Arnheim, *J. Chem. Phys.* **37,** 1900 (1962).
2. Barrer, R. M., *J. Phys. Chem.*, **61,** 178 (1957).
3. Brandt, W. W., *J. Phys. Chem.*, **63,** 1080 (1959).
4. Kumins, C. A., and J. Roteman, *J. Polymer Sci.*, **55,** 699 (1961).
5. Meares, P., *J. Am. Chem. Soc.*, **76,** 3415 (1954).
6. Ryskin, G. Y., *Zh. Tekh. Fiz.*, **25,** 458 (1955).
7. Van Amerogen, G. J., *J. Appl. Phys.*, **17,** 972 (1946).
8. Barrer, R. M., *Trans. Faraday Soc.*, **35,** 628 (1939).
9. Michaels, A. S., and H. J. Bixler, *J. Polymer Sci.*, **50,** 413 (1961).
10. Ciferri, A., C. A. J. Hoeve, and P. J. Flory, *J. Am. Chem. Soc.*, **83,** 1015 (1961).
11. Kwei, K. P. S., and T. K. Kwei, *J. Phys. Chem.*, **66,** 2146 (1962).

12. Yasuda, A., and V. Stannett, *J. Polymer Sci.*, **57**, 907 (1962).
13. Brandt, W. W., *J. Polymer Sci.*, **41**, 403 (1959).
14. Jeans, J., *An Introduction to the Kinetic Theory of Gases*, Cambridge Univ. Press, London, 1950, p. 183.
15. Rogers, C. E., J. A. Meyer, V. Stannett, and M. Szwarc, in *Permeability of Plastic Films and Coated Paper to Gases and Vapors*, Tappi Monograph Series, No. 23, Technical Association of the Pulp & Paper Industry, 1962, Chap. 2.
16. Ito, Y., *Kobunshi Kagaku*, **18**, 1 (1961), *Chem. Abstr.*, **55**, 27947 (1961).
17. Allen, G., D. Sims, and G. J. Wilson, *Polymer*, **2**, 375 (1961).
18. Kambour, R. P., and F. L. Pilar, paper presented at the 140th Meeting, American Chemical Society, Chicago, Illinois, September 1961.

Résumé

La corrélation générale entre $\Delta H^{\ddagger}/T$ et log D_0 dans la diffusion des gaz à travers les polymères est discutée en des termes d'énergie libre linéaire. On montre que la constante de diffusion D peut être représenté par log $D = k\alpha +$ constante, où k est un paramètre caractéristique du gaz diffusant et α un paramètre caractéristique du polymère. Les relations entre les caractéristiques structurelles des gaz et les polymères, et les paramètres correspondants k et α sont discutés. On suggère également quil' existe des relations d'énergie libre linéaire identique pour la constante de perméabilité (P) et la coefficient de solubilité (S).

Zusammenfassung

Die allgemeine Korrelation zwischen $\Delta H^{\ddagger}/T'$ und log D_0 bei der Diffusion von Gasen durch Polymere wird als lineare Frei-Energie-Benziehung diskutiert. Es wird gezeigt, dass die Diffusionskonstante, D, als log $D = k\alpha +$ Const, ausgedrückt werden kann, wo k ein für das diffundierende Gas charakteristischer Parameter und α ein solcher für das Polymere ist. Die Beziehungen zwischen der Struktur der Gase und Polymeren und den entsprechenden Parametern, k und α, werden diskutiert. Weiters wird die Möglichkeit der Verwendung ähnlicher Freier-Energie-Beziehungen für die Behandlung der Permeabilitätskonstanten (P) und des Löslichkeits-koeffizienten (S) erwähnt.

Received January 11, 1963

JOURNAL OF POLYMER SCIENCE: PART A VOL. 2, PP. 965–972 (1964)

Compositions in Equilibrium Two Phases of Polymer–Solvent Mixture Systems

TSUNEO YOSHINO and KENJI FUJISAWA, *Basic Research Laboratories, Toyo Rayon Co., Ltd., Kamakura, Kanagawa, Japan*

Synopsis

The compositions in equilibrium two-liquid phases of polymer–solvent mixture systems have been studied from the standpoint of preferential adsorption of one solvent component by measuring φ_{out}, v', and V/m for toluene–isobutanol–polystyrene systems. Here φ_{out} is the volume fraction of toluene in the solvent mixture outside the adsorbed regions surrounding polymer molecules; v' is the volume of hypothetical toluene layers per unit weight of polymer substance, when the adsorbed regions are divided into pure toluene layers and the remaining parts with solvent composition equal to φ_{out}, keeping the amount of toluene in the adsorbed regions unchanged; and V/m is the volume of solvent per unit weight of polymer substance. v' is observed to be equal for both the polymer-poor and polymer-rich phases and independent of polymer concentration, so far as the polymer concentration in the latter phase is smaller than 0.2 g./cc. solvent. φ_{out} is found to be also equal for the both phases. These observations show that the ternary system at a temperature is approximated by a binary system consisting of polymer molecules which are composed of true polymer molecules and the toluene layers surrounding them, and solvent mixture outside the toluene layers. When V/m and v' in the polymer-rich phase are plotted against decreasing φ_{out}, v' begins to decrease at $\varphi_{out} = 0.6$, where the change of V/m along a steep curve for $\varphi_{out} > 0.6$ is slowed down. This suggests that after the polymer-rich phase is deprived of most of the solvent outside the adsorbed regions the adsorbed regions begin to lose solvent. The magnitude of the adsorbed regions per unit weight of polystyrene in a dilute solution with $\varphi_{out} > 0.6$ is estimated to be about 5 cc./g. from V/m of a polymer-rich phase with $\varphi_{out} = 0.6$.

Phase separation of a system consisting of a single polymer component in a binary solvent mixture is involved in numerous operations in polymer chemistry. The compositions of the two phases depend on the nature of the components and the constraint imposed upon the system. Based on some hypotheses, equations to compute the compositions of the equilibrium phases are derived equating the chemical potentials of the both phases.[1] The equations, however, cannot be solved, if preferential adsorption by polymer of solvent molecules is taken into account.

When a polymer substance is dissolved in a mixture of two solvents A and B to form a uniform dilute solution, the volume fraction of A in the regions surrounding the polymer molecules, φ_{in}, is generally different from that outside the regions, φ_{out}, and that in the original solvent mixture, φ.

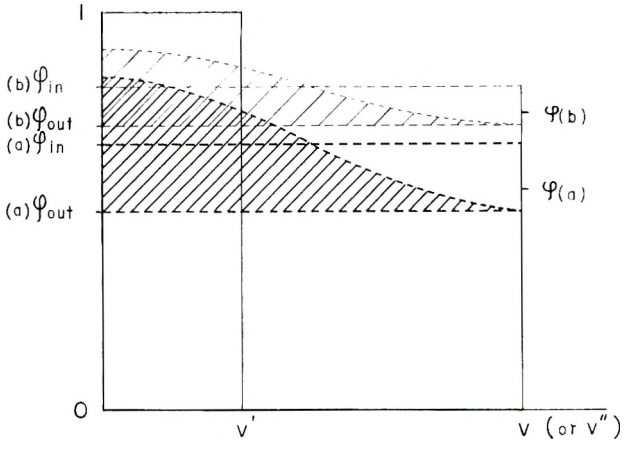

Fig. 1. Schematic diagram for the relations between v, v', v'', φ, φ_{in}, and φ_{out}. The shaded parts express the volumes of the preferentially adsorbed A solvent per unit weight of polymer, $v(\varphi_{in}-\varphi_{out})$, for two cases, a and b. The slopes on the shaded parts represent the change of toluene concentration with distance from a polymer molecule in the adsorbed region.

Assuming an invariant volume of the solvent mixture V for the adsorption, we have the relation

$$mv\varphi_{in} + (V-mv)\varphi_{out} = \varphi V \tag{1}$$

where m is the mass of the dissolved polymer and mv the total volume of the solvent regions surrounding the polymer molecules. The size of v can be taken arbitrarily. The volume of the A component preferentially adsorbed by the solute of unit weight is defined by $(\varphi_{in} - \varphi_{out})v$, and has a definite value for a definite condition in spite of the arbitrary size of v. When the adsorbed regions are regarded to be composed of pure A solvent layers and the remaining parts with solvent composition equal to that outside the adsorbed regions φ_{out}, keeping the amount of A solvent in the adsorbed regions unchanged, the volume v' of the hypothetical A solvent layers per unit weight of polymer substance is given by

$$(\varphi_{in}-\varphi_{out})v = (1-\varphi_{out})v' \tag{2}$$

The relations between φ, φ_{in}, φ_{out}, v, and v' are illustrated in Figure 1.

If the polymer solution is brought into contact with another solvent mixture of A and B without polymer and if the solvent mixture is chosen in such a way that no diffusion through the interface occurs before slow diffusion of polymer molecules, then it may be concluded that the volume fraction of A in the mixture, φ', is equal to φ_{out}. However when the polymer concentration is very high as in one of two equilibrium liquid phases, it is possible that all the solvent molecules are under the influence of polymer molecules and that the solvent composition in a region remotest from polymer molecules in the solution is different from the composition φ' of a sol-

vent mixture of A and B without polymer, which is in equilibrium with the concentrated solution with respect to solvent composition. If φ' is used as φ_{out}, however, the amount of A component preferentially adsorbed $(\varphi_{in} - \varphi_{out})v$ and the volume of A solvent layers v' per unit weight of polymer can be defined even for the concentrated solution as well as for dilute solutions.

The purpose of the present work is to find the relation between polymer concentrations and solvent compositions of two liquid phases in equilibrium through the measurement of v' defined as mentioned above.

Experimental

Measurements were carried out for toluene–isobutanol–polystyrene systems of various compositions to utilize some of the results previously obtained for systems consisting of the same components. Polystyrene was prepared in benzene at 60°C., azobisisobutyronitrile being used as the polymerization initiator. The polymer was precipitated twice with methanol from benzene solution to remove the low molecular weight fraction which is considered to make difficult the measurement of φ_{out} of a polystryrene solution by diffusing into a solvent layer poured on the solution. The molecular weight as obtained by viscosity measurements was 21×10^4.

Isobutanol was added to a toluene solution of polystyrene in a graduated glass bottle and the temperature of the mixture was raised to form a uniform solution. The temperature was then slowly lowered and the solution was allowed to stand over a week at 20°C. to separate into two layers with a clear interface. If required, the separation was stimulated by vibrating the glass bottle. Compositions near the critical point were avoided because they make worse the phase separation.

Since the polymer-poor phase is easier to treat than the viscous polymer-rich phase, polymer concentration and solvent composition were measured for the former phase and those for the latter were derived from them. The initial polymer concentration and solvent composition were selected so as to make the volume ratio of the polymer-poor phase to the polymer-rich phase as small as possible to reduce errors in deriving the composition of the polymer-rich phase. The polymer concentration in the polymer-poor phase was determined by evaporating solvent in vacuum, and the composition of the solvent trapped by liquid nitrogen was determined by refractive index measurement. The composition of a toluene–isobutanol mixture without polymer which is in equilibrium at 20°C., with respect to solvent composition, with the polymer-rich or the polymer-poor phase was determined by the diffusion method described previously.[2]

When the polymer concentration in a polymer-poor phase is small, the solvent composition of the phase φ is nearly equal to the composition outside the adsorbed regions φ_{out} as shown later, and the difference between them, $\varphi - \varphi_{out}$, is considered to decrease further with decreasing polymer concentration. In such a case φ and φ_{out} of the phase are equal to the sol-

vent composition φ' of a solvent mixture without polymer, which is in equilibrium, with respect to solvent composition, with the polymer-rich phase in equilibrium with the polymer-poor phase. The volume v' of pure toluene layers surrounding polymer molecules in the polymer-rich phase, therefore, can be evaluated from the solvent composition of the polymer-poor phase and the solvent composition and the polymer concentration for the whole system by inserting them into eq. (1) as φ_{out}, φ, and m/V, respectively. The solvent composition φ of the polymer-poor phase used here was evaluated directly from the refractive index of the phase corrected for small contribution of the solute.

Since a polymer-rich phase with polymer concentration m/V larger than 0.5 g./cc. is very viscous and it might occlude part of the polymer-poor phase, the observed values of the polymer concentration m/V and the solvent composition φ of the polymer rich phase might be smaller than the true ones. The volume of pure solvent layers per unit weight of polymer v', however, is not affected by these errors so far as the composition of the occluded portion is equal to that of the upper layer of the polymer-rich phase.

Results and Discussion

We shall denote V, m, φ, φ_{out}, and v' of a polymer-poor phase by V_1, m_1, φ_1, φ_{out_1} and v'_1, respectively, and those of the other phase in equilibrium by V_2, m_2, φ_2, φ_{out_2}, and v'_2, respectively. φ and φ_{out} refer to toluene fractions in the systems treated here. The observed values of V_1/V_2, m_1/V_1, and φ_1 of the systems for which φ_{out_1} and φ_{out_2} were measured by the diffusion method, and the values of m_2/V_2 and φ_2 derived from them are shown in Table I together with the observed values of φ_{out_1} and φ_{out_2} which are almost the same. The volume of toluene layers per unit weight of polymer in the polymer-rich phase, v'_2, was evaluated from these values and shown in Figure 2. The values of v'_2 are almost unchanged as seen in Figure 2 for a wide range of polymer concentration up to $m_2/V_2 = 0.23$ g./cc., where φ_{out_2} is about 0.6 and changes slightly with change of polymer concentration in the polymer-rich phase.

Owing to small polymer concentration in the polymer-poor phase, the

TABLE I

Compositions in Equilibrium Two Phases of Toluene–Isobutanol–Polystyrene Systems for Which φ_{out_1} and φ_{out_2} Were Measured by the Diffusion Method

V_1/V_2	m_1/V_1, g./cc.	m_2/V_2, g./cc.	φ_1	φ_2	φ_{out_1}	φ_{out_2}
5.05	0.0126	0.114	0.628	0.672	0.624	0.625
3.38	0.0081	0.142	0.622	0.679	0.618	0.618
2.53	0.0055	0.172	0.614	0.688	0.612	0.611
7.00	0.0035	0.179	0.616	0.690	0.614	0.608
4.49	0.0028	0.196	0.609	0.696	0.607	0.603
3.34	0.0024	0.228	0.603	0.699	0.601	0.591

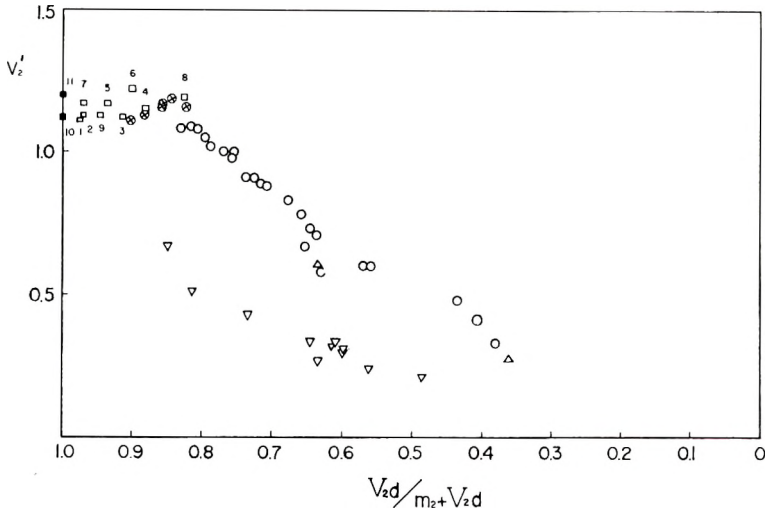

Fig. 2. Volume of the toluene layers v' or v'_2, per unit weight of polymer in relation to volume fraction of solvent, $Vd/(m+Vd)$ or $V_2d/(m+V_2d)$, where d is the density of the polymer: (O) v'_2 obtained by equating φ_1 to φ_{out}; (⊗) v'_2 obtained by the diffusion method; (□, ■) v' obtained by the diffusion method and by the light scattering method, respectively, for a solution without conjugate equilibrium phase (Points bearing a number correspond to points in Fig. 3 with the same number); (△, ▽) volumes of the acetone layers and the dioxane layers in the polymer-rich phases of acetone–cyclohexane–polyvinyl acetate and dioxane–isopropanol–polyvinyl acetate systems, respectively, derived from the observed results of Patat et al.[3]

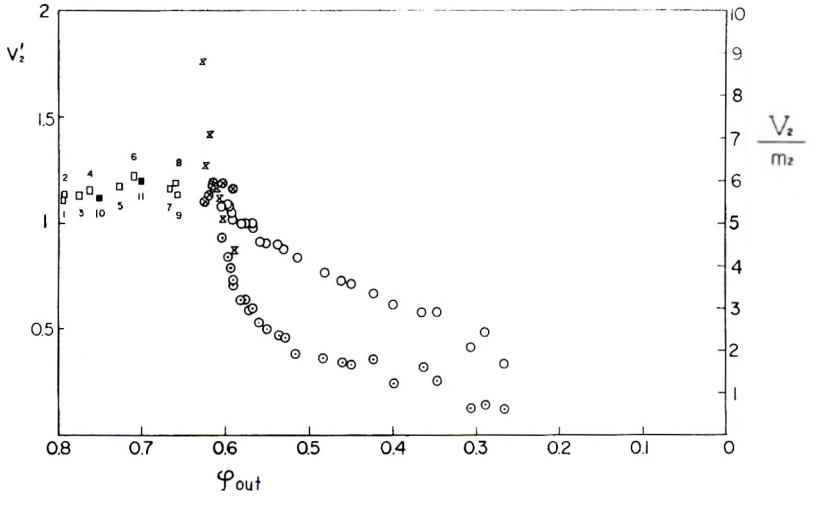

Fig. 3. Volume of the toluene layers v'_2 and volume of the total solvent V_2/m_2 per unit weight of polymer in the polymer-rich phase in relation to solvent composition outside the adsorbed regions φ_{out}: (O), (⊗), (□) have the same meanings as in Fig. 2; (⊙), (▽/△) V_2/m_2 values; (O) and (⊙) and (▽/△) at equal φ_{out} are measured for the same solution.

observed value of $\varphi_1 - \varphi_{out_1}$ is too small to evaluate v'_1 with sufficient accuracy to compare with v'_2. Therefore v'_1 was estimated by a method described below. The values of v' obtained by the diffusion method for single-phase solutions without conjugate equilibrium phases are almost independent of polymer concentration in a range between 2 and 22% and of solvent composition φ_{out} in a range between 0.66 and 0.79, as shown in Figures 2 and 3. Since these v' values are also nearly equal to the value of v' obtained[2] by the light-scattering method for an infinitely dilute solution of nearly the same solvent composition, and since v' for a solution with $m/V = 0.22$ and $\varphi_{out} = 0.66$ is, as seen from Figures 2 and 3, equal to v'_2 of a polymer-rich phase with nearly the same polymer concentration but with a different solvent composition ($\varphi_{out} = 0.59$), v'_1 of a polymer-poor phase with $\varphi_{out} = 0.60$–0.63 and $m_1/V_1 = 0.002$–0.012 g./cc. may be regarded to have nearly the same value as v' observed for single-phase solutions without conjugate equilibrium phases.

The mean molecular weight of the dissolved polymer may be different between the polymer-poor and polymer-rich phases. We can, however, compare v'_1 with v'_2, because v' is independent of molecular weight.[2] Since v'_2 is equal to v'_1, and φ_{out_1} is equal to φ_{out_2} as mentioned before, the solvent composition in the two phases, φ_1 and φ_2, is expressed by

$$\varphi_i = \varphi_{out} + (1 - \varphi_{out})m_i v'/V_i \qquad i = 1,2 \tag{3}$$

and, if $m_1/V_1 \ll m_2/V_2$, by

$$\varphi_2 = \varphi_1 + (1 - \varphi_1)m_2 v'/V_2 \tag{4}$$

The equalities of v' and of φ_{out} in two liquid phases in equilibrium simplify considerations for a ternary system, because the ternary system at a temperature is expressed as a "binary" system consisting of polymer with pure A solvent layers on it and solvent mixture outside the layers whose composition is expressed by φ_{out}. The solvent composition φ_{out} is a constraint imposed upon the system as the temperature is.

The magnitude of v, which appears in eqs. (1) and (2), can be taken arbitrarily so far as it is larger than v'. We shall define v'' as the minimum volume of adsorbed regions per unit weight of polymer substance which contains preferentially adsorbed toluene of a definite amount nearly equal to $v(\varphi_{in} - \varphi_{out})$. Since v' is independent of polymer concentration in dilute solutions, the size of v'' may be also independent of polymer concentration. In a concentrated solution it might be supposed that a particular site adjacent to a polymer segment is occupied by another polymer segment, in probability nearly equal to the volume fraction of polymer substance, leading to diminution of v' and v''. The observed value of v' is, however, practically unchanged by polymer concentration up to $m/V = 0.23$ g./cc., showing that polymer chains do not contact appreciably with each other. This constancy of v' also seems to show that an adsorbed region is not

shared by several polymer segments and v'' has still the same magnitude as in a dilute solution.

The volume of the toluene layers per unit weight of polymer substance v'_2 in a polymer-rich phase of high polymer concentration can be evaluated independent of V_2/m_2, the volume of solvent mixture per unit weight of polymer in the polymer rich phase. When v'_2 and V_2/m_2 are plotted against φ_{out} as shown in Figure 3, the curve of V_2/m_2 is very steep for φ_{out} larger than 0.6, although v'_2 remains almost unchanged. When φ_{out} reaches 0.6, the decrease of V_2/m_2 with decreasing φ_{out} is slowed down, and v'_2 begins to decrease. These observations make us suppose that at $\varphi_{out} = 0.6$ the polymer-rich phase is deprived of most of the solvent which exists between adsorbed regions at higher φ_{out}, and that the adsorbed regions begin to lose solvent with further decrease of φ_{out} as revealed by the diminution of v'. It is reasonable that the change of φ_{out} required for removal of solvent from adsorbed regions is larger than that required for removing from outside the regions. The size of adsorbed regions v'' per unit weight of polymer substance in a polymer solution with φ_{out} larger than 0.6 and with m/V smaller than 0.2 g./cc. is estimated to be around 5 cc./g. from the polymer concentration of a polymer-rich phase with $\varphi_{out} = 0.6$, in which the aforementioned changes in the v' and V_2/m_2 curves take place.

As can be seen from Figure 2, the observed value of v'_2 at polymer concentrations larger than 0.23 g./cc. is nearly proportional to $V_2d/(m_2 + V_2d) - a$, where d is the density of polystyrene and a is a constant of small value around 0.2. Compositions of equilibrium two-liquid phases of a ternary system have scarcely been measured. It is possible, however, to calculate m_1/V_1, m_2/V_2, φ_1, and φ_2 for polyvinyl acetate–acetone–cyclohexane systems and m_2/V_2, φ_1, and φ_2 for polyvinyl acetate–dioxane–isopropanol systems from the results obtained by Patat and Traexler.[3] Approximating φ_{out} by φ_1 because of small polymer concentration* in the upper phase, the values of v'_2 for acetone layers and dioxane layers are evaluated and shown in Figure 2. We see in the figure that the value of v'_2 is nearly proportional to $V_2d/(m_2 + V_2d) - a$ in accordance with the present results for toluene–isobutanol–polystyrene systems.

Although the present measurements were carried out only for toluene–isobutanol–polystyrene systems, the relations obtained here for the compositions of equilibrium two-liquid phases are considered to be applicable to other ternary systems consisting of different components.

References

1. For example, P. J. Flory, *Principles of Polymer Chemistry*, Cornell Univ. Press. Ithaca, N. Y. 1953, p. 549; H. Tompa, *Polymer Solutions*, Butterworths London, 1956, p. 187.

2. Yoshino, T., and H. Tanzawa, *J. Chem. Phys.*, **36**, 2382 (1962).

3. Patat, F., and G. Traexler, *Makromol. Chem.*, **33**, 113 (1959); see especially Table IV and Figures 4 and 5.

* m_1/V_1 is unknown for polyvinyl acetate–dioxane–isopropanol systems, but it is assumed to be zero because of the large isopropanol/dioxane ratio in the polymer-poor phases.

Résumé

On a étudié les compositions, dans deux phases liquides en équilibre, de mélanges polymère–solvant d'un point de vue d'une adsorption préférentielle d'un des solvants, ceci en mesurant φ_{out}, v' et V/m définis plus loin pour des systèmes toluène-isobutanol-polystyrène. φ_{out}: fraction de volume de toluène dans le mélange des solvants en dehors des régions adsorbées entourant les molécules de polymère; v': volume des couches hypothétiques de toluène par unité de poids de substance polymérique lorsque les régions adsorbées sont divisées en couches de toluène pur et les parties restantes avec une composition du solvant égale à φ_{out}, tout en gardant la quantité de toluène inchangée dans les régions adsorbées; V/m: volume de solvant par unité de la substance polymérique. On observe que v' est égal pour les phases riches et pauvres en polymère et indépendant de la concentration en polymère, aussi longtemps que la concentration en polymère est inférieure à 0.2 g par cc de solution. On trouve également que φ_{out} est égal pour les deux phases. Ces observations montrent qu'on peut, à une température donnée, approcher le systeme ternaire au moyen d'un système binaire constitué de molécules polymériques qui sont constituées de vraies molécules de polymère et des couches de toluène qui les entourent, et du mélange de solvants à l'extérieur des couches de toluène. Lorsqu'on exprime V/m et v' dans la phase riche en polymère en fonction des valeurs décroissantes de φ_{out}, v' commence à décroître pour $\varphi_{out} = 0.6$ valeur à laquelle la variation de V/m au long de la courbe pour $\varphi_{out} > 0.6$ diminue. Ceci fait suggérer que lorsque la phase riche en polymére est dépourvue de la plus grande partie du solvant qui se trouve hors des régions adsorbées, ces régions commencent à perdre du solvant. La grandeur des régions adsorbées par unité pondérale de polystyrène dans une solution diluée pour $\varphi_{out} > 0.6$ est estimée aux environs de 5 cc par gramme à partir de V/m d'une phase riche en polymère avec $\varphi_{out} = 0.6$.

Zusammenfassung

Die Zusammensetzung der beiden Gleichgewichts-Flüssigkeitsphasen in einem Polymer-Lösungsmittelgemisch-System wurde in bezug auf die bevorzugte Adsorption einer Lösungsmittelkomponente durch Messung der unten definierten Grössen φ_{aussen}, v' und V/m für das System Toluol-Isobutanol-Polystyrol untersucht. φ_{aussen}: Volumbruch von Toluol im Lösungsmittelgemisch ausserhalb der die Polymermoleküle umgebenden Adsorptionsschicht; v': Volumen der hypothetischen Toluolschichten pro Gewichtseinheit Polymersubstanz bei Aufteilung der Adsorptionsschicht in eine reine Toluolschicht und einen restlichen Teil mit der Lösungsmittelzusammensetzung gleich φ_{aussen}, unter Aufrechterhaltung der ungeänderten Toluolmenge in der Adsorptionsschicht; V/m: Lösungsmittelvolumen pro Gewichtseinheit Polymersubstanz. v' erweist sich als gleich für die polymerarme und polymerreiche Phase und als unabhängig von der Polymerkonzentration, solange die Polymerkonzentration in der polymerreichen Phase kleiner als 0,2 g/cm³ ist. φ_{aussen} ist ebenfalls für beide Phasen gleich. Diese Beobachtungen zeigen, dass das ternäre System bei einer gegebenen Temperatur durch ein binäres, aus wahren Polymermolekülen mit der sie umgebenden Toluolschichte und Lösungsmittelgemisch ausserhalb der Toluolschichte bestehendes System angenähert wird. Beim Auftragen von V/m und v' in der polymerreichen Pase gegen abnehmendes φ_{aussen} beginnt v' bei $\varphi_{aussen} = 0{,}6$ abzunehmen, wo die Änderung von V/m entlang einer steilen Kurve für $\varphi_{aussen} > 0{,}6$ abgeschwächt wird. Das zeight, dass nach Entzug des grössten Teils des Lösungsmittels auserhalb der Adsorptionsschicht aus der polymerreichen Phase die Adsorptionsschichte selbst Lösungsmittel zu verlieren beginnt. Die Grösse der Adsorptionsschicht pro Gewichtseinheit Polystyrol in verdünnter Lösung mit $\varphi_{aussen} > 0{,}6$ wird aus V/m einer polymerreichen Phase mit $\varphi_{aussen} = 0{,}6$ zu rund 5cc/g bestimmt.

Received January 14, 1963

JOURNAL OF POLYMER SCIENCE: PART A VOL. 2, PP. 973–982 (1964)

Mechanism of the Mechanical Degradation of Cellulose*

RONALD L. OTT, *The Institute of Paper Chemistry, Appleton, Wisconsin*

Synopsis

From electron spin resonance spectra of a ball-milled cellulose sample, it was established that the mechanical degradation of air-dry cellulose was characterized by the formation of free radicals. It was shown that iodine increased the rate of mechanical degradation, presumably by preventing the recombination of at least some of the radicals formed during grinding. Since no difference in iodine consumption during grinding was observed between air-dry and oven-dry cellulose samples, it was concluded that heterolytic cleavage of cellulose molecules did not occur. The formation of benzyl iodide and cyclohexyl iodide was observed when cellulose was ground with iodine in toluene and cyclohexane, respectively. It is possible that either chain transfer reactions between cellulose radicals and solvent molecules account for the halogenation of the solvent or that the halogenation is due to a hypoiodite structure formed by the reaction of cellulose alkoxy radicals with iodine.

The mechanism by which cellulose is mechanically degraded has been the subject of conflicting theories since the degradation was first observed by Waentig in 1921.[1] Mechanically activated hydrolysis or oxidation reactions,[1–3] heterolytic mechanical rupture of primary bonds to form macroions,[3] and homolytic mechanical rupture of primary bonds to form macroradicals[4] have all been suggested.

This paper reports evidence which establishes that free radicals are formed during the mechanical degradation of air-dry cellulose by ball-milling and suggests that heterolytic mechanical rupture of chemical bonds does not accompany the homolytic cleavage.

EXPERIMENTAL

Reagents

Cellulose. High viscosity, acetate-grade cotton linters (Type 1-AR-2300) supplied by Buckeye Cellulose Corp. in sheet form were used. Approximately 1500 g. were ground in a Wiley mill to pass through a plate having 0.040-in. diameter holes. The intrinsic viscosity of the nitrated linters in ethyl acetate was 28.2 dl./g. at zero rate of shear. The number-

* A portion of a thesis submitted in partial fulfillment of the requirements of The Institute of Paper Chemistry for the degree of Doctor of Philosophy from Lawrence College, Appleton, Wis., June, 1963. This work was carried out under the direction of Edward J. Jones.

average degree of polymerization calculated from the Immergut correlation,[5] $[\eta] = 0.38 \times 10^{-4}\bar{M}_n^{1.03}$, was 1710.

Air-dry samples (5.8% moisture on an oven-dry basis) were withdrawn from the total sample stored in a humidity room held at 72°F. and 50% R.H. Oven-dry samples were prepared by drying air-dry samples for 3 hr. at 105°C., placing them in absolute ethanol overnight, drying the samples again for 3 hr. at 105°C., placing them in cyclohexane, and drying the samples once again for 3 hr. at 105°C. prior to use.

Solvents. Practical-grade cyclohexane was washed three times with concentrated sulfuric acid and once with water, dried with calcium chloride, and distilled. The product was treated with silica gel prior to use. Distilled, spectral-grade carbon tetrachloride and distilled reagent-grade toluene were used. Cellulose viscosities were determined in Ecusta 1.0*M* cupriethylenediamine diluted volumetrically to 0.5*M*.

Iodine and Radioiodine I^{131}. Baker reagent-grade iodine was used without further treatment. Stock solutions of iodine and iodine I^{131} in organic solvents were prepared by an exchange reaction between iodine and sodium radioiodide. An aqueous solution containing 2 or 3 mcuries of NaI^{131} was diluted to 5 ml. and placed in a 50-ml. extraction funnel fitted with a Teflon stopcock. This solution was shaken 4 or 5 times with 20-ml. portions of a solution of iodine in cyclohexane or carbon tetrachloride containing 10 g. of iodine per liter. The organic layers were collected, dried with calcium chloride, and stored until used. Well over 90% of the radioactivity was transferred to the iodine by this method.

Apparatus

The vibratory ball mill constructed by Busche[6] in accordance with specifications of the National Bureau of Standards mill[7] was employed. The grinding jar of approximately 1-liter capacity was machined from 440-F stainless steel, a heat-treatable material which can be hardened to Rockwell C 59. Stainless steel balls (1/4 in.) of the same material and hardness were used to minimize surface attrition of the balls.

The Varian electron spin resonance spectrometer at the Institute of Enzyme Research in Madison, Wisconsin was used. This instrument had a magnet with a 6-in. diameter pole and a field strength of 3300 g.

Radiation was counted with a Tracerlab model TGC-5 self-quenching Geiger tube connected to a Berkeley model 2000 decimal scaler. The counting efficiency using this equipment was about 0.1%.

For solvent analysis, an Aerograph model 110-C gas chromatograph with a 6-ft. Carbowax 20M (a polyethyleneglycol) column was employed. Thermal conductivities were recorded by a Minneapolis-Honeywell 143 × 58 high-speed recorder.

Electron Spin Resonance Spectroscopy

The grinding jar was charged with 5 g. of air-dry cellulose and 2800 g. of balls under a nitrogen atmosphere, the jar was sealed, and the cellulose was

ground for 36 hr. After grinding, the jar was opened under a nitrogen atmosphere and the sample was transferred to a small vessel and sealed. The vessel was placed in dry ice and transported to Madison. In Madison, the sample was transferred to a thin-walled quartz tube (3 mm. i.d.). During the transfer the sample was exposed to atmospheric oxygen.

Electron spin resonance (ESR) spectra of the sample were determined by using a phase-sensitive detection technique by which the 3-cm. microwave was modulated at a frequency of 100 kcycles/sec. with an amplitude which was small compared to the line width of the signal. As the main magnetic field was varied, a pen recorder plotted the first derivative of the radiofrequency power absorbed by the sample with respect to the main field strength as a function of the magnetic field strength. Measurements were made at a temperature of 120°K. about 5 hr. after grinding. ESR spectra of the empty quartz tube and a cellulose sample that had been ground and allowed to stand for eight days in the presence of oxygen were also determined.

Degradation in the Presence of Cyclohexane

Three runs in which air-dry cellulose was ground for 18–29 hr. in cyclohexane were made. The grinding jar was charged with 3.29 g. of air-dry cellulose, 2250 g. of balls, and 300 ml. of cyclohexane, and the jar was thoroughly flushed with prepurified nitrogen. The contents were then ground in a cold room held at 4°C. The equilibrium temperature reached during milling was about 14°C. Three runs in which a 5-g. sample of oven-dry cellulose was ground for 18–30 hr. were also made. In these runs, the solvent-exchanged sample which had been dried for 3 hr. at 105°C. was charged directly from the oven into the grinding jar.

After each run, the intrinsic viscosity $[\eta]$ of the ground samples was determined. About 0.2 g. of sample was dried at 105°C. and dissolved in 50 ml. of cupriethylenediamine. The specific viscosity, η_{sp}, was determined as a function of concentration at 25°C. in a Cannon dilution viscometer. The solvent time for the viscometer was about 300 sec. The intrinsic viscosity was obtained by linear extrapolation of log η_{sp}/C versus concentration curves.

Degradation in the Presence of Iodine

Runs were made in which 5.29-g. samples of air-dry cellulose were ground under nitrogen with 2250 g. of balls in 300 ml. of carbon tetrachloride containing about 0.1, 0.5, or 2.0 g. of iodine per liter. Runs were also made in which 5.29-g. samples of air-dry cellulose and 5.00-g. samples of oven-dry cellulose were ground under dry nitrogen in cyclohexane containing 2.0 g./l. iodine and enough radioiodine to give a count of 10,000–20,000 counts/min.

The intrinsic viscosity of the samples ground in carbon tetrachloride was determined in 0.5*M* cupriethylenediamine as previously reported. After grinding in cyclohexane, the slurry was separated from the balls and the

volume recovered was measured. The slurry was then diluted to 300 ml. with solvent and counted in a 400-ml. beaker using the dip counter. All counts were made with the counter immersed to the same depth in the center of the beaker. During the counting, the slurry was stirred magnetically.

After counting, the slurry was filtered on a sintered glass filter and about 0.6 g. of the ground cellulose was removed for viscosity determination. The remainder was dispersed in 75 ml. of carbon tetrachloride and dissolved in 100 ml. of 65% sulfuric acid. Then excess iodine was extracted from the sulfuric acid layer with additional portions of carbon tetrachloride. The sulfuric acid was then diluted to 300 ml. with water and counted as before. Also, the total value of carbon tetrachloride used to extract the excess iodine was determined and this phase was then extracted with 1*M* thiosulfate, dried with calcium chloride, and counted. Background counts were determined on 300 ml. of water or 300 ml. of carbon tetrachloride.

The total viscosity sample was dried at 105°C. and about 0.2 g. was dissolved in 0.5*M* cupriethylenediamine. The specific viscosity as a function of concentration and intrinsic viscosity was determined as previously reported.

The iodine consumed by the cellulose was taken to be the sum of the iodine in the sulfuric acid layer that could not be extracted with carbon tetrachloride and the iodine in the carbon tetrachloride extract that could not be extracted with thiosulfate. (The latter was less than 20% of the former.) The fraction of the total initial free iodine that reacted with the cellulose was then equal to the ratio of the counts in these two phases to the total count prior to extraction since no appreciable radiochemical decay of I^{131} occurred over the period of time these counts were made. To determine iodine consumption per gram of cellulose, corrections for the cellulose unrecovered after grinding and the cellulose removed for the viscosity sample were made.

Solvent Analysis after Grinding Cellulose with Iodine

It was observed that after grinding air-dry cellulose with iodine in cyclohexane, a residual count remained in the cyclohexane after the excess iodine had been extracted with 1*M* sodium thiosulfate. The experiment was repeated by grinding 5.29 g. of air-dry cellulose for about 18 hr. under nitrogen in 300 ml. of different solvents containing 2 g. of iodine per liter. Benzene, toluene, and ethylbenzene were used. After each run, the total slurry was counted as before, and the slurry was filtered. The solvent was extracted with 1*M* thiosulfate and counted again. Residual counts in these solvents also remained.

To determine if halogenation of the solvent had occurred, the cyclohexane from two such runs was concentrated about 50 times by distillation and was gas chromatographed. A known solution containing 100 μl. of cyclohexyl iodide per liter of cyclohexane was also chromatographed. A thermal conductivity peak in the unknown corresponding to the cyclohexyl iodide peak in the known was observed. Enough of this unknown material for

ultraviolet analysis was then collected by chromatographing several portions of the grinding solvent and bubbling the exit helium through 3 ml. of cyclohexane as the unknown material left the column. Ultraviolet spectra of the unknown material and a known solution of cyclohexyl iodide in cyclohexane were determined from 240 to 300 mμ with the use of a Beckman model DU spectrophotometer.

A similar experiment was conducted with toluene and benzyl iodide. In this experiment, the unknown material in the solvent after grinding, which gave a thermal conductivity peak similar to benzyl iodide when gas chromatographed, was collected in cyclohexane and its ultraviolet spectrum was determined from 240 to 300 mμ.

RESULTS AND DISCUSSION

Electron Spin Resonance Spectroscopy

The electron spin resonance spectrum of the ball-milled cellulose sample appears in Figure 1. Because the ESR spectra of the empty quartz tube and of the cellulose sample that had been ground and allowed to stand for eight days showed no paramagnetic absorption, this spectrum indicates the presence of at least two types of radicals in the sample, A and B, with the possibility that a third type, C, also exists.

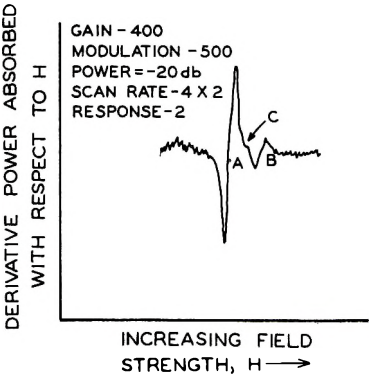

Fig. 1. Electron spin resonance spectra for a ball-milled cellulose sample.

Values for the spectroscopic splitting factor for these radicals were not determined because only the current through the magnet was recorded and the actual field strength was unknown.

Degradation of Cellulose in the Presence and Absence of Iodine

The results from the runs in which cellulose was ground with iodine in carbon tetrachloride and cyclohexane, plotted as intrinsic viscosity versus grinding time, appear in Figures 2 and 3. It may be seen that the rate of degradation is increased as the iodine concentration in carbon tetrachloride

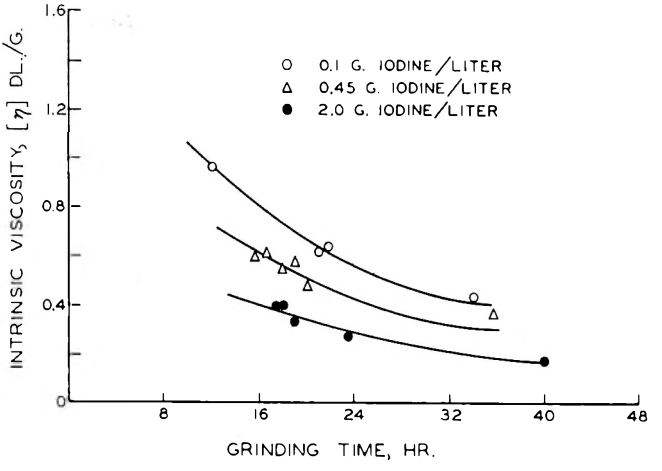

Fig. 2. Cellulose intrinsic viscosity as a function of grinding time for the degradation of cellulose in carbon tetrachloride.

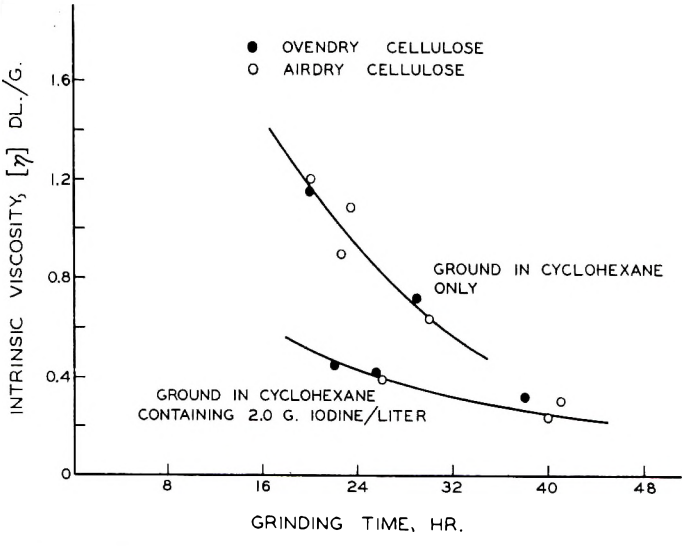

Fig. 3. Cellulose intrinsic viscosity as a function of grinding time for the degradation of cellulose in cyclohexane.

increases from 0.1 to 2.0 g./l. and as the iodine concentration in cyclohexane increases from 0 to 2.0 g./l. Since the same limiting viscosity, 0.15 dl./g., is reached when cellulose is ground for about 190 hr. in the presence and absence of iodine, it is concluded that the increased rate of degradation in the presence of iodine is not due to a secondary chemical degradation involving iodine. Rather, the iodine accelerates the degradation by preventing the recombination of at least some of the macroradicals formed during the milling of cellulose.

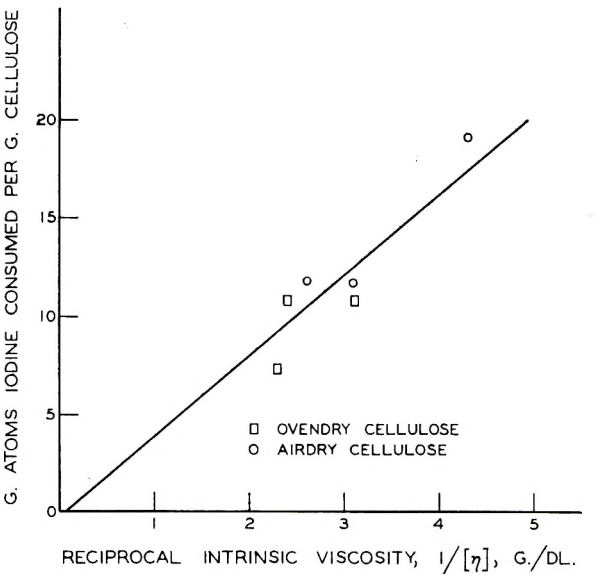

Fig. 4. Iodine consumption during grinding as a function of the degree of degradation.

It is not thought that heterolytic scission of cellulose molecules accompanies the homolytic cleavage. If macroions are formed during the grinding of cellulose, it is almost certain that they are terminated by water molecules. Air-dry cellulose contains about 10 times the required water to terminate the macroions formed by the heterolytic, mechanical degradation of cellulose from a D.P. of 1710 to a D.P. of 20. Therefore, one might expect differences in the rate of degradation and in the iodine consumption during grinding between oven-dry and air-dry cellulose samples if heterolytic scission occurred. However, Figures 3 and 4 indicate that no such differences can be observed.

Solvent Analysis after Grinding Cellulose with Iodine

Data showing the presence of iodide in the solvent after grinding cellulose with iodine are given in Table I. In the case of cyclohexane, the iodine reacted with the solvent is very nearly equal that combined with the cellulose.

The results of the gas chromatography and ultraviolet analyses showed that iodide present in cyclohexane was cyclohexyl iodide and the iodide present in toluene was benzyl iodide. The halogenation of the aliphatic hydrocarbon and the aromatic hydrocarbon in the side chain indicated that a free radical mechanism was involved.

It was first thought that direct halogenation of the solvent by the iodine had occurred.[8] This idea was rejected, however, when it was found that no halogenation of the solvent was observed when glucose was ground for 48 hr. in the presence of toluene and cyclohexane containing 2.0 g. of iodine per liter.

It was then concluded that the halogenation of the solvents was either the result of chain transfer reactions between cellulose radicals and solvent molecules or the result of the reaction of an organic hypoiodite with the solvents. Presumably, this hypoiodite could be formed *in situ* by the reaction of iodine with cellulose alkoxy radicals present as the result of the homolytic cleavage of cellulose molecules and the glycosidic links. Hammond,[9] in studying the reactions of benzyl peroxide with iodine, has noted that halogenation of the solvent occurs and has suggested that a benzoyl hypoiodite type of structure accounts for the halogenation.

TABLE I
Iodine Concentration in Solvent After Grinding Cellulose with Iodine

Grinding time, hr.	Solvent	Iodide concentration during grinding, g./l.	100-sec. counts		Indicated iodide concentration in solvent, g./l.
			Total slurry after grinding	Solvent after thiosulfate extraction[a]	
26	Cyclohexane	2.0	13,100	116	1.8×10^{-2}
17.5	Cyclohexane	2.0	20,500	119	1.2×10^{-2}
17.5	Benzene	2.0	20,000	57	0.6×10^{-2}
16.75	Toluene	2.0	17,700	60	0.7×10^{-2}
19	Ethylbenzene	2.0	11,200	59	1.1×10^{-2}

[a] Corrected for background count which was usually about 30 counts/min. and losses which occurred during extraction and drying.

In polymerizing monomer systems where the chain transfer constants of various solvents have been determined, it has been observed that ethylbenzene is much more reactive than cyclohexane toward many different polymer radicals.[10] Therefore, if a chain transfer reaction involving cellulose radicals and solvent molecules accounts for the halogenation of the solvent, one might expect significantly more iodide present after grinding cellulose with iodine in ethylbenzene than after grinding in cyclohexane.

Since the data in Table I indicate that there is no significant difference in the amount of iodide in ethylbenzene and cyclohexane after grinding cellulose with iodine, there is some evidence that a chain transfer reaction does not account for solvent halogenation. However, because of the large differences between the polymerizing monomer systems and the cellulose–iodine–solvent system, the use of chain transfer constant data for the former to eliminate the possibility of a chain transfer reaction occurring in the latter may not be valid.

There is no evidence that *in situ* organic hypoiodites halogenate by a radical mechanism, although they are known to be effective halogenating agents.[11] Therefore, the halogenation of solvents during the grinding of cellulose with iodine cannot be definitely attributed to a hypoiodite intermediate. Certainly, if a hypoiodite intermediate is involved, the halogenation involves a more complex reaction than simple dissociation of the hy-

poiodite into atomic iodine and an alkoxy radical because atomic iodine is not capable of direct halogenation of aliphatic hydrocarbons.

The formation of alkoxy radicals at the glycosidic links during the milling of cellulose forms the basis for an interesting alternative theory to account for the actual rupture of carbon–carbon bonds within the ring during the ball-milling of cellulose.[12] This has been attributed to actual mechanical rupture of carbon–carbon bonds, but certainly such reasoning can be criticized on the basis that a cellulose molecule subjected to a shear force will almost certainly break at the weakest point, the freely rotating glycosidic link, rather than in the stable, six-membered ring. Alkoxy radicals are known to decompose by carbon–carbon bond fission as follows:[13]

$$R—R'CHO \rightarrow R\cdot + R'CHO \text{ or } R'\cdot + RCHO$$

Also, when alkoxy radicals derived from alicyclic alcohols decompose, carbon–carbon fission in the ring occurs. For example, cyclohexyl radicals decompose to give $\cdot CH_2(CH_2)_4CHO$. Therefore, it is suggested that reactions involving decomposition of cellulosic alkoxy radicals formed during milling accounts for the isolation of three-, four-, and five-carbon fragments from the endgroups of ball-milled cellulose.

The author wishes to thank Dr. Helmut Bienert at the Institute of Enzyme Research, Madison, Wisconsin for his help and cooperation in obtaining the electron spin resonance spectra.

References

1. Waentig, P., *Textil-Forsch.*, **3**, 154 (1921).
2. Meyer, K., *Natural and Synthetic Polymers*, Interscience, New York–London, 1954, p. 398.
3. Grohn, H., *J. Polymer Sci.*, **30**, 551 (1958).
4. Howsmon, J., and R. Marchessault, *J. Appl. Polymer Sci.*, **1**, 313 (1959).
5. Immergut, E., B. Rånby, and H. Mark, *Ind. Eng. Chem.*, **45**, 2483 (1953).
6. Busche, L., Ph.D. Thesis, The Institute of Paper Chemistry, 1960.
7. Forziati, F., W. Stone, J. Rowen, and W. Appel, *J. Res. Natl. Bur. Std.*, **45**, 109 (1950).
8. Perry, E., and C. Feldman, *J. Polymer Sci.*, **54**, 518 (1961).
9. Hammond, G., *J. Am. Chem. Soc.*, **72**, 3737 (1950).
10. Walling, C., *Free Radicals in Solution*, Wiley, New York–London, 1957, pp. 152, 157.
11. Anbar, M., and D. Ginsburg, *Chem. Revs.*, **54**, 925 (1954).
12. Assarson, A., B. Lindberg, and O. Theander, *Acta Chem. Scand.*, **13**, 1231 (1959).
13. Gray, P., and W. Williams, *Chem. Revs.*, **59**, 239 (1959).

Résumé

Au départ du spectre de résonance de spin électronique d'un échantillon de cellulose moulue, il a été établi que la dégradation mécanique de la cellulose dans l'air sec est caractérisée par la formation de radicaux libres. On a montré que l'iode accroît la vitesse de dégradation mécanique, vraisemblablement en empêchant la recombinaison d'au moins quelques uns de radicaux formés au cours du broyage. Vu qu'aucune différence de consommation d'iode n'est observée au cours du broyage des échantillons de cellulose à l'air sec et de cellulose sèchée au four, on en a conclu que la scission hétérolytique des molécules de cellulose n'avait pas lieu. On a observé la formation d'iodure

de benzyle et de cyclohexyle lorsque la cellulose est broyée avec de l'iode respectivement dans le toluène et le cyclohexane. Il est possible soit que les réactions de transfert de chaîne entre les radicaux de la cellulose et les molécules de solvant rendent compte de l'halogénation du solvant, soit que l'halogénation est due à une structure hypoiodite formée par la réaction de radicaux alcoyloxy- de la cellulose avec l'iode.

Zusammenfassung

Elektronspinresonanz-Spektren einer in der Kugelmühle gemahlenen Celluloseprobe zeigten, dass der mechanische Abbau einer lufttrockenen Cellulose durch die Bildung freier Radikale charakterisiert wird. Zusatz von Jod erhöhte, vermutlich durch Verhinderung der Rekombination zumindest einiger der beim Mahlen gebildeten Radikale, die Geschwindigkeit des mechanischen Abbaus. Da zwischen lufttrockenen und ofengetrockneten Celluloseproben kein Unterschied des Jodverbrauches während des Mahlens beobachtet wurde, wird angenommen, dass keine heterolytische Spaltung der Cellulosemolekel auftritt. Beim Mahlen von Cellulose mit Jod in Toluol bzw. Cyclohexan wurde die Bildung von Benzyljodid bzw. Cyclohexyljodid beobachtet. Es erscheint möglich, dass entweder Kettenübertragungsreaktionen zwischen Celluloseradikalen und Lösungsmittelmolekeln für die Halogenierung des Lösungsmittels verantwortlich sind, oder dass die Halogenierung durch eine bei der Reaktion von Cellulose-Alkoxyradikalen mit Jod gebildete Hypojoditstruktur bewirkt wird.

Received January 14, 1963

JOURNAL OF POLYMER SCIENCE: PART A VOL. 2, PP. 983–1000 (1964)

Thermal and Photochemical Degradation of Poly(*n*-butyl Methacrylate)

N. GRASSIE and J. R. MacCALLUM, *The Chemistry Department, The University, Glasgow, Scotland*

Synopsis

Like poly(methyl methacrylate), poly(*n*-butyl methacrylate) yields monomer as the predominating volatile product of thermal degradation at 250°C. Unlike poly(methyl methacrylate) which gives quantitative yields of monomer, however, poly(*n*-butyl methacrylate) only degrades to monomer to an extent of approximately 40%. On prolonged heating the residue becomes progressively more stable. The clue to this behavior is given by the fact that traces of 1-butene are detectible among the volatile products and anhydride structures in the residue. Thus depolymerization and ester decomposition to acid proceed simultaneously during the thermal degradation of this polymer. Competition between these two processes is a general property of methacrylates, with poly(methyl methacrylate) and poly(*tert*-butyl methacrylate) representing the two extremes of behavior. This interference by ester decomposition prevents a quantitative comparison of the thermal depolymerization of the poly(alkyl methacrylate) series but it has been possible to show that as in poly(methyl methacrylate) the depolymerization process in poly(*n*-butyl methacrylate) is initiated thermally at the chain ends. When copolymers of *n*-butyl methacrylate and methacrylic acid are heated to 250°C., conversion of acid to anhydride is rapid and complete. Yet the polymer degrades to the same extent as ester homopolymer. On the other hand, preheating the copolymer at 170°C. has an inhibiting effect on subsequent degradation at 250°C. Rapid heating to 250°C. apparently results in intermolecular anhydrides which can be liberated in a depolymerization reaction. Preheating at 170°C. allows acid units to migrate along the polymer chain so that intramolecular anhydride structures can be formed by elimination of water between adjacent acid units. These are the true inhibitors of depolymerization. Unlike the thermal reaction, the photochemically initiated depolymerization to monomer at 170°C. is quantitative. That also appears to be a general property of poly-(alkyl methacrylates) and even applies to poly(*tert*-butyl methacrylate) which thermally undergoes almost quantitative ester decomposition. There is no self-inhibition as in the thermal reaction. As in the thermal degradation, however, the presence of methacrylic acid units in the polymer has no effect, but preheating depresses the rate of depolymerization. Certain features of these reactions lead to the conclusion that ester decomposition in poly(*n*-butyl methacrylate), unlike that in poly(*tert*-butyl methacrylate) is a radical process occurring in direct competition with depolymerization. This is supported by the observation that during the polymerization of *n*-butyl methacrylate at 30°C., isobutene is produced and acid units appear in the polymer. A unified picture of ester decomposition during polymerization and depolymerization is presented in terms of such a radical mechanism. Mechanisms are also suggested to explain self-inhibition in the thermal reaction and the inhibiting effect of preheating acid/ester copolymers on both their thermal and photochemical depolymerizations.

The methyl and *tert*-butyl esters are the only members of the polymethacrylate series whose thermal degradations have been studied experimentally in detail. Poly(methyl methacrylate) yields monomer exclusively.[1] Poly(*tert*-butyl methacrylate), on the other hand, undergoes ester decomposition followed by elimination of water from the resulting acid so that the predominating volatile products are isobutene and water while the involatile residue is poly(methacrylic anhydride).[2] At the same time, reproducible yields of monomer of the order of 1% are obtained.

The methacrylate esters are of particular interest as a series since they allow, through polymerization and particularly through copolymerization experiments, a study to be made of the effects on radical reactivity of small, well defined changes in chemical structure. But precisely the same radicals take part in the monomer producing chain depolymerization reactions which are typical of these polymers. Degradation studies would therefore appear to offer a third possible approach to such reactivity investigations.

Poly(*n*-butyl methacrylate) is an interesting starting point for such experiments because, like poly(methyl methacrylate), it is a primary ester although with more bulky side chains comparable in size with those of poly(*tert*-butyl methacrylate).

EXPERIMENTAL

Monomers

n-Butyl methacrylate (I.C.I. Ltd.) was washed four times with 5*N* caustic soda to remove stabilizer (hydroquinone), four times with distilled water, dried for 24 hr. over anhydrous sodium sulfate and finally filtered and distilled under reduced pressure (b.p. 55–58°C. at 25 mm.). The infrared spectrum of the resulting monomer was identical with that reported by Davison.[3] This evidence, and the fact that only one peak was obtained on the gas-liquid chromatogram, were accepted as sufficient proof of purity.

Methacrylic acid (I.C.I. Ltd.) was freed from inhibitor by distillation under reduced pressure (b.p. 60°C./10 mm.). Both monomers were stored at −16°C. prior to use.

Preparation of Polymers

Details of the preparations of *n*-butyl methacrylate homopolymers and ester/acid copolymers are given in Table I.

The initiator was 2,2′-azoisobutyronitrile, and polymerizations were carried out in absence of air. Poly(*tert*-butyl methacrylate) was prepared as previously described.[2]

Reactivity ratios for the *n*-butyl methacrylate/methacrylic acid system have not previously been reported. Values reliable and accurate enough for the present purpose may be calculated by using the Alfrey-Price *Q-e* scheme[4] and data which exist for the copolymerization of methacrylonitrile

TABLE I
Preparation of Polymers

Polymer	Initiator (w/v), %	Preparation	Composition of copolymer (ester/acid)	Molecular weight $\times 10^{-5}$	Temperature of polymerization, °C.
NB 1	0.05	Bulk	—	11.0	60
NB 2	0.50	Bulk	—	4.6	60
NB 4	0.20	$\frac{\text{Monomer}}{\text{Benzene}} = 1/10$	—	0.4	80
NB 6	0.03	$\frac{\text{Monomer}}{\text{Benzene}} = 1/2$	—	1.1	80
CNB 1	0.50	Bulk	99:1		60
CNB 2	0.50	Bulk	90:10		60

with methacrylic acid and its esters.[5] These values are $r_1 = 0.82$; $r_2 = 1.11$ (methacrylic acid, M_1; *n*-butyl methacrylate, M_2).

Polymers were precipitated and twice reprecipitated by methanol from acetone solution. They were dried by prolonged storage in vacuum.

Degradation Methods

Thermal degradations were carried out on a dynamic molecular still modified as described by Grant and Grassie.[6] In each experiment 0.2–0.3 g. of polymer was used, being covered by 60–80 mesh copper powder (10–12 g.) to ensure uniform heating.

For photochemical experiments the dynamic molecular still was modified by incorporating a quartz window in the lid. The polymer was in the form of film approximately 0.003 cm. in thickness. An Osram 125-w. mercury arc lamp with glass envelope removed was used as light source.

By the use of filters it was shown by Cowley and Melville[7] that the photodepolymerization of poly(methyl methacrylate) was initiated by the 2537 A. radiation emitted by this lamp. By similar methods it was ascertained that the photochemical degradation of poly(*n*-butyl methacrylate) is similarly initiated. Measurement of the ultraviolet absorption of poly(*n*-butyl methacrylate) using a Perkin-Elmer 137 instrument showed that at least 95% of 2537 A. radiation is transmitted by the films used in degradation experiments. Thus there can be no significant "skin effect."

Analysis of Products of Degradation

Products of degradation were examined by infrared spectroscopy and gas–liquid chromatography. Infrared measurements were made with the use of a Perkin-Elmer Model 13 double-beam instrument with rock salt prism. Volatile products were measured either in a 10 cm. gas cell or using a drop of the liquid compressed between rock salt plates. Residual polymer was examined either in chloroform solution or as a powder dispersed in KCl.

Gas–liquid chromatograms of volatile products were obtained by using a

Pye-Argon instrument with an ionization detector. All measurements were qualitative.

Number-average molecular weights were obtained by using a modified Fuoss-Mead osmometer.[8]

RESULTS AND DISCUSSION

Thermal Degradation of Homopolymer

At 220°C., the depolymerization reaction in poly(methyl methacrylate) prepared using benzoyl peroxide as a catalyst, is initiated at the unsaturated chain ends formed in the disproportionation termination reaction.[1,9] The chain ends terminated by catalyst fragments are quite stable. Thus at 220°C., 50% of the polymer molecules are degradable. On raising the temperature to 280°C. the remainder of the polymer depolymerizes smoothly, the reaction being initiated at the saturated chain ends formed in the termination process during polymerization. When the polymerization is carried out in benzene solution, chain transfer occurs which has the effect of decreasing the proportion of molecules having unsaturated ends.[9] Thus the rate of degradation and the proportion of the polymer degradable at 220°C. are reduced. For poly(methyl methacrylates) of similar structure, differing only in molecular weight, the rate of depolymerization is independent of molecular weight up to values of the order of 150,000. Thereafter the rate decreases with increasing molecular weight.

The behavior of poly(*n*-butyl methacrylate) is quite different, as shown in Figure 1. Thus materials prepared in benzene solution degrade at a

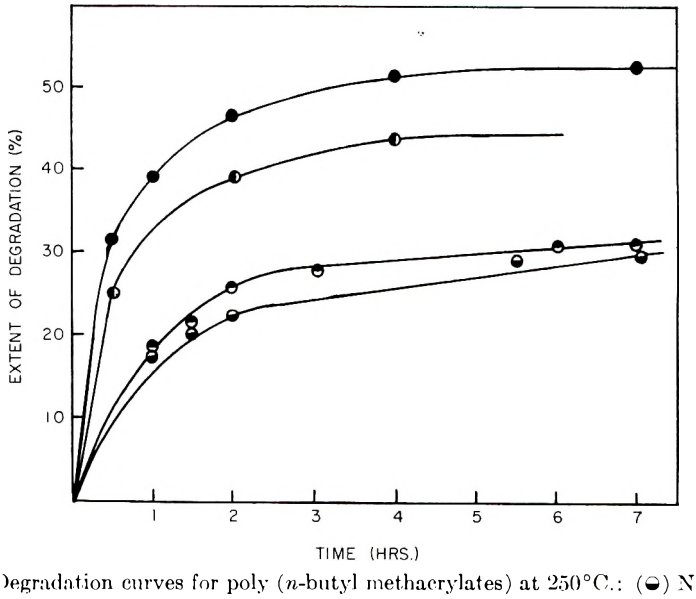

Fig. 1. Degradation curves for poly (*n*-butyl methacrylates) at 250°C.: (◒) NB1; (◓) NB2; (●) NB4; (◐) NB6.

TABLE II
Cracking Patterns of Butenes Compared with Unknown Butene (Ionizing Voltage = 50 e.v.)

Mass/charge ratio	1-Butene	*cis*-2-Butene	*trans*-2-Butene	Isobutene	Unknown butene
56	38.5	50.2	47.8	44.5	40.1
55	17.5	22.0	22.0	16.0	16.0
41	100	100	100	100	100
39	34.9	36.8	35.9	44.9	36.0
28	29.4	32.1	32.4	21.8	30.0
27	30.9	34.9	35.1	21.7	29.8

faster rate, these rates in general decreasing with increasing molecular weight. Similarly, the extent of degradation at 250°C. is limited, this limit being greater for lower molecular weight polymers. Even on raising the temperature to over 300°C., depolymerization still does not go to completion; instead the residue becomes progressively more stable. These polymers are different in basic structure to the poly(methyl methacrylates) mentioned above to the extent that in the preparation of the former azo bis isobutyronitrile was used as initiator while the latter were initiated by benzoyl peroxide. In view of the well established mechanism of depolymerization of poly(methyl methacrylate) these differences should not be expected to have the effects described above.

Examination of the volatile products of degradation by gas–liquid chromatography showed that besides monomer, small amounts of butene are produced. The various butenes are not readily distinguishable by this means, but mass spectrometric analysis gives a cracking pattern closely similar to that of 1-butene, as shown in Table II.

Butene-1 is of course the olefin which is to be expected in an ester decomposition reaction in poly(*n*-butyl methacrylate) analogous to that which occurs in poly(*tert*-butyl methacrylate). The strong carbonyl absorption at 1720 cm.$^{-1}$ in the infrared spectrum of the polymer makes detection of acid or anhydride carbonyl peaks difficult, however, except at advanced stages of reaction. After extensive degradation at 260°C., carbonyl region spectra were obtained as shown in Figure 2. Grant and Grassie[6] have shown that twin carbonyl peaks in this range are characteristic of six-membered ring anhydrides such as glutaric anhydride and of intermolecular anhydrides such as acetic anhydride but that these may be distinguished by the relative intensities of the two peaks. Thus for six-membered ring anhydrides the peak with the lower wave number has the higher intensity. The converse holds for intermolecular anhydrides. The wavelengths and relative intensities of the peaks illustrated in Figure 2 are in fact identical with those found for degraded poly(methacrylic acid) which is a glutaric type anhydride thus proving the presence of six-membered ring anhydride units of the type which would be formed as a result of ester decomposition of adjacent units and subsequent elimination of water.

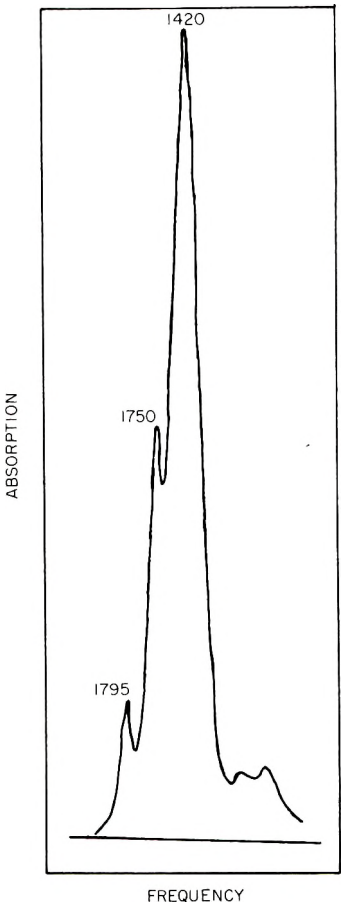

Fig. 2. Carbonyl region infrared spectrum of thermally degraded poly (*n*-butyl methacrylate).

The possibility of some intermolecular structures being formed, resulting in a small amount of crosslinking, is not, of course, precluded. Indeed, at these advanced stages of volatilization at which anhydride structures become identifiable, the polymer becomes progressively more insoluble in chloroform, the insoluble portion existing as a highly swollen gel.

This sequence of reactions in poly(*n*-butyl methacrylate) is at least superficially similar to that which occurs during the thermal degradation of poly(*tert*-butyl methacrylate). Grassie and Grant[2] showed that in this latter polymer a small amount of depolymerization to monomer occurs initially. The main process, however, is ester decomposition to polymethacrylic acid and isobutene. The acid units then react to form mostly cyclic anhydride units which are responsible for inhibiting the chain depolymerization reaction. The final product is an insoluble polyanhydride. Thus the only apparent difference between the *n*-butyl and *tert*-butyl esters is one of degree. Poly(*n*-butyl methacrylate) is comparable with

poly(methyl methacrylate), in that the predominant process is depolymerization, but the small amount of anhydride which is formed as the ultimate product of ester decomposition can effectively inhibit the reaction and ultimately stop it completely. This competition between depolymerization and ester decomposition is probably a general property of methacrylate esters with poly(methyl methacrylate) and poly(*tert*-butyl methacrylate) representing the two extremes of behavior. A brief examination of the thermal degradation of poly(ethyl methacrylate) indicated a close similarity to that of poly(*n*-butyl methacrylate).

This sort of behavior precludes a detailed comparison of the thermal depolymerizations of the various polymethacrylates, but since insolubility does not set in until fairly late in the reaction, molecular weights can be measured in the early stages. For polymer NB2, which was prepared in bulk, the molecular weight has been shown to decrease in proportion to the extent of degradation up to 26% conversion to monomer. This is a strong indication that the reaction, like that in poly(methyl methacrylate), is initiated at chain ends but that the chain length of the depolymerization process is considerably less than the polymer chain length. This is not sufficient evidence, however, to allow any discussion of the reasons why benzene-transferred polymers degrade faster and to a greater extent than bulk polymers as illustrated in Figure 1.

Thermal Degradation of Copolymers with Methacrylic Acid

In view of the close connection between stabilization and the formation of anhydride structures it is obviously of interest to study the degradation of copolymers of *n*-butyl methacrylate and methacrylic anhydride. This cannot be done directly since the bifunctional methacrylic anhydride molecule gives rise to crosslinked, insoluble copolymer. Anhydride units were usefully introduced into poly(*tert*-butyl methacrylate), however, by heating its copolymer with methacrylic acid above 170°C.[2] The effect of preheating at 170°C. on the stability of two such copolymers of *n*-butyl methacrylate with 1% and 10%, respectively, of methacrylic acid, is illustrated by the data in Table III. There is clearly a trend towards

TABLE III
Effect of Preheating on the Extent of Degradation of *n*-Butyl Methacrylate/Methacrylic Acid Copolymers

Polymer	Time preheating at 170°C., hr.	Degradation after 2 hr. at 250°C., %
Homopolymer	—	29.0
CNB 1	0	36.0
CNB 1	1	33.0
CNB 2	0	28.4
CNB 2	1/2	27.0
CNB 2	2	23.1
CNB 2	4	22.0

greater stability with increasing periods of preheating, but surprisingly, the unpreheated copolymers are comparable in stability with pure poly(*n*-butyl methacrylate), in spite of the fact that infrared spectral measurements confirm that anhydride formation is taking place at 170°C. and is in any case complete by the time the degradation temperature of 250°C. is reached.

Thus, the presence of anhydride structures in the polymer is not in itself sufficient for inhibition to occur. Indeed, although *n*-butyl methacrylate is the only liquid product of copolymer degradation identifiable by infrared methods, gas–liquid chromatographic analysis indicates small traces of a high boiling constituent with the same retention time as monomeric methacrylic anhydride. Since the methacrylic acid units in these ester rich copolymers must be widely separated from one another the anhydride formed must be predominantly intermolecular. The two vinyl groups in any anhydride monomer unit are thus polymerized into separate polymer chains. They should therefore be expected to behave individually like disubstituted ethylenic monomer units and thus be separately liberated during depolymerization as has been shown for glycol dimethacrylate units copolymerized into poly(methyl methacrylate) molecules.[10] Thus monomeric methacrylic anhydride would be liberated if both chains underwent depolymerization.

Where effective inhibition does occur, it is clear from the homopolymer experiments described above that intramolecular anhydrides are always present and the reasons for such inhibition have been discussed previously by Grassie and Grant.[2] Two ways in which these may be produced during the preheating period have also been discussed. Either exchange can occur between adjacent acid and ester groups thereby making it possible for acid units to migrate along the chains, or, as was shown to occur during poly(*tert*-butyl methacrylate) degradation, an acid unit in the chain can catalyze decomposition of an adjacent ester grouping. Since, however, there is no significant difference in the rate characteristics of thermal depolymerization at 250°C. between ester homopolymer and unpreheated ester/acid copolymer it is clear that the anhydride structures producing inhibition in homopolymer and unpreheated copolymers are produced in quite a different way. This is confirmed by the fact that once depolymerization stops in a homopolymer, there is no further significant production of anhydride or butene in spite of the fact that the large majority of the ester units in the residual polymer chains are intact. Thus depolymerization and ester decomposition in this polymer are closely linked and it seems probable on this evidence that ester decomposition must be explained in terms of a radical mechanism which is in direct competition with depolymerization.

Photochemical Degradation of Homopolymer

At 170°C., poly(*n*-butyl methacrylate) was found to be completely converted to monomer by ultraviolet irradiation. A search for other

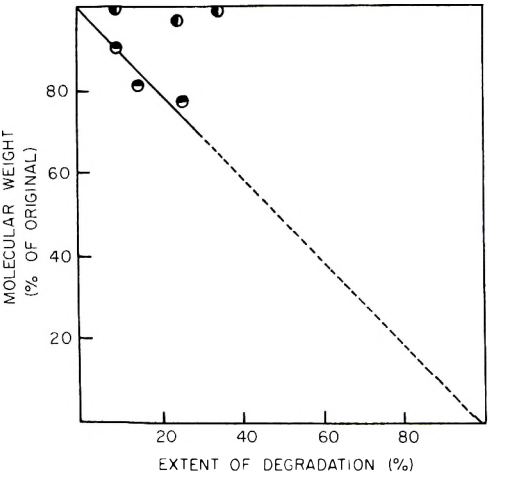

Fig. 3. Effect of degradation on the molecular weight of poly (*n*-butyl methacrylate): (◓) NB2; (◐) NB6.

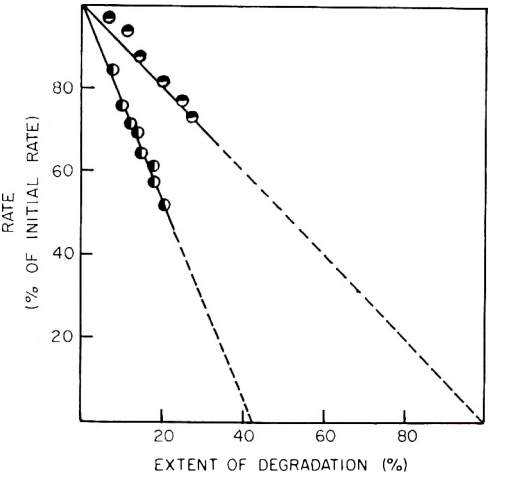

Fig. 4. Effect of degradation on the rate of degradation of poly (*n*-butyl methacrylate): (◓) NB2; (◐) NB6.

products, particularly butene and methacrylic acid, yielded negative results, although their identification is made particularly difficult by the relatively large concentrations of monomer. Figure 3 illustrates the changes in molecular weight which occur in two polymers of widely different molecular weight. These results indicate an end-initiated reaction[1] with a kinetic chain length lying somewhere between the molecular chain lengths of these two materials. During the investigation of both the photo and thermally initiated degradation of poly(methyl methacrylate),[1,7,9] a good deal of information was gained about the type of chain end through which initiation occurs by studying the rate changes during the course of the reaction and particularly by a comparison of polymers prepared from bulk monomer

and in benzene solution. The behaviors of two such poly(*n*-butyl methacrylates) are compared in Figure 4. Obviously in bulk polymer all the molecules are degradable, while in polymer prepared under conditions where transfer to benzene is possible, about 40% of the molecules are degradable. Since the chain ends terminated by phenyl groups (from benzene) and the saturated structures formed by transfer and in the disproportionation termination process are stable in poly(methyl methacrylate it is reasonable to suppose that they are also stable in poly(*n*-butyl methacrylate). The only other types of ends present are the initiator residues and unsaturated ends formed by disproportionation. The only chain end structure common to all molecules in a bulk polymer is that incorporating the initiator fragment and if these were centers of initiation of depolymerization, a curve extrapolating to 100% degradation as in the diagram is to be expected.

Grassie and Vance[9] have shown how, from measurements of molecular weight, the proportions of the various end structures in polymer prepared in benzene solution may be calculated. Using their method it can be shown that 16% of the molecules in polymer NB6 are terminated by initiator fragments and 16% have unsaturated ends formed by disproportionation. On the assumption that the former as well as the latter are sites for photoinitiation of depolymerization the experimental value of approximately 40% for the proportion of degradable molecules is in good agreement with theory.

All the *n*-butyl methacrylate polymers used in the present work were prepared using 2,2′-azoisobutyronitrile as initiator so that the end terminated by an initiator fragment will have the structure,

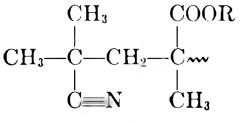

which may be photochemically labile. Unfortunately, no methyl methacrylate polymers initiated in this way were studied in the earlier work.[7] An example of the initiator system having a profound effect on degradation characteristics is found in the work of Bywater[11] in which he finds poly(methyl methacrylate) initiated and terminated by hydroxyl groups to be particularly unstable thermally. On the whole, however, the question of the effect of polymerization initiators on polymer stability is one which has received little attention to the present time.

Photochemical Degradation of Copolymers with Methacrylic Acid

The effect of preheating *n*-butyl methacrylate/methacrylic acid copolymers on the rate of their photochemically initiated depolymerization is illustrated in Figure 5. Thus the rate of depolymerization of unpreheated copolymer is comparable with that for homopolymer whose rate is not significantly affected by preheating. Preheating progressively depresses

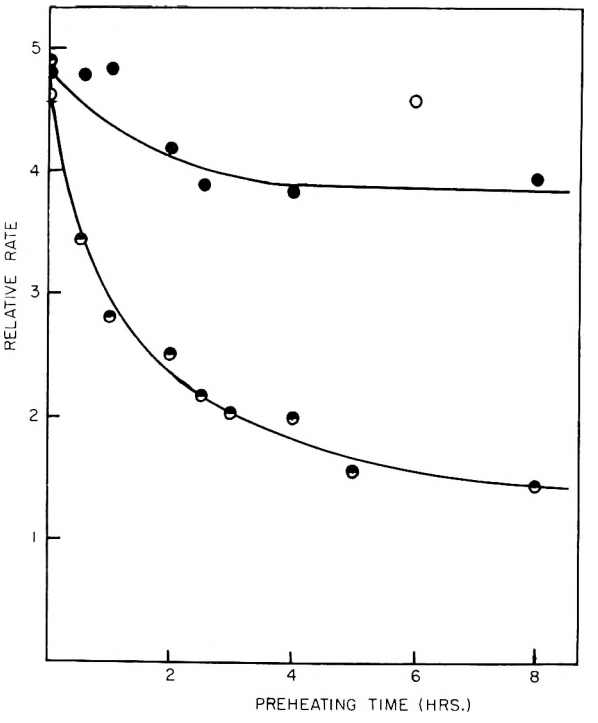

Fig. 5. Effect of preheating at 170°C. on the initial rate of photodepolymerization at 170°C. of *n*-butyl methacrylate homopolymer and copolymers with methacrylic acid: (○) NB2; (●) CNB1; (◓) CNB2.

the rate of depolymerization of the copolymers. The residue is always at least partially insoluble, indicating some intermolecular anhydride formation. The liquid products are acidic and their infrared spectrum shows broad absorption and small peaks in the 2500–3400 cm.$^{-1}$ region which is characteristic of acid hydroxyl groups and is presumably due to methacrylic acid. It was never possible to detect anhydrides in the liquid products by either infrared spectroscopy or gas–liquid chromatography although this does not preclude the presence of low concentrations in view of the strong ester carbonyl absorption in the infrared spectrum of these copolymers. By contrast with the thermal reaction at 250°C. it is clear that at the lower temperature of photochemical degradation there is no self inhibition of the depolymerization reaction by some intramolecular anhydride-producing radical process occurring in direct competition with depolymerization. Preheating, on the other hand, has precisely the same effect as in the thermal reaction and must be associated with the production of intramolecular anhydrides.

Photochemical Degradation of Poly(*tert*-butyl Methacrylate)

The ability to depolymerize quantitatively to monomer under the initiating influence of ultraviolet radiation is apparently a general property of

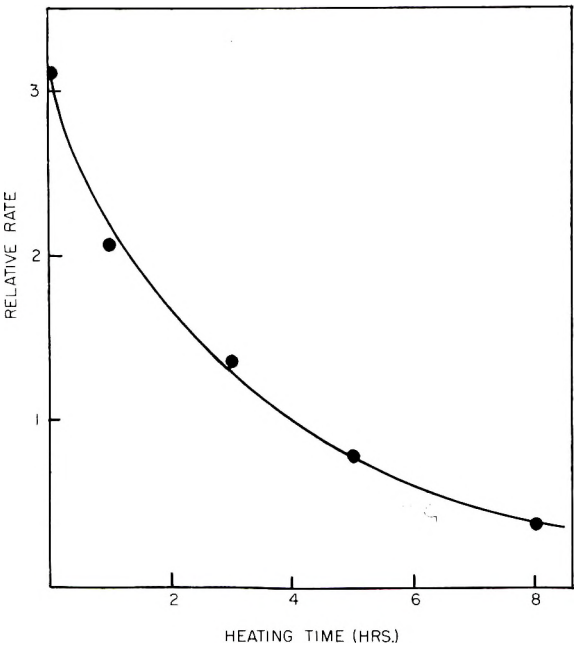

Fig. 6. Effect of preheating at 178°C. on the initial rate of photodepolymerization of poly(*tert*-butyl methacrylate) at 170°C.

poly(alkyl methacrylates). Even poly(*tert*-butyl methacrylate) which undergoes almost quantitative ester decomposition on heating to 200°C. gives yields of monomer close to 100% under 2537 A. irradiation at 170°C. This temperature is very close to the threshold of thermal degradation[2] in which isobutene and water are evolved consecutively leaving anhydride units in the residue. Thus it is possible by controlled preheating to introduce anhydride units, which are mainly intramolecular, into the polymer chain. Figure 6 shows the effect of preheating a sample of poly(*tert*-butyl methacrylate) at 178°C. on the initial rate of degradation. With increasing time of preheating, and thus increasing numbers of intramolecular anhydride links, the polymer becomes more stable to photodepolymerization.

Ester Decomposition during Polymerization of *n*-Butyl Methacrylate at 30°C.

During their study of the thermal polymerization of *n*-butyl methacrylate, Burnett, Evans, and Melville[12] observed that bubbles of gas were evolved and the polymer was insoluble in monomer, although soluble in polar solvents. The gas was not identified, but it was suggested that it might be butene or carbon dioxide. Their experiments were repeated using 100 ml. of monomer, sealed in vacuum, thermostated at 30°C., and carried to 10% conversion. Examination of the gas by gas–liquid chromatography proved it to be butene. The polymer which had precipitated

from the monomer was twice reprecipitated from acetone solution by methanol and dried by prolonged storage in vacuum. Broad hydroxyl peaks at approximately 3000 cm.$^{-1}$ in the infrared spectrum of this polymer, which are unaffected by further storage in vacuum, revealed that traces of acid were present. There is no possibility that the molecular ester decomposition reaction can occur at this temperature. In addition, the fact that solutions of poly(*n*-butyl methacrylate) are perfectly stable at 30°C. and the obvious close association of butene and acid production makes it clear that polymerizing radicals are involved. Since the same radicals are involved in polymerization as occur during depolymerization at higher temperatures these observations are clearly further support for the contention that anhydride formation during thermal degradation is the ultimate result of a similar radical reaction.

Mechanism of Ester Decomposition

The molecular mechanism for the decomposition of carboxylic acid esters into acid and olefine was first suggested by Hurd and Blunk[9,13] and elaborated by McColl[14] in terms of a six-membered cyclic transition state,

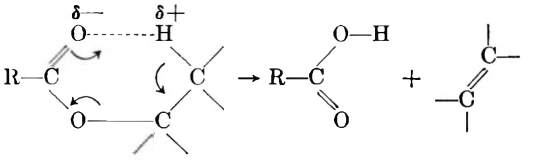

The bulk of the evidence available for low molecular weight esters supports this molecular theory and McColl suggests that the rate-determining step is the formation of the hydroxyl bond, not the breaking of the alkyl oxygen bond. In order that this sort of reaction may occur it is necessary that the ester should possess a hydrogen atom on the β carbon atom of the alcohol residue. The stability of esters to this sort of breakdown is in the order primary > secondary > tertiary,[15] and the temperatures at which the rates of reaction become appreciable have been quoted as 350, 310, and 250°C., respectively. In the polymeric carboxylic acid ester field, Grassie[16] has studied the decomposition of poly(vinyl acetate), a primary ester, at 213°C. and Grant and Grassie[2] the decomposition of poly(*tert*-butyl methacrylate), a tertiary ester, at 200°C. Both of these undergo ester decomposition by a nonradical process. This apparent enhanced instability of these two materials is due to favorable steric influences resulting from the occurrence of the reaction in a polymer chain environment. This is associated with catalytic effects, on adjacent units, of the residues from units which have already decomposed. In this way both reactions assume overall autocatalytic properties. Such behavior is not evident in the ester decomposition reaction in poly(*n*-butyl methacrylate), yet the reaction can clearly occur at 30°C at a measurable rate which is over 300°C. lower than the temperature quoted above for primary esters. Clearly a different mechanism is involved and the evidence

discussed in previous sections of this paper suggests a radical process. It is in fact possible to give a unified picture of ester decomposition in *n*-butyl methacrylate polymerization at 30°C. and during the degradation of its polymer within the framework of a single radical process.

It is proposed that the sequence of reactions which results in ester decomposition during polymerization at 30°C. is as follows:

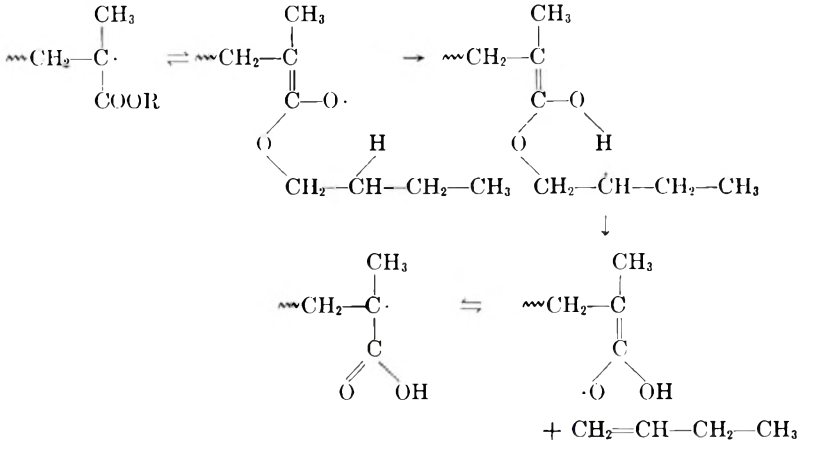

The growing polymer radical reacts in its alternative canonical form, abstracting, as in the molecular ester decomposition process and through a six-membered ring transition state, the β-hydrogen atom of the alcohol residue. Intramolecular disproportionation ensues liberating isobutene, and the resulting radical may add monomer to continue polymerization, a unit of methacrylic acid thus becoming incorporated into the polymer chain in accordance with the experimental evidence. Reaction of a growing polymer radical in an alternative resonance form has its precedents. Thus the ketone-imine structures in polymethacrylonitrile result from reaction of the growing polymer radical in the form,[17]

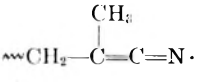

and it has been suggested, although not proved, that the weak links in polystyrene may be the result of reaction of the polystyryl radical in one of the forms,[18]

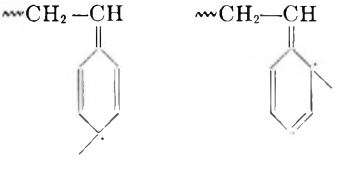

In the photochemically initiated depolymerization reaction at 170°C. in which the same kind of poly(*n*-butyl methacrylate) radicals are involved, precisely the same sequence of reactions may occur, but the methacrylic

acid unit is capable of being liberated in a depolymerization process as the appearance of methacrylic acid among the products of the photodegradation of unpreheated ester/acid copolymers has shown. In fact, neither butene nor methacrylic acid were detected among the products of photodegradation of pure homopolymer. Even at 30°C. the yields are low, however, and it may be that at the higher temperature the increased thermal motion of the ester side chain has the effect of inhibiting the hydrogen abstraction step in the reaction so that the relative yield of isobutene and methacrylic acid are very much lower at 170°C. than at 30°C. In any case, as already pointed out, their identification is made particularly difficult by the relatively large concentrations of monomer.

At the higher temperature of the thermal degradation the depolymerization reaction becomes self-inhibiting due to the formation of terminal anhydride structures. Since about 50% of the polymer is depolymerized to monomer before inhibition is complete and since only one terminal anhydride group per polymer molecule is sufficient to inhibit the reaction completely it is clear that the amount of anhydride formation is relatively very small. The first step in the self-inhibiting process will be the production of a terminal acid unit as at low temperatures. At these higher temperatures, however, it seems probable that further reaction can occur with an adjacent ester unit to product anhydride, butene, and water,

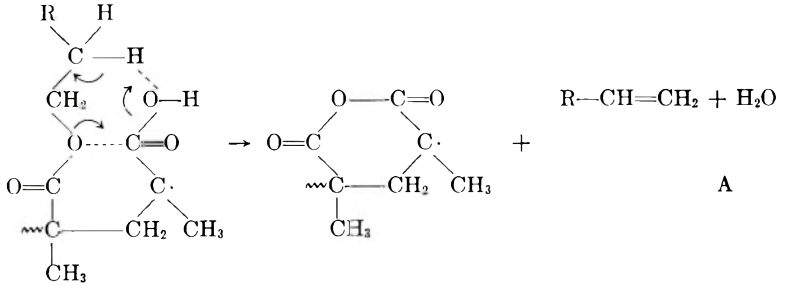

As previously discussed,[6] inhibition is most probably the result of an equilibrium which will be set up between this anhydride radical and the radical which is the product of the liberation of one further ethylenic unit from the chain end.

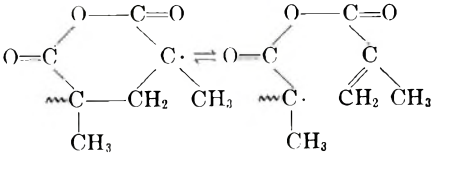

It remains to offer a plausible mechanistic explanation for the inhibiting effect of preheating at 170°C. on both the photoinitiated reaction at 170°C. and the thermal reaction at 250°C. It may be thought somewhat surprising that preheating at 170°C. has such a profound effect on the thermal reaction at 250°C. since any reaction proceeding at 170°C. should go very

much faster during the period of heating at 250°C. Yet the rates of degradation of homopolymer and unpreheated copolymer are comparable. Since intermolecular anhydride formation is rapid at temperatures appreciably above 170°C. it is reasonable to deduce that the inhibiting effect of preheating is associated with acid units and can no longer occur when these are converted to anhydride. It was for reasons of this kind that it was deduced that at preheating temperatures acid units are capable of migration along the copolymer chains.[2] Thus adjacent pairs of acid units would soon appear even in copolymer of low acid content, and being adjacent could eliminate water to form a cyclic anhydride. This is known to occur rapidly in poly(methacrylic acid) at 170°C.[6]

A reasonable mechanism for acid migration can be formulated, which, like reaction A, is favored stereochemically and the first step of which is probably proton migration.

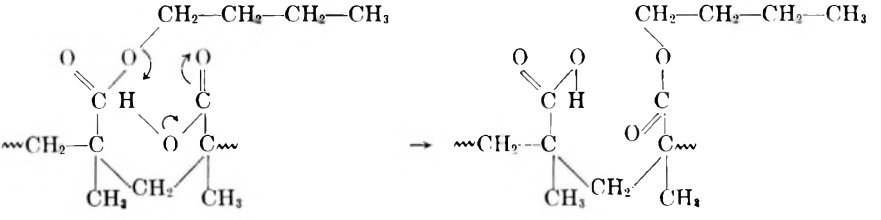

Mechanisms involving the concerted movement of electrons in this way are typical of thermal reactions.

One of the authors (J. R. M.) thanks the Department of Scientific and Industrial Research for a Research Award during the tenure of which this work was carried out.

References

1. Grassie, N., *Chemistry of High Polymer Degradation Processes*, Butterworth, London, 1956.
2. Grant, D. H., and N. Grassie, *Polymer*, **1**, 445 (1960).
3. Davison, W. H. T., and G. R. Bates, *J. Chem. Soc.*, **1953**, 2607.
4. Alfrey, T., and C. C. Price, *J. Polymer Sci.*, **2**, 101 (1959).
5. Cameron, G. G., D. H. Grant, N. Grassie, J. E. Lamb, and I. C. McNeill, *J. Polymer Sci.*, **36**, 173 (1959).
6. Grant, D. H., and N. Grassie, *Polymer*, **1**, 125 (1960).
7. Cowley, P. R. E. J., and H. W. Melville, *Proc. Roy. Soc. (London)*, **A210**, 461 (1952); *ibid.*, **211**, 320 (1952).
8. Masson, C. R., and H. W. Melville, *J. Polymer Sci.*, **4**, 337 (1949).
9. Grassie, N., and E. Vance, *Trans. Faraday Soc.*, **49**, 184 (1953).
10. Grassie, N., and H. W. Melville, *Proc. Roy. Soc. (London)*, **A199**, 22 (1949).
11. Bywater, S., *J. Phys. Chem.*, **57**, 879 (1953).
12. Burnett, G. M., P. Evans, and H. W. Melville, *Trans. Faraday Soc.*, **49**, 1096 (1953).
13. Hurd, C. D., and F. M. Blunk, *J. Am. Chem. Soc.*, **60**, 2419 (1938).
14. Maccoll, A., *J. Chem. Soc.*, **1958**, 3398.
15. Rudy, C. E., and P. Fugassi, *J. Phys. Chem.*, **52**, 357 (1948).
16. Grassie, N., *Trans. Faraday Soc.*, **48**, 379 (1952); *ibid.*, **49**, 835 (1953).
17. Grassie, N., and I. C. McNeill, *J. Polymer Sci.*, **27**, 207 (1958).
18. Cameron, G. G., and N. Grassie, *Makromol. Chem.*, **53**, 72 (1962)

Résumé

De même que dans le cas du polyméthacrylate de méthyle, la dégradation thermique à 250° du polyméthacrylate de *n*-butyle fournit du monomère comme produit volatil principal. Le polyméthacrylate de méthyle donne un rendement quantitatif en monomère. Par contre, le polyméthacrylate de *n*-butyle dégrade en monomère jusqu'à environ 40% de conversion. En chauffant plus longtemps le résidu, celui-ci devient progressivement plus stable. L'explication de ce comportement peut être donné par le fait que l'on trouve des traces de 1-butène dans les produits volatils et des structures anhydrides dans le résidu. Ainsi, dans la dégradation thermique de ce polymère, la dépolymérisation et la décomposition de l'ester en acide, se produisent simultanément. La compétition entre ces deux processus est une propriété générale des méthacrylates; dans cette série, le polyméthacrylate de méthyle et le polyméthacrylate de *tert.*-butyle ont un comportement limite. L'interférence due à la décomposition de l'ester empêche une comparaison quantitative de la dépolymérisation thermique dans la série des polyméthacrylates d'alcoyle. Néanmoins, on a pu démontrer que, aussi bien dans le polyméthacrylate de méthyle, que dans le polyméthacrylate de *n*-butyle, le processus de la dépolymérisation est initié thermiquement aux extrémités de la chaîne. Quand on chauffe jusqu'à 250°C des copolymères du méthacrylate de *n*-butyle et de l'acide méthacrylique, la conversion de l'acide en anhydride s'effectue rapidement et de façon quantitative. D'autre part le préchauffage du copolymère jusqu'à 170°C a un effet inhibiteur sur la dégradation à 250°C. Apparemment, des anhydrides intermoléculaires résultent du chauffage rapide jusqu'à 250°C; ceux-ci peuvent être mis en liberté par la réaction de dépolymérisation. Le préchauffage à 170°C permet la migration des unités acides le long de la chaîne polymérique, de façon a ce que des structures anhydrides intramoléculaires soient formées par élimination d'eau entre deux unités voisines. Ceux-ci sont les vrais inhibiteurs de la dépolymérisation. Contrairement à la réaction thermique, la dépolymérisation en monomère à 170°C, initiée photochimiquement, est quantitative. Ceci également semble une propriété générale des polyméthacrylates d'alcoyle, même du polyméthacrylate de *tert.*-butyle, qui, thermiquement, subit une décomposition presque totale de l'ester. Il n'y a pas d'auto-inhibition comme il y en a dans la réaction thermique. De même que dans la réaction thermique, la présence d'unités d'acide méthacrylique dans le polymere n'a pas d'effet, mais la préchauffage diminue la vitesse de dépolymérisation. Certains faits dans ces réactions nous permettent de conclure que la décomposition de l'ester dans le poly-méthacrylate de *n*-butyle est un processus radicalaire, en compétition directe avec la dépolymérisation, contrairement au polyméthacrylate de *tert.*-butyle. Ceci est confirmé par le fait que durant la polymérisation du méthacrylate de *n*-butyle à 30°C, il y a production d'isobutène et apparition d'unités acides dans le polymère. On présente un schéma général de la décomposition de l'ester durant la polymérisation et la dépolymérisation, suivant un tel mécanisme radicalaire. On suggère aussi des mécanismes pour expliquer l'auto-inhibition dans la réaction thermique et l'effect inhibiteur du préchauffage de copolymeres acide/ester, sur leur décomposition thermique et photochimique.

Zusammenfassung

So wie Polymethylmethacrylat liefert auch Poly-*n*-butylmethacrylat beim thermischen Abbau bei 250°C als flüchtiges Produkt hauptsächlich Monomeres. Abweichend vom Polymethylmethacrylat, das eine quantitative Ausbeute an Monomerem liefert, wird aber Poly-*n*-butylmethacrylat nur zu etwa 40% zum Monomeren abgebaut. Bei längerem Erhitzen wird der Rückstand zunehmend stabiler. Dieses Verhalten lässt sich auf Grund der Tatsache verstehen, dass unter den flüchtigen Produkten Spuren von 1-Buten und im Rückstand Anhydridstrukturen auftreten. Während des thermischen Abbaus dieses Polymeren tritt also gleichzeitig Depolymerisation und Esterzersetzung auf. Die Konkurrenz zwischen diesen beiden Prozessen ist eine allgemeine

Eigenschaft der Methacrylate, wobei Polymethylmethacrylat und Poly-*tert*-butylmethacrylat die beiden Grenzfälle repräsentieren. Die Störung durch die Esterzersetzung macht einen quantitativen Vergleich der thermischen Depolymerisation in der Reihe der Polyalkylmethacrylate unmöglich; es konnte aber gezeigt werden, dass der Depolymerisationsprozess beim Poly-*n*-butylmethacrylat, ebenso wei beim Polymethylmethacrylat, thermisch an den Kettenenden gestartet wird. Beim Erhitzen von Copolymeren von *n*-Butylmethacrylat und Methacrylsäure auf 250°C tritt rasche und vollständige Umwandlung der Säure ins Anhydrid ein. Das Polymere wird aber im gleichen Ausmass abgebaut wie das Esterhomopolymere. Andrerseits hat das Vorerhitzen des Copolymeren auf 170°C einen inhibierenden Einfluss auf den darauffolgenden Abbau bei 250°C. Rasches Erhitzen auf 250°C führt offenbar zur intermolekularen Bildung von Anhydriden, die in einer Depolymerisationsreaktion in Freiheit gesetzt werden können. Vorerhitzen auf 170°C ermöglicht eine Wanderung der Säurebausteine entlang der Polymerkette, so dass sich durch Eliminierung von Wasser zwischen benachbarten Säurebausteinen intramolekulare Anhydridstrukturen bilden können. Diese bilden die eigentlichen Depolymerisationsinhibitoren. Im Gegensatz zur thermischen Reaktion verläuft die photochemisch gestartete Depolymerisation zum Monomeren bei 170°C quantitativ. Auch das scheint eine allgemeine Eigenschaft von Polyalkylmethacrylaten zu sein und trifft sogar für Poly-*tert*-butylmethacrylat zu, das thermisch eine fast quantitative Esterzersetzung zeigt. Die bei der thermischen Reaktion auftretende Selbstinhibierung fehlt hier. Ebenso wie beim thermischen Abbau hat jedoch die Anwesenheit von Methacrylsäurebausteinen im Polymeren keinen Einfluss, das Vorerhitzen setzt aber die Depolymerisationsgeschwindigkeit herab. Gewisse Merkmale dieser Reaktionen führen zu dem Schluss, dass die Esterzersetzung bei Poly-*n*-butyl-methacrylat, ungleich der bei Poly-*tert*-butylmethacryl ataufretenden, eine Radikalreaktion ist, die als direkte Konkurrenzreaktion zur Depolymerisation auftritt. Eine Stütze dafür bildet die Beobachtung, dass während der Polymerisation von *n*-Butylmethacrylat bei 30°C Isobuten gebildet wird und im Polymeren Säurebausteine auftreten. Ein einheitliches Bild der Esterzersetzung währed der Polymerisation und Depolymerisation wird anhand eines solchen Radikalmechanismus enteworfen. Auch zur Erklärung der Selbstinhibierung bei der thermischen Reaktion und des inhibierenden Einflusses der Vorerhitzung von Säure-Estercopolymeren auf die thermische und photochemische Depolymerization werden Mechanismen angegeban

Received January 15, 1963

JOURNAL OF POLYMER SCIENCE: PART A VOL. 2, PP. 1001–1015 (1964)

An Interpretation of Gaseous Diffusion Through Polymers Using Fluctuation Theory

A. T. DiBENEDETTO and D. R. PAUL, *Department of Chemical Engineering, University of Wisconsin, Madison, Wisconsin*

Synopsis

An amorphous polymer is visualized as an ensemble of N independent, n-center polymer segments. An ergodic hypothesis and a canonical ensemble are utilized in determining the probability of a given volume fluctuation within the polymer. The thermal energy change associated with a given volume fluctuation is calculated and related to the activation energy for gaseous diffusion. Polymer segment lengths were in the range of 6–20 A. and appeared to decrease with increasing temperature in the case of natural rubber. The results were interpreted to show that the activation energy for gaseous diffusion in rubbery polymers went into the breaking of cohesive bonds between parallel polymer segments while in glassy polymers it went into both the breaking of cohesive bonds and the compressing of the surrounding segments. It is felt that it may be possible to relate gaseous diffusion, self-diffusion, and viscous flow to the thermodynamic and molecular properties of an amorphous polymer.

Introduction

A cell model was previously used to describe the structure-insensitive properties of amorphous high polymers.[1,2] The amorphous polymer was characterized as a homogeneous, one-component phase containing N identical n-center polymer segments, each of which was acted upon by a "cylindrically" symmetric square well potential. A center is some simple structural unit along the polymer chain (e.g., —CH_2— in polyethylene). Molecular constants, p–V–T behavior, glass transition temperatures, and cohesion energy densities were predicted from a minimum of experimental data.[1] The model was then extended in order to characterize the diffusion of slightly soluble gases through the polymers.[2] A sorbed gas molecule was visualized as a three-dimensional harmonic oscillator trapped at an equilibrium site by surrounding bundles of parallel polymer segments. A diffusion jump occurred when four parallel polymer segments separated sufficiently to create a cylindrical void into which the gas molecule could move. As a first approximation it was assumed that a void volume of $(\pi/4)d_g^2 l$ accompanied a diffusional jump of l units of length by a gas molecule of diameter d_g. The possibility of equivalent (or larger) void volumes of different dimensions participating in the diffusional process was not considered.

It is recognized that the measured value of any thermodynamic property for a material is really the mean (or most probable) of a wide range of values that exist in the system of particles. One may visualize any given segment in an amorphous polymer as having a random, but restrained, motion centered about an imaginary lattice point, with the volume per segment fluctuating about a stationary average value. It is possible to statistically relate the size of a given fluctuation to the energy required to cause it. This kind of an approach, irrespective of any model, has been used to explain the temperature dependence of viscosity of polymers[3] and more recently has been extended to characterize gaseous diffusion through polymers.[4]

In this paper a statistical theory of fluctuation is used to obtain the activation energy for gaseous diffusion through polymers as a function of gas diameter and the thermodynamic properties of the solid. A comparison with previous work on the lattice model[2] shows an excellent consistency between the two approaches.

Theory

Consider an amorphous polymer as an ensemble of N independent n-center polymer segments. A center corresponds to a single structural unit along the polymer chain (e.g., —CH_2— in polyethylene). The structure is divided into N unit cells (systems), each of which has an average cell volume of $nv_0 = 2\lambda\rho^2 n$. It is possible to construct an ensemble of N such systems whose condition at any time can be specified by a density of distribution, f_N, which is a function of all the coordinates in phase space and time.[5]

$$f_N = f(q_1 \ldots q_N, p_1 \ldots p_N, t) \tag{1}$$

The mean value for any observable property of the whole ensemble at a specific time is then:

$$<F(q_1 \ldots q_N, p_1 \ldots p_N, t)> = \frac{\int \ldots \int F \cdot f_N dq_1 \ldots dq_N, dp_1 \ldots dp_N}{\int \ldots \int f_N dq_1 \ldots, dp_1 \ldots dp_N} \tag{2}$$

For an equilibrium ensemble, one may write a canonical distribution function for the ensemble in terms of the total energy of one of the systems in the ensemble.

$$f_N(e) = C \exp \{-e/kT\} \tag{3}$$

It also follows from this form of f_N, that the probability of measuring a certain value for a property of the system is correctly given by the probability of occurrence of that value of the property in the ensemble. Thus eq. (2) will also give the average value, $<F>$, for the system. Equation (3) is satisfactory when there is a large number of particles in each system.

It is assumed that a sorbed gas molecule will diffuse along the axis of four parallel polymer segments when a volume fluctuation of $\delta(nv)$, $\delta(nv) =$

$(\pi/4)d_g^2\ 2\lambda n$, or greater, occurs in a unit cell. The amount of excess energy, δe, that must be localized in order to cause such a fluctuation is then interpreted as an activation energy for the fluctuation. The measured activation energy for the diffusion of a gas molecule of diameter d_g, ΔE_D, is an average of the activation energies for all volume fluctuations large enough to allow a diffusional jump.

The problem that arises in utilizing a canonical distribution function for an ensemble of N independent n-center polymer segments, is that the "system" is a single, n-center segment (the unit cell). The canonical distribution function [eq. (3)] is derived for a system of many particles. On the other hand, during the time it takes to measure the activation energy for gaseous diffusion, each unit cell of the polymer will exhibit an infinite number of fluctuations. It is therefore assumed that for a polymer consisting of an equilibrium ensemble of N identical, n-center polymer segments, the fluctuation of states of one polymer segment over an infinite period of time (relative to the frequency of the fluctuations) is the same as the fluctuation of states for the entire ensemble at a specific time and, furthermore, these fluctuations can be described by the canonical distribution function for the ensemble.

Then, the probability of finding a polymer segment in a given state 1, regardless of the states of the other systems and neglecting the presence of the gas molecules, is:

$$W_1 = f_1(e_1) = C \exp\left\{-e_1/kT\right\} \tag{4}$$

The total probability of all states with a specific value of a particular variable, say v, is:

$$W(v) = \sum_{i=i(v)} C \exp\left\{-e_i/kT\right\} \tag{5}$$

The summation is for all states which are compatible with the assigned value of v. Equation (5) may be rewritten to give:

$$\begin{aligned} W(v) &= C \exp\left\{\frac{1}{kT}\left[kT \ln \sum_i \exp\left(\frac{e_i}{kT}\right)\right]\right\} \\ &= C \exp\left\{-na(v)/kT\right\} \end{aligned} \tag{6}$$

The quantity $na(v)$ is the Helmholtz energy for an n-center polymer segment when it has a volume v. The probability of getting a volume fluctuation, $\delta(nv) = nv - nv_0$, is then:

$$\begin{aligned} W(\delta nv) &= \frac{W(nv)}{W(nv_0)} = \exp\left\{-(na - na_0)/kT\right\} \\ &= \exp\left\{-\frac{\delta na}{kT}\right\} \end{aligned} \tag{7}$$

If (nu_0) is the thermal energy of a polymer segment at its "equilibrium" volume of nv_0 and (nu) is the thermal energy of the segment when it has a

volume nv, the amount of energy that must be localized in order to produce the fluctuation $\delta(nv)$ is:

$$\delta nu = n(u - u_0) = \text{excess thermal energy required to produce } \delta nv \quad (8)$$

The average excess thermal energy associated with all fluctuations larger than $\delta(nv)$ is then:

$$<\delta nu> = \frac{\int_{\delta v}^{\infty} \delta(nu) \exp\{-\delta na/kT\} d(\delta v)}{\int_{\delta v}^{\infty} \exp\{-\delta a/kT\} d(\delta v)} \quad (9)$$

From our "ergodic" hypothesis, this average excess thermal energy associated with all fluctuations in time larger than $\delta(nv)$, is equal to the average excess thermal energy associated with the same fluctuations for the entire ensemble at a specific time. For the ensemble of N n-center segments:

$$N <\delta nu> = <\delta nU> \quad (10a)$$

$$N\delta nv = \delta nV \quad (10b)$$

$$N\delta na = \delta nA \quad (10c)$$

Then, the average excess internal energy is:

$$<\delta nU> = \frac{\int_{\delta nV}^{\infty} (nU) \exp\{-\delta nA/RT\} d(\delta nV)}{\int_{\delta nV}^{\infty} \exp\{-\delta nA/RT\} d(\delta nV)} \quad (11)$$

It is assumed that the activation energy for the diffusion of a gas of "collision diameter" d_g, ΔE_D, is equal to the average excess energy associated with all volume fluctuations greater than $\delta nv = (\pi/4)d_g{}^2 2\lambda n$.

$$\Delta E_D = <\delta nU> \quad (12)$$

In the region where δnU does not vary too rapidly with volume and the main dependence on the probability of the variable is given by the exponential factor, it is plausible to expand both the internal energy and the Helmholtz energy in Taylor series:

$$U - U_0 = \delta U = \left(\frac{\partial U}{\partial V}\right)_{\substack{T \\ V=V}} \delta V + \left(\frac{\partial^2 U}{(\partial V)^2}\right)_{\substack{T \\ V=V_0}} \frac{(\delta V)^2}{2} + \left(\frac{\partial^3 U}{\partial V^3}\right)_{\substack{T \\ V=V_0}} \frac{(\delta V)^3}{6} + \ldots \quad (13)$$

It can be shown thermodynamically[7] that the first partial derivative of eq. (13) is:

$$(\partial U/\partial V)_T = (\beta T/\kappa) - p_{\text{ext}} \quad (14)$$

It is reasonable to assume that $(\beta T/\kappa)$ is constant for all polymers at constant temperature, (i.e., $\beta T/\kappa$ is independent of pressure), so that eq. (13) may be written as:

$$\delta U = [(\beta T/\kappa) - p_{ext}]\delta V + (V_0/\kappa)\sum_{j=0}^{\infty}(-1)^j[j!/(j+2)!](\delta V/V_0)^{j+2} \tag{15}$$

Similarly, assuming that the compressibility, κ, is independent of pressure, one obtains:

$$\delta A = -p_{ext}\delta V + (V_0/\kappa)\sum_{j=0}^{\infty}(-1)^j[j!/(j+2)!](\delta V/V_0)^{j+2} \tag{16}$$

Substituting eqs. (12–16) into eq. (11), one may obtain an expression for the activation energy as a function of the thermodynamic properties of the polymer and the collision diameter of the diffusing gas.

$$\Delta E_D^* = \frac{V^*\int_{d_g^{*2}}^{\infty}\left[\left(\beta^* - \frac{p^*}{V^*}\right)\nu^* + \sum_{j=0}^{\infty}(-1)^j\frac{j!}{(j+2)!}\nu^{*j+2}\right] \times \exp\left\{-V^*\sum_{j=0}^{\infty}(-1)^j\frac{j!}{(j+2)!}\nu^{*j+2}\right\}\exp\{p^*\nu^*\}d\nu^*}{\int_{d_g^{*2}}^{\infty}\exp\left\{-V^*\sum(-1)^j\frac{j!}{(j+2)!}\nu^{*j+2}\right\}\exp\{p^*\nu^*\}d\nu^*} \tag{17}$$

The following dimensionless variables have been introduced:

$$\Delta E_D^* = \Delta E_D/RT \tag{18a}$$

$$\beta^* = \beta T \tag{18b}$$

$$d_g^{*2} = (2\lambda)(\pi/4)d_g^2(N/V_0) \tag{18c}$$

$$V^* = nV_0/\kappa RT \tag{18d}$$

$$p^* = (p_{ext})nV_0/RT \tag{18e}$$

$$\nu^* = \delta V/V_0 = \delta v/v_0 \tag{18f}$$

The potential energy of an n-center polymer segment is estimated as:[1]

$$\varphi_{TC} = (4n\epsilon^*p^*/2\lambda)[0.77(v^*/v)^{11/2} - 2.32\,(v^*/v)^{5/2}] \tag{19}$$

Equation (19) is plotted in Figure 1. Most of the polymers we are dealing with are in the range of (v/v^*) between 1.0 and 1.1. Previous work, based on this potential energy function,[2] indicates that a diffusional jump in amorphous polymers (e.g., polyvinyl acetate) is on the order of $2\lambda n \doteq 10$–15 A. This figure is in reasonable agreement with the work of others.[4,6] The cell volumes, nv_0, are thus in the range of 300–700 A.^{3}. For small gas molecules such as helium (d_g = 2.58 A.) and argon (d_g = 3.47 A.), volume fluctuations large enough to result in a diffusional jump start at values of $\delta nv/nv_0$ equal to 0.1 to 0.3 or at values of v/v^* in the range

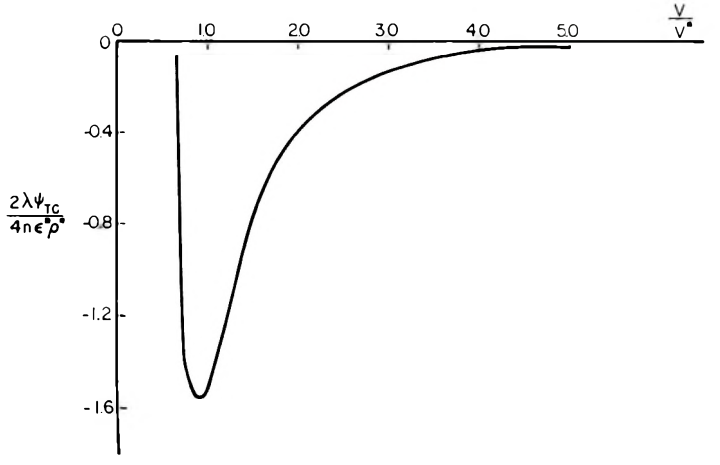

Fig. 1. Total potential energy of a polymer segment.

of 1.1 to 1.4. If the probability function, W, has a reasonably sharp peak, the contributions to the integrals of eq. (17) by volume fluctuations beyond $v/v^* = 2.0$ (or ν^* beyond 1.0) should be negligible. For a typical polymer $nV_0/N = nv_0 \approx 500$ A.^{3}, $\kappa \simeq 5 \times 10^{-11}$ cm.^{2}/dyne, and thus $V^* \approx 250$. At one atmosphere of external pressure $p^* \approx 0.01$ and thus $\exp\{p^*\nu^*\} \approx 1.0$. The probability function is then:

$$W \doteq \exp -250\left(\frac{1}{2}\nu^{*2} - \frac{1}{6}\nu^{*3} + \frac{1}{12}\nu^{*4} - \ldots\right) \tag{20}$$

In going from $\nu^* = 0.3$ to $\nu^* = 0.6$ the probability, W, has decreased by a factor of about 2×10^{10}. Hence we may neglect values of ν^* greater than 1.0, and therefore eq. (17) may be solved in closed form. Differentiating eq. (16), one obtains:

$$\begin{aligned} d\left(\frac{\delta nA}{RT}\right) &= V^*\left\{\sum_{i=0}^{\infty}(-1)^i\frac{\nu^{*i+1}}{i+1}\right\}d\nu^* - p^*d\nu^* \\ &= [-p^* + V^*\ln(1+\nu^*)]d\nu^* \qquad \nu^* \leqslant 1.0) \end{aligned} \tag{21}$$

Solving with the boundary condition $\delta nA = 0$ at $\nu^* = 0$ one obtains:

$$\frac{\delta nA}{RT} = V^*(1+\nu^*)\ln(1+\nu^*) - (V^* + p^*)\nu^* \tag{22}$$

Equation (17) may then be rewritten as:

$$\Delta E_D = \frac{\left[V^*\int_{d_0^{*2}}^{1.0}\left\{\left(\beta^* - \frac{p^*}{V^*}\right)\nu^* + (1+\nu^*)\ln(1+\nu^*) - \nu^*\right\} \times (1+\nu^*)^{-V^*(1+\nu^*)}\exp\{V^* + p^*\}\nu^*d\nu^*\right]}{\int_{d_0^{*2}}^{1.0}(1+\nu^*)^{-V^*(1+\nu^*)}\exp\{V^* + p^*\}\nu^*d\nu^*} \tag{23}$$

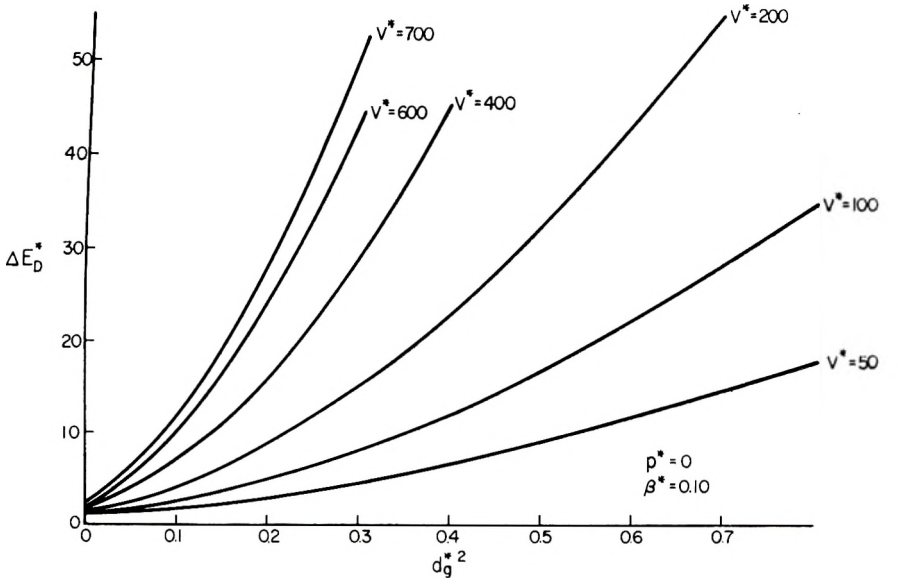

Fig. 2. Activation energy for gaseous diffusion in amorphous polymers.

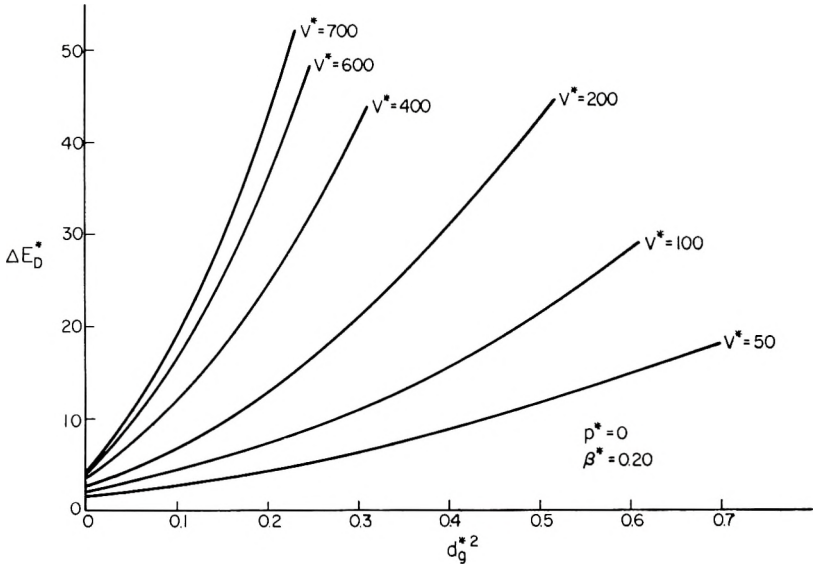

Fig. 3. Activation energy for gaseous diffusion in amorphous polymers.

The assumptions inherent in equation (23) are: (*a*) the fluctuation of states over an infinite period of time for a single polymer segment is the same as the fluctuation of states for a system of N identical polymer segments at a specific time and, furthermore, these fluctuations can be described by the canonical distribution function for an ensemble of systems; (*b*) the isothermal compressibility, κ, and the thermal expansion coefficient,

β, are independent of pressure (i.e., $(\partial\kappa/\partial v)_T = (\partial\beta/\partial v)_T \cong 0$); (c) the presence of the gas molecules in the polymer may be ignored; (*d*) the measured activation energy is equal to the "average" energy that must be localized on an n-center polymer segment to cause a volume fluctuation greater than a certain size.

Figures 2 and 3 are plots of the reduced activation energy, ΔE_D^*, as a function of the square of the reduced gas diameter, d_g^{*2}, for a few typical values of the reduced parameters V^* and β^*. The parameter involving the external pressure, p^*, may be taken as zero for all systems at atmospheric pressure.

Results

Gaseous diffusion data from several sources[4,6,8,9] are listed in Table I. The thermodynamic data required for the analysis are averages from a variety of literature sources and are listed in Table II. The collision diameters for a number of simple gases based on viscosity data (for dilute gases) and a Lennard-Jones 6–12 potential are listed in Table III.[11,12]

Experimental reduced activation energies for gaseous diffusion are plotted as a function of reduced gas diameter. Typical results for a "rubbery" solid and a "glassy" solid are illustrated in Figures 4 and 5, respectively. The theoretical curves refer to those obtained from eq. (23) for the fluctuation analysis and from eq. (19) for the molecular model analysis.[2] The model approach equated the activation energy for diffusion of a gas molecule of diameter d_g with the change in average potential energy of molecular interaction accompanying a volume change of $2\lambda n(\pi/4)d_g^2$. Predicted average values for the length of a polymer segment are listed in Table IV.

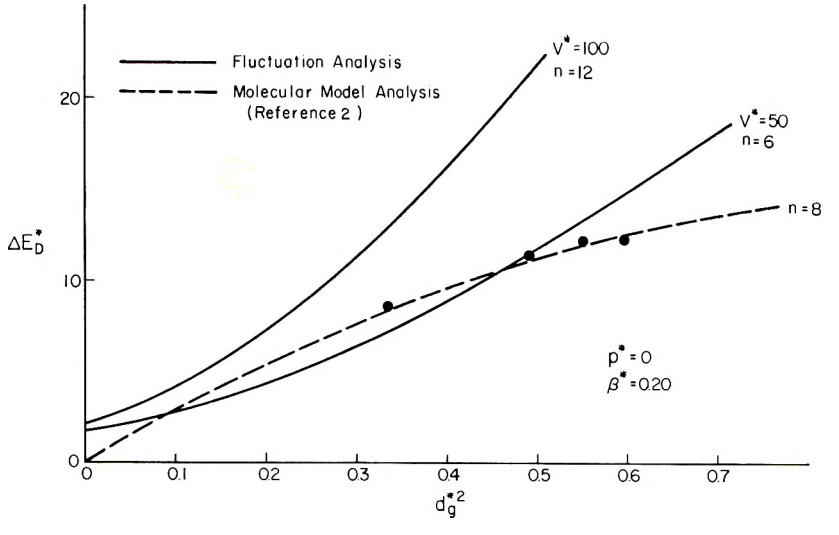

Fig. 4. Activation energies for gaseous diffusion in polybutadiene (rubbery).

TABLE I
Activation Energies for Gaseous Diffusion Through Polymer Films

Polymer	Temp., °K.	ΔE_D, kcal./mole									Reference
		He	H_2	O_2	N_2	CO_2	Ne	A	CO	H_2O	
Polybutadiene	298–323		5.1	6.8	7.2	7.3					8,9
Natural rubber	273		7.1								8,9
	285	5.1	6.7		10.7						
	298	4.7	6.3	8.9	9.4	9.6					
	308	4.4	6.0		8.8						
	323	4.0	5.8		7.9						
	343	3.3			6.6						
Neoprene	298–323		7.5	9.4	10.3	10.8					9
Polyisobutene	298–323		7.6	10.8	11.6	11.7					9
Polyvinyl acetate	<290	4.16	5.17	11.09			7.36	11.38			6
	290–299	0.0	5.72	6.50			3.16	7.96			
	>299	5.35	7.50	14.49			8.46	16.50			
VYHH copolymer (87% PVC/13% PVA)	280–360	7.58	6.84	10.63		20.56 (Above 302)	10.19		17.05		4
Polyvinyl chloride	298									10.0	9

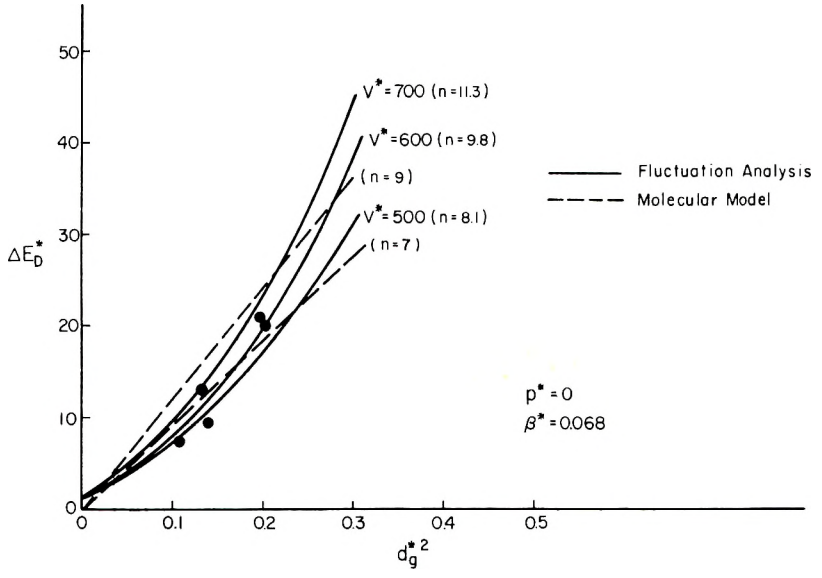

Fig. 5. Activation energies for gaseous diffusion in polyvinyl acetate (glassy).

Within the certainty of the experimental data and for the gases that were studied, the two approaches give approximately the same values for the lengths of polymer segments involved in gaseous diffusion. It should be noted that the segmental lengths of all the elastomers and amorphous polymers listed, for every gas studied, are of about the same size. Although it is

TABLE II
Thermodynamic Data for Some Linear Polymers

Polymer	$\beta \times 10^4\ \kappa^{-1}$ at 25°C.[a]	$\kappa \times 10^{11}$, cm.²/dyne[b]	v, cc./g.[a]	V_0, cc./ mole centers[c]	2λ[d]
Polybutadiene	6.7	7.25	1.12	15.1	1.25
Natural rubber	5.7	6.2	1.07	17.6	1.18
Neoprene	5.2	5.0	0.81	17.8	1.20
Polyisobutene	5.8	6.8	1.09	30.5	1.16
Polyvinyl chloride[e]	3.0	2.9	0.71	22.0	1.25
Polyvinyl acetate[e]	2.5 (at 0°C.)	2.6	0.85	36.6	1.25
VYHH copolymer[e]	2.65 (at 0°C.)		0.736	24.1	1.25
	5.74 (at 50°C.)	3.25	0.751	24.6	1.25

[a] From various sources, mainly Wood.[10]

[b] Estimated from cohesion energy density, $CED \simeq \beta T/\kappa$.

[c] The molecular weight of an "average" center is obtained by taking the mer weight and dividing by the number of carbon atoms per mer along the main polymer chain.

[d] Estimated from either fiber periods or Courtauld molecular models.

[e] From measurements below the glass transition.

TABLE III
Collision Diameters for Simple Gases

Gas	d_g, A.	$(\pi/4)d_g^2$, A.^{2}
He	2.58	5.23
Ne	2.86	6.43
H_2	2.92	6.70
A	3.47	9.47
O_2	3.54	9.85
CO	3.71	10.81
N_2	3.75	11.05
CO_2	3.90	11.95

TABLE IV
Average Length of Polymer Segments

Polymer	$2\lambda n$, A.		Average temp., °K.
	From molecular model	From eq. (23)	
Polybutadiene	10	6–8	300
Natural rubber	13	15	273
	12	14	285
	11	11	308
	8	6	343
Neoprene	11	8–12	300
Polyisobutene	14	16–20	300
Polyvinyl chloride	20	17	300
Polyvinyl acetate	8–11	10–14	273
VYHH copolymer	7–10	10–18	273

difficult to generalize on the basis of the small amount of data obtained from the literature and because of the uncertainty of what is meant by "gas diameter" and "activation energy," the implication is that all of the internal processes of diffusion and flow within amorphous polymers might be controlled by the motion of polymer segments whose lengths are primarily a function of temperature. On the basis of van Amerongen's data on the effects of temperature on activation energy,[8] these analyses show that the average segmental length appears to be decreasing with increasing temperature. The decrease in activation energy is therefore related to the decrease in the short-range molecular order within the polymers.

Although there is reasonable agreement between the two theoretical approaches in the range of fluctuations required for diffusion of simple gases, differences are apparent in the limits of large and small fluctuations. In the limit of zero gas diameter, the activation energy predicted by the molecular model is zero since the activation energy was defined as the average change in potential energy accompanying a volume change of $2\lambda n(\pi/4)d_g^2$. The potential energy function was defined in such a way that this change was equal to the energy required to overcome the cohesive forces between polymer segments. The compression of the surrounding

segments and the interaction of the gas molecule with the surroundings were neglected. Thus as the fluctuations become large and the average attractive forces become small, the predicted activation energy tapers off to a constant value which represents the total cohesion energy of a segment. In the limit of zero gas diameter, the activation energy predicted by the fluctuation analysis is a positive value since the activation energy was defined as the excess energy associated with all fluctuations larger than the minimum size of $2\lambda n(\pi/4)d_g^2$. This excess, localized energy was written as a power series of the volume fluctuation [eq. (15)] which shows the energy increasing very rapidly with the size of the fluctuation. Ignoring the presence of the gas molecule is implicit in the development, but no assumptions were made as to the mechanism responsible for the changing energy. If one wishes to put an interpretation on eq. (15), it might be said that the total internal energy change associated with the volume change is the work required to overcome the cohesive forces of the segment to its surroundings and the work required to compress the surroundings. Thus, as the volume of the fluctuation increases, the amount of compression increases sharply, and the predicted activation energy continues to rapidly rise in spite of the fact that the cohesion forces are now negligible.

It is interesting to note that the activation energies for gaseous diffusion in the rubbery polymers, polyisobutene, neoprene, natural rubber and polybutadiene, were almost exactly predicted by the molecular model (see Figure 4, for example), while the activation energies for gaseous diffusion in the glassy polymers, VYHH copolymer and polyvinyl acetate, followed the theoretical curves of the fluctuation analysis much more closely. This is interpreted to mean that when a polymer is well above its glass transition temperature, there is sufficient mobility for the structure to readjust to a volume fluctuation without having to compress surrounding bundles of polymer segments. Thus, eq. (15) is a poor representation of the excess thermal energy, since no further expenditure of energy is required in rubbery solids once the cohesive forces holding the polymer segment are overcome. On the other hand, when a polymer is below (or even around) the glass transition temperature, the mobility of the surrounding bundles of polymer segments is not sufficient to readjust to the volume fluctuation and therefore the fluctuation can occur only if work is done to compress the surroundings. Then eq. (15) is a very reasonable representation of the fluctuation energy.

These concepts are very appealing, to us at least, because they give a very simple interpretation to a variety of superficially different kinds of diffusion data for amorphous polymers. If they are correct concepts, there is hope, at least, that one can tie the phenomena of gaseous diffusion, self diffusion and viscous flow to the thermodynamic and molecular properties of the polymer. To show restraint, however, it should be emphasized that the analysis in this paper (and the prior two[1,2]) is based on "average" values for the physical properties of the polymers, an assumption that the diffusion data were truly obtained from the amorphous forms of these

polymers (or that one could neglect diffusion in crystallite region if they were present), that the diameters for the gases in the polymers were reasonably represented by the values of Table III and that the activation energy change could truly be equated to either the average potential energy change (the molecular approach) or the average excess fluctuation energy (thermodynamic approach).

It is our opinion that the first and second of these factors are very reasonable assumptions. The matter of what gas diameter to choose is a difficult question to resolve. A number of different sources of values were tried, including diameters based on viscosity data, virial coefficient data, molecular models, and diameters referred to gases at infinite temperature. It was found that as long as one is consistent, the choice of source does not change the general results. A more fundamental question is whether any of these sources are useful for characterizing a gas in a polymer. The assumption of a molecule as a penetrable sphere is very reasonable in the gaseous state, but when a gas molecule is trapped in a solid polymer it is questionable whether the geometry of nonspherical molecules such as hydrogen, oxygen and carbon dioxide can be simplified. The literature data are not precise enough to resolve this point. The final question of whether one can equate activation energies to the specified variables is a question of interpretation and should be given further thought.

In summary, interpretations of gaseous diffusion through polymers have been presented from both a molecular model and a statistical fluctuation viewpoint. Both interpretations give very similar results and when combined, give an insight into the nature of transport processes in an amorphous polymer.

This project has been supported in part by the Research Committee of the Graduate School from funds supplied by the Wisconsin Alumni Research Foundation and also from funds supplied by the Shell Fellowship in Chemical Engineering.

Appendix

β = Volumetric coefficient of thermal expansion $(°K.)^{-1}$
δF = Delta F, the difference between two states $F_1 - F_0$
d_g = Collision diameter of gas molecule, A.
ϵ^* = Energy parameter for the 6–12 potential, ergs/center
ΔE_D = Activation energy for gaseous diffusion, kcal./mole
φ_{TC} = Interaction potential energy, ergs/center
κ = Coefficient of isothermal compression, $cm.^2$/dyne
2λ = Chain length per center, A.
n = Number of centers per polymer segment
N = Avogadro's number, molecules/mole
p_{ext} = External pressure
ρ^* = Distance parameter for the 6–12 potential, A.
T = Absolute temperature, °K.
v^* = Volume parameter for the 6–12 potential = $2\lambda\rho^2$, $A.^3$

v = Volume per center, A.^{3}/center
R = Gas constant, cal./mole-°K.
f_N = General density of distribution function for an ensemble
e = Total energy for one system of an ensemble, ergs
k = Boltzmann constant, ergs/molecule-°K.
W = Probability function
a = Helmholtz energy per average center, ergs/center
u = Thermal energy per center, ergs/center
V = Total volume of a system cc./mole of centers
A = Total Helmholtz energy, cal./mole of centers
U = Total thermal energy, cal./mole of centers
ΔE_D^* = Dimensionless activation energy = $\Delta E_D/RT$
β^* = Dimensionless thermal expansion coefficient = βT
d_g^{*2} = Dimensionless gas diameter = $2\lambda(\pi/4)d_g^2(N/V_0)$
V^* = Dimensionless average volume for a polymer segment = $nV_0/\kappa RT$
p^* = Dimensionless external pressure = $p_{ext}nV_0/RT$
v^* = Dimensionless volume fluctuation = $\delta v/v_0$
F_0 = Mean thermodynamic value for property at a given temperature and pressure

References

1. DiBenedetto, A. T., *J. Polymer Sci.*, **A1**, 3459 (1963).
2. DiBenedetto, A. T., *J. Polymer Sci.*, **A1**, 3477 (1963).
3. Bueche, F., *J. Chem. Phys.*, **21**, 1850 (1953).
4. Kumins, C. A., and J. Roteman, *J. Polymer Sci.*, **55**, 683, 699 (1961).
5. Tolman, R. C., *The Principles of Statistical Mechanics*, Oxford University Press, 1938, Chap. III, p. 46; Chap. XIV, p. 638.
6. Meares, P., *J. Am. Chem. Soc.*, **76**, 3415 (1954).
7. Glasstone, S., *Textbook of Physical Chemistry*, 2nd Ed., Van Nostrand, 1946, p. 479.
8. van Amerongen, G. J., *J. Polymer Sci.*, **5**, 307 (1950).
9. Houwink, R., *Elastomers and Plastomers*, Vol. I, Elsevier, Amsterdam, 1950, Chap. 6.
10. Wood, L. A., *J. Polymer Sci.*, **28**, 319 (1958).
11. Hirschfelder, J., C. F. Curtiss, and R. B. Bird, *The Molecular Theory of Gases and Liquids*, Wiley, New York, 1954, p. 1110.
12. Trautz, M., A. Melster, R. Zink, *Ann. Physik* [5], **7**, 409 (1930).

Résumé

On se représente un polymère amorphe comme un ensemble de N segments de polymère, indépendants, à n-centres. On utilise une hypothèse ergodique, et un ensemble canonique afin de déterminer la probabilité d'une fluctuation de volume donné dans un polymère. On calcule le changement d'énergie thermique associé à une fluctuation de volume donné et rapporté à l'énergie d'activation pour la diffusion gazeuse. Les longueurs des segments de polymère sont dans un domaine de 6 à 20 A et diminuent avec l'augmentation de température dans le cas du caoutchouc naturel. On interprète ces résultats afin de montrer que l'énergie d'activation pour la diffusion gazeuse dans les polymères caoutchouteux conduit à la cassure des liens de cohésion entre les segments parallèles de polymères tandis que dans un polymère vitreux elle conduit à la cassure des

liens de cohésion et à la compression des segments environnants. On remarque qu'il est possible de relier la diffusion gazeuse, la "self"-diffusion et l'écoulement visqueux aux propriétés thermodynamiques et moléculaires d'un polymère amorphe.

Zusammenfassung

Ein amorphes Polymeres wird als ein Ensemble von N unabhängigen, n-zentrigen Polymersegmenten betrachtet. Zur Bestimmung der Wahrscheinlichkeit einer gegebenen Volumsschwankung innerhalb des Polymeren wird eine Ergodenhypothese und ein kanonisches Ensemble herangezogen. Die mit einer gegebenen Volumsschwankung verbundene Änderung der thermischen Energie wird berechnet und zur Aktivierungsenergie für die Gasdiffusion in Beziehung gesetzt. Die Polymersegmentlängen lagen im Bereich von 6 bis 20 A und schienen im Falle des Naturkautschuks mit steigender Temperatur abzunehmen. Die Ergebnisse wurden dahingehend interpretiert, dass die Aktivierungsenergie der Gasdiffusion in kautschukartigen Polymeren zur Spaltung von Kohäsionsbindung zwischen parallelen Polymersegmenten aufgewendet wird, während bei Polymeren im Glaszustand eine Spaltung von Kohäsionsbindungen und eine Kompression der umgebenden Segmente notwendig ist. Es scheint möglich zu sein, Gasdiffusion, Selbstdiffusion, und viskoses Fliessen zu den thermodynamischen und molekularen Eigenschaften eines amorphen Polymeren in Beziehung zu bringen.

Received January 14, 1963

JOURNAL OF POLYMER SCIENCE: PART A VOL. 2, PP. 1017–1021 (1964)

Copolymerization of Diethyl Phosphonoalkyl Acrylates*

C. G. OVERBERGER and E. SARLO, *Department of Chemistry, Polytechnique Institute of Brooklyn, Brooklyn, New York*

Synopsis

Diethylphosphonomethyl acrylate, diethylphosphonomethyl methacrylate, and 1-diethylphosphonoethyl acrylate were copolymerized by radical catalysis with methyl methacrylate and, in one case, methyl acrylate. The reactivity ratio values indicate that the phosphorous-containing monomers enter into the copolymer somewhat less readily than methyl acrylate or methyl methacrylate. Both electronic and steric effects may be operative.

INTRODUCTION

The utilization of organophosphorus monomers and polymers has been almost entirely studied in industrial laboratories. The patent literature indicates their use as coatings,[1] adhesives,[2] plasticizers,[3] flame retardents,[4] and ion-exchange resins.[5] Since polymethylmethacrylate filling materials have been quite widely used for dental restortions, it was of interest to prepare several phosphorus-containing acrylates which might find use in tooth restorations. Because much of the enamel and dentine of the tooth its hydroxyapatite, better adhesion might possibly be obtained by the incorporation of the polar phosphonate moiety into the resin filling material. Further, transesterification might occur between the tooth filler and the phosphate present in the dentine and enamel of the tooth, thereby enhancing the adhesive properties of the polymer.

It was also of interest to determine the reactivity ratios of the phosphorous-containing acrylates in vinyl copolymerization, in order to gain some knowledge of the influence of the phosphonate group in a radical addition reaction. The following communication reports the results of these copolymerizations using methyl methacrylate and, in one case, methyl acrylate as the comonomers.

RESULTS AND EXPERIMENTAL

Monomers

Diethylphosphonomethyl acrylate (I), diethylphosphonomethyl methacrylate (II), and 1-diethylphosphonoethyl acrylate (III), and the poly-

* This paper comprises a portion of a dissertation submitted by E. Sarlo in partial fulfillment of the requirements for the degree of Doctor of Philosophy in the Graduate School of the Polytechnic Institute of Brooklyn.

mers derived therefrom were prepared as previously reported.[6] The pertinent physical constants appear in Table I. Methyl acrylate and methyl methacrylate were distilled immediately before use.

TABLE I
Physical Constants of Diethylphosphonoalkyl Acrylates I, II, and III

Monomer	B.p., °C./mm. Hg	n_D^{25}	Yield, %	P, % Calcd.	P, % Found
I	108–110/0.6	1.4340	35	13.94	13.90
II	92–94/0.3	1.4398	46	13.11	12.73
III	90–93/0.05	1.4363	30	13.11	12.82

Copolymerizations

The copolymerizations were carried out in 5 in. glass tubes. The monomers were weighed out directly in the polymerization tubes which were then immersed in an acetone–dry ice bath and evacuated by means of an oil pump with intermittent flushing with nitrogen. The tubes were then sealed under vacuum and placed in a constant temperature oil bath. Azobisisobutyronitrile was employed as a free radical source in a concentration of 0.3–0.4 wt.-% in each case. The data are given in Tables II–V. The reactivity ratios were calculated by the method of Mayo and Lewis.[7] The values are given in Table VI.

TABLE II
Copolymerization of Diethylphosphonomethyl Acrylate (M_1) and Methyl Acrylate (M_2) at 75°C.

Charge composition M_1/M_2	Copolymer composition m_2/m_1	Conversion, %	P, %
2.830	0.745	12	10.76
			10.90
1.407	1.139	11	9.67
0.829	1.690	1	8.43
			8.39

TABLE III
Copolymerization of Diethylphosphonomethyl Acrylate (M_1) and Methyl Methacrylate (M_2) at 75°C.

Charge composition M_1/M_2	Copolymer composition m_2/m_1	Conversion, %	P, %
2.07	1.21	15	9.02
			9.00
0.99	2.33	10	6.83
			6.76
0.265	7.79	10	3.08
			3.09

TABLE IV
Copolymerization of Diethylphosphonomethyl Methacrylate (M_1) and Methyl Methacrylate (M_2) at 68°C.

Charge composition M_1/M_2	Copolymer composition m_2/m_1	Conversion, %	P, %
1.07	1.53	9	8.02
			7.89
0.27	5.58	8	3.87
			3.93
0.64	2.43	9	6.48
			6.48

TABLE V
Copolymerization of 1-Diethylphosphonoethyl Acrylate (M_1) and Methyl Methacrylate (M_2) at 65°C.

Charge composition M_1/M_2	Copolymer composition m_2/m_1	Conversion, %	P, %
1.12	2.47	10	6.41
1.12	2.42	10	6.47
0.32	6.95	4.4	3.35
			3.30
0.36	6.56	6	3.47
			3.46

TABLE VI
Copolymerization Results

Monomer 1	Monomer 2	r_1	r_2
Diethylphosphonomethyl acrylate	Methyl acrylate	0.29 ± 0.05	0.88 ± 0.09
Diethylphosphonomethyl acrylate	Methyl methacrylate	0.27 ± 0.01	1.88 ± 0.03
Diethylphosphonomethyl methacrylate	Methyl methacrylate	0.50 ± 0.03	1.43 ± 0.05
1-Diethylphosphonoethyl acrylate	Methyl methacrylate	0.15 ± 0.03	2.02 ± 0.05

DISCUSSION

The synthesis and polymerization of vinylphosphonates has been reported by several investigators.[8-10] Their ability to polymerize and copolymerize by radical catalysis was reported to be relatively poor. Arcus and Matthews[11] found that diethyl vinylphosphonate was slow to enter into radical-initiated copolymerization with styrene, the reactivity ratios being 3.25 for styrene and 0.0 for the phosphonate. The effect of both temperature and initiator concentration was found to be small. It was also noted that the degree of polymerization increased as the styrene content in the feed increased. Lindsey[12] and Marvel[9] also showed that

dimethyl 1-propene-2-phosphonate was less prone to enter the growing copolymer than either styrene, methyl methacrylate, or butadiene in radical copolymerization. Butler and Berlin[13] suggested that the unreactivity and the low molecular weight of poly(diphenylvinylphosphine oxide) were due to enolic structures involving expansion of the phosphorus shell as well as the steric requirement of the phosphoryl group.

From the data tabulated in Table VI, it appears that the phosphonoacrylates enter into the copolymer somewhat less readily than do the alkyl acrylates and methacrylates. The first result indicates that diethylphosphonomethyl acrylate is less reactive than methyl acrylate toward a diethylphosphonomethyl acrylate free radical and that both are equally reactive toward a methyl acrylate free radical, i.e., $r_1 = k_{11}/k_{12} = 0.29$; $r_2 = k_{22}/k_{21} = 0.88$. The copolymerizations of the phosphonoacrylates with methyl methacrylate show that the former compounds are less prone to enter into the copolymer than are the latter. The r_1 values in these cases are of the same order of magnitude as in the case of diethylphosphonomethyl acrylate with methyl acrylate, indicating the same tendency for a phosphonoacrylate monomer to add to a phosphonoacrylate free radical. The overall reactivity values are similar to those reported by Sandberg and Bovey[14] for 1,1-dihydroperfluorobutyl acrylate (M_1) and methyl methacrylate (M_2) where $r_1 = 0.25$ and $r_2 = 1.40$.

The diminished ability of the phosphorus-containing acrylates to enter the copolymer can be partially explained in terms of electronic and steric effects. Substituents two to three atoms distant from the polymerizable vinyl group are known in some cases[15] to effect copolymer composition. Both electronic and steric effects have been invoked by Toy[16] to explain the polymerization behavior of various substituted diallyl alkylphosphonates, R—(O)—P— $(O—CH_2—CH=CH_2)_2$. As the size of R increased, the tendency for the formation of gum to soft gel-like polymer increased. The electronegative character of R also appeared to influence the course of polymerization even though it was rather far removed from the allylic group. Rabinowitz[17] found that diethyl 2-vinyloxyethylphosphonate gave a low molecular weight polymer when treated with di-*tert*-butyl peroxide. A fiftyfold variation in the initiator concentration had no effect on the molecular weight. Cationic initiation failed completely, thus showing a marked difference between this monomer and 2-chloroethyl vinyl ether.

Since methyl acrylate is more reactive toward a diethylphosphonomethyl acrylate radical than is the diethylphosphonomethyl acrylate monomer, a steric requirement on the part of both the incoming monomer and the growing radical might affect the copolymer composition. Molecular models indicate some crowding in the phosphorus-containing acrylates, while the terminal phosphonoacrylate radical may exhibit a penultimate effect caused by partial shielding by the phosphoryl oxygen and/or by the ethoxy groups each of which is six atoms away from the radical site.[13,18]

The phosphonate group may also be deactivating the monomer through its electron withdrawing ability in copolymerizations with acrylate types; that is, there is no polar driving force. Thus the electronegative character of phosphonates causes effects similar to those caused by carbonyl and nitro groups.[19]

References

1. Toy, A. D. F. and K. H. Rattenbury (to Victor Chemical Works), U.S. Pat. 2,714,100 (July 26, 1955).
2. Brandner, J. D. (to Atlas Powder Co.), Can. Pat. 509,645 (Feb. 1, 1955).
3. Toy, A. D. F. (to Victor Chemical Works), U.S. Pat. 2,691,567 (Oct. 25, 1949).
4. Schuyten, H. A., J. W. Weaver, and J. D. Reid, *Ind. Eng. Chem.*, **47**, 1433 (1955).
5. Daul, G. C., and J. D. Reid (to U.S. Secy. of Agriculture), U.S. Pat. 2,609,360 (Sept. 2, 1952).
6. C. G. Overberger and E. Sarlo, *J. Org. Chem.*, **26**, 4711 (1961).
7. Mayo, F. R., and F. M. Lewis, *J. Am. Chem. Soc.*, **66**, 1594 (1944).
8. Pike, J. M., and R. A. Cohen, *J. Polymer Sci.*, **44**, 374 (1955).
9. Marvel, C. S., and J. C. Wright, *J. Polymer Sci.*, **8**, 255 (1952).
10. Kosolapoff, G. M., *J. Am. Chem. Soc.*, **70**, 1971 (1948).
11. Arcus, C. L., and R. J. S. Matthews, *J. Chem. Soc.*, **1956**, 4607.
12. Lindsey, R. V. (to E. I. du Pont de Nemours & Co.), U.S. Pat 2,439,214 (April 6, 1948).
13. Butler, G. B. and K. D. Berlin, *J. Org. Chem.*, **26**, 2537 (1961).
14. Sandberg, C. L., and F. A. Bovey, *J. Polymer Sci.*, **15**, 553 (1955).
15. Petrova, G. A., G. A. Shtraikhman, and A. A. Vansheĭdt, *Zh. Fiz. Khim.*, **33**, 1246 (1959).
16. Toy, A. D. F., and R. S. Cooper, *J. Am. Chem. Soc.*, **76**, 2193 (1954).
17. Rabinowitz, R., *J. Org. Chem.*, **26**, 5152 (1961).
18. Newman, M. S., *Steric Effects in Organic Chemistry*, Wiley, New York, 1956, p. 206.
19. Crofts, P. C., *Quart. Revs.*, **12**, 341 (1958).

Résumé

On a effectué la copolymérisation radicalaire de l'acrylate de diéthylphosphoroéthyle, du méthacrylate de diéthylphosphonométhyle et de l'acrylate de 1-diéthylphosphonométhyle avec le méthacrylate de méthyle et, dans un cas, avec l'acrylate de méthyle. On a constaté, grâve aux valeurs des rapports de réactivité que les monomères qui contiennent du phosphore, copolymérisent un peu moins facielment que l'acrylate de méthyle ou que le méthacrylate de méthyle. On peut attribuer ceci tant aux effets stériques qu'électroniques.

Zusammenfassung

Diäthylphosphonomethylacrylat, Diäthylphosphonomethylmethacrylat und 1-Diäthylphosphonoäthylacrylat wurden radikalisch mit Methylmethacrylat und, in einem Fall, mit Methylacrylat copolymerisiert. Der Wert des Reaktivitätsverhältnisses zeigt, dass die phosphorhältigen Monomeren etwas weniger leicht ins Copolymere eintreten als Methylacrylat oder Methylmethacrylat. Dafür können elektronische und sterische Effekte verantwortlich sein.

Received January 18, 1963

BOOK REVIEW

N. G. GAYLORD, Editor

The Effect of Ionizing Radiation on High Polymers (Russian Tracts on Advanced Mathematics and Physics, Vol. 13), T. S. Nikitina, E. V. Zhuravskaya, and A. S. Kuzminsky, Gordon and Breach, New York, 1963, vi + 90 pp. $4.95.

This volume is a translation by Scripta Technica Inc. of a work originally published in the USSR. One might say of this book that it is "too little and too late." It is only ninety pages in over-all length and the last twenty-odd pages are devoted to tables of formulations and radiations effects on commercial plastics and elastomers. The coverage of the literature is only through 1958 so that much of the data is out of date. The book provides only the briefest and cursory review of this field and offers nothing which has not been written much earlier and with greater depth. This volume is certainly much inferior to similar efforts by Bovey, Charlesby, and Chapiro. The reviewer had hoped to find a more extensive review of the Russian research work in this field but even this proved to be a disappointment for only twenty-seven of two hundred and four references are to Russian work. Actually, this is little more than an English translation of a Russian review of non-USSR publications.

The translation itself is well done and very easily readable with a minimum of technical errors. It is unfortunate that so much time was devoted to translation of such outdated and nonsignificant material.

The reviewer cannot recommend this work from any standpoint. The paper is of poor quality, the print is too small, and the bibliography is not bound but appears on a separate, removable sheet.

D. S. Ballantine

Brookhaven National Laboratory
Associate Universities, Inc.
Upton, New York

ERRATUM

Some Considerations on the Kinetics of the Acid Hydrolysis of Poly- and Oligo-saccharides

(article in *J. Polymer Sci.*, **C2**, 97–107, 1963)

By ALEXANDER MELLER

Research Laboratory, Australian Paper Manufacturers Limited, Melbourne, Australia

On page 101, para. 3, line 18 the literature reference should read 23.

On page 102 in Table I under column 5, top line should read 4.6×10^{16}; under column 6, lines 18 and 19, should read 22.

On page 104 caption of Figure 4 should read: Relationship between $\log k$ and $1/T$ and H_0 for cellobiose in sulfuric acid solutions: (□) $\log k \times 10^4$ vs. $1/T$, 8% H_2SO_4, data of Rogovin and Konkin;[22] (X) $\log k \times 10^4$ vs. $1/T$, 1N H_2SO_4, data of Sharples[20] and Senju and Shimizu;[21] (●) $\log k \times 10^4$ vs. $-H_0$, 40°C., data of Novikova and Konkin[1] and Noto La Diega.[16]